

Dissertation

**MECHANISM OF ACTION STUDIES ON THE FR-900482 CLASS OF  
ANTITUMOR ANTIBIOTICS**

Submitted by

Scott Raymond Rajski

Department of Chemistry

In partial fulfillment of the requirements

for the degree of

Doctor of Philosophy

Colorado State University

Fort Collins, Colorado

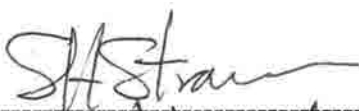

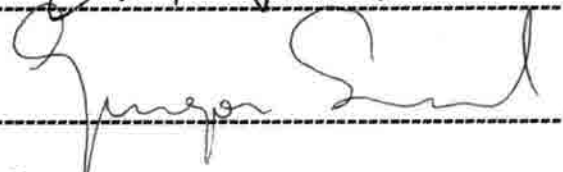

Summer 1997

Colorado State University

March 13, 1997

WE HEREBY RECOMMEND THE DISSERTATION PREPARED UNDER OUR SUPERVISION BY SCOTT R. RAJSKI ENTITLED " MECHANISM OF ACTION STUDIES ON THE FR-900482 CLASS OF ANTITUMOR ANTIBIOTICS" BE ACCEPTED AS FULFILLING IN PART THE REQUIREMENTS FOR THE DEGREE OF DOCTOR OF PHILOSOPHY.

Graduate Research Committee Members

  
-----  
  
-----  
  
-----  
  
-----

-----  
ADVISOR

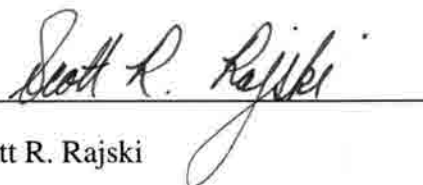
-----  
DEPARTMENT HEAD

## ABSTRACT OF DISSERTATION

### MECHANISM OF ACTION STUDIES ON THE FR-900482 CLASS OF ANTITUMOR ANTIBIOTICS

The interactions of members of the FR-900482 class of antitumor antibiotic agents with DNA has been examined. Importantly, the first *in vitro* demonstration of nucleic acid interstrand cross-linking has been reported and the DNA base pair sequence specificity of the cross-linking event has been elucidated. These agents demonstrate a high degree of selectivity for 5'-CG-3' sequences of DNA. As such, bio-mechanistic analogy between these compounds and the clinically employed compound Mitomycin C has been shown. Efforts have also examined extensively the ability of these agents to give rise to orientation isomers of each respective cross-link and their different properties.

DNA-protein cross-linking by these agents has also been examined. A sequence-specific DNA-peptide binding motif has been identified which undergoes drug-mediated DNA-protein cross-linking. This is the first reported instance of a mitosene based-minor groove DNA-protein cross-link event. Significantly, the motif examined is characteristic of tissues which bear striking similarity to those of cancerous cell lines.



Scott R. Rajski

Department of Chemistry

Colorado State University

Fort Collins, Colorado 80523

## Acknowledgments

The interdisciplinary nature of this project mandated the use of resources not typically associated with a "straight" chemistry project. In this regard, the author would like to thank Dr. Joseph Corisini and Dr. Margaret Kovach of the Jonathon Carlson group in Microbiology. These individuals had a tremendous impact upon the early successes of this project and were fundamental in fostering the foundation for the author's understanding of molecular biology techniques and principles. In line with this, Dr. Jon Carlson also provided invaluable input and willingly addressed what should have seemed like an astounding number of questions.

With regard to members of the chemistry department the author would like first and foremost to thank certain members of the faculty. Prof. Williams has stated that a measure of one's success is the ability (or inability) to use every possible resource at hand to achieve specific goals. With this in mind, it can be said with great certainty that some of the most valuable resources at CSU are Dr. Louis S. Hegedus, Frank R. Stermitz and Marc M. Greenberg. These faculty members have provided excellent examples of professionalism and dedication to excellence in their field. Not only have they been willing to discuss scientific problems (sometimes in great length), but they have also offered valuable general advice pertaining to career paths and the like. The amount of time this took was often considerable and did not go unnoticed. It is truly remarkable that individuals who have so little time in which to do an infinite number of tasks manage to spend so much time with students. I consider myself very fortunate to have been associated with these individuals.

The author would like to extend a special token of gratitude to past and present members of the Williams' research group. These people have provided many long hours



of entertainment (often unexpected), companionship and support over the years and continue to be the source of intellectual stimulation. Particularly giving with respect to time and effort have been Dr. Mark Flanagan, Mr. Tracy Tippie, Dr. Greg Miknis, Dr. Glenn Fegley, Ms. Renee Gallegos, Dr. Juan San-Cevera, and Ms. Kathleen Halligan. The friendships fostered by these individuals are among those most valued.

Members of the Greenberg group are also to be thanked for providing a valuable source of scientific exchange. Gary Cook, Tracy Matray, and Dustin McMinn, in addition to being the hardest working students in Chemistry, were kind enough to allow ideas/experiments to be continually bounced off of them. This too can be said of Dr. Marc "Chief" Greenberg. The kindness of these extremely driven and talented people is gratefully acknowledged.

Technically speaking, the author would like to thank Don Dick for conducting all mass spectral analyses, Mr. Eric Dodson for taking time to perform cyclic voltametry experiments and engaging the author in helpful discussions, the Fujisawa Pharmaceutical Corporation for providing authentic FR-900482, and Dr. T. Bradner of Bristol Myers-Squibb for a sample of mitomycin C. Additionally, the author would like to recognize Mr. Samuel Rollins for extensive efforts with respect to the molecular modeling studies. Sam also provided a great deal of helpful input into the analysis of the resulting structures. Shelly Swanson is also to be acknowledged for assistance starting from day one of the author's involvement with CSU. Her friendly attitude and willingness to assist with the daily tasks has been invaluable throughout the author's graduate stay.

The author would also like to thank Professor Robert M. Williams for providing lab space, chemicals and the extensive financial support required by the studies discussed herein. Dr. Williams' enthusiasm at the outset of the project balanced with a hands-off approach later on provided a great opportunity by which to learn problem-solving skills not attainable in many other scenarios. His willingness to allow the author to pursue his own intellectual interests and to actively involve the author in proposal renewals, paper writing,

and interactions with visiting professors fostered a learning experience far exceeding that gained by benchwork alone. Additionally, Dr Williams' interest and ability to pursue research problems at the leading edge of chemical/biological research has been exemplary. His reluctance to be confined within a narrow window of expertise is directly responsible for this author's exposure to and interest in a vast amount of science not traditionally associated with chemistry.

Lastly, the author would like to express appreciation for the continual support and interest of his father and family (inclusive of Diane, Jason and "Grandma" Kelly). Additionally the author would like to recognise Ms. Tricia Cecil's patience and tolerance. These individuals' never-wavering support and encouragement is lovingly appreciated.

## **Dedication**

This dissertation is dedicated to the memory of my grandparents (Erma and Raymond) and to their eldest child Douglas, my father. No lessons are more important than those bestowed upon me by them.

## TABLE OF CONTENTS

<b>Chapter 1 INTRODUCTION</b>	<b>1</b>
1. DNA-DNA Crosslinking ( <i>A Review</i> )	1
1.1. Origin and Biological Significance	1
1.2. Inherently reactive agents not requiring activation	7
1.2.1. Nitrogen Mustards and Related Structures	7
1.2.2. Chloroethylating agents	14
1.2.2.1. Nitrosoureas	15
1.2.2.2. Triazenes	17
1.2.2.3. Alkyl Sulfonates	20
1.2.3. Epoxide Containing agents	21
1.2.3.1. Diepoxybutane	23
1.2.3.2. Carzinophilin/Azinomycin B	25
1.2.4. <i>cis</i> -Diamminedichloroplatinum (II)	28
1.2.5. Dimeric monoalkylating agents as interstrand cross-linkers	35
1.2.5.1. Carzinophilin A and Isochrysohermidin	36
1.2.5.2. Bizelesin (U-77,779) and related structures	38
1.2.5.3. Pyrrolo[1,4]benzodiazepine Dimers	42
1.2.5.4. Dinuclear <i>cis</i> platin compounds	44
1.3. Photoactivated Compounds	46
1.3.1. Psoralens	46
1.4. Oxidatively Activated Agents	52
1.4.1. Cyclophosphamide	54
1.4.2. N,N,N',N',N',N'-hexamethylmelamine (HMM) and related compounds	58
1.4.3. Pyrrolizidine alkaloids	62
1.5. Hypoxia Specific Agents (reductively activated)	70
1.5.1. "Masked" Nitrogen mustards ( N-oxides and nitroaromatics)	72
1.5.2. Transition metal complexes	76
1.5.3. Anthracyclines	79
1.5.4. Aziridinybenzoquinones	89
1.5.5. Mitomycin C and related structures	93
1.6. Conclusions/summary	111
1.7. References	113

## Chapter 2 DNA-DNA Interstrand Crosslinking by FR-900482 and related compounds

2.1.	Background	136
2.2.	Results & Discussion	140
2.2.1.	Activation studies	140
2.2.2	Comparison of cross-linking efficiency by FR-900482 and FR-66979	150
2.2.3.	DNA Sequence specificity studies: Relevance to a "mitosene" intermediate	154
2.2.4.	Studies directed at elucidation of a reactive leuco-FR-66979 intermediate enroute to FR-66979 mediated interstrand cross-linking	166
2.2.5.	Verification of Orientational Isomerism in the FR-66979 mediated 5'-CG-3' cross-link	176
2.2.6.	Assignment of "mitosene core" orientation with respect to gel mobility of cross-linked <b>template 3</b>	186
2.2.7.	Detection of DNA kinking/bending induced by FR-66979 as assayed by DNA ligation.	191
2.2.8.	Detection of Drug-induced hyperreactive DNA regions	192
2.2.9.	Molecular Modeling of FR-66979 cross-link orientation isomers	196
2.2.10.	Reaction of orientation isomers of FR-66979 cross-link with Alu I restriction endonuclease	199
2.3.	Conclusion/Significance	205

## Chapter 3 DNA-protein cross-linking mediated by the FR-900482 class of antitumor antibiotics

3.1.	Background	207
3.1.1.	Minor groove-binding proteins	208
3.1.2.	The HMG proteins	214
3.2.	Results & Discussion	219
3.2.1.	DNA monoalkylation model studies pertinent to DNA-protein cross-linking by reductively activated FR-66979	219

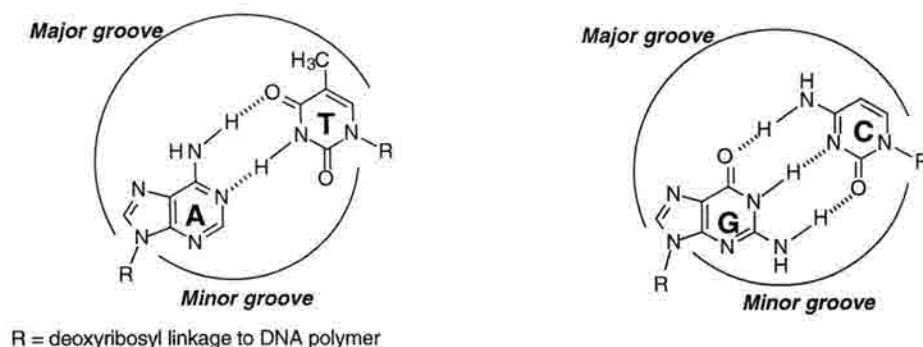
3.2.2. Initial Efforts toward DNA-peptide cross-linking by reductively activated <b>314</b> : Modeling and Rationale	225
3.2.3. Reactions of non-self-complementary DNA substrates with functionalized HMG binding domain peptides	230
3.2.4. HMG peptide-DNA cross-linking by reductively activated FR-66979	236
3.3. Conclusion/Significance	243
<b>Chapters 2 &amp; 3 references</b>	245
<b>Chapter 4 Experimentals</b>	257
4.1. General methods	258
4.2. Specialized procedures (in the order as they appear in chapters 2 & 3)	265
<b>Appendices</b>	297
<i>Appendix Listing</i>	
<b>Figure 5-1</b> Desferal and Fe <sup>2+</sup> vs. Fe <sup>3+</sup> reactions of <b>312</b> with linearized PBR322	299
<b>Table 5-1.</b> Summary of ISC yields from Figure 5-1.	300
<b>Figure 5-2</b> Large format image of Fig. 2-14 (Fe(II)-EDTA footprinting of FR-66979 cross-linked <b>templates 1</b> and <b>2</b> )	301
<b>Figure 5-3</b> Fe(II)-EDTA Footprinting for FR-900482, FR-66979, FK-973 cross-linked <b>templates 1</b> and <b>2</b>	302
<b>Figure 5-4</b> Large format image of Fig. 2-15 (Fe(II)-EDTA footprinting of FR-66979 cross-linked <b>templates 1</b> and <b>2</b> - ODN <b>3</b> 5'-labeled)	303
<b>Figure 5-5</b> Reactions of <b>template 1</b> with HPLC fractionated crude FR-66979	304
<b>Figure 5-6</b> Reactions of <b>template 1</b> with FR-66979 derived mitosenes <b>352</b> , <b>353</b>	305
<b>Figure 5-7</b> Reactions of FR-66979, FR-900482, FK-973 with <b>template 3</b>	306
<b>Figure 5-8</b> Reactions of FR66979 with self-complementary ODN <b>7</b>	307
<b>Figure 5-9</b> Fe(II)-EDTA Footprint analysis of orientation isomers of FR-66979 cross-linked <b>template 3</b>	308
<b>Figure 5-10</b> UV vs. Temp. plots for orientation isomers of FR-66979 cross-linked <b>template 3</b>	309

<b>Figure 5-11</b> T4 DNA Ligase reactions with orientation isomers of FR-66979 cross-linked <b>template 3</b>	310
<b>Figure 5-12</b> DEPC hyperreactivity reactions of FR-66979 cross-link orientation isomers of <b>template 3</b> (5'-end-labeled on <b>ODN 4</b> strand)	311
<b>Figure 5-13</b> Chloroacetaldehyde (CAA) reactions with orientation isomers of cross-linked <b>template 3</b>	312
<b>Figure 5-14</b> Verification of C10 connectivity to slow orientation isomer of FR-66979 cross-linked <b>template 7</b>	313
<b>Figure 5-15</b> Alu I digestions of MC cross-linked <b>template 7</b> orientation isomers	314
<b>Figure 5-16</b> Non-Denaturing gel analysis of FR-66979 monoalkylated <b>template 3</b>	315
<b>Figure 5-17</b> Band-shifting of self-complementary <b>ODN 13</b> with cysteinylated BD peptide <b>375a</b>	316
<b>Figure 5-18</b> Piperidine digestions of <b>375a-ODN 16'</b> (5'-end-labeled) complex	317
<b>Figure 5-19</b> DNA exchange of radiolabeled drug-dependent DNA-peptide cross-link	318
<b>Figure 5-20</b> Piperidine digestions of <b>376-ODN 16'</b> and <b>376-ODN 16</b> drug-mediated complexes (each ODN 3' end-labeled)	319

## Chapter 1- Introduction

### 1.1. Origin & Biological Significance

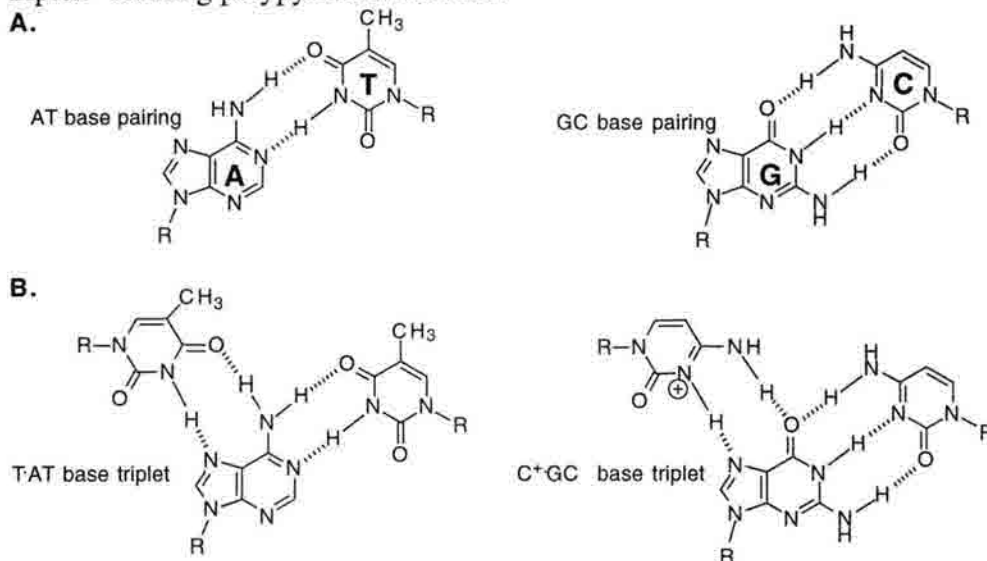
The double helical structure of deoxyribonucleic acid (DNA) represents the richest source of information within a living organism. Importantly, its sequence codes not only for protein/enzyme synthesis *via* the process of translation, but it also codes for RNA synthesis, which, in light of the discovery of ribozymes, is likely to play a much larger cellular role than previously believed.<sup>1</sup> Composed of the four nucleotides deoxyadenosine, deoxyguanosine, deoxycytidine, and deoxythymidine (dA, dG, dC, and dT respectively) DNA is a rather uniform structure when compared to proteins for which there are 20 amino acids to choose from upon translation. The vast majority of naturally occurring DNA is in the canonical B-form, consisting of the two polynucleotide strands wound about a common axis with a right-handed twist.<sup>2</sup> The duplex is roughly 20 Å in diameter with the two strands running antiparallel to each other.<sup>2</sup> The core contains the nitrogenous bases while the sugar-phosphate chains occupy the periphery so as to minimize electrostatic repulsions between the two strands.



**Figure 1-1.** Depiction of major and minor grooves within B-DNA as viewed from top to bottom of the duplex. Grooves are defined with respect to the glycosyl linkage of each base to its respective deoxyribose. See Figure 1-4 (page 8) for base numbering scheme.



Two hydrogen bonding motifs exist for DNA; the Watson and Crick model which is by far the most relevant in considering B-DNA duplexes; and the Hoogsteen motif which is favored under slightly acidic conditions (Fig. 1-2.).<sup>3</sup> Hoogsteen bonding also requires multi-valent cations in order to reduce electrostatic repulsions between the phosphate backbone of the Watson-Crick duplex and the negatively charged backbone of the "triplex" forming polypyrimidine strand.<sup>3</sup>



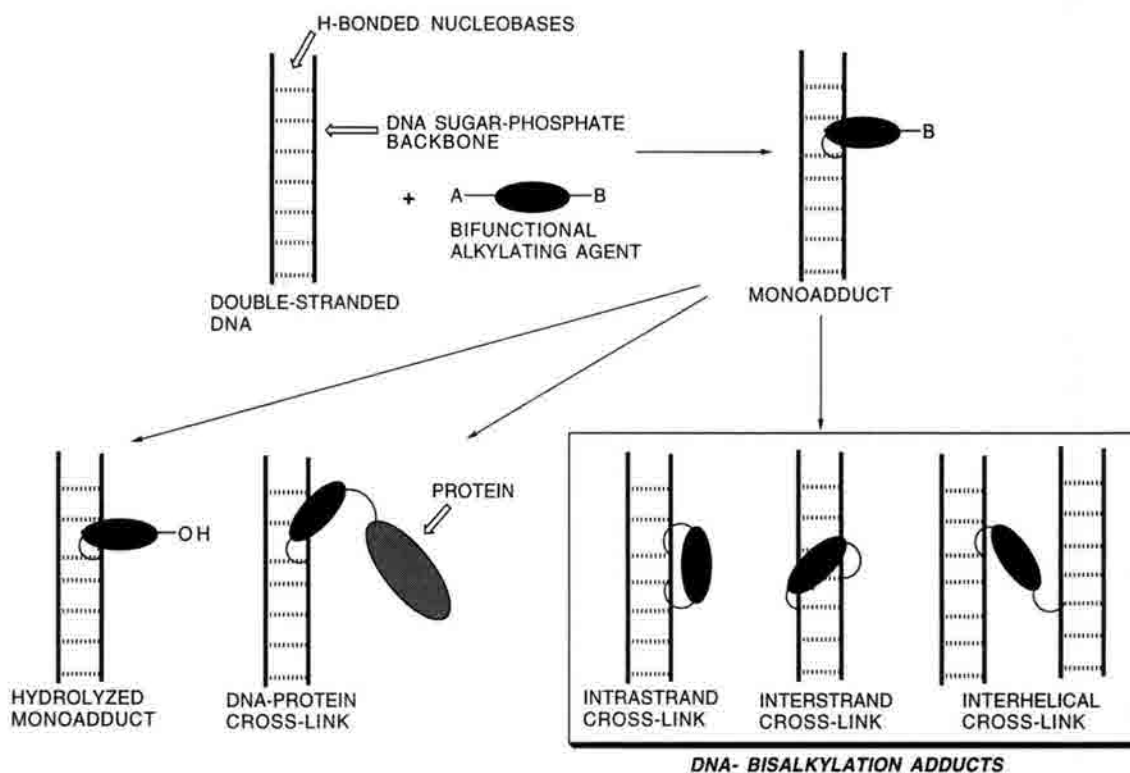
**Figure 1-2.** (A) Watson-Crick A-T and G-C base pairs; and (B) Hoogsteen hydrogen bonding motif for pyrimidines bound in the major groove to the Watson-Crick bonded GC and AT pairs.

Hydrogen bonding is crucial to the ability of the two strands to stay annealed to each other which, in turn, is critical for a host of macromolecular interactions necessary for the survival of the organism. Some such interactions involve the recognition of specific DNA duplex structures by proteins responsible for tumor suppression<sup>4</sup>, transcription activation<sup>5</sup>, and DNA repair<sup>6</sup>, to name just a few. Equally important is the ability of the two strands to separate from one another.

The necessity that DNA be able to undergo strand separation was first hinted at by Watson and Crick in the statement: "It has not escaped our notice that the specific pairing we have postulated immediately suggests a possible copying mechanism for the genetic material."<sup>7</sup> Not long after their ground-breaking paper in which this comment appeared,

they did indeed demonstrate that one DNA strand could act as the template for synthesis of the complementary strand.<sup>8</sup> Since then a great deal has been learned about the intricacies of DNA replication. A host of different enzymes are involved and numerous functions must be performed. At its most rudimentary level of understanding ( and that most relevant to the issue of DNA interstrand cross-linking) DNA is replicated by DNA polymerases which utilize single-stranded DNA as a template upon which the complementary strand is synthesized.<sup>9</sup> This synthesis is dictated by Watson-Crick base pairing of an incoming nucleotide with the template strand thus affording a new strand capable of annealing with the original template. Absolutely crucial is the progressive separation of the two parental strands leading to the synthesis of their complements yielding two semi-conservatively replicated "daughter" strands.<sup>10</sup> The point at which parental strand separation occurs is referred to as the replication fork. The replication fork has held the interest of biologists and chemists alike in that its viability is critical to DNA replication. To block it is to halt replication thus inflicting a catastrophic event upon the organism.<sup>11</sup>

The vast majority of clinically employed alkylating agents behave as electrophilic traps for macromolecular nucleophiles. Such nucleophiles often include amino acids such as cysteine, lysine, tyrosine and threonine. Additionally, the nucleobases of DNA and RNA represent likely targets. It is often the case that bifunctional alkylating agents may give rise to a number of different lesions, including those depicted in Figure 1-3.<sup>12</sup> Although knowledge of the biological consequences of such lesions is increasing, it is generally agreed that the formation of interstrand cross-links represents by far the most toxic of all alkylation events, since this results in seizure of the replication fork.<sup>11</sup>



**Figure 1-3.** Mechanistic pathway for DNA functionalization by interstrand cross-linking agents. A and B represent electrophilic moieties within the compound of interest.

That interstrand cross-links (ISCs) completely shut down replication has been demonstrated on several occasions. In 1969 Lawley *et al.* found that T7 phage were much less infective of an *E. coli* host after reaction with the sulfur mustard di-2-chloroethyl sulfide than by its monohalogenated analog.<sup>13</sup> Phage inactivation occurred with an average of 7 monoalkylations per phage resulting in 1.3 equivalents of interstrand cross-link (note that not all monoalkylations can result in cross-links due to geometric specificity constraints). However, utilizing the singly electrophilic mustard, a total of 280 alkylations per phage were required to achieve a similarly low level of infectivity. More recently, Patierno and Manning have demonstrated the DNA base-specific arrest of T7 DNA polymerase at sites of chromium mediated interstrand cross-linking.<sup>14</sup> Utilizing ascorbate reduction of hexavalent chromium to the trivalent state (5-60uM in Cr(III)) between 2-40 chromium adducted sites were formed per 1000 nucleotides (nts.) of substrate DNA. Of these lesions 18.5 percent resulted in polymerase arrest.

Chromium binds not only the nucleobases, but also the phosphate backbone (giving rise to interhelical binding events). However, only the chromium bound bases were capable of polymerase arrest and of these, only the interstrand cross-link sites terminated polymerase activity, thus accounting for the 18.5 % "arrest ratio".

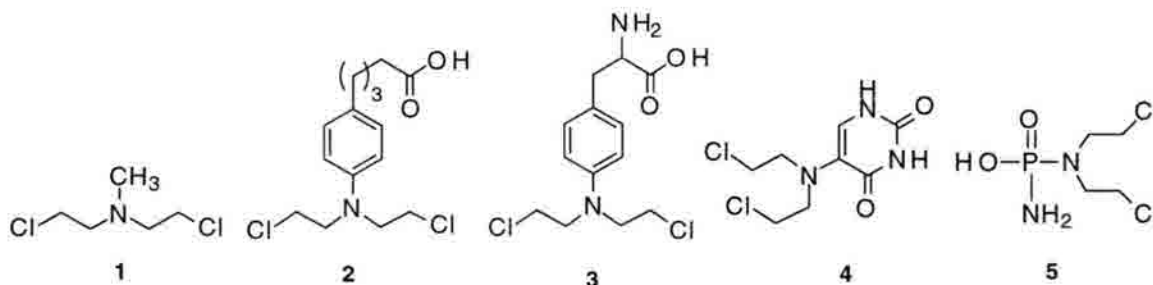
DNA interstrand cross-linking agents comprise an extremely important class of clinical agents not only in the treatment of cancers, but also for diseases such as psoriasis, and various anemias.<sup>15</sup> Their ability to induce DNA-protein cross-links has also been exploited in molecular recognition studies aimed at understanding DNA-protein interactions.<sup>11c,16</sup> The importance of these agents and their biological activities has, in many cases, been known for several decades. For example, DNA-DNA interstrand and DNA-protein cross-linking was achieved in the early 1960's.<sup>17</sup> However, the ability to elucidate the functionalities involved at the atomic level has been realized only recently, due largely to the advent of solid phase oligodeoxyribonucleotide (ODN) synthesis, and the discovery of restriction endonucleases. Arguably, the isolation of drug-DNA complexes following enzymatic digestion of large DNAs (bacterial plasmids, calf thymus, etc) represents an exception to this statement. However, the inherent instability and extremely low yields of many interstrand lesions has hampered characterization *via* this method. Additionally, the enzymatic digestion/isolation route has only provided information pertaining to the nucleotide-drug-nucleotide complex but not the influence of flanking sequences or tertiary structure of the target DNA. In this vein, solid phase ODN synthesis and exploitation of restriction endonucleases has allowed studies aimed at understanding the interactions necessary for interstrand cross-linking by many agents about which very little was previously known. This knowledge has been used to design more efficient and/or selective agents and has also allowed the design of cross-linking agents from the simple dimerization of DNA mono-alkylating agents. Triple helix formation has also been employed in the design of cross-linking agents vastly more discriminating in selectivity than the parental compound. Given this, it seems surprising that no reviews have appeared

in the literature pertaining to cross-linking agents. This chapter, in addition to providing some background regarding the significance of DNA interstrand cross-linking, seeks to provide a brief overview of compounds (or classes thereof) capable of DNA cross-linking. Particular emphasis has been placed upon the molecular recognition studies of the last ten years, a great deal of which has been possible for the reasons stated above. The four subsections cover; 1) Inherently labile compounds ; 2) Photoactivated agents; 3) Oxidatively activated cross-linkers; and 4) Reductively activated agents. Numerous compounds reviewed are structurally similar to those in subsection 1.2. but have been modified to fall into one of the other three subsections. In many cases this was done in order to increase the clinical utility of the parent compound.

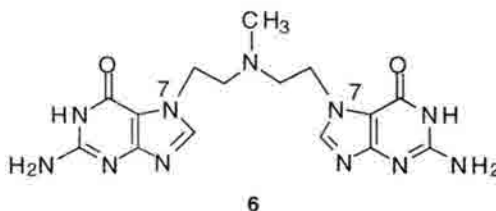
## 1.2. INHERENTLY REACTIVE AGENTS

### 1.2.1. The Nitrogen Mustards

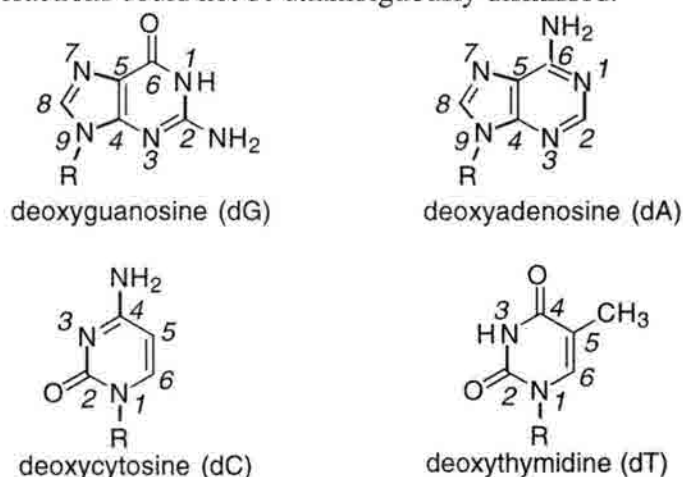
The nitrogen mustards represent the earliest and perhaps most extensively studied of the DNA interstrand cross-linking agents.<sup>11b</sup> Despite their long history, mechlorethamine **1** and chlorambucil **2** are two of the most heavily employed clinical anti-cancer agents in use today.<sup>18</sup> Along with a number of other mustard based structures (**3-5**), their high degree of cytotoxicity is attributed to their ability to induce DNA interstrand cross-links thereby inhibiting replication. In the case of mechlorethamine, this was originally inferred from the anomalously fast renaturation kinetics of mustard treated DNA.<sup>17a</sup> Though these compounds have been studied and clinically exploited for over 30 years, they still provide an area of extremely intense and progressive investigation.



The site specificity of the mustards was originally assigned as being the 5'-GC-3' sequence within canonical B-form DNA. This was based on the isolation of the lesion **6** in which two guanine residues are bridged *via* their respective N<sup>7</sup> atoms by one mechlorethamine derived pentylene chain.<sup>19</sup> The original isolation involved reaction of mechlorethamine **1** with the simple monomer GMP (guanosine monophosphate), and was soon followed by experiments involving isolation from mechlorethamine treated yeast RNA.<sup>20</sup>



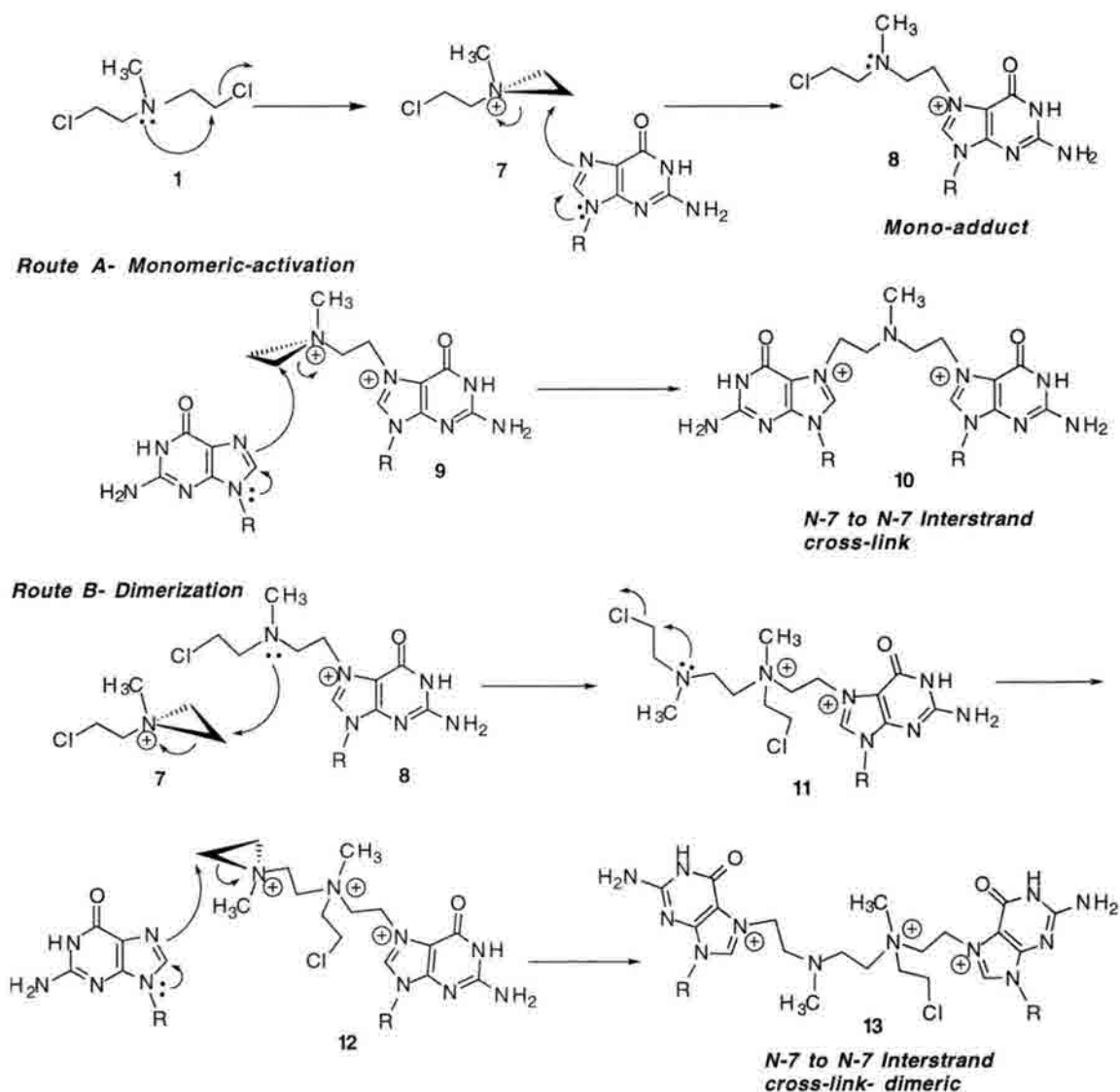
From the RNA experiments it was postulated that **6** was the result of interstrand bis-alkylation at the sequence 5'-GC-3'. Assumed to be a uni-molecular reaction with respect to the mustard, this assignment was later substantiated by the molecular modeling studies of Lewensohn *et al.* for a closely related compound.<sup>21</sup> These studies strongly suggested the ideal N<sup>7</sup> to N<sup>7</sup> distance match of 5'-GC-3' for cross-linking by mechlorethamine within the interstrand motif. On these grounds alone the mechanistic origin of **6** was assigned as being interstrand, although in fact, the possibility of interhelical or intrastrand interactions could not be unambiguously dismissed.



**Figure 1-4.** Deoxynucleotide numbering system where R = deoxyribose.

The early 1990's represented a time of intense study in the area of molecular recognition by the nitrogen mustards. The Grueneberg and Hopkins groups independently reported that the distal deoxyguanosines of 5'-GNC-3' (N= dA,dG,dC, or dT) are cross-linked much more efficiently by **1** than is 5'-GC-3'.<sup>22</sup> This discovery revealed the true sequence selectivity of the mustards and in doing so, pointed out an important dilemma pertaining to the mechanism of ISC formation by the mustards.

The nitrogen mustards covalently cross-link DNA *via* a sequence of aziridinium (**7**) formation followed by alkylation (to afford **8**) and then presumed repetition of the cycle to ultimately afford *bis*-alkylated material (**10**).<sup>23</sup>



**Figure 1-5.** Proposed Mechanisms of DNA-DNA interstrand cross-link formation by mechlorethamine **1**.

Molecular modeling of the unstrained pentylene tether resulting from such a mechanism suggests a "greatest" distance of 5.1 Å.<sup>20</sup> Given that the planes occupied by adjacent base pairs within canonical B-DNA are separated by roughly 3.4 Å, to span three bases (as in 5'-GNC-3') would require a minimum possible distance (assuming a single perpendicular line) of 6.8 Å.<sup>20</sup> This, in conjunction with the fact that **6** had never been unambiguously shown to arise from interstrand linking, led to conjecture involving dimerization of **1** *enroute* to the 5'-GNC-3' cross-link. Such a lesion would easily account for this specificity and would result in minimal perturbation of the B-DNA target structure.

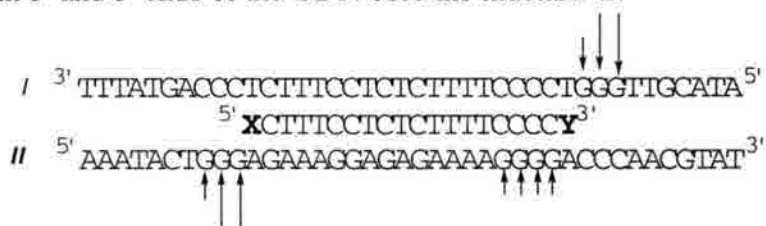


In 1993 the Hopkins group presented results which refuted the possibility of such a dimerization manifold *enroute* to cross-linking by **1**.<sup>23</sup> Utilizing ODN duplexes of differing sizes, it was found that **1** was incapable of interhelical cross-linking as judged by the absence of "crossed" adducts in reactions involving multiple DNA substrates. More importantly, the isolation and characterization of **6** was repeated using ODNs in which predominant cross-linking was relegated to 5'-GNC-3' thus fortifying the monomeric cross-linking route depicted in Figure 1-5. That this was the sole lesion isolated strongly suggested the inoperability of mechlorethamine dimerization involved in ISC generation. Furthermore, the correlation of **6** with the 5'-GNC-3' cross-link points out that the nitrogen mustards likely induce a high degree of structural distortion to their DNA targets. In doing so, the mustards represent a unique departure from most DNA reactive agents whose base pair selectivities are dictated largely by minimization of target distortions. This phenomenon will likely account for investigations into the DNA repair pathways necessary to repair mustard induced cross-links. Additionally, while the nature of this distortion is not currently known, it is likely to exert considerable influence upon DNA:protein interactions within the vicinity of the cross-link. This is anticipated to provide valuable information pertaining to the cytotoxicity of these and other DNA reactive agents.

Despite their clinical importance, the usefulness of many DNA-modifying drugs is often limited by a number of pharmacological deficiencies resulting from the reactivity of the agent. Low affinity for the target molecule of interest (in this case DNA) and rapid quenching *via* hydrolysis prior to DNA alkylation or hydrolysis of the monoadduct, place severe restrictions on the potential utility of DNA reactive agents. Efforts to increase the target affinity of the mustards have produced a number of successes and continue to provide an area of intense interest.

Utilizing the reactivity of chlorambucil **2**, triple helix approaches to genome-specific cross-linking have been examined. Kutyaev *et al.* have shown that the polypyrimidine ODN 5'-CTTTCCTTCTCTTTTCCCC-3' tethered at either the 3' or 5' end

with **2**, was capable of covalently linking the synthetic ODN to one strand of the target duplex or the other.<sup>24</sup> Interstrand cross-linking of the target duplex was seen only in the case where both 5' and 3' ends of the ODN bore the mustard **2**.

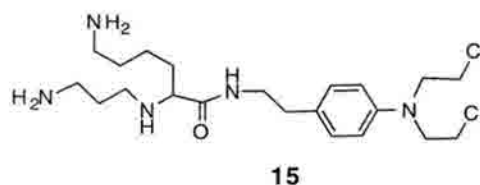
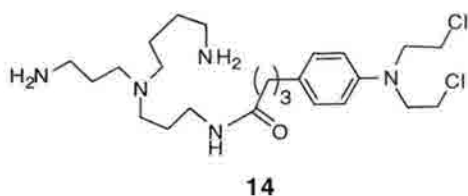


**Figure 1-6.** Histogram of observed base labile lesion formation for ODN-**2** conjugate upon reaction with the strand I/II Watson-Crick duplex.

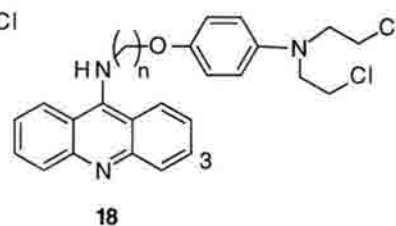
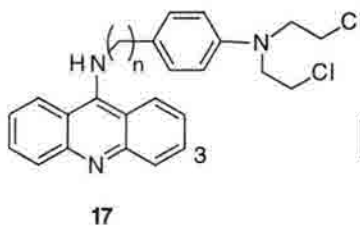
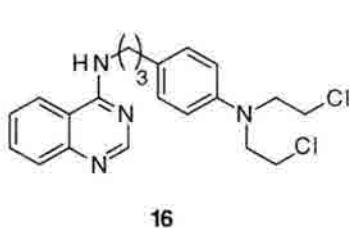
That no interstrand cross-link was observed for a mono-functionalized ODN is directly related to the absence of 5'-GNC-3' within the vicinity of either end of the functionalized polypyrimidine ODN. Strand II proximal to **Y** does bear 5'-GNC-3', however, the aminohexyl moiety employed to tether **2** places the mustard too far away for "normal" interstrand cross-linking to occur. The lesions derived from either *mono* or *bis*-alkylation were attributable to N<sup>7</sup> alkylation on one of several possible dG residues proximal to the 3' or 5' ODN terminus, as depicted by the histogram resulting from piperidine treatment of the alkylation adducts. Chlorambucil functionalization at the ODN 3' end gives rise to base labile alkylations on both sides of the Watson-Crick duplex. Major cleavage sites are seen in strand I while minor cleavage is detected on strand II. This is most likely due to a high degree of flexibility imparted by the aminohexyl linker upon the ODN-mustard conjugate allowing **2** to inflict DNA damage by folding back over to the 5' side of the ODN-**2** connection.

In a much simpler vein, Cohen *et al.* synthesized the chlorambucil-spermidine conjugate **14** in hopes that under physiological pH, the polycationic spermidine chain would associate with the duplex DNA target thus increasing the target affinity of the chlorambucil moiety.<sup>25</sup> Additionally, the observation that many cancer cell lines possess polyamine uptake systems made the choice of spermine or spermidine conjugation an attractive means of enhancing *in vivo* drug delivery.<sup>26</sup> In fact, what was observed was a

much greater efficiency of interstrand cross-linking (*in vitro*) by **14** versus the parent compound **2** although biological activity profiles (*in vivo*) revealed poor cellular uptake of the conjugate. In similar efforts, Stark and Meadows devised the slightly altered conjugate **15** which also demonstrated unexpectedly low cytotoxicity against BL6 melanoma cells and equally poor polyamine uptake.<sup>27</sup>



In addition to increasing drug-to-target affinity by attachment to potential hydrogen bonding groups or cationic matrices, the appending of DNA intercalating groups has also been examined. By tethering an intercalating chromophore to the drug of interest, drug affinity for the DNA substrate is considerably increased *via* the  $\pi$ -stacking interactions of the nucleobases with the attached chromophore. Prakash and co-workers have recently demonstrated this approach by conjugation of aniline mustards to a number of quinazoline and 9-aminoacridine chromophores (**16-18**).<sup>28</sup>



In all cases, the tethered mustards resulted in a much greater degree of monoalkylation than that seen with the untethered analogs. On average, only one cross-link was observed per 20 monoalkylation events. This rate of cross-linking closely parallels that of the native mustards and represented a rather disappointing result. It was believed that by increasing the inductive electron density of the aniline, facilitation of both DNA alkylation events would ensue. This was not the case with interstrand *bis*-alkylation, but to some extent this was in fact observed with the initial monoalkylation. Substitution

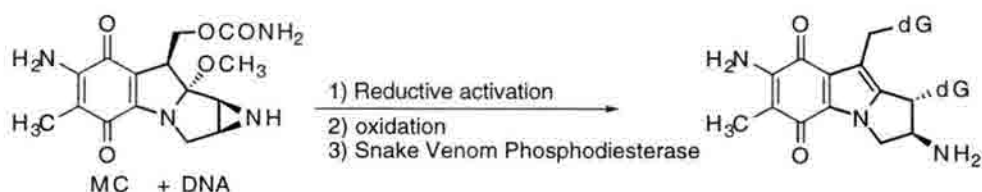
*para* to the mustard resulted in the following order of reactivity ; **17** > **18** > thioether analog of **18** > sulfoxide analog of **18**. In fact, the sulfoxide (SO<sub>2</sub>) analog of **18** yielded no discernible DNA-drug adducts. Of **17**, **18**, and the thioether analog of **18**, the thioether was found considerably less efficient at *in vitro* interstrand cross-linking than were **17** and **18** and *in vivo* activity was much lower as well. It is noteworthy that these three tethered compounds showed much higher cytotoxicity values than the untargeted mustards. Drugs bearing the core structure of either **17** or **18** (n was variable from 2 to 5) were much more potent (optimal dose of 20-30mg/kg) than was the aniline mustard chlorambucil **2** (optimal dose 225mg/kg) or any other untethered mustards. On the other hand, the thioether and sulfoxide congeners of **18** showed weak *in vivo* activity.

The Prakash study also investigated the differential alkylation studies of structures **17** and **18** from the perspective of tether length (n) alteration and its influence upon DNA base selectivity.<sup>28</sup> These studies, in conjunction with evaluation of the quinazoline **16**, revealed that the aminoacridine-mustard conjugates were capable of adenine alkylation. This work represented the first demonstration of adenine alkylation by any of the nitrogen mustards. Experimental work in addition to evaluation of CPK models indicated that use of short tethers (3-4 atoms total) induced a degree of rigidity to the conjugate. This rigidity orients the mustard group at right angles to the acridine plane thereby placing the electrophilic mustard in line with the guanosine N<sup>7</sup> of the sequence 5'-GTA-3' (preferred monoalkylation site). Use of longer tethers, however removes this rigidity thus giving rise to the observed adenine N<sup>7</sup> alkylation on the complementary strand (3'-CAT-5'). Later studies by Denny *et. al.* in 1994 revealed that the lesion previously assigned as adenine N<sup>7</sup> by the Prakash group was in fact not N<sup>7</sup> but rather adenine N<sup>1</sup>.<sup>29</sup> Utilizing a "singly-armed" (only one chloroethyl group on the aniline nitrogen) version of compound **18** (with n = 5) it was demonstrated that connectivity to adenine N<sup>1</sup> (demonstrating *the first example* of any agent that selectively alkylates this position), was formed in greater than 90% yield. This amazing selectivity is proposed to result from acridine intercalation with concomitant

projection of the mustard-acridine tether into the major groove thus giving rise to base pair distortions. Such distortions would likely result in increased access to the normally hydrogen-bonded/deactivated adenine N<sup>1</sup> adjacent to the site of intercalation. From these efforts it becomes clear that initiatives to increase drug:DNA affinity often provide frameworks upon which to design and construct new drugs of higher efficacy or altered selectivity. Although no examples have appeared in the literature, it seems likely that the targeting of new DNA sequences by the aminoacridine-mustard conjugates offers fertile ground for research and will no doubt increase the utility of the nitrogen mustards.

### 1.2.2. CHLOROETHYLATING AGENTS

The majority of DNA interstrand cross-linking agents give rise to lesions which bear a distinct structural similarity to the DNA reactive starting material (*ie*- the cross-linking agent). One such example is that of interstrand cross-linking by mitomycin C in which the cross-link bears the indoloquinone core of the original starting material.<sup>30</sup> However, some instances do exist in which the cross-linking agent undergoes dramatic

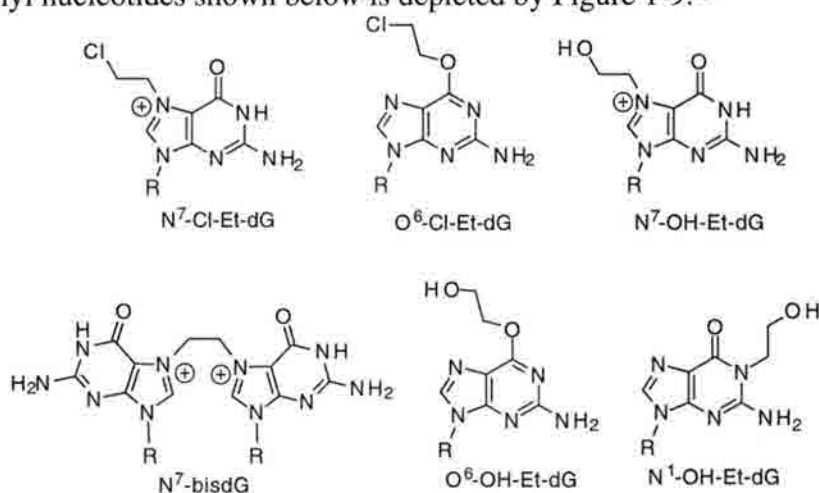


**Figure 1-7.** Generic scheme for DNA cross-linking by reductively activated Mitomycin C (MC). Note that ISC lesion retains the majority of the mitomycin core structure.

decomposition or metabolism thereby releasing the active cross-linking agent (now representing only a fraction of the starting material's structure). The lesions generated are often very simple in structure and bear little similarity to the transient parent compound. Examples include the nitrosoureas, triazenes, and the alkylsulfonates.

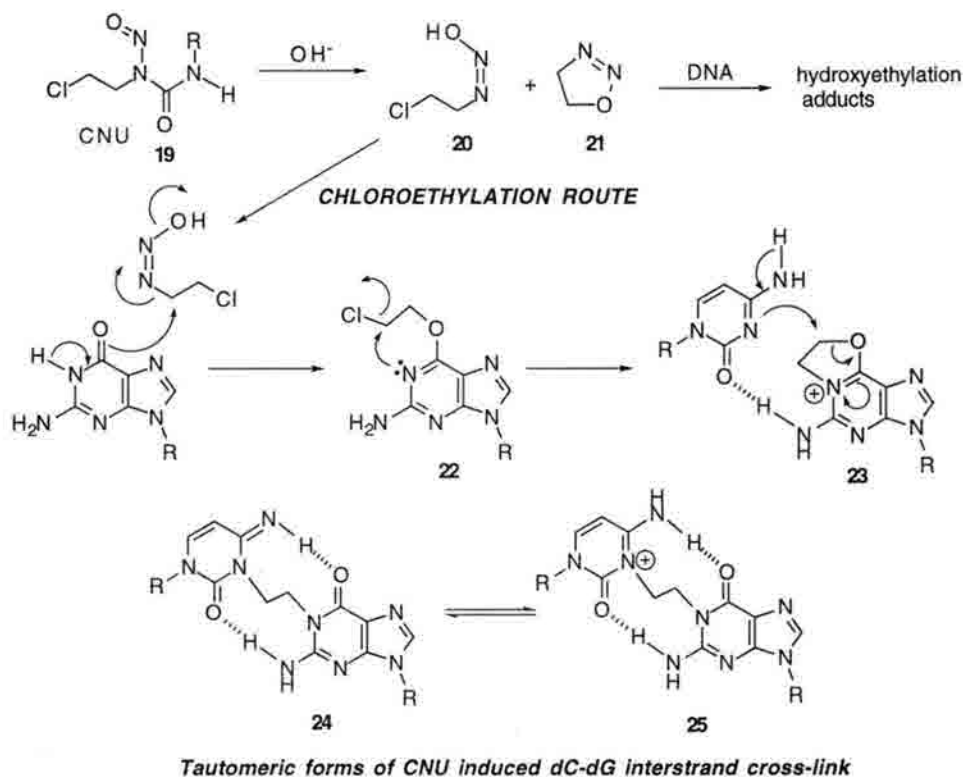
### 1.2.2.1. Nitrosoureas

Chloroethylnitrosoureas (CENU's) are clinical antineoplastic agents employed specifically in the treatment of brain tumors.<sup>31</sup> Although these agents are capable of inducing numerous alkylation adducts (Figure 1-8), it is the formation of an ethane linkage between the N<sup>1</sup> of deoxyguanosine and the N<sup>3</sup> of its base pairing partner deoxycytosine which gives rise to the critical interstrand cross-link.<sup>32</sup> The generally accepted mechanism by which these agents decompose in aqueous solution to generate the chloroethyl and hydroxyethyl nucleotides shown below is depicted by Figure 1-9.<sup>33</sup>



**Figure 1-8.** Commonly observed adducts resulting from CENU treatments of double-stranded DNA.<sup>34</sup>

Mechanistic uncertainties involve the formation of the active chloroethylating moiety and that of the O<sup>6</sup> to N<sup>1</sup> chloroethyl group shift (**22** to **24**) depicted in Figure 1-9.<sup>32c</sup> The importance of a chloronium ion in monoalkylation of deoxyguanosine O<sup>6</sup> has been implied though never demonstrated experimentally.<sup>32b</sup> Alternatively, one may envision the direct S<sub>N</sub>2 attack shown in Figure 1-9 resulting in loss of N<sub>2</sub> and water.

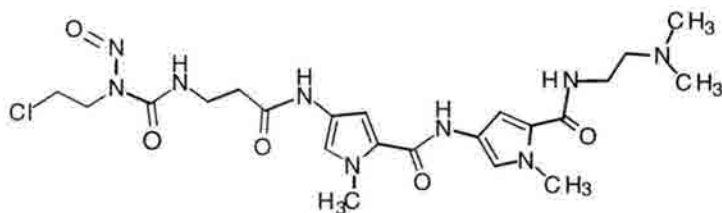


**Figure 1-9.** Mechanism of chloroethylnitrosourea decomposition resulting in dC-dG interstrand cross-link.

The interstrand lesion had the structure shown in Figure 1-9. However, the questionable reactivity of dG N<sup>1</sup> (and amide nitrogens in general) led Kohn *et al.* to propose that dG chloroethylation proceeds *via* initial O<sup>6</sup> chloroethylation followed by rearrangement to the N<sup>1</sup> alkylated material.<sup>35</sup> This was substantiated by studies involving the DNA repair enzyme O<sup>6</sup>-methylguanine-DNA methyltransferase.<sup>36</sup> Known to remove substituted ethyl groups from dG O<sup>6</sup> and dT O<sup>4</sup>, this enzyme was incapable of CNU cross-link reversal. However, when included in the cross-link reaction, the enzyme completely shut down cross-link formation. In earlier support of this, Kohn *et al.* had demonstrated that in mammalian cell lines possessing reduced capacity to repair O<sup>6</sup> alkylguanosine, CNU induced cross-linking was observed at much higher levels than in normal cells.<sup>37</sup> This phenomenon has also been demonstrated more recently by the Gold group.<sup>38</sup> Utilizing conjugates of the general form **26**, they found that chloronitrosourea induced cross-links were formed preferentially in 9L cell lines lacking O<sup>6</sup> methyltransferase



activity versus those which possess normal levels of the DNA repair enzyme. Interestingly, tethering of CNU to the minor groove binding peptide shown in **26** resulted in a decreased level of cross-link formation over that of the untethered CNU. Mismatching of the CNU (major groove alkylator) and the polypyrrole peptide (minor groove binding at dA rich sites) results in the formation of a new minor groove alkylation (at adenine N<sup>3</sup>) at the expense of major groove alkylation (required *enroute* to dG-dC cross-linking). That adenine N<sup>3</sup> alkylation does not give rise to any of the DNA cross-links observed with **26** has been inferred but not unambiguously demonstrated. As with the acridine tethered aniline mustards, attempts to simply increase target-drug affinities resulted in the inadvertent design of a new alkylation specificity. Although demonstration of adenine-dependent cross-linking by **26** or related analogs has not yet appeared, this represents a potentially fruitful area for study.

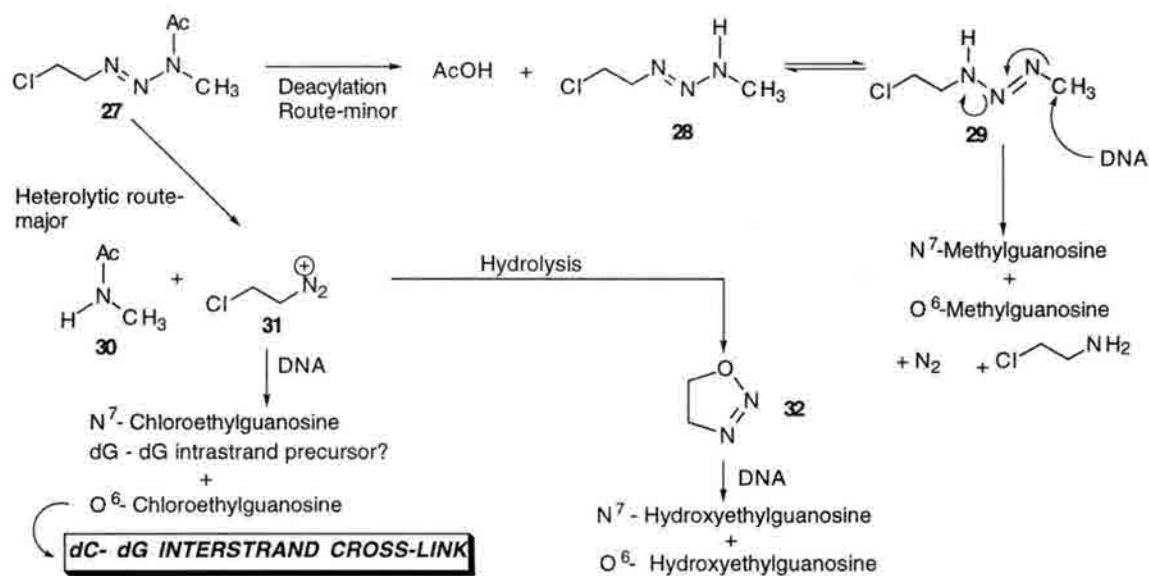
**26**

### **1.2.2.3. Triazenes**

The chemical decomposition of the 1,3-dialkyl-3-acyltriazenes has received a great deal of attention owing to the biological activity of the degradation products involved. These compounds result in the transfer of the N<sup>1</sup> and N<sup>3</sup> alkyl groups to the reactive deoxyguanosine N<sup>7</sup> and O<sup>6</sup> positions.<sup>39</sup> Two degradative routes have been demonstrated (Figure 1-10).<sup>40</sup> Immediate deacylation followed by tautomerization resulting in transfer of the N<sup>3</sup> alkyl group represents the minor pathway while heterolytic scission of the N<sup>2</sup>-to-N<sup>3</sup> bond results in generation of the alkanediazonium. Generation of the diazonium followed by DNA alkylation or hydrolysis (also giving rise to dG adducts) ensues and completes the major pathway of triazene decomposition. In the case where the N1 alkyl group is



chloroethyl, quenching of the diazonium yields chloroethylation at either dG N<sup>7</sup> or O<sup>6</sup>. As with the nitrosoureas, O<sup>6</sup> chloroethylation ultimately gives rise to the dG - dC interstrand cross-link while the N<sup>7</sup> event may result in the dG-dG intrastrand lesion should there be another deoxyguanosine proximal to the initial N<sup>7</sup> lesion.<sup>41</sup>

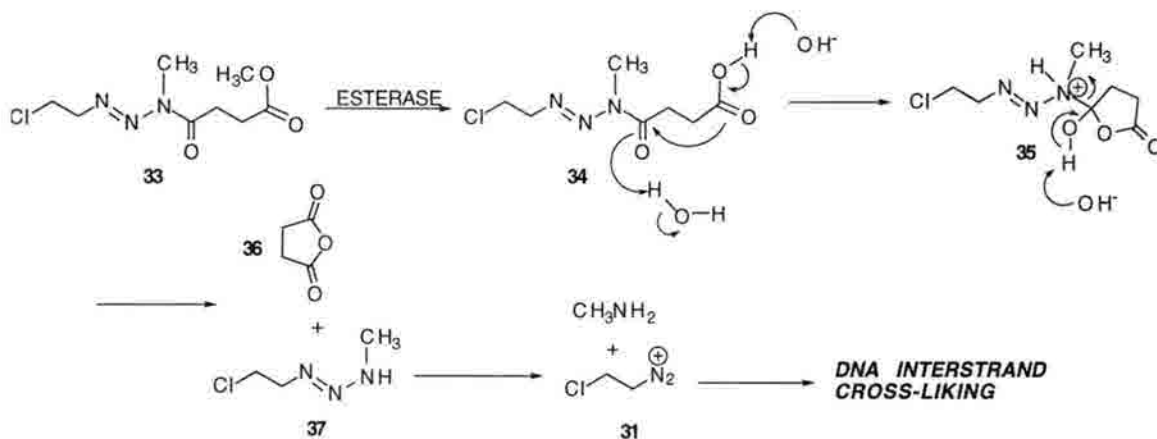


**Figure 1-10.** Degradation of 1,3-dialkyl-3-acyltriazenes to afford DNA alkylation adducts.

Kroeger Smith *et al.* have recently shown that a high degree of control over the deacylation route may be obtained by using an N3 attached acyl group bearing a terminal methyl ester.<sup>42</sup> Enzymatic conversion of the ester to the corresponding acid allows cyclization followed by release of the N3 methyl triazene which may then result in guanosine alkylation by either the major and to a lesser extent, the minor pathway shown in Figure 1-10.

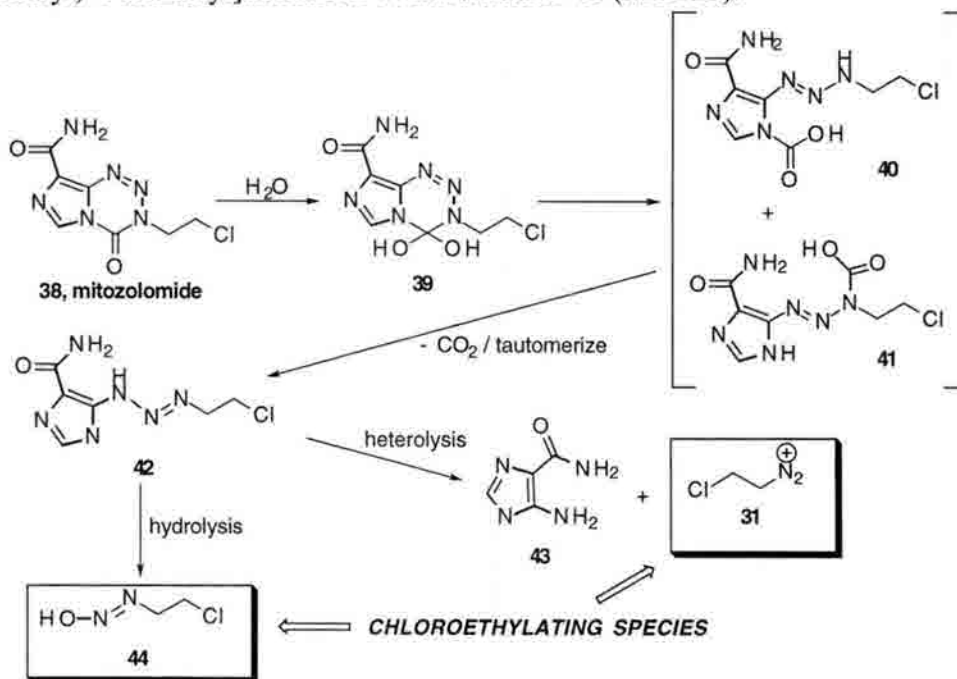
Using a similar strategy of acyl group functionalization on N3 of the triazene, Schmidt and co-workers selectively targeted gastrin receptor (GR) expressing tumor cells.<sup>43</sup> GR is expressed in a number of human cancers (one example being colon adenocarcinoma) and a critical factor in the recognition of gastrointestinal peptides by this receptor is the C-terminus sequence Trp-Met-Asp-Phe amide. Using the conjugate N-[3-benzyl-3-(carboxy-propanoyl)-1-(2-chloroethyl)triazene]-β-Ala-Trp-Met-Asp-Phe amide,

cytotoxicity was directed selectively at the gastric AR42J cancer cells. A549 human lung cancer cells (not capable of GR expression) were completely unaffected by the conjugate.<sup>43</sup>



**Figure 1-11.** Enzymatic activation of triazene decomposition enroute to DNA interstrand cross-linking.

Based upon the proposed ring cleavage of the cyclic triazenes under physiological conditions, the cyclic triazenyylimidazoles have prompted investigation and have been found to closely resemble acyclic triazenes in their DNA cross-linking ability. Representative of the cyclic triazenyylimidazoles, mitozolomide **38** (Figure 1-12) is simply a prodrug of 5-[3-(2-chloroethyl)-1-triazenyl]imidazole-4-carboxamide **41** (MCTIC).<sup>44a</sup>

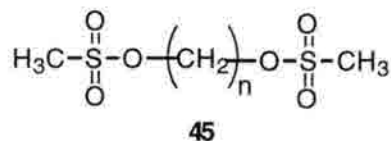


**Figure 1-12.** Mitozolomide decomposition pathway.

Despite enhanced stability relative to MCTIC (and thus less reactive towards cross-linking), mitozolomide has proven extremely effective against TLX5 lymphoma, B16 melanoma, colon 26, colon 38 and L1210 leukemia (resistant to cyclophosphoramide) cell lines.<sup>44b</sup> Indeed a number of very promising DNA cross-linking agents have been designed with the general structure of mitozolomide in mind, all of which operate upon the basic mechanism of chloroethylation to afford dC-dG cross-links.

### 1.2.2.3. Alkyl sulfonates

As stated earlier, the correlation between biomolecule alkylation and therapeutically useful agents relies heavily on the electrophilicity of those agents. This realization was brought about no doubt by the nitrogen mustards and was the impetus for the study of alkyl sulfonates. Particular emphasis was originally placed upon the potential DNA cross-linking ability of the "homo-bifunctional" sulfonates many of which consisted of sulfonylated cyclic or acyclic alkanes.<sup>45</sup> Many of these agents are active against numerous cancer cell lines, though the exact mechanisms by which they effect cytotoxic action has not been thoroughly elucidated.<sup>46</sup> Busulfan **45a** and its related congeners **45b,d-f** represent the only di-sulfonyl compounds shown conclusively to effect ISC formation.<sup>47</sup> Characterization of the lesion obtained from busulfan treated DNA has revealed the generation of 1,4-bis-(7-guanyl)butane as well as, 7-(4-hydroxybutyl)guanosine upon hydrolysis of the modified DNA.<sup>47</sup>

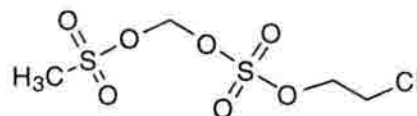


- a:**  $n = 4$ , **Busulfan**
- b:**  $n = 1$
- c:**  $n = 2$
- d:**  $n = 9$
- e:**  $n = 8$
- f:**  $n = 6$

Concomitant with the development of the bis-(methanesulfonates), monosulfonic agents were examined as a means of chloroethyl introduction into DNA. The 2-chloroethyl methane-sulfonates received considerable attention but were fraught with low activities in the tumor cell lines chosen. So too were the vast majority of 2-chloroethyl alkene/arene sulfonates examined. The next generation of sulfonates afforded vast improvements in activity against leukemia P388 cell lines over that seen with the 2-chloroethyl

methanesulfonates. These agents, the 2-chloroethyl chloroethane-sulfonates in turn, gave rise to the development of 2-chloroethyl-(methyl-sulfonyl)-methanesulfonate (clomesone, **46**). Studies by the Kohn, Pegg, and Smith groups have confirmed that **46** does, in fact chloroethylate dG N<sup>1</sup> (via O<sup>6</sup> transfer as per Figure 1-9) *enroute* to formation of the anticipated dC-dG interstrand cross-link.<sup>32b,48</sup> Some differences regarding general reactivity patterns exist between **46** (the most prevalent

of the sulfonate chloroethylating agents) and the chloronitrosoureas and triazenes. Firstly, **46** is much more selective in its DNA specificity. The vastly predominant product from reaction of calf thymus

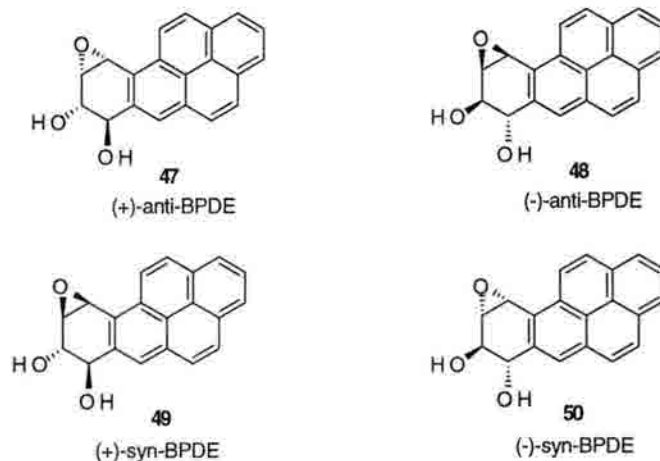


**46, clomesone**

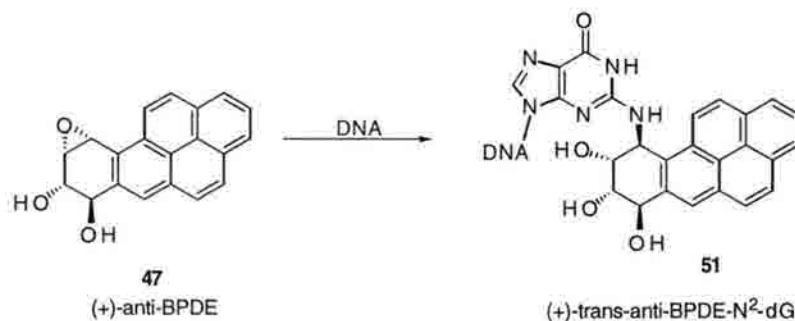
DNA with **46** is N<sup>7</sup>-chloroethylguanosine whereas both the triazenes and nitrosoureas produce a wide array of adducts (many incapable of interstrand cross-linking) as shown in Figure 1-8.<sup>49a</sup> Additionally, **46**, (and all the alkyl sulfonates in general) is devoid of carbamylation activity (a common side reaction seen in chloronitrosourea treated proteins), this being a route leading to non-selective toxicities resulting in the therapeutically unproductive consumption of drug.<sup>49b</sup> The chloroethylsulfonates (specifically **46**-based structures) thus represent the most efficient of the chloroethylating agents owing largely to the specificity of alkylation.

### 1.2.3. EPOXIDE-CONTAINING AGENTS

It has been realized for a long time that epoxides represent potent DNA alkylating moieties. This reactivity has been demonstrated most vividly by the benzo [α]pyrenes which, in mammals undergo oxidative metabolism to the four stereoisomers **47-50** of the carcinogenic 7,8-dihydroxy-9,10-epoxy-7,8,9,10-tetrahydrobenzo[a]-pyrene BPDE. Bearing the activated benzylic epoxide, these compounds are highly reactive towards DNA forming numerous adducts; the predominant ones (both *in vivo* and *in vitro*) resulting from



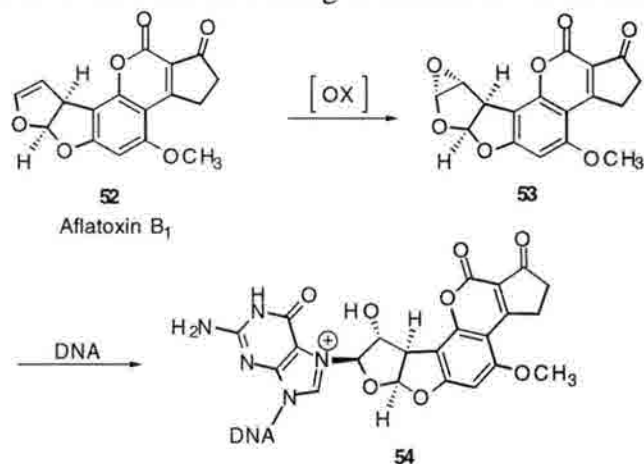
epoxide opening and subsequent connection of the bulky BPDE C-10 to DNA *via* the exocyclic amine N<sup>2</sup> of deoxyguanosine.<sup>50</sup> Surprisingly, only the (+)-anti-BPDE dG lesion results in carcinogenic/ mutagenic cellular events while alkylation of the other stereoisomers has comparatively little biological significance.<sup>51</sup>



The lesion **51** blocks RNA<sup>52</sup> and DNA<sup>53</sup> polymerases and very recently has been shown to inhibit the DNA helicase activity (necessary for replication) of the bacteriophage T7 gene 4 protein in addition to blocking dNTPase activities as well.<sup>54</sup>

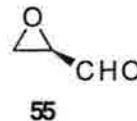
The *in vivo* generation of epoxides *via* cytochrome P-450 oxidation is a common theme in epoxide biochemistry; prime examples being the oxidative activation of aflatoxin B alkylation, shown below<sup>55</sup>, and the conversion of glycidyl ethers to glycidaldehyde.<sup>56</sup> Much simpler epoxides (not resulting from metabolic activation) are also capable of DNA alkylation. Examples include propylene oxide<sup>57</sup>, styrene oxide and trichloropropylene oxide.<sup>58</sup> The DNA residues most susceptible to alkylation by these agents include dG N<sup>7</sup>, dA N<sup>6</sup>, and

dC N<sup>3</sup>. It is noteworthy that most examples of DNA modifying epoxides result only in monoalkylation adducts. Even more interesting is that review of the literature reveals little



**Figure 1-13.** Oxidative activation of aflatoxin B<sub>1</sub> and ensuing reaction with deoxyguanosine.

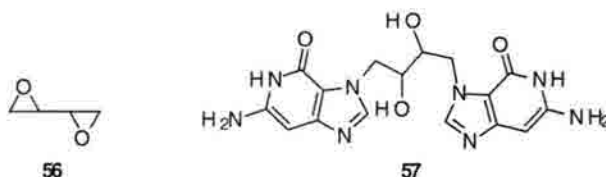
or no mechanistic detail pertaining to the mechanism of action of the few known epoxide cross-linking agents. One case in point is glycidaldehyde **55**. Although it is often reported as a DNA cross-linking agent<sup>59c</sup>, no structure elucidation (of the ISC lesion) has been achieved nor has there even been a DNA sequence assignment for its preferred ISC site. Its reactions with dA and dG have been thoroughly studied but data pertaining to any interstrand events of importance has been extremely elusive.<sup>59</sup> Given this, glycidaldehyde will not be discussed in this chapter though the interested reader is referred to reference 59 for insight into its ring extension reactions (analogous to chloroacetaldehyde) with dA and dG and the importance of **55** in probing DNA structure perturbations.



#### **1.2.3.1. Diepoxybutane**

Diepoxybutane (DEB, **56**) is the simplest of the epoxide cross-linking agents and the first epoxide to be reported as carcinogenic.<sup>60</sup> Lawley and Brookes proposed that DEB behaves similarly in its cross-linking behavior to the N-mustards.<sup>61</sup> This was based upon the 1967 isolation of the diol **57** implicating two dG N<sup>7</sup> residues as those responsible for the interstrand event.<sup>61</sup> As with the mustards, the original supposition was that 5'-GC-3'

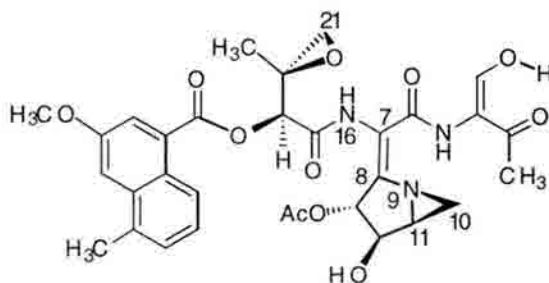
was the preferred DNA sequence targeted by DEB. More recently, Millard and White have shown using synthetic ODN's of varying sequences that indeed, the preferred sequence for cross-linking by DEB is 5'-GNC-3' thus refuting the proposal put forth by Lawley and Brooks.<sup>62</sup>



Interesting to note is that diepoxybutane (DEB), unlike the nitrogen mustards, cross-links a number of different sequences, the order of reactivity being 5'-GGCC-3' >>TGCA, TCGA >CCGG >TATA with the 5'-GNC-3' (*ie.*- 5'-GGCC-3') predominating over the next reactive sequence by 4-fold. Piperidine cleavage of cross-linked material confirmed N<sup>7</sup> base-labile alkylation at both dG residues involved in the cross-link. This finding refutes the original 5'-GC-3' specificity assignment but more surprisingly points out a discrepancy pertaining to the molecular distances available within B-form DNA. As discussed previously with the N-mustards, the N<sup>7</sup>-to-N<sup>7</sup> distance within the targeted 5'-GNC-3' sequence of B-DNA greatly exceeds that which can be spanned by the cross-linking agent. A best case scenario dictates that 6.8 Å separates the N<sup>7</sup> moieties (assuming retention of base stacking interactions) while the minimized pentylene chain of mechlorethamine affords a distance of only 5.1 Å between the terminal electrophilic sites. The DEB case is even shorter in that it lacks the central nitrogen present with mechlorethamine and all the N-mustards. Thus, the target 5'-GNC-3' must substantially distort in order to accomodate the DEB induced cross-link. How this occurs and the implications with respect to subsequent DNA-protein (repair?) interactions has yet to be addressed and most certainly represents an area of interest with respect to molecular recognition of small molecules and the different forms (B-DNA and otherwise) of DNA.

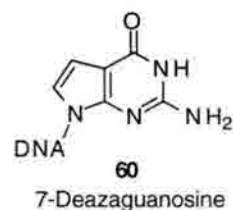
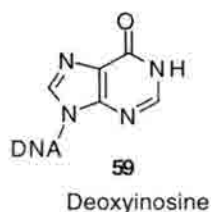
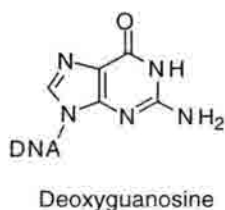
### 1.2.3.2. Carzinophilin/Azinomycin B

Considerably more complex than any other epoxide cross-linking agent carzinophilin (**58**, also called azinomycin B) possesses not only the labile epoxide, but also bears the novel bicyclic aziridinopyrrolidine in conjugation with the C6 amide. Isolated from broths of *Streptomyces sahachiroi* this potent antitumor antibiotic was recently shown to be identical in structure to azinomycin B which is isolated from *Streptomyces griseofuscus* S42227.<sup>63</sup>



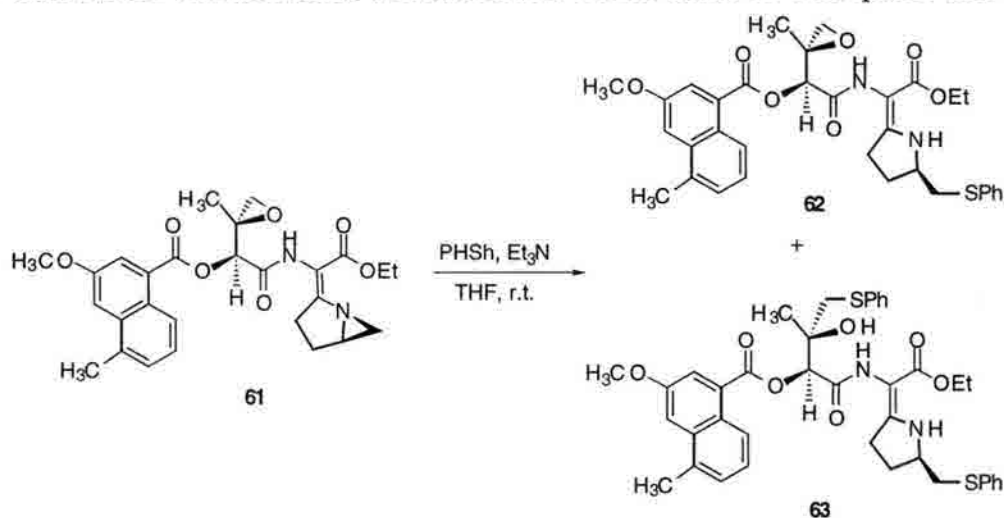
**58, Carzinophilin / Azinomycin B**

To date, the only mechanism of action studies have been carried out by the Armstrong group. It has been determined that DNA cross-linking specificity is for 5'-GNC-3' and 5'-GNT-3' in which the N<sup>7</sup> moieties of two deoxyguanosines (in the case 5'-GNC-3') or the N<sup>7</sup> of one deoxyguanosine and the N<sup>7</sup> of the neighboring deoxyadenosine (the 5'-GNT-3' case) are alkylated.<sup>64</sup> These assignments were derived from examination of piperidine labile sites of cleavage, as well as the use of ODN substrates bearing the modified bases deoxyinosine and 7-deazaguanosine in probing the effects of functional group deletions on cross-linking efficiency. Additionally, treatment of cross-linked substrates with the chemical nuclease reagent (1,10-phenanthroline) copper was used to confirm connectivity assignments derived from the piperidine reactions.

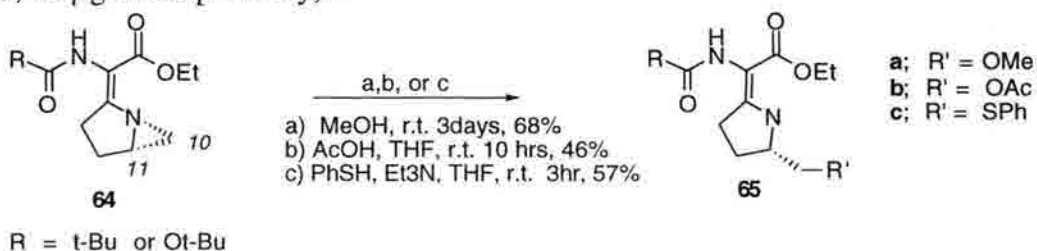




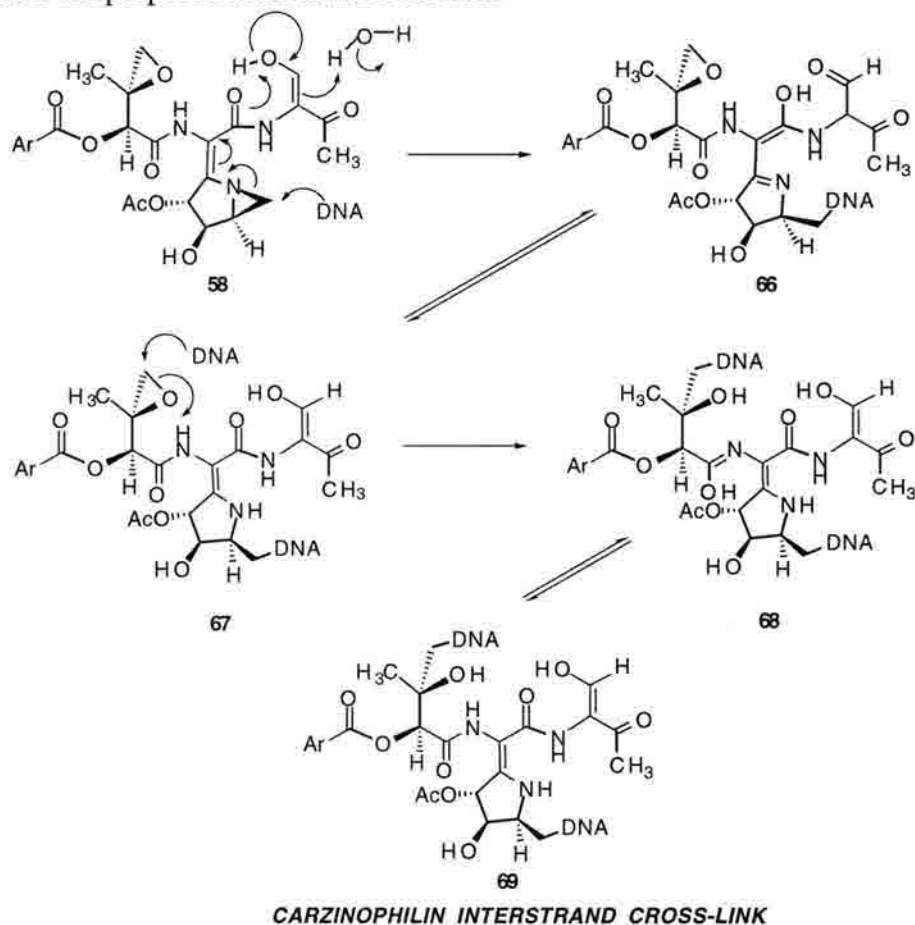
The alkylation sites on DNA have been assigned, but no assignments regarding drug connectivities have been reported. Terashima *et al.* have recently reported the generation of ring opened structures **62** and **63** upon treatment of synthetic intermediate **61** with thiophenol and triethylamine at room temperature.<sup>65</sup> This transformation is consistent with the anticipated lability of the epoxide and aziridine rings of the natural product and has prompted the mechanism of action proposed by Terashima depicted in Figure 1-14. Particularly susceptible to ring-opening is the aziridine, given the preponderance of **62** over **63** in cases where reaction times were shortened. From this it is anticipated that **63** is



derived by way of **62** and thus aziridine cleavage gives rise to the initial monoadduct *enroute* to interstrand cross-linking. This is further supported by the conversion of aziridine **64** to the ring-opened adducts **65a-c** under extremely mild conditions *via* nucleophilic attack of the aziridine C10 position. Further, *in vitro* cytotoxicity assays against P388 murine leukemia utilizing **61**, **62** and **63** demonstrated prominent values for **61** ( $\text{IC}_{50} = 0.0023\mu\text{g/ml}$ ) while **62** and **63** demonstrated much weaker activities ( $\text{IC}_{50} = 0.035, 1.9\mu\text{g/ml}$  respectively).<sup>65</sup>



According to the mechanism proposed by Terashima,<sup>65</sup> conjugation of the aziridine nitrogen with the N5-C6 amide likely activates this position for initial DNA attack at C10 leading to the imine monoadduct **66** (Figure 1-14). Tautomerization restores the enamine **67** which *may* then undergo attack at epoxide C21 in an intramolecularly assisted fashion *via* deprotonation of amide N16. Tautomerization of the resulting imideate **68** back to the amide yields the proposed interstrand cross-link.

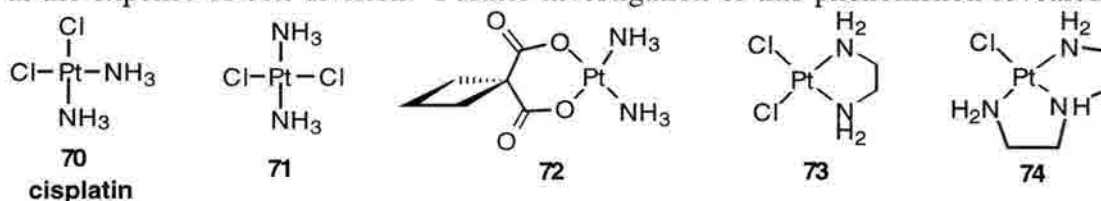


**Figure 1-14.** Terashima model for DNA interstrand cross-linking by carzinophilin. Regiospecificity and reaction ordering derived from synthetic reactivity studies.<sup>65</sup>

Despite the compelling nature of this mechanism and its resulting covalencies, the amount of supporting evidence has been limited. No DNA-drug lesion has been isolated nor have extensive DNA-binding studies been performed aside from the original Armstrong findings. As such, carzinophilin represents a novel natural product due not only to its complex structure but also due to its relatively unknown mechanism of DNA interaction.

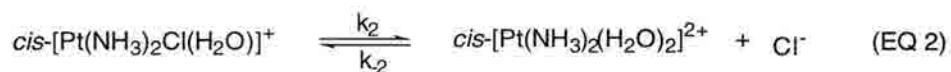
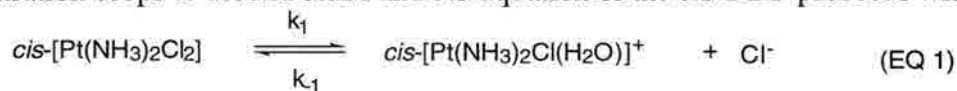
### 1.2.4. CIS-DIAMMINEDICHLOROPLATINUM (II)

*Cis*-diamminedichloroplatinum (II) (*cis*-platin or *cis*-DDP, **70**) was originally described 150 years ago but has only within the last 30 years been recognized as a potent anti-tumor agent.<sup>66</sup> The cytotoxic properties of this and numerous analogues have been attributed to its ability to form both inter- and intrastrand cross-links within deoxyguanosine-rich runs of DNA. Interestingly, its biological activity was initially observed in electrochemical studies involving the effects of electric fields on the growth rates of *E. coli*.<sup>67</sup> Cells exposed to electric currents (aerobic conditions) in the presence of  $\text{NH}_4\text{Cl}$  underwent abnormal filament elongation (as much as 300 times the normal length) at the expense of cell division. Further investigation of this phenomenon revealed that



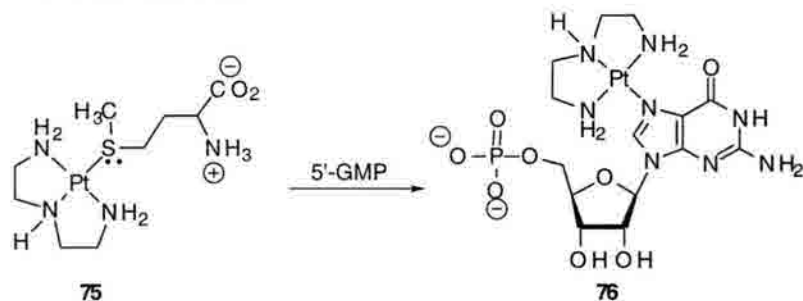
generation of *cis*-DDP (in addition to the trans-isomer **71**) from electrolysis at the platinum electrodes was responsible for the abnormal cellular behavior.<sup>68</sup> Despite extensive studies and clinical trials leading to the drug's FDA approval in 1979 the mechanism of action of *cis*-DDP has continued to provide fertile ground for intense investigations. Particular emphasis of late has involved the ability of **70** to induce DNA mutations<sup>69</sup> and to radically alter DNA-protein binding motifs.<sup>70</sup>

Evidence suggests that *cis*-DDP undergoes sequential chloride displacements *via* a two step hydration process. Studies with  $[\text{Pt}(\text{en})\text{Cl}_2]$  **73** have shown that chloride displacement does not occur in plasma (where chloride ion concentration is about 100mM) but rather, it occurs upon membrane penetration.<sup>71</sup> Once inside the cell the chloride concentration drops to around 5mM and *bis*-aquation of the *cis*-DDP proceeds with  $k_1$  and



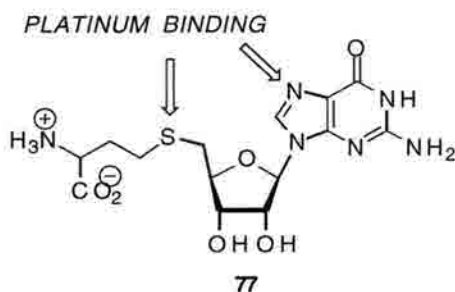
neutral *cis*-DDP to the positively charged hydroxy species which in turn, is attracted to the negatively charged DNA target *via* electrostatic interactions. The rate-limiting hydrolysis is then followed by nucleotide binding, for which the rate of dissociation is extremely slow. In light of this, binding of *cis*-DDP to its target sequences has been assigned as a kinetic rather than thermodynamically driven process.<sup>66a</sup>

More recent studies by the Reedijk and Sadler groups<sup>73,74</sup> have shown that thiol and thioether containing peptides and proteins may play an equally important role in the activation and transport of *cis*-DDP to its ultimate target. Sulfur ligands possess a much higher affinity for Pt (II) than do most nitrogen ligands and this principle has been used to great therapeutic advantage in the removal of toxic Pt(II) upon administration of therapeutically designed sulfur nucleophiles.<sup>73</sup> In contrast to this, the Sadler group has recently demonstrated that platinated methionine **75** was capable of selective platinum transfer to the N<sup>7</sup> of 5'-guanosine monophosphate (5' GMP) to afford **76**.<sup>74</sup> Attempts to effect Pt(II) transfer to any of the other three deoxynucleotides (dA, dT, or dC) yielded no conversion of **75** to the unplatinated amino acid. Additionally, reactions involving both methionine and 5' GMP showed that generation of **75** was preferred over the direct N<sup>7</sup> platination of 5' GMP but that over time **76** is formed as the thermodynamic product thus releasing the unbound thioether.



Reedijk *et al.* have demonstrated that upon release of methionine in the conversion **75** to **76**, it is likely that platination may occur again and the cycle repeated thus suggesting that the process may be catalytic with respect to the thioether.<sup>75</sup> This is suggested based upon the intramolecular platinum transfer from the sulfur of S-guanosyl-L-homocysteine

**77** to the guanosyl N<sup>7</sup> followed by a second platination at the previously occupied sulfur. The initial kinetically driven thioether platination of **77** proceeds with a  $t_{1/2}$  of 2 hours while the isomerization to N<sup>7</sup> is considerably slower ( $t_{1/2}$  = 10 hours). That migration proceeds *via* an associative mechanism (five-coordinate transition state) is supported by the



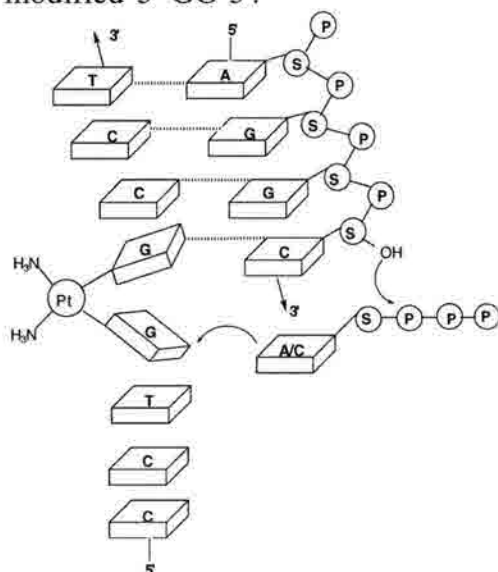
second order rate constants observed by Sadler *et al.* in the intermolecular conversion of **75** to **76** and is typical of many known substitution reactions of square planar Pt(II) complexes.<sup>76</sup>

These data taken together comprise a meaningful (albeit very recent) picture of how *cis*-DDP maybe transported to its nucleic acid target sequences. This mechanism is enticing too in that different cell types possess vastly different electrolyte compositions which could have bearing on the effectiveness of the *bis*-aquation route to *cis*-DDP activation. For instance, liver cells possess [Cl<sup>-</sup>] in excess of 150mM which would hinder platinum hydrolysis thus limiting DNA adduction.<sup>74</sup> The viability of *cis*-DDP activation *via* sulfhydryl or thioether complexation however, may afford a means of both delivery and activation towards DNA binding. Such a motif may involve the platination of select cysteines or methionines within a monoclonal antibody targeted to a specific tissue or protein.

Although the intrastrand lesion is by far the major and perhaps the most interesting adduct, the induction of interstrand cross-links has also received considerable attention. The predominant DNA adducts (intrastrand) obtained upon treatment with *cis*-platin are the *cis*-[Pt(NH<sub>3</sub>)<sub>2</sub>{d(GpG)-N<sup>7</sup>(1),-N<sup>7</sup>(2)}](G\*G\*), *cis*-[Pt(NH<sub>3</sub>)<sub>2</sub>{d(GpNpG)N<sup>7</sup>(1),N<sup>7</sup>(3)}], and *cis*-[Pt(NH<sub>3</sub>)<sub>2</sub>{d(ApG)-N<sup>7</sup>(1),-N<sup>7</sup>(2)}] (A\* G\*) accounting for > 90% of the DNA platination sites.<sup>77a</sup> The N<sup>7</sup>-N<sup>7</sup> intrastrand cross-link at 5'-GG-3' comprises roughly 65% of the adduction while the N<sup>7</sup> atoms of adjacent pyrimidines 5'-AG-3' account for another 15%.<sup>77b</sup> The remaining products consist of the intrastrand 1,3 cross-link at 5'-GNG-3' as

well as the interstrand lesion between the opposing N<sup>7</sup> atoms of the sequence 5'-GC.<sup>77c</sup> Though all intrastrand lesions have been shown capable of inducing mutations in the genome, it is widely recognized that the 5'-GG-3' adduct is extremely lethal and is probably the source of *cis*-DDP cytotoxicity. Platination of 5'-GG-3' induces upon the DNA polymer a high degree of structural distortion as evidenced by the destacking of these adjacent dG residues to afford a dihedral angle between the ring planes of 76-87°. <sup>78</sup> Both 5'-GG-3' and 5'-AG-3' intrastrand lesions bend the helix of duplex DNA by 32-35° and it is known that the 5'-GG-3' event bends the helix in the direction of the major groove despite retention of the hydrogen bonding network to the complementary deoxycytosine residues. <sup>78,79</sup> Helix perturbation is found to be much more profound with respect to the 5'- side of the principal GG target in that this G undergoes a G to T transversion upon introduction of the 5'-GG-3' *cis*-DDP lesion into bacteriophage substrates. <sup>78</sup> That the 3' dG inflicts no such mutation in the replication of the original DNA substrate indicates that, like apyrimidinic/apurinic (AP) sites in DNA, the platinated 5'-dG represents a "noninformational" or rather a "misinformational" site to the DNA polymerase responsible for complementary strand synthesis. <sup>80</sup>

**Figure 1-15.** Mechanism of polymerase driven G to T transversion at 5'dG of *cis*-DDP modified 5'-GG-3'.



Polymerase insertion of deoxyadenosine at such a site follows with the established default mechanism and ultimately results in the net G to T transversion. <sup>78,80</sup> That the intrastrand 5'-GG *cis*-DDP represents a mutational hot-spot detracts from the lesion's ability to halt polymerase activity altogether. Polymerase seizure is believed to be the source of cytotoxic activity while mutational activity is felt to cause

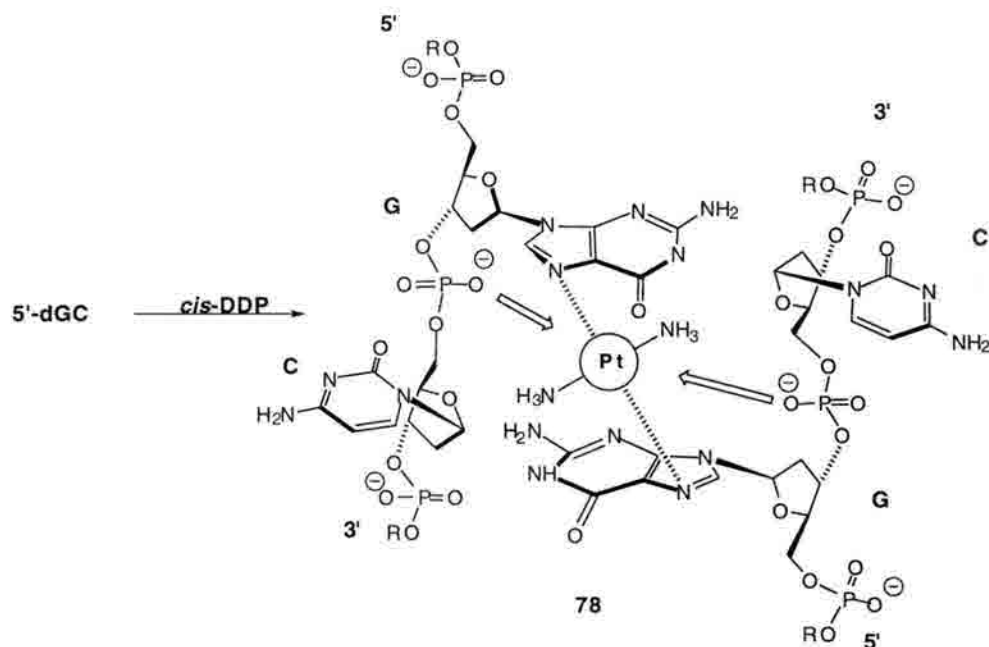
development of secondary tumor formation upon therapy with *cis*-DDP. As such, efforts have been focused on the generation Pt(II) agents capable of shutting down polymerase and other enzymatic processes while avoiding detrimental mutation events. Emphasis has been placed upon the ability to form dinuclear Pt complexes which optimize DNA *interstrand* cross-linking events while avoiding *intrastrand* distortional processes.<sup>81</sup>

The high degree of target distortion induced upon DNA modification with *cis*-DDP is not limited to the *intrastrand* event. The *interstrand* lesion produced upon binding the diagonally displaced N<sup>7</sup>s of 5'-GC-3' accounts for 5-10 % of the total platination products and has been shown to produce significant conformational perturbations within the substrate DNA. These distortions have been recently probed with respect to *E. coli* RNA polymerase (prokaryotic) and wheat germ RNA polymerase II (eukaryotic) elongation reactions involving the *inter-* and *intrastrand* platination events. Leng *et al.* have shown that DNA substrates bearing either the *cis*-d(G\*TG\*) *intrastrand* or *cis*-d(G\*C/G\*C) *interstrand* cross-link irreversibly shut down transcription at the site of platination.<sup>70a</sup> Termination was also observed several nucleotides ahead of the *interstrand* lesion suggesting that the presence of the *cis*-DDP lesion was not the sole reason for transcription blockage. That some DNA perturbation was induced by the lesion and was the cause of this "pre-lesion" block was supported by the efficient polymerase bypass of the same DNA substrate bearing monoadduction with chloro(diethylenetriamine)platinum (II). Severe structural distortion at the *interstrand* 5'-GG cross-link site had been suggested based upon molecular modeling, chemical hyperreactivity probes and gel electrophoresis (DNA conformational analysis) but had not yet been demonstrated to alter enzymatic processes dependent upon the modified DNA.<sup>77b,c,82</sup>

Drobny and Hopkins have recently reported the solution structure of the *cis*-DDP *interstrand* cross-linked substrate [d(CATAGCTATG)<sub>2</sub>].<sup>79</sup> Confirming earlier reports that the *interstrand* lesion induces an 80° unwinding of the DNA target and that considerable bending is induced as well, they also uncovered structural features never previously shown



to result from small molecule-DNA interactions. Of particular interest was the determination that at interstrand cross-linked 5'-GC-3' both cytosines are flipped completely out of the duplex leaving each N<sup>7</sup> platinated deoxyguanosine completely unpaired. Additionally, the NMR data generated indicates that the *cis*-DDP bridge resides in the minor groove of the duplex and that a highly localized change from right-handed B-DNA to left-handed Z-DNA occurs at this same Pt(II) bridge. This is in stark contrast to previous models for the *cis*-DDP interstrand cross-link which place the bridge in the major groove and allows retention of hydrogen bonding/ $\pi$  stacking of the modified bases within the constraints of B-DNA. Stabilization of the Z-DNA structure induced upon *cis*-DDP binding relies heavily upon electrostatic interactions of the phosphate oxyanions of each GC linkage (O-Pt distance = 3.2 Å) as depicted by Figure 1-16 below.

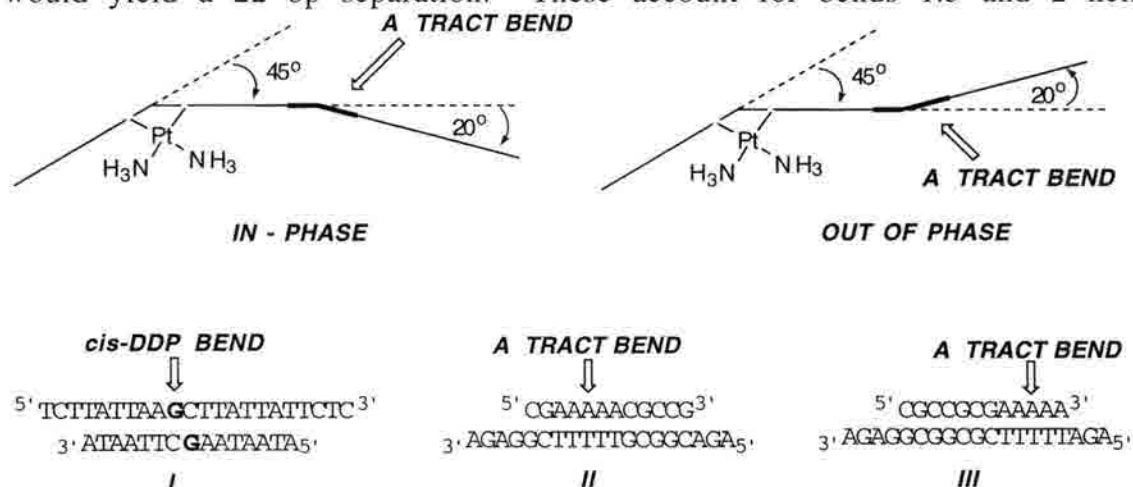


**Figure 1-16.** Structural distortion of 5'-GC upon *cis*-DDP mediated ISC formation (Drobny and Hopkins <sup>79</sup>).

In addition to the structural elucidation of the interstrand lesion, the NMR derived prediction that DNA bending be in the direction of the minor groove versus the major groove (as previously assigned based upon modeling studies placing the Pt(II) core in the major groove) was confirmed utilizing a T4 DNA ligase assay. It is known that A tracts



induce an approximate  $20^\circ$  bend (in the center of the A tract) in DNA towards the minor groove and that this distortion gives rise to electrophoretic retardation.<sup>82</sup> In order to determine the direction of groove bending induced by *cis*-DDP the ODN I (Figure 1-17) was interstrand cross-linked with *cis*-DDP and then ligated into both ODN II and ODN III each of which bear A tracts. Ligation into ODN II would afford a 17 bp separation between cross-link site and the bend site inherent to the A tract while ligation into ODN III would yield a 22 bp separation. These account for bends 1.5 and 2 helix



**Figure 1-17.** T4 DNA Ligase experiment with A tract bends "in phase" or "out of phase" with *cis*-DDP induced helix bending.

turns removed from each other assuming roughly 10.4 bp per helical turn. Thus, sites of interest are either "in phase" with each other (the 22 bp situation) or "out of phase" with each other. That *cis*-DDP mediated DNA bending was in the direction of the major or minor groove could thus be ascertained since bending (in phase substrate) in the same direction as that known for the A tract would afford a much more bent (electrophoretically retarded) structure than that seen for the "out of phase" case in which the two types of bends cancel each other. Additionally, bending towards the major groove would afford conformationally "neutral" ligation adducts in the "in phase" case resulting in minimal gel retardation or perhaps mobility enhancement depending on the extent of *cis*-DDP curvature induction. Comparison of electrophoretic mobilities between the "in-phase" and "out of

phase" ligation adducts revealed that, in fact, the " in phase" products were considerably more retarded than the " out of phase" ODN's. The ensuing minor groove assignment was thus consistent with the NMR-derived structure and further substantiated its relevance.

Most importantly, this work points out numerous mechanistic questions pertaining to the efficacy of *cis*-DDP and its analogs. Particularly intriguing, and very relevant to DNA cross-linking agents in general, are the issues of 1) the step-wise bond formation involved in going from mono-adduct to cross-link; 2) conformational changes within the DNA target necessary for this conversion ; and 3) the potential detrimental properties of an interstrand lesion or intrastrand lesion owing to perturbed DNA structure (ie- mutational events), not inflicted by a simple mono-adduction.

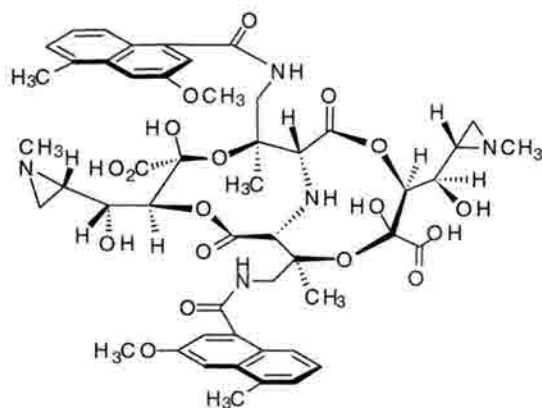
### 1.2.5. DIMERIC CROSS-LINKING AGENTS

Chemical cross-linking of DNA by small molecules suffers from several drawbacks. Firstly, most small molecules possess recognition motifs dependent upon only 2 or 3 bases of the target DNA sequence.<sup>12</sup> This lack of selectivity in many cases means that modification may occur not only in a region or genome of interest, but may also inflict undesired damage upon an otherwise innocuous substrate. Secondly, the means by which these molecules are attracted to their targets is somewhat limited due to the limited number of favorable drug: DNA interactions possible owing to the small size of the drug. A vivid example of this is the considerably lower binding affinity ( $k_a$ ) of peptide fragments of a DNA binding protein versus that of the intact protein for a given DNA operator (recognition) domain.<sup>83</sup> Thirdly and most importantly, is the much slower rate of reaction for the second DNA modification event versus that of the initial DNA mono-adduction.<sup>84</sup>

A strategy used commonly by nature in increasing site-specificity and binding affinity of nucleic acid-binding proteins is that of dimerization, both covalent and non-covalent.<sup>85</sup> Non-covalent dimerization in proteins often involves a "dimerization domain". In addition to the presence of a recognition domain these "domains" are responsible for

extremely high binding affinities typically on the order  $10^9$  -  $10^{12}$  M<sup>-1</sup>.<sup>85</sup> The concept of dimerization has also been exploited by nature *enroute* to DNA cross-linking agents.

#### 1.2.5.1. Carzinophilin A & Isochrysohermidin

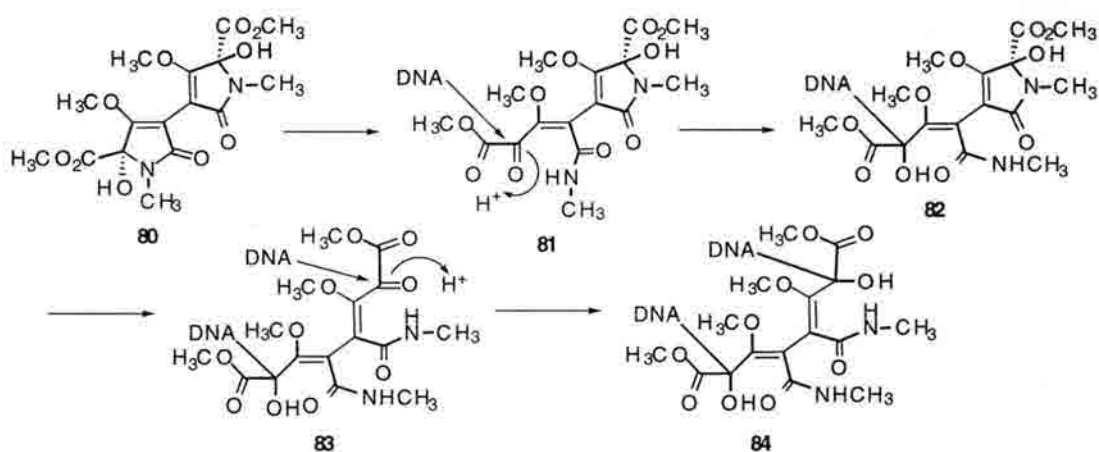


79, carzinophilin



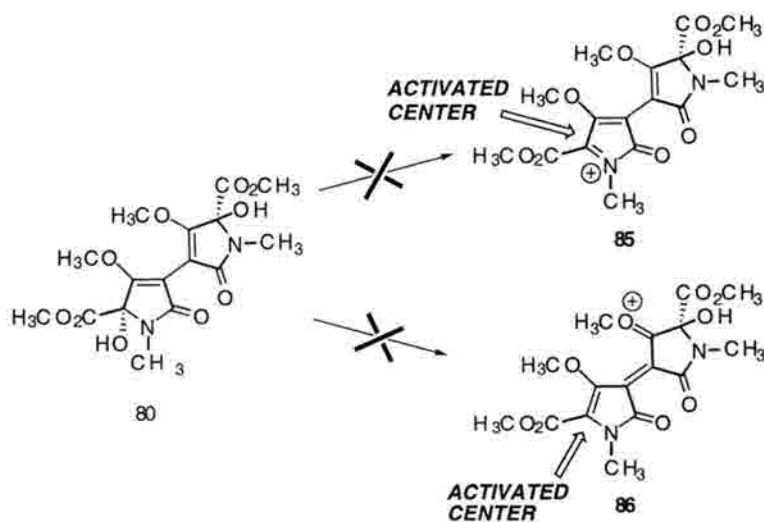
80, isochrysohermidin

Carzinophilin A (79) is an antitumor antibiotic isolated from *Streptomyces sahachiroi* and bears a distinct similarity to the previously discussed azinomycin B.<sup>86</sup> Particularly striking about both structures is the presence of the substituted naphthalene moieties which have been proposed to greatly enhance drug-DNA affinities *via* intercalation. While azinomycin B/carzinophilin benefits from only one aromatic moiety, 79 possesses two naphthalene moieties spaced 10 Å apart thus allowing *bis*-intercalation at contiguous sites in a *syn*-fashion.<sup>87</sup> The presumed mechanism of cross-linking by carzinophilin A involves initial intercalation followed by ring opening of each aziridine upon S<sub>N</sub>2 attack by each strand of the duplex.<sup>86</sup> The exact structure of the lesion has not yet been elucidated but degradative studies have confirmed the acid-catalyzed lability of each aziridine (with retention of the peptide backbone) and fluorescence enhancements substantiate that *bis*-intercalation occurs upon titration with calf thymus DNA.<sup>86</sup> Similarly, the lesion resulting from DNA alkylation with isochrysohermidin (80) has not been elucidated though mechanistic data has been generated to suggest a likely mechanism of action.<sup>88</sup>



**Figure 1-18.** Proposed mechanism of DNA cross-linking by isochrysohermidin.<sup>88</sup>

Boger *et al.* in presenting a novel total synthesis of isochrysohermidin reported the slow pH dependent formation of DNA interstrand cross-links into linearized  $\phi$ X174 DNA.<sup>88</sup> That *d,l*- and *meso*-isochrysohermidin all demonstrated equivalent cross-linking efficiencies under acidic (pH 4.2) or basic (pH 8.7) conditions, which were markedly decreased at neutral (pH 6-7) suggests the generation of the ring-opened amido ketones **81** and **83** as the electrophilic agents. Formation of the acylimminium **85** via dehydration and subsequent quenching by a nucleobase is unlikely in that basic conditions would deter such a process.

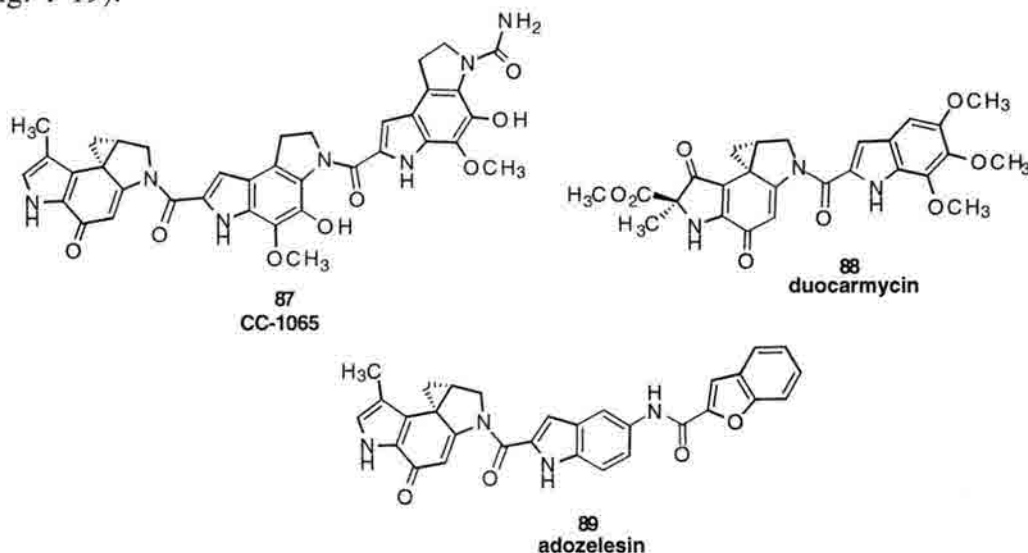


Likewise, generation of **86** *via* methoxy group assistance of one pyrrole to the other is unlikely due to the poor leaving group ability of hydroxide and the preferential donation into the neighboring amide carbonyl of the same pyrrole unit. Experimentally, the pH dependence observed argues against the importance of **86** as a relevant intermediate.<sup>88</sup>

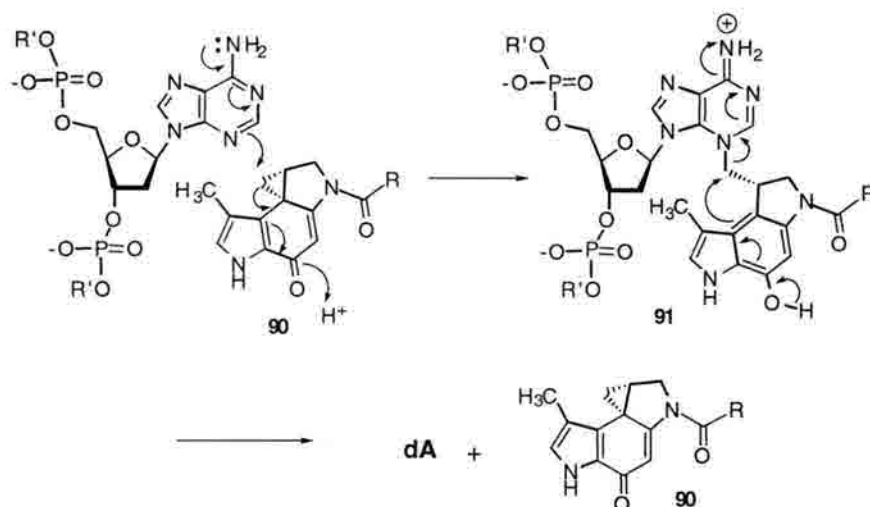
That both carzinophilin A and isochrysohermidin cross-link DNA *via* the equivalent of two mono-alkylation events has spurred a great deal of interest in the generation of synthetic cross-linking dimers.

#### 1.2.5.2. Biselezin ( U-77,779) and related structures

The cyclopropylpyrroloindoles (CPIs) have received considerable attention as extremely potent DNA monoalkylating agents. Of particular notoriety are CC-1065 **87**, duocarmycin **88**, and adozelesin **89** all of which induce selective adenine N<sup>3</sup> alkylation (Fig. 1-19).

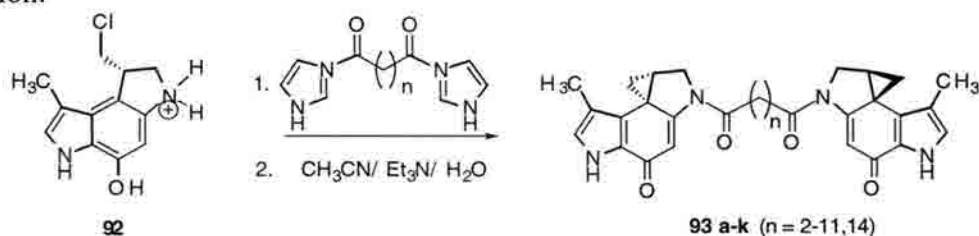


It is well established that S<sub>N</sub>2 attack upon the cyclopropane methylene unit generates the phenol adduct **91** (Fig. 1-19).<sup>89a</sup> This reversible process in turn, gives rise to base- and heat-labile lesions leading to DNA strand scission.<sup>89</sup> Exploitation of these agents as potential interstrand cross-linkers was originally reported by Mitchell *et al.* in which generation of **93a-k** was achieved by reaction of **92** (two equivalents) with one equivalent of the *bis*-imidazole of the required diacid.<sup>90</sup>



**Figure 1-19.-** Reversibility of DNA alkylation by cyclopropylpyrroloindoles

Additionally, dimers enantiomeric at one or both CPI units were constructed. Of these dimers all enantiomeric derivatives were devoid of cross-linking activity while only **93 b,d,e** and **g** gave rise to the gel-retarded restriction fragments<sup>91</sup> indicative of cross-link formation.



Notably, **93 b**, and **d** at 1.7 $\mu$ M concentrations gave rise to comparable amountsof cross-linked material as that achieved with 17 $\mu$ M of trimethylpsoralen. Reaction of the restriction fragments of interest with **93 e**, and **g** afforded considerably less cross-linked material (as assayed by alkaline agarose gel electrophoresis) but still demonstrated the novelty of CPI dimerization in altering the mode of action of the parent structure.

Bizelesin (**94**) represents the second generation of dimeric CPI compounds.<sup>92</sup> Unlike the methylene tethered CPI dimers, bizelesin possesses the rigid bis(indolecarboxylic acid) linker which allows a 6 to 7 bp span between alkylation sites while occupying the intervening minor groove between the terminal alkylation sites.



Like CC-1065 (**87**), the bizelesin CPI units selectively alkylate the adenine N<sup>3</sup> of the sequence 5'-TTA-3'. As such, bizelesin preferentially cross-links the sequence 5'-\*TAATTA-3' (A indicates one of the cross-linking sites while \* indicates the thymine opposite the other cross-linked adenine) though other sequences which place the two adenines of interest the same distance from each other have been noted.<sup>93</sup> Hurley *et al.* have shown that bizelesin may also cross-link the sequence 5'-TTAGTTA-3' at the same residues observed with the shorter substrate lacking the central dG-dC base pair.<sup>94</sup> Surprisingly, this sequence undergoes cross-linking preferentially to the shorter 5'-TAATTA-3' despite a considerably greater distance between the targeted adenine N<sup>3</sup> residues.

<sup>1</sup>H NMR and inosine substitution (for the central dG) experiments reveals that the exocyclic N<sup>2</sup> hydrogen of guanosine (not H-bonded to the complementary cytosine) allows an extremely strong hydrogen bond with the ureylene carbonyl which benefits from coplanarity with the dG exocyclic amine.<sup>94</sup> Once established, this bond shows quantitative occupancy within the duplex adduct (even at 500° K) and essentially locks the bizelesin linker moiety within the minor groove. Additionally, twisting of the urenyl linker almost 90° out of the *bis*-indole plane was found to induce considerable curvature of the dimer thus facilitating the minor groove fit. Given this, it has been postulated that, upon monoalkylation, bizelesin undergoes hydrogen bonding to the central dG (*via* N<sup>2</sup> interactions). This, in turn, pulls bizelesin down into the minor groove allowing distortion of the alkylated adenine towards the center of the duplex thus reducing the distance between the respective adenine N<sup>3</sup> residues. This perturbation in target structure mediated by the

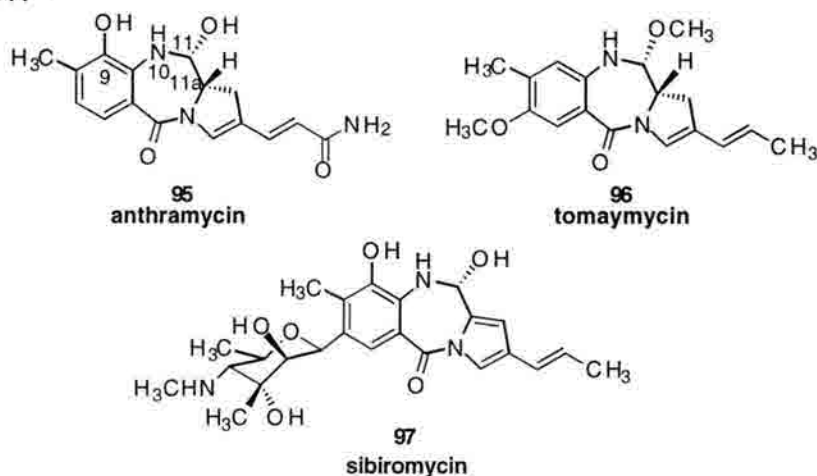
urenyl linker affords an N<sup>3</sup> to N<sup>3</sup> distance in the 7-bp system comparable to that seen with the 6-bp target.

These results, coupled with studies aimed at understanding the principle of 5'-TAATTA-3' recognition point out the importance of the dimerization motif chosen. Within the 5'-TAATTA-3' sequence, inherent instability of the central A·T step leads to base pair opening. Once opened, hydrogen bonding of the ureylene amido protons and the bases stabilize the transient Hoogsteen and open base-pair conformations thus facilitating cross-link specificity. That the ureylene moiety exerts such a strong influence upon the sequence selectivity of bizelesin suggests that dimerization offers enhanced specificity not due just to the compounding of monomer-DNA interactions, but also the result of linker-DNA interactions as well. Bizelesin represents a novel example of this concept and the importance of these interactions is reflected in the efficiency with which bizelesin selectively inflicts *bis*-alkylation upon 5'-TTAGTTA-3'. Hurley and co-workers have reported that bizelesin does not form detectable amounts of monoalkylated material upon reaction with 5'-TTAGTTA-3'.<sup>94</sup> Instead, only the direct conversion of native double-stranded DNA to covalently cross-linked substrate is observed for reaction aliquots analyzed at 0.5, 1, 2, 5, 7, 9, 12, 14, 24, 34, and 72 hours respectively. That this has not been the case for efforts involving the shorter 6 bp substrates lacking the central dG-dC pair argues well for the importance of the dG-to-linker contacts observed with 5'-TTAGAAT-3'. Considerable quantities of monoalkylation adducts have been reported for other target sequences<sup>93a</sup> and thus point out less pharmacologically important targets given the relative ease with which monoadducts may be repaired<sup>6a</sup> and their inability to stop strand separation events.<sup>9-11,13,14</sup>



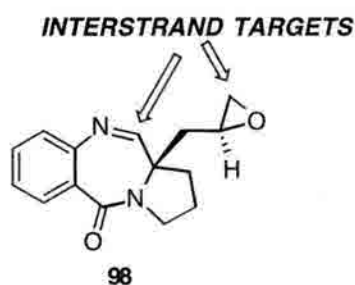
### 1.2.5.3. Pyrrolobenzodiazepine Dimers

The pyrrolo[2,1-c][1,4]benzodiazepines (PBDs) comprise a class of antitumor antibiotic natural products which includes anthramycin **95**, tomaymycin **96**, and sibiromycin **97**.<sup>95</sup>

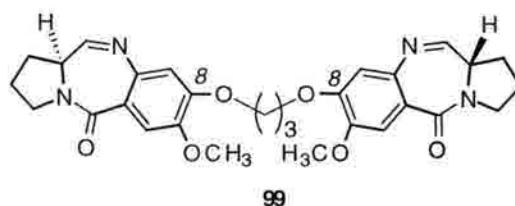


Conversion of the carbinolamine at C-11 to the corresponding imine affords reversible alkylation in the minor groove of the exocyclic N<sup>2</sup> amine of deoxyguanosine within duplex DNA. Minor groove binding is promoted by the PBD twist resulting from the S configuration at the bicyclic C11a position and related congeners bearing the phenolic 9-OH further benefit from hydrogen bonding with the O<sup>2</sup> of the cytosine complementary to the alkylated guanosine.<sup>96</sup> Sibiromycin lacks the S stereochemistry at C-11a (due to the pyrrolic nature of this moiety) but the amino-sugar compensates for this by providing attractive electrostatic interactions with the anionic backbone of DNA.<sup>97</sup> PBD monomers are efficient inhibitors of DNA and RNA synthesis<sup>98a</sup> and have proven to be highly sequence selective with a preference for purine-G-purine triplets.<sup>98b</sup> These agents have also received considerable attention as DNA anchoring systems for non-specific DNA cleaving agents such as Fe(II)-EDTA.<sup>99</sup> Additionally, conjugation to the 5'-AATT-3' minor groove-binding agent netropsin has been pursued as a means of enhancing the specificity of DNA modification by anthramycin.<sup>100</sup>

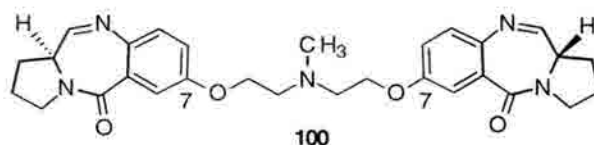
Bifunctional PBDs such as **98** have been prepared with the intention of effecting *bis*-alkylation but have met with only minimal success.<sup>95</sup> Considerably more fruitful has



been the generation of PBD dimers resulting from linker connection to the phenolic moieties of two PBC cores. Hartley and Thurston have shown that the dimers involving PBD linkage through their C8 positions *via* the flexible 1,3-alkanedioldioxy ether are extremely efficient interstrand cross-linkers.<sup>101</sup> Particularly effective is the propane-dioldioxy ether linked dimer **99**. After only 2 hours at 37°C, **99** induces detectable cross-linking (as assayed by alkaline agarose gel electrophoresis using linearized PBR322 DNA) down to 10pM concentration (drug:nucleotide ratio = .025) while at 0.4μM (drug-to-nucleotide ratio = 1.0) greater than 90% of the linear substrate is cross-linked. By comparison, **99** is 50 times more efficient than either mechlorethamine or *cis*-DDP and



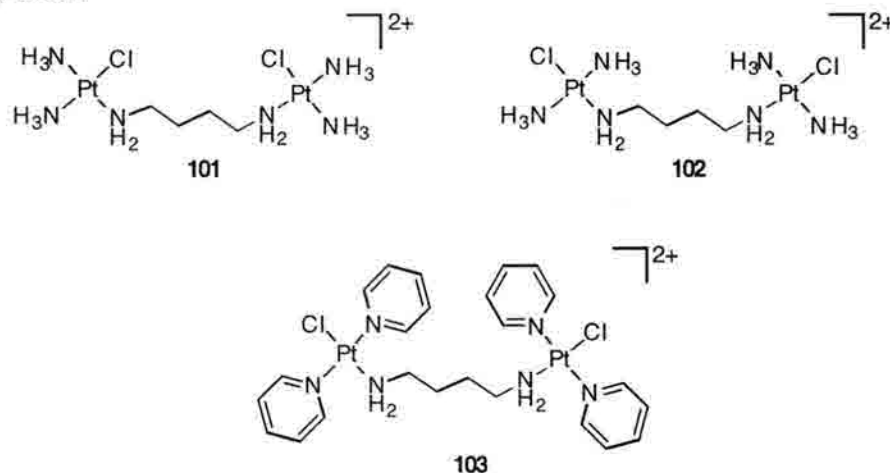
rivals the alkylation efficiency of the CPI dimers described above. More interestingly, cross-linking was found to be irreversible. This is in stark contrast to the weaker binding C7-linked dimer **100** examined by Suggs *et al.*<sup>102</sup> Thus, in the case of **99**, dimerization enhances the efficacy of each PBD monomer not only by increasing drug:DNA affinities, but also by preventing loss of the relevant lesion to hydrolytic decomposition. Additionally, it is interesting to note that the altered means of dimerization (C7 vs. C8 connectivities) led to different reactivities with respect to DNA alkylation.



Although **99** gave rise to DNA cross-links that migrated analogously to double-stranded standards, **100** afforded DNA adducts which migrated considerably slower than psoralen cross-linked standards. That such adducts were attributable to interhelical events seems a likely explanation for this phenomenon and points out a potentially useful mechanistic difference which is potentiated by the chosen means of dimerization.<sup>103</sup>

#### 1.2.5.4. Dinuclear *cis*-DDP analogues

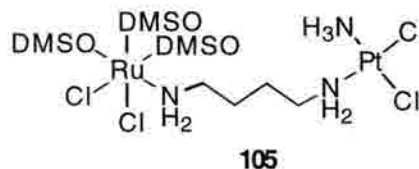
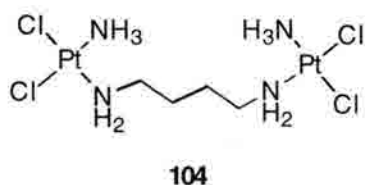
As mentioned previously, the interstrand lesion resulting from reaction of *cis*-DDP with 5'-GC-3' results in massive distortion of the B-DNA target which very likely limits the utility of this compound as an interstrand cross-linking agent. Similarly, the intrastrand lesion while forming much more readily than the interstrand lesion, induces mutational events *via* the distortion of its nucleic acid target. These detrimental issues have been addressed by the generation of dinuclear Pt complexes which possess two Pt (II) centers each of which carries only one chloro ligand thus relegating each Pt (II) capable of only one coordination event.<sup>81a</sup> Farrell *et al.* have recently synthesized the dinuclear complexes **101**, **102**, and **103** and studied their respective interactions with calf thymus DNA and a small 49 bp ODN.<sup>81a</sup>



Owing to the presence of the pyridyl ligands, **103** induces a much higher degree of DNA unwinding than that seen with either of the ammonia-bound complexes, as well as the mononuclear *trans*-[PtCl<sub>2</sub>(py)<sub>2</sub>]. Similarly, **103** stabilizes B-form DNA while the other

complexes induce B-Z transitions upon DNA binding. These alterations likely involve the ability of **103** to undergo  $\pi$ -stacking interactions upon DNA association which in turn, disfavors the Z-DNA conformation. Importantly, ISC formation is very efficient for all three complexes with yields of 80%, 52%, and 41% for **101**, **102**, and **103** respectively. Further, only **102** (the *trans* isomer) was capable of intrastrand adduction. That the diamine chain in **102** can be rotated around the two Pt square planes to afford simultaneous dG N<sup>7</sup> binding in the sequence 5'-GGCC-3' is the proposed origin of the intrastrand capability of **102**.<sup>16</sup> The *cis* placement of the chlorides (as in **101**) with respect to the diamine linker prohibits (after the initial DNA connection) the butanediamine chain from achieving an orientation necessary for the intrastrand connectivity. As such, interstrand cross-linking has been very successfully achieved while avoiding the undesired distortional processes inherent to the mononuclear complexes.<sup>81a</sup> Importantly, such dinuclear Pt(II) complexes have been shown to be extremely effective against tumor cell lines which have become resistant to monomeric *cis*-DDP.<sup>104</sup>

The ability to form heterodimers of mono- or di-chloro Pt(II) amine complexes and dichloro Ru(II) has allowed the generation of agents which interstrand or intrastrand cross-link a given DNA substrate with one end while giving rise to protein adducts at the other end.<sup>16a</sup> This methodology has been elegantly demonstrated *enroute* to the formation of DNA-protein cross-links between the repair enzymes UvrA and UvrB and a synthetic ODN treated with the homodimers **102**, **104**, or, the heterodimeric **105**.<sup>16a</sup>



The UvrABC nuclease system acts to initiate the process of nucleotide excision repair leading ultimately to DNA repair of damaged nucleotides.<sup>6a</sup> UvrA and UvrB form a 2:1 complex in solution that has been shown to travel along DNA in an ATP-dependent

fashion. Arrival at a site of damage induces structural reorganization of the trimeric assembly resulting in loss of the UvrA dimer. Retention of the resulting UvrB-DNA complex signals to UvrC the precise location of damage. UvrC, in turn, induces dual incisions upon the phosphodiester backbone bracketing the lesion of interest. Demonstration that both UvrA and UvrB are in intimate contact with the DNA and its initially formed Pt(II) lesion (as the recognized site of damage) manifests itself in the observed DNA-protein cross-links obtained using **102,104**, and **105**. Specifically, cross-linking of both the UvrA/UvrB complex and lone UvrB to the ODN was obtained upon treatment with either **104** or **105**. Cross-linking of the UvrA dimer to the platinum-modified ODN ensued using any three of the dinuclear complexes thus further demonstrating the versatility of this approach. In this fashion, the dimerization of transition metal complexes represents a novel means of not only effecting DNA interstrand cross-links, but of also inducing site-specific suicide DNA lesions *enroute* to enzyme inactivation.

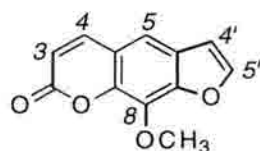
The versatility of the dinuclear metal complexes brings to light an additional strength to the strategy of dimerization; that being diversity. The mixing and matching of dimerized moieties not only allows the previously discussed issues to be addressed (with respect to ISC formation), but also allows elaboration on the themes of specificity and affinity. As evidenced with the metal complexes above, even basic mechanisms of action can be radically altered based upon the choice of the monomeric units involved in dimer construction.

### **1.3. PHOTOACTIVATED CROSS-LINKING AGENTS**

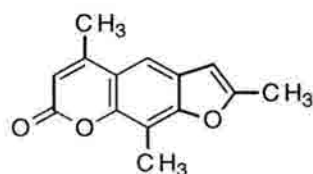
#### **1.3.1. Psoralens**

To date, the psoralens are the only class of compounds known to induce ISCs upon photolysis. This naturally occurring class of aromatic compounds consists of a furan ring fused to a coumarin.<sup>105</sup> They are found predominantly in plants from the *Umbelliferae*,

*Rutacea*, and *Leguminosae* families, but have also been isolated from microorganisms including fungi.<sup>106</sup> The two most heavily studied psoralens, 8-methoxypsoralen (8-MOP, **106**), and 4,5',8-trimethylpsoralen (Me<sub>3</sub>psoralen, **107**) are found as fungal metabolites.<sup>106</sup> Clinically, the psoralens are employed in the treatment of psoriasis, vitilago, and cutaneous T-cell lymphoma (CTCL).<sup>107</sup> They have also proven efficacious for the treatment of diseases associated with autoimmune disorders, organ rejections, and the AIDS-Related Complex.<sup>107</sup>



**106**  
**8-MOP**

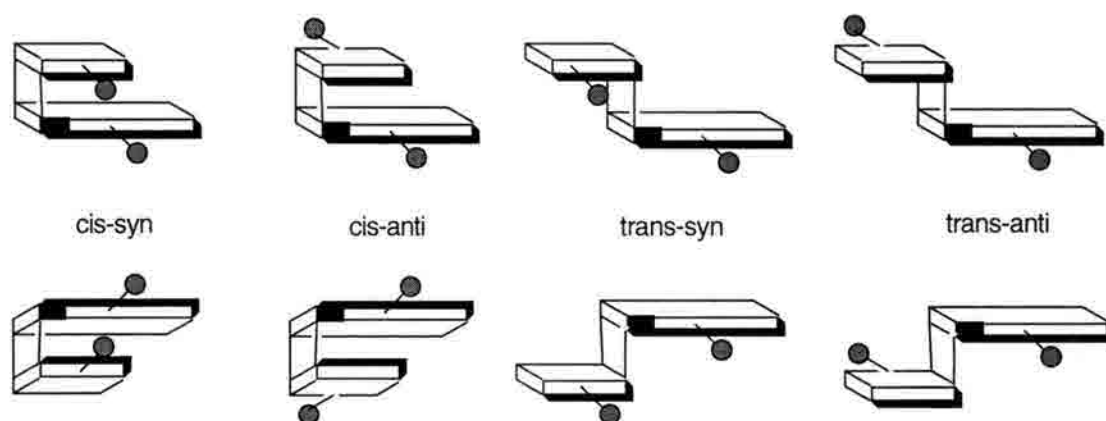


**107**  
**Me<sub>3</sub>psoralen**

It is proposed that in addition to ISC generation, these agents express favorable activity by inducing A to C mutations which enhance immunogenicity in tumor cells.<sup>108,109</sup> The sequence 5'-GGGATTTCACCC is an essential enhancer motif in murine lymphoma cells but not in the host HeLa cells. Its binding to the transcription factor NF- $\kappa$ B results in activation of transcription; an action traditionally associated with proliferation of non-tumorigenic cells. Briegel *et al.* have shown that in the case of the IL-2 gene of murine lymphoma cells, mutation of the boldface **A** to C in this sequence converts a weak binding site (for the T-cell restricted NF- $\kappa$ B) into a strong one resulting in release of NF- $\kappa$ B from the inhibiting factor I $\kappa$ B.<sup>108</sup> Induction of the transcription factor gives rise to increased production of non-tumorigenic cells thus allowing for an increased immunological response. This represents a unique application of mutation induction by a DNA reactive agent. Unlike *cis*-DDP which induces detrimental mutations, the psoralens may express the majority of their preferred biological activity *via a mutational pathway* which enhances the immune status of host cells.

In addition to the clinical applications, the psoralens have been used extensively in probing the secondary and tertiary structures of DNA and RNA.<sup>106</sup> Similarly, psoralen-DNA monoadducts have been used as probes for DNA-protein interactions *via* the generation of DNA-protein cross-links.<sup>110</sup> Solid phase synthesis of psoralen functionalized ODNs has been achieved upon generation of psoralen tethered phosphoramidites.<sup>111</sup> Additionally, biotinylated psoralens have been used for non-isotopic labeling of DNA.<sup>112</sup> They have also been used to inactivate viruses and other pathogens *via* irreversible nucleic acid interactions which spare the function of proteinaceous cellular subunits.<sup>113</sup>

Induction of ISCs into duplex DNA requires three distinct steps. Initially, the planar tricycle intercalates into the duplex between the two bases of either 5'-TA or 5'-AT. Such binding to synthetic ODNs is particularly strong with dissociation constants ( $K_d$ ) on the order of  $6.6 \times 10^{-6}$  M.<sup>114</sup> Upon the absorption of a quantum of light, either the 4',5'-furan double bond or the 3,4-pyrone double bond can undergo photocycloaddition to the 5,6-double bond of a thymidine.<sup>115</sup> Reaction of the pyrone results in destruction of the coumarin nucleus resulting in a low lying triplet state for the resulting monoadduct. This state is unreactive towards the second photocycloaddition due to its rapid relaxation to the

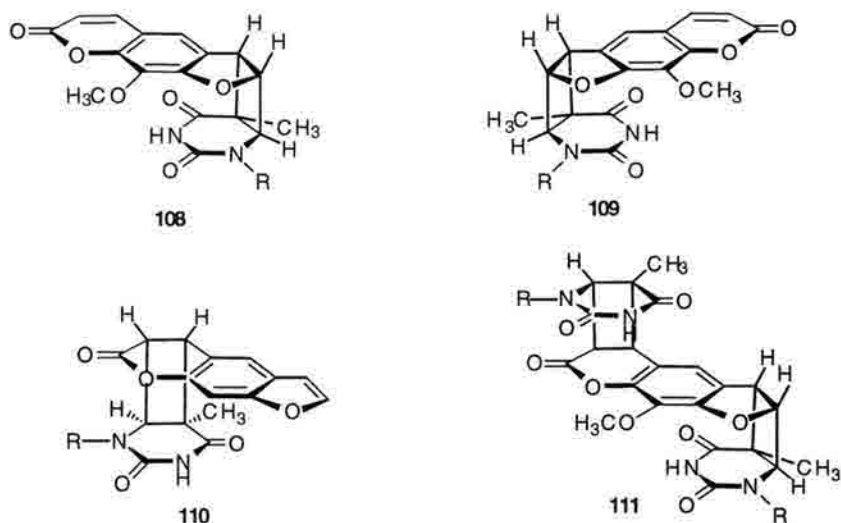


**Figure 1-20.** Representation of the 8 possible configurational isomers for 8-MOP-thymine monoadducts (*enroute* to the ISC). The large slabs represent 8-MOP with the furan end designated with the black marker and the C8 methoxy group as the shaded handle. Thymine is represented by the smaller slabs with the shaded handle representing N1. Isomers on the top row are mirror images of the isomers on the bottom row.



ground state. Thus, destruction of the coumarin nucleus abrogates ISC formation. However, retention of the pyrone (*via* the initial photocyclization involving the furan) allows the intact coumarin to absorb a second quantum of light leading to local excitation of the 3,4-double bond to the excited triplet ( $\pi$  to  $\pi^*$  transition) which cyclizes with the 5,6-double bond of the adjacent pyrimidine thus affording the ISC.

The photoreaction of thymidine with psoralens may occur from either the 3'-side or 5'-side of the thymidine base depending upon the displacement of the psoralen (pso). Monoadduct formation within either cross-linkable site 5'-TpA (3' face) or 3'-TpA (5' face) results in the generation of enantiomeric thymine adducts. While a number of isomers is possible, as shown in Figure 1-20, the *cis-syn* configuration is most readily formed due to severe restrictions on the modes of psoralen intercalation imposed by the duplex conformation.



Chirality of the deoxyribosyl unit renders these monoadducts as a mixture of diastereomers. Exemplary in this stereoselectivity is 8-MOP **106**. Reaction of **106** with 5'-TpA or 5'-ApT yields two furan-side monoadducts **108** and **109**, with concomitant generation of only one pyrone adduct **110** (C-8 methoxy not shown for clarity).<sup>106</sup> Additionally, thymidine-8-MOP-thymidine cross-links have been isolated as a mixture of two diastereomers each of which bears the *cis-syn* stereochemistry as per **111**. This



stereochemical relationship has been observed for numerous psoralens and is very likely general to all linear furocoumarins.<sup>116</sup>

Psoralens have been used to non-covalently increase ODN binding affinities *enroute* to triple-helix motifs. Likewise, psoralen specificity has been enhanced *via* triple-helix strategies. Such instances of covalent attachment of a psoralen tethered ODN to a given DNA target illustrates the symbiotic relationship between the two halves of the conjugate.<sup>117</sup> For instance, the Thuong group has demonstrated that psoralen conjugation to 5'-TTTTCCTCTCCCCTCT-3' (C=5-methylcytosine) affords an ODN capable of inhibition of gene expression.<sup>118</sup> The functionalized polypyrimidine binds (*via* Hoogsteen base pairing) to the site (operator sequence) normally occupied by the transcription factor NF- $\kappa$ B which activates transcription from the IL-2R $\alpha$  promoter. Photolysis at 365nm selectively anchors the ODN proximal to the operator and thus increases the localized concentration of the ODN to its target sequence. Inhibition of transcription by the ODN-pso conjugate occurred upon *in vitro* photolytic cross-linking followed by electroporation/transfection into HSB2 T-cell tumor lines. Additionally, *in vitro* transcription assays were performed with the cross-linked plasmid (IL-2R $\alpha$  CAT) as were *in vivo* assays in which the ISC was induced following introduction of the ODN-pso conjugate into the cell line. Both assays revealed a high degree of ISC induction (70-80%) and subsequent transcription inhibition.

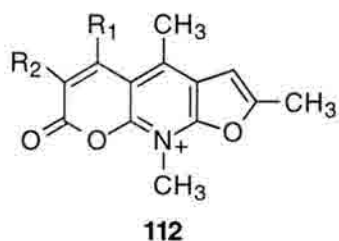
Thuong *et al.* have applied a similar approach towards targeted interstrand cross-linking of HIV proviral DNA.<sup>119</sup> Psoralen conjugation to the 5' phosphate of 5'-TTTTC-TTTTCCCCCCT-3' afforded a conjugate capable of triplex formation with two 16 bp homopurine runs of the HIV proviral genome. Each homopurine run overlaps the recognition/cleavage site of Dra I restriction endonuclease and subsequently, represented a novel target for ODN-pso conjugate binding. Construction of pBT1 and pLTR plasmid DNAs resulted from insertion of HIVBRUCG proviral fragments into the commercially available pUC19 and pBR322 plasmids. The pLTR substrate contained 4 Dra I sites (5'-

TTTAAA) one of which extends three base pairs into the triplex region. Plasmid pBT1 contained 14 Dra I sites of which two were within the triplex domain. Efforts involving Dra I cleavage of pLTR revealed that the conjugate (unphotolyzed) was capable of slight Dra I inhibition at short incubation times, but that over time, complete cleavage of the substrate occurred. The reversibility of triple-helix formation responsible for this observation was averted upon photolysis. Irradiation at 20, 40, and 330 seconds resulted in irreversible ODN-*ps*o binding as evidenced by complete Dra I blockage at the cleavage site in question. Similarly, the same phenomenon was observed with the pBT1 substrate. Additionally, reaction of this substrate with the conjugate (following irradiation) afforded an unanticipated Dra I inhibition site resulting from triplex formation involving only 8 consecutive triplets. This was ultimately attributed to the inability of contiguous cytosines to undergo protonation at the experimental pH of 6.9. Thus a plasmid site capable of triple helix formation with only the 5'-TTTTCTTT-3 portion of the ODN-*ps*o conjugate was detected *via* unintentional photo-induced ISC formation.<sup>119</sup>

That recent efforts have involved only the conjugation of psoralens to other molecules of interest is not the case. The ability to fine tune psoralen reactivity *via* synthetic manipulations has been demonstrated. The general trends observed place particular importance upon functionalization at carbons 3,4',5 and 8. Methylation of the 4,5'-, and 8- position enhances the intercalative binding affinity, as well as, the quantum yield of cycloaddition over that of the unsubstituted case.<sup>120</sup> However, methyl ether incorporation at C8 dramatically slows the photochemistry, hence, the much slower DNA alkylation by 8-MOP versus **107**.<sup>120b</sup> Methyl group placement at C4 results in near quantitative monoadduct formation at the furan side of the chromophore in contrast to 8-MOP which gives up to 20% pyrone monoadduct. This is attributed to steric clashes involving the C4 methyl and the thymidine C5 methyl with which the pyrone side would normally react.<sup>121</sup> Strong electron donating or withdrawing groups at C5 and C8 greatly reduces or completely obliterates reactivity with DNA.<sup>120b</sup> Analogous substitution at C3

has a similar result.<sup>122</sup> However, positively charged groups placed at the C4' and C5 enhance both non-covalent DNA associations as well as covalent modification events.<sup>123</sup>

Recent synthetic efforts have focused on generation of psoralens with enhanced light absorption properties, longer lived and more easily achieved excited states and greater water solubility characteristics.<sup>114</sup> This has involved the synthesis of heterocyclic analogs in which sulfur or selenium replaces the endocyclic oxygens,<sup>124</sup> as well as, the construction of N-methyl azapsoralens of the form **112** ( $R_1 = \text{CH}_3$  or H,  $R_2 = \text{CH}_3$  or H) possessing vastly improved water solubility.<sup>125</sup> That these compounds possess the attributes which motivated their synthesis has not yet been shown.



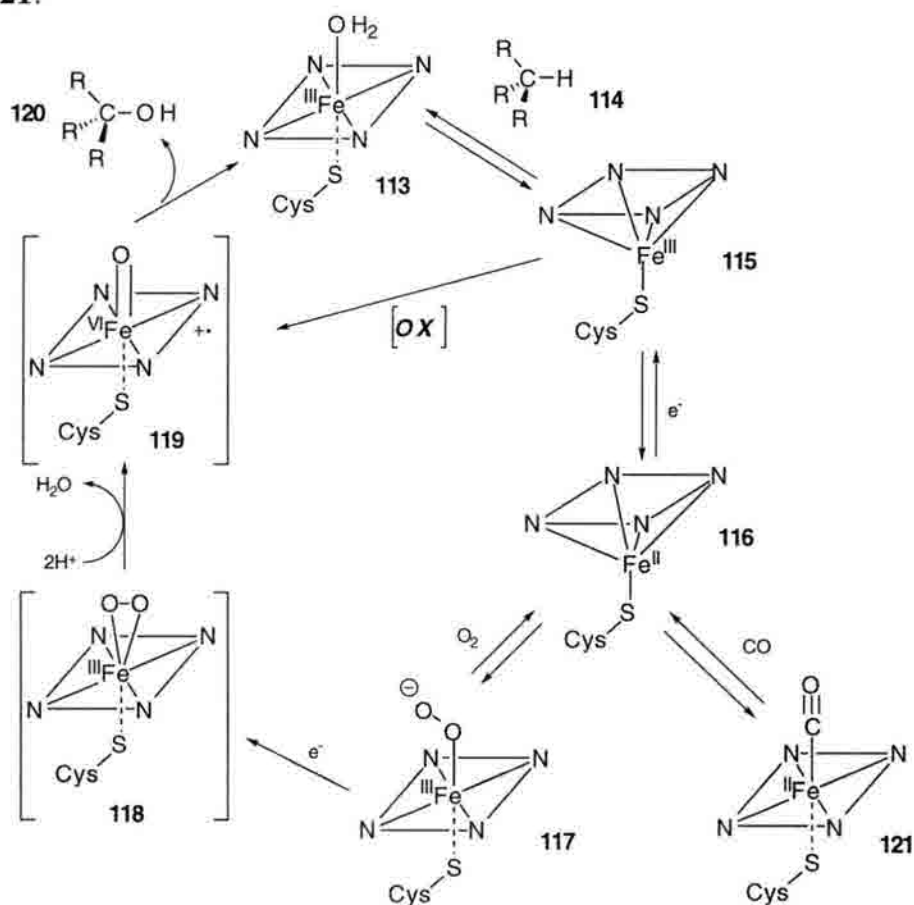
#### 1.4. OXIDATIVELY ACTIVATED AGENTS

The cytochrome P450 group of monooxygenases is a superfamily of enzymes which consists of more than 153 genes represented in 27 families, 10 of which occur in mammals.<sup>126</sup> Oxidative transformations catalyzed by cytochrome P450 include carbon hydroxylation, heteroatom hydroxylation, heteroatom dealkylations (*via* aldehyde generation), oxidations of  $\pi$ -systems, and conversion of aldehydes or alcohols to the corresponding acids.<sup>127</sup> In a general sense, the thermodynamic parameters of the oxygenation event may be represented by Eq. 3.



This transformation involves two extremely high energy barriers, namely, dissociation of the dioxygen bond (460 kJ/mol), and dissociation of the carbon-hydrogen bond of the substrate (420 kJ/mol).<sup>128</sup> By breaking down the overall process into several discrete steps, cytochrome P450 affords the net transformation requiring only 40-70

kJ/mol.<sup>128</sup> This is largely due to the weakening of the O-O bond upon binding of dioxygen to the heme iron in the active site. As depicted by Figure 1-21, the mechanism of substrate oxidation involves (1) binding of the substrate **114** to the enzyme resulting in conversion of the low spin six coordinate species **113** to the high spin five coordinate **115**, (2) 1-electron reduction of the iron by the flavoprotein NADPH cytochrome P450 reductase to yield **116**, (3) reaction of the ferrous iron with O<sub>2</sub> to yield the unstable (FeO<sub>2</sub>)<sup>+2</sup> complex **117**, (4) addition of a second electron from either NADPH-cytochrome P450 reductase or cytochrome b<sub>5</sub> affording **118** (5) heterolytic scission of the FeO-O(H) bond to yield the (FeO) compound **119**, (6) oxidation of the substrate (regenerating Fe<sup>+3</sup>), and (7) release of the oxidized substrate **120** from the enzyme.<sup>129</sup> Alternatively, binding of carbon monoxide instead of O<sub>2</sub> may occur in step (3) thus yielding the monoxide bound species **121**.

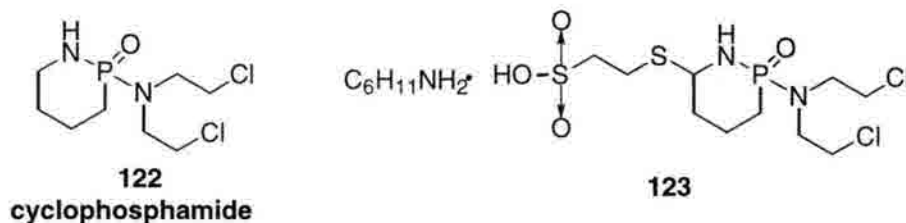


**Figure 1-21.** Proposed Mechanism of Xenobiotic oxidation by Cytochrome P450.

Significantly, numerous enzymes are capable of oxidative transformations.<sup>130</sup> It is generally agreed however, that cytochrome P450 is the predominant species responsible for hepatic activation of DNA alkylating agents. Resulting from its dual versatility and natural abundance, the vast majority of studies dealing with oxidative activation of drugs have directly addressed issues pertinent to P450. These include mechanistic issues such as substrate stereochemistry and corresponding rates of oxidation, P450 overexpression, and P450 inhibition (either by enzyme inactivation or overexpression of competing reductases). Detailed below are the three principal classes of interstrand cross-linking agents whose efficacy is cytochrome P450 mediated.

#### **1.4.1. Cyclophosphamide**

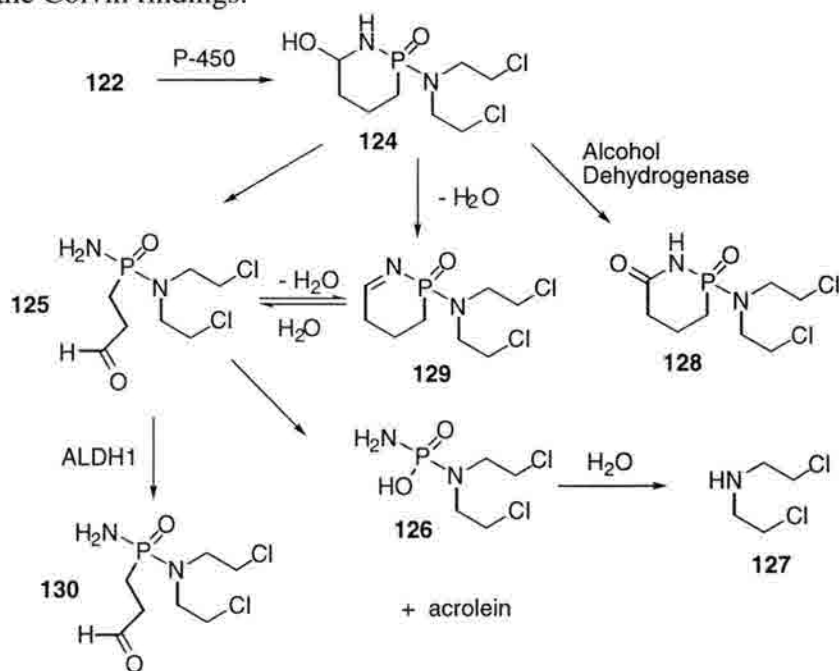
Cyclophosphamide (CP, **122**) was among the first agents recognized as requiring metabolic activation *enroute* to biomolecule modification. Since its discovery in 1958, it has become the most widely used chemotherapeutic of the alkylating class.<sup>131</sup> Cyclophosphamide and related oxazaphosphorines undergo oxidation at the C4 position (adjacent to the cyclic nitrogen) to yield the corresponding 4-OH-CP **124**, which spontaneously undergoes reversible ring-opening to afford the biologically active aldophosphamide **125** (Figure 1-22).<sup>132</sup> Once generated, the AP intermediate **124** may



undergo several different transformations. Alcohol dehydrogenase mediated oxidation of **124** yields the amide **128** and has been shown to be a means by which DNA alkylation is shut down. Oxidation (*via* aldehyde dehydrogenase ALDH1) of the ring-opened **125** to the corresponding acid **130** also represents a non-productive metabolic pathway with respect to ISC formation. Alternatively, elimination of the phosphoryl moiety from

aldehyde **125** affords the mixture of phosphoramidate mustard **126** and acrolein. Hydrolysis of the phosphoramidate mustard yields the secondary amine version of mechlorethamine **127** commonly referred to as nor-HN2.

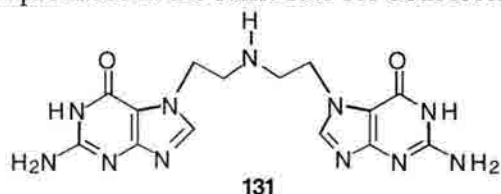
Elucidation of the interstrand lesion formed upon reaction of activated CP with DNA revealed **131** as the relevant interstrand lesion.<sup>133</sup> Originally believed to arise from cross-linking by nor-HN2, Colvin *et al.* have shown that phosphoramidate mustard **126** is the actual cross-linking agent formed upon CP metabolism.<sup>134</sup> Additional studies by Hemminki have shown nor-HN2 to be a very poor alkylating agent thereby further substantiating the Colvin findings.<sup>134</sup>



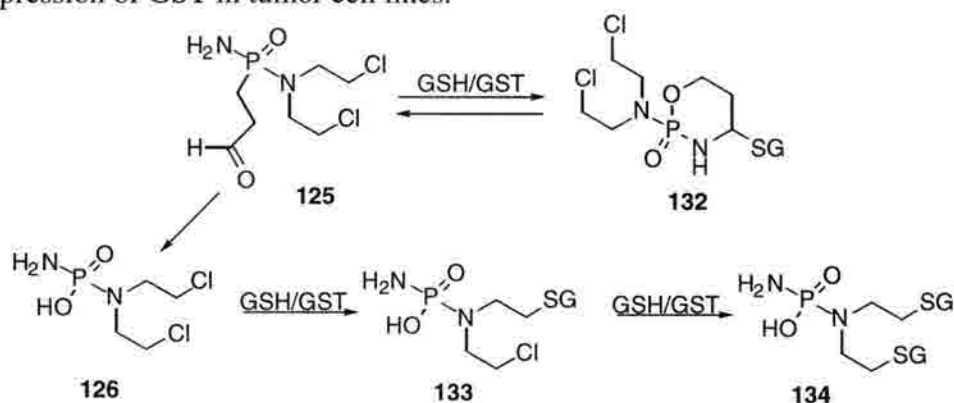
**Figure 1-22.** Mechanism of oxidative degradation of **122** to DNA reactive metabolites.

In addition to elucidation of the metabolic activation of CP, efforts to define other mechanistic aspects of CP's mechanism of action have been undertaken. The specific cytochrome P-450 enzymes responsible for the *in vivo* activation of CP have been identified.<sup>135</sup> These include CYP2B1, CYP2C6, CYP2C11, and CYP3A1 in the case of adult rat liver.<sup>135</sup> Similarly, CYP2B6, CYP3A4, and several of the CYP2C class enzymes have been implicated in the human liver activation pathways.<sup>135</sup> Additionally, it is proposed that only the oxidized 4-OH-CP can cross cell-membranes whereas the native

"pro-drug" cannot.<sup>136</sup> *In vivo* studies have demonstrated that oxidation/metabolism of the S enantiomer of CP proceeds at a faster rate than CP bearing the R configuration at phosphorus although ALDH1 inactivation of both stereoisomers of 4-OH-CP *via* conversion to the keto form proceeds at the same rate for both isomers.<sup>137</sup>



Recent efforts have focused on the issues of drug resistance and activation/deactivation pathways *via* gene over-expression. It is well established that one means of resistance to biological alkylating agents is the increased production of glutathione and higher levels of glutathione S-transferase over those seen in normal cells.<sup>138</sup> Normally present intracellularly at concentrations up to 5-10 mM, this tripeptide very often competes with DNA for drug binding. Importantly, increased levels of glutathione S-transferase (GST) have been found in tumor cell lines which have developed resistance to CP, as well as other alkylating agents such as the N-mustards and *cis*-DDP. Dirven *et al.* have shown that GSH readily forms the adducts shown below in Figure 1-23.<sup>138</sup> Additionally, GST enhances the formation 4-glutathionylcyclophosphamide 2-4 times over that of the nonenzymatic rate. These efforts have suggested that CP resistance may likely result from overexpression of GST in tumor cell lines.



**Figure 1-23.** Mechanism of cyclophosphoramide inactivation by glutathione/glutathione S-transferase. GSH= glutathione, GST= glutathione S-transferase.



Studies by the Dalla-Favera group have demonstrated induction of maphosphamide resistance upon *in vitro* overexpression of ALDH1.<sup>139</sup> Cloning of the full-length human ALDH1 cDNA and introduction *via* retroviral vectors into human (U937) and murine (L1210) hematopoietic cell (HPC) lines endowed these cell lines with resistance to the activated CP congener **123**. Increases in maphosphamide resistance were 4 to 10 times above control transduced HPCs. As such, this gene strategy revealed that the ALDH1 mediated conversion of **124** to the keto intermediate is likely implicated in the development of drug resistance not only to CP, but to other oxidatively activated drugs as well. This identifies the ALDH1 gene as a previously unidentified member of the drug-resistance gene family that includes the DHFRr and MDR1 genes.<sup>140</sup> More importantly, this methodology may provide a means of increasing CP resistance in cell lines which undergo undesired CP reactions upon clinical administration. For instance, the introduction of genetically engineered bone marrow cells expressing genes of therapeutic relevance has been suggested as a means of inhibiting myelosuppression in CP therapies.

Gene overexpression techniques have been used to probe the avenues by which CP resistance is induced. These same strategies have also been exploited *enroute* to selective drug activation. The effectiveness of the oxazaphosphorines is limited by the hematopoietic, renal, and cardiac toxicity that accompanies the distribution of the liver-activated metabolites. A method of bypassing this problem has been demonstrated by Waxman and Chen.<sup>135</sup> Introduction of the liver cytochrome P450 gene CYP2B1 into human breast MCF-7 cancer cells was found to induce a high degree of cytotoxicity towards both CP and its analogue ifosfamide (IFA). This is particularly significant since MCF-7 cells possess little or no endogenous CYP enzyme activity, but instead express high levels of NADPH cytochrome P450 reductase. Cell cycle analysis revealed that CP-arrested the CYP2B1 transfected cells but not the CYP2B1-negative cells. That CP-mediated cell cycle arrest was CYP2B1-mediated was further supported by the loss of cytotoxicity upon cell treatment with metapyrone, a known heme binding ligand.

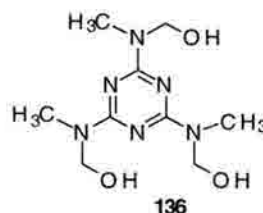
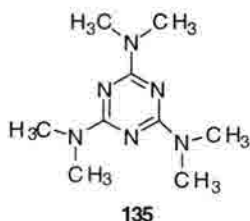


Cytotoxicity to adjacent tumor cells lacking the P450 gene was also observed. This anti-tumor effect was attributed to transfer of toxic CP metabolites through cell-cell contacts as well as through the medium. Additionally, this gene expression, when treating MCF-7 tumors grown in nude mice gave rise to a 15-20 fold greater CP *in vivo* cytotoxicity.

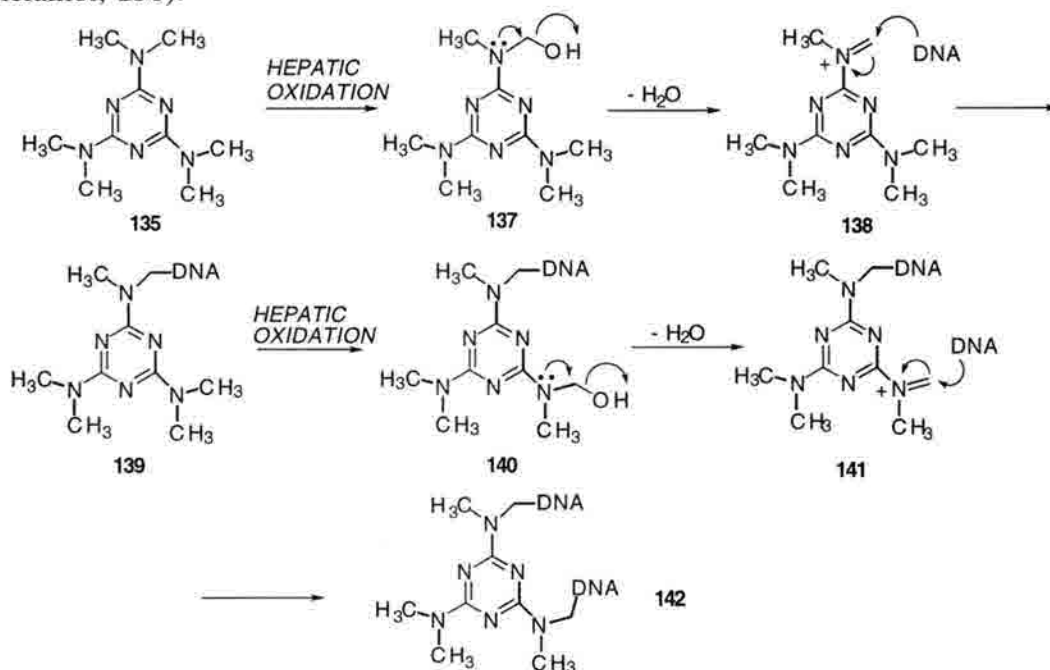
In addition to breast cancer cell lines, Chen *et al* have applied this same strategy towards selective targeting of glioblastomas.<sup>141</sup> The most common malignant primary brain tumor, glioblastoma is considered incurable, with multimodal therapeutic approaches (surgery, radiation, chemotherapy) increasing survival times by only a matter of months. Overexpression of P450 2B1 gene (C6-P450) in C6 glioma cells afforded cells highly sensitive to CP both *in vitro* and *in vivo*. Diffusion/transfer of toxic CP metabolites occurs as in the MCF-7 case with CP (500  $\mu$ M) induced tumor cell death observed after 3 hours. This represents a novel tumor killing strategy wherein target selectivity arises not only from the drug itself, but also from the selective expression of "activating" enzymes. Still further, the Chen studies have shown the relevance of a "bystander" effect by which toxic drug metabolites generated in one tumor cell may inflict damage upon another nearby tumor cell. Thus, the need for quantitative transfection of the gene to be expressed is not necessary to elicit the desired therapeutic response.

#### 1.4.2. N,N,N',N',N',N'-hexamethylmelamine and Related Structures

Hexamethylmelamine (HMM,135) is an antitumor agent shown to be effective against a number of different human tumor cell lines. It is active against metastatic breast cancer, lymphoma, cervical cancer and bladder cancers.<sup>142</sup> Additionally, it has received considerable attention in the treatment of ovarian cancer and to a lesser degree, lung carcinomas.



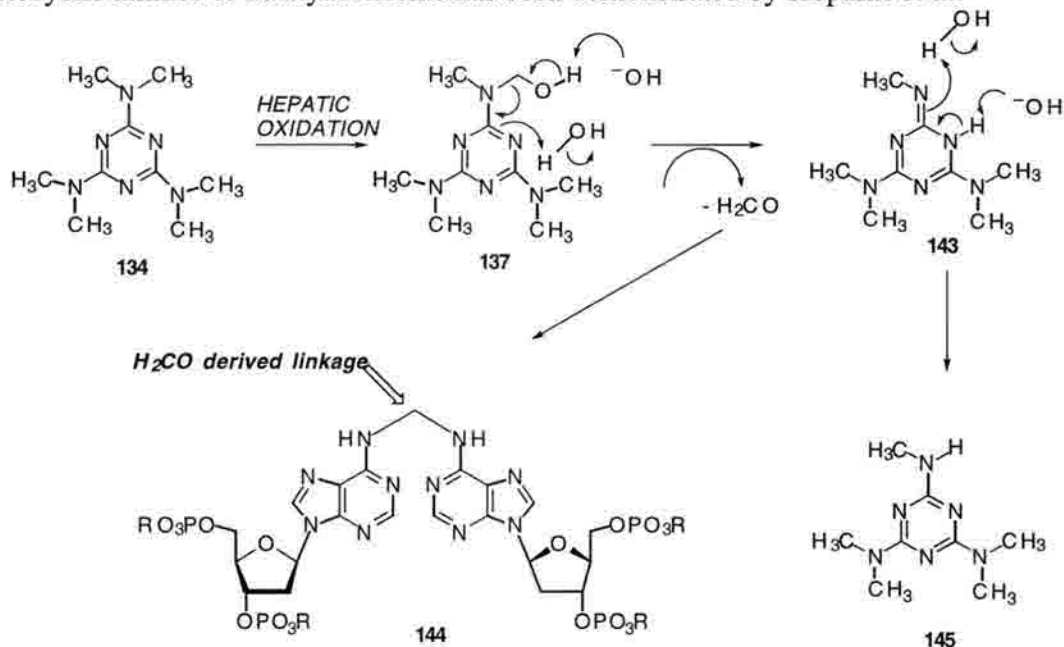
Upon hepatic oxidation by cytochrome P450, N-demethylation occurs *via* initial hydroxylation followed by dehydration (Figure 1-24).<sup>143</sup> The resulting imminium is a potent DNA alkylating agent and it is likely that this species undergoes subsequent DNA alkylation. Stemming from these observations involved in DNA modification by hexamethylmelamine, has been the generation of N<sup>2</sup>,N<sup>4</sup>,N<sup>6</sup>-trimethylmelamine (trimelamol, **136**).<sup>143</sup>



**Figure 1-24.** Mechanism of activation of hexamethylmelamine and subsequent DNA modifications.

The tris-hydroxylated analog **136** is much more water soluble than its predecessor and circumvents the need for oxidative activation. That trimelamol mimics the mechanism of action of hexamethylmelamine and structurally related congeners has been stipulated by the known metabolic pathway leading to demethylation of each trimelamine exocyclic nitrogen *via* P450-mediated carbinolamine formation.<sup>143</sup> Little is known about the mechanism of action of the parent compound HMM, however, some data (*in vitro*) has been generated pertaining to the reaction of trimelamol with linearized plasmid PBR322 DNA.<sup>144</sup>

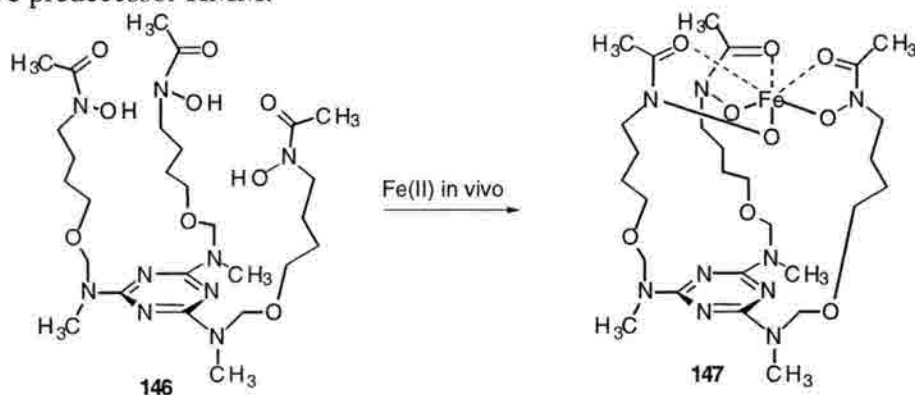
Hartley and Thurston have addressed the concern that ISC formation by trimelamol (and HMM by induction) may result not from covalent attachment of DNA to the drug, but rather may involve formaldehyde-mediated cross-linking (resulting from deformylation of **137**).<sup>144</sup> That formaldehyde cross-links 5'-AT *via* methylene bridging of the two N<sup>6</sup> exocyclic amines of deoxyadenosine has been demonstrated by Hopkins *et al.*<sup>145</sup>



The viability of interstrand cross-linking *via* formaldehyde was probed in two ways.<sup>144</sup> Firstly, it was demonstrated that in the presence of thiophenol, trimelamol gave rise exclusively to the trisubstituted thioether adduct. No deformylation adducts were obtained nor was any methylene-bridged *bis*-thiophenol product detected. Additionally, reactions of the 5'- <sup>32</sup>P end-labeled PBR322 with concentrations of formaldehyde analogous to those that would be present in trimelamol reactions wherein ISC formation was readily detected, were completely devoid of cross-linked material. Taken together, these findings strongly implicate trimelamol as the DNA binding agent. Preliminary evidence has suggested that the drug-DNA covalency is minor groove-dependent since piperidine reactions of cross-linked material failed to reveal any base-labile sites resulting from facile depurination or depyrimidation (facilitated by base alkylation). This is in contrast to many of the alkylating agents which selectively alkylate the deoxyguanosine N<sup>7</sup>

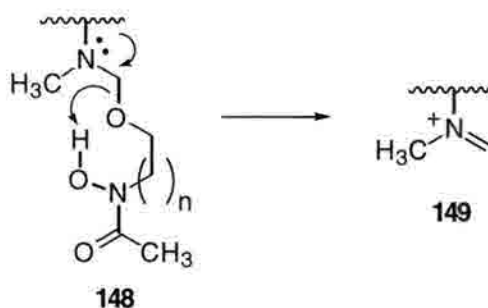
position (the DNA amine bearing the greatest negative character) thus giving rise to base-labile lesions in a fashion analogous to that used in Maxam-Gilbert DNA sequencing.<sup>146</sup> That the two alkylation events leading to ISC generation proceed in rapid succession and perhaps simultaneously has been suggested. Like mechlorethamine, the second alkylation (typically rate-limiting for many cross-linking agents) appears too fast to be measured thus suggesting that monoalkylation brings the highly activated imminium species of the "second arm" in close enough proximity to the second strand such that almost immediate reaction occurs, presumably with little or no structural perturbation of the target duplex.

The high degree of efficiency with which trimelamol inflicts ISCs upon duplex DNA has provided the impetus for improved delivery systems of this drug. While approaches such as anti-sense, triplex and peptide conjugations have received attention with other cross-linking agents, these strategies have not yet been applied to trimelamol or its oxidative predecessor HMM.



An alternative strategy has recently been reported by Miller and Ramurthy wherein synthesis of the trimelamol siderophore **146** was achieved.<sup>147</sup> Iron-sequestering siderophores are readily recognized and actively transported into cells which might not otherwise allow delivery of the molecule in the absence of the siderophore. Once inside the cell, iron is released for use by the organism and the siderophore is likely metabolised and discarded.<sup>148</sup> As such, the incorporation of a DNA damaging moiety into such a molecule allows active transport into the cell followed by nucleic acid modification. Such a strategy converts drugs which had previously relied on passive diffusion (and to which resistance

maybe developed) into much more interactive agents. Specifically, Miller *et al.* envisioned that once inside the cell, the trimelamol would release the siderophore tether and in so doing would generate the DNA reactive imminium species **149**. Initial studies with **146** have revealed that growth delay of *E. coli* X580 cells is induced by the siderophore conjugate. This is consistent with other siderophore conjugates (not ISC agents) studied by the Miller group and is suggestive of iron complex recognition by the outer membrane receptors followed by transport into the cell and subsequent DNA damage. To date, no further details have been reported on this pathway to ISC generation.

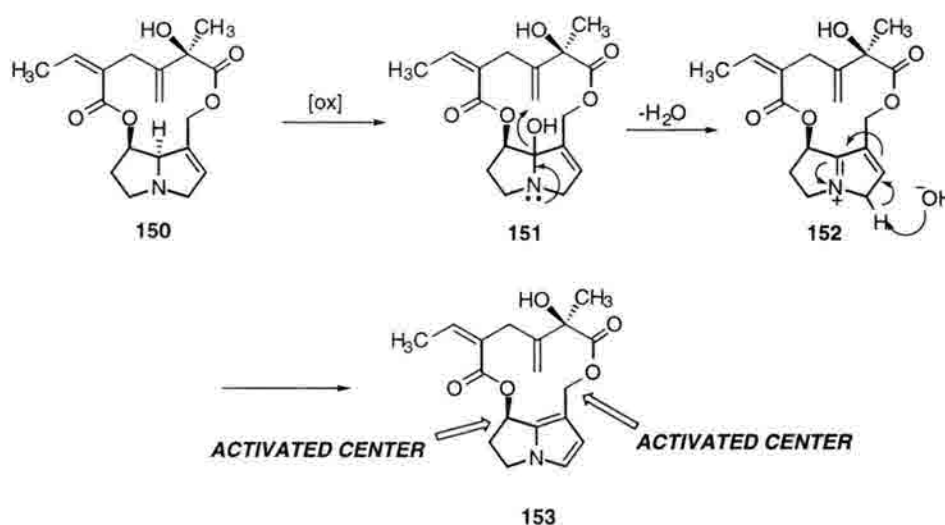


### 1.4.3. Pyrrolizidine Alkaloids

The pyrrolizidine alkaloids comprise one of the most abundant classes of biologically active natural products. As constituents of over 6000 species of plants with wide morphological and geographical diversity, these compounds (of which over 200 varieties have been reported) express poisonous activities of endemic proportions.<sup>149</sup> Particularly common to tropical regions such as the Caribbean and Africa, poisonings have not been completely averted in the U.S. An interestingly rich source of poisoning events in the U.S. has been through the use of herbal medicines. Despite their poisonous traits, these agents have provided a fruitful avenue by which to examine oxidative, selective DNA *bis*-alkylation. An additional means by which these compounds express biological activity is through the formation of DNA-protein cross-links.<sup>150</sup> Ironically, indicine N-oxide possesses potent antitumor activities against acute refractory leukemias and various solid tumors, despite the fact that it does not efficiently cross-link DNA.<sup>151</sup> That the degree of

hepatotoxicity displayed is minimal compared to other PAs is likely due to a preference for DNA-protein cross-link formation in lieu of ISC formation (after hepatic oxidation).

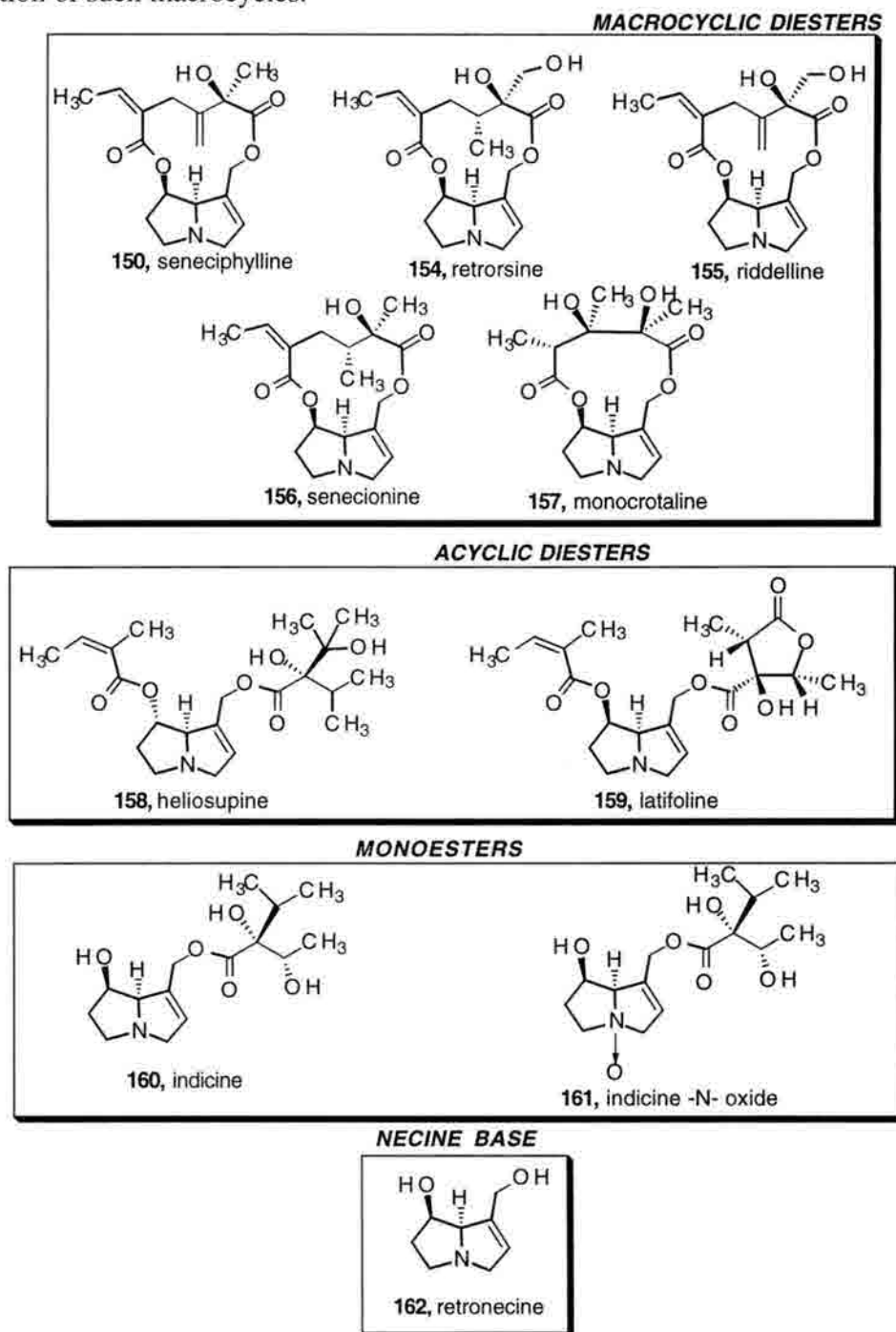
Cytochrome P-450 oxidation affords two major products: the reactive, highly toxic pyrrole and the less toxic N-oxide. Generation of the pyrrolic moiety is proposed to occur as outlined by the oxidative transformation of **150** to **153**. This results in electrophilic activation at the C-7 and C-9 ester substituents *via* conjugation with the pyrrole nitrogen lone pair. That such a species is extremely reactive was recently evidenced by Niwa *et al.*<sup>152</sup> Upon oxidation of monocrotaline **157** to dehydromonocrotaline **166** it was found that the pyrrole was completely hydrolyzed within 1 minute in aqueous media at room temperature.



**Figure 1-25.** Mechanism of oxidative PA activation.

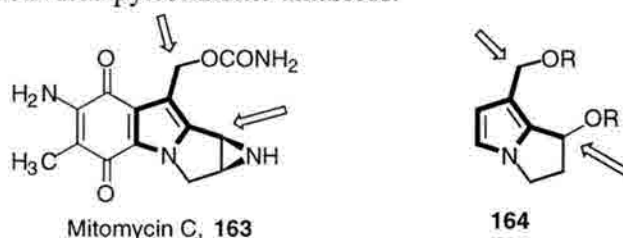
DNA cross-linking has been demonstrated with monocrotaline **157**, and its oxidation product dehydromonocrotaline **166**, as well as the pyrrolic metabolites of retronecine **162**, senecionine **156**, seneciophylline **150**, and ridelline **155** and the diacetates **167-169**. In general, those PAs bearing the  $\alpha,\beta$ -unsaturated 12-membered macrocyclic necic diester are more potent cross-linkers than PAs lacking analogous cyclic structure and/or the  $\alpha,\beta$ -unsaturation.<sup>151</sup> The origin of this preference is unknown, though it is possible that DNA modifications other than those involving C7 and C9 are

possible. Particularly intriguing is the possibility for 1,4-addition to the  $\alpha,\beta$ -unsaturated ester portion of such macrocycles.



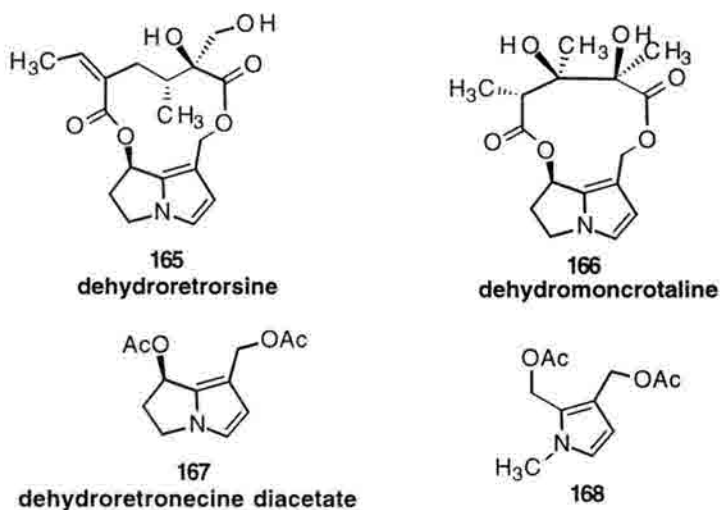
**Figure 1-26.** Some of the representative biologically active pyrrolizidine alkaloids.<sup>151</sup>

The structural similarities between the mitomycins and pyrrolizidine alkaloids and their repercussions on DNA base specificity was first suggested by Iyer and Szybalski some 30 years ago.<sup>153</sup> This was in line with the proposed specificity for reductively activated mitomycin C for which the alkylating "business end" of the molecule closely resembles that of the activated dehydro-PAs. Placement of the carbamate at the indoloquinone C10 and the presence of the aziridine at C1 parallels the leaving group placements in the activated pyrrolizidine alkaloids.



**Figure 1-27.** Structural analogy highlight between the mitomycins and PAs.

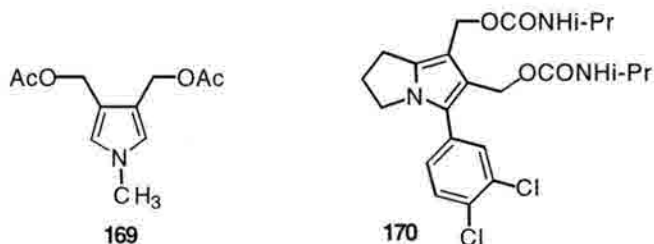
Only recently, however, has data been generated to support the hypothesis that activated pyrrolizidine alkaloids target the same sequences of DNA as those targeted by mitomycin C.<sup>154</sup> Utilizing dehydroretrorsine **165**, dehydromonocrotaline **166**, dehydroretronecine diacetate **167**, and 2,3-bis-(acetoxymethyl)-1-methyl pyrrole **168**, Hopkins *et al.* have demonstrated that ISC formation by these representative PAs proceeds with a high degree of selectivity for 5'-CG-3'.<sup>154</sup>





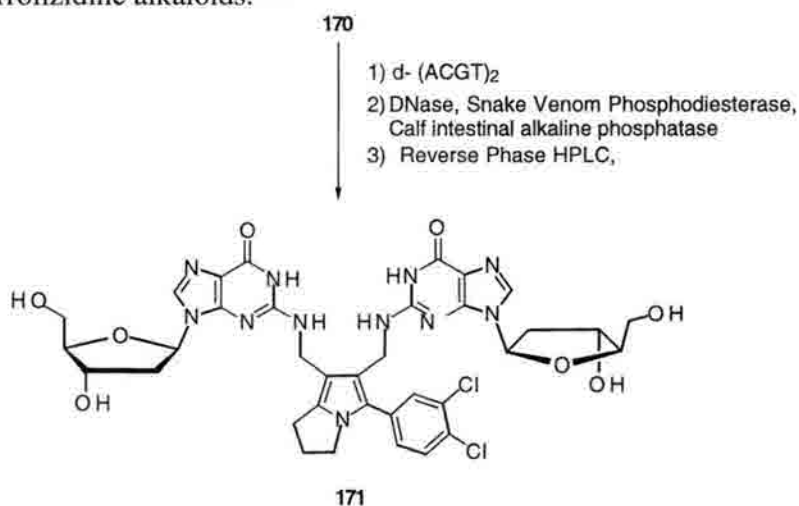
For **167** and **168**, Fe (II)-EDTA footprinting revealed the interstrand cross-links to involve drug connectivities involving the adjacent deoxyguanosines of 5'-CG-3'. Additionally, **167** was found to be capable of ISC formation at the sequence 5'-GC-3' and the **168**-mediated cross-linking event showed very little, if any, dependence upon the flanking bases of the 5'-CG-3'. For instance, in the case of methyl-pyrrole **168**, cross-linking of 5'-TCGA-3' and 5'-GCGC-3' proceeded with similar efficiencies. This is in stark contrast to the sequence preferences observed for mitomycin C wherein only 5'-CG-3' serves as the template for ISC formation, with a strong dependence upon the base sequence on either side of the 5'-CG-3' motif. That **167** and **168** both showed preference for 5'-CG-3' suggests similar connectivities for these lesions and those induced by the mitomycins. However, the added sequence promiscuity of the simpler agents suggests that they lack some of the molecular recognition constituents inherent to the mitomycins. Thus, while preferred connectivities may be conserved based on reactivity arguments, the molecular recognition elements pertinent to the enhanced specificity of the mitomycins over the PA analogs in this study represent candidates for a contribution to, but not solely responsible for, the mitomycin lesions formed with 5'-CG-3'.

More recently Hopkins and Woo have addressed the issue of regiochemistry involved in cross-linking of 5'-CG-3' within small synthetic ODNs.<sup>155</sup> In addition to the methyl pyrrole **168**, the regioisomeric pyrrole **169** was examined as was the di-urethanyl compound **170**.

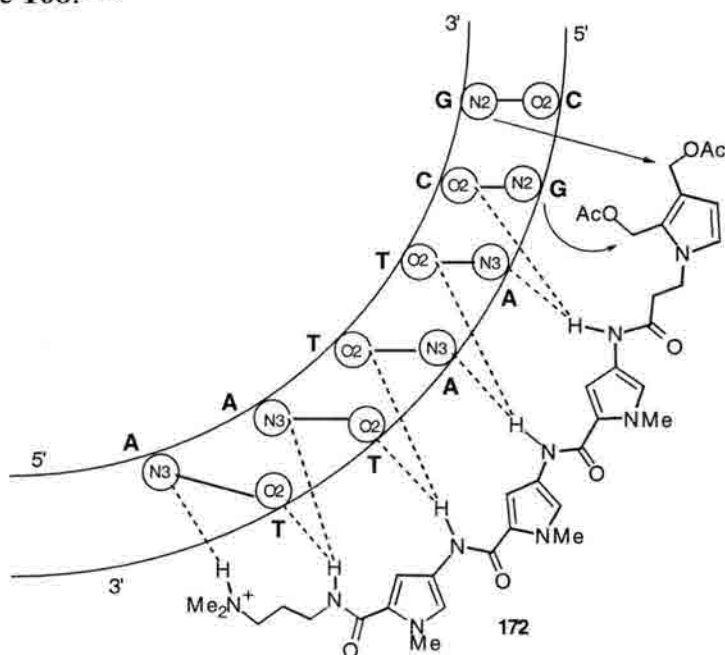


Utilizing a series of inosine substituted ODNs and large scale preparation of **170** cross-linked 5'-(ACGT)<sub>2</sub> the importance of the exocyclic N<sup>2</sup> amines of the dGs contained within 5'-CG-3' was revealed. Simply stated, incorporation of inosine at one or both dG

residues within the self-complementary ODN 5'-TATAATACGTATTATA-3' completely abrogated ISC formation upon treatment with **168**, **169**, and **170**. In combination with the earlier Fe(II)-EDTA fragmentation results, this demonstrated the necessity of dG N2-drug interactions *enroute* to DNA *bis*-alkylation. Alternatively, reaction of **170** with 5'-(ACGT)<sub>2</sub> followed by enzymatic degradation down to the nucleoside-drug adduct followed by HPLC mass spectrometry and UV analysis revealed the **169**-mediated cross-link to result from the lesion **171**. Although not a natural product, **170** had been shown to possess excellent antitumor activities, likely resulting from structural and mechanistic analogies to the pyrrolizidine alkaloids.<sup>156</sup>



Spectrophotometric analyses (UV and MS) of the resulting lesion was consistent with the structure assignment **171** as verified by comparison to a synthetically derived sample of **171**. Both the enzymatically obtained material and the synthetic sample displayed identical retention times by reverse phase HPLC and migrated as one distinct entity following co-injection. Importantly, this represented the first isolation/elucidation of the *bis*-nucleoside adducts responsible for DNA interstrand cross-linking by any members (or analogs thereof) of the pyrrolizidine alkaloid class. Further, it substantiates the assertion that the pyrrolizidine alkaloids interstrand cross-link DNA in a fashion similar to the mitomycins.



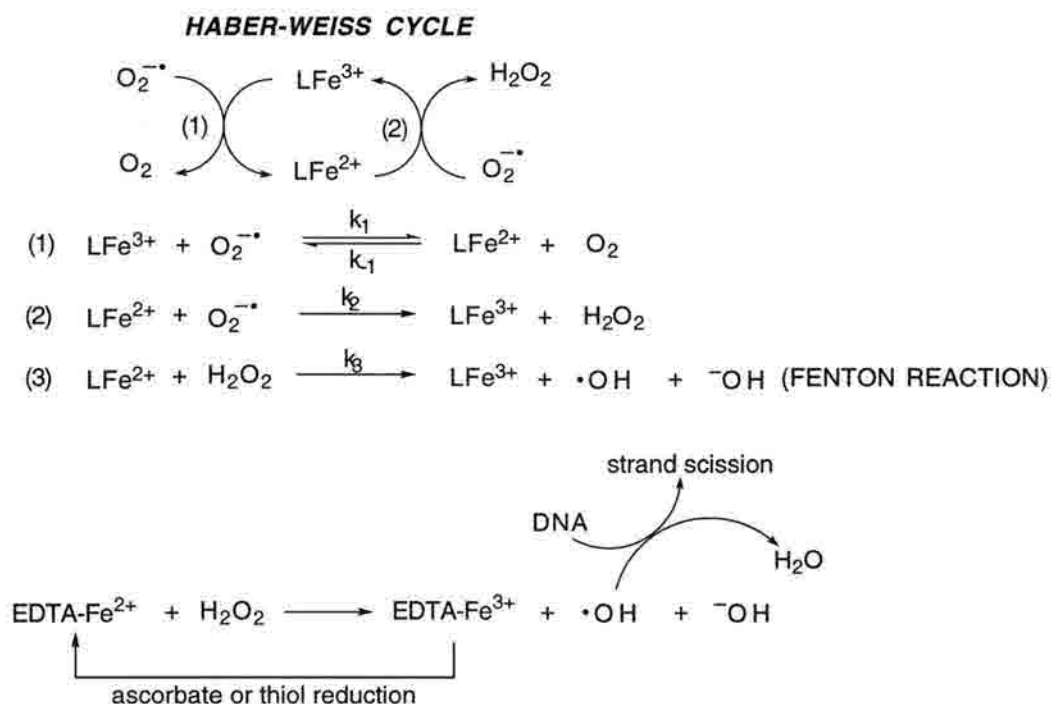
Initial studies were performed using Eco RI linearized plasmid pBluescript II KS which bears some 27 runs of four sequential A or T residues proximal to 5'-CG-3' boxes. Utilizing this substrate, efficient ISC formation was obtained at concentrations as low as 10 nM ( conjugate:bp ratio of 0.03). Subsequent efforts with several ODNs revealed that the sequence 5'-(GATCGAATTCGATC)<sub>2</sub> gave optimal cross-linking with an astounding 67% yield of the ISC. Inosine substitution at either dG residue flanking the 5'-AATT-3' abrogated ISC formation thus suggesting retention of the known alkylation pathway

exerted by the methyl pyrrole. That DNA connectivity to the cross-linking moiety was conserved in the conjugate was verified upon scale up and subsequent enzymatic digestion. All spectral data generated for the conjugate mediated lesion was consistent with the regiochemical assignments previously made with the untethered **168**.

Although the conjugation methodology presented provides a highly efficient and selective means of ISC induction, such strategies have not yet been applied to oxidatively activated conjugates. This likely represents the next frontier in the selective delivery and bioactivation of various drugs. Indeed initial efforts with mitomycin C conjugated oligonucleotides have shown this to be a viable means of delivery for redox-activated drugs.<sup>158</sup>

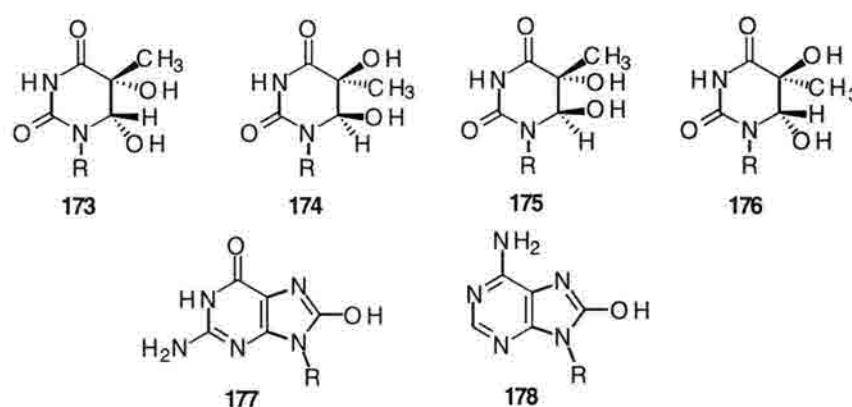
### 1.5. HYPOXIA-SELECTIVE AGENTS (REDUCTIVELY ACTIVATED)

The proposed mode of action for radiation-based therapies (still the most successful non-invasive means of treatment for most cancers) relies on the abundance of oxygen within the tissue of interest.<sup>159</sup> Exposure of oxygenated tissues to ionizing radiation affords superoxide which in turn produces the highly reactive hydroxyl radical species *via* iron-mediated dismutation of hydrogen peroxide and subsequent Fenton chemistry.<sup>160</sup> Alternatively, direct generation of hydroxyl radical mediates cellular damage and provides another entry to Fenton/Haber-Weiss redox cycling.<sup>160</sup> Diffusion of the highly reactive hydroxyl radical inflicts damage upon phospholipids, proteins, and most notably, the nucleic acids. Reaction with DNA affords a wide array of base-oxidized nucleotides (Figure 1-29)<sup>161</sup> and leads also to indiscriminate strand scission of the phosphodiester backbone.<sup>162</sup>



**Figure 1-28.** Fenton/Haber-Weiss redox cycling outline.

Superoxide dismutation is facilitated by a wide array of iron complexes and represents the only kinetically significant step in the net conversion of dioxygen to hydroxyl radical. The most heavily studied Fe(II)-EDTA system possesses a rate-limiting  $k_1$  of  $76 \text{ M}^{-1}\text{sec}^{-1}$  at neutral pH affording a steady state of Fe(II)-EDTA since  $k_2 > k_{-1} > k_3 \gg k_1$ .<sup>163</sup> Radiation therapy, though a highly effective means of treating diseases inherent to oxygenated tissues, often suffers from decreased efficiency upon the development of solid tumors.



**Figure 1-29.** Common base oxidized nucleotides resulting from reaction with hydroxyl radical. R = deoxyribsyl connection to DNA polymer.

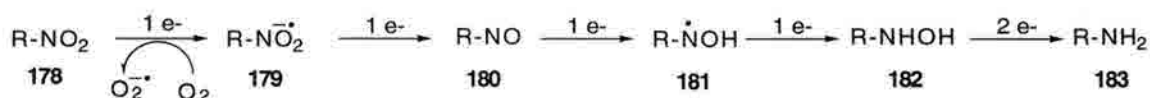
It is well established that hypoxic cells (those lacking oxygen) exist in solid tumors and that these cells are resistant to the cytotoxic effects of ionizing radiation. The gene expression and subsequent secretion of angiogenesis factors *enroute* to the development of a solid tumor's own blood supply is necessary for tumor growth.<sup>164</sup> The inefficiency of this process mandates that many of the tumor cells are greater than  $150\mu\text{m}$  from the nearest blood vessel and are therefore oxygen deficient. This "diffusion-limited" hypoxia results from the rapid metabolism of oxygen by cells proximal to the blood vessel thus depleting the supply for the more distal tumor cells.<sup>165</sup> Alternatively, the closing off of blood vessels (either host vessels for tumor generated vessels) by simple constriction due to tumor growth leads to "perfusion hypoxia".<sup>165</sup> Importantly, the generation of hypoxia is not limited to neoplastic cells. Anaerobic bacteria and other parasitic organisms have been

proposed targets for hypoxia selective agents (HSAs) which like neoplasms, maintain the presence of reductive enzymes such as cytochrome P450 reductase, DT diaphorase and others while possessing much lower than normal levels of oxygen.<sup>166</sup>

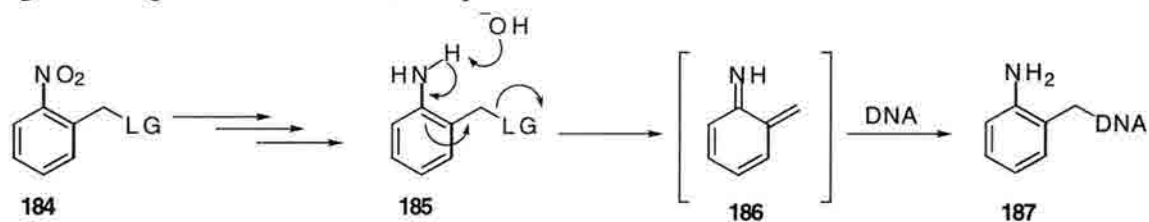
Most HSAs rather than undergoing selective reduction, undergo reduction events in all cells which are reversible in the presence of molecular oxygen (*via* superoxide generation). Hence, in the absence of O<sub>2</sub>, the activated reduction product is long-lived enough to inflict macromolecular damage resulting in cytotoxicity. It has been demonstrated that agents possessing reduction potentials in the range -300mV to -450mV are accessible to enzymatic reduction *in vivo*.<sup>167</sup> These can be categorized into three classes; (1) nitro- and aza- aromatics, (2), quinone-containing agents, and (3) transition metal complexes. Application of these reducible functionalities has been applied to the design (both man-made and naturally occurring) of the following "prodrugs".

#### 1.5.1. Masked Nitrogen Mustards

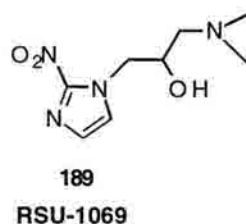
Owing to their structural simplicity and high degree of reactivity with nucleic acids, the nitrogen mustards have received considerable attention with respect to prodrug design. As with cyclophosphamide (essentially an oxidatively activated N-mustard derivative), the tethering of mustard moieties to redox active organic functionalities has allowed the generation of highly specific DNA cross-linking agents. Particularly successful has been the employment of nitro- and aza-aromatic chemistry. Several reports of nitroaromatic alkylating prodrugs have appeared, all of which undergo reduction *via* the conversion of **178** to **183**.<sup>168</sup>



Nitrobenzyl compounds bearing leaving groups at the benzylic position have shown hypoxic selectivities in cell culture and are proposed to behave as nucleic acid alkylating agents *via* generation of the iminoquinone methide **186**.<sup>169</sup>



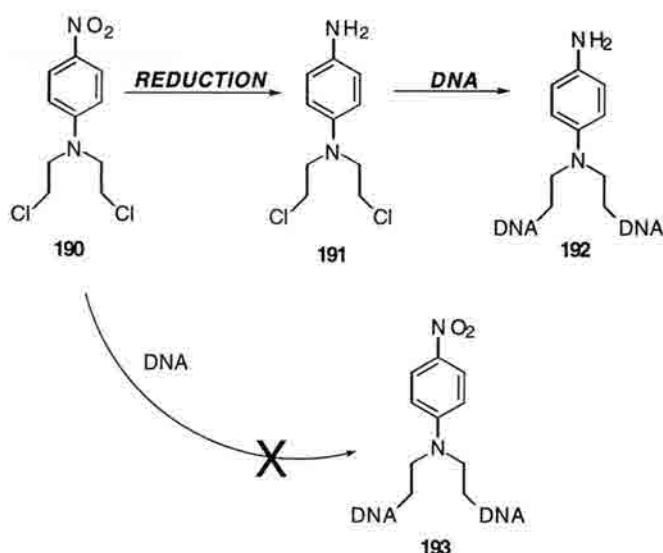
Additionally, the conversion of the electron-withdrawing nitro group to the donating amine or intermediate hydroxylamine has been used as a means of reductively activating substituted nitroimidazoles towards DNA *mono*- and *bis*-alkylation.<sup>170</sup> Misonidazole **188** is a known DNA monoalkylating agent whose cytotoxicity is reductively driven. Unlike other nitroaromatics, the critical intermediate is not the free amine but rather



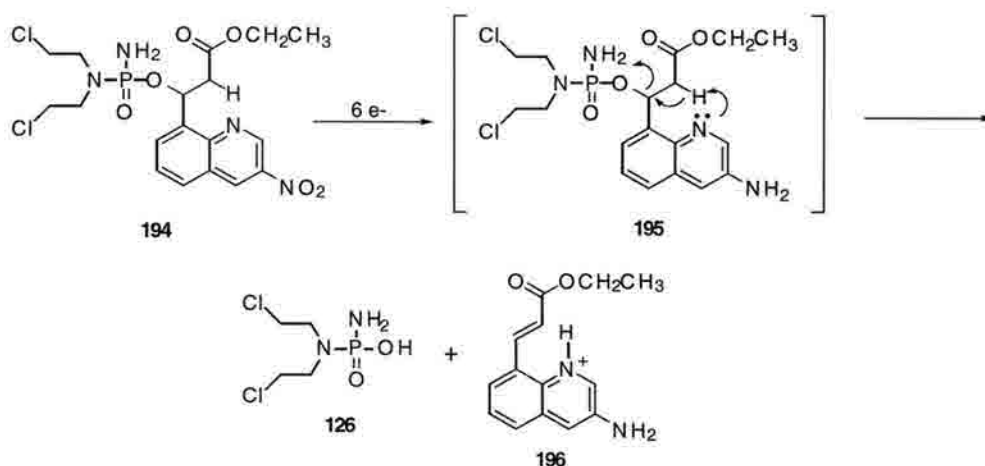
the partially reduced hydroxylamine.<sup>171</sup> The identity of the lesion is not known but likely involves alkylation of the hydroxylated side chain *via* assistance from the hydroxylamine moiety. Within the realm of ISC generation, RSU 1069 (**189**) undergoes initial ring-opening of the aziridine to afford monoadducts under aerobic conditions.<sup>170</sup> Once anchored to the DNA, reduction of the nitro functionality gives rise to a second electrophilic site which undergoes nucleophilic attack by the complementary strand to yield interstrand cross-linked material.<sup>170</sup>

With respect to the "protection" of nitrogen mustards, many derivatives of the nitroaniline chloromustards have been examined.<sup>172</sup> Conjugation of the nitrogen mustard lone pair with the *p*-nitro group abrogates aziridinium formation required for efficient ISC formation.



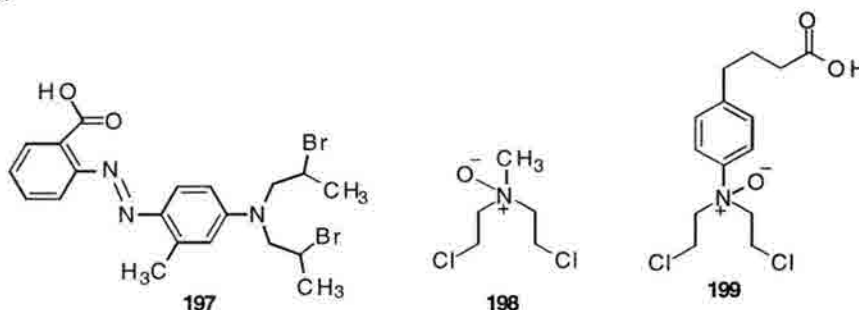


However, conversion of the nitro group to either the hydroxylamine or the fully reduced amine deconjugates this lone pair thus facilitating the formation of the requisite aziridinium. Similarly, the nitroquinoline **194** is an extremely stable compound. Six-electron reduction of the nitro group considerably alters the electron density of the quinoline ring system.<sup>173</sup> A reflection of this electronic change is the considerably enhanced basicity of the cyclic nitrogen. Intramolecular base-catalyzed rearrangement subsequent to nitro group reduction facilitates elimination of phosphoramidate mustard which, as discussed previously, is the DNA-reactive intermediate involved in cyclophosphamide cytotoxicity.

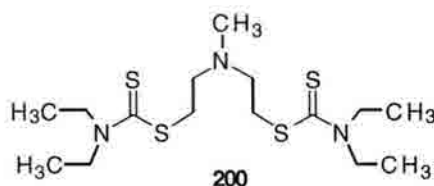


**Figure 1-30.** Reductive activation of **194**.

In addition to nitroaromatic conjugation methodologies, the N-mustards have been tethered to aza-aromatics in order to achieve similar results. One such example reported by Wilman *et al.* is depicted by **197**.<sup>174</sup> Conceptually, reduction of the azo functionality was envisioned to yield the free aniline mustard which, by analogy to the nitro systems, would effect selective DNA bis-alkylation. This was in fact the case for the Wilman study in which **197** and structurally related analogs demonstrated selective liver cytotoxicity.<sup>174</sup> The design of hypoxia selective N-mustards has not not been relegated only to nitro or aza-aromatics.



The conversion of nitrogen mustards to the corresponding N-oxides has been pursued. N-oxidation considerably lowers the  $pK_a$  of an amine (roughly 5 units) and effectively deletes nucleophilic characteristics. In line with this concept, compounds such as **198** and **199** have been designed as reductively activated prodrugs of mechlorethamine and chlorambucil respectively. Connors *et al.* have shown that nitromin **198** undergoes enzymatic reduction (under anaerobic conditions) with resultant increases in unscheduled DNA synthesis of JB1, BL8 and Walker 256 carcinoma cell lines.<sup>175</sup>



Additionally, anaerobic enzymatic reduction by rat liver microsomal extracts followed by trapping of the *bis*-electrophilic mustard with diethyldithiocarbamate (DDC) afforded the adduct **200**. Under aerobic conditions, little, if any, nitromin was DDC

derivatized while the DDC-mechlorethamine adduct was obtained in > 90% yield. The reducing microsomal system examined can use either NADH or NADPH to effect reduction. Analogously, purified cytochrome P450 reductase was able to reduce nitroimin in the absence of any other microsomal proteins.

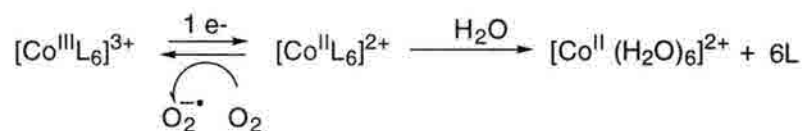
Taken together, these findings strongly suggest that N-oxide functionalization of mechlorethamine provided an effective means of masking the reactivity of the parent compound while allowing a reductive "unmasking" route to selective activation. Conversely, Shervington and Mann have shown that this strategy fails with the chlorambucil analog **199** which shows no hypoxia selectivity *enroute* to DNA modification.<sup>176</sup>

### **1.5.2. Transition Metal Complexes**

Activation of HSAs ensues upon one-electron reduction, but may also follow in the case of two-electron reduction. Examples of two-electron reductases include NAD(P)H:quinone oxidoreductases (DT diaphorase) and xanthine dehydrogenase both of which reduce quinones and nitroheterocycles under aerobic conditions.<sup>177</sup> Such a case is deleterious to the reductive selectivity of such agents since the whole concept of selectivity is based on the facile reoxidation of the one-electron-reduced species with concomitant generation of superoxide. The two-electron reduction scenario bypasses this oxygen-reversible stage thus abrogating selectivity.

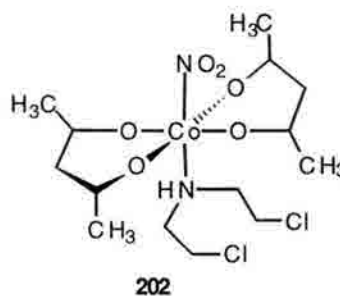
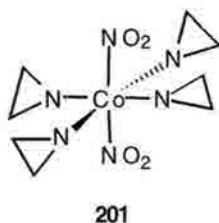
One means of avoiding inadvertant drug toxicities resulting from irreversible two electron reduction processes has involved the construction of transition metal complexes which are capable of only one-electron reduction events. Denny *et al.* have shown that Co(III) complexes are particularly attractive in this manifold.<sup>178</sup> The d<sup>6</sup> low-spin electronic configuration of octahedral Co(III) complexes renders them kinetically inert. For instance CoIII(NH<sub>3</sub>)<sub>6</sub> possesses a half-life of  $6 \times 10^9$  s with respect to aquation.<sup>179</sup> However, one

electron reduction (reduction potentials typically in the range of -200 to -400 mV) results in a highly labile Co(II) complex capable of rapid ligand exchange.<sup>180</sup>

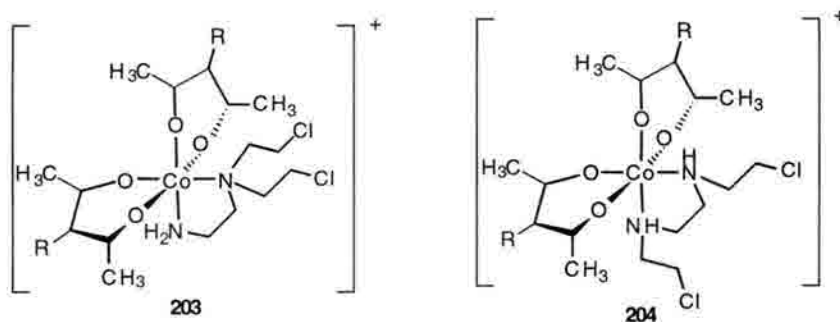


**Figure 1-31.** Reduction promoted ligand release from Co(III) complexes.

However, this process is essentially irreversible since the resulting  $[\text{Co}(\text{H}_2\text{O})_6]^{2+}$  is extremely stable with respect to back oxidation ( $E^0 = +1800\text{ mV}$ ).<sup>178b</sup> The ability to control the substitutionally labile  $\text{Co(II)L}_6$  relies heavily upon the nature of the ligands used, with monodentate ligands demonstrating extremely facile exchange thus giving rise to the oxidatively inert hexaqua species. Indeed, initial studies by the Denny group<sup>178c</sup> revealed that the complexes **201** and **202**, while capable of reductive activation towards DNA alkylation, showed no selectivity for hypoxic cells due to the insufficient stability of the  $\text{Co(II)L}_6$  complex.



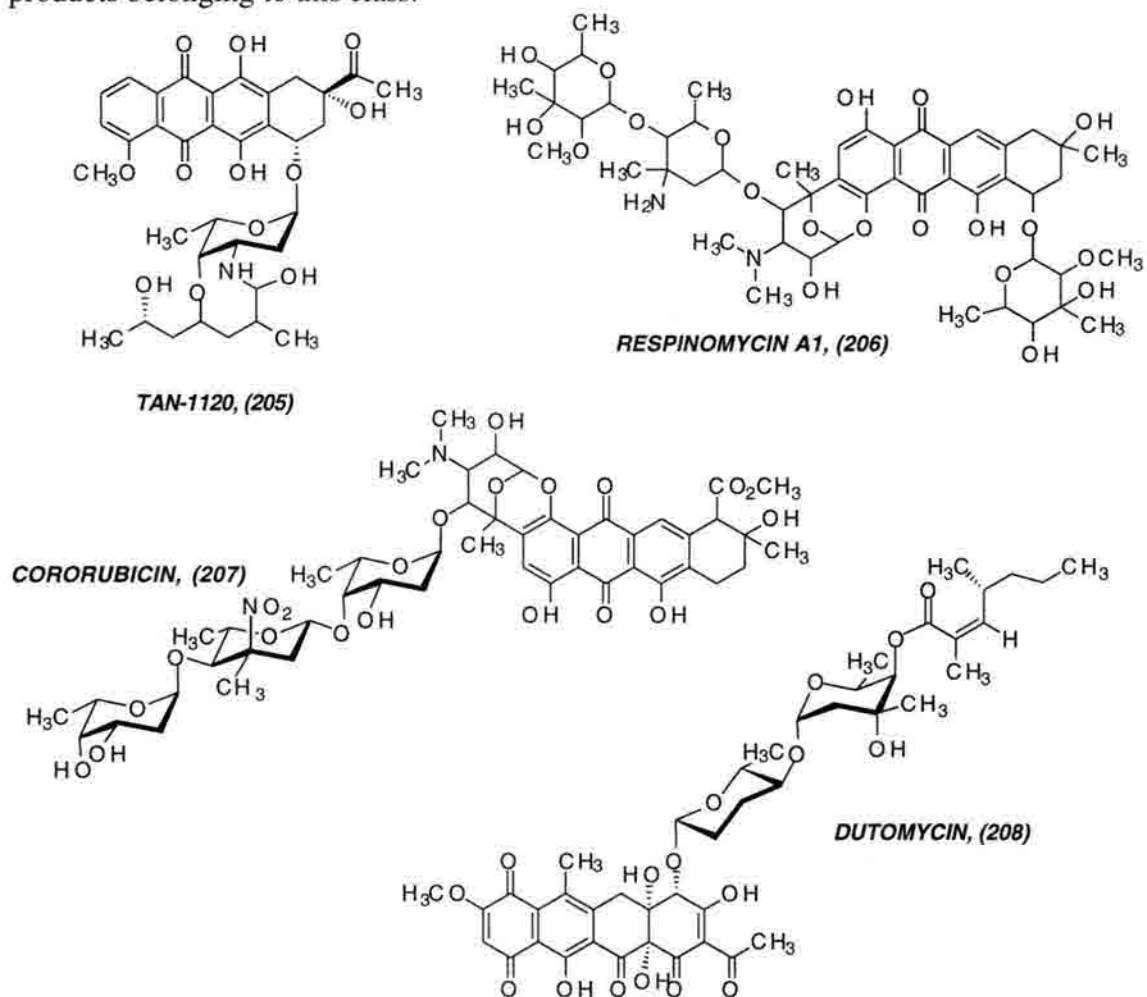
More recent accounts reveal that the use of polydentate ligands stabilizes the reduced Co(II) species thus allowing the oxygen-reversibility needed to achieve hypoxic selection.<sup>178b</sup> The design of metal complexes **203** and **204** follows from the concept of N-oxidation of reactive mustards in that coordination of the nitrogen lone pair to Co(III) shuts down aziridinium formation.<sup>178b</sup> Variations of the R groups from H, to methyl, ethyl or propyl was observed to considerably alter the reduction potentials of the respective analogs which in turn influenced the cytotoxicity properties observed.



Surprisingly, only the parent compound **203** ( $R=H$ ) possessed a reduction potential ( $E^0 = -310$  mV) within the physiological range previously stated, with the methyl, ethyl, and propyl analogs possessing reduction potentials of  $-42$ ,  $-460$ , and  $-500$  mV respectively. The methyl, ethyl, and propyl congeners of **204** possessed reduction potentials of  $-305$ ,  $-350$ , and  $-385$  mV respectively while the unsubstituted case was well outside the potential window with a potential of  $-235$  mV. The hypoxic selectivities of these compounds was determined in UV4 cell cultures. Though **203** possessed minimal potency in this assay, the methyl-substituted analog was very selective towards hypoxic cells despite possessing a reduction potential outside the physiological window. All compounds of the general structure **203** were considerably more potent than the **204**-based compounds likely owing to the ability of the *N,N*-bis(2-chloroethyl)ethylenediamine (DCE) ligand to induce monoadducts and ISCs *via* the mechlorethamine pathway.<sup>181</sup> That this is in fact the case has not been shown and the authors postulate that the enhanced cytotoxicities observed are due to more facile DCE release upon Co(III) reduction versus that observed with the *N,N'*-bis(2-chloroethyl)-ethylenediamine (BCE) complexes. In either event, the utility of Co(III)L<sub>6</sub> complexes as a means of selectively targeting hypoxic cells has been demonstrated and represents a novel approach towards reductive drug activation.

### 1.5.3. Anthracyclines

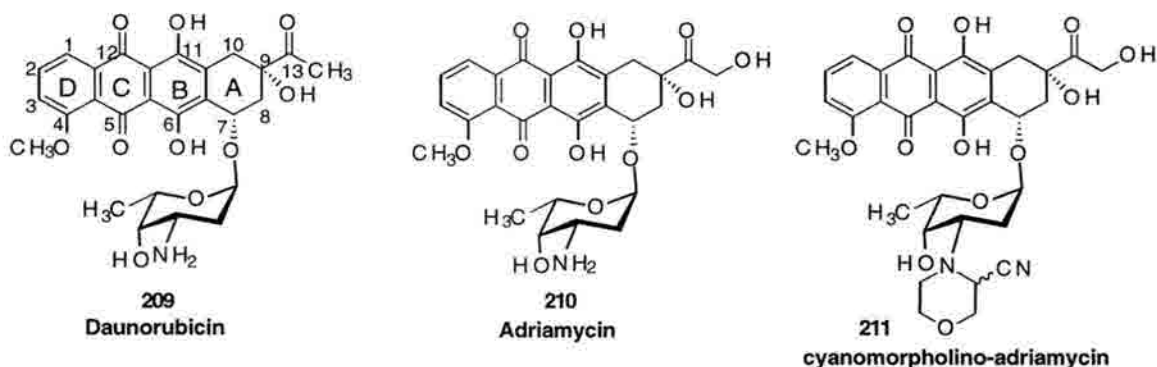
Possessing the tetracyclic quinophenolic ring system with the tethered aglycone, the anthracyclines represent a structurally diverse and clinically important class of antitumor antibiotics.<sup>182</sup> The investigation of synthetic derivatives of adriamycin (**210**) alone has resulted in the synthesis of more than 2000 compounds over the last 25 years.<sup>183</sup> Additionally, isolation from fermentation broths continues to reveal the multitude of natural products belonging to this class.



Recently isolated additions to the anthracycline group of compounds include TAN-1120 (**205**) (from *Streptomyces triangulatus*)<sup>183a</sup>, respinomycin A1 (**206**)<sup>183d</sup> (from *Streptomyces* sp. RK-483), cororubicin (**207**) (from *Micromonosporasp. JY16*)<sup>183c</sup>, and dutomycin (**208**) (from *Streptomyces* sp. 1725)<sup>183b</sup>. All of these compounds demonstrate potent cytotoxicities against several tumor cell line, but most striking is the ability of

cororubicin to generate superoxide in N18-RE-105 hybridoma cells (rat retina x mouse neuroblastoma cells) as detected by *in vitro* nitro blue tetrazolium (NBT) reduction.<sup>183c</sup> It is clear that the members of the anthracycline class of natural products exhibit vastly different chemistries and that these likely potentiate the biological significance of the individual anthracyclines. Common to all the anthracyclines, however is the ability to intercalate between the base pairs of DNA.

That the anthracyclines are avid DNA intercalating agents was first described crystallographically by Wang *et al.* in 1987.<sup>185</sup> The structure of a 2:1 complex between daunorubicin **209** and 5'-d(CGTACG)<sub>2</sub> was reported at near atomic (1.2Å) resolution and showed drug intercalation of the extended chromophore between the 5'-CG-3' steps at both ends of a distorted B-DNA duplex. The chromophore penetrates the double helix with the



D ring protruding into the major groove and the amino sugar lying in the minor groove. Later studies revealed the relevance of this binding motif to several anthracyclines and also demonstrated the importance of certain drug-DNA interactions inherent to this mode of binding.<sup>186</sup>

Particularly intriguing was the finding that anthracyclines devoid of the O9 hydroxyl were not biologically active.<sup>186</sup> This was proposed to be a reflection of lower binding affinity due to the absence of the critical hydrogen bonding network involving the O9 hydroxyl hydrogen and the N<sup>3</sup> and N<sup>2</sup> nitrogens of the deoxyguanosine adjacent to the aglycone. The importance of an intercalative binding mechanism has been shown by

numerous workers and has been suggested as the predominant means of DNA association. Additionally, the intercalative mode of binding is very often accompanied by attractive DNA contacts involving the tethered aglycones in a fashion reminiscent of enediynes such as calicheamicin and other amino-sugar antibiotics such as chromomycin.<sup>187</sup>

Evidence suggests that the anthracyclines operate *via* several different modes of action. Impairment of topoisomerase II activity, membrane-related effects and redox-mediated DNA damage have all been implicated as manifestations of anthracycline biological activity.<sup>188</sup> Of these, topoisomerase impairment has received the most attention. Inhibition of enzyme activity follows from self-inflicted endonucleolytic DNA double-strand breaks. Binding to a given duplex, topoisomerase II induces strand scission of each strand by forming a transient covalent bond with the 5' phosphoryl end of the broken strand and a tyrosine of each subunit of the 170kDa homodimeric protein.<sup>189</sup> Formation of this "cleavage complex" allows another intact duplex to pass through the opening created in the topoisomerase II-bound strand.<sup>189</sup> Subsequent ligation of the broken strands ensues leading to enzyme release. Stabilization of the cleavage complex by the anthracyclines prohibits ligation and thus affords the arrested drug-DNA complex as a dead-end in the supercoiling process.<sup>188</sup> That this occurs at clinically relevant concentrations has been demonstrated for adriamycin and is proposed to be pertinent to the mechanism of action of numerous other anthracyclines.

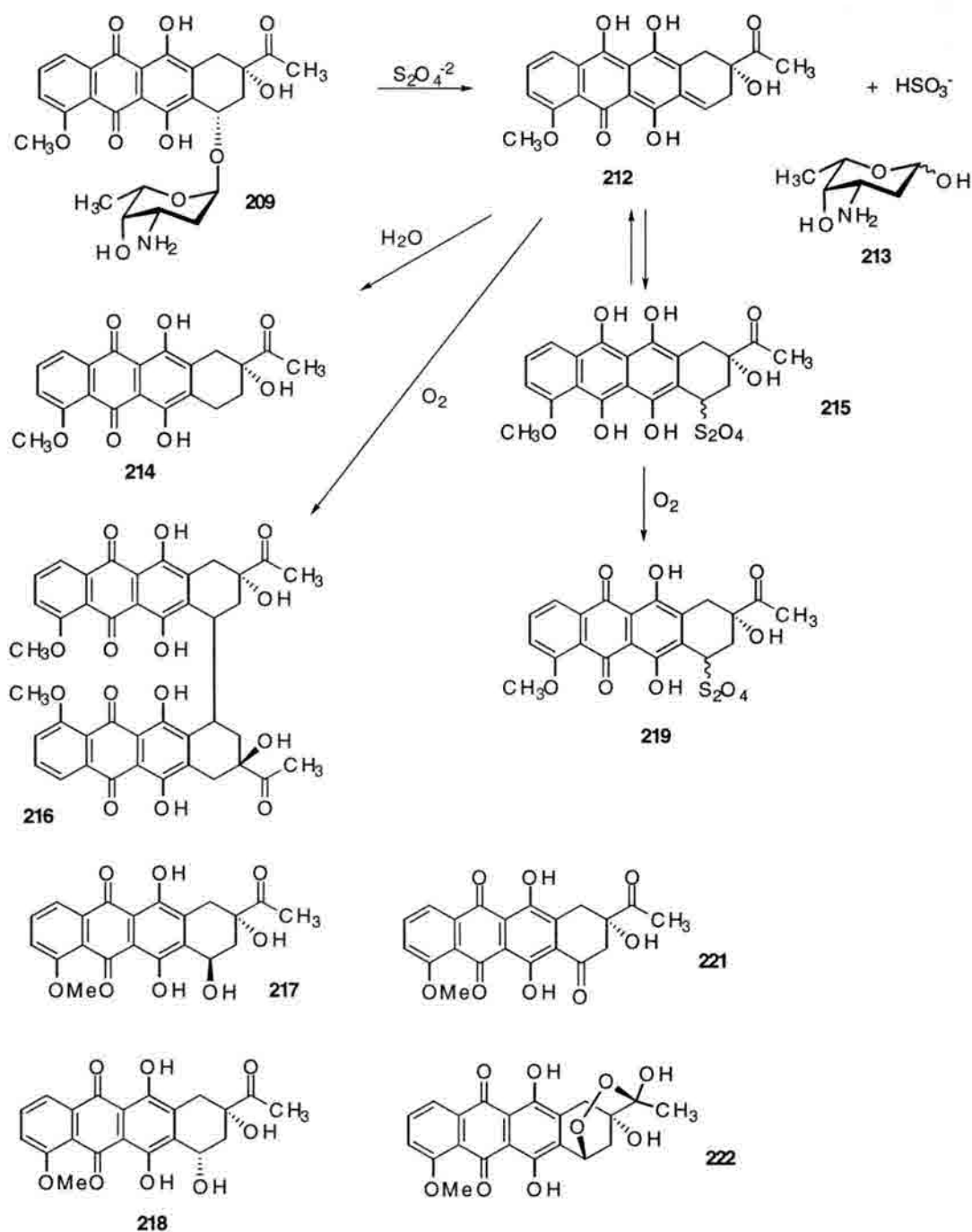
Membrane effects associated with the anthracyclines result from drug affinities for the negatively charged phospholipids and resultant alteration of membrane functions. These interactions (not involving radical damage or intercalative processes) at subcytotoxic levels serve to promote cell growth in both human and murine tumor cell lines. However, higher drug concentrations inhibit growth.<sup>190</sup> This has been attributed to excessive growth rates resulting from overstimulation of the membrane-mediated signaling mechanism responsible for growth; in effect, out-stripping of the cellular resources results leading to ultimate growth inhibition and eventual cell death. Surprisingly, despite some 20 years of



clinical use and research, little is known about the specifics of this mechanism of cytotoxicity for the anthracyclines.

Anthracycline mediated oxidative DNA damage has been implied due not only to the detection of non-protein-associated strand scission products, but also to the tendency of the anthracyclines (specifically adriamycin) to induce severe cardiomyopathy.<sup>188</sup> Heart tissue is known to activate adriamycin at several sites including the cytosol, mitochondria and sarcoplasmic reticulum.<sup>191</sup> Additionally, these tissues possess very low levels of the peroxide detoxification enzyme catalase. These facts coupled with the known inactivation of glutathione peroxidase (another peroxide-counteracting enzyme) by adriamycin, demonstrate the origin of anthracycline induced cardiomyopathy. Not only does the drug stimulate superoxide generation, but it also shuts down (or avoids) the repair mechanisms by which oxidative damage is typically averted.<sup>191</sup>

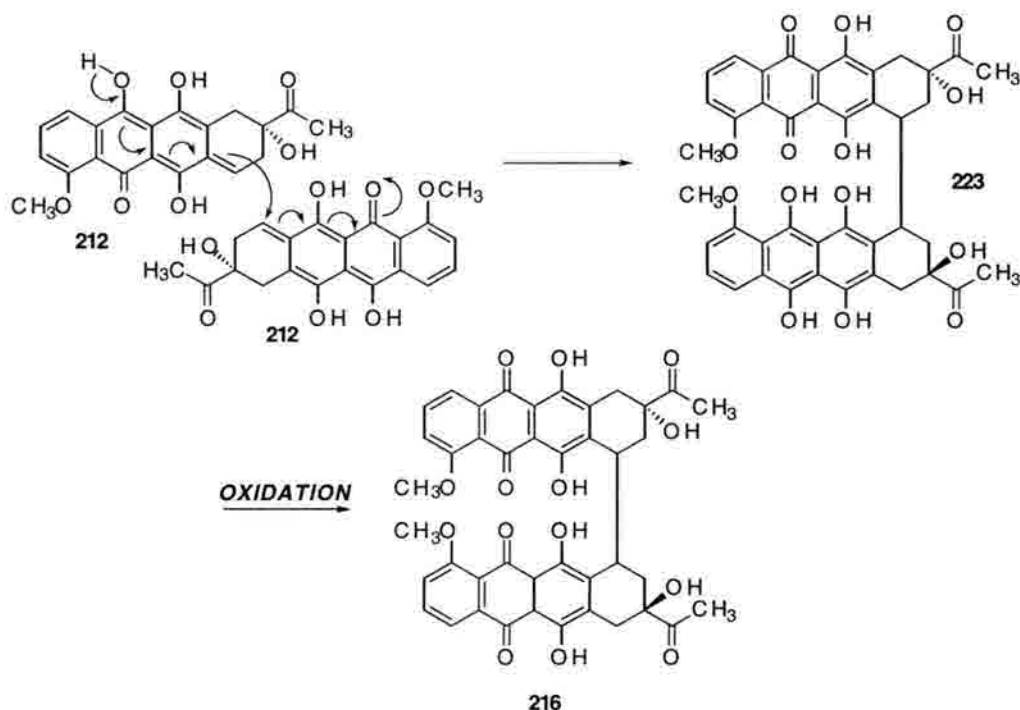
Perhaps the most interesting chemistry demonstrated by the anthracyclines lies in their ability to undergo redox conversion to quinone methides. The inefficiency of aerobic reduction stems from the rate limiting quinone reduction ( $E^0 = -300\text{mV}$ ) and the almost immediate conversion of this species back to the quinone with concomitant superoxide formation (rate constant  $k = 10^8\text{mol/L}^{-1}\text{s}^{-1}$ ).<sup>188</sup> However, as stated previously, the absence of oxygen facilitates retention of the activated species. Elegant studies by Koch *et al.* have shown that anaerobic reduction of daunomycin (**209**) with sodium dithionite affords a wide array of adducts as shown in Figure 1-32.<sup>192</sup> This anaerobic chemistry is highly substituent-dependent especially with respect to the 11 position. Indeed, the quinone methide stemming from reduction of 7,11-dideoxydaunomycin is considerably less reactive with protic solvents than is the analogous compound bearing the C-11 hydroxyl and is thus much longer lived than the hydroxylated congener. That these compounds dimerize upon reduction has been demonstrated and is very often the predominant *in vitro* reaction pathway.<sup>193</sup>



**Figure 1-32.** Product distribution of duanomycin reduction by sodium dithionite.

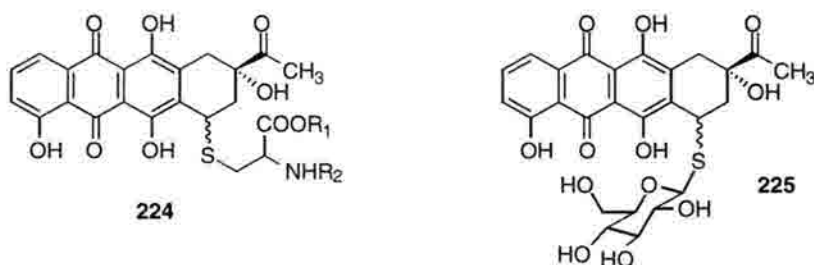
Dimerization is proposed to result from one of two mechanisms. The possibility of radical generation at C7 followed by recombination has been suggested as has the condensation of two activated quinone methides wherein one nucleophilically adds to another (Figure 1-33). The ability of these dimeric compounds to induce biological

activity has not been disproved. However, that the quinone methide generated upon aglycone release is an efficient electrophilic trap (with selective addition to the C7 position) for biologically relevant nucleophiles has been shown by several groups.

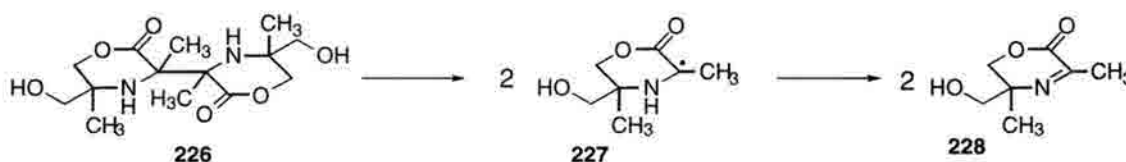


**Figure 1-33.** Mechanism of quinone methide dimerization *enroute* to duanomycin dimer **216** (Figure 1-32).

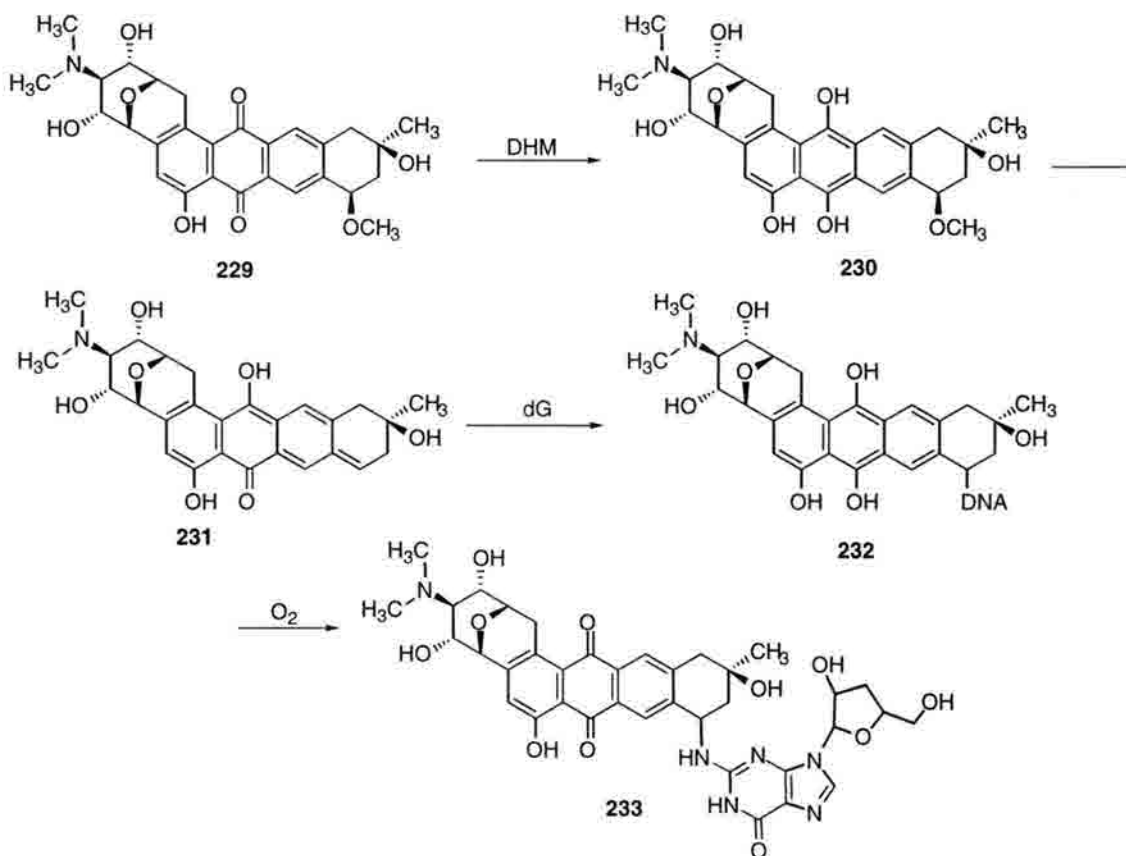
Fisher and Ramakrishnan have shown that anaerobic reduction of daunomycin with substoichiometric amounts of NADPH provides the quinone methide which is efficiently trapped by thiolate nucleophiles such as N-acetyl,L-cysteine, N-(t-butoxycarbonyl)-L-cysteine and 1-thio- $\beta$ -D-glucose providing the pair of C7 diastereomers for the respective products **224** and **225**.<sup>194</sup>



The resulting thioethers were typically obtained in 65% yield with the major products bearing the *S* stereochemical configuration at the 7 position. Nucleic acid alkylation studies by Koch and Egholm revealed that reduction of manogaril with the one electron reducing agent bi(3,5-dimethyl-5-(hydroxymethyl)-2-oxomorpholin-3-yl) (DHM-3 dimer, **226**) in the presence of deoxyguanosine yields the C7 nucleoside-substituted **233**.<sup>195</sup> Interestingly, none of the dG N<sup>7</sup> alkylated material was found nor were any of

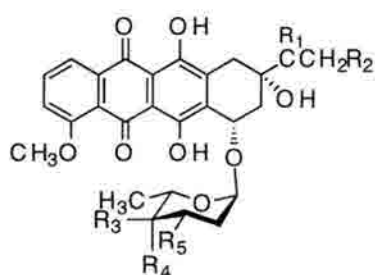


the nucleoside hydroxyls tethered to the anthracycline chromophore. Additionally, analogous reaction conditions in the presence of the other purine nucleoside deoxyadenosine failed to afford any drug-nucleoside conjugates.



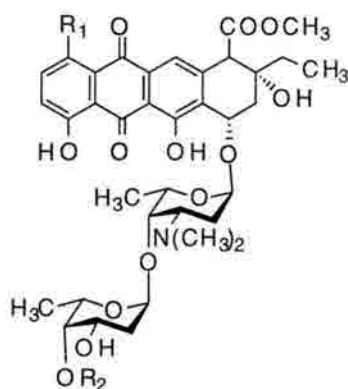
Recent studies by Skladanowski and Konopa have revealed that numerous members of the anthracycline class antibiotics induce interstrand cross-links into DNA.<sup>196</sup> Incorporation of <sup>14</sup>C-methyl-thymidine into the cellular DNA of HeLaS<sub>3</sub> cells was used as a means of detection for DNAs with abnormal renaturation kinetics following a cell:drug incubation period of 3 hours at 37°C. From these studies it was found that members of both the class I and class II anthracyclines inflicted ISCs upon HeLa cellular DNA (Figure 1-34).

#### CLASS I ANTHRACYCLINES



Compound	R <sub>1</sub>	R <sub>2</sub>	R <sub>3</sub>	R <sub>4</sub>	R <sub>5</sub>	% ISC
Adriamycin	=O	OH	H	OH	NH <sub>2</sub>	72.6
Daunomycin	=O	H	H	OH	NH <sub>2</sub>	53.6
Epirubicin	=O	OH	OH	H	NH <sub>2</sub>	50.0
Ixorubicin	=O	OH	H	I	NH <sub>2</sub>	76.9
4'-amino-Adria	=O	H	H	NH <sub>2</sub>	OH	10.0
Rubidazone	<div><div><div>O</div><div>=N-N</div><div>H</div></div><div>C(=O)C<sub>6</sub>H<sub>5</sub></div></div>	H	H	OH	NH <sub>2</sub>	25.0

#### CLASS II ANTHRACYCLINES



Compound	R <sub>1</sub>	R <sub>2</sub>	% ISC
Aclacinomycin	H		66.7
Cinerubin A	OH		35.0
Marcellomycin	H		> 70.0

**Figure 1-34.** Representative class I and class II anthracyclines known to interstrand cross-link HeLaS<sub>3</sub> cellular DNAs.<sup>196</sup>

The class I anthracyclines are nucleolar non-selective, inhibiting both DNA and nucleolar precursor ribosomal RNA (NO-RNA) synthesis at approximately equivalent concentrations while the class II compounds inhibit NO-RNA synthesis at concentrations 200-1300 fold lower than those required to inhibit DNA synthesis.<sup>197</sup> That members of

either class express biological activity *via* ISC formation has led to intense efforts aimed at the elucidation of the resulting lesions and the mechanisms responsible for their generation.

Reductive quinone methide formation explains the ability of the anthracyclines to induce monofunctional binding, but is not obligate for ISC induction by all anthracyclines. One case in point originally disclosed by Westendorf *et al.* and recently elaborated upon by Phillips and Cullinane is that of (cyanomorpholino)-adriamycin **211**.<sup>198</sup> Utilizing a degradative exonuclease III digestion assay, **211** was found to induce intrastrand cross-links at the sequence 5'-GG-3' on either strand of the alkylated duplex ODN (enzyme stop sites at the sequence 5'-CC-3' was considered diagnostic for alkylation of the 5'-GG-3' of the complementary strand).<sup>198b</sup> The intrastrand lesion is preferentially formed over the interstrand (involving alkylation at both dG residues of 5'-GC-3') *bis*-alkylation by a factor of ten and both events have been shown to involve alkylation of the N<sup>2</sup> of each deoxyguanosine residue.<sup>199</sup> Cross-linking of Eco RI linearized plasmid pSP64 with **210** did not require reductive conditions and afforded heat labile adducts which readily decomposed upon heating to 60-70°C for ten minutes.<sup>199</sup> The observed decomposition was attributed not to DNA strand scission, but rather to reversible release of the anthracycline chromophore from the duplex substrate. More important, was the *ability to induce ISCs without any exogenous reductants*. This substantiated earlier studies by Begleiter *et al.* in which DNA cross-links were isolated from drug-treated L5178Y murine lymphoma cells.<sup>200</sup> Notably, the *in vitro* plasmid reactions called for relatively high drug concentrations (micromolar) whereas the cellular studies required only nanomolar concentrations, thus suggesting the importance of metabolic activation. That the **211**-induced ISCs were obtained without reductive activation and show a high degree of reversibility at higher temperatures is suggestive of an adduct resulting from amination formation between the drug and the dG N<sup>2</sup>. Additionally, retention of both the anthracycline chromophore and the morpholino moiety supports the proposal that the ISC results partly from cyano displacement followed by addition of dG N<sup>2</sup> to the resulting

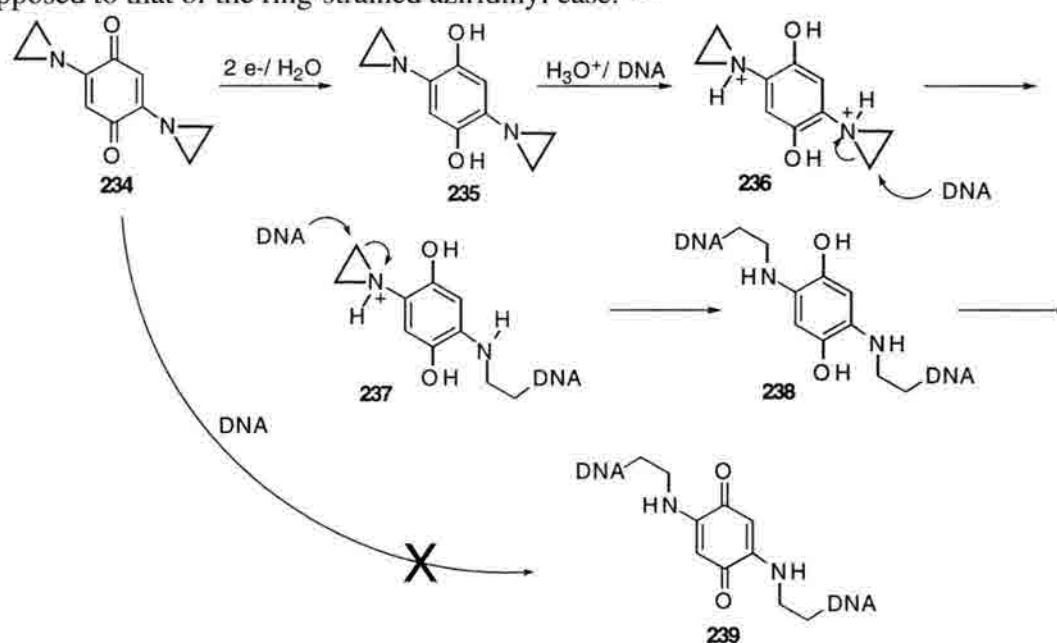
iminium species.<sup>199</sup> Although the viability of this mechanism is clear (based on analogy to DNA alkylation by Saframycin A), it only accounts for one of the two alkylation events necessary for ISC production. The second event remains unclear, but may involve simple Schiff base formation involving the C-13 ketone and the N<sup>2</sup> of the other deoxyguanosine involved in cross-linking. Given that the extended chromophore remains intercalated between the bases of interest, it is likely that the drug functionalities responsible for DNA alkylation be placed above and below the plane of the tetracycle. This, in combination with the relative reactivities of drug functional groups suggests that it is these "side chains" that endow **211** with interstrand cross-linking activity.

Studies by the Phillips group have addressed the ability of adriamycin **210** to induce similarly unstable cross-links into synthetic ODN's.<sup>183,201</sup> Contrary to the morpholino substituted anthracycline, *adriamycin displays the absolute requirement of an exogenous reductant in order to efficiently cross-link DNA*. Concentrations as high as 5-10mM are required with reducing agents such as dithiothreitol, glutathione and  $\beta$ -mercaptoethanol.<sup>183</sup> Additionally, the rate of cross-link formation is dependent upon the concentration of Fe(III).<sup>201b</sup> This most likely stems from the inability of intercalated anthracyclines to undergo reduction due to steric constraints inherent to the DNA bound species.<sup>188</sup> However, formation of the extremely stable anthramycin-Fe(III) complex affords a species still capable of intercalation, but now possessing a redox shuttling system.<sup>188</sup> It is proposed that reduction of the drug bound Fe(III) to Fe(II) gives rise to the intramolecularly reduced semi-quinone radical which is then electrophilically activated. Adriamycin mediated ISC's have been mapped to the sequence 5'-GC-3' using  $\lambda$ -exonuclease and are dependent upon the exocyclic N<sup>2</sup> amines of the deoxyguanosine residues on each strand of the duplex.<sup>201b,c</sup> However, the structure of the lesion has not been solved and more interestingly, no structurally related examples exist for which any corresponding ISC lesions have been elucidated. As such, the molecular mechanism by

which the anthracyclines interstrand cross-link DNA is largely unknown and thus represents a novel area of study given the widespread clinical use of the anthracyclines.

#### 1.5.4. Aziridinylbenzoquinones

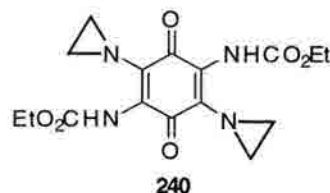
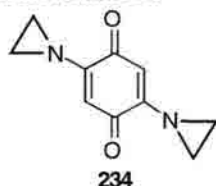
The aziridinylquinones represent perhaps the simplest of the mitomycin C-like prodrugs. Reduction of the quinone results in the transition from a nonaromatic quinone to the aromatic semiquinone or hydroquinone (1- and 2- electron reductions respectively). The resulting altered electronic distribution no longer invokes conjugation of the nitrogen lone pair electrons with the respective carbonyls.<sup>202</sup> As such, this substantially enhances the basicity of the aziridinyl nitrogens thus facilitating protonation of each tertiary amine.<sup>202</sup> This activation process vastly enhances aziridine electrophilicity thus affording a species capable of facile DNA alkylation. Following alkylation, autoxidation ensues thus restoring the quinone moiety. Importantly, autoxidation of the *bis*-alkylated species back to the quinone (as in the anthracycline case) is favored over the parent hydroquinones due to the increased electron donation from the acyclic amines into the aromatic hydroquinone as opposed to that of the ring-strained aziridinyl case.<sup>202</sup>



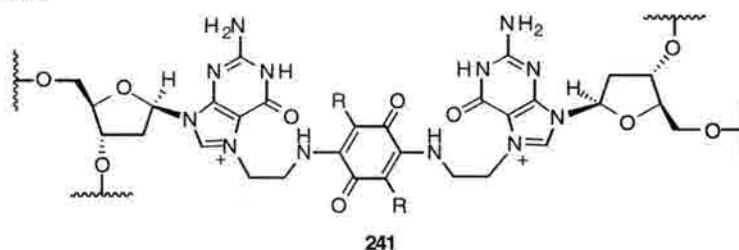
**Figure 1-35.** Reductive mechanism of DNA interstrand cross-linking by the diaziridinylquinones.



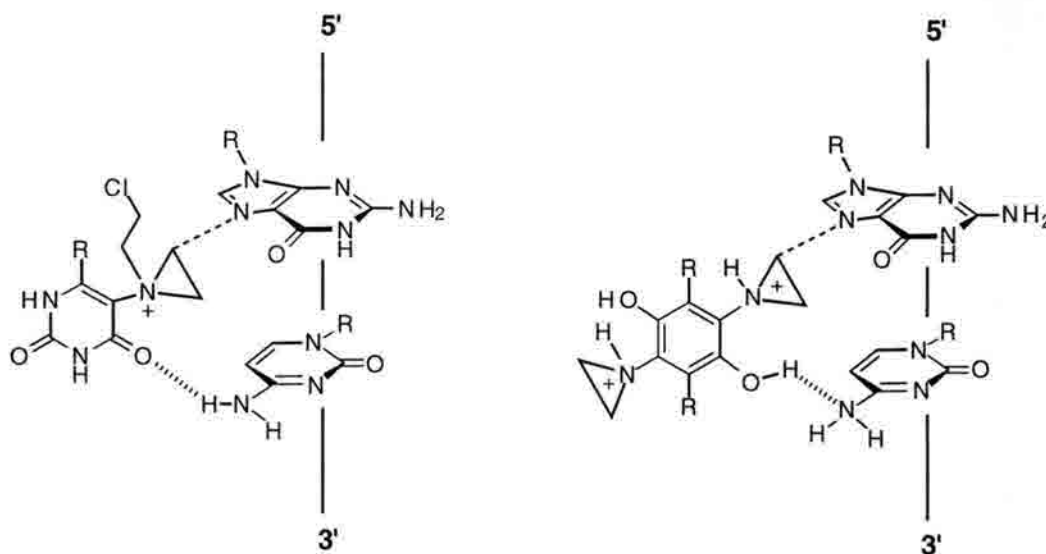
Of the diaziridinylquinones, the most heavily studied are the simple unfunctionalized diaziridinylquinone **234** (DZQ) and the more clinically promising 2,5-bis(1-aziridinyl)-3,6-bis(carboethoxyamino)-1,4-benzoquinone **240** (AZQ). AZQ is particularly interesting since it is one of the few therapeutic agents known to be active against human brain tumors.<sup>203</sup>



Hopkins and co-workers have recently described the lesion structure resulting from reaction of various synthetic ODN's bearing the sequences 5'-GN<sub>n</sub>C-3' (n=0,1 or 2) with both DZQ and AZQ.<sup>204</sup> Enzymatic digestion followed by HPLC, UV, and mass spectral analyses reveal the previously assigned structures to be consistent with those of the isolated lesions resulting from connectivities to both N<sup>7</sup> atoms of the two cross-linked dG residues as shown by **241**.

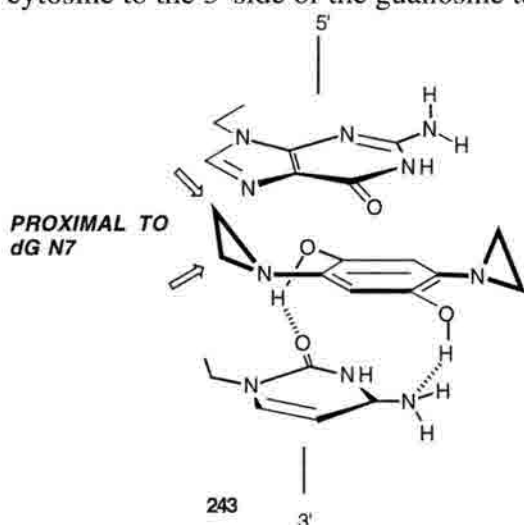


Concurrent with elucidation of these covalencies, studies have been directed at understanding the non-covalent interactions inherent to the reaction of these agents with DNA. For instance, DZQ (**234**) when in the quinone oxidation state, demonstrates DNA alkylation patterns very similar to most structurally related analogs.<sup>205</sup> However, reduced **234** reacts exclusively at 5'-GC-3' with a particularly strong preference for 5'-TGC-3'.<sup>205</sup> The nature of this radical transition in sequence selectivity has not been unambiguously defined. However, the analogous selectivities of DZQ and uracil mustard (**242**) in which both share a high degree of selection for 5'-PyGC-3' has prompted the proposed non-covalent motif shown in Figure 1-36.<sup>205</sup>



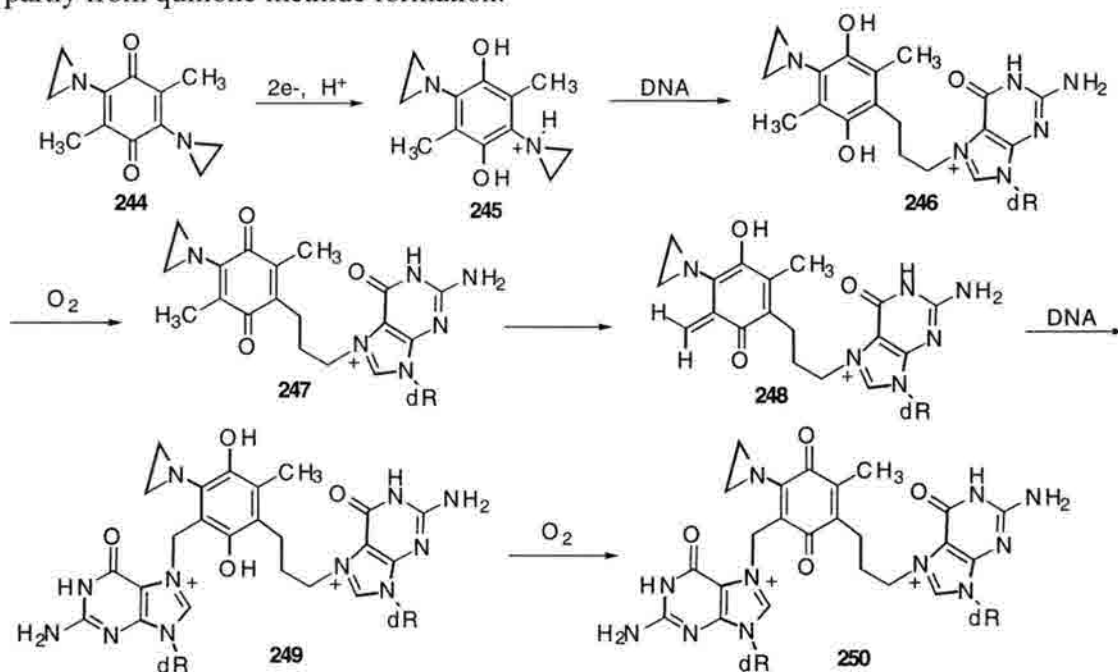
**Figure 1-36.** Proposed 5'-GC-3' binding motifs for activated uracil mustard (**242**) and activated DZQ (**234**).

Both cases involve ISC formation *via* major groove N<sup>7</sup> alkylations of the opposing deoxyguanosines on each strand of the duplex and indeed this model is consistent with at least one N<sup>7</sup> alkylation. That unreduced DZQ (structurally more similar to uracil mustard than the reduced form) did not show the same specificity as the reduced form has raised questions pertaining to the motif shown in Figure 1-36. An alternative rationale derived from molecular modeling studies has shown that the activated DZQ core readily undergoes hydrogen bonding between the hydroquinone hydroxyls and the O<sup>2</sup> and C<sup>4</sup>-NH<sub>2</sub> of the cytosine to the 3' side of the guanosine target base as in the complex **243**.<sup>205,206</sup> In this



fashion, the reactive carbon of the aziridine is positioned within bond-forming distance of the dG N<sup>7</sup> above the plane of the hydroquinone. That only the hydroquinone of DZQ could undergo such a binding mechanism suggests the validity of this view, though an unambiguous demonstration of this motif has not been reported.

In addition to alkylation of the major groove N<sup>7</sup> of deoxyguanosine, some instances of adenine alkylation have been noted.<sup>206</sup> Enzymatically reduced DZQ alkylates not only deoxyguanosine, but also shows a preference for adenines within 5'-(A/T)AA-3' runs. The methylated 2,5-dimethyl DZQ (**244**) readily monoalkylates 5'-GC-3' in line with most DZQ based structures. However, reduction with either ascorbate or DT-diaphorase affords a species highly selective for 5'-TAA-3'. The resulting lesion gives rise to base labile sites as demonstrated through piperidine digestion. More precisely, it appears that the major groove adenine N<sup>7</sup> is the modified moiety since the presence of 10mM Mg<sup>2+</sup> abrogates adenine alkylation (*via* minor groove N<sup>3</sup> coordination). The origin of this altered selectivity has not been determined, but dG alkylation with such analogs has been found to result partly from quinone methide formation.<sup>202</sup>



**Figure 1-37.** Proposed mechanism of 2,5-dimethyldiaziridinylquinone reaction with DNA *via* dual aziridine ring opening followed by oxidation and quinone methide formation.

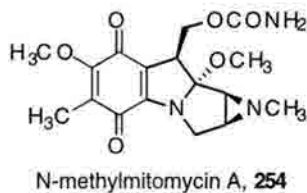
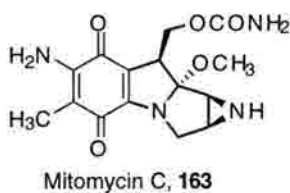
Butler *et al.* have shown that **244** is capable of ISC formation at the sequence 5'-TGC-3' and that this process requires the initial reduction of the quinone.<sup>202</sup> Computer modeling has revealed that aziridine ring-opening by the first dG brings the *para*-situated methyl group much closer to the N<sup>7</sup> of the opposing dG. Oxidation followed by quinone

methide formation ensues and subsequent Michael addition by the second strand affords the cross-linked adduct **250** shown in Figure 1-37. That oxidation of the initially formed monoadduct is required for ISC generation by **244** strongly supports this theory, although structural elucidation of the resulting lesion still has not been reported. Additionally, the fate and/or role of the second aziridine ring is not known in this quinone methide route to *bis*-alkylation.

The diaziridinylquinones have received considerable attention with respect to the design of 2,5-substituted analogs, but for the most part, little attention has been paid towards the design of peptide or DNA conjugates. As with the anthracyclines, this is likely due to the complexity of such a conjugate which requires not only the desired drug-target interactions, but which must still be capable of the desired activation process. Surprisingly, the mitomycins, for which the diaziridinylquinones may be thought of as mechanistic and structural predecessors<sup>207</sup>, have received attention with respect to such conjugation methodologies despite their considerably more complex structures.<sup>158</sup>

#### **1.5.5. Mitomycin C and Related Structures**

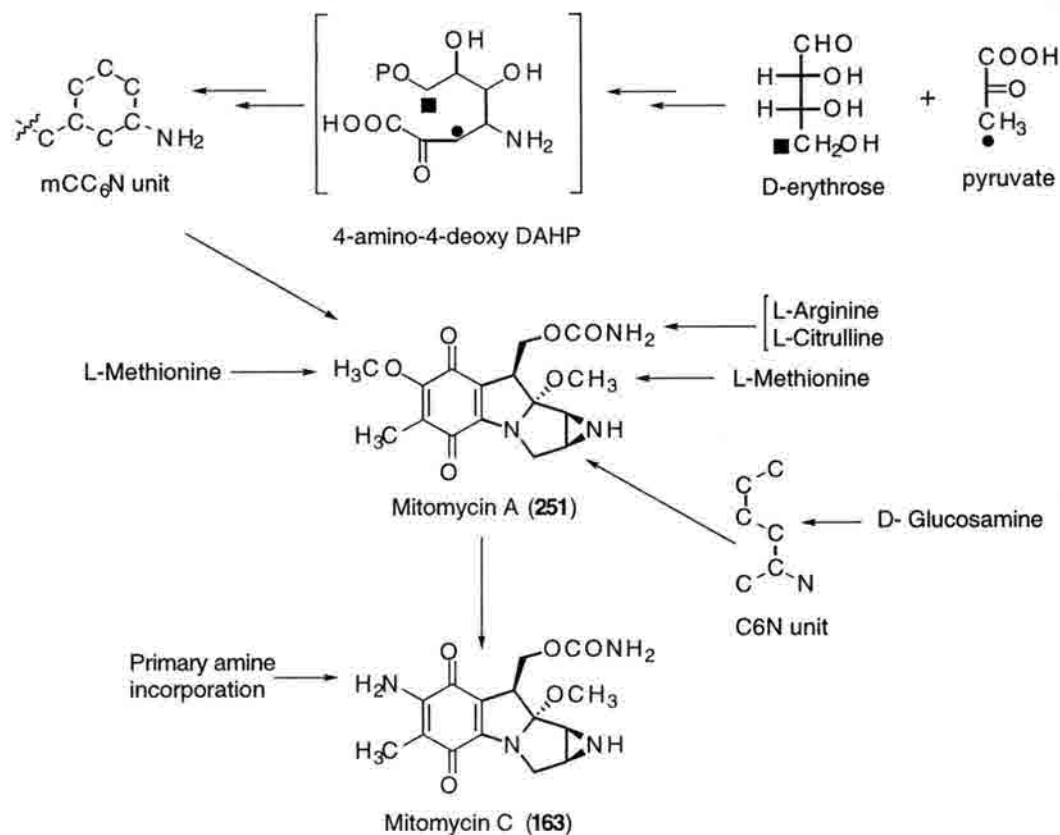
The mitomycins display a wide array of substitution patterns inherent to the core pyrrolo-[1,2a]-indole structure. Originally isolated in Japan by Hata *et al.*, mitomycins A and B were quickly recognized as potent antibacterial and antitumor agents.<sup>208</sup> The 1956 isolation of these compounds from broths of *Streptomyces caespitosus* was followed two years later by the isolation of mitomycin C (MC, **163**) from the same bacterium at the Kyowa Hakko corporation. In 1960, the aziridinyl N-methylated analog of MC, porifomycin **253** was isolated from *Streptoverticillium ardens*. In 1962 the same four compounds were isolated from broths of *Streptomyces verticillatus* as was the biologically inactive pentacyclic mitiromycin.



More recent additions to the mitomycins include N-methylmitomycin A reported in 1981<sup>212a</sup> and the equilibrium mixture of isomitomycin A (**256**) and albomitomycin A (**257**) which ultimately affords mitomycin A (**251**) as the thermodynamically favored isomer.<sup>212b</sup>



In addition to the isolation of mitomycin congeners from "native" broths, the doping of these broths with biosynthetic "synthons" has yielded a wide array of "unnatural" mitomycins. Bush *et al.* have demonstrated that supplementing the normal fermentation medium for *Streptomyces caespitosus* with various primary amines results in two types of mitomycin analogues.<sup>213</sup> The first type is analogous to mitomycin C with the exception that primary amine incorporation at the quinone C7 position is observed. Alternatively, the mitomycin isolated is analogous to mitomycin B with the primary amine incorporated once again at the C-7 position. Broth supplementation with methylamine, ethylamine, propylamine, propargylamine and 2-methylallylamine gave rise to mitomycin C analogues all of which possessed greater activities against L1210 lymphatic leukemia cells in mice than the related mitomycin B congeners.

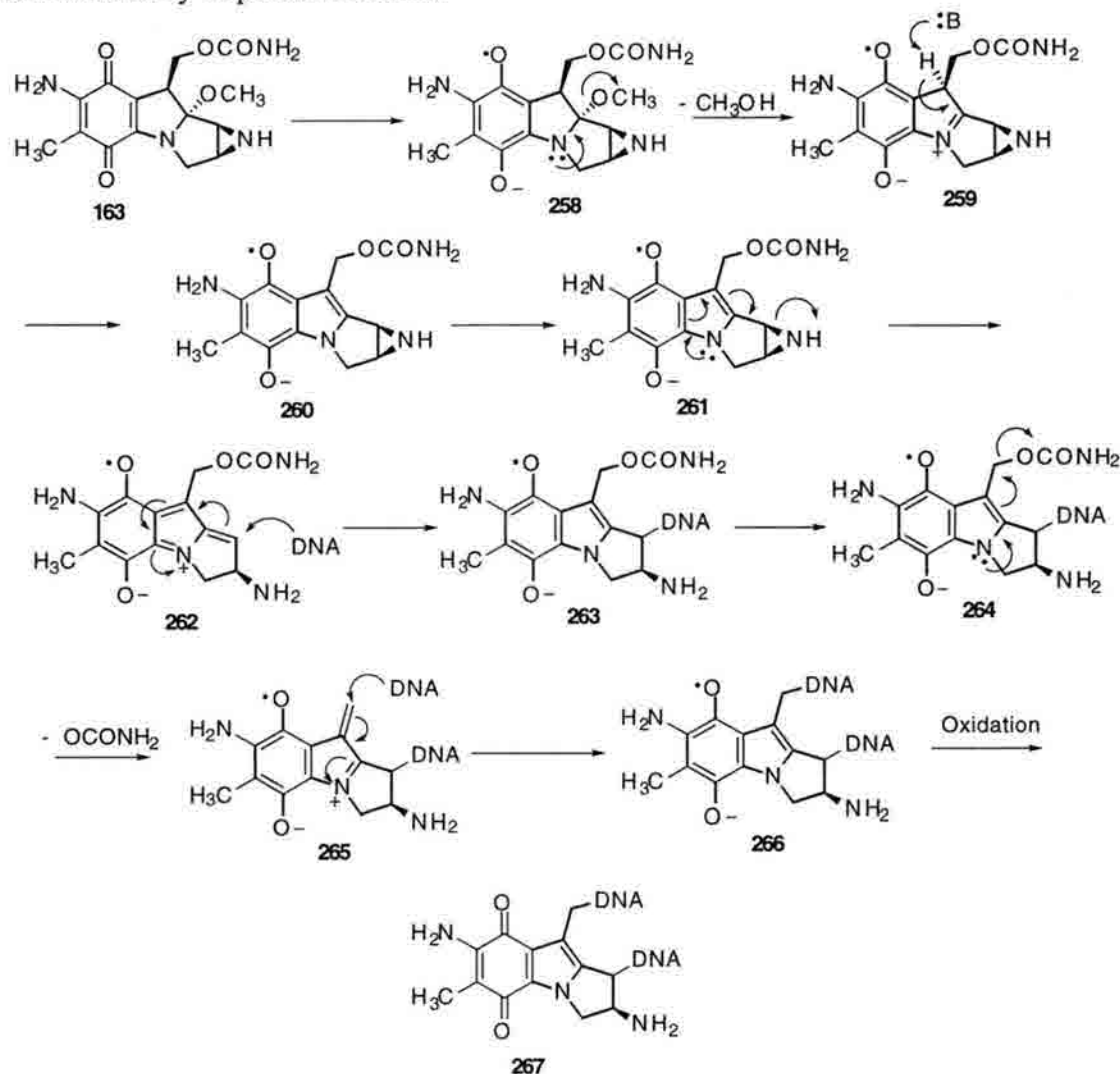


**Figure 1-38.** Proposed biosynthetic pathway to mitomycin C.<sup>214</sup>

Outlined in Figure 1-38, biosynthetic studies have shown that the 6 carbon chain from C10 to C3 containing the aziridine of the natural product is derived from D-glucosamine.<sup>214a</sup> The carbamate derives from citrulline and the O-methyl group at C9a is donated from methionine.<sup>214b</sup> The quinone is believed to originate from glucose *via* pyruvic acid.<sup>214b</sup> Importantly mitomycin C is derived by way of mitomycin A *via* the biosynthetic route proposed by Hornemann.<sup>215</sup> As such, broth supplementation has been viewed as a viable means of continued generation of new mitomycin analogues, particularly with respect to C7 functionalization.

Like the other quinone-containing DNA interstrand cross-linking agents, the mitomycins benefit from extraordinary stability in the absence of exogenous reductants. However, quinone reduction affords a species capable of facile DNA alkylation as well as superoxide production and subsequent oxidative DNA damage.<sup>216</sup> The activated

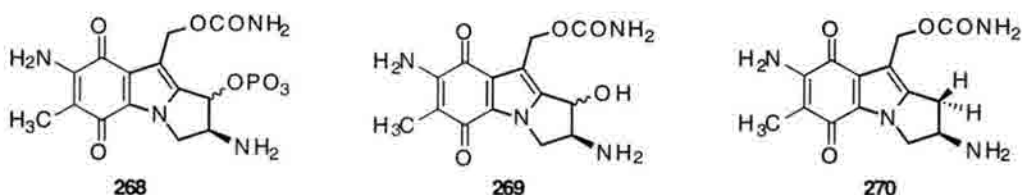
"aziridinomitosenes" core has been shown to react principally with deoxyguanosine *enroute* to a wide array of possible lesions.<sup>217</sup>



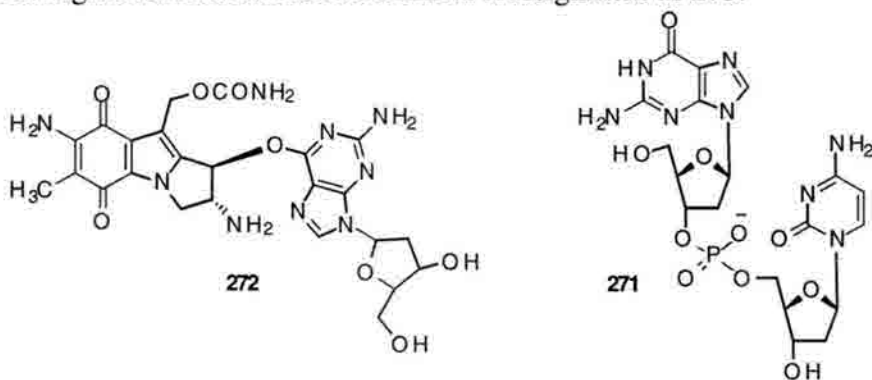
**Figure 1-39.** Proposed mechanism of DNA cross-linking by one electron reductive activation of mitomycin C.

Preliminary mechanism of action studies revealed that the mitomycins shut down DNA synthesis and also induced phosphodiester strand scission within cellular DNAs. Particularly interesting were the Iyer and Szybalski studies which demonstrated that cell death was not a consequence of the strand scission events.<sup>153</sup> Rather, it was attributed to the formation of interstrand cross-links as evidenced by the anomalously fast renaturation kinetics of mitomycin C-treated bacterial DNA.<sup>153</sup> Fragmentation studies with mitomycin modified DNAs revealed that cross-linking was extremely rare with only one ISC per

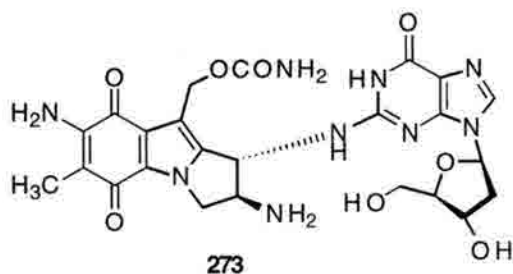
20,000 base pairs of DNA.<sup>153</sup> Additionally, the failure to induce ISC*s in vitro* without the presence of cell lysates suggested that cellular activation was required for drug action.<sup>153</sup> Indeed, Iyer and Szybalski demonstrated that the normally inert mitomycin was capable of DNA cross-linking upon treatment with chemical reductants such as H<sub>2</sub>/Pd/C, NaBH<sub>4</sub>, or sodium dithionite and that this reaction demonstrated differing efficiencies with different DNA substrates. The different CG content of *S. Lutea* (a high GC content genome) versus *C. johnsonii* (34 % CG) DNAs led to much more efficient cross-linking of the former substrate.<sup>153,218</sup> The first adducts isolated from the reductive activation of mitomycin C were reported by Tomasz and co-workers.<sup>219</sup> Reduction of MC with rat liver microsomes and NADPH in phosphate buffered aqueous solutions afforded the aziridine ring-opened adducts **268 -270**.



The preference for GC runs of DNA was elaborated upon *via* the elegant studies of Tomasz and Nakanishi in which enzymatic digestions of the mitomycin-modified dinucleotide dGC (**271**) and subsequent HPLC purification revealed **272** as a presumed monoalkylated intermediate in the pathway to cross-link formation.<sup>220</sup> This represented the first documentation of an MC-nucleotide adduct although subsequent studies<sup>219</sup> mandated its regiochemical and stereochemical reassignment as **273**.

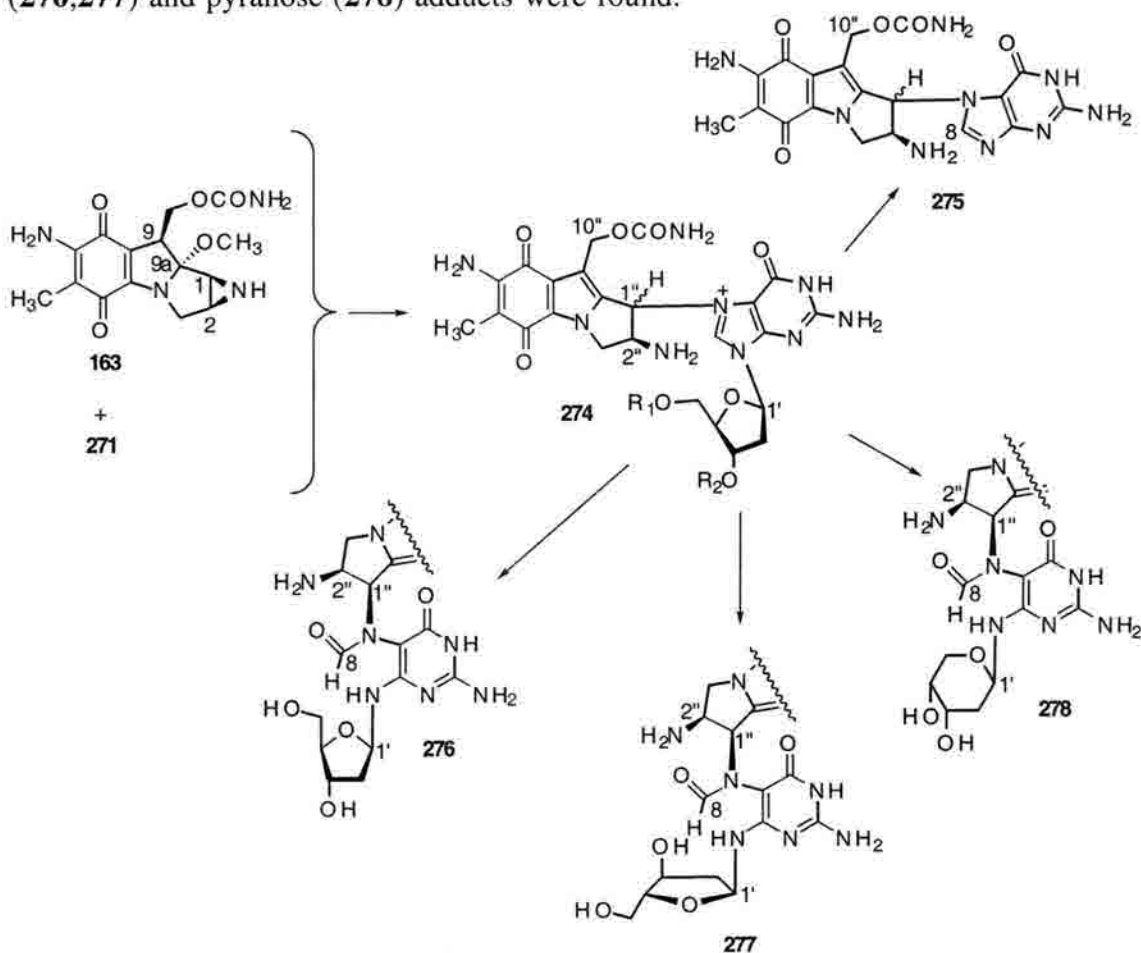






Later studies by Nakanishi *et al.* revealed that MC could alkylate DNA *via* acid-catalyzed pathways in addition to the reductive methodologies previously demonstrated.<sup>30,221</sup>

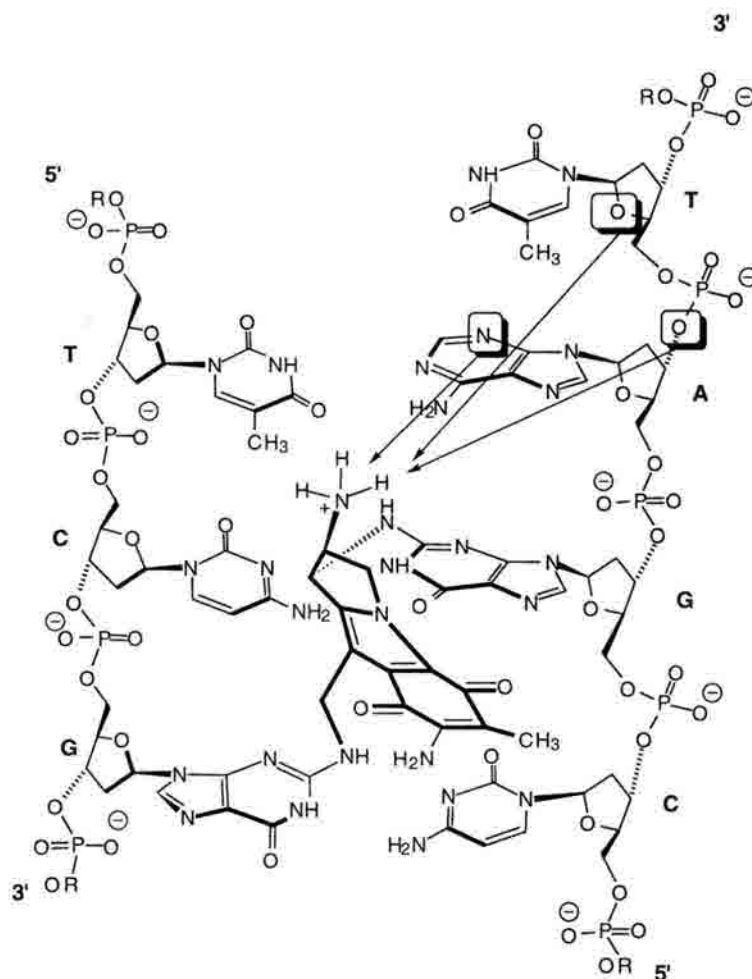
Acidic activation requiring  $\text{pH} \leq 5$  induced both monofunctional binding and cross-linking. Generation of 1-substituted-2 $\beta$ ,7-diaminomitosenes was effected with a remarkable change in selectivity from dG N<sup>2</sup> alkylation to the dG N<sup>7</sup> event. The imidazolium formed upon N<sup>7</sup> alkylation gave rise to not only the deribosylated lesion **275** (leading to DNA strand scission), but also the N-formylated adducts arising from hydrolysis at the purine C8 position. Both furanose (**276,277**) and pyranose (**278**) adducts were found.



**Figure 1-40.** MC-DNA product distribution under acidic activation conditions.

Extensive molecular modeling of both interstrand cross-linked 5'-CG-3'-containing oligodeoxyribonucleotides and monoalkylated ODNs has been performed. Molecular mechanics simulations of the 5'-CG-3' cross-link in the computer-generated decamer d(GCATCGATGC)<sub>2</sub> was carried out by Tomasz and Verdine (Figure 1-41).<sup>30</sup> This model showed the comfortable fit of the MC derived mitosene within the minor groove of B-DNA. No distortions of the sugar-phosphate backbone were detected and all glycosidic torsion angles proximal to the cross-link conformed to the usual *anti* configuration.<sup>30</sup> Additionally, the C-G base-pairing was maintained in both drug-modified pairs although slight alteration of the propeller-twisting of each alkylated base was observed.<sup>30</sup> Twisting of the C10" bound dG was reduced and twisting of the C1" bound dG was increased relative to B-DNA. This is believed to be a function of the approximate 0.3 Å difference in bonding distances between the mitosene and the intra-duplex dG N<sup>2</sup>-dG N<sup>2</sup> box resulting in slight spreading apart of the duplex at the expense of propeller twisting.

Within the decamer examined, the mitosene N2 ammonium function appears to be involved in considerable hydrogen bonding interactions with three atoms on the same strand to which the C1" is attached.<sup>30</sup> Particularly noteworthy are contacts with the N<sup>3</sup> and O<sup>3'</sup> of the deoxyadenosine residue below and the O<sup>4'</sup> of the deoxythymidine residue two bases below. The base-pairing interactions of both strands are intact, but some degree of reorganization has occurred with respect to the C1" bound strand. This is facilitated by the proximity to the mitosene N2 ammonium group. The minor groove is compressed to widths of 8.1 and 9.5 Å (as determined by phosphorus-to-phosphorus distances) immediately below the cross-link and returns to the normal values of 11.1- 11.9 Å in the rest of the duplex.<sup>30</sup>



**Figure 1-41.** Mechanical modeling of MC cross-linked d(GCATCGATGC)<sub>2</sub>. Only partial structure of the DNA duplex is shown and interstrand hydrogen-bonding interactions are not shown for the purposes of clarity. Intra-strand DNA-drug contacts are highlighted involving the aziridinyI N2.<sup>30</sup>

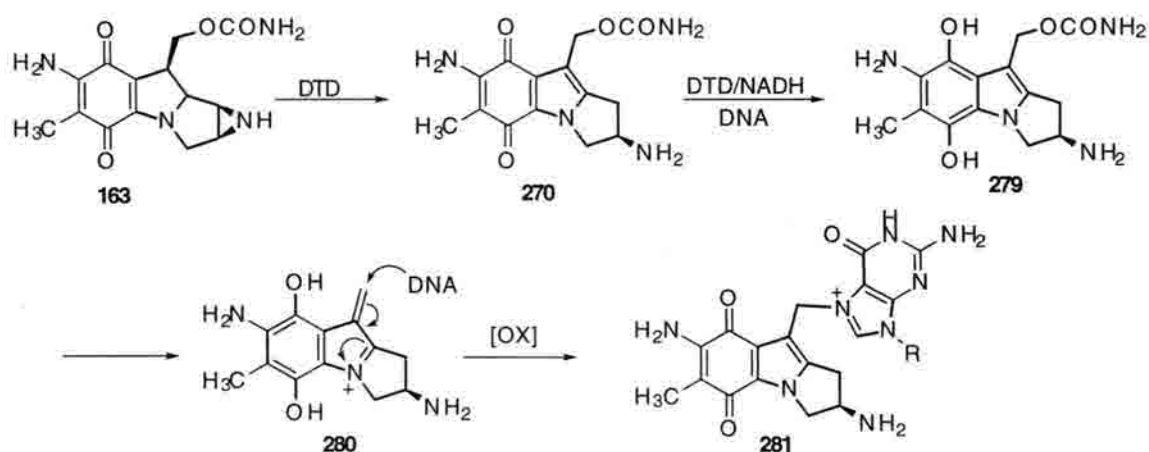
Recent <sup>1</sup>H NMR examination of MC cross-linked 5'-d(T<sup>1</sup>A<sup>2</sup>C<sup>3</sup>G<sup>4</sup>T<sup>5</sup>A<sup>6</sup>) has more rigorously addressed the solution structure of the MC cross-link than was possible *via* the Verdine modeling study.<sup>222</sup> Like the modeling study, interproton distance constraints obtained by Tomasz and co-workers verify the retention of all H-bonding interactions between the two DNA strands and also confirm the *anti* conformations of the glycosidic bonds.<sup>222a</sup> Strikingly, the 1H derived data suggests that the substrate DNA does, however deviate from that of normal B-DNA. The sugar protons on adjacent nucleotides are 5 Å apart in B-DNA and as such NOEs are not found between sugar H1' protons on adjacent residues. However, NOEs were detected between the sugar H1' protons of G10 and T11.

A similar result was obtained involving the same protons of G4 and T5.<sup>222a</sup> As such, MC cross-link formation was found to be facilitated, in part, by alteration of the phosphodiester backbone of the G10-T11 and the G4-T5 steps which brings the sugar rings at these positions into closer proximity than expected for retention of the B-form structure. Strikingly, measurement of phosphorus resonances revealed that MC complex formation results in distortions in the phosphate backbone also at the G10-T11 step and its complementary G4-T5 step.<sup>222a</sup> This, in combination with the recognized alignment of the MC aromatic chromophore toward the G10-T11 step of the T<sup>7</sup>-A<sup>8</sup>-C<sup>9</sup>-G<sup>10</sup>-T<sup>11</sup>-A<sup>12</sup> strand rather than with the center of the minor groove, allows for slight widening of the minor groove in contrast to preceding mechanical modeling studies.

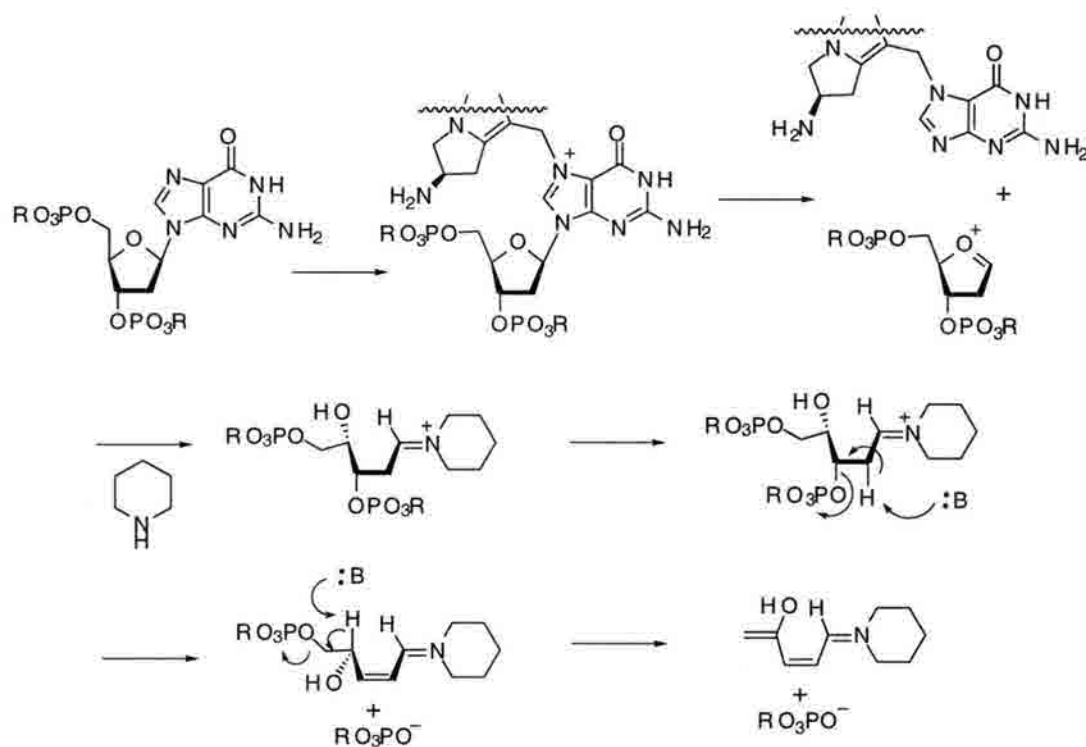
Like the MC interstrand cross-link, the solution structure of MC monoalkylated DNA also undergoes non-symmetrical stacking of the chromophore ring system with principally one of the two DNA strands.<sup>223</sup> Indeed many of the traits inherent to the interstrand cross-link are also observed with the monoadduct. One notable difference is that the MC monoadduct displays rapid exchange of the MC dG exocyclic amino protons.<sup>223</sup> This is in stark contrast to the very slow exchange rate seen for the cross-link. As such, it has been reasoned that the MC dG monoadduct is much more solvent accessible than in the case of *bis*-alkylated DNA substrates. The monoalkylated MC chromophore is positioned in the minor groove and the indoloquinone system lies at an approximate 45° angle with respect to the helix axis. The DNA substrate examined (in this case a 9-mer self-complementary ODN 5'-d(ICACGTCIT)<sub>2</sub>) possessed base-pairs displaced by approximately -3.0 Å towards the major groove thus allowing the minor groove positioning of the MC derived mitosene. This data is consistent with the interstrand structural data in that retention of the hydrogen-bonding network between the two strands was observed and that the O-10" atom of the MC carbamate side-chain forms a critical H-bond with the exocyclic amino group of the non-alkylated dG residue proximal to the alkylated deoxyguanosine.<sup>223</sup>

The vast majority of studies pertaining to interstrand cross-linking by the mitomycins have exploited chemical reducing agents such as sodium borohydride or sodium dithionite under anaerobic conditions. Such assays have revealed that ISC formation proceeds almost exclusively at 5'-CG-3' sequences with some variation in efficiency based upon the flanking bases on either side of the two-base sequence.<sup>224</sup> Additionally, cytosine methylation of the 5'-CG-3' enhances the extent of cross-linking.<sup>225</sup> Absolutely critical to mitomycin induced cross-linking is the presence of the two exocyclic N<sup>2</sup> amines of the adjacent deoxyguanosines on either strand.<sup>217,218</sup>

Contrary to results utilizing chemical reduction, enzymatic reduction by one-electron reductants such as xanthine oxidase or NADPH-cytochrome c reductase results in monoadduct formation which accounts for more than 90% of the DNA-bound drug.<sup>226</sup> Additionally, aerobic chemical reduction methodologies result in base-labile lesions *via* presumed dG N<sup>7</sup> alkylation involving aziridine ring cleavage and pursuant C1 substitution.<sup>227</sup> Gibson and co-workers have shown that dG N<sup>7</sup> alkylation occurs not only upon acidic activation, but may also be facilitated by DT-diaphorase (DTD)-mediated reduction.<sup>228</sup> Under aerobic conditions, this two electron reductase has been implicated in the DNA *mono-* and *bis-*alkylation events, as well as, glutathione conjugation reactions with mitomycin C.<sup>228</sup> Surprisingly, the major product of DTD metabolism is the 2,7

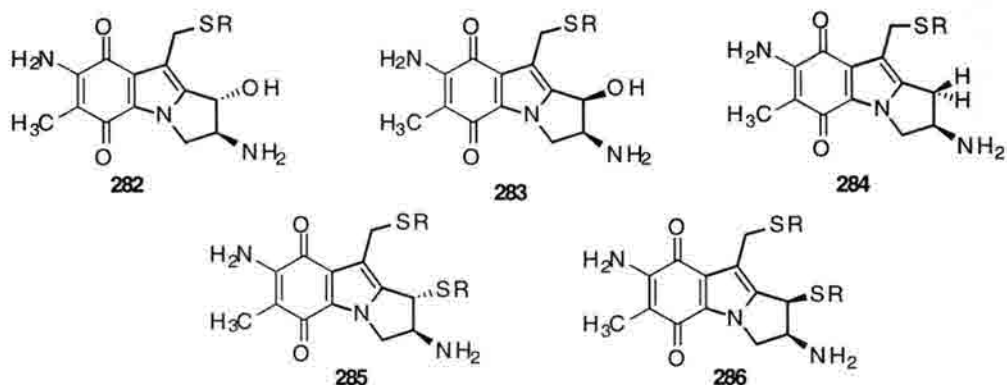


Substrate **270**, upon reduction with DTD is capable of only monoalkylation *via* loss of the carboxamide to afford the Michael acceptor **280**. No longer capable of cross-linking (due to *a priori* destruction of the aziridine) **279** readily alkylates dG N<sup>7</sup> moieties preferentially within 5'-GG-3' and 5'-GTC-3' sequences thus giving rise to base-labile lesions (Fig. 1-42.).<sup>228</sup> The reaction requires both DTD and NADH and shows a marked dependence upon pH with optimal alkylation observed at pH 5.8. Proton-assisted loss of the carbamate has been proposed as the root of the observed pH dependence.

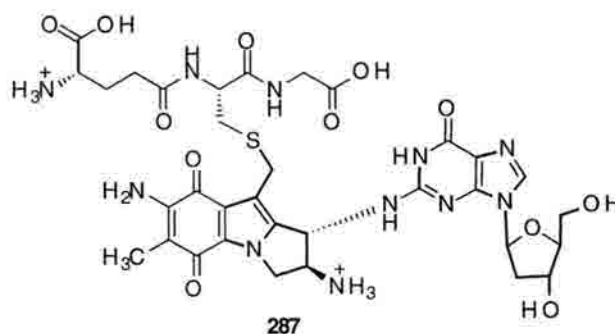


**Figure 1-42.** Mechanism of depurination followed by base mediated DNA strand scission.

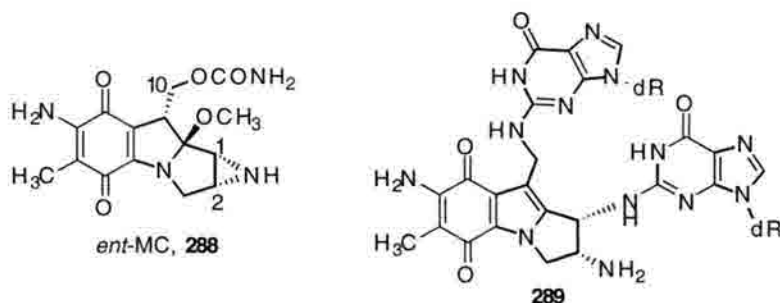
In addition to studies pertaining to sequence selectivities of the mitomycins (much of which will be discussed later), the reactions of mitomycin C with various nucleophiles of biological consequence have been explored. Tomasz and Sharma have shown that reaction of reductively-activated mitomycin C with glutathione, mercaptoethanol and N-acetylcysteine affords *mono*- and *bis*-thiolated compounds **282-286**.<sup>229</sup>



The reactions absolutely required the presence of an additional reducing agent aside from the chosen thiols and in fact, the thiols studied were incapable of mitomycin reductive activation even at concentrations as high as 50mM in thiol. Unreduced MC (**163**) was completely inert towards thiolation. An interesting observation was that, though incapable of MC reduction, glutathione was found to radically accelerate the rate of MC reduction by "slow" reductants such as cytochrome *c* reductases and H<sub>2</sub>/PtO<sub>2</sub>.<sup>229a</sup> Additional studies have shown that sodium dithionite reduction of MC in the presence of *M. luteus* DNA and glutathione affords the ternary complex **287**.<sup>229b</sup> The same lesion was isolated following PtO<sub>2</sub> activation procedures, contrary to the belief that thiol poisoning of the catalyst would abrogate MC activation. Additionally, reduction of the monoalkylated ODN 5'-ACACG\*T-CAT-3' (G\* denotes the mitomycin bound dG residue) in the presence of 50mM glutathione also produced the ternary complex following enzymatic digestion and HPLC purification.<sup>229b</sup>



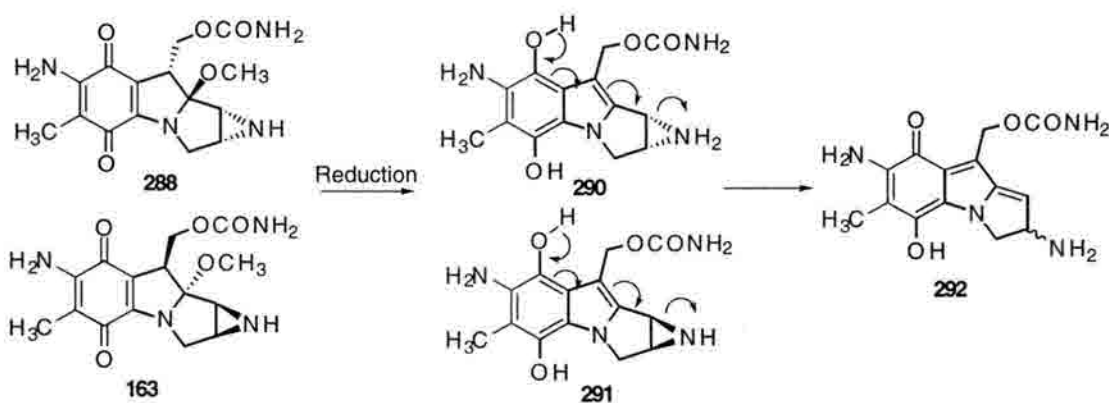
Concomitant with the thiol alkylation studies, the Tomasz group, in collaboration with Fukuyama, demonstrated that the 5'-CG-3' selectivity demonstrated by the mitomycins is dictated largely by the initially formed C1"  $\alpha$  linkage to the first dG.<sup>230</sup> The solution structures of synthetic ODN duplexes containing both the 5'-CG-3' interstrand cross-link and the monoadduct had been determined by 2-D NMR as well as molecular modeling.<sup>222,223</sup> Consistent with earlier proposals, the structures revealed that the monoadduct assumes an orientation within the minor groove in which the C10 carbamate is positioned in the 5'-direction (upstream) from the initially alkylated dG. Given the observed orientation of the monoadduct, only that dG N<sup>2</sup> of the complementary strand would be capable of C10 alkylation thus affording the cross-link. The alternative alignment wherein the carbamate is directed to the 3'-side (downstream) of the initially alkylated dG could give rise to the interstrand cross-link such that 5'-GC-3' specificity was obtained. That such specificity had never been observed was attributed to the chirality of the drug C1"- $\alpha$ -linkage to the N<sup>2</sup> atom of first alkylated dG though a thorough examination of this was lacking. Alternatively, this specificity was proposed to result from favorable hydrogen bonding interactions involving the C10-oxygen atom of the MC C10-carbamate and the exocyclic guanosine N<sup>2</sup> in the non-bonding strand at the 5'-CG-3' bonding site (Figure 1-42).<sup>224,226</sup>



In order to probe this issue more thoroughly, reactions involving the reductive activation and subsequent DNA alkylation chemistry of *ent*-MC (**288**) were pursued.<sup>230</sup> Surprisingly, the resulting interstrand cross-link was formed and found to bear the  $\alpha$ -stereochemistry (giving the 1",2" *cis*-product **289**) at the C1" position analogous to that

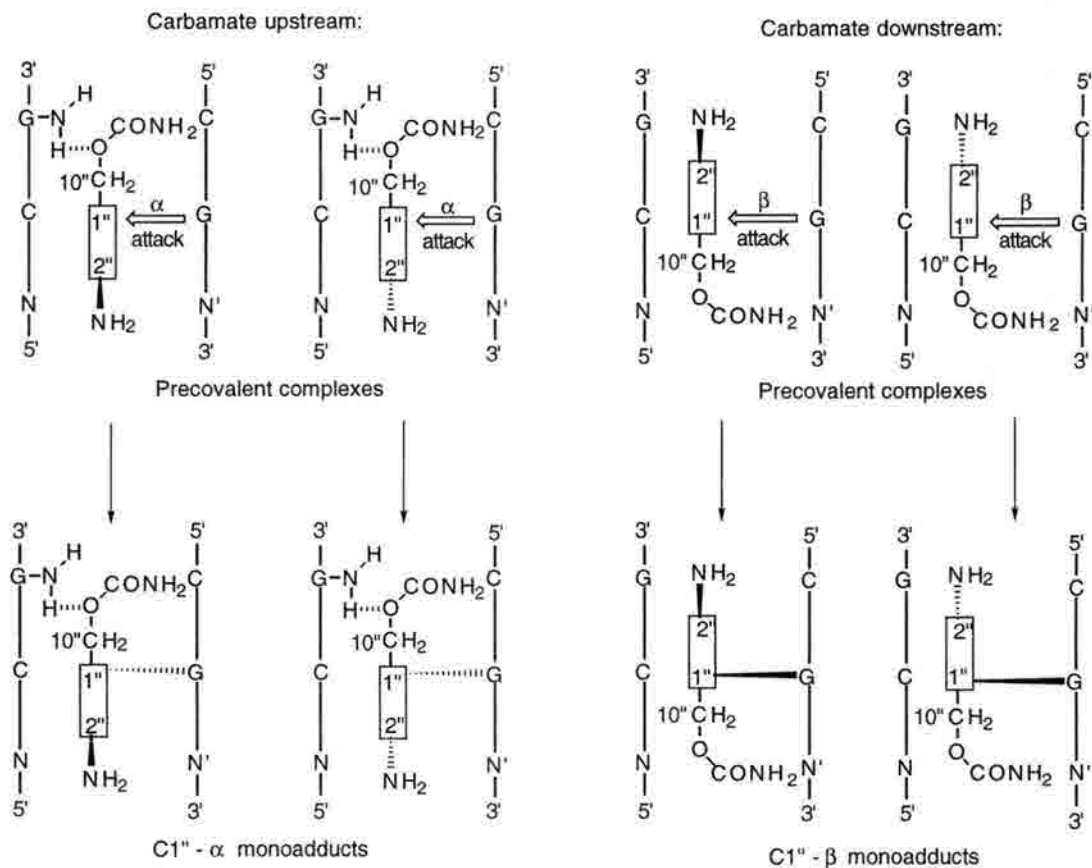


seen with the native mitomycins. This refuted the proposal that the aziridine stereochemistry of the natural products was responsible for the stereospecific  $\alpha$ -face attack by the first dG residue. Moreover, it suggests that the quinone methide is the species to undergo monoalkylation in an  $S_N1$  fashion. The chiral minor groove of 5'-CG-3' binds to both quinone methides using a similar motif which gives rise to the stereospecific attack upon the prochiral quinone methide C1 by deoxyguanosine on the  $\alpha$ -face of the mitomycins.



Importantly, once in place, the C1" stereochemistry sets the mitosene core within the 5'-CG-3' sequence so as to allow only the carbamate upstream positioning. In this motif, 5'-CG-3' behaves similarly to an enzyme active site *via* chirality induction upon an achiral center.<sup>230</sup> That the proposed carbamate-dG N<sup>2</sup> hydrogen bond exists has been shown by NMR studies, but equally important is the demonstration that substitution of the potential H-bond-donating dG amine with inosine (lacking N<sup>2</sup>) affords retention of only the upstream orientation upon 5'-CG-3' monoalkylation.<sup>222a</sup> As such, considerable evidence has been presented to suggest the importance of the stereospecific first addition to the activated mitosene with respect to interstrand cross-linking by the mitomycins.

The generation of synthetic analogues of the mitomycins has represented a fruitful area for study and the immense effort put forth warrants much greater consideration than is available within this discussion. The interested reader is referred to the synthetic endeavors described in reference 231.



**Figure 1-43.** Non-covalent interactions of "aziridinomitosenes" within 5'-CG-3' leading to stereospecific  $\alpha$ -face attack at C1. (C1''- $\beta$ -mono or *bis*-alkylation adducts are not experimentally observed)<sup>230</sup>

As with many other redox-activated agents, the mitomycins have received little attention with respect to bioconjugate chemistry. To date, only two instances of MC conjugation to DNA binding ODNs have appeared. Tomasz and Maruenda have demonstrated that a number of 5'-functionalized ODNs were capable of reductively activated minor groove alkylation events.<sup>158a</sup> The single-stranded target ODNs underwent hybridization with the MC-tethered complements and upon treatment with NADPH-cytochrome c reductase readily formed the covalently bound duplex.

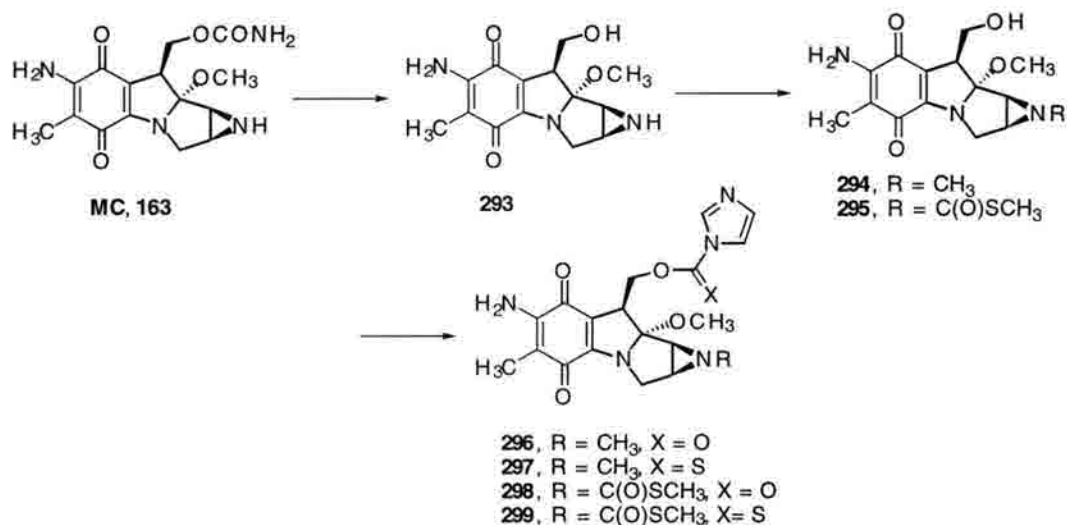


**Figure 1-44.** MC conjugate binding to single-stranded ODN.<sup>158a</sup>

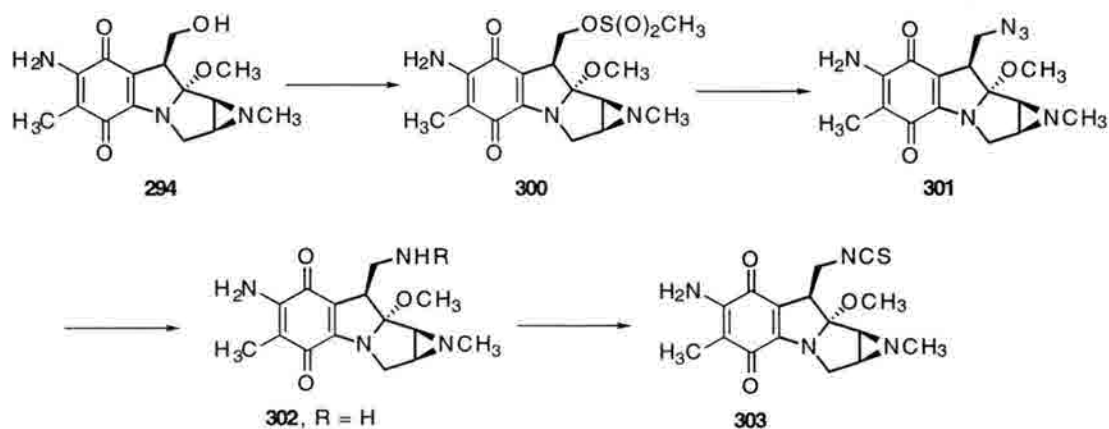
Target alkylation was found to occur exclusively at dG N<sup>2</sup> and was relegated to the 3 dG residues proximal to the MC core. The preferred alkylation site was G15 ( 3rd from the 3' target terminus), though substitution of G-15 with inosine shifted the alkylation chemistry to G16 and G-18 despite the fact that neither one is involved in base pairing with the conjugate.

Kohn *et al.* have shown that conjugation of various mitomycin core structures to phosphorothioate oligodeoxyribonucleotides could be achieved involving conjugation *via* the mitomycin C10 position to afford a conjugate capable of facile C1 alkylation.<sup>158b</sup> This was in contrast to the Tomasz study in which the MC unit was tethered through the C7 position so as to leave the DNA-alkylation chemistry at C1 and C10 intact.<sup>158a</sup> The use of oligodeoxyribonucleotides containing phosphorothioate units instead of the phosphodiester backbone was sought as a means of inhibiting exo- and endo-nuclease activities.

Several strategies were envisioned by which to effect conjugation of the MC chromophore to the ODNs of interest. The first involved decarbamylation of MC (**163**) with sodium methoxide to afford **293**. This was followed by functionalization of the aziridinyl nitrogen with dimethyl sulfate or methyl chlorothiolformate to yield the N-substituted mitomycins **294** and **295**. Conversion of **294** and **295** to the carbonylimidazoles **296-299** was effected upon treatment with either 1,1'-carbonyldiimidazole or 1,1'-thiocarbonyl-diimidazole.

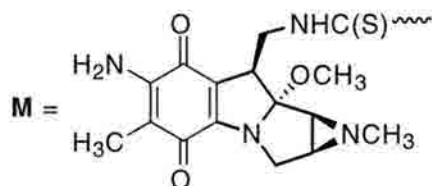


Alternatively, conjugation of the aminohexyl functionalized oligodeoxy-ribonucleotides was envisioned to occur *via* ODN addition to the isothiocyanate **303**. Substrate **303** was derived from decarbamoyl MC (**294**) by mesylation of the C10 alcohol, displacement with sodium azide and subsequent reduction to the amine (PtO<sub>2</sub>, H<sub>2</sub>) in pyridine followed by air oxidation to ultimately afford **302**. Conversion of **302** to the isothiocyanate **303** was effected upon treatment with 2-pyridyl thionocarbonate (DPT). Conjugation efforts emphasized the reactions of **297**, and **299** with H<sub>2</sub>N-(CH<sub>2</sub>)<sub>6</sub>-P(S)(OH)-GGCC-CCGTGGTGGCTCCAT. Difficulties associated with these, and the other activated carboimidazoles **296** and **298** ultimately led however, to the exclusive use of isothiocyanate **303** as the mitomycin of choice for phosphorothioate conjugations.



Reaction of **303** with amino-hexyl functionalized ODNs of varying length and sequence composition gave rise to the conjugates **304-311** all of which were intended as antisense strands to a 30 bp long region from the coding region of the human FGFR1 gene. Bearing the sequence 5'-AGATGGAAAAGAAATTGCATGCAGTGCCG-3', the sense strand of this region was intended as the target for conjugate-mediated inhibition of high-affinity bFGF binding to smooth muscle cells. This activity was in fact confirmed with all mitomycin-bearing conjugates inhibitin the proliferation of culture human aortic smooth muscle cells at concentrations as low as 1  $\mu$ M. Although interstrand cross-linking was presumed to not be a likely mechanism of action for these conjugates, it was clear that conjugation of **303** to each ODN was capable of endowing the conjugate with inhibitory attributes far exceeding those of the untethered oligos.

ACCTTTTCTTTAACGTACGTCACGG-P(S)(OH)-(CH <sub>2</sub> ) <sub>6</sub> NH-M	<b>304</b>
TACCTTTTCTTTAACGTACGTCACG-P(S)(OH)-(CH <sub>2</sub> ) <sub>6</sub> NH-M	<b>305</b>
CTACCTTTTCTTTAACGTACGTCAC-P(S)(OH)-(CH <sub>2</sub> ) <sub>6</sub> NH-M	<b>306</b>
TCTACCTTTTCTTTAACGTACGTCA-P(S)(OH)-(CH <sub>2</sub> ) <sub>6</sub> NH-M	<b>307</b>



ACCTTTTCTTTAACGTACGTCACGG-P(S)(OH)-(CH <sub>2</sub> ) <sub>6</sub> NH-M	<b>308</b>
TACCTTTTCTTTAACGTACGTCACG-P(S)(OH)-(CH <sub>2</sub> ) <sub>6</sub> NH-M	<b>309</b>
CTACCTTTTCTTTAACGTACGTCAC-P(S)(OH)-(CH <sub>2</sub> ) <sub>6</sub> NH-M	<b>310</b>
TCTACCTTTTCTTTAACGTACGTCA-P(S)(OH)-(CH <sub>2</sub> ) <sub>6</sub> NH-M	<b>311</b>

These studies have clearly shown the amenability of the mitomycins with respect to bioconjugate approaches to drug delivery. Although the specific mechanism of action of the conjugates was not examined, these efforts (in combination with the system examined

by Tomasz) represent one of the more progressive aspects of mitomycin research. More intriguing however, is the mechanistic and structural analogies between the mitomycins and the recently discovered FR-900482 class of drugs detailed in chapters 2 and 3. The discovery of the FR-900482 class of compounds may thus be viewed as representing the most recent chapter in mitomycin research efforts.

## 1.6. CONCLUSION

The DNA interstrand cross-linking agents represent one of the most potent categories of antitumor antibiotics. This is due largely to the ability of such compounds to shut down DNA strand separation events crucial to replication and transcription. In addition to unique DNA sequence recognition properties resulting from structural considerations, many of these agents preferentially target specific regions based upon "activation" processes which are unique to a physiological region of interest. In addition to synthetic manipulations of the drug core structure aimed at enhancing or changing such activation processes, molecular biology has also come to play a role in selective drug triggering. The methodology of selective drug activation *via* protein over-expression is perhaps the most progressive field of study with respect to the DNA cross-linking agents. Also important has been the design/discovery of cross-linking agents based upon the concept of dimerization. The ability of the synthetic chemist to mix and match monoalkylating subunits of a dimeric agent clearly represents an important area for future research. Despite some thirty years of intense research, the interstrand cross-linking agents still represent an area of great therapeutic promise and intense interest. The interstrand cross-linking agents discussed herein are summarized below in Table 1-1.

**Table 1-1.** Summation of DNA-DNA interstrand cross-linking agents and their interactions within duplex DNA.

Agent or class thereof	agent #	interstrand cross-link specificity	related analogues	DNA groove occupancy
N-mustards	<b>1-5</b>	dG N <sup>7</sup> -dG N <sup>7</sup>	<b>14 - 18</b>	major
chloroethylnitroso-ureas (CNU)	<b>19</b>	dC N <sup>3</sup> -dG N <sup>1</sup>	<b>26</b>	major
1,3-dialkyl-3-acyltriazene	<b>27</b>	dC N <sup>3</sup> -dG N <sup>1</sup>	<b>38, 41</b>	major
Busulfan	<b>45a</b>	dG N <sup>7</sup> -dG N <sup>7</sup>	<b>45b - f</b>	major
clomesone	<b>46</b>	dC N <sup>3</sup> -dG N <sup>1</sup>	-	major
glycidaldehyde	<b>55</b>	not known	-	not known
diepoxybutane	<b>56</b>	dG N <sup>7</sup> -dG N <sup>7</sup>	-	major
carzinophilin/azinomycin B	<b>58</b>	dG N <sup>7</sup> -dG N <sup>7</sup> dG N <sup>7</sup> -dA N <sup>7</sup>	-	major
<i>cis</i> -diammine-dichloroplatinum (II)	<b>70</b>	dG N <sup>7</sup> -dG N <sup>7</sup>	<b>71 - 74</b>	major
carzinophilin A	<b>79</b>	not known	-	not known
isochrysohermidin	<b>80</b>	not known	-	not known
cyclopropylpyrrolo-indole dimers	<b>93a-k</b>	dA N <sup>3</sup> - dA N <sup>3</sup>	-	minor
Bizelesin	<b>94</b>	dA N <sup>3</sup> - dA N <sup>3</sup>	-	minor
pyrrolobenzo-diazepine dimers	<b>99,100</b>	dG N <sup>2</sup> -dG N <sup>2</sup>	-	minor
dinuclear <i>cis</i> -DDP dimers	<b>101-103</b>	dG N <sup>7</sup> -dG N <sup>7</sup>	<b>104,105</b>	major
8-methoxypsoralen	<b>106</b>	dT C <sup>5,6</sup> -dT C <sup>5,6</sup>	-	major
4,5',8-trimethyl-psoralen	<b>107</b>	dT C <sup>5,6</sup> -dT C <sup>5,6</sup>	-	major
cyclophosphamide	<b>122</b>	dG N <sup>7</sup> -dG N <sup>7</sup>	<b>123</b>	major
hexamethylmelamine	<b>135</b>	not known	<b>136,146</b>	minor
pyrrolizidine alkaloids	<b>150, 154-162</b>	dG N <sup>2</sup> - dG N <sup>2</sup>	<b>168-172</b>	minor
RSU-1069	<b>189</b>	not known	-	not known
aza-aromatic N-mustards	<b>197</b>	dG N <sup>7</sup> -dG N <sup>7</sup>	-	major
nitromin	<b>198</b>	dG N <sup>7</sup> -dG N <sup>7</sup>	-	major
chlorambucil N-oxide	<b>199</b>	dG N <sup>7</sup> -dG N <sup>7</sup>	-	major
Co(III)-mustards	<b>201-204</b>	dG N <sup>7</sup> -dG N <sup>7</sup>	-	major
daunorubicin	<b>209</b>	dG N <sup>2</sup> - dG N <sup>2</sup>	see Fig. 1-34	minor
adriamycin	<b>210</b>	dG N <sup>2</sup> - dG N <sup>2</sup>	see Fig. 1-34	minor
cyanomorphilino-adriamycin	<b>211</b>	dG N <sup>2</sup> - dG N <sup>2</sup>	see Fig. 1-34	minor
AZQ/DZQ	<b>234, 240</b>	dG N <sup>7</sup> -dG N <sup>7</sup>	-	major
mitomycins	<b>163, 251-254</b>	dG N <sup>2</sup> - dG N <sup>2</sup>	-	minor



## 1.7. REFERENCES

1. (a) *Self-Splicing of Group I Introns*, Cech, T.R., *Annu. Rev. Biochem.* (1990) **59**, 543. (b) *Structure and Activities of Group II Introns*, Michel, F.; Ferat, J.L., *Annu. Rev. Biochem.* (1995) **64**, 435; (c) Cech, T.R., (1993) In *The RNA World* (Gesteland R.F.; Atkins, J.F.; Eds.) pp. 239, Cold Spring Harbour, New York.
2. Voet, D., Voet J. G., (1990) *Biochemistry*. John Wiley & Sons, New York, pp 793-804.
3. (a) *Sequence-Specific Cleavage of Double Helical DNA by Triple Helix Formation*, Moser, H. D., Dervan, P.B. *Science* 1987, **238**, 645; (b) *Formation of a Three-Stranded Polynucleotide Molecule*, Felsenfeld, G., Davis, D.R., Rich, A. *J. Am. Chem. Soc.* 1957, **79**, 2023 ; (c) Felsenfeld, G., Miles, H.T. *Annu. Rev. Biochem.* 1967, **36**, 407.
4. *The Tumor Suppressor Genes*, Levine, A.J., *Annu. Rev. Biochem.* (1993) **65**, 623. and references cited therein.
5. (a) *Mechanisms of Transcriptional Synergism Between Distinct Virus-Inducible Enhancer Elements*, Maniatis, T.; Thanos, D.; Du, W., *Cell* (1993) **74**, 887; (b) *Transcription Factors: Structural Families and Principles of Recognition*, Pabo, C.O.; Sauer, R.T., *Annu. Rev. Biochem.* (1992) **61**, 1053.
6. (a) *DNA Excision Repair*, Sancar, A., *Annu. Rev. Biochem.* (1996) **65**, 43; (b) *O6-methylguanine Inhibits the Binding of Transcription Factors to DNA*, Bonfanti, M.; Broggini, M.; Prontera, C.; D'Incalci, M., *Nucleic Acids Research* (1991) **19**, 5739; (c) *Metal Dependence of Transcriptional Switching in Escherichia coli Ada*, Myers, L.C.; Jackow, F.; Verdine, G.L., *J. Biol. Chem.* (1995) **270**, 6664; (d) *Methylation Dependent Functional Switch Mechanism Newly Found in Escherichia coli Ada Protein*, Ohkubo, T.; Sakashita, H.; Sakuma, T.; Kainosho, M.; Sekiguchi, M.; Morikawa, *J. Am. Chem. Soc.* (1994) **116**, 6035.
7. (a) *Molecular structure of nucleic acids*, Watson, J.D. ; Crick, F.H.C., *Nature* (1953) **171**, 737.
8. *Genetic Implications of the Structure of Deoxyribonucleic Acid*, Watson, J.D.; Crick, F.H.C., *Nature* (1953) **171**, 964.
9. (a) *Eukaryotic DNA Replication*, Campbell, J.L., *Annu. Rev. Biochem.* (1986) **55**, 733; (b) *Single-stranded DNA Binding Proteins Required for DNA Replication*, Chase, J.W., Williams, K.R., *Annu. Rev. Biochem.* (1986) **55**, 103; (c) *DNA Replication*, Kornberg, A., *J. Biol. Chem.* (1988) **263**, 1; (d) *Prokaryotic DNA Replication Systems*, Nossal, N.G., *Annu. Rev. Biochem.* (1983) **52**, 581.
10. *The Replication of DNA in Escherichia Coli*, Meselson, M., Stahl, F.W., *Proc. Natl. Acad. Sci.* (1958) **44**, 671.



11. For excellent general reviews pertaining to the biological relevance of DNA interstrand cross-linking see (a) Kohn, K.W. (1994) in *Topics in Structural & Molecular Biology : 3) Molecular Aspects of Anti-cancer Drug Action* (Neidle, S., & Waring, M., Eds.) pp 315, Verlag Chemie GmbH, D-6940, Weinheim ; (b) *Alkylation of DNA and its Aftermath*, Lawley, P.D., *BioEssays* (1995) **17**, 561; (c) *Biological Relevance and Consequences of Chemical- or Metal-Induced DNA Cross-Linking*, Paustenbach, D.J., Finley, B.L., Kacew, S., *Proc. Soc. for Experimental Biology and Medicine*. (1996) **211**, 211; (d) *The Effects of DNA Covalent Adducts on in Vitro Transcription*, Gniazdowski, M., Cera, C., *Chem. Rev.* (1996) **96**, 619.
12. *Sequence Preferences of DNA Interstrand Cross-Linking Agents: Importance of Minimal DNA Structural Reorganization in the Cross-Linking Reaction of Mechlorethamine, Cisplatin, and Mitomycin C*, Hopkins, P.B.; Millard, J.T., Woo, J.; Weidner, M.F.; Kirchner, J.J.; Sigurdsson, S.T.; Raucher, S., *Tetrahedron* (1991) **47**, 2475.
13. *Inactivation of Bacteriophage T7 by Mono- and Difunctional Sulphur Mustards in Relation to Cross-linking and Depurination of Bacteriophage DNA*, Lawley, P.D.; Lethbridge, J.H.; Edwards, P.A.; Shooter, K.V., *J. Mol. Biol.* (1969) **39**, 181.
14. *Base-specific Arrest of in Vitro DNA Replication by Carcinogenic Chromium: Relationship to DNA Interstrand Cross-Linking*, Bridgewater, L.C.; Manning, F.C.R.; Patierno, S.R., *Carcinogenesis* (1994) **15**, 2421.
15. (a) Perone, V.B., *Microbial Toxins* (1972) **8**, 71; (b) Parrish, J.A.; Fitzpatrick, T.B.; Tanenbaum, L.; Pathak, M.A., *N. Engl. J. Med.* (1974) **291**, 1207; (c) Dall'Acqua, F.; Caffieri, S., *Photochem. Photobiol.* (1988) **10**, 1; (d) *Psoralen Photobiology*, Gasparro, F.P., *Photochem. Photobiol.* (1996) **63**, 553; (e) Parrish, J.A.; Stern, R.S.; Pathak, M.A.; Fitzpatrick, T.B. (1982) *Photochemotherapy of Skin Diseases*. In *The Science of Photomedicine* (Eds. Regan, J.D., Parrish, J.A.) pp. 595, Plenum Press, New York.
16. (a) *Homodinuclear (Pt,Pt) and Heterodinuclear (Ru,Pt) Metal Compounds as DNA-Protein Cross-Linking Agents: Potential Suicide DNA Lesions*, Van Houten, B.; Illenye, S.; Qu, Y.; Farrell, N., *Biochemistry* (1993) **32**, 11794; (b) *Photoreactivity of Platinum (II) in Cisplatin-Modified DNA Affords Specific Cross-Links to HMG Domain Proteins*, Lippard, S.J., Kane, S.A., *Biochemistry* (1996) **35**, 2180.
17. (a) *Reversible DNA*, Geiduschek, E.P., *Proc. Natl. Acad. Sci. U.S.A.* (1961) **47**, 950; (b) *A Molecular Mechanism of Mitomycin Action: Linking of Complementary DNA Strands*, Iyer, V.N.; Szybalski, W., *Proc. Natl. Acad. Sci. U.S.A.* (1963) **50**, 355; (c) *Inter-strand Crosslinking of DNA by Nitrogen Mustard*, Kohn, K.W.; Spears, C.L.; Doty, P., *J. Mol. Biol.* (1966) **19**, 266.
18. (a) *The Biological Actions and Therapeutic Applications of the B-Chloroethyl Amines and Sulfides*, Gilman, A.; Phillips, F.S., *Science* (1946) **103**, 409; (b) Haskel, C.M., *Cancer Treatment*, (2nd edition), (1990) Saunders, Philadelphia.
19. *The Alkylation of Guanosine and Guanylic Acid*, Brookes, P.; Lawley, P.D., *J. Chem. Soc.* (1961), 3923.
20. Brookes, P.; Lawley, P.D., *Biochem. J.* (1961), **80**, 496.

21. *Formation and Removal of DNA Cross-Links Induced by Melphalan and Nitrogen Mustard in Relation to Drug-induced Cytotoxicity in Human Melanoma Cells*, Hansson, J.; Lewensohn, R.; Ringborg, U.; Nilsson, B. *Cancer Res.* (1987) **47**, 2631.
22. (a) *Mechlorethamine Cross-Links Deoxyguanosine Residues at 5' GNC Sequences in Duplex DNA Fragments*, Hopkins, P.B.; Raucher, S.; Millard, J.T., *J. Am. Chem. Soc.* (1990) **112**, 2459; (b) *Synthesis of a Duplex Oligonucleotide Containing a Nitrogen Mustard Interstrand DNA-DNA Cross-Link*, Ojwang, J.O.; Grueneberg, D.A.; Loechler, E.L. *Cancer Research* (1989) **49**, 6529.
23. *Covalent Structure of a Nitrogen Mustard-Induced DNA interstrand Cross-Link: An N7-to-N7 Linkage of Deoxyguanosine Residues at the Duplex Sequence 5'-d(GNC)*, Rink, S.M.; Solomon, M.S.; Taylor, M.J.; Sharanabasava, R.B.; McLaughlin, L.W.; Hopkins, P.B., *J. Am. Chem. Soc.* (1993) **115**, 2551.
24. *Efficient, Specific Interstrand Cross-Linking of Double-Stranded DNA by a Chlorambucil-Modified, Triplex-Forming Oligonucleotide*, Kutayavin, I.V.; Gamper, H.B.; Gall A.A.; Meyer, R.B. Jr., *J. Am. Chem. Soc.* (1993) **115**, 9303.
25. (a) *Targeting of Cytotoxic Agents by Polyamine Synthesis of a Chlorambucil-Spermidine Conjugate*, Cohen, G.M.; Cullis, P.M.; Hartley, J.A.; Mather, A.; Symons, M.C.R.; Wheelhouse, R.T., *J. Chem. Soc., Chem. Commun.* (1992) 298; (b) *Targeting of Tumor Cells and DNA by a Chlorambucil-Spermidine Conjugate*, Holley, J.P.; Mather, A.; Wheelhouse, R.T.; Cullis, P.M.; Hartley, J.A.; Bingham, J.P.; Cohen, G.M., *Cancer Res.* (1992) **52**, 4190.
26. (a) *Polyamine Metabolism and Function*, Pegg, A.E.; McCann, P.P., *Am. J. Physiol.* (1982) **243**, C212; (b) *Polyamine Transport in Mammalian Cells*, Seiler, N.; Dezuere, F., *Int. J. Biochem.* (1990) 211; (c) *Polyamines in Rapid Growth and Cancer*, Janne, J.; Poso, H.; Raina, A., *Biochim. Biophys. Acta* (1978) **473**, 241; (d) *Antiproliferative Properties of Polyamine Analogues: A Structure-Activity Study*, Bergeron, R.J.; McManis, J.S.; Liu, C.Z.; Feng, Y.; Weimar, W.R.; Luchetta, G.R.; Wu, Q.; Ortiz-Ocasio, J.; Vinson, J.R.T.; Kramer, D.; Porter, C., *J. Med. Chem.* (1994) **37**, 3464.
27. *Synthesis and Evaluation of Novel Spermidine Derivative as Targeted Cancer Chemotherapeutic Agents*, Stark, P.A.; Thrall, B.D.; Meadows, G.G.; Abdel-Monem, M.M., *J. Med. Chem.* (1992) **35**, 4264.
28. *DNA-Directed Alkylating Ligands as Potential Antitumor Agents: Sequence Specificity of Alkylation by Intercalating Aniline Mustards*, Prakash, A.S.; Denny, W.A.; Gourdie, T.A.; Value, K.K.; Woodgate, P.D. Wakelin, L.P.G., *Biochemistry* (1990) **29**, 9799.
29. *Identification of the Major Lesion from the Reaction of an Acridine-Targeted Aniline Mustard with DNA as an Adenine N1 Adduct*, Boritzki, T.J.; Palmer, B.D.; Coddington, J.M.; Denny, W.A., *Chem. Res. Toxicol.* (1994) **7**, 41.
30. Gregory L. Verdine, Ph.D. thesis Columbia 1986. and references therein.

31. (a) *Nitrosourea Chemotherapy for Primary Malignant Gliomas*, Levin, V.A.; Wilson, C.B., *Cancer Treat. Rep.* (1976) **60**, 719; (b) Prestayko, A.W.; Crooke, S.T.; Baker, L.H.; Carter, S.K.; Schein, P.S., Eds. (1981) In *Nitrosoureas: Current Status and New Developments*, Academic Press, New York.
32. *Sequence-selective Depurination, DNA Interstrand Cross-Linking and DNA Strand Break Formation Associated with Alkylated DNA*, Prakash, S.S.; Gibson, N.W., *Carcinogenesis* (1992) **13**, 425; (b) *DNA Sequence Selectivity of Guanine-N7 Alkylation by Three Antitumor Chloroethylating Agents*, Hartley, J.A.; Gibson, N.W. Kohn, K.W. Mattes, W.B., *Cancer Research* (1986) **46**, 1943; (c) *Formation of the Cross-Link 1-[N<sup>3</sup>-Deoxycytidyl],2-[N<sup>1</sup>-deoxyguanosinyl]-ethane in DNA Treated with N,N'-Bis(2-Chloroethyl)-N-Nitrosourea*, Tong, W.P.; Kirk, M.C.; Ludlum, D.B., *Cancer Research* (1982) **42**, 3102.
33. *Reaction of N-(2-Chloroethyl)-N-nitrosoureas with DNA: Effect of Buffers on DNA Adduction, Cross-Linking and Cytotoxicity*, Chen, F.X.; Bodell, W.J.; Liang, G.; Gold, B., *Chem. Res. Toxicol.* (1996) **9**, 208.
34. *DNA Alkylation by the Haloethylnitrosoureas: Nature of Modifications Produced and their Enzymatic Repair or Removal*, Ludlum, D.B., *Mutation Res.* (1990) **233**, 117.
35. *Interstrand Cross-linking of DNA by 1,3-Bis(2-chloroethyl)-1-nitrosourea and Other 1-(2-haloethyl)-1-nitrosoureas*, Kohn, D.W., *Cancer Res.* (1977) **37**, 1450.
36. *Cross-Linking of DNA Induced by Chloroethylnitrosourea is Prevented by O<sup>6</sup>-Methylguanine-DNA Methyltransferase*, Robins, P.; Harris, A.L.; Goldsmith, I.; Lindahl, T., *Nucleic Acids Res.* (1983) **11**, 7743.
37. *DNA cross-linking and monoadduct repair in nitrosourea-treated human tumour cells*, Erickson, L.C.; Laurent, G.; Sharkey, N.A.; Kohn, K.W., *Nature* (1980) **288**, 727.
38. *DNA Cross-linking, Sister Chromatid Exchange and Cytotoxicity of N-2-Chloroethylnitrosoureas Tethered to Minor Groove Binding Peptides*, Gold, B.; Bodell, W.J.; Chen, F.X.; Zhang, Y.; Church, K.M., *Carcinogenesis* (1993) **14**, 935.
39. *Base Sequence Selectivity in the Alkylation of DNA by 1,3-Dialkyl-3-acyltriazines*, Kroeger-Smith, M.B.; Taneyhil, L.A.; Michejda, C.J.; Smith, R.H. Jr., *Chem. Res. Toxicol.* (1996) **9**, 341 and references cited therein.

40. Excellent papers describing both decomposition routes are (a) *1,3-Dialkyl-3-Acyltriazenes: Products and Rates of Decomposition in Acidic and Neutral Aqueous Solutions*, Smith, R.H. Jr.; Wladkowski, B.D.; Herling, J.A.; Pfaltzgraff, T.D.; Pruski, B.; Klose, J.; Michejda, C.J., *J. Org. Chem.* (1992) **57**, 654; (b) *Novel Cross-Linking Alkylating Agents, 1-(2-Chloroethyl)-3-methyl-3-acyltriazene*s, Smith, R.H. Jr.; Mehl, A.F.; Shantz, D.L. Jr.; Chmurny, G.N.; Michejda, C.J., *J. Org. Chem.* (1988) **53**, 1467; (c) Lown, J.W.; Koganty, R.R.; Bhat, U.G.; Chauhan, S.M.S., (1986) *Isolation and Characterization of Electrophiles from 2-haloethylnitrosoureas forming cytotoxic DNA Cross-Links and Cyclic Nucleotide Adducts and the analysis of Base Site-Selectivity by ab initio calculations*. In *The Role of Cyclic Nucleic Acid Adducts in Carcinogenesis and Mutagenesis* (Singer, B.; Bartsch, H.; Eds.) IARC Publications No. 70, pp 136 International Agency for Research on Cancer, Lyon; (d) *Structure-Activity Relations of (2-Chloroethyl)nitrosoureas. 2. Kinetic Evidence of a Novel Mechanism for the Cytotoxically Important DNA Cross-Linking Reactions of (2-Chloroethyl)nitrosoureas*, Buckley, N.; Brent, T.P., *J. Am. Chem. Soc.* (1988) **110**, 7520.
41. *Formation of the Cross-Linked Base, Diguanylethane, in DNA Treated with N,N'-Bis(2-chloroethyl)-N-nitrosourea*, Ludlum, D.B.; Tong, W.P., *Cancer Res.* (1981) **41**, 380.
42. *Specificity of DNA Alkylation by 1-(2-Chloroethyl)-3-alkyl-3-acyltriazene*s Depends on the Structure of the Acyl Group: Kinetic and Product Studies, Kroeger Smith, M.B.; Schmidt, B.F.; Czerwinski, G.; Taneyhill, L.A.; Snyder, E.J.; Kline, A.M.; Michejda, C.J.; Smith, R.H. Jr., *Chem. Res. Toxicol.* (1996) **9**, 466.
43. *Peptide-linked 1,3-dialkyl-3-acyltriazene*s: Gastrin Receptor Directed Antineoplastic Alkylating Agents, Schmidt, B.F.; Hernandez, L.; Rouzer, C.; Czerwinski, G.; Chmurny, G.; Michejda, C.J., *J. Med. Chem.* (1994) **37**, 3812.
44. (a) *Differential cytotoxicity and DNA-damaging effects produced in human cells of the Mer<sup>+</sup> and Mer<sup>-</sup> phenotypes by a series of alkyltriazenylimidazoles*, Gibson, N.W.; Hartley, J.; LaFrance, R.J.; Vaughan, K., *Carcinogenesis* (1986) **7**, 259; (b) *Experimental Antitumor Activity against Murine Tumor Model Systems of 8-Carbamoyl-3-(2-chloroethyl)imidazo[5,1-d]-1,2,3,5-tetrazin-4(3H)-one (Mitozolomide), a Novel Broad-Spectrum Agent*, Hickman, J.A.; Stevens, M.F.G.; Langdon, S.P.; Fizames, C.; Lavelle, F.; Atassi, G.; Lunt, E.; Tilson, R.M., *Cancer Res.* (1985) **45**, 3008.
45. Bedford, P.; Fox, B.W., *Biochem. Pharmacol.* (1983) **32**, 2297.
46. (a) Hartley, J.A.; Fox, B.W., *Cancer Chemother. Pharmacol.* (1986) **17**, 56; (b) *Mechanisms of Toxicity of Hepsulfan in Human Tumor Cell Lines*, Pacheco, D.Y.; Cook, C.; Hincks, J.R.; Gibson, N.W., *Cancer Res.* (1990) **50**, 7555; (c) *Comparison of the Mechanism of Action of Busulfan with Hepsulfan, a New Antileukemic Agent, in the L1210 Cell Line*, Pacheco, D.Y.; Stratton, N.K.; Gibson, N.W., *Cancer Res.* (1989) **49**, 5108.
47. (a) Brookes, P.; Lawley, P.D., *Biochem. J.* (1961) **80**, 496; (b) *Crosslinking of DNA by Busulfan: Formation of Diguanyl Derivatives*, Tong, W.P.; Ludlum, D.B., *Biochim. Biophys. Acta* (1980) **608**, 174.



48. (a) *2-Chloroethyl (Methylsulfonyl)methanesulfonate (NSC-338947), a More Selective DNA Alkylating Agent Than the Chloroethylnitrosoureas*, Gibson, N.W.; Hartley, J.A.; Strong, J.M.; Kohn, K.W., *Cancer Res.*, (1986) **46**, 553; (b) *Effect of O<sup>6</sup>-Alkylguanine Pretreatment on the Sensitivity of Human Colon Tumor Cells to the Cytotoxic Effects of Chloroethylating Agents*, Pegg, A.E.; Dolan, M.E.; Young, G.S., *Cancer Res.*, (1986) **46**, 4500; (c) *Effect of O<sup>6</sup>-Methylguanine on DNA Interstrand Cross-Link Formation by Chloroethylnitrosoureas and 2-Chloroethyl(methylsulfonyl)methanesulfonate*, Dolan, M.E.; Pegg, A.E.; Hora, N.K.; Erickson, L.C., *Cancer Res.*, (1988), **48**, 3603; (d) *Formation of DNA Interstrand Cross-Links by the Novel Chloroethylating Agent 2-Chloroethyl(methylsulfonyl)methanesulfonate: Suppression by O<sup>6</sup>-Alkylguanine-DNA Alkyltransferase Purified from Human Leukemic Lymphoblasts*, Brent, T.P.; Lestrud, S.O.; Smith, D.G.; Remack, J.S., *Cancer Res.*, (1987) **47**, 3384.
49. (a) *Identification of 7-(2-hydroxyethyl)guanine as a product of alkylation of calf thymus DNA with Clomesone*, Struck, R.F.; Alexander, J.A.; McCain, D.M.; Shealy, Y.F.; Rose, L.M., *Biochem. Pharmacol.*, (1991) **41**, 457; (b) Kann, H.E., Jr. In *Nitrosoureas: Current Status and New Developments*; Prestayko, A.W.; Baker, L.H.; Crooke, S.T.; Carter, S.K.; Schein, P.S., Eds.; Academic: Orlando, FL, 1981; pp 95-105.
50. (a) *Alkylation of Polyguanylic Acid at the 2-Amino Group and Phosphate by the Potent Mutagen (±)-7b,8a-Dihydroxy-9b,10b-epoxy-7,8,9,10-tetrahydro-benzo[a]pyrene*, Moore, P.D.; Koreeda, M., *J. Am. Chem. Soc.* (1976) **98**, 6720; (b) *Base Sequence-Dependent Bends in Site-Specific Benzo[a]pyrene Diol Epoxide-Modified Oligonucleotide Duplexes*, Liu, T.; Xu, J.; Tsao, H.; Li, B.; Xu, R.; Yang, C.; Smin, S.; Moriya, M.; Geacintov, N.E., *Chem. Res. Toxicol.* (1996) **9**, 255; and references cited therein.
51. (a) *Mutagenic Selectivity at the HPRT Locus in V-79 Cells: Comparison of mutations caused by Bay-region Benzo[a]pyrene 7,8-diol-9,10-epoxide Enantiomers with high and low Carcinogenic Activity*, Wei, S.J.C.; Chang, R.L.; Hennig, E.; Cui, X.X.; Merkler, K.A.; Wong, C.Q.; Yagi, H.; Conney, A.H., *Carcinogenesis* (1994) **15**, 1729; (b) *Mutation in Mammalian Cells by Stereoisomer of Anti-benzo[a]pyrene diol Epoxide in Relation to the Extent and Nature of the DNA Reaction Products*, Brookes, P.; Osborne, M.R., *Carcinogenesis* (1982) **3**, 1223; (c) *Differences in Mutagenicity of the Optical Enantiomers of the Diastereomeric Benzo[a]pyrene 7,8-diol-9,10-epoxides*, Wood, A.W.; Chang, R.L.; Levin, W.; Yagi, H.; Thakker, D.R.; Jerina, D.M.; Conney, A.H., *Biochem. Biophys. Res. Commun.* (1977) **77**, 1389; (d) *Double-Stranded DNA Stereoselectively Binds Benzo[a]pyrene Diol Epoxides*, Meehan, T.; Straub, K., *Nature* (1979) **277**, 410.
52. (a) *Template Activity of Calf Thymus DNA Modified by a Dihydrodiol Epoxide Derivative of Benzo[a]pyrene*, Leffler, S.; Pulkrabek, P.; Weinstein, I.B., *Biochemistry* (1977) **16**, 3133; (b) *Effect of Carcinogenic Adducts on Transcription by T7 RNA Polymerase*, Nath, S.T.; Lee, M.S.; Romano, L.J., *Nucleic Acids Res.* (1987) **15**, 4257; (c) *Site-Specific Benzo[a]pyrene Diol Epoxide-DNA Adducts Inhibit Transcription Elongation by Bacteriophage T7 RNA Polymerase*, Choi, D.J.; Marino-Alessandri, D.J.; Geacintov, N.E.; Scicchitano, D.A., *Biochemistry* (1994) **33**, 780.

53. (a) *Inhibition of DNA Synthesis in vitro by Binding of Benzo[a]pyrene Metabolite Diol Epoxide I to DNA*, Mizusawa, H.; Kadefuda, T., *Nature* (1979) **279**, 75; (b) *Inhibition of DNA Synthesis by an Electrophilic Metabolite of Benzo[a]pyrene*, Busbee, D.L.; Joe, C.O.; Norman, J.O.; Rankin, P.W., *Proc. Natl. Acad. Sci. U.S.A.* (1984) **81**, 5300; (c) *Influence of Template Strandedness on in vitro Replication of Mutagen-Damaged DNA*, Larson, K.L.; Strauss, B.S., *Biochemistry* (1987) **26**, 2471.
54. (a) *Benzo[a]pyrene-DNA Adducts Inhibit Translocation by the Gene 4 Protein of Bacteriophage T7*, Brown, W.C.; Romano, L.J., *J. Biol. Chem.* (1989) **263**, 6748; (b) *Benzo[a]pyrene-DNA Adducts Inhibit the DNA Helicase Activity of the Bacteriophage T7 Gene 4 Protein*, Yong, Y.; Romano, L.J., *Chem. Res. Toxicol.* (1996) **9**, 179.
55. (a) *Aflatoxin B<sub>1</sub> -2,3-oxide as a Probable Intermediate in the Covalent Binding of Aflatoxins B<sub>1</sub> and B<sub>2</sub> to Rat Liver DNA and Ribosomal RNA in Vivo*, Swenson, D.H.; Lin, H.K.; Miller, E.C.; Miller, J.A., *Cancer Res.* (1977) **37**, 172; (b) *Photochemical Epoxidation of Aflatoxin B<sub>1</sub> and Sterigmatocystin: Synthesis of Guanine Containing Adducts*, Büchi, G.; Fowler, K.W.; Nadzan, A.M., *J. Am. Chem. Soc.* (1982) **104**, 544; (c) *Sterigmatocystin-DNA Interactions: Identification of a Major Adduct Formed after Metabolic Activation in Vitro*, Essigmann, J.M.; Barker, L.J.; Fowler, K.W.; Francisco, M.A.; Reinhold, V.N.; Wogan, G.N., *Proc. Natl. Acad. Sci. U.S.A.* (1979) **76**, 179.
56. *Hydrolysis of Bisphenol A Diglycidylether by Epoxide Hydrolases in Cytosolic and Microsomal Fractions of mouse Liver and skin: Inhibition by Bisepoxycyclopentylether and the Effects upon the Covalent Binding to Mouse Skin DNA*, Bently, P.; Bieri, F.; Kuster, H.; Muakkassah-Kelly, S.; Sagelsdorff, P.; Staubli, W.; Waechter, F., *Carcinogenesis* (1989) **10**, 321.
57. *Alkylation by Propylene Oxide of Deoxyribonucleic Acid, Adenine, Guanosine and Deoxyguanylic Acid*, Lawley, P.D.; Jarman, M., *Biochem. J.* (1972) **126**, 893.
58. *Alkylation Products of DNA Bases by Simple Epoxides*, Hemminki, K.; Paasivirta, J.; Kurkirinne, T.; Virkki, L., *Chem.-Biol. Interactions* (1980) **30**, 259.
59. (a) *Determination of the Structure of the Adduct from Guanosine and Glycidaldehyde*, Nair, V.; Turner, G.A., *Tetrahedron Lett.* (1984) **25**, 247; (b) *Reaction of DNA with Glycidaldehyde: Isolation and Identification of a Deoxyguanosine Reaction Product*, Van Duuren, B.L.; Lowengart, G., *J. Biol. Chem.* (1977) **252**, 5370; (c) *Structure Determination of Adducts from the Reaction of (R)-Glycidaldehyde and Guanosine*, Watson, W.P.; Kennedy, G.; Golding, B.T., *Carcinogenesis* (1990) **11**, 865; (d) *Non-B DNA Structure: Preferential Target for the Chemical Carcinogen Glycidaldehyde*, Kohwi, Y., *Carcinogenesis* (1989) **10**, 2035.
60. *Cytotoxic Agents: II, Bis-epoxides and related compounds*, Hendry, J.A.; Rose, F.L.; Homer, R.F.; Walpole, A.L.; *Br. J. Pharmacol.* (1951) **6**, 235.
61. *Interstrand Cross-linking of DNA by Difunctional Alkylating Agents*, Lawley, P.D.; Brookes, P., *J. Mol. Biol.* (1967) **25**, 143.

62. *Diepoxybutane Cross-Links DNA at 5'-GNC Sequences*, Millard, J.T.; White, M.M., *Biochemistry* (1993) **32**, 2120.
63. (a) Hata, T.; Koga, F.; Sano, Y.; Kanamori, K.; Matsumae, A.; Sugawara, R.; Shima, T.; Ito, S.; Tomizawa, S., *J. Antibiot., Ser. A, (Tokyo)*, (1954) **7**, 107; (b) Yokoi, K.; Nagaoka, K.; Nakashima, T., *Chem. Pharm. Bull.* (1986) **34**, 4554; (b) Matsumoto, M.; Oono, J.; Yokoi, K.; Ishizeki, S.; Nakashima, T., *J. Antibiot.* (1986) **39**, 1527; (c) Ishizaki, S.; Ohtsuka, M.; Irinoda, K.; Nagaoka, K.; Nakashima, T., *J. Antibiot.* (1987) **40**, 60.
64. *Novel Interstrand Cross-Links Induced by the Antitumor Antibiotic Carzinophilin/Azinomycin B*, Armstrong R.W.; Salvati, M.E.; Nguyen, M., *J. Am. Chem. Soc.* (1992) **114**, 3144.
65. *Synthesis, Chemical Property, and Cytotoxicity of the Carzinophilin Congeners Carrying a 2-(1-Acylamino-1-alkoxycarbonyl)methylidene-1-azabicyclo-[3.1.0]-hexane System.*, Hashimoto, M.; Matsumoto, M.; Yamada, K.; Terashima, S., *Tetrahedron Lett.* (1994) **35**, 2207.
66. For excellent reviews on cisplatin see: (a) *Improved Understanding in Platinum Antitumor Chemistry*, Reedijk, J., *J. Chem. Soc., Chem. Commun.*, (1996) 801; (b) *Structural Aspects of Platinum Anticancer Drug Interactions with DNA*, Sherman, S.E.; Lippard, S.J., *Chem. Rev.* (1987) **87**, 1153; (c) Lippard, S.J. (1991) in *Platinum and Other Metal Coordination Compounds in Cancer Chemotherapy* (Howell, S.B., Ed.) pp 1-10, Plenum Press, New York.
67. Rosenberg, B.; VanCamp, L.; Krigas, T. *Nature* (1965) **205**, 698.
68. *The Inhibition of Growth or Cell Division in Escherichia coli by Different Ionic Species of Platinum (IV) Complexes*, Rosenberg, B.; VanCamp, L.; Grimley, E.B.; Thomson, A.J., *J. Biol. Chem.* (1967) **242**, 1347.
69. (a) *Base-pair substitution hotspots in GAG and GCG nucleotide sequences in Escherichia coli K-12 induced by cis-diamminedichloroplatinum (II)*, Brouwer, J., van de Putte, P.; Fichtinger-Schepman, A.M.J.; Reedijk, J., *Proc. Natl. Acad. Sci. U.S.A.* (1981) **78**, 7010; (b) Bubley, G.J.; Ashburner, B.P.; Teicher, B.A., *Mol. Carcinogenesis* (1991) **4**, 397; (c) *In Vitro Mutational Specificity of Cisplatin in the Human Hypoxanthine Guanine Phosphoribosyl-transferase Gene*, Cariello, N.F.; Swenberg, J.A.; Skopek, T.R., *Cancer Res.* (1992) **52**, 2866.
70. (a) *Spectrum of DNA-Platinum Adduct Recognition by Prokaryotic and Eukaryotic DNA-Dependent RNA Polymerases*, Corda, Y.; Job, C.; Anin, M.F.; Leng, M.; Job, D., *Biochemistry* (1993) **32**, 8582; (b) Brown, S.J.; Kellett, P.J.; Lippard, S.J., *Science* (1993) **261**, 603; (c) Treiber, D.K.; Zhai, X.; Jantzen, H.M.; Essigman, J.M., *Proc. Natl. Acad. Sci. U.S.A.* (1994) **91**, 5672; (d) *Specific Binding of Chromosomal Protein HMG1 to DNA Damaged by the Anticancer Drug Cisplatin*, Pil, P.M.; Lippard, S.J., *Science* (1992) **256**, 234.
71. Lim, M. C.; Martin, R.B., *J. Inorg. Nucl. Chem.* (1976) **38**, 1911.

72. (a) *Chlorotriammineplatinum(II) Ion. Acid Hydrolysis and Isotopic Exchange of Chloride Ligand*, Aprile, F.; Martin, D.S., *Inorg. Chem.* (1962) **1**, 551; (b) *cis-Dichlorodiammineplatinum(II). Acid Hydrolysis and Isotopic Exchange of the Chloride Ligands*, Reishus, J.W.; Martin, D.S., *J. Am. Chem. Soc.* (1961) **83**, 2457.
73. (a) Dedon, P.C.; Qazi, R.; Borch, R.F., (1986) In *Biochemical Mechanisms of Platinum Antitumour Drugs* (McBrien, D.C.H.; Slater, T.F., Eds.) pp 199, IRL Press, Oxford.
74. *Intermolecular Displacement of S-Bound L-Methionine on Platinum (II) by Guanosine 5'-monophosphate: Implications for the Mechanism of Action of Anticancer Drugs*, Barnham, K.J.; Djuran, M.I.; Murdoch, P.D.S.; Sadler, P.J., *J. Chem. Soc. Chem. Commun.* (1994) 721.
75. *Unprecedented Migration of [Pt(dien)]<sup>2+</sup> (dien = 1,5-diamino-3-azapentane) from Sulfur to Guanosine-N<sup>7</sup> in S-Guanosyl-L-homocysteine (sgh)*, van Boom, S.S.G.E.; Reedijk, J., *J. Chem. Soc., Chem. Commun.* (1993) 1397.
76. Wilkins, R.G. (1991) In *Kinetics and Mechanism of Reactions of Transition Metal Complexes.*, pp 235 VCH, Weinheim.
77. (a) *Structure and Isomerization of an Intrastrand Cisplatin-Cross-Linked Octamer DNA Duplex by NMR Analysis.*, Yang, D.; van Boom, S.S.G.E.; Reedijk, J.; van Boom, J.H.; Wang, A.H.-J., *Biochemistry* (1995) **34**, 12912; (b) *Interstrand Cross-Links are Preferentially Formed at the d(GC) sites in the Reaction Between cis-diamminedichloroplatinum (II) and DNA*, Lemaire, M.A.; Schwartz, A.; Rahmouni, A.R.; Leng, M., *Proc. Natl. Acad. Sci. U.S.A.* (1991) **88**, 1982; (c) *Base Sequence-Independent Distortions Induced by Interstrand Cross-Links in cis-diamminedichloroplatinum (II)-Modified DNA*, Malinge, J.M.; Pérez, C.; Leng, M., *Nucleic Acids Res.* (1994) **22**, 3834.
78. *Mutagenicity and Genotoxicity of the Major DNA Adduct of the Antitumor Drug cis-Diamminedichloroplatinum (II)*, Bradley, L.J.N.; Yarema, D.J.; Lippard, S.J.; Essigmann, J.M., *Biochemistry* (1993) **32**, 982 and references cited therein.
79. *Solution Structure of a Cisplatin-Induced DNA Interstrand Cross-Link*, Huang, H.; Zhu, L.; Reid, B.R.; Drobny, G.P.; Hopkins, P.B., *Science* (1995) **270**, 1842.
80. For a detailed overview of mutagenic events resulting from generation of abasic sites in DNA see: *Mutagenesis by Apurinic/Apyrimidinic Sites*, Loeb, L.A.; Preston, B.D., *Annu. Rev. Genet.* (1986) **20**, 201.
81. (a) *Effects of Geometric Isomerism and Ligand Substitution in Bifunctional Dinuclear Platinum Complexes on Binding Properties and Conformational Changes in DNA*, Farrell, N.; Appleton, T.G.; Qu, Y.; Roberts, J.D.; Soares Fontes, A.P.; Skov, K.A.; Wu, P.; Zou, Y., *Biochemistry* (1995) **34**, 15480; (b) *A Novel DNA Structure Induced by the Anticancer Bisplatinum Compound Cross-linked to a GpC Site in DNA*, Yang, D.; van Boom, S.S.G.E.; Reedijk, J.; van Boom, J.H.; Farrell, N.; Wang, A.H.-J., *Nature Structural Biology* (1995) **2**, 577.



82. (a) *DNA Bending at Adenine-Thymine Tracts*, Crothers, D.M.; Wu, H.M.; Koo, H.S., *Nature* (1986) **320**, 501; (b) *DNA Bend Direction by Phase Sensitive Detection*, Zinkel, S.S.; Crothers, D.M., *Nature* (1987) **328**, 178.
83. *Sequence-Specific DNA Binding by a Short Peptide Dimer*, Talanian, R.V.; McKnight, J.C.; Kim, P.S., *Science* (1990) **249**, 769.
84. *An Agarose Gel Method for the Determination of DNA Interstrand Cross-linking Applicable to the Measurement of the Rate of Total and "Second-Arm" Cross-link Reactions*, Hartley, J.A.; Berardini, M.D.; Souhami, R.L., *Anal. Biochem.* (1991) **193**, 131.
85. Barton, J.K., personal communication.
86. *Structure and Function of the Antitumor Antibiotic Carzinophilin A: The First Natural Intercalative Bisalkylator*, Lown, W.J., Hanstock C.C., *J. Am. Chem. Soc.* (1982) **104**, 3213.
87. Dugas, H., (1996) In *Bioorganic Chemistry: A Chemical Approach to Enzyme Action*, pp 146., Springer, New York.
88. *d,l- and meso-Isochrysohermidin: Total Synthesis and Interstrand DNA Cross-Linking*, Boger, D.L.; Baldino, C.M., *J. Am. Chem. Soc.* (1993) **115**, 11418.
89. (a) *Chemistry of Thermal Degradation of Abasic Sites in DNA. Mechanistic Investigation on Thermal DNA Strand Cleavage of Alkylated DNA*, Sugiyama, H.; Fujiwara, T.; Ura, A.; Tashiro, T.; Yamamoto, K.; Kawanishi, S.; Saito, I., *Chem. Res. Toxicol.* (1994) **7**, 673; (b) *DNA Interstrand Cross-Links Induced by Cyclopropylpyrroloindole Antitumor Agent Bizelesin Are Reversible Upon Exposure to Alkali*, Lee, C.-Soon.; Gibson, N.W., *Biochemistry* (1993) **32**, 9108.
90. *Interstrand DNA Cross-Linking with Dimers of the Spirocyclopropyl Alkylating Moiety of CC-1065*, Mitchell, M.A.; Johnson, P.D.; Williams, M.G.; Aristoff, P.A., *J. Am. Chem. Soc.* (1989) **111**, 6428.
91. The alkaline agarose gel electrophoresis assay was applied in the detection of gel-retarded (interstrand cross-linked) Hae III restriction digest fragments of the plasmid DNA ØX174. Generation of slow mobility fragments was judged by comparison to control samples devoid of drug treatment.
92. The synthesis of Bizelesin followed the promising results obtained with the aliphatically linked dimers of general structure **93**. See: *Synthesis and DNA Cross-Linking by a Rigid CPI Dimer*, Mitchell, M.A.; Kelly, R.C.; Wicnienski, N.A.; Hatzenbuehler, N.T.; Williams, M.G.; Petzold, G.L.; Slightom, J.L.; Siemieniak, D.R., *J. Am. Chem. Soc.* (1991) **113**, 8994.
93. (a) *Nucleotide Preferences for DNA Interstrand Cross-Linking Induced by the Cyclopropylpyrroloindole Analogue U-77,779*, Gibson, N.W.; Lee, C.-Soon., *Biochemistry* (1993) **32**, 2592. (b) *Cross-Linkage by "Intact" Bizelesin and Bisalkylation by the "Separated Halves" of the Bizelesin Dimer: Contrasting Drug Manipulation of DNA Conformation (5'-TAATTA-3') Directs Alkylation Toward Different Adenine Targets*, Seaman, F.C.; Chu, J.; Hurley, L., *J. Am. Chem. Soc.* (1996) **118**, 5383.

94. *Determination of the Structural Role of the Internal Guanine-Cytosine Base Pair in Recognition of a Seven-Base-Pair Sequence Cross-Linked by Bizelesin*, Thompson, A.S.; Fan, J.Y.; Sun, D.; Hansen, M.; Hurley, L.H., *Biochemistry* (1995) **34**, 11005.
95. *Design and Synthesis of Potential DNA Cross-Linking Reagents Based on the Anthramycin Class of Minor Groove Binding Compounds*, Confalone, P.N.; Huie, E.M.; Ko, S.S.; Cole, G.M., *J. Org. Chem.* (1988) **53**, 482.
96. (a) Hurley, L.H.; Reck, T.; Thurston, D.E.; Lanley, D.R., *Chem. Res. Toxicol.* (1988) **1**, 258; (b) Barkley, M.D.; Thomas, T.J.; Maskos, K.; Remers, W.A., *Biochemistry* (1991) **30**, 4421; (c) Kohn, K.W.; Glaubiger, D.; Spears, C.L., *Biochim. Biophys. Acta* (1974) **361**, 288.
97. *Pyrrolo(1,4)benzodiazepine Antitumor Antibiotics: In Vitro Interaction of Anthramycin, Sibiromycin and Tomaymycin with DNA Using Specifically Radiolabelled Molecules*, Hurley, L.H.; Gairola, C.; Zmijewski, M., *Biochim. Biophys. Acta* (1977) **475**, 521.
98. (a) *Pyrrolo[1,4]benzodiazepine Antitumor Antibiotics; Chemistry, Interactions with DNA and Biological Implications*, Hurley, L.H.; Thurston, D.E., *Pharm. Res.* (1984) **2**, 52. and references cited therein; (b) *DNA Sequence Specificity of the Pyrrolo[1,4]benzodiazepine Antitumor Antibiotics. Methidiumpropyl-EDTA-iron (II) Footprinting analysis of DNA Binding Sites for Anthramycin and Related Drugs.*, Hertzberg, R.P.; Hecht, S.M.; Reynolds, V.L.; Molineux, I.J.; Hurley, L.H., *Biochemistry* (1986) **25**, 1249.
99. *Synthesis of a Novel GC-Specific Covalent-Binding DNA Affinity-Cleavage Agent based of Pyrrolobenzodiazepines (PBDs)*, Thurston, D.D.; Morris, S.J.; Hartley, J.A., *J. Chem. Soc., Chem. Commun.* (1996) 563.
100. *Design of B-DNA Cross-Linking and Sequence-Reading Molecules*, Walker, W.L.; Kopka, M.L.; Filipowsky, M.E.; Dickerson, R.E.; Goodsell, D.S., *Biopolymers* (1995) **35**, 543.
101. *Rational Design of A Highly Efficient Irreversible DNA Interstrand Cross-Linking Agent Based on the Pyrrolobenzodiazepine Ring System*, Bose, D.S.; Thompson, A.S.; Ching, J.; Harley, J.A.; Berardini, M.D.; Jenkins, T.C.; Neidle, S.; Hurley, L.H.; Thurston, D.E., *J. Am. Chem. Soc.* (1992) **114**, 4939.
102. *Synthesis and DNA Crosslinking Ability of a Dimeric Anthramycin Analog*, Farmer, J.D. Jr.; Rudnicki, S.M.; Suggs, W.J., *Tetrahedron Lett.* (1988) **29**, 5105.
103. The rate and extent of DNA denaturation involved in alkaline agarose electrophoresis is likely to be much greater for an interstrand cross-linked restriction fragment than would be expected for an interhelical product in which the denaturation process involves two duplexes as opposed to just one. Additionally, interhelical joining of one duplex already bearing an interstrand lesion to another duplex (with or without its own interstrand lesion) would give a much slower adduct than a single interstrand cross-linked duplex.

104. Manzotti, C.; Pezzoni, G.; Giuliani, F.; Valsecchi, M.; Farrell, N.; Tognella, S., *Proc. AACR* (1994) **35**, 2628.
105. *Mutagenesis Induced by Site Specifically Placed 4'-hydroxymethyl-4,5',8-trimethylpsoralen Adducts*, Piette, J.; Gamper, H.B.; van de Vorst, A.; Hearst, J.E., *Nucleic Acids Research* (1988) **16**, 9961.
106. *Psoralens as Photoactive Probes of Nucleic Acid Structure and Function: Organic Chemistry, Photochemistry, and Biochemistry*, Cimino, G.D.; Gamper, H.B.; Isaacs, S.T.; Hearst, J.E., *Annu. Rev. Biochem.* (1985) **54**, 1151.
107. (a) *Psoralen Photobiology: Recent Advances*, Gasparro, F.P., *Photochemistry and Photobiology* (1996) **63**, 553; (b) *Psoralen-protein Photochemistry-The Forgotten Field*, Gasparro, R.P.; Chimenti, S.; Schmitt, I.M., *J. Photochem. Photobiol. B Biol.* (1995) **27**, 101; (c) *Treatment of Cutaneous T-cell Lymphoma by Extracorporeal Photochemotherapy*, Edelson, R.I.; Berger, C.L.; Gasparro, F.P., *N. Engl. J. Med.* (1987) **316**, 297; (d) Gasparro, F.P., (1994) *Extracorporeal Photochemotherapy-Clinical Aspects and the Molecular Basis for Efficacy*. Landes Press, Georgetown, TX.
108. *One Base Pair Change Abolishes T Cell-Restricted Activity of a  $\kappa$ B-like Protoenhancer Element from the Interleukin 2 Promoter*, Briegel, K.B.; Hentsch, B.; Pfeuffer, I.; Serfling, E., *Nucleic Acids Research* (1991) **19**, 5929.
109. The A to C transversion is the second most commonly observed 8-MOP induced mutation. See: *Mutagenesis by 8-Methoxypsoralen and 5-Methylangelicin Photoadducts in Mouse Fibroblasts: Mutations at Crosslinkable Sites by Monoadducts as well as Cross-Links*, Gunther, E.J.; Yeasky, T.; Gasparro, F.P., *Cancer Res.* (1995) **55**, 1283.
110. *Laser-Induced Protein-DNA Cross-Links via Psoralen Furanoside Monoadducts*, Sastry, S.S.; Spielmann, P.H.; Hoang, Q.S.; Phillips, A.M.; Sancar, A.; Hearst, J.H., *Biochemistry* (1993) **32**, 5526.
111. Glen Research 1995-1996 Product Listing
112. *Biotinylated Psoralen Derivative for Labeling Nucleic Acid Hybridization Probes*, Levenson, C.; Watson, R.; Sheldon, E.L., *Methods in Enzymology* (1990) **184**, 577.
113. *The photoactivation of an RNA animal virus, vesicular stomatitis virus, with the aid of newly synthesized psoralen derivatives*, Hearst, J.E.; Thiry, L., *Nucleic Acids Research* (1977) **4**, 1339.
114. This dissociation constant was for 4'-aminomethyl-4,5',8-trimethylpsoralen (AMT) reported in Isaacs, S.T.; Shen, C.-K.J.; Hearst, J.E.; Rapoport, H., *Biochemistry* (1977) **16**, 1058.
115. *Isolation and Characterization of Pyrimidine-Psoralen Photoadducts from DNA*, Straub, K.; Kanne, D.; Hearst, J.E.; Rapoport, H., *J. Am. Chem. Soc.* (1981) **103**, 2347.

116. *Photoreaction of 5-Methoxypsoralen with Thymidine and the Thymine Moiety of Isolated and Saccharomyces cerevisiae DNA. Characterization and Measurement of the two cis-syn Furan Side Monocycloadducts*, Anselmino, C.; Averbeck, D.; Cadet, J., *Photochemistry and Photobiology* (1995) **62**, 997.
117. For other studies in which psoralens were used in triplex/anti-sense methodologies see: (a) *Template-Directed Modification of Single-Stranded DNA by Psoralen-Tethered Oligonucleotides: Sites of Photoadduct Formation Analyzed by Sequence-Specific and Sequence-Random Cleavage*, Woo, J.; Hopkins, P.B., *J. Am. Chem. Soc.* (1991) **113**, 5457; (b) *Triplex Formation by a Psoralen-Conjugated Oligodeoxyribonucleotide Containing the Base Analog 8-Oxo-Adenine*, Miller, P.S.; Bi, G.; Kipp, S.A.; Fok, V.; Delong, R.K., *Nucleic Acids Research* (1996) **24**, 730.
118. *Inhibition of Gene Expression by Triple Helix-Directed DNA Cross-Linking at Specific Sites*, Brigoriev, M.; Praseuth, D.; Guieysse, A.L.; Robin, P.; Thuong, N.T.; Helene, C.; Harel-Bellan, A., *Proc. Natl Acad. Sci. U.S.A.* (1993) **90**, 3501.
119. *Oligodeoxynucleotide-Directed Photo-induced Cross-Linking of HIV Proviral DNA via Triple-Helix Formation*, Giovannangeli, C.; Thuong, N.T.; Helene, C., *Nucleic Acids Research* (1992) **20**, 4275.
120. (a) *4'-Methylangelicins: New Potential Agents for the Photochemotherapy of Psoriasis*, Dall'Acqua, F.; Vedaldi, D.; Bordin, F.; Baccichetti, F.; Carlassare, F., *J. Med. Chem.* (1983) **26**, 870. ; (b) Isaacs, S.T.; Chun, C.; Hyde, J.E.; Rapoport, H.; Hearst, J.E., (1982) In *Trends in Photobiology* ( Helene, C.; Charlier, M.; Montenay-Garestier, Th. ; Laustriat, G., Eds.) pp 279-94, Plenum Press, New York.
121. *Isolation and Characterization of Pyrimidine-Psoralen-Pyrimidine Photodiadducts from DNA*, Kanne, D.; Straub, K.; Hearst, J.E.; Rapoport, H., *J. Am. Chem. Soc.* (1982) **104**, 6754.
122. Vedaldi, D.; Dall'Acqua, F.; Caffieri, S.; Rodighiero, G., *Photochem. Photobiol.* (1980) **30**, 547.
123. Hearst, J.E.; Rapoport, H.; Isaacs, S.; Shen, C.-K.J. (1979) *U.S. Patent No. 4,169,204*.
124. *Synthesis of Monosulphur and Monoselenium Analogues of Psoralen*, Jakobs, A.E.; Christiaens, L.E.; Renson, M.J., *Tetrahedron* (1994) **50**, 9315.
125. *Azapsoralens. Synthesis of 8-Azapsoralens*, VanSickle, A.P.; Rapoport, H., *J. Org. Chem.* (1990) **55**, 895.
126. *Evolution of the P450 Gene Superfamily: Animal-Plant Warfare; Molecular Drive and Human Genetic Differences in Drug Oxidation*, Gonzalez, F.J.; Neber, D.W., *Trends Genet.* (1990) **6**, 182.
127. For an excellent review of the mechanisms involved in these transformations see: Foye, W.O.; Lemke, T.L.; Williams, D.A., (1995) *Principles of Medicinal Chemistry*. Williams & Wilkins, Baltimore, pp 104-111.

128. *Mechanism of the Cytochrome P-450 Catalyzed Hydroxylation-Thermodynamic Aspects and the Nature of the Active Oxygen Species*, Jung, C.; Ristau, O., *Pharmazie* (1978) **33**, 329.
129. Cytochrome P-450 and Chloroperoxidase: Thiolate-Ligated Heme Enzymes. Spectroscopic Determination of Their Active Site Structures and Mechanistic Implications of Thiolate Ligation, Dawson, J.H.; Sono, M., *Chem. Rev.* (1987) **87**, 1255.
130. Xanthine Oxidase, alcohol dehydrogenase and aldehyde dehydrogenase are just a few examples of non P-450 enzymes capable of effecting oxidation.
131. Struck, R.F. (1995) In *Cancer Chemotherapeutic Agents* (Foye, W.A.; Ed.) pp. 114, American Chemical Society, Washington D.C., USA.
132. (a) *Investigation of the Mechanism by which Cyclophosphamide Alters Cytochrome P450 in Male Rats*, McClure, M.T.; Stupans, I., *Biochemical Pharmacol.* (1992) **43**, 2655; (b) *In Situ Preparation and Fate of cis-4-Hydroxycyclophosphamide and Aldophosphamide: <sup>1</sup>H and <sup>31</sup>P NMR Evidence for Equilibrium of cis- and trans-4-Hydroxycyclophosphamide with Aldophosphamide and Its Hydrate in Aqueous Solution*, Hoye, T.R.; Swanson, T.A.; Borch, R.F., *J. Med. Chem.* (1984) **27**, 490; (c) *The Mechanism of Activation of 4-Hydroxycyclophosphamide*, Millard, J.A.; Borch, R.F., *J. Med. Chem.* (1987) **30**, 427.
133. *Identification of Cyclophosphamide-DNA Adducts in Rat Embryos Exposed in Vitro to 4-Hydroperoxyxlophosphamide*, Mirkes, P.E.; Brown, N.A.; Kajbaf, M.; Lamb, J.H.; Farmer, P.B.; Naylor, S., *Chem. Res. Toxicol.* (1992) **5**, 382. and references cited therein.
134. *Metabolism of Oxazaphosphorines*, Sladek, N.E., *Pharmacol. Ther.* (1988) **37**, 301. and references cited therein.
135. *Sensitization of Human Breast Cancer Cells to Cyclophosphamide and Ifosfamide by Transfer of a Liver Cytochrome P450 Gene*, Waxman, D.J.; Chen, L.; Chen, D.; Kufe, D.W., *Cancer Res.* (1996) **56**, 1331.
136. *Deactivation of Cyclophosphamide Metabolites by Sulfhydryl Compounds*, Draeger, U.; Peter, G.; Hohorst, H.J., *Cancer Treat. Rep.* (1976) **60**, 355.
137. *Effect of Stereochemistry on the Oxidative Metabolism of the Cyclophosphamide Metabolite Aldophosphamide*, Habib, A.D.; Boal, J.H.; Hilton, J.; Nguyen, T.; Chang, Y.H.; Ludeman, S.M., *Biochemical Pharmacol.* (1995) **50**, 429.
138. *Involvement of Human Glutathion S-Transferase Isoenzymes in the Conjugation of Cyclophosphamide Metabolites with Glutathione*, Dirven, H.A.; van Ommen, B.; van Bladeren, P.J., *Cancer Res.* (1994) **54**, 6215.
139. *Induction of Cyclophosphamide-Resistance by Aldehyde-Dehydrogenase Gene Transfer*, Dalla-Favera, R.; Gianni, A.M.; Magni, M.; Shammah, S.; Schiro, R.; Mellado, W., *Blood* (1996) **87**, 1097.



140. (a) *Isolation and Expression of an Altered Mouse Dihydrofolate Reductase cDNA*, Simonsen, C.C.; Levinson, A.D., *Proc. Natl. Acad. Sci. U.S.A.* (1983) **80**, 2495; (b) *A Retrovirus Carrying an MDRI cDNA Confers Multidrug Resistance and Polarized Expression of P-glycoprotein in MDCK Cells*, Pastan, I.; Gottesman, M.M.; Ueda, K.; Lovelace, E.; Rutherford, A.V.; Willingham, M.C., *Proc. Natl. Acad. Sci. U.S.A.*, (1988) **85**, 4486.
141. *Gene-Therapy for Malignant Gliomas Using Replication Incompetent Retroviral and Adenoviral Vectors Encoding the Cytochrome-P450 2B1 Gene Together with Cyclophosphamide*, Manome, Y.; Wen, P.Y.; Chen, L.; Tanaka, T.; Dong, Y.; Yamazoe, M.; Hirshowitz, A.; Kufe, D.W.; Fine, H.A., *Gene Therapy* (1996) **3**, 513.
142. *Hexamethylmelamine: An Evaluation of its role in the Therapy of Cancer*, Legha, S.S.; Slavik, M.; Carter, S.K., *Cancer* (1976) **38**, 27.
143. *Studies on the Stability of Trimelamol, a Carbinolamine-containing Antitumor drug*, Jackson, C.; Crabb, T.A.; Gibson, M.; Godfrey, R.; Saunders, R.; Thurston, D.E., *J. Pharm. Sci.* (1991) **80**, 245.
144. *N<sup>2</sup>,N<sup>4</sup>,N<sup>6</sup>-Tri(hydroxymethyl)-N<sup>2</sup>,N<sup>4</sup>,N<sup>6</sup>-Trimethylmelamine (Trimelamol) is an Efficient DNA Cross-linking Agent In Vitro*, Jackson, C.; Hartley, J.A.; Jenkins, T.C.; Godfrey, R.; Saunders, R.; Thurston, D.E., *Biochem. Pharmacol.* (1991) **42**, 2091.
145. *Formaldehyde Preferentially Interstrand Cross-Links Duplex DNA through Deoxyadenosine Residues at the Sequence 5'-d(AT)*, Huang, H.; Solomon, M.S.; Hopkins, P.B., *J. Am. Chem. Soc.* (1992) **114**, 9240.
146. Maxam-Gilbert sequencing relies on the ability of abasic sites to give rise to piperidine-mediated phosphodiester bond cleavage.
147. *Framework-Reactive Siderophore Analogs as Potential Cell-Selective Drugs. Design and Syntheses of Trimelamol-Based Iron Chelators*, Ramurthy, S.; Miller, M.J., *J. Org. Chem.* (1996) **61**, 4120.
148. Hider, R.C., *Struct. Bonding* (Berlin) (1990) **58**, 25.
149. *Trifunctional Reagents for Substrate-Protein Conjugation: Application to Pyrrolizidine Alkaloids*, Kurth, M.J.; Milco, L.A.; Miller, B.R., *Tetrahedron* (1992) **48**, 1407.
150. *Pyrrolizidine Alkaloid-Induced DNA-Protein Cross-Links*, Kim, H.Y.; Stermitz, F.R.; Coulombe, R.A. Jr., *Carcinogenesis* (1995) **16**, 2691.
151. *Structural Influences on Pyrrolizidine Alkaloid-Induced Cytopathology*, Kim, H.Y.; Stermitz, F.R.; Molyneux, R.J.; Wilson, D.W.; Taylor, D.; Coulombe, R.A. Jr., *Toxicology and Applied Pharmacology* (1993) **122**, 61.
152. *Alkylation of Nucleosides by Dehydromonocrotaline, the Putative Toxic Metabolite of the Carcinogenic Pyrrolizidine Alkaloid Monocrotaline*, Niwa, H.; Ogawa, T.; Yamada, K., *Tetrahedron Lett.* (1991) **32**, 927.

153. (a) *A molecular mechanism of mitomycin action: linking of complementary DNA strands*, Iyer, V.N.; Szybalski, W.A., *Proc. Nat. Acad. Sci., U.S.A.* (1963) **50**, 355; (b) *Mitomycins and Porfiromycin: Chemical Mechanism of Activation and Cross-Linking of DNA*, Iyer, V.N.; Szybalski, W., *Science* (1964) **145**, 55.
154. *Sequence Preferences of DNA Interstrand Cross-Linking Agents: dG-to-dG Cross-Linking at 5'-CG by Structurally Simplified Analogues of Mitomycin C*, Weidner, M.F.; Sigurdsson, S.T.; Hopkins, P.B., *Biochemistry* (1990) **29**, 9225.
155. *DNA Interstrand Cross-Linking of Pyrrole-Based Bifunctional Electrophiles: Evidence for a Common Site in DNA*, Woo, J.; Sigurdsson, S.T.; Hopkins, P.B., *J. Am. Chem. Soc.* (1993) **115**, 3407.
156. *Synthesis and Antileukemic Activity of 5-Substituted 2,3-Dihydro-6,7-bis(hydroxymethyl)-1 H- pyrrolizine Diesters*, Anderson, W.K.; Corey, P.F.; *J. Med. Chem.* (1977) **20**, 812.
157. *Affinity Cross-Linking of Duplex DNA by a Pyrrole-Oligopeptide Conjugate*, Sigurdsson, S.T.; Rink, S.M.; Hopkins, P.B., *J. Am. Chem. Soc.* (1993) **115**, 1263.
158. (a) *Antisense Sequence-Directed Cross-Linking of DNA Oligonucleotides by Mitomycin C*, Maruenda, H.; Tomasz, M., *Bioconjugate Chem.* (1996) **7**, 541; (b) *Design, Synthesis, and Evaluation of Mitomycin-Tethered Phosphorothioate Oligodeoxynucleotides*, Huh, N.; Rege, A.A.; Yoo, B.; Kogan, T.P.; Kohn, H., *Bioconjugate Chemistry* (1996) **7**, 659.
159. *Effects of Ionizing Radiation in DNA; the Role of Oxygen*, Boon, P.J.; Cullis, P.M.; Symon, M.C.R.; Wren, B.W., *J. Chem. Soc. Perkin Trans.* (1984) **2**, 1393
160. *Single- and Double-Strand Break Formation in DNA Irradiated in Aqueous Solution: Dependence on Dose and OH Radical Scavenger Conditions*, Siddiqi, M.A.; Bothe, E., *Radiation Research* (1987) **112**, 449.
161. Box, H.C.; Schroder, E.A.; Budzinski, E.E. (1995) in *Radiation Damage in DNA: Structure/Function Relationships at Early Times* (Fuciarelli, A.F.; Zimbrick, J.D., Eds.) pp 285-290, Battelle Press, Columbus.
162. *Mechanisms of Bleomycin-Induced DNA Degradation*, Stubbe, J.; Kozarich, J.W., *Chem. Rev.* (1987) **87**, 1107.
163. *Mechanism of Oxidation of Ferrous Polydentate Complexes by Dioxygen*, Brown, E.R.; Mazzrella, J.D., *J. Electroanal. Chem.* (1987) **222**, 173.
164. *Induction of angiogenesis during the transition from hyperplasia to neoplasia*, Folkman, J.; Watson, K.; Ingver, D.; Hanahan, D., *Nature* (1988) **339**, 58.
165. Coleman, C.N., *J. Natl. Cancer Inst.* (1988) **50**, 310.
166. *Chemotherapeutic Attack of Hypoxic Tumor Cells by the Bioreductive Alkylating Agent Mitomycin C*, Keyes, S.R.; Heimbrook, D.C.; Fracasso, P.M.; Rockwell, S.; Sligar, S.G.; Sartorelli, A.C., *Adv. Enzyme Reg.* (1985) **23**, 291.

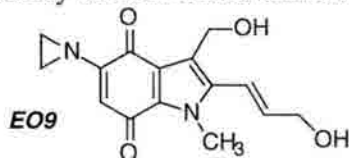
167. *Oxygen Diffusion and the Distribution of Cellular Radiosensitivity in Tumours*, Tannock, I.F., *Br. J. Radiol.* (1972) **45**, 515.
168. Connors, T.A.(1983) In *Structure-Activity Relationships of Antitumour Agents*; (Reinhoudt, D.N.; Connors, T.A.; Pinedo, H.M.; van der Poll, K.W.; Eds.) pp. 47-59 Nijhoff, Hague, The Netherlands.
169. (a) *Pulse Radiolytic Kinetics Study of the Decay of  $\alpha$ -Methyl-Substituted Benzoquinone Radical Anions: A Possible Mechanistic Model for Bioreductive Alkylation*, O'Shea, K.E.; Fox, M.A., *J. Am. Chem. Soc.* (1991) **113**, 611; (b) *Nitrobenzyl Halides and Carbamates as Prototype Bioreductive Alkylating Agents*, Teicher, B.A.; Sartorelli, A.C., *J. Med. Chem.* (1980) **23**, 955.
170. *Induction of DNA Crosslinks In Vitro Upon Reduction of the Nitroimidazole-Aziridines RSU-1069 and RSU-1131*, O'Neill, P.; McNeil, S.S.; Jenkins, T.C., *Biochemical Pharmacol.* (1987) **36**, 1787.
171. McClelland, R.A.; Fuller, J.R.; Seaman, N.E.; Rauth, A.M.; Battistella, R., *Biochem. Pharmacol* (1984) **33**, 303.
172. Denny, W.A. (1995) In *Cancer Chemotherapeutic Agents* (Foye, W.A.; Ed.) pp. 491-493, American Chemical Society, Washington D.C., USA.
173. *Nitroheterocycle Reduction as a Paradigm for Intramolecular Catalysis of Drug Delivery to Hypoxic Cells*, Firestone, A.; Mulcahy, R.T.; Borch, R.F., *J. Med. Chem.* (1991) **34**, 2933.
174. Wilman, D.E.V., *Biochem. Pharmacol.* (1980) **29**, 2919.
175. *Reduction of Nitroimin to Nitrogen Mustard: Unscheduled DNA Synthesis in Aerobic or Anaerobic Rat Hepatocytes, JB1, BL8 and Walker Carcinoma Cell Lines*, Connors, T.A.; White, I.N.H.; Suzanger, M.; Mattocks, A.R.; Bailey, E.; Farmer, P.B., *Carcinogenesis* (1989) **10**, 2113.
176. *Synthesis of Novel N- and S- Mustards as Potential Pro-drugs Activated by Bioreductive Processes*, Mann, J.; Shervington, L.A., *J. Chem. Soc. Perkin Trans. 1*, (1991) 2961.
177. (a) *The Nitroreductase Enzyme in Walker Cells that Activates 5-(aziridin-1-yl)-2,4-dinitrobenzamide (CB 1954) to 5-(aziridin-1-yl)-4-hydroxylamino-2-nitrobenzamide is a Form of NAD-(P)H Dehydrogenase (quinone)(EC1.6.99.2)*, Knox, R.J.; Boland, M.P.; Friedlos, F.; Coles, B.; Southan, C.; Roberts, J.J., *Biochem. Pharmacol.* (1988) **37**, 4671; (b) *Dinitropyrene Nitroreductase Activity of Purified NAD(P)H-quinone Oxidoreductase: Role in Rat Liver Cytosol and Induction by Aroclor-1254 Pretreatment*, Hajos, A.K.D.; Winston, G.W., *Carcinogenesis* (1991) **12**, 697.



178. (a) *Design and Synthesis of Cobalt (III) Nitrogen Mustard Complexes as Hypoxia Selective Cytotoxins. The X-ray Crystal Structure of bis-(3-Chloropentane-2,4-dionato)(RS-N,N'-bis(2-chloroethyl)ethylenediamine)-cobalt(III)Perchlorate, [Co(Clacac)<sub>2</sub>(bce)]ClO<sub>4</sub>*, Ware, D.C.; Wilson, W.R.; Denny, W.A.; Rickard, C.E.F., *J. Chem. Soc., Chem. Commun.* (1991) 1171. (b) *Hypoxia Selective Antitumor Agents. 7. Metal Complexes of Aliphatic Mustards as a New Class of Hypoxic Selective Cytotoxins. Synthesis and Evaluation of Cobalt (III) Complexes of Bidentate Mustards*, Ware, D.C.; Palmer, B.D.; Wilson, W.R.; Denny, W.A., *J. Med. Chem.* (1993) **36**, 1839; (c) *Synthesis and Characterization of Aziridine Complexes of Cobalt(III) and Chromium(III) Designed as Hypoxia-Selective Cytotoxins. X-ray Crystal Structure of trans-[Co(Az)<sub>4</sub>(NO<sub>2</sub>)<sub>2</sub>]Br·2H<sub>2</sub>O·LiBr*, Ware, D.C.; Siim, B.G.; Robinson, K.J.; Denny, W.A.; Brothers, P.J.; Clark, G.R., *Inorg. Chem.* (1991) **30**, 3750.
179. Atwood, J.D. (1985) In *Inorganic and Organometallic Reaction Mechanisms*, pp. 87, Brooks & Cole, Monterey CA.
180. *Kinetics of Ammonia Detachment from Reduced Cobalt (III) Complexes based on Conductometric Pulse Radiolysis*, Simic, M.; Lilie, J., *J. Am. Chem. Soc.* (1974) **96**, 291.
181. Recall that *bis*(2-chlorethyl)amine is only minimally active as a DNA cross-linking agent as found with the cyclophosphamide studies by Colvin (reference 134). As such, ISC induction by the Co(II) complexes may not be the actual cause for the differential cytotoxicities observed. That ISC formation occurs using these complexes has not been unambiguously demonstrated.
182. Arcamone, F., (1984) , *Doxorubicin, Anticancer Antibiotics*, Academic Press, New York; b) Arcamone, F., *Med. Res. Rev.* (1984) **4**, 153.
183. *Formation of Adriamycin-DNA Adducts in Vitro*, Cullinane, C.; Cutts, S.M.; van Rosmalen, A.; Phillips, D.R., *Nucleic Acids Res.* (1994) **22**, 2296.
184. (a) *TAN-1120, A New Anthracycline with Potent Angiostatic Activity*, Nozaki, Y.; Hida, T.; Iinuma, S.; Ishii, T.; Sudo, K.; Muroi, M.; Kanamaru, T., *J. Antibiotics* (1993) **46**, 569; (b) *Dutomycin, A New Anthracycline Antibiotic From Streptomyces*, Xuan, L.J.; Xu, S.H.; Zhang, H.L.; Xu, Y.M., *J. Antibiotics* (1992) **45**, 1974; (c) *Cororubicin, A New Anthracycline Antibiotic Generating Active Oxygen in Tumor Cells*, Ishigami, K.; Hayakawa, Y.; Seto, H., *J. Antibiotics* (1994) **47**, 1219; (d) *Respinomycin A1, A New Anthracycline Antibiotic*, Ubukata, M.; Tanaka, C.; Osada, H.; Isono, K., *J. Antibiotics* (1991) **44**, 1274.
185. *Interactions Between an Anthracycline Antibiotic and DNA: Molecular Structure of Daunomycin complexed to d(CpGpTpApCpG) at 1.2 Å Resolution*, Wang, A.H.-J.; Ughetto, G.; Quigley, G.J.; Rich, A., *Biochemistry* (1987) **26**, 1152.
186. Wang, A.H.-J., (1993) In *Molecular Aspects of Anticancer Drug-DNA Interactions*, (Neidle, S.; Waring, M., Eds.) pp. 35-38., CRC Press, Boca Raton.

187. For examples of other DNA interactive drugs which bind *via* sugar-DNA interactions see: (a) *Calicheamicins: Discovery, Structure, Chemistry, and Interaction with DNA*, Lee, M.D.; Ellestad, G.A.; Borders, D.B., *Acc. Chem. Res.* (1991) **24**, 235.
188. *The Molecular Pharmacology of Doxorubicin in Vivo*, Cummings, J.; *Eur. J. Cancer* (1991) **27**, 532.
189. *DNA Topoisomerases*, Wang, W.A., *Annu. Rev. Biochem.* (1985) **54**, 665.
190. *Stimulation of Growth in Human and Murine Cells by Adriamycin*, Vichi, P.; Tritton, T.R., *Cancer Res.* (1989) **49**, 248.
191. Sengupta, S.K. (1995) In *Cancer Chemotherapeutic Agents* (Foye, W.A.; Ed.) pp. 210-217, American Chemical Society, Washington D.C., USA.
192. *Reduction of Daunomycin and 11-Deoxydaunomycin with Sodium Dithionite in DMSO. Formation of Quinone Methide Sulfite Adducts and the First NMR Characterization of an Anthracycline Quinone Methide*, Gaudiano, G.; Frigerio, M.; Sangsurasak, C.; Bravo, P.; Koch, T.H., *J. Am. Chem. Soc.* (1992) **114**, 5546.
193. (a) *Spectroscopic and Kinetic Evidence for the Tautomer of 7-Deoxyalkylavinone as an Intermediate in the Reductive Coupling of Aclacinomycin A*, Kleyer, D.L.; Gaudiano, G.; Koch, T.H., *J. Am. Chem. Soc.* (1984) **106**, 1105; (b) *Formation and Reaction of the Quinone Methide from Reductive Cleavage of the Antitumor Drug Menogaril*, Boldt, M.; Gaudiano, G.; Haddadin, M.J.; Koch, T.H., *J. Am. Chem. Soc.* (1989) **111**, 2283.
194. *7-Deoxydaunomycinone Quinone Methide Reactivity with Thiol Nucleophiles*, Ramakrishnan, K.; Fisher, J., *J. Med. Chem.* (1986) **29**, 1215.
195. *Coupling of the Anthracycline Antitumor Drug Menogaril to 2'-Deoxyguanosine Through Reductive Activation*, Egholm, M.; Koch, T.H., *J. Am. Chem. Soc.* (1989) **111**, 8291.
196. *Interstrand DNA Crosslinking Induced by Anthracyclines in Tumour Cells*, Skladanowski, A.; Konopa, J., *Biochemical Pharmacol.* (1994) **47**, 2269.
197. *Discovery and Development of Anthracycline Antitumour Antibiotics*, Lown, W.J., *Chem. Society Reviews* (1993) 165.
198. (a) Westendorf, J.; Groth, G.; Steinheider, G.; Marquardt, H., *Cell Biol. Toxicol.* (1985) **1**, 87; (b) *Sequence Specificity of (Cyanomorpholino)adriamycin Adducts in Human Cells*, Cullinane, C.; Phillips, D.R., *Biochemistry* (1994) **33**, 6207.
199. *Thermal Stability of DNA Adducts Induced by Cyanomorpholinoadriamycin in Vitro*, Cullinane, C.; Phillips, D.R., *Nucleic Acids Res.* (1993) **21**, 1857.
200. *Characterization of the DNA-DNA Cross-Linking Activity of 3'-(3-Cyano-4-morpholinyl)-3'-deaminoadriamycin*, Jesson, M.I.; Hohnston, J.B.; Robotham, E.; Begleiter, A., *Cancer Res.* (1989) **49**, 7031.

201. (a) *Use of Oligonucleotides to Define the Site of Interstrand Cross-Links Induced by Adriamycin*, Cutts, S.M.; Phillips, D.R., *Nucleic Acids Res.* (1995) **23**, 2450; (b) *Stability of Adriamycin-Induced DNA Adducts and Interstrand Cross-Links*, van Rosmalen, A.; Cullinane, C.; Cutts, S.M.; Phillips, D.R., *Nucleic Acids Res.* (1995) **23**, 42; (c) *Does Adriamycin Induce Interstrand Cross-Links in DNA?* Cullinane, C.; van Rosmalen, A.; Phillips, D.R., *Biochemistry* (1994) **33**, 4632.
202. *Cross-Linking and Sequence Specific Alkylation of DNA by Aziridinyquinones. 1. Quinone Methides*, Mayalarp, S.P.; Hargreaves, R.H.J.; Butler, J.; O'Hare, C.C.; Hartley, J.A., *J. Med. Chem.* (1996)**39**, 531.
203. *Randomized Comparison of Diaziquone and Carmustine in the Treatment of Adults with Anaplastic Glioma*, Schold, S.C., Jr.; Herndon, J.E.; Burger, P.C.; Halperin, E.C.; Vick, N.A.; Cairncross, J.G.; Macdonald, D.R.; Droghda, E.J.; Morawetz, R.; Bigmer, D.D.; Mahaley, M.S., Jr., *J. Clin. Oncol.* (1993) **11**, 77.
204. (a) *DNA-DNA Interstrand Cross-Linking by 2,5-Bis(1-aziridiny)-3,6-bis(carbethoxyamino)-1,4-benzoquinone: Covalent Structure of the dG-to-dG Cross-Links in Calf Thymus DNA and a Synthetic DNA Duplex*, Alley, S.C.; Hopkins, P.B., *Chem. Res. Toxicol.* (1994) **7**, 666; (b) *DNA Interstrand Cross-Linking by 2,5-Bis(1-aziridiny)-1,4-benzoquinone: Nucleotide Sequence Preferences and Covalent Structure of the dG-to-dG Cross-Links at 5'-d(GN<sub>n</sub>C) in Synthetic Oligonucleotide Duplexes*, Alley, S.C.; Brameld, K.A.; Hopkins, P.B., *J. Am. Chem. Soc.* (1994) **116**, 2734.
205. *DNA Cross-Linking and Sequence Selectivity of Aziridinybenzoquinones: A Unique Reaction at 5'-GC-3' Sequences with 2,5-Diaziridiny-1,4-benzoquinone upon Reduction*, Harley, J.A.; Berardini, M.; Ponti, M.; Gibson, N.W.; Thompson, A.S.; Thurston, D.E.; Hoey, B.M.; Butler, J., *Biochemistry* (1991) **30**, 11719.
206. *Alteration in DNA Cross-Linking and Sequence Selectivity of a Series of Aziridinybenzoquinones after Enzymatic Reduction by DT-Diaphorase*, Lee, C.S.; Hartley, J.A.; Berardini, M.D.; Butler, J.; Siegel, D.; Ross, D.; Gibson, N.W., *Biochemistry* (1992)**31**,3019.
207. An interesting aziridinyquinone which bears a striking similarity to mitomycin C in both cross-linking ability and structural similarity is the indoloquinone EO9.



For a recent citation see: *Indoloquinone DO9: DNA Interstrand Cross-Linking upon Reduction by DT-Diaphorase or Xanthine Oxidase*, Maliepaard, M.; Wolfs, A.; Groot, S.E.; deMol, N.J.; Janssen, L.H.M., *British Journal of Cancer* (1995) **71**, 836.

208. (a) *Mitomycin, a New Antibiotic from Streptomyces*. I. , Hata, T.; Sano, Y.; Sugawara, R.; Matsumae, A.; Kanomori, K.; Shima, T.; Hoshi, T., *J. Antibiotics*, Ser. A. (1956) **9**, 141; (b) *Mitomycin, a New Antibiotic from Streptomyces*. II. *Description of the strain.*, Sugawara, R.; Hata, T., *J. Antibiotics*, Ser. A. (1956) **9**, 147.
209. *Isolation of New Fractions of Antitumor Mitomycins.*, Wakagi, S.; Marumo, H.; Tomoka, K.; Shimizu, G.; Kata, E.; Kamada, H.; Kudo, S.; Fugimoto, Y., *Antibiot. and Chemoth.*, (1958) **8**, 228.
210. *Porfiromycin, a New Antibiotic. II. Isolation and Characterization.*, Herr, R.R.; Bergy, M.E.; Eble, T.E.; Jahnke, H.K., *Antimicrobial Agents Ann.* (1961) **1960**, 23.
211. *Isolation and Characterization of Mitiromycin and Other Antibiotics Produced by Streptomyces Vericillatus*, Lefemine, D.V.; Dann, M.; Barbatschi, F.; Hausmann, W.K.; Zbinovsky, V.; Monnikendam, P. Adam, J.; Bohonos, N., *J. Am. Chem. Soc.* (1962) **84**, 3184.
212. *Albomitomycin A and Isomitomycin A: Products of Novel Intramolecular Rearrangement of Mitomycin A*, Kono, M.; Saitoh, Y.; Shiriahata, K.; Arai, Y.; Ishii, S., *J. Am. Chem. Soc.* (1987) **109**, 7224.
213. *New Mitomycin Analogs Produced by Directed Biosynthesis*, Bush, J.A.; Claridge, C.A.; Doyle, T.W.; Nettleton, D.E.; Moseley, J.E.; Kimball, D.; Kammer, M.F.; Veitch, J., *J. Antibiotics* (1986) **XXXIX**, 437.
214. (a) Sekiguchi, M.; Takagi, Y., *Biochim. Biophys. Acta.* (1960) **41**, 434; (b) *D-Glucosamine and L-Citrulline. Precursors in Mitomycin Biosynthesis by Streptomyces Verticillatus*, Hornemann, U.; Kehrer, J.P., Nunez, C.S.; Ranieri, R.L., *J. Am. Chem. Soc.* (1974) **96**, 320.
215. Hornemann, U., (1981) *Biosynthesis of the mitomycins*. In *Antibiotics. IV. Biosynthesis*. (Corcoran, J.W., Editor) pp. 295-312, Springer-Verlag, New York.
216. (a) *Generation of hydroxyl radical by anticancer quinone drugs, carbazilquinone, mitomycin C, aclacinomycin A and adriamycin, in the presence of NADPH-cytochrome c reductase*, Komiyama, T.; Kikuchi, T.; Sugiura, Y., *Biochem. Pharmacol.* (1982) **31** 3651; (b) *The mechanism of action of quinone antibiotics*, Lown, J.W., *Molec. Cell. Biochem.* (1983) **55**, 17; (c) *Generation of Reactive Oxygen Radicals through Bioactivation of Mitomycin Antibiotics*, Sartorelli, A.C.; Pritsos, C.A., *Cancer Res.* (1986) **46**, 3528; (d) *DNA Strand Scission by Enzymatically Reduced Mitomycin C- Evidence for Participation of the Hydroxyl Radical in the DNA Damage*, Hamana, K.; Terokubota, S.; Sugioka, K.; Kawada, K.; Nakano, M.; Ikegami, Y., *Biochemistry International* (1985) **10**, 301.
217. For excellent reviews on the alkylation chemistry of the mitomycins see: (a) *Mitomycin Antitumour Agents- A Review of Their Physicochemical and Analytical Properties and Stability*, Beijnen, J.H.; Lingeman, H.; Underberg, W.J.M.; Vanmunster, H.A., *Journal of Pharmaceutical and Biomedical Analysis* (1986) **4**, 275; (b) *Mitomycin C: small, fast and deadly (but very selective)*, Tomasz, M., *Chemistry & Biology* (1995) **2**, 575.
218. Melissa S. Egbertson, Ph.D. thesis Yale University 1989.

219. *Reassignment of the Guanine-Binding Mode of Reduced Mitomycin C*, Tomasz, M.; Lipman, R.; Verdine, G.; Nakanishi, K., *Biochemistry* (1986) **25**, 4337.
220. *Full Structure of a Mitomycin C Dinucleoside Phosphate Adduct. Use of Differential FT-IR Spectroscopy in Microscale Structural Studies*, Tomasz, M.; Lipman, R.; Snyder, J.K.; Nakanishi, K., *J. Am. Chem. Soc.* (1983) **105**, 2059.
221. *Reaction of Acid-Activated Mitomycin C with Calf Thymus DNA and Model Guanines- Elucidation of the Base-catalyzed Degradation of N<sup>7</sup>-Alkylguanine Nucleosides*, Tomasz, M.; Lee, M.S.; Lipman, R.; Nakanishi, K.; Verdine, G.L., *Biochemistry* (1987) **26**, 2010.
222. (a) *NMR and Computational Characterization of Mitomycin Cross-Linked to Adjacent Deoxyguanosines in the Minor Groove of the d(TACGTA)-d(TACGTA) Duplex*, Norman, D.; Live, D.; Sastry, M.; Lipman, R.; Hingerty, B.E.; Tomasz, M.; Broyde, S.; Patel, D.J., *Biochemistry* (1990) **29**, 2861; (b) *Conformations of the Noncovalent and Covalent Complexes between Mitomycins A and C and d(GCGCGCGCGC)<sub>2</sub>*, Rao, S.N.; Singh, U.C.; Kollman, P.A., *J. Am. Chem. Soc.* (1986) **108**, 2058; (c) *Conformations of Complexes between Mitomycins and Decanucleotides. 3. Sequence Specificity, Binding at C-10, and Mitomycin Analogues*, Remers, W.A.; Rao, S.N.; Wunz, T.P.; Kollman, P.A., *J. Med. Chem.* (1988) **31**, 1612.
223. *Solution Structure of the Monoalkylated Mitomycin C-DNA Complex*, Sastry, M.; Fiala, R.; Lipman, R.; Tomasz, M.; Patel, D.J., *J. Mol. Biol.* (1995) **247**, 338.
224. *Recognition between Mitomycin C and Specific DNA Sequences for Cross-Link Formation*, Tomasz, M.; Lipman, R.; Borowy-Borowski, H., *Biochemistry* (1990) **29**, 2999.
225. *Cytosine Methylation Enhances Mitomycin C Cross-Linking*, Millard, J.T.; Beachy, T.M., *Biochemistry* (1993) **32**, 12850.
226. *Recognition of Specific DNA Sequences by Mitomycin C for Alkylation*, Kumar, S.; Lipman, R.; Tomasz, M., *Biochemistry* (1992) **31**, 1399.
227. *Studies on the Bonding Specificity for Mitomycin C-DNA monoalkylation Processes*, Li, V.; Kohn, H., *J. Am. Chem. Soc.* (1991) **113**, 275.
228. *Sequence-Selective Alkylation and Cross-Linking Induced by Mitomycin C upon Activation by DT-Diaphorase*, Prakash, A.S.; Ross, D.; Beall, H.; Gibson, N.W., *Biochemistry* (1993) **32**, 5518.
229. (a) *Conjugation of Glutathione and Other Thiols with Bioreductively Activated Mitomycin C. Effect of Thiols on the Reductive Activation Rate*, Sharma, M.; Tomasz, M., *Chem. Res. Toxicol.* (1994) **7**, 390; (b) *Effects of Glutathione on Alkylation and Cross-Linking of DNA by Mitomycin C. Isolation of a Ternary Glutathione-Mitomycin-DNA Adduct*, Sharma, M.; He, Q.Y.; Tomasz, M., *Chem. Res. Toxicol.* (1994) **7**, 401.



230. *Alkylation and Cross-Linking of DNA by the Unnatural Enantiomer of Mitomycin C: Mechanism of the DNA-Sequence Specificity of Mitomycins*, Gargiulo, D.; Musser, S.S.; Yang, L.; Fukuyama, T.; Tomasz, M., *J. Am. Chem. Soc.* (1995) **117**, 9388.
231. (a) *Antitumor-Activity and Toxicity in Animals of Bmy-25282, a New Mitomycin Derivative*, Bradner, W.T.; Catino, J.J.; Florczyk, A.P.; Rose, W.C.; Schurig, J.E.; Huftalen, J.B., *Cancer Research* (1985) **45**, 6475; (b) *Synthesis of Mitomycin C Analogs. 1. Introduction of the Urethane Function at C-10 of the Pyrrolo(1,2-A) Indole Skeleton*, Dijksman, W.C.; Egberink, R.J.M.; Reinhoudt, D.N.; Verboom, W., *J. Org. Chem.* (1985) **50**, 3791; (c) *Preparation and Antitumor Activity of New Mitomycin A Analogs*, Sami, S.M.; Bradner, W.T.; Iyengar, B.S.; Remers, W.A., *J. Med. Chem.* (1987) **30**, 168; (d) *Synthesis of 9-epi-Mitomycin B: The First Inversion of the C-9 Stereochemistry in Mitomycin B*, Kasai, M.; Kono, M.; Shirahata, K., *J. Org. Chem.* (1989) **54**, 5908; (e) *Mitomycin Derivatives Having Unique Condensed Ring Structures*, Arai, H.; Kanda, Y.; Ashizawa, T.; Morimoto, M.; Gomi, K.; Kono, M.; Kasai, M., *J. Antibiotics* (1994) **47**, 1312; (f) *Mitomycin C Analogues with a Substituted Hydrazine at Position 7. Synthesis, Spectral Properties, and Biological Activity*, Sawhney, K.N.; Kohn, H., *J. Med. Chem.* (1989) **32**, 248.

## Chapter 2

### DNA Interstrand Cross-Linking by FR-900482 and Related Compounds

#### 2.1 Background

The recently discovered anti-tumor antibiotics FR-900482 (**312**) and the dihydro congener, FR-66979 (**314**), obtained from the fermentation harvest of *Streptomyces sandaensis* No. 6897 at Fujisawa Pharmaceutical Co., Japan, bear close structural similarity to the clinically-employed bioreductive alkylating agent mitomycin C (MC, **163**).<sup>1</sup> In preliminary clinical studies, it was shown that FR-900482 (4-formyl-6,9-dihydroxy-14-oxa-1,11-diazatetracyclo[7.4.1.0.0]tetradeca 2,4,6 triene 8-yl-methyl-carbamate) and the derived triacetate, FK973 (**313**), are *ca* three-fold more potent than mitomycin C and have significantly lower toxicity.<sup>2</sup> FK973 has recently been shown to form DNA-DNA interstrand cross-links and DNA-protein cross links in L1210 cells.<sup>3</sup> Even more intriguing is that both FK973 and FR-900482 are active against multidrug-resistant (including MC) P388 cells.<sup>2a,c</sup>



Like the mitomycins, **312-314** also require reductive activation both *in vivo* and *in vitro*.<sup>4</sup> However, in contrast to mitomycin C, these compounds do not produce single-strand DNA breaks typically associated with superoxide production upon bioreduction.<sup>2c,d,5</sup> The inability of these agents to take part in Fenton/Haber Weiss

chemistry (leading to DNA strand scission) most likely abrogates other damaging events such as phospholipid oxidations.<sup>6</sup> The relatively low host toxicity of the Fujisawa drugs in clinical trials relative to MC may thus be correlated to the incapacity of these substances to cause indiscriminate oxidative damage to DNA and other cellular targets.<sup>5</sup> Since FK973 and MC both share the ability to cross-link DNA, it is very clear that the lack of adventitious redox cycling chemistry inherent in the bioreductive activation of **312-314** has not compromised their potential efficacy as antitumor drugs relative to MC.

The inability to induce DNA single-strand breaks (SSBs) is likely due to the absence of the quinone functionality <sup>2d,3a</sup>, obligate for the reductive unmasking of the potent, *bis*-electrophilic mitosene from MC.<sup>7</sup> In the Fujisawa drugs, it appears that the reductively labile functionality is the N-O bond of the unique hydroxylamine hemi-ketal. Given the therapeutic potential of these agents coupled with both their unusual structures and relationship to MC, a great deal of effort has been directed towards the synthesis of the natural products<sup>8,9</sup> as well as preliminary mechanistic studies concerning the biological mode of action of these secondary metabolites.<sup>10</sup> Both issues have been the focus of intense efforts within the Williams group, some of which are detailed herein.

FR-900482 and FR-66979 both exist as a mixture of diastereoisomers **315** $\alpha$  and  $\beta$ .<sup>1a</sup> The tautomeric equilibrium resulting from the labile hydroxylamine hemiketal at C8 affords **315** $\alpha$  as the major constituent of the FR-900482 mixture.<sup>1a</sup> The equilibrium between **315**  $\alpha$  and **315**  $\beta$  for FR-900482 (R = CHO) is sensitive to pH but favors **315** $\alpha$ , particularly at low pH. This results from an intramolecular hydrogen bond between the bridged hydroxylamine oxygen and the aziridine NH, which is not allowed in the  $\beta$  form.<sup>1a</sup> Conversely, the stereoisomeric mixture of acetates **313** $\alpha$  and  $\beta$  equilibrates such that the  $\beta$  form is favored in a ratio of 79:7.

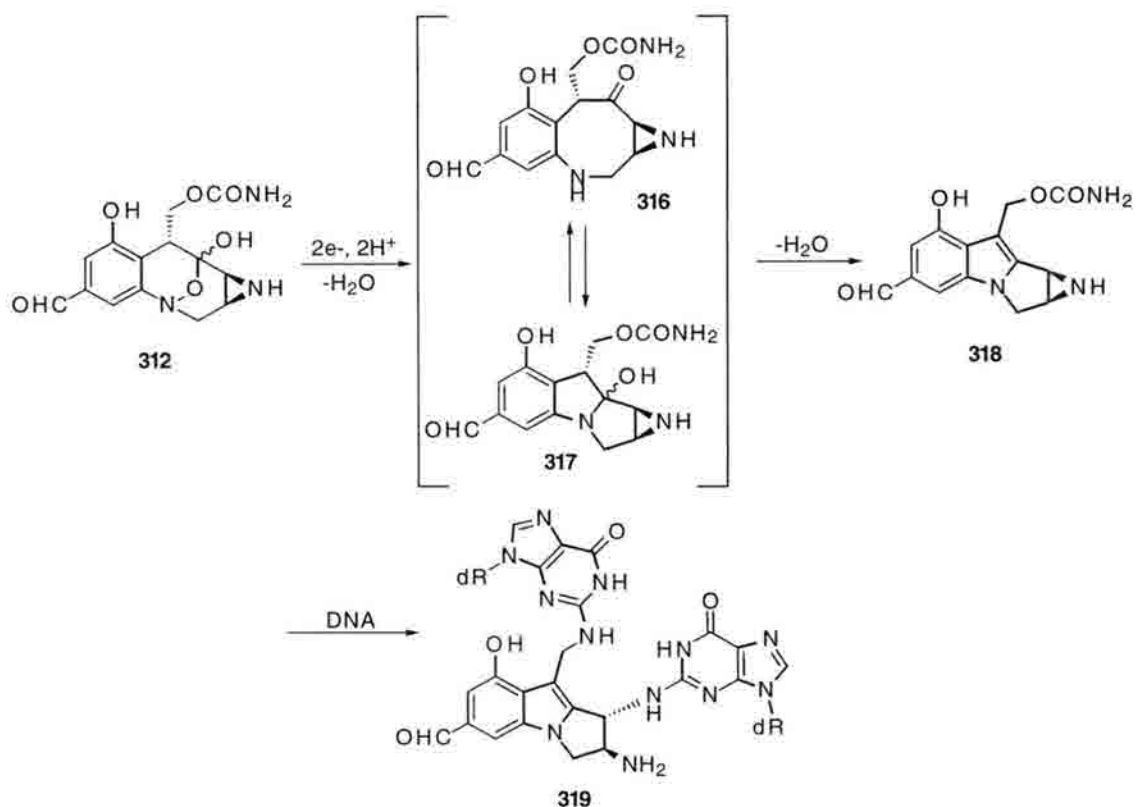




**Table 2-1.** 315 $\alpha$ :315 $\beta$  ratios for various pH conditions<sup>1a</sup>

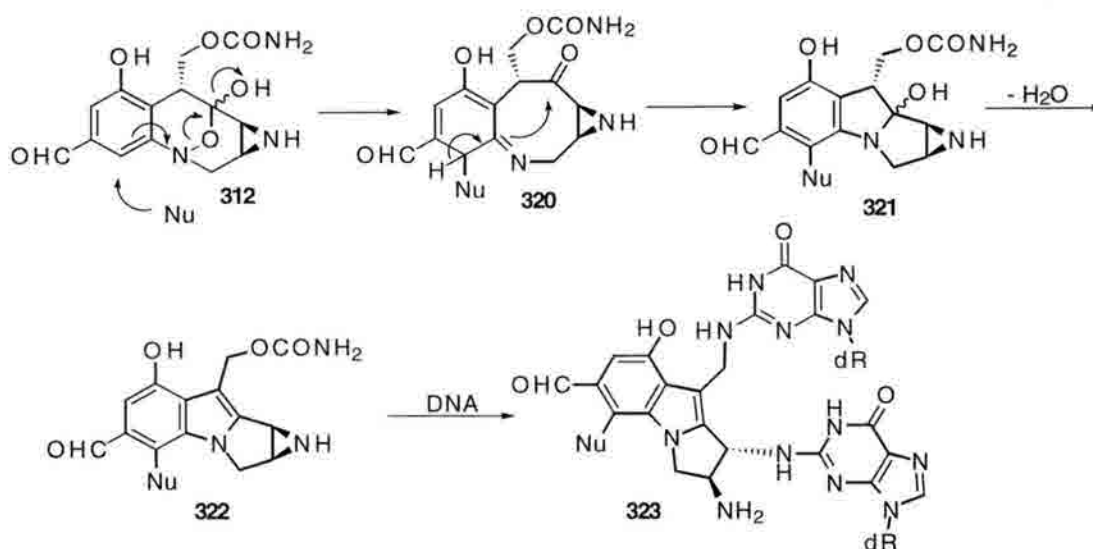
pH	Buffer system	Ratio (315 $\alpha$ : 315 $\beta$ )
1.0	0.1 N HCl	1:0
2.0	0.1 M NaOAc-HCl	12:1
4.0	0.1 M NaOAc-HCl	6:1
7.0	0.1 M KH <sub>2</sub> PO <sub>4</sub>	2.3: 1
9.0	0.1 M Tris-HCl	3: 1

Prior to the work detailed herein, mechanistic proposals pertaining to how these aziridinoepoxybenzazocines interstrand cross-link DNA relied heavily on a mitomycin-like pathway.<sup>7</sup> Particularly intriguing was the means by which activation to the DNA-reactive species might occur. Goto and Fukuyama were the first to propose reductive activation of **312 enroute** to DNA cross-linking (Fig. 2-1) in a preliminary synthetic approach to these substances.<sup>9i</sup> Deriving from the known ability of the mitomycins to undergo electrophilic activation *via* either one or two-electron reduction of the quinone moiety,<sup>7,11</sup> this proposal invoked a mechanism of action for the FR class of compounds analogous to that previously demonstrated for the mitomycins. Reductive cleavage of the N-O bond was proposed to generate aniline derivative **316** which was expected to rapidly cyclize (to **317**) and dehydrate to aziridonomitosen **318**. Related and extensive work<sup>7</sup> on structurally similar mitosenes generated from MC provided ample precedent for the expectation that interaction of **318** with DNA would afford the bis-alkylated DNA species **319**. If this proposal proved correct, the 5'-CG-3' cross-linking sequence specificity for mitosenes derived from MC would also be anticipated for the FR-900482-generated DNA interstrand cross-links.



**Figure 2-1.** Fukuyama and Goto proposal for reductive activation and subsequent DNA interstrand cross-linking by the FR-900482 class of antitumor natural products.<sup>9i</sup>

Alternatively, Danishefsky and McClure proposed that activation of the FR-900482 class of compounds might follow a nucleophilically-triggered motif.<sup>9c,12</sup> Addition of some biologically-relevant nucleophile (presumably a proteinaceous thiol or amine) to the aromatic C2 was envisioned to induce heterolytic cleavage of the hydroxylamine hemiketal with concomitant loss of water. Following rearomatization or coinciding with it, the expected ring closure would yield carbinolamine **321**. Dehydration of **321** would then afford the highly reactive aziridinomitosenes **322** capable of *bis*-alkylation at the activated C1 and C10 positions (mitomycin numbering system). DNA alkylation by this species would yield a lesion similar to that invoked by the Fukuyama proposal with the notable exception of substitution at the aryl C2 position (FR-900482 numbering system).



**Figure 2-2.** Danishefsky and McClure proposal for nucleophilic activation pathway to DNA interstrand cross-linking by FR900482 and related compounds.<sup>9c</sup>

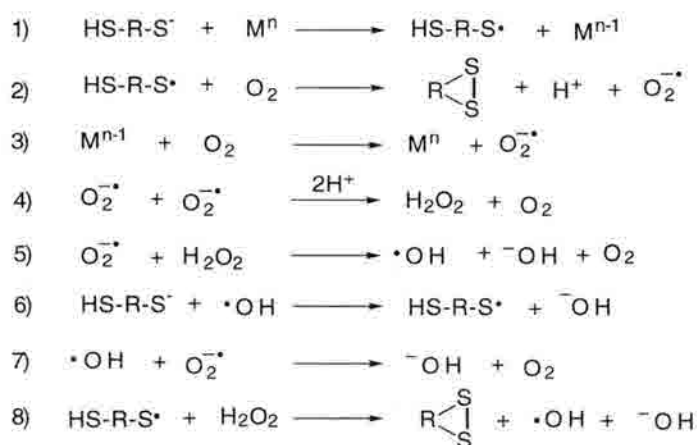
## 2.2 Results & Discussion

### 2.2.1. Activation Studies

Paramount to efforts aimed at elucidation of the mechanism of action of the FR-900482 class of drugs was the ability to induce activation *in vitro*. Efforts by Fujisawa demonstrated quite clearly the ability of these agents to form DNA-DNA and DNA-protein cross-links in L1210 leukemia and other tumor cell lines.<sup>2,3</sup> However, FK973 (**313**) formed no detectable interstrand DNA-DNA or DNA-protein cross-links when isolated nuclei of cells were exposed to the drug. This suggested that cytosolic (presumably reductive or oxidative) activation was required by the FR class compounds in order to inflict DNA damage.<sup>2c,d,3b</sup> The nature of the drug-induced lesions was known in only very general terms. Issues such as DNA/amino acid specificities and potential activation pathways were not addressed in any detail. Consequently, initial efforts focused on the ability of FR-900482 and structurally-related compounds to induce interstrand cross-links into plasmid DNAs for which the possibility of lesion detection was deemed extremely high due to the sheer number of potential cross-link sites. Given the mechanistic uncertainties pertaining to FR drug activation, we elected to study the more abundant FR-900482 with a

variety of reductants and nucleophiles amenable to the aqueous conditions deemed physiologically relevant. Hind III linearization of pBR322 DNA from *E. coli*. afforded a substrate for which ISC induction could easily be detected *via* alkaline agarose gel electrophoresis using methodology developed by Cech.<sup>13</sup>

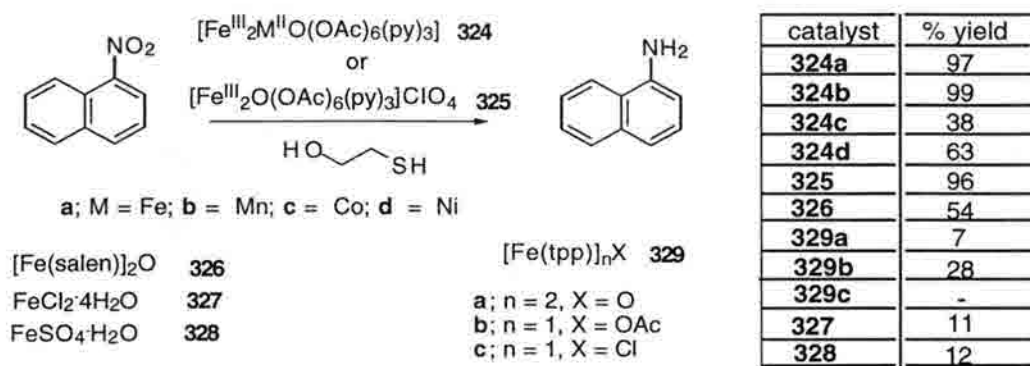
The physiological preponderance<sup>14</sup> of thiols and disulfides prompted the investigation of simple thiols such as dithiothreitol (DTT),  $\beta$ -mercaptoethanol ( $\beta$ -MET), and glutathione (GSH) with respect to FR-900482 activation. Thiols are readily converted to disulfides in the presence of oxygen, resulting in the concomitant reduction of molecular oxygen to superoxide.<sup>15</sup>



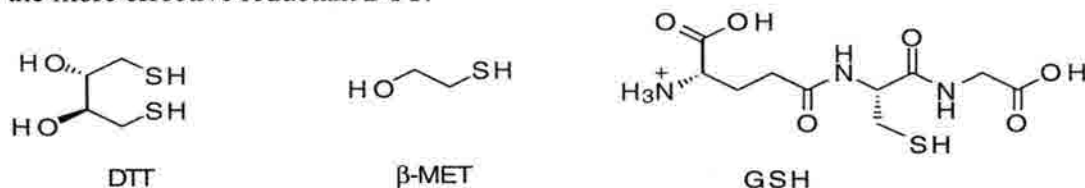
**Figure 2-3.** Proposed mechanism for the aerobic oxidation of thiols to disulfides.

The first step involves metal reduction (typically either  $\text{Fe}^{3+}$  or  $\text{Cu}^{2+}$ ) to afford an  $\text{M}^{n-1}$  species along with the resultant thiyl radical. Single electron transfer from the thiyl radical to endogenous oxygen yields superoxide and the corresponding disulfide.<sup>15</sup> Additionally, the  $\text{M}^{n-1}$  species may undergo oxidation *via* reaction with oxygen to produce superoxide or it may effect reduction of some other reactant. Particularly well noted are  $\text{Fe}^{3+}/\text{Fe}^{2+}$ -mediated reductions of nitroaromatics. Miura *et al.* have shown that catalysts **324a-d** and **325** very efficiently convert a wide array of nitroaromatic compounds to the corresponding amines upon the addition of  $\beta$ -mercaptoethanol.<sup>16</sup> In addition to

nitronaphthalene reduction, these complexes catalyzed the quantitative oxidative conversion of thiophenol to diphenyldisulfide in the presence of molecular oxygen. Precipitation of the iron-thiol complex and subsequent  $^{57}\text{Fe}$  Mossbauer spectroscopy indicated an  $\text{Fe}^{2+}/\text{Fe}^{3+}$  ratio of 56:44 thus implicating the thiol-ligated metal complex as the active reductant. This suggests that the active species which transfers electrons to the nitro compound is the reduced metal catalyst and not the transiently formed superoxide or thiyl radical species. Related work by Endo and co-workers<sup>17</sup> have addressed similar reactions under aqueous conditions using exclusively  $\text{Fe}^{2+}$ .

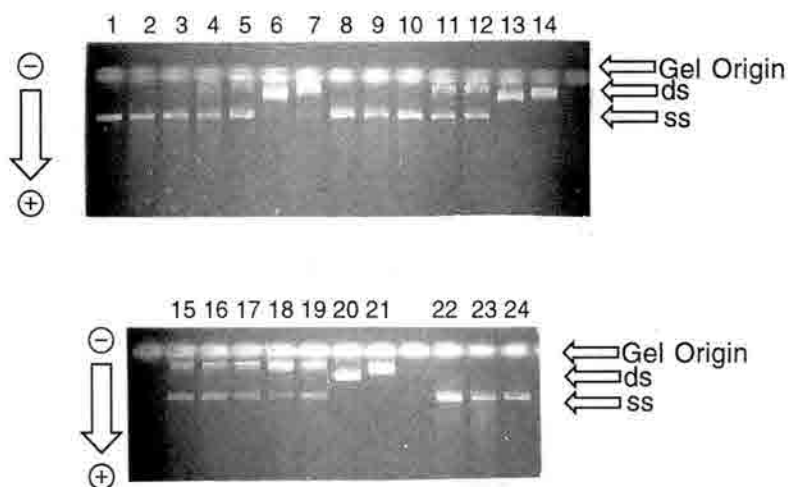


Our initial efforts involved analysis of cross-linking efficiency by FR900482 in the presence of dithiothreitol and  $\beta$ -mercaptoethanol. Given the vastly different reduction potentials of the two<sup>18</sup>, we believed that a reductively driven process would benefit from the more effective reductant DTT.



As shown in Figure 2-4, comparison of dithiothreitol (DTT) and  $\beta$ -mercaptoethanol ( $\beta$ -MET) containing reactions revealed that, in general, the more potent reductant DTT ( $E^\circ = -0.36$  V) afforded the higher cross-linking efficiency. Reactions 1 mM in FR900482 demonstrated  $\geq 99\%$  interstrand cross-link (ISC) formation in the presence of 10 mM DTT

as opposed to 72.7% for the analogous mercaptoethanol ( $E^0 = -0.207$  V) reaction (Figure 2-4 lanes 6 and 7). Similar differences in (ISC) induction were observed upon comparison of lanes 11 and 12 (53.1 % with DTT and 39.3% with  $\beta$ -MET respectively), as well as lanes 18 and 19 (93.3 % with DTT vs. 58.5 % with  $\beta$ -MET). These findings substantiated a potential redox pathway *enroute* to DNA cross-linking by FR900482, but did not refute potential nucleophilic activation.



**Figure 2-4.** Reactions of **312** with linearized pBR322 in the presence of dithiothreitol and  $\beta$ -mercaptoethanol. All reactions carried out in 10mM phosphate buffer, pH 8.0. Reactions were incubated 37°C 24 hours prior to electrophoresis. **Lane 1)** 1mM **312**; **Lane 2)** 1mM **312** + 0.1mM DTT; **Lane 3)** 1mM **312** + 0.1mM  $\beta$ -MET; **Lane 4)** 1mM **312** + 1mM DTT; **Lane 5)** 1mM **312** + 1mM  $\beta$ -MET; **Lane 6)** 1mM **312** + 10 mM DTT; **Lane 7)** 1mM **312** + 10 mM  $\beta$ -MET; **Lanes 8 - 14** same loadings as **lanes 1-7** except [**312**] = 10 mM. **Lanes 15-21** same loadings as **lanes 1-7** except [**312**] = 50 mM. **Lanes 22-23)** DNA only, DNA + 10 mM DTT, and DNA + 10 mM  $\beta$ -MET controls respectively. ss refers to single-stranded pBR322 whereas ds denotes interstrand cross-linked material. Arrows to left side of image denote the direction of electrophoresis.

**Table 2-2.** Summary of FR-900482 reactions with Hind III linearized pBR322 in the presence of DTT and  $\beta$ -mercaptoethanol ( See Figure 2-4 for electrophoretic image)

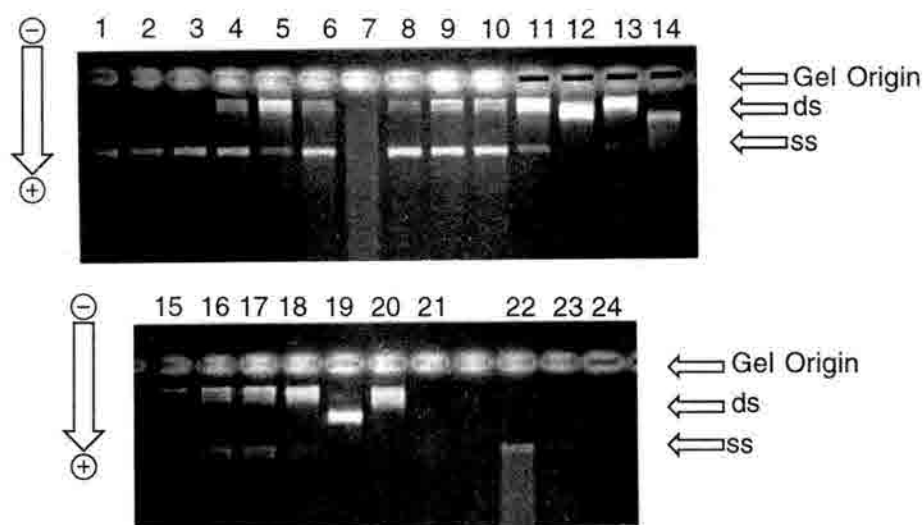
Entry	[FR-900482]	[ DTT]	[ $\beta$ -MET]	% ISC <sup>a</sup>
1	1 mM	-	-	-
2	1 mM	100 $\mu$ M	-	-
3	1 mM	-	100 $\mu$ M	-
4	1 mM	1 mM	-	20.0
5	1 mM	-	1 mM	28.0
6	1 mM	10 mM	-	$\geq 99$
7	1 mM	-	10 mM	72.7
8	10 mM	-	-	$\leq 1$
9	10 mM	100 $\mu$ M	-	$\leq 1$
10	10 mM	-	100 $\mu$ M	$\leq 1$
11	10 mM	1 mM	-	53.1
12	10 mM	-	1 mM	39.3
13	10 mM	10 mM	-	$\geq 99$
14	10 mM	-	10 mM	$\geq 99$
15	50 mM	-	-	45.8
16	50 mM	100 $\mu$ M	-	47.4
17	50 mM	-	100 $\mu$ M	66.7
18	50 mM	1 mM	-	93.3
19	50 mM	-	1 mM	58.5
20	50 mM	10 mM	-	$\geq 99$
21	50 mM	-	10 mM	$\geq 99$

<sup>a</sup>Determined by measurement of respective optical densities for each band of interest

Reactions with glutathione ( a very nucleophilic reducing agent) revealed that DNA cross-linking by FR900482 was slightly favored by glutathione (GSH) over  $\beta$ -MET (Fig. 2-5). Substitution of GSH for  $\beta$ -MET typically afforded a 5-10% enhancement in cross-linking. This was contradictory to the results of Figure 2-4 wherein the more effective reductant effected substantially higher ISC yields than the more nucleophilic (less reducing) thiol. Both GSH and  $\beta$ -MET gave rise to similar yields of cross-linked pBR322 supportive of a redox mediated process. Drug activation inherant to a nucleophile-triggered pathway would have been *substantially favored by glutathione* (vs.  $\beta$ -MET). Additionally,



glutathione's more potent reducing ability in comparison to  $\beta$ -MET could offer an explanation for the observed difference in ISC induction. As in Figure 2-5 the greatest difference in ISC formation between reactions containing glutathione and MET is 20% (lane 4 vs. lane 5). On average a difference of 8.2% cross-linking efficiency was observed with the two thiols, strongly indicative of reduction potential differences rather than nucleophilicity differences.



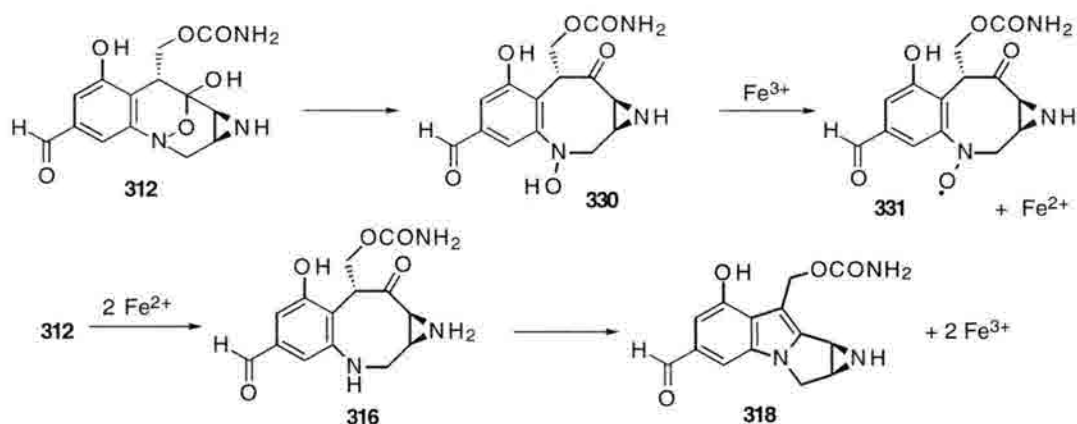
**Figure 2-5.** Reactions of **312** with linearized pBR322 in the presence of glutathione and mercaptoethanol. All reactions carried out as described in Fig. 2-4. **Lane 1)** 1mM **312**; **Lane 2)** 1mM **312** + 1mM  $\beta$ -MET; **Lane 3)** 1mM **312** + 1mM glutathione; **Lane 4)** 1mM **312** + 5mM  $\beta$ -MET; **Lane 5)** 1mM **312** + 5mM glutathione; **Lane 6)** 1mM **312** + 10 mM  $\beta$ -MET; **Lane 7)** 1mM **312** + 10 mM glutathione; **Lanes 8 - 14** same loadings as **lanes 1- 7** except [ **312** ] = 10 mM. **Lanes 15-21** same loadings as **lanes 1-7** except [ **312** ] = 50 mM. **Lanes 22-24)** DNA control, DNA + 10 mM  $\beta$ -MET control and DNA + 10 mM glutathione control respectively. No slow mobility material was noted in **lanes 22-24**.

**Table 2-3.** Summary of FR-900482 reactions with Hind III linearized pBR322 in the presence of glutathione and  $\beta$ -mercaptoethanol (Figure 2-5)

Entry	[FR-900482]	[ $\beta$ -MET]	[glutathione]	% ISC
1	1 mM	-	-	-
2	1 mM	1 mM	-	< 1
3	1 mM	-	1 mM	< 1
4	1 mM	5 mM	-	58.3
5	1 mM	-	5 mM	79.0
6	1 mM	10 mM	-	17.1
7	1 mM	-	10 mM	decomposition
8	10 mM	-	-	16.0
9	10 mM	1 mM	-	61.7
10	10 mM	-	1 mM	66.2
11	10 mM	5 mM	-	84.9
12	10 mM	-	5 mM	$\geq 99$
13	10 mM	10 mM	-	94.6
14	10 mM	-	10 mM	$\geq 99$
15	50 mM	-	-	76.1
16	50 mM	1 mM	-	75.4
17	50 mM	-	1 mM	72.3
18	50 mM	5 mM	-	93.8
19	50 mM	-	5 mM	$\geq 99$
20	50 mM	10 mM	-	$\geq 99$
21	50 mM	-	10 mM	decomposition.

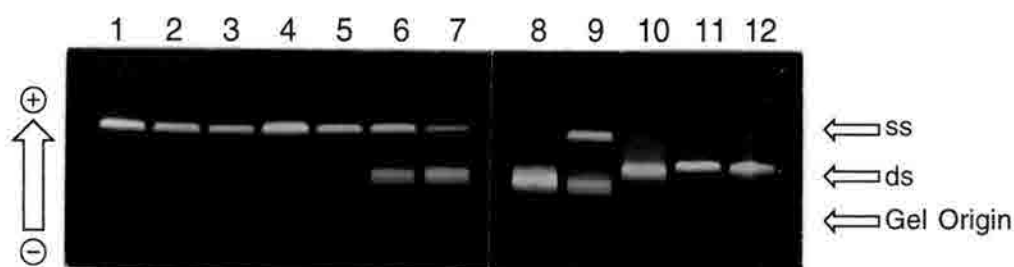
Given the importance of  $\text{Fe}^{3+}$  within Fenton/Haber-Weiss redox cycling and its role in the oxidation of thiols to the corresponding disulfides<sup>15,16</sup>, a viable means by which to probe a possible redox manifold involved alteration of  $\text{Fe}^{3+}$  concentrations in the cross-linking reactions. As shown in Figure 2-7, reaction of **312** with  $\text{Fe}^{3+}$  in concentrations ranging from 1  $\mu\text{M}$  to 1 mM produced a marked increase in double-stranded material with progressively increasing  $\text{Fe}^{3+}$  concentration. This most likely resulted from thiol reduction of  $\text{Fe}^{3+}$  to  $\text{Fe}^{2+}$  followed by FR900482 reduction/activation as per the Fukuyama model. This was found for not only those reactions involving  $\beta$ -mercaptoethanol, but was also

visible in **312** + Fe(III)-EDTA control reactions. Comparison of drug only (lane 5) and drug + thiol (lane 9) reactions (both in the presence of 100  $\mu$ M Fe(III)-EDTA) revealed that the presence of thiol radically increased the extent of cross-linking observed over the case not containing thiol and that this increase exceeded simple additive affects. The synergism thus witnessed in the thiol + Fe(III)-EDTA reactions offered strong evidence that FR-900482 activation followed a reductive pathway. Two facts supported this reasoning. *First, the thiol mediated reduction of  $Fe^{3+}$  to  $Fe^{2+}$  is known to effect the reduction of nitroaromatics to the corresponding amines.<sup>16,17</sup> Secondly, were nucleophilic thiol additions responsible for drug activation, then the addition of  $Fe^{3+}$ /EDTA would have greatly reduced the amount of ISC induction due to increased conversion of the nucleophilic thiol to the "inert" disulfide thereby quenching the activating agent.*



**Figure 2-6.** Proposed mechanism by which **312** undergoes Fe(III)-EDTA mediated reductive activation.

The ability of **312** to interstrand cross-link pBR322 in the presence of Fe(III)-EDTA indicates that FR900482 and structurally related compounds *may* undergo "self-activation" in the presence of metal ions.  $Fe^{3+}$  readily undergoes reduction by hydroxylamines to afford  $Fe^{2+}$  complexes.<sup>19</sup> As discussed previously,  $Fe^{2+}$  complexes are capable of facile nitroaromatic reduction.<sup>16,17</sup> Thus, a mechanism wherein  $Fe^{3+}$  is reduced to  $Fe^{2+}$  which then reduces FR-900482 (see Fig. 2-6) is completely consistent with the literature and seems viable based upon the data generated.



**Figure 2-7.** Reactions of **312** with linearized pBR322 in the presence of Fe(III)-EDTA and/or  $\beta$ -mercaptoethanol ( $\beta$ -MET) (See Table 2-4 for yield quantiations). All reactions carried out in 10mM phosphate buffer, pH 8.0. Reactions were incubated 37°C 4 hours prior to electrophoresis. **Lane 1**) control DNA ; **Lane 2**) 10 mM **312**; **Lane 3**) 10mM **312** + 10mM  $\beta$ -MET ; **Lane 4**) 10mM  $\beta$ -MET control ; **Lane 5**) 10 mM **312** + 1  $\mu$ M Fe(III)-EDTA ; **Lane 6**) 10mM **312** + 10  $\mu$ M Fe(III)-EDTA; **Lane 7**) 10mM **312** + 100  $\mu$ M Fe(III)-EDTA; **Lane 8**) 10mM **312** + 1 mM Fe(III)-EDTA ; **Lanes 9-12** same loadings as **lanes 5-8** and contained 10mM  $\beta$ -MET.

**Table 2-4.** Summary of reactions of FR-900482 with linearized pBR322 in the presence of  $\beta$ -mercaptoethanol and/or Fe(III)-EDTA. ( see Figure 2-7 above for electrophoretic image).

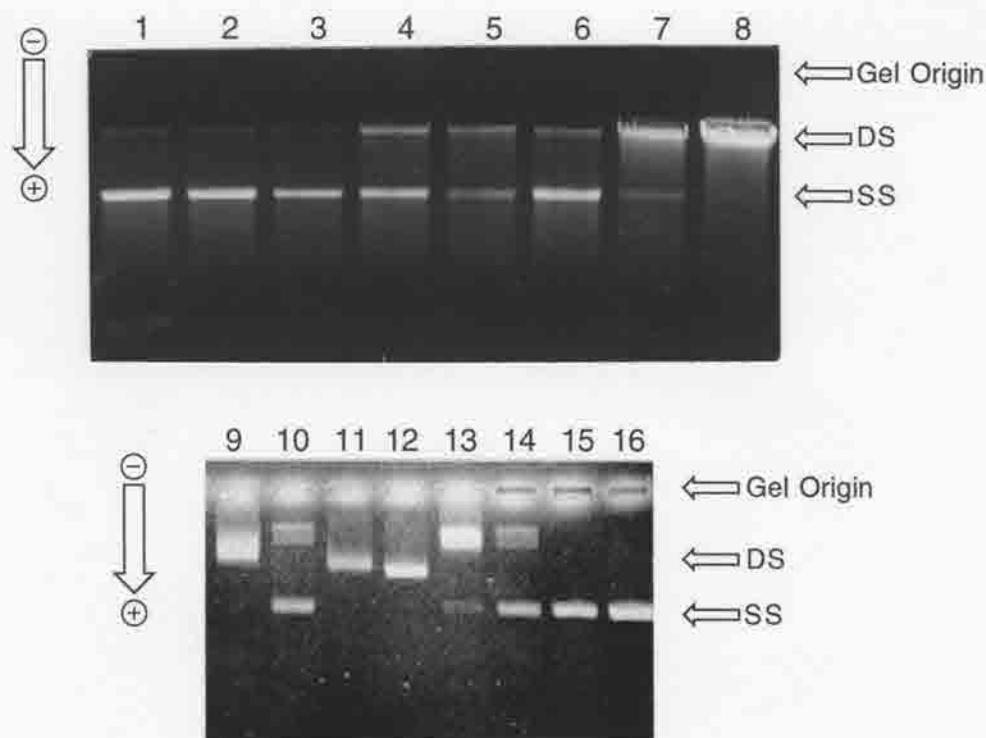
Entry	[FR-900482]	[ $\beta$ -MET]	[FeCl <sub>3</sub> -EDTA]	%ISC induction
1	-	-	-	-
2	10 mM	-	-	-
3	10 mM	10 mM	-	-
4	-	10 mM	-	-
5	10 mM	-	1 $\mu$ M	11.5
6	10 mM	-	10 $\mu$ M	33.5
7	10 mM	-	100 $\mu$ M	71.6
8	10 mM	-	1 mM	$\geq 99$
9	10 mM	10 mM	1 $\mu$ M	54.2
10	10 mM	10 mM	10 $\mu$ M	$\geq 99$
11	10 mM	10 mM	100 $\mu$ M	$\geq 99$
12	10 mM	10 mM	1 mM	$\geq 99$

In addition to elucidation of  $\text{Fe}^{3+}/\text{Fe}^{2+}$  redox shuttling with respect to FR-900482 activation, we were also concerned with the findings of Figures 2-4 and 2-5. Strong evidence had been generated to support a reductive manifold *enroute* to DNA cross-linking by **312**. However, the generation of slow mobility DNA in lanes 8 and 15 of Figure 2-4 and lane 15 of Figure 2-5 (containing neither thiol or  $\text{Fe}^{3+}$ ) could not be explained. Initial hypotheses involved incomplete DTT removal after pBR322 Hind III digestion, however, reactions using gel purified pBR322 yielded the same result.

The critical role of  $\text{Fe}^{3+}$  and/or  $\text{Fe}^{2+}$  in the activation process suggested that adventitious  $\text{Fe}^{3+}$  in the reactions may have been responsible for the observed slower mobility DNA.<sup>20</sup> To probe this possibility, reactions were performed in the presence of the iron chelating agent desferal. Desferal forms a hexa-coordinate complex with  $\text{Fe}^{3+}$  that excludes iron-associated water and uncouples the oxidation of  $\text{Fe}^{2+}$  from the Fenton redox cycle.<sup>21</sup> It possesses a high affinity for  $\text{Fe}^{3+}$  ( $\log k_f = 30.7$ ) and as such was deemed a good candidate for shutting down or inhibiting potential  $\text{Fe}^{2+}/\text{Fe}^{3+}$  redox shuttling.<sup>21</sup> Reactions 10 mM in FR-900482 containing 10  $\mu\text{M}$  desferal suffered a roughly 30% decrease in ISC efficiency over the case not involving desferal (see Appendix Figure. 5-1 and Table 5-1). No exogenous iron ( $\text{Fe}^{3+}$  or  $\text{Fe}^{2+}$ ) was used, and neither reaction contained added reductants. As such, the implication that **312** at concentrations  $\geq 10$  mM could act to cross-link DNA *by itself* was refuted. More likely, it appears that adventitious metals (presumably  $\text{Fe}^{3+}$  and/or  $\text{Cu}^{2+}$ ) are capable of redox interaction with **312** in a fashion leading to the DNA reactive species. The expected low efficiencies of this process would explain why those reactions containing a high excess of **312** are affected.

### **2.2.2. Comparison of DNA interstrand cross-linking efficiencies by natural products FR-900482 and FR66979**

Concomittant with the section 2.2.1. studies, efforts were directed at examination of the other natural product **314**. The intention of these studies was to determine the importance of the benzylic aldehyde of FR-900482 in facilitating formation of the DNA-reactive species. Deprotonation at *C7 enroute* to mitosenes **318** and/or **322** was proposed to be greatly enhanced due to the presence of the C12 aldehyde. One means of probing this was to compare the relative cross-linking efficiencies of the aldehyde **312** and the benzylic alcohol **314**.<sup>10a</sup> Due to its low natural abundance from fermentation, FR-66979 (**314**) was prepared by reduction of the more available FR900482 (**312**) by catalytic hydrogenation at 1 atmosphere. Experiments involving the two natural products once again exploited alkaline denaturing agarose gel electrophoresis as a means of readily detecting interstrand cross-linked material. Shown in Figure 2-8, **312** afforded only marginal cross-linking activity at concentrations 1-10 mM. As discussed previously, this was the likely result of adventitious metals. At [**312**] = 50 mM (lanes 5 & 8) a marked decrease in activity both in the presence and absence of thiol was noted as compared to the 1-10 mM cases. In line with the findings of section 2.2.1., significant cross-link formation became evident at [**312**] = 1-10 mM in the presence of equimolar amounts of thiol (lanes 7,8). FR-66979 (**314**) showed significant cross-link formation at concentrations as low as 100  $\mu$ M *in the absence of thiol* (lane 14). More significantly, the addition of thiol to FR-66979 reactions did not result in appreciable enhancement of ISC formation ( lane 10 vs. 14 and 9 vs. 13) as evidenced for **312** (lanes 3 vs. 6). At 1-10 mM, **314** (w/o added reductant) completely cross-linked the pBR322 substrate (lanes 11 and 12). Additionally, at [drug]=50mM, **314** resulted in quantitative cross-linking and did not exhibit any of the inhibitory characteristics that **312** had demonstrated (lanes 3-5 and 6-8).



**Figure 2-8.** Reactions of **312** and **314** with linearized pBR322 in the presence or absence of  $\beta$ -mercaptoethanol ( $\beta$ -MET). All reactions were carried out at 37°C for 24 h. in 10 mM phosphate buffered saline (PBS). **Lanes 1 and 16** are DNA control lanes. **Lanes 2 and 15** are both 1mM  $\beta$ -MET lanes. **Lanes 3-5** are 1.0, 10, and 50 mM FR-900482 (**312**) respectively. **Lane 6** is 1mM **312** + 1.0 mM thiol. **Lane 7** is 10 mM **312** + 10 mM thiol whereas **lane 8** is 50 mM **312** + 10 mM thiol. **Lane 9** is 1.0 mM FR-66979 + 1.0 mM thiol. **Lane 10** is 0.1 mM **314** + 0.1 mM thiol. **Lanes 11-14** are reactions involving only **314** in decreasing concentrations. **Lane 11** is 50 mM **314**; **lane 12** is 10 mM **314**; **lane 13** is 1.0 mM **314**, and **lane 14** is 0.1 mM **314**.

From these results, it followed that, **314** did not require exogenous chemical activation (such as reduction) to cross-link DNA. On the other hand, **312** was comparatively inactive in and of itself and required 1 molar equivalent of reductant to significantly cross-link DNA.

To probe the possible chemical role of the thiol with **312** more closely, reactions of **312** with 2-mercaptoethanol; DTT; and glutathione at 37°C for 24 h in D<sub>2</sub>O (all 5 mM in thiol and 5 mM in drug) were followed by <sup>1</sup>H nmr spectroscopy and TLC. Under these conditions, no evidence for any reaction was detected. Similarly, incubation of **312** (3.3 mM) with 2'-deoxyguanosine-5'-monophosphate (3.3 mM) in D<sub>2</sub>O at 37°C for 24 h. in



either the presence or absence of stoichiometric thiol resulted in no detectable reaction. Parallel experiments with **314** similarly resulted in no detectable reaction products. Similar studies have recently been reported by Hopkins and Paz.<sup>4a</sup>

**Table 2-5.** Summary of FR-900482 and FR-66979 reactions with Hind III linearized pBR322 in the presence or absence of  $\beta$ -mercaptoethanol (Figure 2-8)

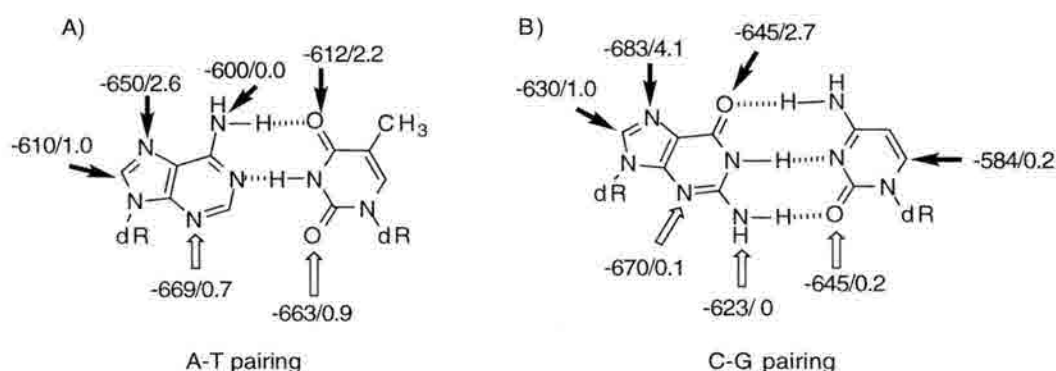
Entry/lane	[FR-900482]	[FR-66979]	[ $\beta$ -MET]	% ISC
1	-	-	-	-
2	-	-	1 mM	-
3	1 mM	-	-	25.2
4	10 mM	-	-	63.0
5	50 mM	-	-	9.1
6	1 mM	-	1 mM	96.1
7	10 mM	-	10 mM	$\geq 99$
8	50 mM	-	10 mM	28.6
9	-	1 mM	1 mM	$\geq 99$
10	-	0.1 mM	0.1 mM	58.7
11	-	50 mM	-	$\geq 99$
12	-	10 mM	-	$\geq 99$
13	-	1.0 mM	-	93.8
14	-	0.1mM	-	42.4
15	-	-	1 mM	-
16	-	-	-	-

In the context of the mechanisms proposed in Figures 2-1 & 2-2, our results indicated that one possible pathway for the activation of **312** may involve two-electron reduction to **314** which, as shown above, would directly effect cross-linking; **314** appeared to possess the correct oxidation state to induce ISCs. This raised the question of the inherent reducibility of the N-O bond (**312** to **317**, Figure 2-1) *in vitro* and *in vivo*.<sup>22</sup> The stability of both **312** and **314** to powerful nucleophilic thiols in the presence or absence of the mononucleotide under conditions that led to quantitative DNA cross-links once again disfavored the viability of nucleophilic activation (**312** to **320**, Figure 2-2).

Although the conversion of **312** to a mitosene derivative (*via* **314**?) was an alluring hypothesis, our results indicated that **314** and not **312** represented the more intriguing focus of further mechanistic work. Particularly relevant to this reasoning was that **314** seemed to be more closely related to the DNA reactive species responsible for cross-linking. Of the two natural products, **314** represents the more reactive substance by a factor of about 10 (in the absence of thiol) as shown by comparison of lanes 3 and 14. This was confirmed in the presence of thiol as well. Cross-linking of small radiolabeled ODNs (**template 2**-section 2.2.3.) and quantiation *via* liquid scintillation counting revealed that only 1.9% of the substrate was cross-linked by **312** while the yield for cross-linked material resulting from reaction with **314** was 14.3 %. Indeed, the vastly greater reactivity of this species was the impetus for its use in sequence specificity studies.

### 2.2.3. Sequence-Specificity Studies: relevance to a mitosene intermediate.

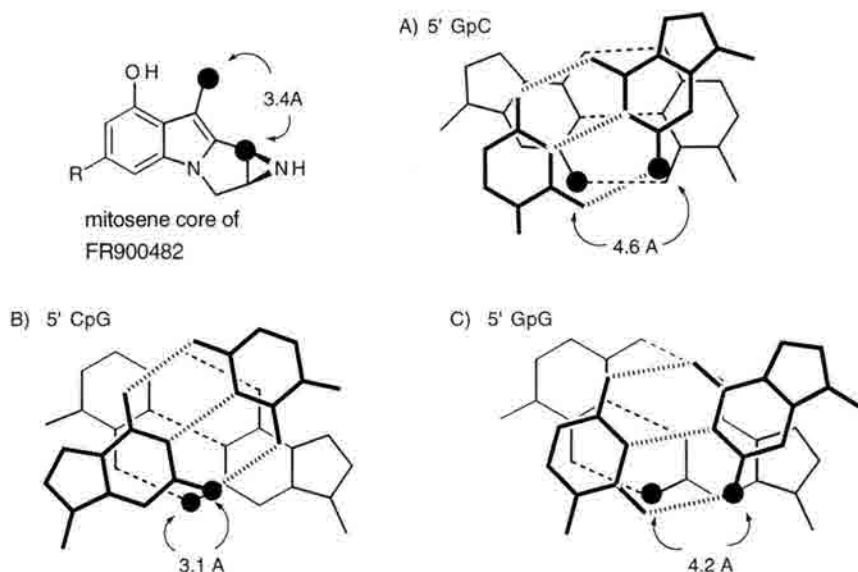
The minor and major grooves of DNA bear considerably different negative potentials. The geometry of the grooves and their location with respect to the helical axis has a major influence on this electrostatic potential as well as the steric accessibilities of the reactive centers.<sup>23</sup> These geometries mandate that for GpC the most negative potential is located within the major groove (specifically N<sup>7</sup>) while for ApT, the minor groove possesses the greatest nucleophilic character.<sup>24</sup> Steric accessibility also bears considerable influence upon the reactivity of these positions with electrophilic agents.<sup>24</sup>



**Figure 2-9.** Electrostatic potentials and calculated accessibilities of major and minor groove moieties within G-C and A-T base pairings. Dark arrows denote major groove sites while outlined arrows denote minor groove sites. The first number of each set denotes base site potentials in units of kcal/mol while the second number expresses the base atom accessibility in units of Å<sup>2</sup>. These values are applicable only to B-DNA and are as calculated by Pullman *et al.*<sup>23</sup>

The DNA sequence-specificity of the mitomycins derives partially, but not completely, from this concept.<sup>25</sup> Within 5'-CG-3', the most nucleophilic residue is the N<sup>7</sup> of dG (the result of additive electrostatic potential and accessibility values).<sup>23</sup> However, placement of the quinone methide (resulting from mitomycin activation) within the major groove fails to result in an N<sup>7</sup>-mediated interstrand cross-link. Rather, the N<sup>7</sup> alkylation event (formed in generally high yields upon two electron reduction of the mitomycin)<sup>26</sup> leads only to monoalkylation thus providing a therapeutically insignificant lesion. Despite a considerably reduced potential and greater steric encumbrance (Figure 2-9) the less nucleophilic minor groove exocyclic amine represents the preferred site of DNA

modification involved in interstrand cross-linking. This stems from the ideal geometric fit of the mitosene within the 5'-CG-3' sequence. The intramolecular distance between the two electrophilic centers of the mitosene (3.4 Å) and the distance between the two deoxyguanosine N<sup>2</sup> amines of duplex substrate (3.1 Å for 5'CpG, Figure 2-10) are ideally matched and thus greatly facilitates the observed 5'CpG specificity observed for the mitomycins.<sup>25,27</sup>



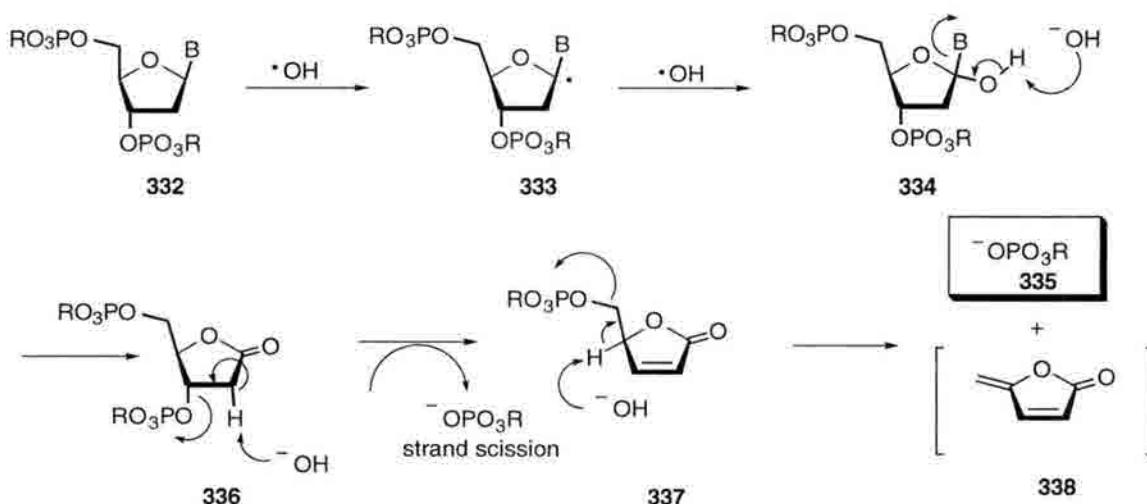
**Figure 2-10.** Molecular distances of adjacent guanosine N<sup>2</sup> amines in sequences of interest. View is from the top of sequence looking down. Bold bonded bases are on top with the thin-lined bases below. Black balls on DNA bases denote exocyclic N<sup>2</sup> positions while black balls on the FR mitosene core denote electrophilically activated centers in line with analogy to the mitomycins.<sup>27</sup>

Although other principles of molecular recognition are involved<sup>25</sup>, this geometric matching of the drug and its target sequence is the largest single contributor to the base-pair specificity observed for the mitomycins (see section 1.5.5.).

In the absence of exogenous reducing agents, FR-900482 does not cross-link DNA.<sup>4,10</sup> As detailed in sections 2.2.4., preparation of FR-66979 from Pd/C catalyzed hydrogenation of FR900482 affords a chemically "pre-activated" FR congener most likely bearing the carbinolamine structure **317**.<sup>4a</sup> Due to the efficacy with which "over-reduced" FR-66979 was found to cross-link both plasmid and synthetic DNAs we opted to determine the base pair specificity of this FR-66979 "analog". This was deemed highly

significant since no mechanistic data for these compounds had been obtained beyond the Fujisawa reports. Additionally, the belief that FR-66979 did not require reductive activation posed intriguing mechanistic questions which could be addressed partially by assignment of DNA specificity.

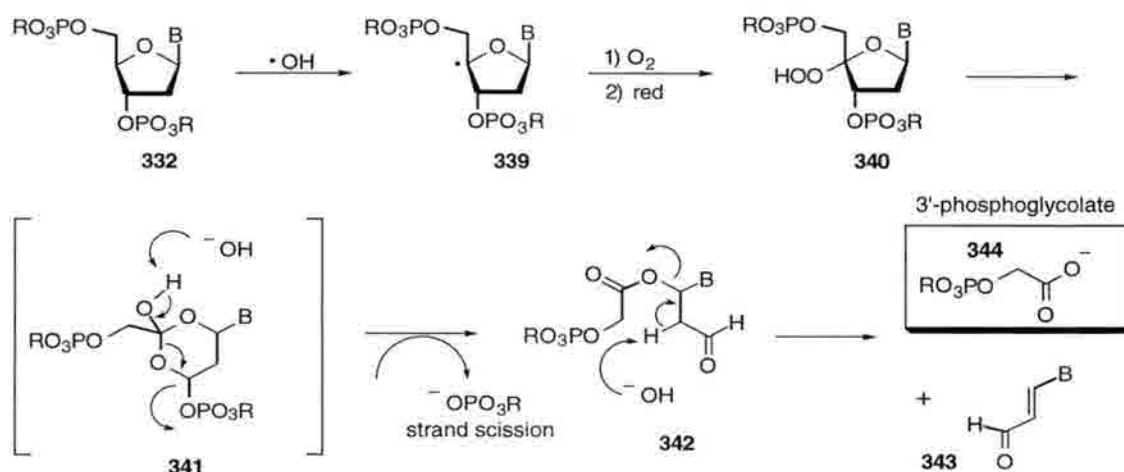
Preliminary efforts toward sequence-specificity assignments involved the exploitation of Fe(II)-EDTA footprinting methodology developed by Tullius and Dombroski<sup>28</sup> and extended by Hopkins.<sup>30</sup> Extension of Fe(II)-EDTA mediated (*via* hydroxyl radical production) DNA scission towards the development of highly selective chemical nucleases has been examined by Dervan and co-workers *via* conjugation of Fe(II)-EDTA to a host of DNA binding ligands.<sup>29</sup> The strand scission process relies on Fenton/Haber-Weiss redox cycling which produces the highly reactive hydroxyl radical.



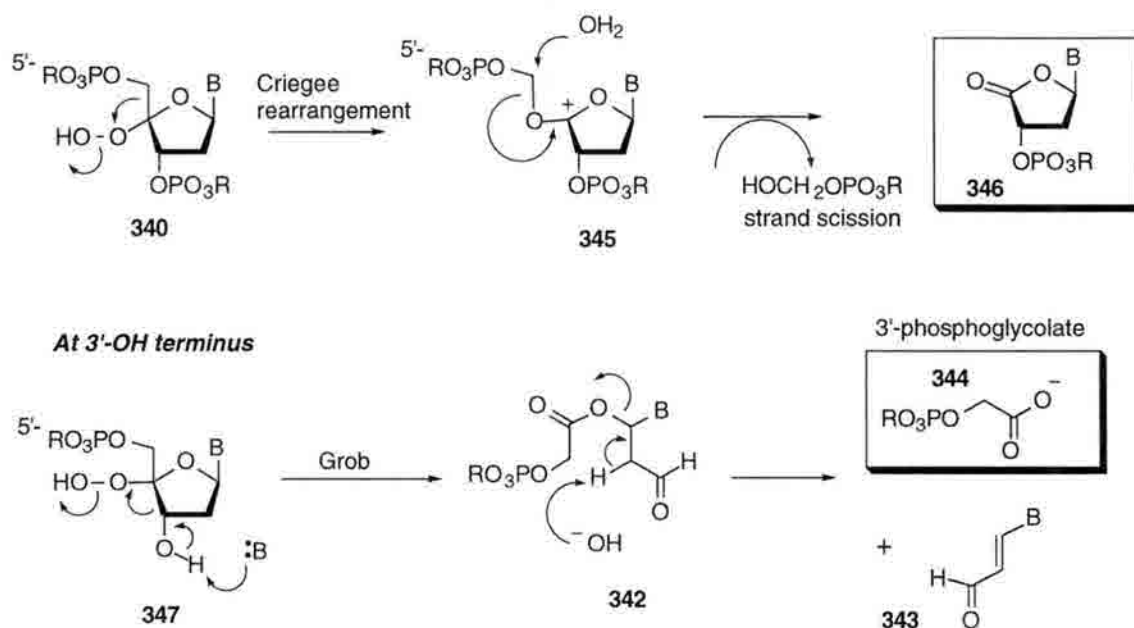
**Figure 2-11.** C1' H-atom abstraction leading to DNA strand scission resulting in 3' phosphate formation.<sup>6</sup>

Hydrogen abstraction at the DNA sugar C1' and C4' results from interaction with the diffusable hydroxyl radical and leads to the DNA strand scission products outlined in Figures 2-11 and 2-12.<sup>6</sup> Recent and extensive work by Giese and co-workers has addressed formation of lactone **346** which results also from the C4' H-abstraction event (Figure 2-13).<sup>6c</sup> These workers have also provided evidence that generation of the 3'

phosphate and 3' phosphoglycolate may result not only from traditional Criegee rearrangement of the C4' hydroperoxide, but may also occur *via* Grob fragmentation (Figure 2-13) of 3'-dephosphorylated nucleotides (**347**).<sup>6c</sup>



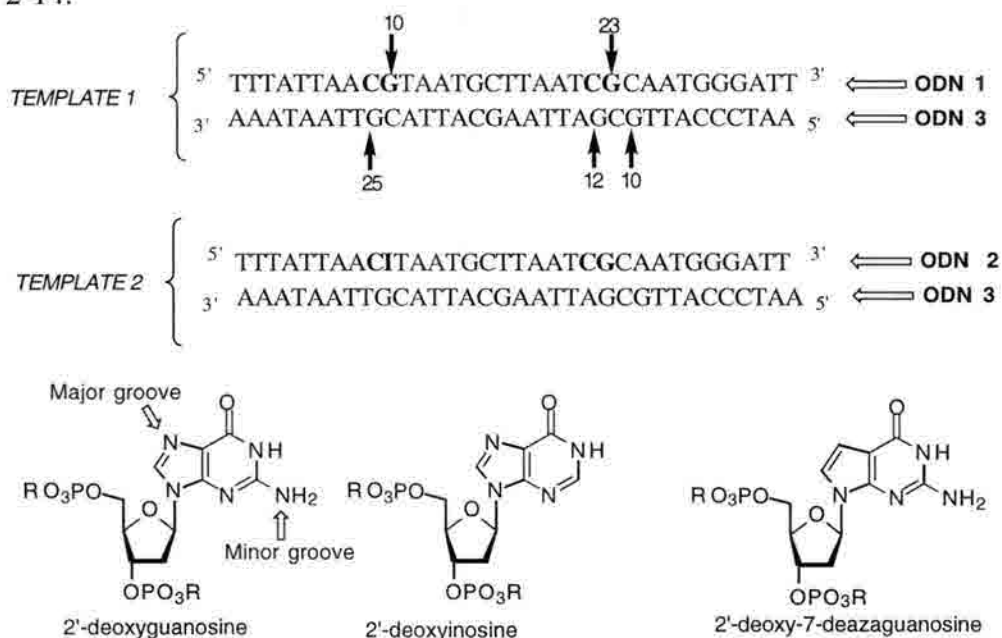
**Figure 2-12.** C4' H-atom abstraction leading to 3' phosphate and 3' phosphoglycolate adducts.<sup>6</sup>



**Figure 2-13.** Giese proposals for C4' H-atom abstraction leading to 5' lactone adduct **346** and 3' phosphate and 3' phosphoglycolate *via* Grob fragmentation.<sup>6c</sup>

Although applicable only to interstrand cross-linked ODNs, the reports by Hopkins *et al.* provided ample support for our studies employing this radical-based means of DNA sequencing.<sup>30</sup> This methodology, in conjunction with DNA base substitution efforts afforded not only a means of base specificity assignments, but also regiochemical determination of the DNA base atoms involved in FR-66979 *bis*-alkylation.<sup>10b</sup>

The substrate 5'-TTTATTAACGTAATGCTTAATCGCAATGGGATT-3' (**ODN 1**) and a modified version bearing inosine (guanosine lacking the N<sup>2</sup> exocyclic amine) at the G-10 position (**ODN 2**) and the mutual complement **ODN 3** strand were synthesized. Cross-linking of 5'-<sup>32</sup>P-labeled **ODNs 1** and **2** to their shared complement followed by isolation and Fe(II)-EDTA digestion rendered the cleavage patterns in lanes 7 and 8 of Figure 2-14.



Barring conjugation to DNA site-specific ligands (DNA-binding peptides, triple-helix forming ODNs, sequence-specific DNA alkylating agents, etc.), the process of Fe(II)-EDTA mediated strand scission is a sequence random event.<sup>29a</sup> Native DNA subjected to Fe(II)-EDTA cleavage affords an equimolar assortment of all fragment sizes up

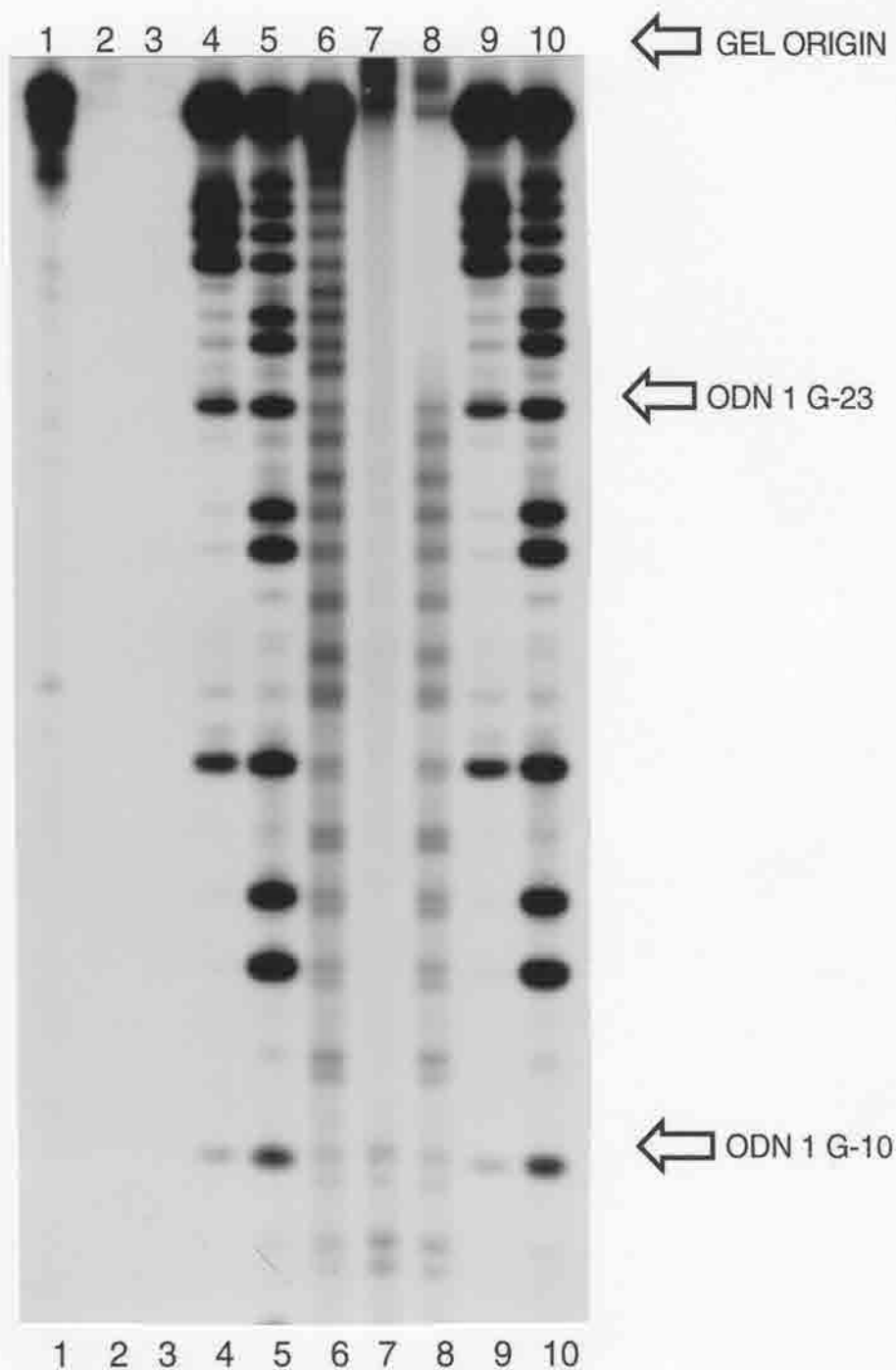


to and including the full-length strand (lane 6, Figure 2-14). Analogous treatment of cross-linked DNA yields short fragments corresponding to cleavage at or to- the radiolabeled side of the alkylated residue.

As such, the observed cleavage pattern revealed by lane 7 of Figure 2-14 was diagnostic for **ODN 1** alkylation at G-10. Conversely, cross-linking and digestion of the **template 2** (bearing inosine at the **ODN 1** G-10 position) revealed G-23 as the primary alkylation site (lane 8, Figure 2-14). This "cleavage shift" resulted from deletion of the exocyclic amine ( $N^2$ ) at the G-10 residue. Installation of inosine at this position halted cross-link formation, thus implicating the  $N^2$  residues of adjacent guanosines (within only the 5'-CG-3' box) exposed in the minor groove, as the sole functionalities responsible for interstrand cross-linking by **314**.

This was in accord with the expectation that *bis*-alkylation of FR-66979 with DNA should occur in the minor groove of DNA and supported the hypothesis that FR-66979 and related congeners cross-link DNA *via* a mitomycin type mechanism. Notably, cross-linking of **ODNs 1** and **2** by FR-900482 and FK973 followed by Fe(II)-EDTA digestion afforded the same results thus demonstrating the generality of the disclosed dG  $N^2$  specificity within 5'-CG-3' (Appendix Figure 5-3).<sup>31</sup>

Complementary strand analysis (Figure 2-15) was performed to ensure that indeed each cross-linkable site within the respective duplexes involved the adjacent deoxyguanosine residues within each 5'-CG-3'. This was accomplished upon 5'-<sup>32</sup>P end-labeling of **ODN 3** (complementary strand to both **ODNs 1** and **2**). Cross-linking followed by Fe(II)-EDTA digestion revealed that for the cross-linked **template 1**, cleavage seizure occurred at the dG-25 of **ODN 3** (lane 7, Fig. 2-15). This corresponds to the dG of 5'-CG-3' previously shown to coincide with cross-link participation of **ODN 1** dG-10. Conversely, cross-linking of **template 2**, in which the now unlabeled strand



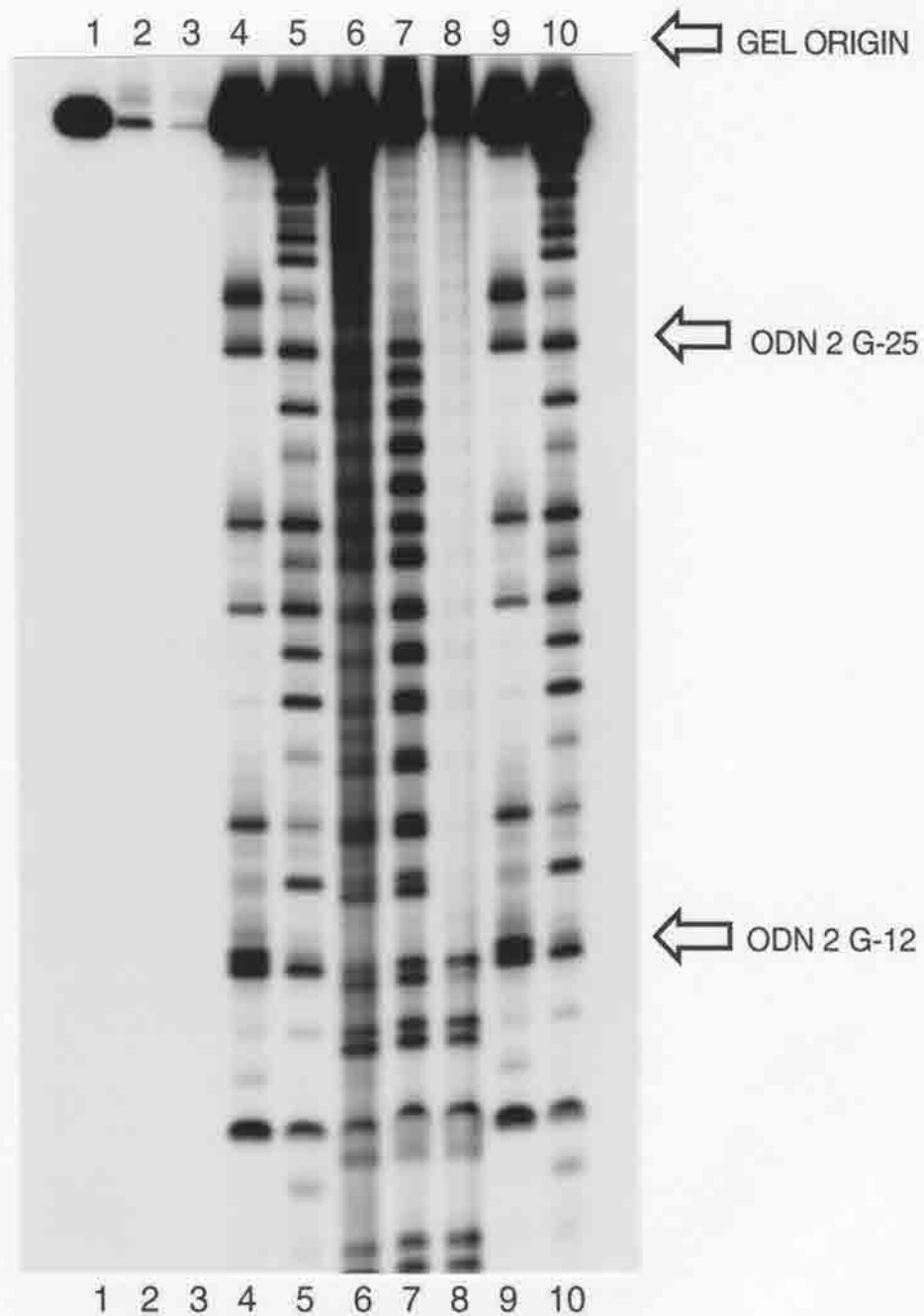
**Figure 2-14.** Autoradiogram of Fe(II)-EDTA footprinting of cross-linked **templates 1** and **2** (labeled at 5' terminus of **ODNs 1** and **2** respectively). **Lanes 1-3**, standard DNA, cross-linked **template 1**, cross-linked **template 2**; **lanes 4** and **9** Maxam-Gilbert G; **lanes 5,10** Maxam-Gilbert G+A. **Lane 6**, 1mM Fe(II)-EDTA control; **Lane 7**, cross-linked **template 1** after 1mM Fe(II)-EDTA digestion; **Lane 8**, cross-linked **template 2** after 1mM Fe(II)-EDTA digestion. Slow mobility cross-link standards in **lanes 2** and **3** (outside of the sequencing region depicted) maybe seen in Appendix Figure 5-2.

(ODN 2) had inosine at position 10, gave rise to cleavage diagnostic for ODN 3 dG-12 alkylation of the labeled complement (lane 8 Figure 2-15). Significantly, the pattern obtained was completely attributable to dG-12 alkylation of ODN 3 with no detectable enhancement in cleavage (see appendix Fig. 5-4) arising from the possible dG-10 alkylation event (from potential 5'-GC-3' cross-linking). Thus, when confronted with the possibility of forming either the 5'-CG-3' cross-link or the 5'-GC-3' cross-link, the active species derived from FR66979 was completely selective for the 5'-CG-3' event.

It is noteworthy that, at the time that these reactions were performed, the ability to resolve the different cross-linked species from one another had not yet been achieved. As such, the cleavage patterns obtained for **template 1** were diagnostic for whichever 5'-CG-3' box underwent preferential cross-link formation within the "bis"-cross-linkable duplex.

The cleavage patterns for cross-linked **template 1** (Figures 2-14 and 2-15) indicate preferential alkylation at the dG-10 5'-CG-3' box of ODN 1 as opposed to the G-23 residue. Equal cleavage at both sites (assuming equitable cross-link formation at both 5'-CG-3' boxes) would yield a pattern corresponding to a G-23 fragment or perhaps a mixture of the two. Assuming that **template 1** suffered alkylation at both 5'dCG boxes, this preference would likely result from the effect of flanking bases. Alternatively, should two different cross-linked species have resulted (one from dG-10 and one from dG-23 of ODN 1), then that proceeding with the greatest efficiency would be expected to result in the predominant cleavage pattern.

Mitomycin C (**163**) undergoes preferential cross-link formation in the order 5'-d(ACGT)>5'-d(TCGA)=5'-d(CCGG).<sup>30d</sup> Since cross-linking of **template 1** in all cases gave rise to the dG-10 oriented cleavage pattern, it was concluded that of the two 5'-CG-3' cross-linkable sites, the 5'-ACGT-3' site underwent preferential cross-link formation. As such, the original interpretation of these results with FR66979 (**314**) followed the trend observed for mitomycin C with respect to flanking sequence preferences thereby supporting the intermediacy of a mitosene.



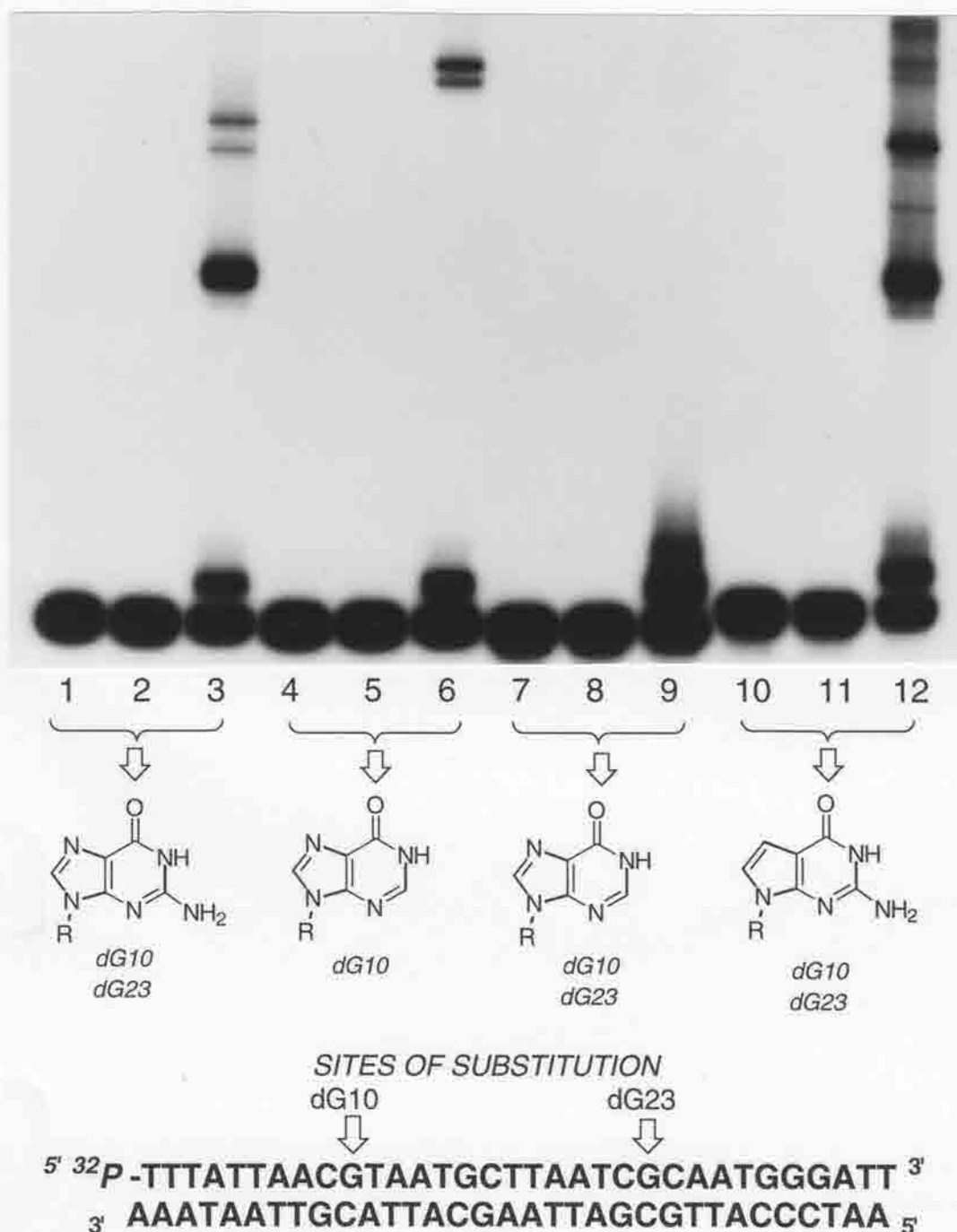
**Figure 2-15.** Autoradiogram of Fe(II)-EDTA footprinting of cross-linked **template 1** and **template 2** ( $^{32}\text{P}$ -labeled at 5' terminus of ODN 3). **Lanes 1-3**, standard DNA, cross-linked **template 1**, cross-linked **template 2**; **lanes 4 and 5** Maxam-Gilbert G, G+A respectively. **Lane 6**, 1mM Fe(II)-EDTA control; **Lane 7**, cross-linked **template 1** after 1mM Fe(II)-EDTA digestion; **Lane 8**, cross-linked **template 1** after 1mM Fe(II)-EDTA digestion. **Lanes 9 and 10** Maxam-Gilbert G, G+A respectively. Slow mobility cross-link standards in **lanes 2 and 3** (outside of the sequencing region depicted) may be seen in Appendix Figure 5-4.

A final venture investigating the role of the N<sup>2</sup> of deoxyguanosine involved synthesis of **template 1** with G-10 and G-23 substituted with 7-deazaguanosine. As shown in Figure 2-16, treatment of this modified template with **314** afforded cross-linked material in yields comparable to those seen with the native dG-containing template. This verified that N<sup>2</sup> and *not* the N<sup>7</sup> of guanosine is responsible for bis-alkylation of the DNA duplex. Additionally, these experiments revealed for the first time that the differing placement of each cross-linkable 5'-CG-3' within **template 1** gave rise to electrophoretically-unique adducts. The ability to separate and assign the positioning of each cross-link site within **template 1** also verified the results of Fe(II)-EDTA footprinting experiments to suggest the preferred cross-linking of 5'-ACGT-3' over 5'-TCGC-3'. Comparison of the two cross-linked species resulting from reaction of **template 1** with FR-66979 clearly shows the enhanced yield of 5'-ACGT-3' cross-linked material over the corresponding 5'-TCGC-3' *bis*-alkylated duplex. The respective cross-link yields of 53.7 % for **ODN 1** G-10 alkylated material and 8.5% for the G-23 cross-link were determined by liquid scintillation of each band.

The combination of base-substitution experiments and Fe(II)-EDTA footprinting afforded a concise means of not only assigning the DNA base pair specificity for interstrand cross-linking by FR66979, but also yielded important information regarding the regiochemistry of DNA bis-alkylation. More precisely, the exocyclic N<sup>2</sup> moieties of each deoxyguanosine of 5'-CG-3' are required and little or no dependence upon any other base atoms has been observed (as derived from Fe(II)-EDTA cleavage patterns). The implication based upon analogy to mitomycin C is that the N<sup>2</sup> atoms of each deoxyguanosine (of 5'-CG-3') undergo drug-mediated alkylation. No covalencies were observed with any other bases, although cross-linking efficiency was strongly influenced by the flanking bases on either side of the cross-linkable 5'-CG-3' and followed a similar trend known for the mitomycins. An interesting observation is the greatly reduced amount

of 3'-phosphoglycolate (in comparison to the 3' phosphate) observed for Fe(II)-EDTA footprinting lanes at the site of drug attachment. The origin of this phenomenon is unknown and to date has not been reported for Fe(II)-EDTA footprinting studies on MC. The C4' H-atom abstraction necessary for 3' phosphoglycolate generation (see Figures. 2-12, 2-13) may undergo either drug-mediated inhibition, or rapid quenching due to proximity of the FR-derived mitosene core .

GEL ORIGIN



**Figure 2-16.** FR-66979 (314) reactions with dG10/dG23 substituted and native ODN 1 duplexes. Base and position substitutions are denoted. Base structures denote base incorporation at sites which are noted directly below each base (guanosine, inosine, or deazaguanosine). **Lanes 1,4,7,10** are ODN standard lanes, **Lanes 2,5,8,11** are 100 mM DTT controls. **Lanes 3,6,9,12** are 10 mM FR66979 + 100 mM DTT reactions. Reactions were incubated 16 hours at 25°C prior to electrophoresis.



#### **2.2.4. Studies directed at elucidation of a reactive FR-66979 intermediate enroute to interstrand cross-linking.**

As discussed in section 2.2.2., we had observed that synthetically derived FR-66979 did not require the addition of exogenous reductants in order to efficiently cross-link (yield of cross-link  $\geq 10\%$ ) either pBR322 or smaller synthetic ODNs used for sequence specificity assignments. Non-reductive instances of interstrand cross-linking had been previously shown for the mitomycins but these reactions called for acidic activation conditions at  $\text{pH} \leq 5$ .<sup>27b</sup> As such, the cross-linking activity of FR-66979 observed could not be attributed to acidic activation pathways since these reactions called for neutral or near neutral pH conditions. Mechanistic proposals concerning a non-reductive route to cross-link formation could justify the existence of two electrophilic sites within the FR-66979 structure but suffered from the argument that the DNA-bound core structure could not possess an indolic structure due to its incorrect oxidation state. More perplexing was that the interstrand cross-link still demonstrated the 5'-CG-3' sequence specificity inherent to a mitomycin like lesion (section 2.2.3.).

Concomitant with our studies of FR-900482 and related compounds, Hopkins and Woo reported that FR-66979 required reductive activation contrary to our findings.<sup>10c</sup> This provided the impetus for insightful studies pertaining to the mechanism of FR66979 reaction with 5'-CG-3'.

Due to its low natural abundance from fermentation, FR-66979 (**314**) had always been prepared by reduction of the more available **312** with either  $\text{NaBH}_4$  or  $\text{H}_2/\text{Pd-C}$ . By chance, prior to this study, the two laboratories had selected different reductants, and had each relied solely upon the one source. Collaborative efforts with Hopkins and Woo required that each group repeat, in part, the work of the other, confirming the observations previously described, those being that FR-66979 (**314**) derived from hydrogenation very

efficiently cross-linked DNA *without an exogenous reductant*; while NaBH<sub>4</sub> derived material was devoid of cross-linking activity without an exogenous reducing agent.<sup>4a</sup>

Initial efforts involved verification of the other group's findings. Indeed, NaBH<sub>4</sub> reduction of FR-900482 afforded the dihydro FR-66979 which, upon reaction with **template 1** (see section 2.2.3.) failed to cross-link the 33 base pair duplex. Additionally, the Hopkins group was able to successfully demonstrate that Pd/C reduction yielded **314** which required no exogenous reductant in order to cross-link the self-complementary substrate 5'-TATAATACGTATTATA-3'. Cross-checking of each group's findings gave way to intense studies in which the "activated" FR-66979 analog and the lesion resulting from its reaction with 5'-CG-3' were examined.

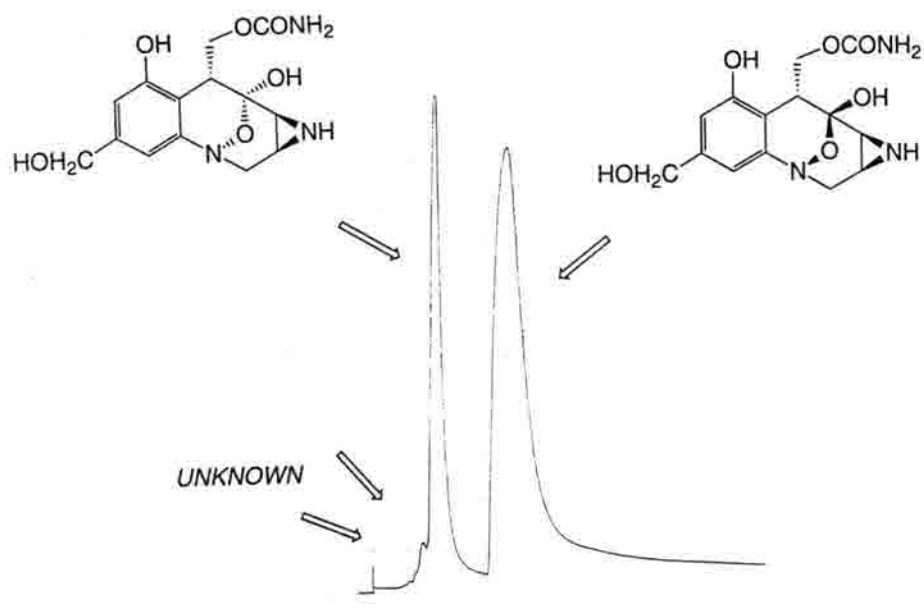
The hypothesis that Pd/C over-reduction of FR-66979 gave rise to the species responsible for the observed cross-linking was substantiated by several findings. First, and perhaps most importantly, we observed that exposure to silica (either purification by preparative TLC or simply stirring in methanolic silica at room temperature) substantially reduced the extent of inherent cross-linking activity. Secondly, it was noted by the Hopkins group that monitoring of H<sub>2</sub>/Pd-C reduction of FR-900482 gave rise to substantial changes in the UV spectrum over time. Conversion of FR-900482 (**312**) to FR-66979 (**314**) was observed within the first 15 minutes of the reaction *via* UV and chromatographic monitoring. However, at time intervals between 1 and 5 hours, a considerable increase in UV absorbance was noted above 300nm and a new band was observed at approximately 250nm. Correspondingly, Hopkins and co-workers noted a sharp decrease in intensity at 215nm representing loss of the FR-66979 chromophore and TLC analysis revealed that the major diastereoisomer of FR-66979 was consumed. That extended exposure to the hydrogenation conditions converted FR-66979 to some other compound was clear based on the dramatic UV changes. The structure and cross-linking activity of this new substance/substances was, however, never assayed or analyzed further by the Hopkins group.<sup>32</sup>

Given this observation, we examined reaction mixtures *via* HPLC in order to visualize and isolate the proposed over-reduction product. Chiral HPLC analysis of **314** readily afforded separation of the major and minor diastereoisomers of FR-66979 as shown in Figure 2-17. However, analysis of crude and PTLC purified synthetic samples of FR-66979 resulted in essentially identical chromatograms (Fig. 2-17). This was the case for **314** derived from H<sub>2</sub>/Pd-C reductions at 1 atm. and 60 psi. Visualization of peaks other than those attributed to diastereoisomerism of FR-66969 led to fractionation/collection of only the minor and major isomers of FR-66979. Disappointingly, re-injection returned not only the other diastereoisomer, but also displayed the presence of what had previously been attributed to possible over-reduction products. Concomitant with HPLC studies, PTLC was also attempted in which all UV detectable fractions were collected and assayed for DNA cross-linking activity. Reaction of each collected fraction with 5'-<sup>32</sup>P-labeled **template 1** for 16 h. failed to afford interstrand cross-linked material as assessed by 20% DPAGE analysis. This resulted from decomposition of the active species and not due simply to separation from the collected fractions (*vide supra*).

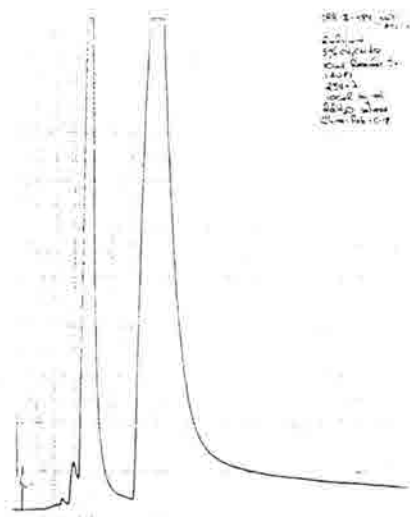
With potential stability and comigration problems in mind, an alternative means of detection of DNA-reactive substances was sought by HPLC/MS. Chiral HPLC was used in-line with positive ion electrospray mass spectrometry to scan the entire chromatogram of crude FR-66979 prepared by H<sub>2</sub> Pd/C conditions for potential masses of interest (indole **318** m/e=289, **317/316** m/e=307).

That FR-66979 over-reduction would afford a DNA-reactive indole of structure **318** was deemed possible (indeed, the Hopkins group favored **318** as the predominant over-reduction product), and would certainly have accounted for the high degree of instability observed. However, studies by Danishefsky and Egbertson had shown that in the mitomycin series, conversion of the mitomycin A (**251**) to the leucoaziridinylmitosene **349** affords an unstable species capable of rapid C1 hydrolysis<sup>33,34</sup>. On the other hand, conversion of mitomycin A to leucomitomycin A (**348**) in which the angular C9a OH is

A)

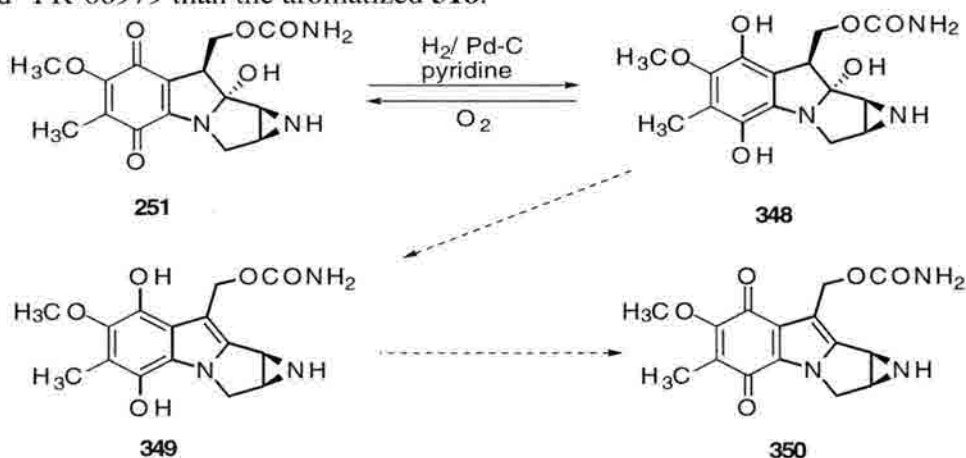


B)



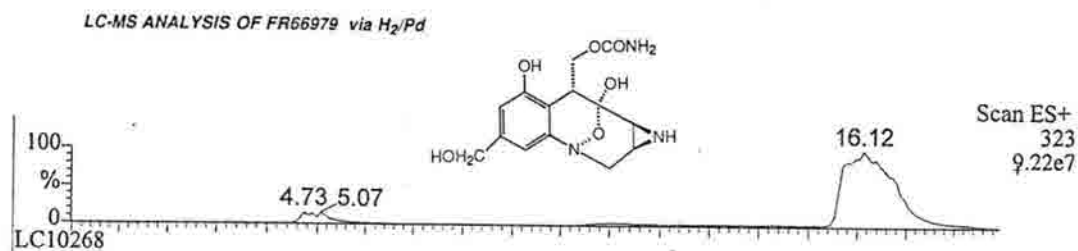
**Figure 2-17.** Reverse-Phase CHIRALPAK WH HPLC chromatograms of FR-66979. A) Crude **314** prepared by Pd/C-H<sub>2</sub>. B) PTLC purified **314** prepared by hydrogenation (mixture of the two diastereoisomers). 5% CH<sub>3</sub>CN, 2mls./min., Detn. 254nm.

retained proceeds in good yields with good stability characteristics observed for **348**. Indeed reoxidation back to **251** is more facile than C9a elimination to **349**. The stability of **348** thus suggested **317** (Fig. 2-1) as a more likely structure corresponding to "over-reduced" FR-66979 than the aromatized **318**.

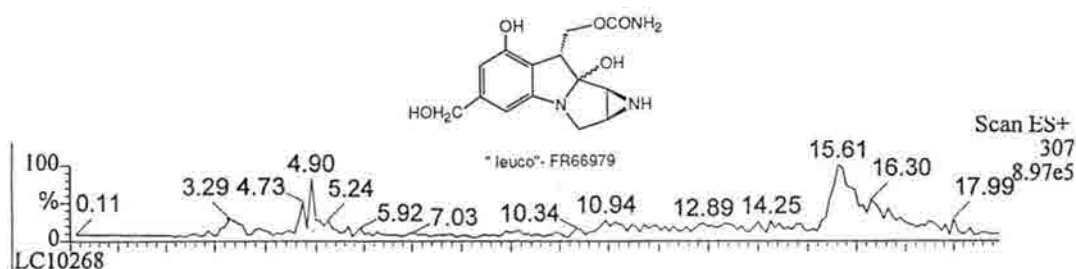


In line with the Danishefsky findings, LC-MS revealed the presence of substances with  $m/e$  307 which comigrated with the major and minor diastereoisomers of FR-66979 (see differing mass scans in Figure 2-18). The existence of indole **318** would be expected to result in signals diagnostic for a compound with  $m/e = 289$ . This was, however, not the case suggesting that **318** may not be a key player in the previously observed reactions of "over-reduced" FR-66979 with DNA. Attempts at fractionation and collection of  $m/e$  307 substances were complicated by the prominence of FR-66979 (due to comigration) in each fraction. Reactions of HPLC fractionated material with DNA traced the majority of "activated" FR-66979 to a peak corresponding to the minor diastereoisomer of **314** (Appendix Fig. 5-5). Importantly, this also supported the assertion that the fast mobility material preceding the minor **314** diastereoisomer (Fig. 2-17.) was devoid of cross-linking activity. This was consistent with the LC-MS data in which a greater percentage of a potential "leuco-FR" compound ( $m/e=307$ ) was found to comigrate with the minor FR-66979 diastereoisomer. Significantly, UV-vis analysis of all fractions failed to show absorbances in the 230 nm range which would have supported the presence of **318**.

A)



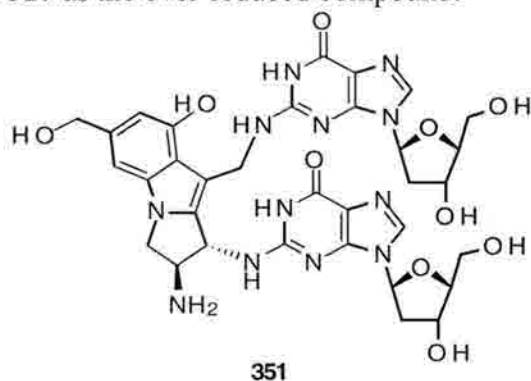
B)



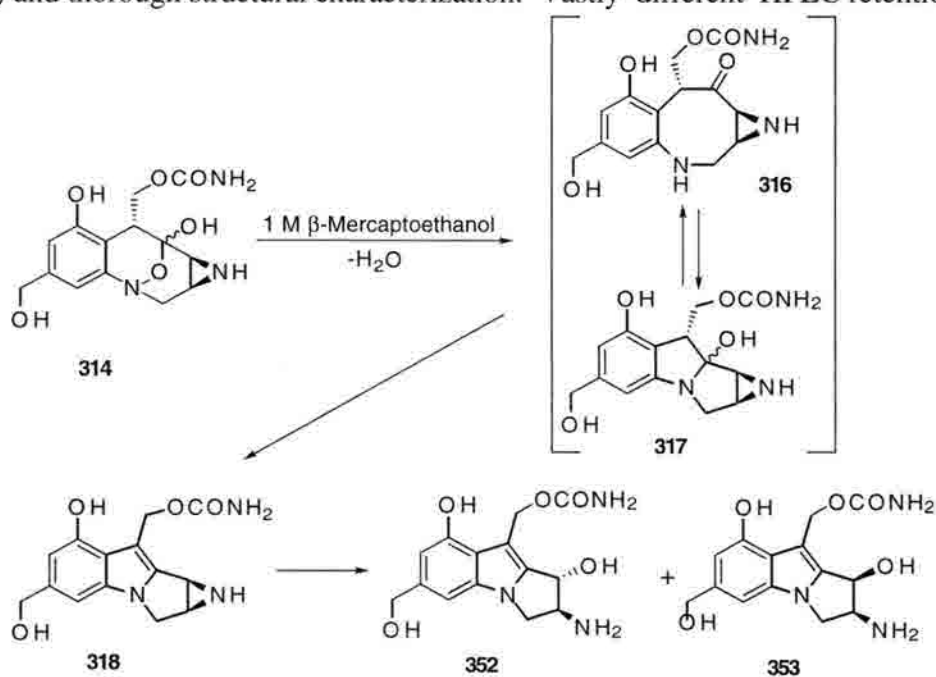
**Figure 2-18.** HPLC/MS scans of CHIRALPAK WH chromatography of crude **314**; A) MS detection of **314**; B) MS scanning of  $m/e = 307$  (potential "leuco"-FR-66979 compound **317** or ring-opened tautomer **316**).

Concomitant with HPLC fractionation studies in our laboratories, the Hopkins group had characterized the lesion responsible for the cross-link and found it to be identical to that derived from *reductively activated* FR-66979. The self-complementary 14-mer 5'-ATAATACGTATTAT-3' was interstrand cross-linked with crude **314** from hydrogenation. The interstrand cross-linked product was isolated from DPAGE and digested. The resulting mixture was then compared with the corresponding hydrolysate from the same DNA cross-linked ODN obtained using dithionite-activated FR-66979 prepared by sodium borohydride reduction. Rigorous structural characterization had proven the latter to contain substance **351**, fully consistent with the reductive activation hypothesis in Figure 2-1. The lesions from these two sources possessed identical HPLC retention times, and gave essentially identical UV spectra and electrospray ionization mass spectra, indicating the identity of the covalent structures of the cross-links formed by these two preparations.<sup>4a</sup> These findings substantiated the proposal that DNA cross-linking by FR-

66979 in the absence of exogenous reductants was attributable to some over-reduction product such as **317** or **318** in the DNA reaction mixtures. This also supported our tentative assignment of **317** as the over-reduced compound.



Attempts to generate the over-reduction product yielded the ring-opened mitosenes **352** and **353** (mw = 307). The mixture was observed in quantitative yield upon exposure of FR-66979 to 1M  $\beta$ -mercaptoethanol at room temperature for 48 hours (Figure 2-19). The initial belief that the thiol-generated substance could actually be the putative reactive intermediate **317** or **318** was refuted based on DNA cross-linking assays (see Appendix Fig. 5-6) and thorough structural characterization. Vastly different HPLC retention times

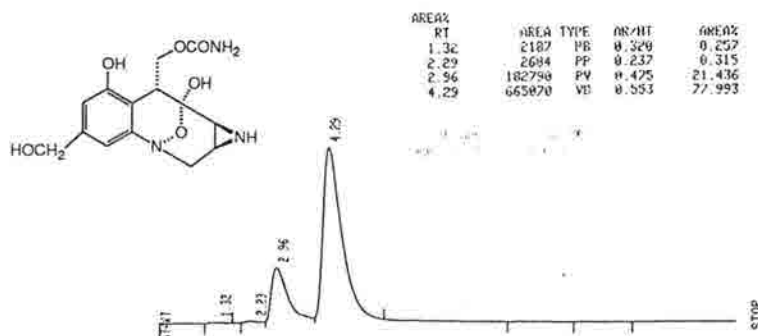


**Figure 2-19.** Thiol mediated reduction of **314** to C1 hydrolyzed mitosenes.

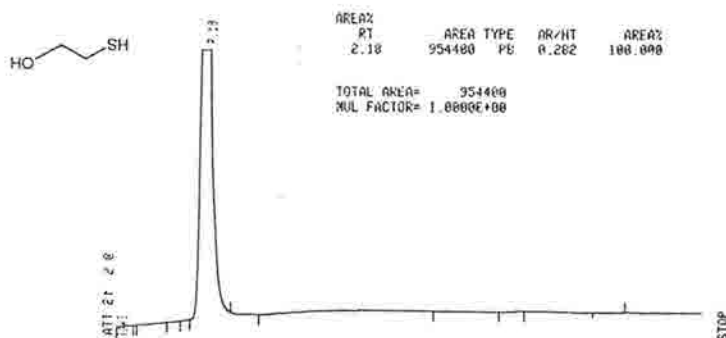


(Fig. 2-20) and UV spectra ( $\lambda$  max = 230nm.) suggested that the  $m/e=307$  peak previously seen to comigrate with FR-66979 *was not* obtained from simple hydrolysis of a potential aziridinomitosenes ( $m/e = 289$ ), but is more likely the carbinolamine **317** whose mass is identical to that of amino alcohols **352** and **353**.

A)



B)



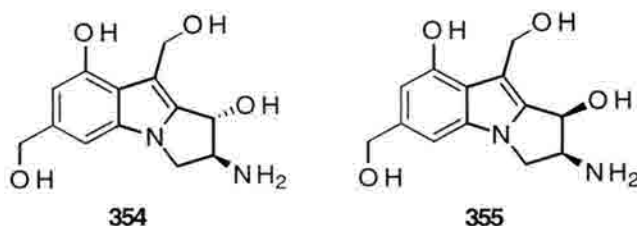
C)

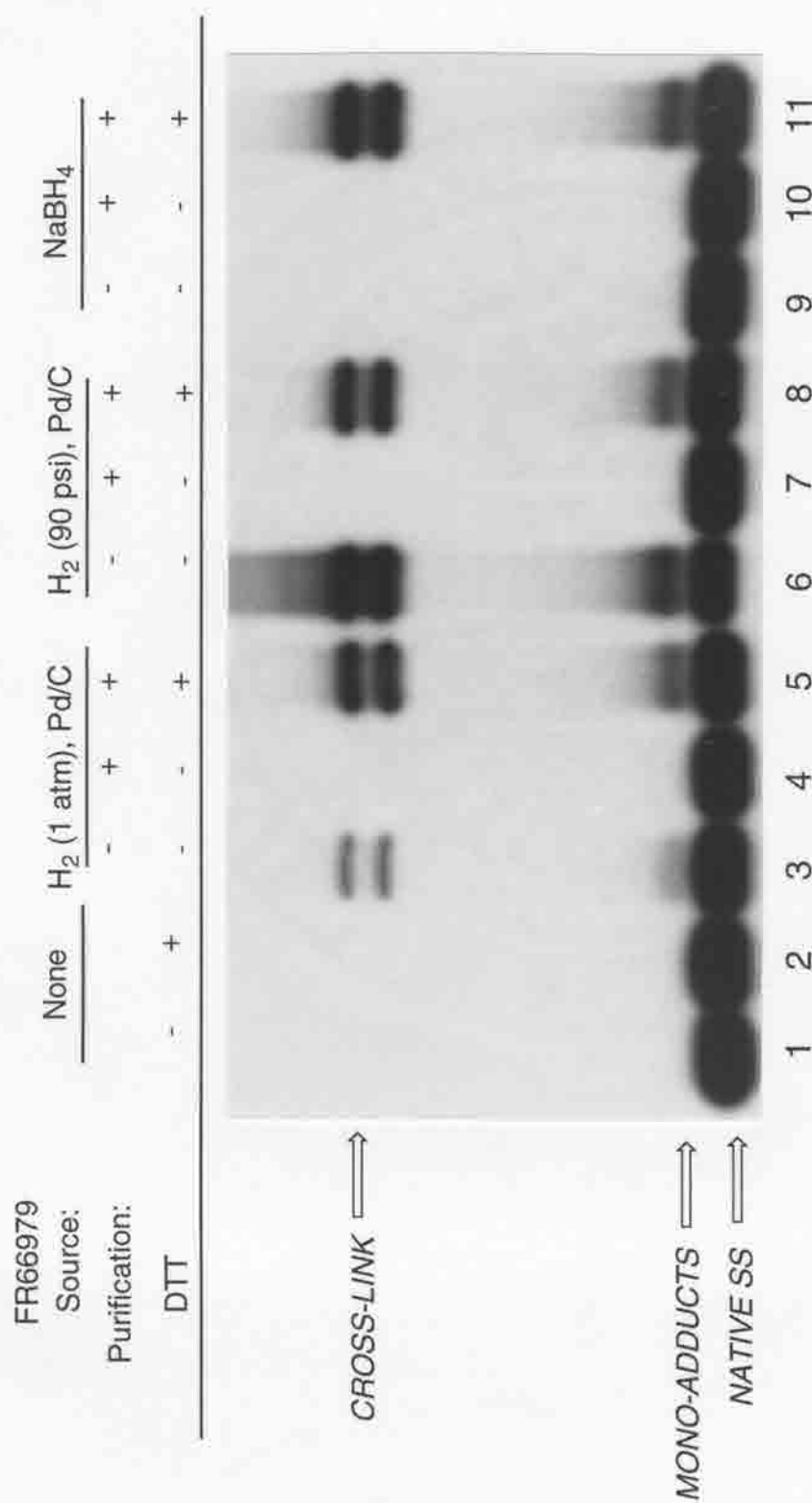


**Figure 2-20.** Reactions of PTLTC purified **314** with  $\beta$ -mercaptoethanol . A) FR-66979 control injection; B)  $\beta$ -MET control injection; C) reaction of FR-66979 with  $\beta$ -MET (1M) for 48 hours. The fast peak shown in panel A is the minor diastereoisomer of FR-66979 and the slow peak is the major diastereoisomer. The two slow moving peaks in panel C represent the mixture of ring-opened mitosenes **352** and **353**.

An alternative approach to effect over-reduction of **314** involved  $\text{H}_2/\text{Pd-C}$  reduction at increased pressures. As shown below in Figure 2-21, reduction of **312** with  $\text{H}_2/\text{Pd-C}$  at 90 psi, rather than 1 atm. afforded significantly more active cross-linking agent, despite the fact that both reactions produced predominantly FR-66979. characterization.

In light of the results generated regarding the attempted over-reduction of FR-66979 it is significant that similar reactions of involving DTT and  $\text{Fe}^{2+}$  have been recently examined by Hopkins and Paz.<sup>4b</sup> Electrospray LC-MS and UV absorbance data confirms the generation of aziridinyl ring-opened mitosenes **354/355** derived from **314**. A departure from the data generated in these laboratories is noted in that **354** and **355** (obtained in the presence of catalytic  $\text{Fe}^{2+}$ ) lack the carbamoyl moiety at C10 (mitomycin numbering). Considering that these compounds were generated after only 5 h., it is surprising that decarbamoylation has occurred while in our experiments (lacking exogenous  $\text{Fe}^{2+}$ ) retention of the carbamate was seen even after 48 hours. This raises interesting questions pertaining to metal ion-assisted decarbamoylation of the FR derived mitosenes and its potential role in DNA modification by these agents.





**Figure 2-21.** Reactions of **template 3** with FR-66979 (**314**) of varying origins. **Lanes 1** and **2** are ODN + 20mM DTT standards respectively. **Lanes 3, 4** and **5** are FR-66979 via 1 atm. H<sub>2</sub>/Pd-C crude, PTLC'd, and PTLC'd + DTT respectively. **Lanes 6, 7**, and **8** are the same sequence as **lanes 3-5**, except hydrogenation was carried out at 90 psi. **Lanes 9-11** are same sequence as **6-8** except FR-66979 was obtained by NaBH<sub>4</sub> reduction of FR-900482 (**312**).

Reactions of crude FR-66979 from H<sub>2</sub>/Pd-C with **template 1** suggested that the over-reduction product was consumed (*via* cross-linking and/or hydrolysis) within 1 hour at room temperature under aqueous conditions. This instability, coupled with problems experienced in the isolation/purification of over-reduced FR66979 deemed the characterization of this proposed DNA-reactive intermediate an issue with limited likelihood for success. Also a consideration, was the presumed low yield of over-reduction product and severely limited quantities of FR-900482 available with which to pursue this issue. As such, complete characterization of the putative cross-linking agent obtained upon H<sub>2</sub>/Pd-C reduction of FR-900482 to FR-66979 was not pursued further. However, a good deal of evidence has been generated to suggest that catalytic hydrogenation of FR-900482 produces carbinolamine **317** which decomposes under aqueous conditions to afford the potent DNA cross-linking (and highly unstable) mitosene **318**.

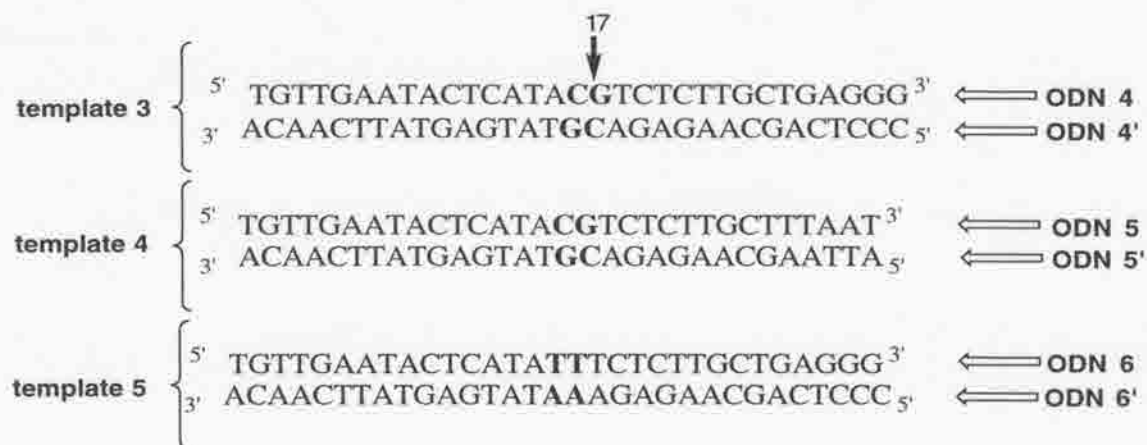
Given that a 200:1 ratio of drug to DNA duplex was employed in cross-linking experiments, a contaminant of only 0.5 mole-% easily overlooked by standard analytical methods, could fully account for the observed cross-linking activities observed by both groups.

#### **2.2.5. Verification of orientational isomerism in the FR-66979 mediated 5'-CG-3' cross-link.**

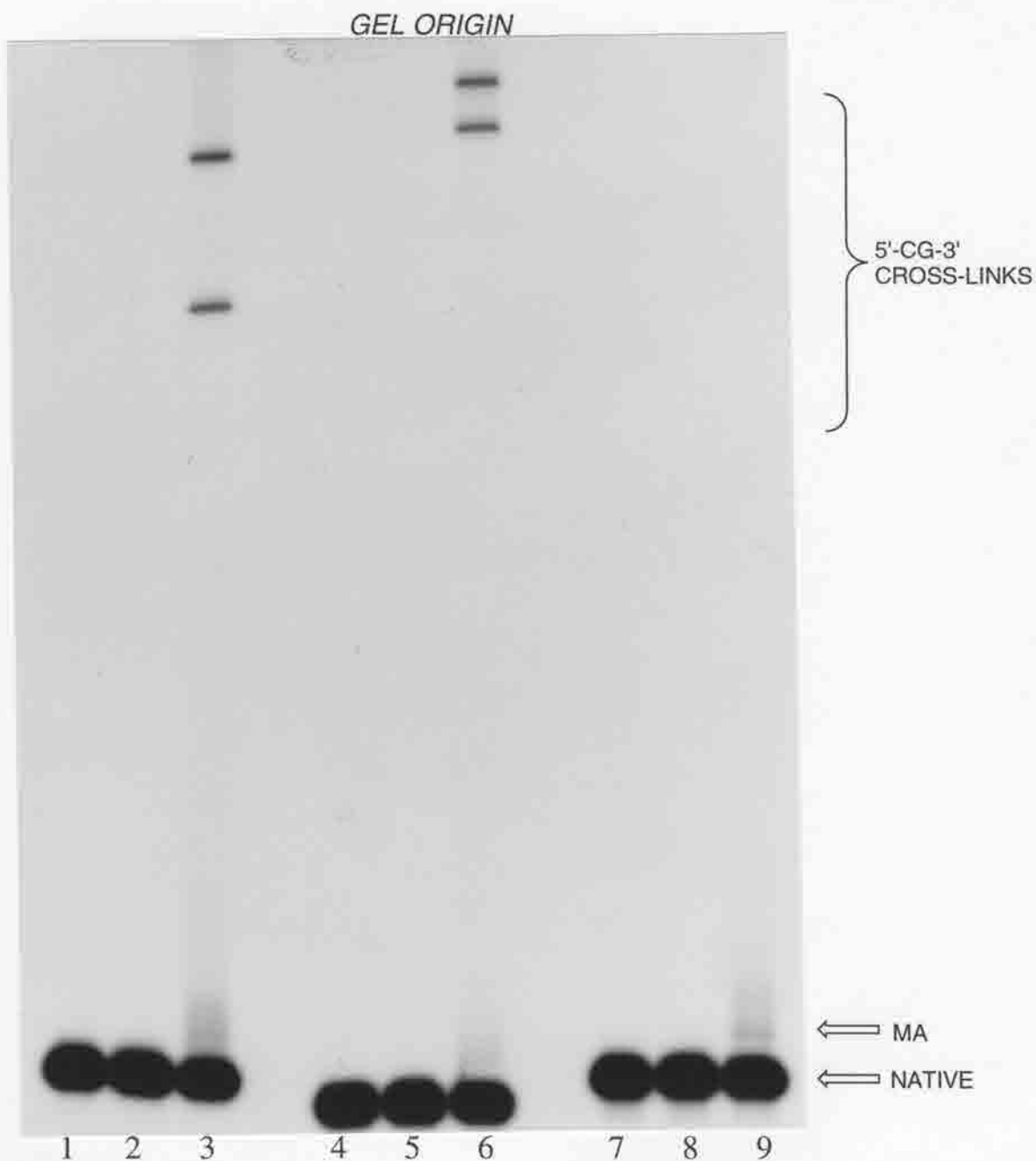
During collaborative efforts with the Hopkins group, reactions in which the preparation and purification methods used to derive **314** from **312** were tested using <sup>32</sup>P-5'-end-labeled 5'-TGTTGAATACTCATACGTCTCTTGCTGAGGG-3' (**ODN 4**) annealed to its complement (to yield **template 3**).<sup>4a</sup> An interesting phenomenon observed in these experiments was the presence of two distinct bands corresponding to cross-linked DNA possessing only one 5'-CG-3' run (Figure 2-21). Preceding the collaborative effort by two years, Hopkins *et al.* had observed that cross-linking of 5'-TATAATCCG-GATTATA-3' with FR-66979 also gave rise to two separate cross-links.<sup>10c</sup> Since this

"multiple-band" phenomenon seemed somewhat general (**312** and **313** followed the same trend -Appendix Fig. 5-7) and had not been previously examined, we sought to address its structural origin and potential implications relevant to the mechanism of action of the FR compounds.

One plausible explanation for the two band pattern observed with **template 3** invoked an over-alkylation phenomenon giving rise to the slower band. Of particular concern was the 5'-GAGGG-3' run at the ODN 3' terminus. By analogy to MC, this sequence posed problems entailing not only possible mono-alkylation, but also intrastrand *bis*-alkylation between two neighboring dG residues.<sup>25</sup> The presence of another interstrand site was considered highly unlikely but, based on the available data, could not be ruled out. To probe these issues two additional oligonucleotides (and their complements) were synthesized. One substrate (**ODN 5**) replaced the 5'-GAGGG-3' run with 5'-TTAAT-3' while the other (**ODN 6**) exchanged the cross-linkable 5'-CG-3' with 5'-TT-3'. These substrates when annealed to their respective blunt-ended complements, afforded **templates 4** and **5** respectively. As a control, the self-complementary 5'-TATTAATAATTAATACGTATTAATTTTAATA-3' (**ODN 7**) was also synthesized. Reaction of **templates 3-5** with FR-66979 and DTT for 16 h. at room temperature was followed by 20% DPAGE analysis. As shown in Fig. 2-22 retention of the two band pattern was found not only for **template 3**, but also for the substrate lacking the dG-rich 3' terminus (**template 4**). The substrate lacking 5'-CG-3' gave no interstrand reaction (lane 9, Figure 2-22) thus ruling out the possibility of another interstrand cross-linkable site. The self-complementary substrate (**ODN 7**) yielded only one band, supportive of, but not verification for potential dG over-alkylation of the original substrate. Retention of



the two band pattern between substrates with and without the 5'-GAGGG-3' terminus suggested that in fact, the observed two band pattern was not due to an over-alkylation process, but rather the melting temperature ( $T_m$ ) dependent separation of orientation isomers of the cross-link. That the self-complementary control yielded a single-sharp cross-link band (Appendix Fig. 5-8) substantiated an orientational isomer phenomenon as both possible orientation isomers would be C2 symmetric and thus electrophoretically indistinguishable.



**Figure 2-22.** FR-66979 cross-link adducts formed with **templates 3,4, and 5**. **Lanes 1,4,7**- DNA controls for **templates 3,4,5** respectively. **Lanes 2,5,8** - DNA + DTT controls in the same order as **lanes 1,4,7**. **Lanes 3,6,9**- Reactions of reductively activated FR66979 with **templates 3,4,5** respectively. MA refers to mono-alkylated 5'-<sup>32</sup>P-labeled ODNs.

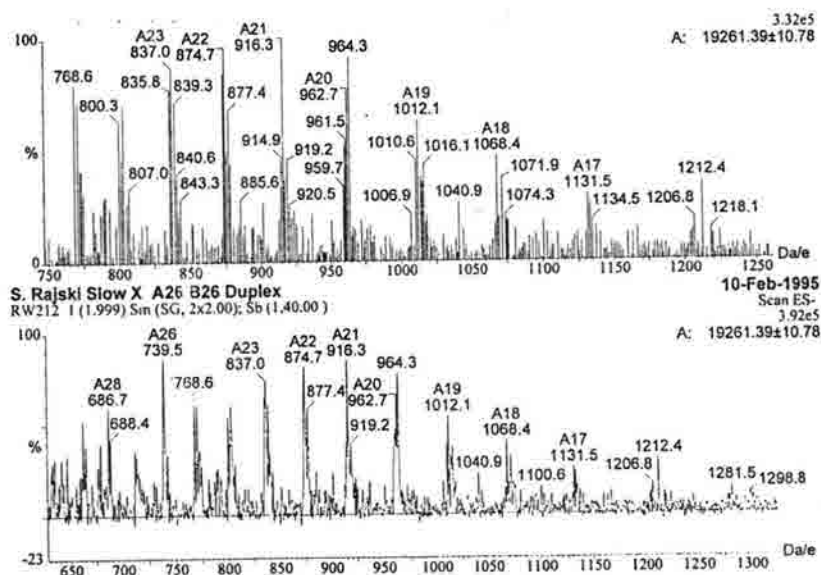


FR-66979 alkylation of a residue other than guanosine was considered unlikely, but would easily explain the ease of separation of the two cross-linked species. Verification of 5'-CG-3' involvement in the cross-linking event for **template 3** was pursued by Fe(II)-EDTA digestion. Each band generated for the **ODN 4** cross-link was isolated and individually subjected to Fe(II)-EDTA footprinting followed by 20% DPAGE. (Appendix Fig. 5.9). Footprinting analysis (Appendix Fig. 5-9) revealed that indeed, each band corresponded to the same singly, site-specific 5'-CG-3' cross-link. Connectivity to 5'-CG-3' was assigned for both strands of the duplex *via* labeling and analysis of each separate selectively 5' labeled duplex (Appendix Fig. 5.9)

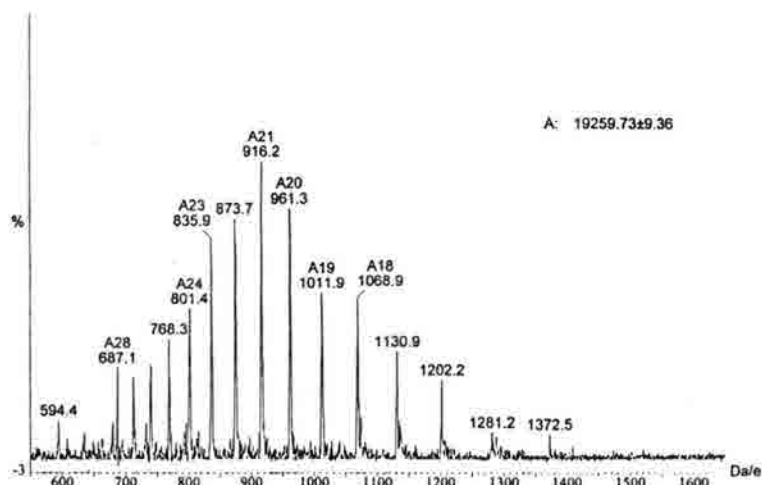
The potential that one of the bands involved dG N<sup>7</sup> connectivity as opposed to exclusive dG N<sup>2</sup> functionalization was investigated by heating to 90°C in 1M piperidine. Piperidine digestion readily converted cross-linked material to a mixture of monoadducts and single-stranded ODNs, but failed to reveal major groove (alkaline-labile) alkylation sites on either strand of each cross-linked species. This supported the anticipated involvement of *both dG N<sup>2</sup> residues* within 5'-CG-3' for each cross-linked band (data not shown).

Unambiguous quantitation of DNA alkylation by reductively activated **314** was ultimately obtained upon mass spectral analysis of each cross-linked adduct. Cross-linking followed by 20% DPAGE afforded the cross-linked material as two separable species. Isolation of each adduct was achieved by elution into 500mM NH<sub>4</sub>OAc/1mM EDTA at 37°C for 1 hour. This was followed by filtration, sample concentration and ion exchange (NH<sub>4</sub><sup>+</sup> for Na<sup>+</sup>) *via* repetitive ethanol precipitation from NH<sub>4</sub>OAc (pH = 5.2). Negative ion electrospray mass spectral analysis of each cross-linked product demonstrated that each product was a mono-adduct of the duplex with the drug; the faster-eluting band gave a molecular ion  $m/z = 19,259.73 \pm 9.36$  and the slower-eluting band gave a molecular ion  $m/z = 19,261.39 \pm 10.78$ ; the calculated mass for the singly cross-linked duplex was  $m/z = 19,259.75$ . This data ( Figure 2-23 ) was uniquely consistent with these products being

(A)



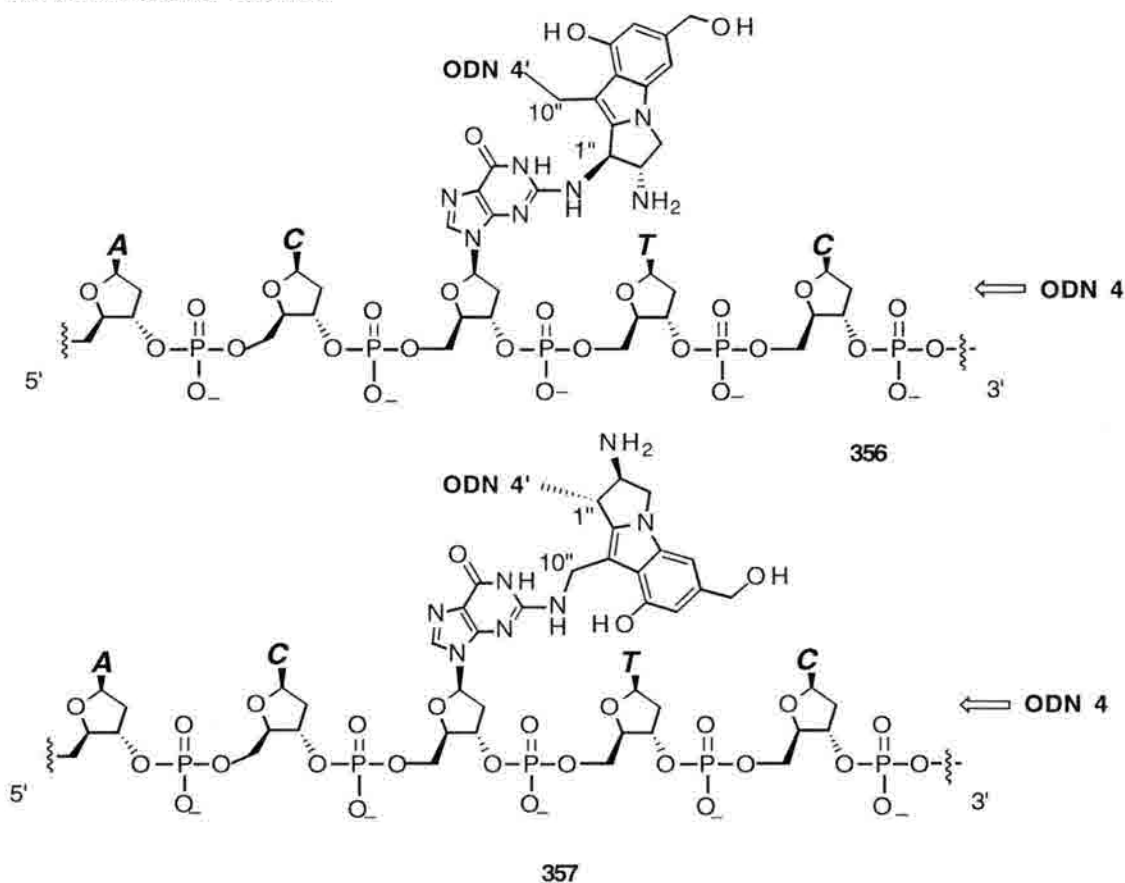
(B)



**Figure 2-23.** Negative Ion electrospray mass spectral analysis of each orientation isomer of FR-66979 cross-linked **template 3**. (A) Mass spectrum corresponding to the slower of the two isomers. (B) Mass spectrum corresponding to the faster of the two isomers. Note that in each spectrum, the number above each signal (preceded by the letter A) represents the number of charges corresponding to the mass signal. As such, each peak corresponds to one value for the total mass of the cross-linked template. The mass of each orientation isomer was obtained by averaging of all masses obtained (# of charges x mass per signal) within a given spectrum. For example the strongest signal in panel B is the A21 peak. The mass corresponding to this species was multiplied by 21 to obtain a value of 19,240.2 Da. for this specific signal.

orientational isomers (**356** and **357**) of the drug cross-linked to the same 5'-CG-3' box within **template 3**. More importantly, it disproved that over-alkylation of **templates 3** and **4** was the origin of the "two-band" pattern observed. In reference to section 2.2.1., this result verified that DTT mediated activation of **314** proceeds through a reductive rather than nucleophilic route since the mass obtained was exclusive of functionalities other than the mitosene-DNA lesion predicted by Fukuyama and Goto.<sup>9i</sup>

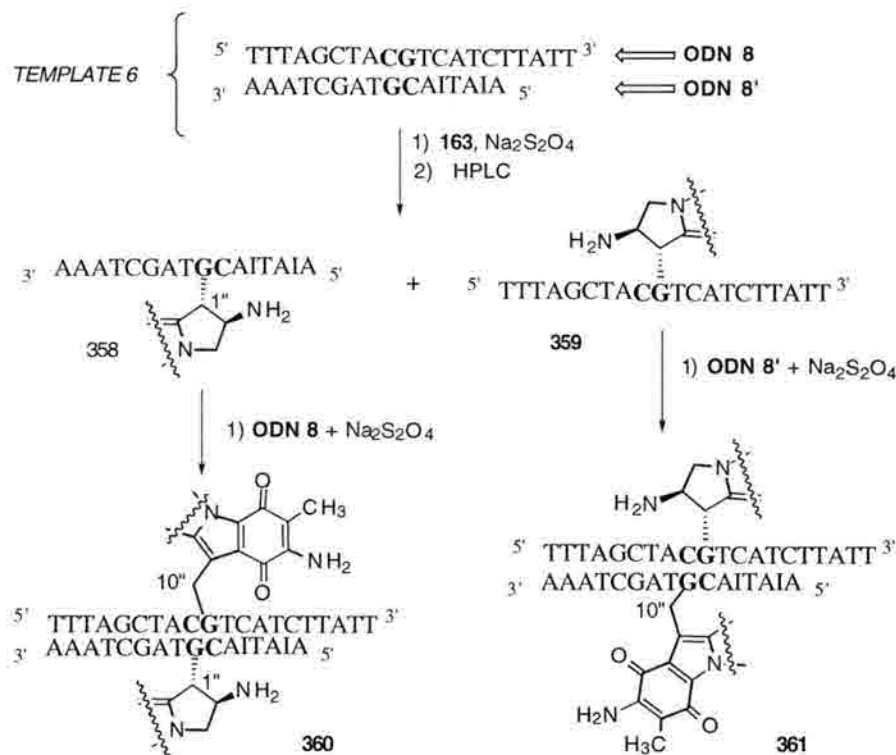
As demonstrated in structures **356** and **357**, the orientation isomers of **314** cross-linked ODNs arise from the fact that *bis*-alkylation of the activated FR core may occur in two orientations which are 180° opposite one another. In the case of **template 3** *bis*-alkylation, **ODN 4** may be alkylated by either the C1 or C10 of activated FR-66979 while the complementary strand (**ODN 4'**) must be alkylated by the center (either C1 or C10) not connected to **ODN 4**.



The origin of the vastly different electrophoretic mobilities observed was highly speculative although it had been demonstrated with psoralen interstrand cross-links that a similar phenomenon is attributable to "differential denaturation" rates of the two psoralen orientation isomers.<sup>35</sup> Kumarasen *et al.* had shown that orientation isomers of 4,5',8-trimethylpsoralen cross-linked 5'-AGCTCCTCTCATCCTGGCCTAG-3' (annealed to its complement) were easily separable by 20% DPAGE.<sup>35</sup> The degree of electrophoretic separation was highly dependent upon the effective  $T_m$  of the duplex. Incorporation of differing numbers and positions of base pair mismatches within the complementary strand was exploited as a means of  $T_m$  variation for a given cross-linked species.<sup>35</sup> The observations that electrophoretic mobility decreased with decreasing  $T_m$  and that orientation isomer separation decreased with decreasing  $T_m$  are both consistent with the trends observed in Figure 2-22. As pointed out by these workers, the complementary bases at the termini for each cross-link band are essentially hydrogen-bonded prior to migration into the gel matrix. ODN hybridization occurs despite heating at 90°C in formamide prior to loading of the sample. This stems from the ability of an interstrand cross-link to behave as a site of nucleation for rapid DNA hybridization immediately following denaturation. As such, slightly different  $T_m$  values for each cross-linked species results in different rates of conversion from double-stranded material to single-stranded form during the course of electrophoresis. This ultimately affords different electrophoretic mobilities for each isomer. While the structural origin of the  $T_m$  difference observed by Kumaresan *et al.* was not assigned, it was concluded that the different orientation isomers of psoralen cross-linked ODNs induce  $T_m$  differences upon the target duplex.

Tomasz and co-workers have shown that reaction of reductively activated **163** with small synthetic ODNs affords a mixture of monoalkylation adducts wherein C1" of the indolomitosene (Figure 2- 24) is attached to one of the two dG residues within duplexed 5'-CG-3'.<sup>36</sup> Isolation of each adduct (two separate strands of the duplex) *via* HPLC and subsequent reaction with the necessary complement afforded each orientation isomer of the

MC cross-link. These efforts culminated in the formation and reactions of each orientation isomer of MC cross-linked **template 6** with the restriction endonuclease Alu I.<sup>36</sup> Interestingly, the separation of orientation isomers of MC cross-linked **template 6** was not possible by electrophoretic means despite a reported<sup>36</sup>  $\Delta T_m$  of 3.1°C between **360** and **361**. The origin of the differing HPLC retention times for each orientation isomer was not elucidated nor was any hypothesis put forth to explain this behavior. Unlike the psoralen case where the cross-link induced helix destabilization was different for each isomer (one cross-link allows the native H-bonding of the 5'-AT-3' box while the other doesn't), the cross-link site for **163**-modified DNA is proposed to be fully base-paired in both orientations.<sup>36</sup>



**Figure 2-24.** Preparation of each MC orientation isomer of **template 6** and connectivity assignments based on digestive/HPLC analysis of each monoadduct. Note that diagrams for each cross-linked species illustrate the pertinent connectivities to *one drug molecule per cross-link*. Partial structures of mitomycin chromophore included for clarity only.

Examination of Figure 2-22 reveals that cross-linking by **314** of **template 3** and **template 4** afforded two orientation isomers of each respective duplex. As mentioned, cross-linking of **template 4** affords orientation isomers much slower in electrophoretic

mobility than the corresponding **template 3** case. Additionally, the effective separation of **template 4** isomers was considerably decreased in comparison to the **template 3** cross-links. This substantiated the belief that FR-66979 orientation isomerism was attributable to  $T_m$  variations between the two orientation isomers of each respective cross-linked duplex. Calculation of the theoretical  $T_m$  values for **templates 3** and **4** using the equation  $T_m = 81.5^\circ\text{C} + 16.6(\log_{10}[\text{Na}^+]) + 0.41(\% \text{ C+G}) - (600/n)$  was carried out where  $[\text{Na}^+]$  is the sodium concentration of the buffer system and  $n$  is the number of nucleotides in the duplex substrate. The values obtained revealed the theoretical  $T_m$  for **template 3** to be  $53.9^\circ\text{C}$ , whereas the theoretical  $T_m$  for **template 4** =  $48.7^\circ\text{C}$ . This was in line with the previous findings of Kumaresan *et al.*<sup>35</sup> and also corroborated the findings depicted in Figure 2-22.

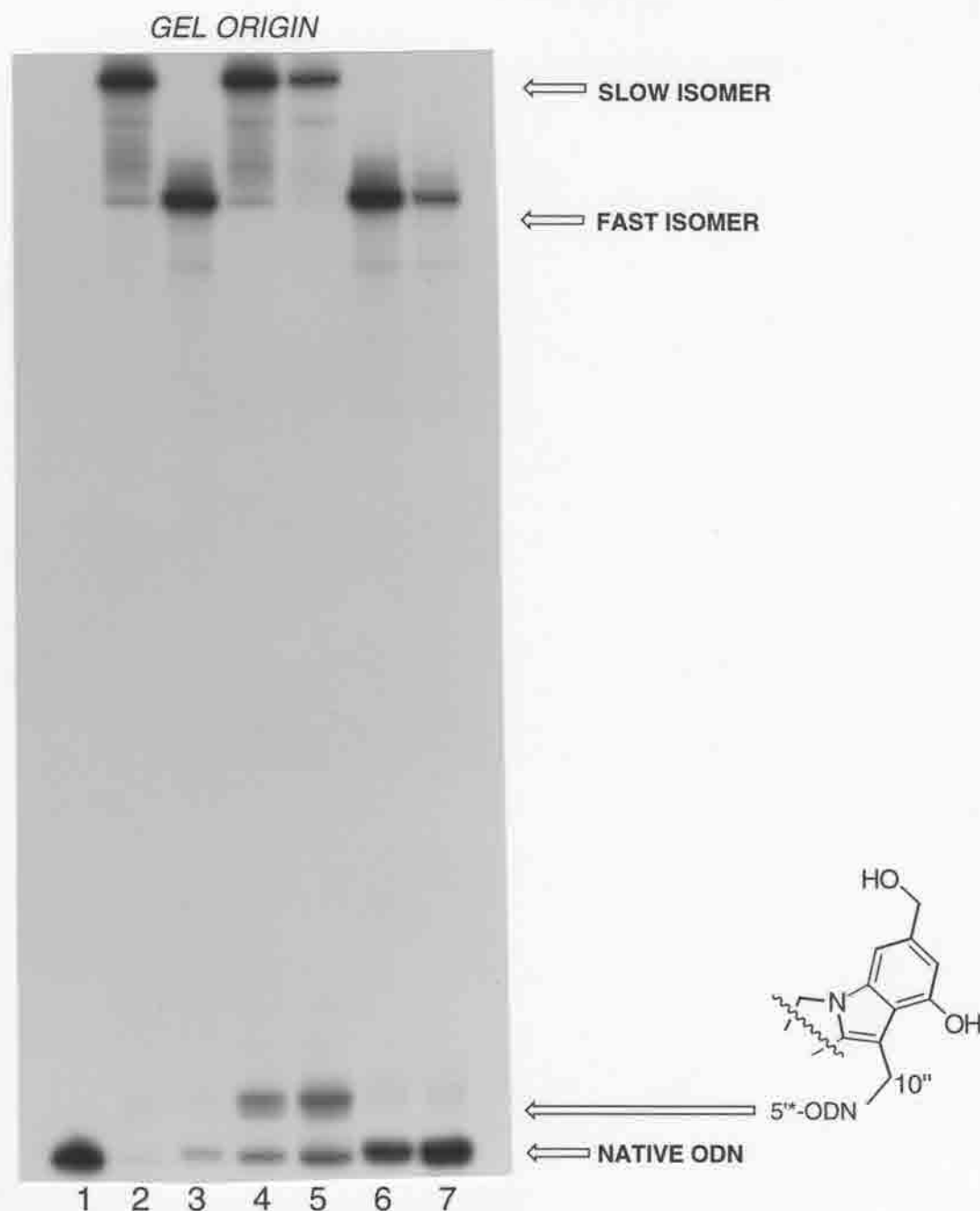
Verification of a potentially significant  $\Delta T_m$  between the orientation isomers of cross-linked **template 3** was sought. In a fashion similar to that used for mass spectral analysis, each orientation isomer of FR-66979 cross-linked **template 3** was isolated *via* elution into 500mM  $\text{NH}_4\text{OAc}$ /1mM EDTA. Following work-up, each sample was rigorously desalted using 30 kDa Amicon microconcentrator tubes *as per* manufacturer's specifications. Measurement of each orientation isomer's UV absorbance at 260nm with increasing temperature was performed to yield melting curves for each cross-linked species from which the points of hyperchromicity were determined (Appendix Fig. 5-10). The melting temperatures obtained for each orientation isomer revealed the slow isomer to have a  $T_m$  of  $77.56^\circ\text{C}$  while the fast isomer had a  $T_m$  of  $79.90^\circ\text{C}$ . The  $T_m$  for native duplex **template 3** was also determined and found to be  $69.9^\circ\text{C}$ . As expected, this was considerably lower than for either cross-link.

With this in mind, it was postulated that the difference in  $T_m$  values observed both spectrophotometrically and electrophoretically may result from a perturbation of DNA structure characteristic of only one orientation isomer. We felt that such a perturbation, while undetectable by Fe(II)-EDTA footprinting, might be revealed by any one of a number of methods capable of detecting site-specific DNA deformations.

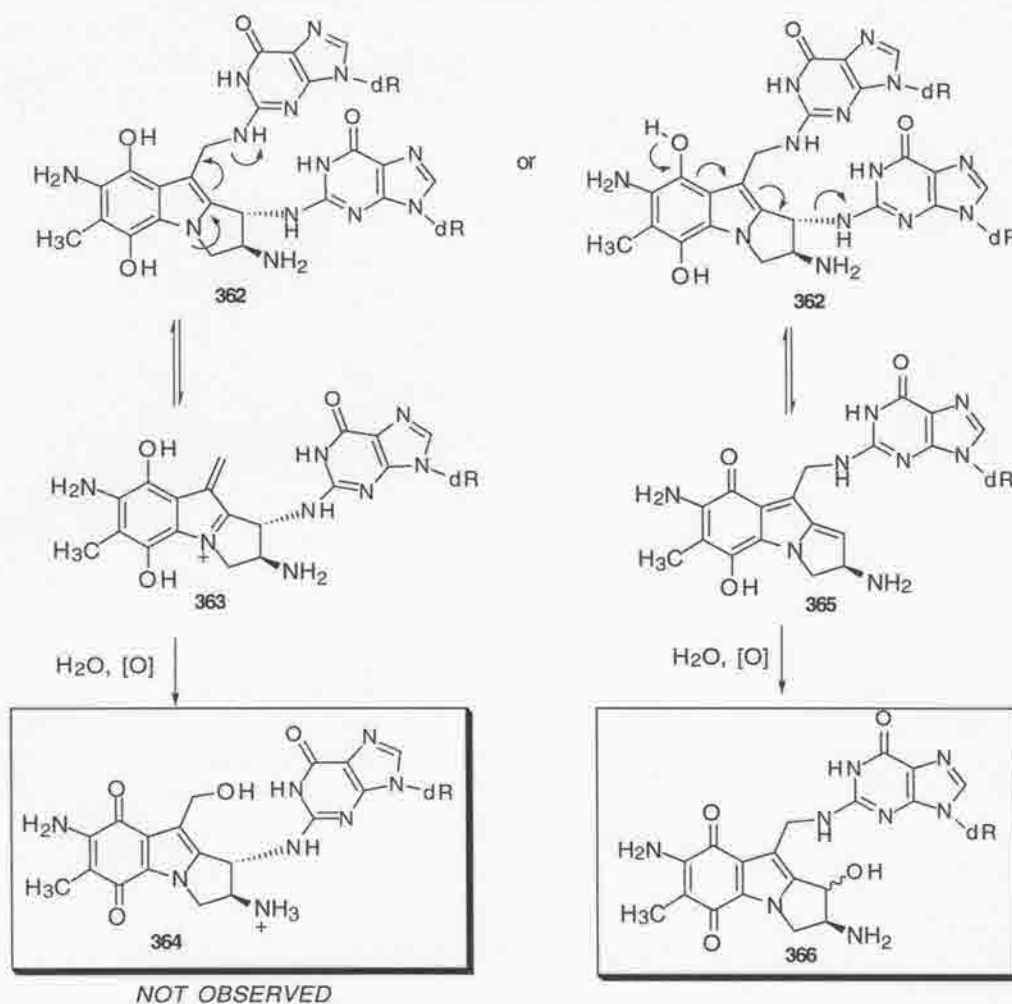
### 2.2.6. Assignment of mitosene orientation with respect to gel mobility of cross-linked template 3.

Efforts to determine if the observed orientation isomers were subject to interconversion were carried out by separating the two isomers and then treating each to denaturing conditions and subsequent re-analysis by 20% DPAGE. It was not anticipated that actual drug-DNA connectivities would be altered. However, if the observed  $T_m$  difference between isomers was a DNA/conformation dependent phenomenon, it was felt that isomer interconversion might be possible. Depicted in Figure 2-25, no evidence for interconversion was observed upon 20% DPAGE analysis of isomers that had been subjected to denaturation at 80°C in 200mM Tris buffer (pH = 7.5). Instead, treatment of each orientation isomer to denaturing conditions yielded DNA products corresponding to selective strand release events. Initial trials involved cross-linked adducts in which **ODN 4** was 5' labeled and its complement ( **ODN 4'** ) left unlabeled. As shown in lanes 4 and 5 of Figure 2-25, generation of low molecular weight material was achieved with some material corresponding to native **ODN 4**, and a large percentage corresponding to monoalkylated material. Of particular interest was that heating of the slow orientation isomer generated presumably C-10" monoalkylated material in preference to the simple native radiolabeled ODN.





**Figure 2-25.** 20% DPAGE of sequential denaturing/renaturation reactions using orientation isomers of **template 3** (5'-labeled on **ODN 4**) cross-linked with **314**. **Lanes 1-3**, standard duplex, slow orientation isomer of cross-linked substrate, fast orientation isomer standards. **Lane 4** depicts the products of heat denaturation at 80 °C for 20 minutes followed by cooling to 25°C (2 h.) for the slow orientation isomer. **Lane 5** is the same as **lane 4** except the slow isomer was put through two iterations of the heating/cooling cycle. **Lanes 6 and 7** are the same as **lanes 4 and 5** respectively as applied to the fast orientation isomer of **314** cross-linked **template 3**.



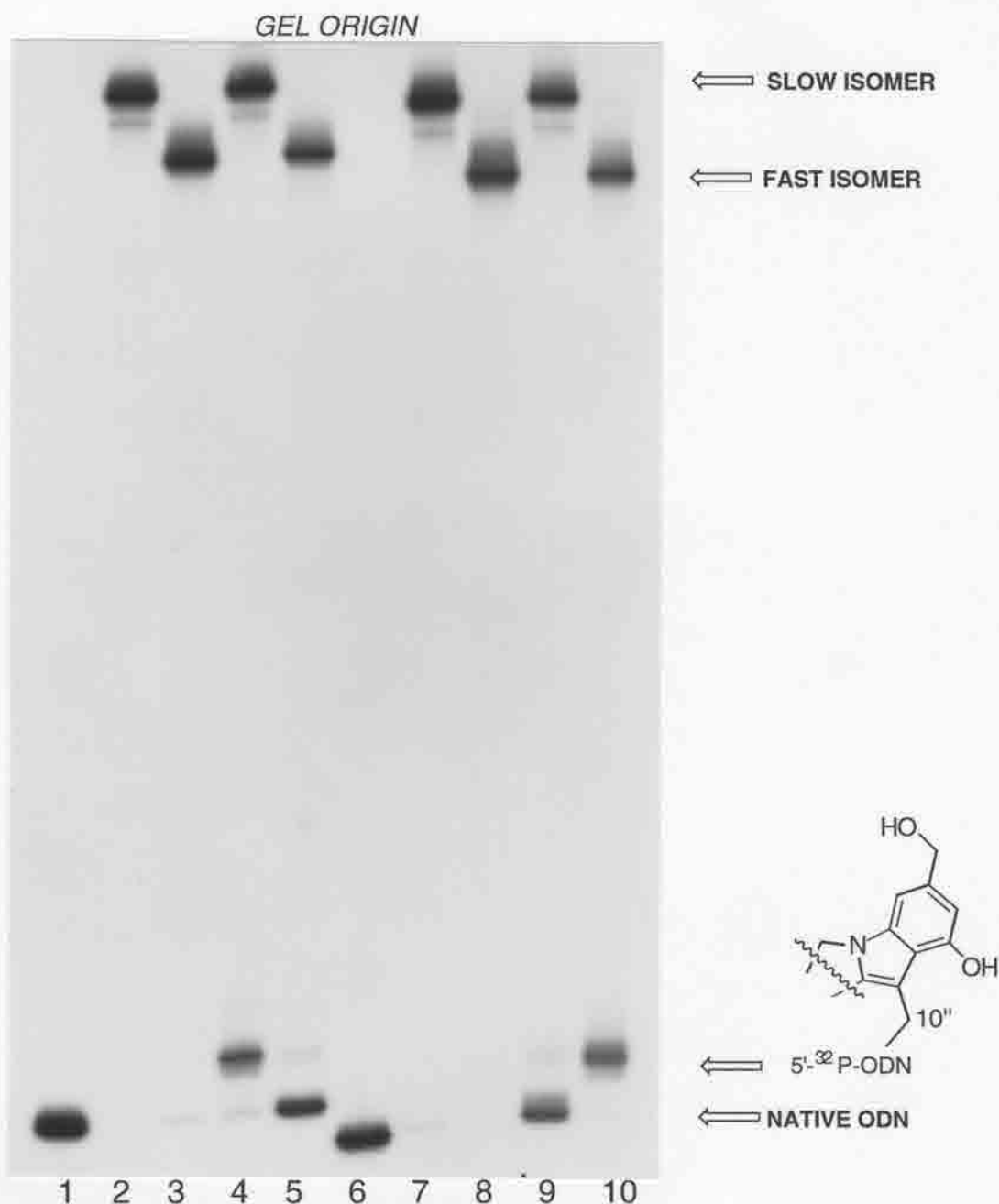
**Figure 2-26.** Differential pathways to DNA strand release by reductively activated MC.<sup>37b</sup>

Kinetic data pertaining to alkylation of MC suggests more facile reversibility of C1" over C-10" in the mitomycin series.<sup>37</sup> This is based largely on the inability to detect (*via* HPLC) the C-10" hydrolyzed mitosene indoloquinone **364** *enroute* to cross-link reversion (Figure 2-26).<sup>37b</sup> The structural and mechanistic analogies between MC and the FR drugs therefore suggest that the slow orientation isomer ( $T_m=77.56^\circ\text{C}$ ) is that corresponding to alkylation in which radiolabeled **ODN 4** is bound to mitosene C-10" derived from **294**. Likewise, the faster of the two isomers ( $T_m=79.90^\circ\text{C}$ ) results from connection of this strand to the more labile C-1". To further verify this result, **ODN 4'** was 5' labeled and the experiment repeated (Fig. 2-27). Conversion of the slow orientation isomer to single-

stranded material demonstrated that while radiolabeled **ODN 4** was converted to mono-alkylated material (lane 4, Fig. 2-27), the radiolabeled complement (**ODN 4'**) was converted directly to native single-stranded material (lane 9, Fig. 2-27). Likewise, the reverse trend was found when the fast isomer was treated to the analagous conditions.

The assumption that FR-66979 demonstrates similar kinetic reversibility rates to those demonstrated by MC (**163**) was substantiated by exposure of the orientation isomers of MC cross-linked **template 3** to reductive conditions amenable to cross-link reversion.<sup>37b</sup> Exposure of the slow orientation isomer of MC cross-linked **template 3** to 100 mM DTT at room temperature for 24 hours revealed that, in fact, this too generated both mono-adduct DNA and native substrate (data not shown).<sup>37b</sup> Analysis of the corresponding fast MC isomer resulted only in generation of single-stranded native substrate.

The ability to assign a given connectivity to each specific orientation isomer represented an interesting and potentially insightful result. The lower  $T_m$  of the slow mobility orientation isomer ( for which drug C10" connectivity was assigned) suggested some distortional process inherant to this orientation of the FR-derived mitosene which was lacking in the other isomer . This rationale led to several attempts at detection/identification of distortional processes specific to the slower orientation isomer.



**Figure 2-27.** 20% DPAGE of sequential denaturing/renaturing reactions using orientation isomers of **template 3** cross-linked with **314**. **Lanes 1-5** substrate is 5'-labeled on **ODN 4** while **lanes 6-10** are 5'-labeled on complementary strand (**ODN 4'**). **Lanes 1-3**, standard duplex, slow orientation isomer of cross-linked substrate, fast orientation isomer standards. **Lane 4** depicts the product of heat denaturation at 80 °C for 20 minutes followed by cooling to 25°C (2 h.) for the slow orientation isomer, while **lane 5** depicts analogous treatment as applied to the fast orientation isomer. **Lanes 6-10** are the same as **lanes 1-5** except that cross-linked substrate is 5'-labeled on **ODN 4'**.

### **2.2.7. Detection of DNA kinking/bending induced by FR-66979 as assayed by DNA ligation.**

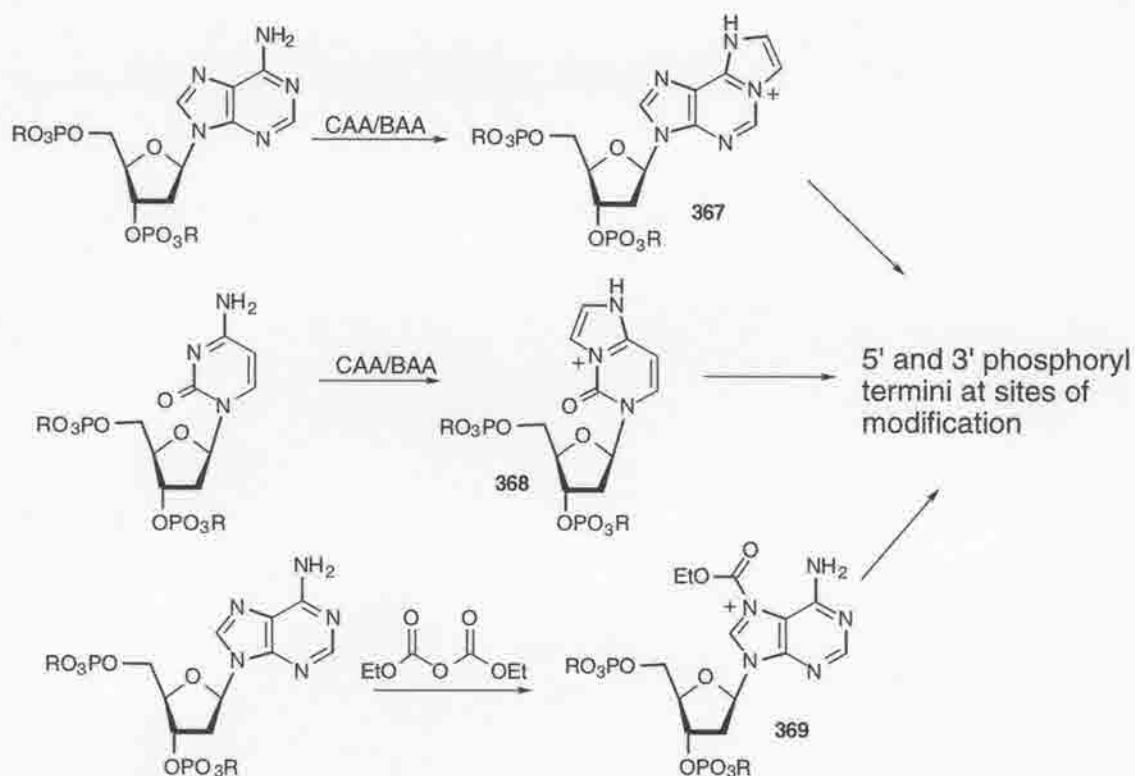
It is well documented that *cis*-platin *inter*- and *intra*-strand cross-links induce severe structure deformations in their respective target DNA's.<sup>38</sup> Given that such deformations have been detected by ligation of the *cis*-platin modified ODNs<sup>38a,39</sup> and analysis by non-denaturing gel electrophoresis (run against unmodified controls), we believed that structure perturbations induced by **314** might be probed in a similar fashion. Alkylation and subsequent isolation of the respective FR-66979 orientation isomers was carried out as previously described and ligations performed using T4 DNA ligase. This enzyme catalyzes the formation of a phosphodiester bond between juxtaposed 5' phosphate and 3' hydroxyl termini in duplex DNA. As such, we anticipated that ligation of the blunt-ended duplex **template 3** with and without FR-66979 modification would yield multimers wherein 5' CG alkylation sites ( potential sites of DNA kinking?) were separated successively by denominators of 33 nucleotides.<sup>40</sup> One complete turn of B-form DNA requires 10.5 base pairs, therefore a length of 33 bases would result in roughly 3 turns of DNA thus placing the 5' CG boxes in-phase with one another resulting in the effects of any perturbation being additive.<sup>38a,39</sup> The presence of such a perturbation would therefore result in differing electrophoretic mobilities of the ligation adducts for one orientation isomer versus ligation adducts of both the other cross-link isomer and standard non-alkylated DNA. This, however, was found not to be the case (Appendix Fig 5-11). No alteration of gel mobility was found for any ligation products obtained from either orientation isomer, nor was any difference seen in the two cross-linked standard lanes. Under the non-denaturing electrophoresis conditions used to analyze the ligase reactions, structure distortions of either orientation isomer would have been evident even in the control lanes. Failure to detect anomalous mobilities of monomeric or multimeric orientation isomers suggests that like mitomycin C<sup>36</sup>, FR-induced cross-links do not significantly alter target DNA structure from that of the normal B-form .

### **2.2.8. Detection of drug-induced hyperreactive DNA regions**

An alternative means of probing structure perturbations is to react the ODN substrate in question with reagents that react preferentially with single-stranded or distorted regions of DNA. This strategy has been used extensively with *cis*-platin modified ODNs and has been very successful due to the highly distorted nature of such adducts.<sup>41</sup> Additionally, single-stranded and Z-DNA regions of plasmid DNAs have been identified *via* this methodology.<sup>42</sup> The identification of nuclease S1-sensitive DNA sites (single-stranded) within chromatin has been particularly relevant to the study of promoter and terminator sequences within supercoiled DNAs.<sup>43</sup>

Numerous reagents have been developed which react preferentially with the more highly exposed reactive moieties of unduplexed bases. Two approaches have been sought. The first entails reaction of the distorted base such that a base labile lesion results which is revealed upon piperidine treatment.<sup>42a</sup> In this vein, the imidazolium of purines can be generated (Fig. 2-28) by carboethoxylation at N<sup>7</sup> with diethylpyrocarbonate (DEPC).<sup>44</sup> Analogously, hydroxylamine reacts with dC residues at the C<sup>4</sup> and C<sup>6</sup> to afford base labile lesions.<sup>42a</sup> Chloroacetaldehyde (CAA) and bromoacetaldehyde (BAA) react with the N<sup>1</sup> and N<sup>6</sup> of deoxyadenosine and the N<sup>3</sup> and N<sup>4</sup> moieties of dC to yield the ring-extended products **367** and **368**.<sup>43,42b</sup> Osmium tetroxide has also received considerable attention since dihydroxylation across the 5,6 double bond of pyrimidines occurs readily.<sup>42a</sup>

A second approach combines the reaction of CAA or BAA and subsequent digestion of the modified substrate with nuclease S1.<sup>43</sup> Reaction of native supercoiled DNA with CAA or BAA affords selective ring extended products with single-stranded runs of dA and dC. Subsequent restriction digestion and radiolabeling affords selectively radiolabeled ODNs bearing the chemically maintained single-stranded/distorted region within the restriction fragment. Digestion with the single-strand specific endonuclease S1 results in strand scission only at those residues whose single-stranded nature in the supercoiled state has been retained *via* reaction with CAA or BAA.<sup>43</sup>



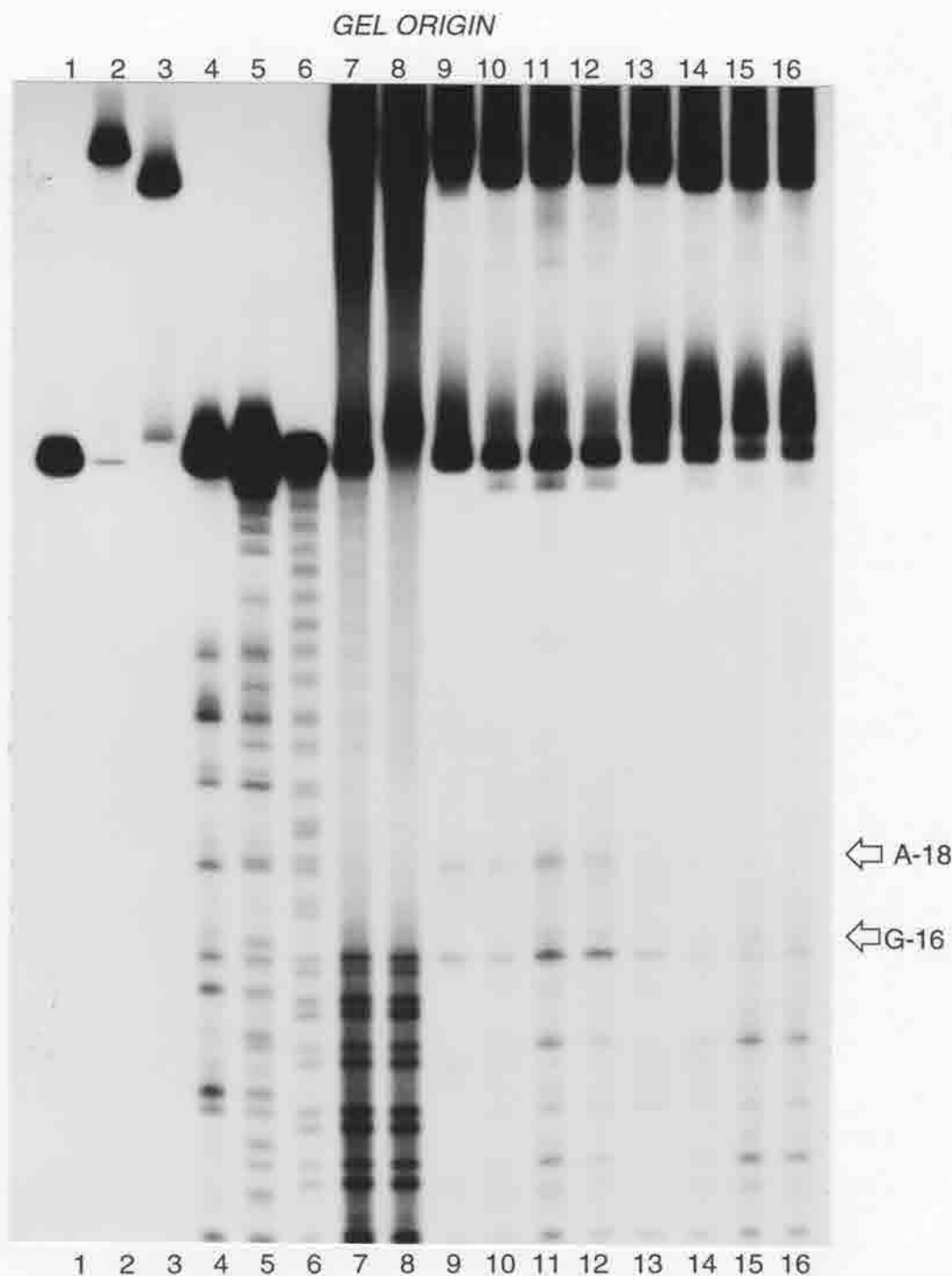
**Figure 2-28.** Representative transformations specific for hyperactive regions of DNA which lead to cationic base-labile lesions.

The cross-linkable 5'-CG-3' of **template 3** resides within the hexameric sequence 5'-TACGTC-3'. Introduction of sequence asymmetry with respect to the cross-link site starts at the boldfaced dT and dC at either terminus of this sequence. The loss of C2 symmetry at these base pairings suggested that a perturbation unique to one orientation isomer but not the other might well manifest itself through alteration of one of these pairings. To probe the possibility that one of the purines involved in these pairings was distorted out of the normal base pairing interactions with its complementary pyrimidine each orientation isomer was reacted with diethylpyrocarbonate (DEPC). Subsequent treatment with 1M piperidine at 80°C for 30 minutes afforded the cleavage patterns revealed in lanes 9-16 of Figure 2-29. Cleavage initiating roughly half-way through either radiolabeled ODN was quite apparent (See Appendix Fig. 5-12 for the **ODN 4** labeled experiment). Both fast and slow orientation isomers demonstrated pronounced cleavage starting at the alkylated dG of the radiolabeled strand and continuing in the 5'-direction.



That only cleavage to the 5' side of the cross-link was observed likely results from 5'-placement of the  $^{32}\text{P}$  label (based upon analogy to Fe(II)-EDTA footprinting of 5'-labeled duplexes - lanes 7 & 8 of the same figures). *Significantly, the absence of site-specific DEPC-dependent strand cuts suggests that base hyperreactivities do not result from either orientation isomer of the FR66979 cross-link. The known influence upon DNA conformation of hyperreactive bases and our inability to detect such regions thus supported the T4 Ligase results. These results were further confirmed via reactions with chloroacetaldehyde which yielded the same result (Appendix Fig. 5-13).*

Notably, base-labile lesions were encountered both at the site of dG alkylation (as confirmed by Fe(II)-EDTA digestion controls in lanes 7 and 8 of Fig. 2-29) and 2 bases to the 3' side of the drug-dG residue. These lesions were observed both in piperidine control reactions and in those reactions containing DEPC. In the case where **ODN 4** was labeled (Appendix Fig. 5-12), the fast isomer demonstrated this pattern while the slow isomer showed no cleavage 3'-from the alkylated dG. Incorporation of the radiolabel on **ODN 4'** revealed the opposite trend (Fig. 2-29). The slow isomer was cut 3'-(at A-18 of **ODN 4'**) from the alkylation site while the fast isomer was not. That the lesions observed occur in a C2 symmetric fashion ( as shown by 5'-labeling of both strands and subsequent analysis) suggests that the specificity of DNA scission may be correlated with the different orientations of the FR-66969 derived mitosene within 5'-CG-3'.

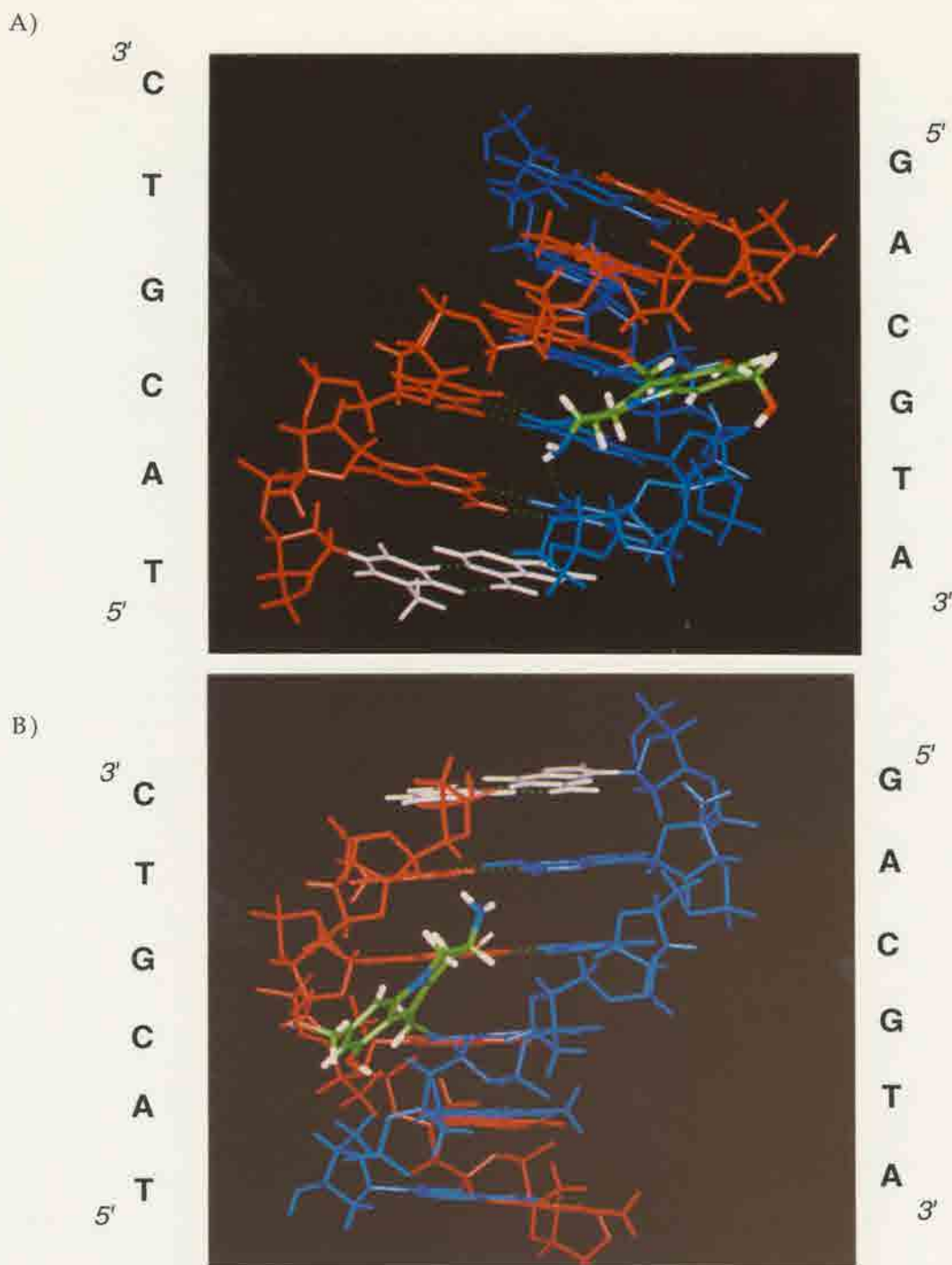


**Figure 2-29**-DEPC sequencing of hyperactive regions in **314** cross-linked **template 3**. **Template 3** was 5'-labeled on ODN **4'**. Base numbering is with respect to the 5' end of ODN **4'**. **Lanes 1-3** are **template 3** standard, slow cross-link and fast cross-link standards respectively; **Lanes 4 & 5**, Maxam-Gilbert G, G+A respectively, **Lane 6** is a 1mM Fe(II)-EDTA digestion standard, **Lanes 7 & 8** are fast and slow cross-links subjected to Fe(II)-EDTA digestion. **Lane 9** is slow orientation isomer subjected to 1M piperidine 80°C; **lanes 10-12** are slow cross-link treated with 5,10, 15  $\mu$ l DEPC respectively then 1M piperidine. **Lanes 13-16** are the same as **lanes 9-12** except using the fast orientation isomer of cross-linked **template 3**.

### **2.2.9. Molecular modeling of FR-66979 cross-link orientational isomers.**

The findings of the T4 DNA ligase, DEPC and CAA hypereactivity studies revealed that the structure of cross-linked **template 3** does not deviate significantly from that of B-form DNA. This, in combination with the ability to assign drug-DNA connectivities to each orientational isomer of cross-linked **template 3**, prompted us to probe additional structural differences between these species by molecular modeling. As discussed, the faster isomer possessed a  $T_m$  of 79.4 °C while the slower isomer demonstrated a  $T_m$  of 77.1°C. This was consistent with the observed electrophoretic properties in that under denaturing conditions, the faster isomer would be expected to possess the more compact structure inherent to double-stranded DNA for a longer period of time than would the lower melting (slower mobility) adduct. It is noteworthy that this same concept had been observed with the comparison of cross-linked substrates bearing a single inosine for guanosine substitution versus cross-linked duplexes bearing only the native deoxynucleotides (Figure 2-16).

Molecular modeling (Figure 2-30) of the 5'-d(GACGTA)<sub>2</sub> sequence cross-linked in both orientations at the 5'-CG-3' box revealed that the slower of the two isomers (Figure 2-30, panel A) allowed not only retention of the fully base-paired deoxyguanosine after alkylation of the mitosene C-10", but that this same adduct allowed for H-bonding between a mitosene N<sup>2</sup> hydrogen and the O<sup>2</sup> of the dT 3'-to the alkylated dG of the same strand.<sup>45</sup> Alternatively, the fast isomer ( higher  $T_m$ ) lacked the drug-to-dT H-bond, but also distorted the mitosene C-1" alkylated guanosine such that the N<sup>2</sup> hydrogen was no longer capable of H-bonding to its complementary cytosine (Figure 2-30, panel B). Notably, distortion of the respective dG residues resulting in disturbed H-bonding was revealed only in those molecular modeling experiments wherein the N<sup>2</sup> moieties of the alkylated deoxyguanosine residues were fixed in space. Experiments in which these sites were not fixed revealed no discernible difference between the two isomers such as distances between the "mitosene"



**Figure 2-30.** Orientation isomers of FR-66979 cross-linked 5'-d(GACGTA)<sub>2</sub>. The sequence 5'-GACGTA-3' is shown in blue while the complement 5'-TACGTC-3' is shown in red. The red strand for each duplex is that which possessed the 5'-AGCT-3' Alu I recognition site to the 5'-side of the *bis*-alkylated 5'-d(CG) box. All hydrogen bonding interactions are highlighted as green dashed lines. (A) Cylindrical bond model of "slow" orientation isomer. Terminal A-T pairing highlighted in white (B) Cylindrical bond model of "fast" orientation isomer. Terminal G-C pairing highlighted in white.

nitrogens and various hydrogen bond acceptors and donors of neighboring bases. The palindromic nature of the 5'-d(ACGT)<sub>2</sub> box supports this finding. This sequence deviates from C2 symmetry only in the context of the right-handed helical twist of the duplex. Importantly, the overall asymmetry of the oligonucleotide duplex examined is what likely facilitates the slight perturbation manifested preferentially by one isomer over the other.<sup>45</sup> That this perturbation equates to the experimentally measured  $T_m$  difference of 2.3°C suggests that a single H-bond difference may exist. The full-length sequence-dependent origin<sup>35,45</sup> of such a perturbation and its relative complexity limits its structural elucidation within our model system. However, potential repercussions of such drug induced DNA distortions are clearly evident as discussed earlier.

An alternative explanation may rely upon the chirality of duplex DNA. Significantly, we have observed that **312**, **313**, and MC also give rise to readily separable orientation isomers of cross-linked ODNs. Given the common aziridiny portion of each drug, it appears that aziridine stereochemistry plays a crucial role in the generation of cross-link orientation isomers of differing  $T_m$ 's. Particularly intriguing is the role played by the chirality of the C2 amine resulting from C1 alkylation. The ability of right-handed DNA to accommodate this asymmetric center may differ depending upon the drug's orientation with respect to the cross-linked substrate. This would not be unlike the pyrrolo[1,4]benzodiazepines in which the (S) stereochemical configuration at C11a enforces a right handed twist which is a major factor in drug-DNA binding prior to alkylation (see section 1.2.5.3.).<sup>46</sup> It is likely that both orientations of the transient quinone methide are bound equally well (hence the 1:1 ratio of isomers observed), but that once attached, mitosene C2 stereochemistry places the aziridiny amine closer to the neighboring dT in one orientation than in the other.

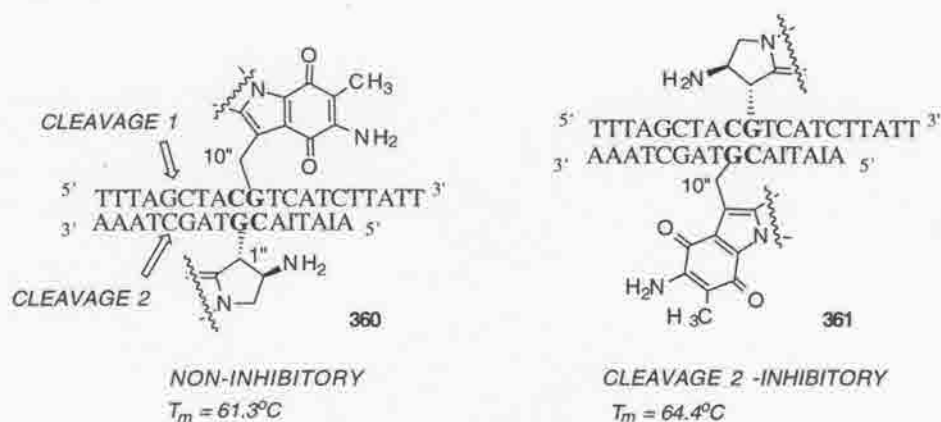
The importance of such interactions although unproven, could explain the amenability of these agents towards the formation of distinct cross-link species which exhibit differential effects upon biological events despite bearing similar connectivities.

#### **2.2.10. Digestion of FR-66979 cross-link orientation isomers with restriction endonuclease Alu I.**

The ability of the FR900482 class of compounds to give rise to clearly different cross-linked species raised questions regarding the origins of the observed electrophoretic differences. Of particular interest was the possibility that the observed orientation isomers may exert differential effects on processes of biological importance owing to their structural differences. The well defined structure constraints of numerous protein:DNA recognition motifs suggested that such interactions might easily be affected by the DNA distortions induced by one or both orientation isomers.

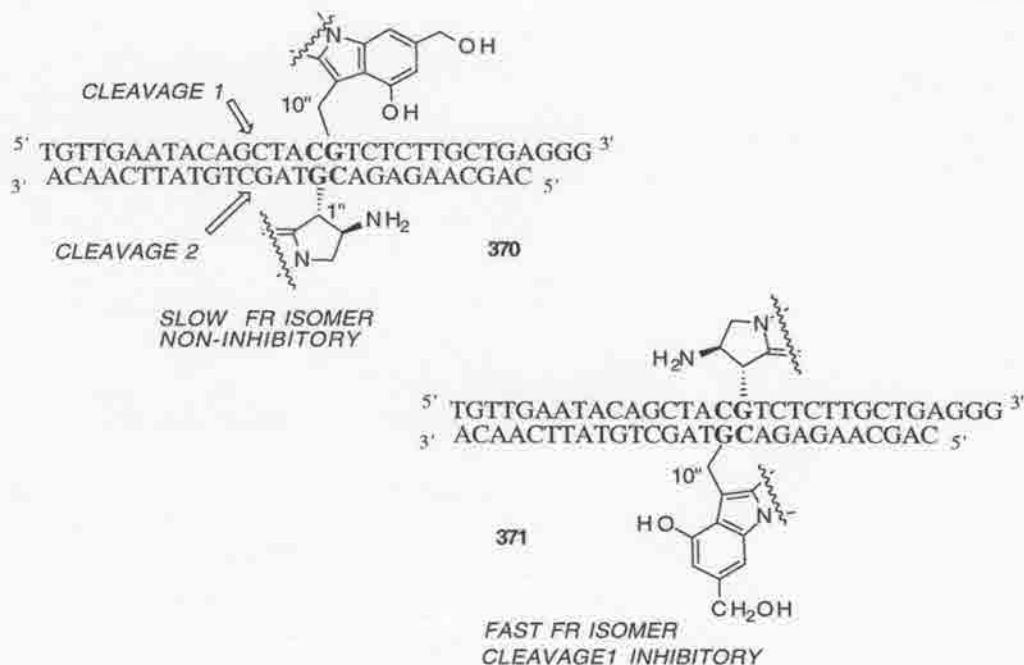
Alu I is a type II endonuclease which recognizes 5'-AGCT-3' and cleaves both strands of the DNA duplex through the central G-to-C phosphodiester linkage.<sup>47</sup> The structure of the Alu I-DNA complex has not been solved and little is known about the mechanism of recognition and cleavage. Like other type II endonucleases such as EcoRI, it is postulated that Alu I is a homodimer with two arms that wrap around the DNA and clamp the backside of each strand directly across the double-stranded helix from each scissile bond.<sup>48</sup> Disruption of either arm is believed to result in loss of DNA cleavage activity. Hurley and co-workers have shown that DNA alkylation by CC-1065 induces an asymmetric effect on DNA conformation which radically alters strand cleavage by Alu I.<sup>47</sup> Remarkably, the effect of this DNA structure alteration extends more than one helix turn away from the site of drug attachment. Similar studies by Tomasz<sup>36</sup> involved placement of the 5'-AGCT-3' recognition sequence one nucleotide 5'-to the MC cross-linkable 5'-ACGT-3'. Utilizing the synthetic ODN 5'-TTTAGCTACGTCATCTTATT-3' (**ODN 8**) and its inosine-substituted complement 3'-AAATCGATGCAITAIA-5' (**ODN 8'**) it was determined that the isomer to which C1" of MC was attached to **ODN 8** inhibited Alu I cleavage of **ODN 8'**.<sup>36</sup> Conversely, attachment of **ODN 8** to the MC C10" failed to inhibit either Alu I cleavage event.



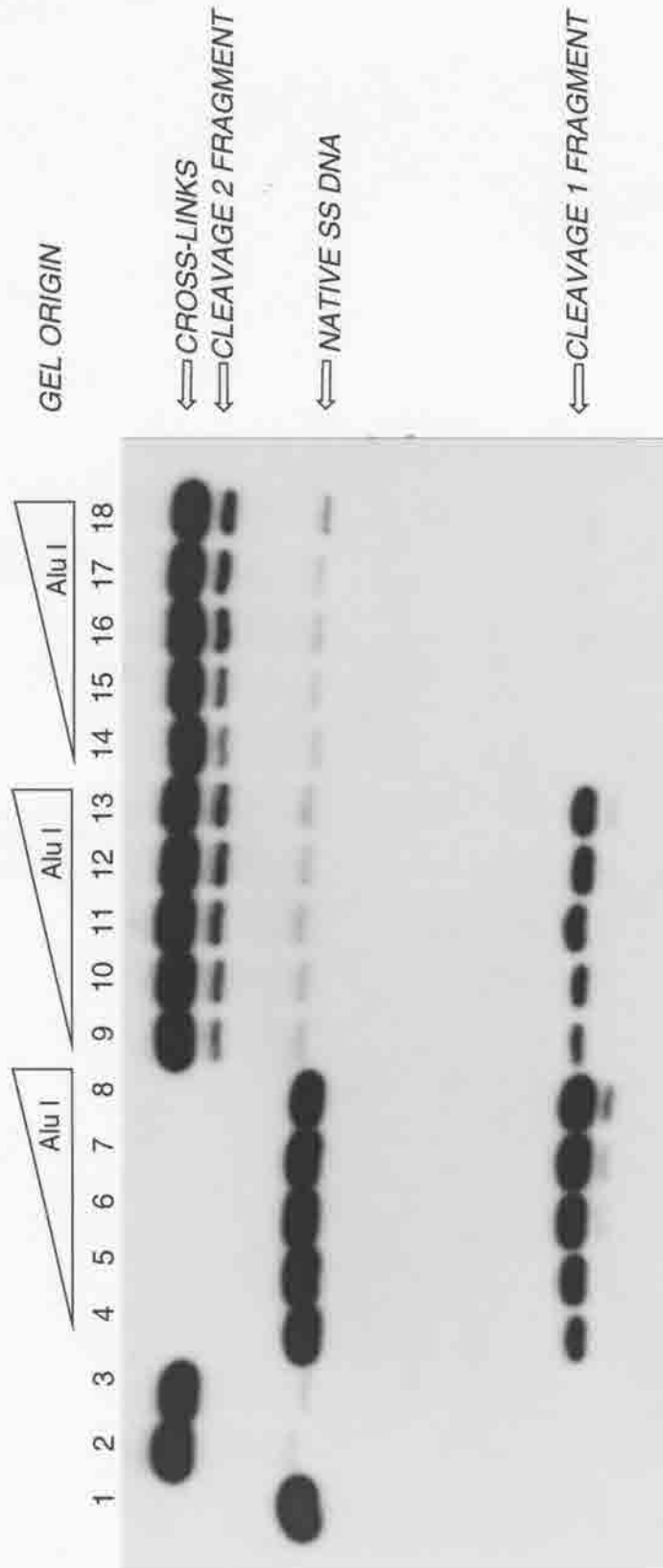


Given the well established ease with which separation of FR-66979 cross-link isomers of **template 3** could be achieved, we incorporated an Alu I site one base 5' of the 5'-ACGT-3' run in **ODN 4**. The resulting oligo 5'-TGTTGAATACAGCTACGTC-TCTTGCTGAGGG-3' (**ODN 9**) and its complement 5'-CCCTCAGCAAAGAAC-GTAGCTGTATTCAACA-3' (**ODN 9'**) were synthesized. The resulting duplex (**template 7**) was cross-linked with reductively activated **314** and the orientation isomers isolated. Conversion of each isomer to the mixture of C10" alkylated mono-adducts and native radiolabeled **ODN 9** revealed that, like **template 3**, the slow mobility isomer was that to which **ODN 9** was mitosene C10" attached (Appendix Fig. 5-14). Incubation of each isomer, as well as a standard duplex control, with 4 units of Alu I for various times gave rise to the autoradiogram depicted by Figure 2-31. Selective 5'-end-labeling of **ODN 9** allowed a means by which to electrophoretically differentiate between Alu I cleavage of the radiolabeled strand (cleavage 1) and cleavage of the complementary **ODN 9'** (cleavage 2). Cleavage of the radiolabeled strand yielded a 12 bp fragment while cleavage of the complement rendered the cross-linked species (retaining the radiolabel) lacking the ODN fragment complementary to the other cleavage product. Thus, the two cleavage events gave rise to easily distinguishable fragments. It is clear that the Alu I cleavage 2 event for each cross-link proceeds with roughly the same efficiency (Figure 2-31 lanes 9-18). However, the faster orientation isomer **371** (higher  $T_m$ ) completely shut down cleavage 1 (Figure 2-31 lanes 14-18).





Consistent with the HPLC results originally published by Tomasz, we observed that only one of the two MC orientation isomers of cross-linked **template 7** inhibited Alu I cleavage of the target duplex. Cleavage 2 was selectively inhibited and cleavage 1 was relatively unaltered from one cross-linked species to the next (Appendix Fig. 5-15). Surprisingly, MC cross-linked **template 7** afforded an enzyme inhibition pattern in which the slow cross-link isomer was that which selectively inhibited the cleavage 2 event. This was in contrast to the published results involving **template 6** in which the higher  $T_m$  cross-link was cleavage 2 inhibitory. By analogy to our own efforts with FR-66979, the slow MC cross-link isomer of **template 7** is the presumed lower  $T_m$  species. Therefore, if the Tomasz correlation of  $T_m$  and enzymatic inhibition was general, then the fast isomer of MC cross-linked **template 7** should have been cleavage 2 inhibitory. That the reverse trend was observed with cross-linked **template 7** thus suggests a fundamental difference in the two ODN substrates **template 6** and **template 7**. It is noteworthy that the Tomasz substrate (**template 6**) possessed an equal number of A-T or C-I base pairs on either side



**Figure 2-31.** 20% DPAGE analysis of restriction fragments obtained from digestion of cross-link orientation isomers of FR-66979 cross-linked **template 7** with Alu I restriction endonuclease (4 units). **Lanes 1-3** standard duplex, slow orientation isomer and fast orientation isomers respectively. **Lanes 4-8** standard duplex treated with Alu I at 1, 2, 5, 10, 30 min. respectively. **Lanes 9-13** contain the slower FR66979 orientation isomer treated with Alu I at 1, 2, 5, 10, 30 minutes while **lanes 14-18** contain the faster orientation isomer subjected to the same digestion as the slow cross-link.

of the cross-link. More importantly, the 5' side of **template 6** (with respect to **ODN 8**) contained a 20% GC content whereas no such residues were located to the 3' side of the MC cross-link. As such **template 6** is 5' (with respect to **ODN 8**) favored with respect to retention of base-pairing on either side of the MC cross-link; **template 6** possesses theoretical  $T_m$ 's of 16.9°C versus -30°C for the 5'- and 3'- sides of the cross-link respectively (with respect to 5' or 3'-orientation of **ODN 8**). Similarly, **template 7** possesses a theoretical  $T_m$  of 47.7°C to the 5' side of the cross-link (with respect to **ODN 9**) and a theoretical  $T_m$  of 30.4°C to the 3' side of the cross-link. This places the higher  $T_m$  situation to the 5' side of the FR-66979 cross-link (with respect to **ODN 9**) in accord with the  $T_m$  asymmetry seen with **template 6**. However, the radically different  $T_m$ s for either side of cross-linked **template 6** in the Tomasz (16.9°C as opposed to -30°C) case may play a role in the Alu I inhibitory trend observed with **template 6** and not observed with the larger substrate (**template 7**).

This may explain the opposite  $T_m$ /cleavage inhibition trend observed for MC cross-linked **templates 6** and **7**. It does not however, explain the selectivity differences seen with MC cross-linked **template 7** as opposed to the analogous FR-66979 system. Indeed, this results most likely from the different structures of each respective lesion and the resulting effects upon the DNA helix. Despite these differences, this confirmed that the observed cleavage selectivities of FR-66979 (opposite to those of MC) was a true effect and not due to artifacts of the assay. That neither **370** or **371** inhibited cleavage 2 represents a novel departure from the known mitomycin literature.

The inhibitory trend observed for FR-cross-linked **template 7** may best be rationalized by the Tomasz proposal pertinent to MC.<sup>36</sup> Tomasz has proposed that placement of the Alu I site one base pair removed from the MC cross-linkable site 5'-ACGT-3' allows the hydrophobic aromatic portion of the derived mitosene to either point to or away from the recognition/cleavage site. This argument was achieved using models for either orientation isomer as reproduced from the NMR-derived model of the central 4-

bp segment of the cross-linked self-complementary hexanucleotide 5'-TACGTA-3'. Significantly, the C2 symmetric nature of this species did not allow differentiation of which MC orientation would be inhibitory. The assignment of the Alu I recognition site positioning with respect to each cross-link was achieved *via* assignment of each orientation isomer mitosene connectivity within **template 6** and its respective Alu I inhibition properties. The resulting MC-DNA connectivity assignments and subsequent modeling (from the NMR-derived structure) was completely in agreement with the motif found for FR-66979. The inhibitory scenario mandates that the quinone portion of MC point towards the enzyme thus interfering with the requisite DNA-protein contacts. Alternatively, placement of the aziridinyl portion of MC in this region minimally influences enzyme recognition and thus does not inhibit strand scission. As such, the results generated with FR-66979 support this notion. As shown in the molecular modeling images of Figure 2-30, it is clear that the faster orientation isomer (that in which **ODN 4** is bound to the C1" of the FR-66979-derived mitosene) places the aromatic chromophore towards the Alu I site. That this orientation would inhibit Alu I was supported not only by our results, but was also supported by the similar findings of Tomasz and co-workers using **template 6** (although the cleavage inhibition was reversed). Connectivity of the radiolabeled strand to the C10" of the mitosene orients the aromatic moiety away from the 5'-AGCT-3 site thus minimizing potentially detrimental drug-enzyme interactions.

Most significantly, with respect to the differing activities of the MC and FR-66979 inhibition trends, is that the fast isomer of FR-66979 cross-linked **template 7** completely shut down the cleavage 1 event. MC, however, only causes enzymatic inhibition and does not prohibit either cleavage. This suggests that the FR-DNA interstrand cross-link may represent a much more potent lesion than the MC cross-link by virtue of an additional biological mode of action. The enhanced ability of FR-66979 to inhibit/shut down protein-

DNA interactions may have a bearing on the lifetime of the interstrand lesion and its resistance to cellular repair mechanisms. This might explain why the FR compounds have been found to be active against numerous mitomycin-resistant cell lines and certainly warrants further attention.

### **2.3- Conclusion**

In summary, the requirement for reductive activation of FR-900482 and FR-66979 has been shown. Surprisingly, interstrand cross-linking of pBR322 with FR-900482 occurs readily in the presence of  $\text{Fe}^{3+}$ . This suggests that a "self-activation" manifold may occur with these compounds which is likely to be dependent upon the presence of the hydroxylamine hemi-ketal. This mode of drug activation was not pursued, but may warrant another interesting departure from the known mitomycin literature. Similar efficiencies with respect to ISC induction by FR-900482 using either  $\text{Fe}^{2+}$  or  $\text{Fe}^{3+}$  complexed with EDTA (see Appendix Table 5-1) suggests that a simple conversion of  $\text{Fe}^{3+}$  to  $\text{Fe}^{2+}$  which then reduces FR-900482 to the DNA-reactive species is not the only manifold by which drug activation occurs during these reactions.

FR-66979 is by far the more active of the two natural products. This is most likely due to more favorable interactions of the C12 benzylic alcohol (as opposed to the aldehyde) with the DNA phosphate backbone since both compounds possess very similar reduction potentials.<sup>22</sup> Additionally, the DNA site specificity/regiochemistry of interstrand cross-linking by these antitumor antibiotics has been elucidated. The sequence 5'-CG-3' is the preferred site of cross-linking and the resulting lesion involves the two adjacent exocyclic amines of each dG residue within this sequence. The cross-linking event occurs wherein the mitosene core can be in either one of two orientations 180° opposite one another. These isomers possess different melting temperatures but do not result in physically discernable distortions of the DNA duplex. Interestingly, the orientation isomers of FR66979 cross-linked DNA give rise to different DNA-protein interactions upon reaction

with Alu I. Significantly, the inhibitory cross-link orientation isomer obtained with FR-66979 completely shuts down the opposite cleavage event from that which is inhibited by MC. This dramatic effect upon protein-DNA interactions may, in part, explain the greater efficacy of the FR drugs as compared to MC.

The capacity of MC to effect non-specific oxidative DNA damage detracts from its utility as a chemotherapeutic. Additionally, facile oxidation of reductively activated MC back to the quinone after mono-alkylation represents a mechanistic hurdle to cross-link formation. The described analogy between MC and the FR drugs thus substantiates the proposal that the FR class of compounds may be a viable replacement for MC since these compounds lack many of the detrimental properties inherent to MC (facile oxidation, superoxide production, etc.) but yet possess the same DNA sequence specificity and requirement for reductive activation.

## Chapter 3

### DNA-protein cross-linking mediated by the FR900482 class of antitumor antibiotics

#### 3.1. Background

Among the initial reports of biological activity of the FR-900482 antitumor antibiotics was that these agents induce DNA-protein cross-links.<sup>2d,3a</sup> The application of alkaline elution methods indicated the time-dependent formation of such cross-links in murine leukemia L1210 cells.<sup>2d,3a</sup> However, the isolation and characterization of such cross-links was not reported. More significantly, the absence of careful structural elucidation of the DNA-protein adducts formed by mitomycin C and the structurally related pyrrolizidine alkaloids has persisted for some thirty years.<sup>49</sup> Given the structural analogy of the mitomycins and the FR drugs, elucidation of the pathway to these lesions was deemed a highly significant undertaking.

DNA sequence-specific binding by proteins has been demonstrated for only a small number of protein-DNA motifs.<sup>50</sup> These are : (i) the helix-turn-helix (HTH) structure of various prokaryotic repressor and activator proteins as well as eukaryotic homeotic gene products; (ii) symmetry-related pairs of  $\alpha$ -helices or a pair of  $\beta$ -strands as found in a bacterial Met repressor protein; (iii) an antiparallel  $\beta$ -sheet found in the G5BP protein; and , (iv) the Zn finger structure originally identified in the transcription factor IIIA protein, but subsequently found in a large number of other eukaryotic regulatory proteins.<sup>50,51</sup> The size and secondary structure of these proteins mandate that DNA-protein interactions occur primarily in the more sterically accessible major groove of duplex DNA. Alternative minor

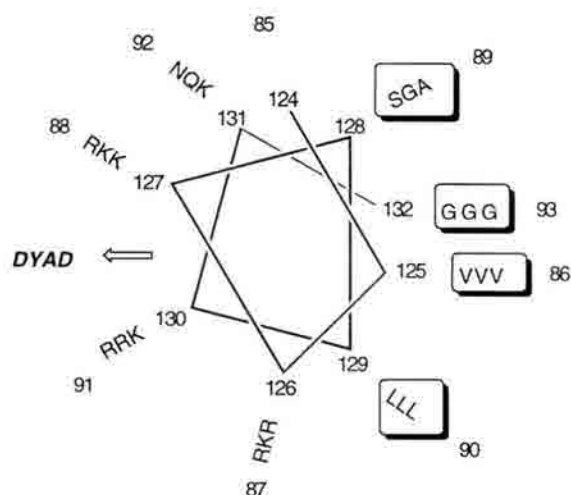


groove sequence-specific binding motifs are much less common and are typically associated with AT rich sequences.<sup>52</sup> This is the result of several factors: specific hydrogen-bonding to adenine and/or thymine bases; the greater negative electrostatic potential in such sequences; the narrowing of the groove in AT regions and oligo(dA) tracts, and the complementarity between groove and ligand curvature.<sup>52a</sup>

### **3.1.1. Minor Groove Binding Protein Motifs**

The minor groove is utilized by several nucleic acid-binding proteins the most prominent of which are: (i) histones H1 and H4;<sup>52b,53</sup> (ii) the pentraxin family of pentameric plasma proteins;<sup>52b</sup> (iii) the N-terminus of protein p6 of the *Bacillus subtilis* phage Ø29;<sup>54</sup> (iv) DNase I;<sup>55</sup> (v) the TATA-binding proteins;<sup>56</sup> (vi) the N-terminal arm of the helix-turn-helix (HTH) engrailed homeodomain protein;<sup>50a,57</sup> and (vii) the N-terminus of the DNA binding domain of *Hin* recombinase enzyme.<sup>58</sup>

- Histones H1 and H4 bear homologous sequences to those observed in the serum amyloid P component (CAP) of the pentraxins.<sup>52b</sup> On the basis of this observation, Turnell *et al.* have proposed a decapeptide motif which specifically recognizes the relatively narrow minor groove of B-form DNA.<sup>52b</sup> Of the conserved regions within the pentraxin family, two have been identified as nucleotide-binding sites which also form a Ca<sup>2+</sup>-binding loop structure. The first of these regions spans residues 136-145 and the second spans amino acids 146 to 158.<sup>52b</sup> A third stretch spanning residues 123-132 is conserved in those pentaxins capable of binding to core particles.<sup>52b</sup> This region is absent in those pentraxins which fail to bind the core particles. Comparison of the sequence with 4,500 sequences in the protein data banks revealed a high degree of homology with only two subsets of sequences; these belonging to histone H1 and histone H4.<sup>52b</sup> From this data, the sequence  $P-V \begin{smallmatrix} RKG \\ KRS \end{smallmatrix} AL \begin{smallmatrix} RN \\ KQ \end{smallmatrix} KG$  has been derived for the common DNA-binding decapeptide of histones H1 and H4 and the pentraxins.



**Figure 3-1.** Projection down the axes of predicted  $\alpha$ -helices. Residues 124-132 in human CRP (inner) and serum amyloid P component (SAP) compared with 85-93 (outer) in gonadal histone H1 from the sea urchin *Parechinus angulosus*. Residues conserved as hydrophobic or small and neutral in the data bank are boxed. The dyad axis is local and relates positively charged and/or dipolar residues (positions 126 and 130 with 131 and 127, respectively). It intersects the helix axis at right angles and intercalates the two turns of the  $\alpha$ -helix.<sup>52b</sup>

The preferred conformation of the decapeptide is proposed to be readily capable of binding to the inner face of the DNA supercoil in the histone H4 case. Additionally, this conformation also allows for histone H1 and SAP binding to the outer face of the DNA *via* common recognition of the minor groove. Analysis of the conserved sequences reveals that nine of the ten residues can form a strongly amphipathic  $\alpha$ -helix (Figure 3-1).<sup>52b</sup> The polar side of the helix is positively charged and accounts for the hydrophilicity of the decapeptide. The side chains of the polar residues are flexible and allow for a closest separation distance between the basic groups of 4Å. Charge-charge and hydrophobic considerations suggest that, in fact the most extended separation is 12Å.<sup>59</sup> Given the width of the minor groove of DNA (9-17Å) and that of the major groove (13-21Å), the configuration of the basic or dipolar residues is most compatible with electrostatic interactions involving the phosphate backbone from across the minor and not the major groove.<sup>60</sup> Indeed, binding is favored by runs of oligo (dA)<sub>n</sub>-(dT)<sub>n</sub> tracts wherein  $n \geq 4$  such that the minor groove is further compressed over that of native heteropolymeric DNA. This has been specifically noted by Satchwell *et al.* in which the preferred (*albeit* truncated) trinucleotide AAA/TTT plays a large role in the binding of the histone octamer to the minor groove of DNA.<sup>61</sup>

In the eukaryotic nucleus, most of the DNA must be tightly bent in order to confine the genome within these organelles. Eukaryotes express minor groove binding histones by which this necessary DNA compression occurs.<sup>53</sup> Both eubacteria and eukaryotes contain DNA-binding proteins which not only compact DNA, but also act to phase chaperone-induced DNA bends which are necessary for transcription.<sup>62</sup> The principal bacterial protein of this class is the HU heterodimer which binds the minor groove of DNA but fails to do so sequence specifically. One homologue, integration host factor (IHF), functions similarly, but does bind to defined sites with higher affinity than for random DNA sequences.<sup>63</sup> HU modulates the binding of IHF to DNA lacking specific IHF-binding sites, as well as to the IHF sites in the replication origin *oriC*.<sup>63</sup> Additionally, HU promotes the assembly of DNA-protein complexes. Interestingly, both HU and IHF bind DNA through the decapeptide motif outlined in Figure 3-1.

A recently discovered nucleoprotein complex in which DNA is wrapped in a superhelical path is that formed by the  $\phi$ 29 p6 protein. This protein binds to the  $\phi$ 29 replication origin thus activating replication initiation. Hermoso and co-workers have shown that the N-terminus forms an amphipathic  $\alpha$ -helix which involves 19 residues.<sup>54a</sup> Like the histone octamer, p6 makes regular minor-groove contacts and induces DNase I hypersensitive sites every 24 base pairs *via* slight widening of the minor groove.<sup>54b,c</sup> Site-directed mutagenesis has revealed that within the 19 amino acid helix the placement of a lysine at residue 2 and arginine at position 6 are both critical to DNA binding.<sup>54a</sup> The binding unit is dimeric and is proposed to wrap the DNA in a right-handed sense. In this respect, p6 differs somewhat from the histones and other nucleoproteins (HU and IHF) which do not appear to rely upon dimerization of the DNA binding  $\alpha$ -helix.

As with most of the DNA-binding proteins, sequence specificity isn't so important as is the shape/conformation of the nucleic acid.<sup>52,53c</sup> One such case in point is the DNA recognition by the nuclease DNase I which selectively recognizes widened minor groove regions.<sup>55</sup> Indeed this property has made DNase I a highly successful probe of ligand-

induced minor groove widening. As mentioned, one example of minor groove widening by the p6 protein is evident based upon regions of DNase I hypersensitivity.<sup>54b,c</sup> The crystal structure of the DNase I-DNA complex shows the enzyme to be bound at a wide minor groove, and the DNA to be bent  $21.5^\circ$  away from the protein.<sup>55</sup> The stacking of a tyrosine residue, Y76, against a deoxyribose at the apex of the bend has been noted and is accountable for much of the DNA distortion.<sup>55</sup> This results in compression of the major groove on the opposite side of the widened minor groove. Such a perturbation is likely necessary to achieve a transition state in which the phosphate is in the catalytic center of the enzyme.

DNA distortion resulting from protein-DNA recognition is a trademark of the nucleoproteins described above and is inherent to DNase I. Particularly severe in its ability to bend DNA is the TATA-binding protein (TBP).<sup>56</sup> The function of TBP is to effect nucleation of the assembly of the pre-initiation complex on promoter elements of genes. In this fashion, TBP acts to facilitate transcription.<sup>64</sup>

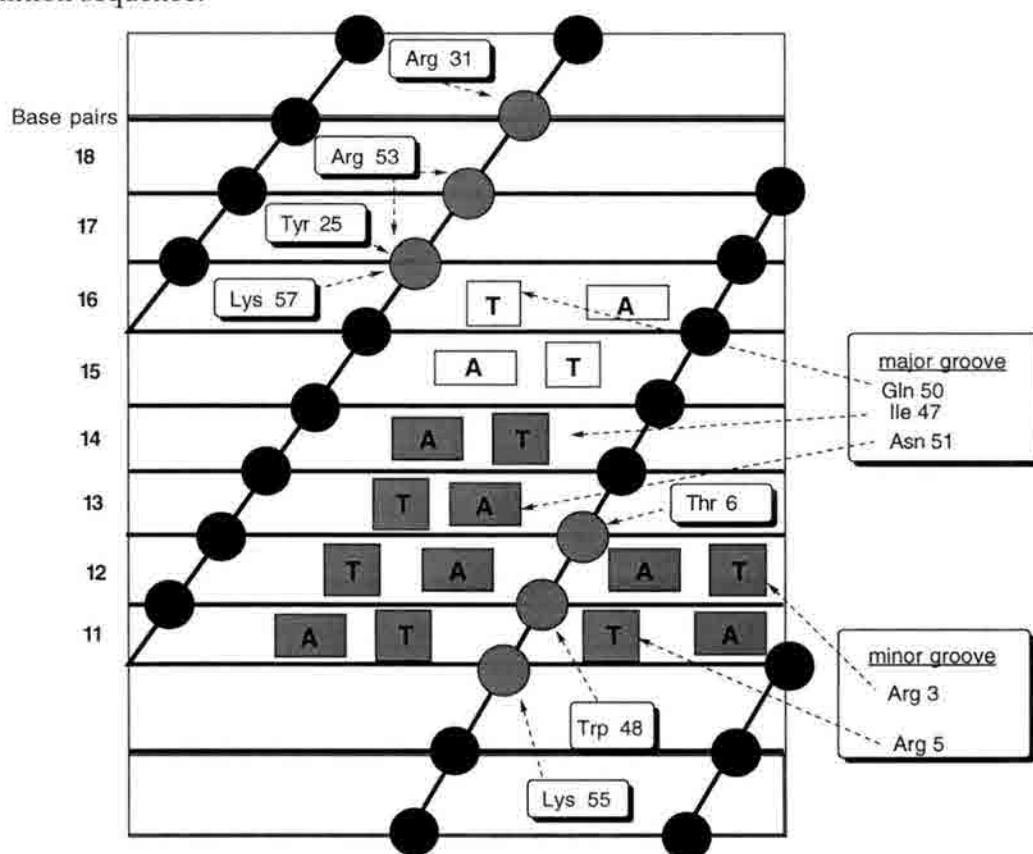
Like DNase I, TBP binds to a widened minor groove. The observed groove widening is a direct result of the  $80^\circ$  net bend induced to the DNA and the resultant unwinding of the base steps proximal to the DNA-protein interface. In the DNase I, case, aromatic residues penetrate the minor groove and facilitate DNA bending.<sup>55</sup> The crystal structure of the TBP-DNA complex has revealed two symmetrically placed  $90^\circ$  kinks at the first and last steps opening towards the minor groove.<sup>56</sup> Both kinks are induced by close juxtapositioning of two phenylalanines. One phenylalanine F73 stacks against a deoxyribose and is in van der Waals contact with the second phenylalanine. Consequently, the second phenylalanine penetrates between the base-pairs external to the contacted ribose thus inducing a kink of  $90^\circ$ . This does not constitute a true intercalation since the phenylalanine is not stacked parallel to the face of the contacted base.<sup>65</sup> Rather, it is aligned at an angle intermediate between stacking and the "edge-to-face" contacts characteristic of interactions between aromatic residues in proteins.<sup>65</sup> The concave surface

of TBP thus bends the DNA away from the body of the protein. This is counter to most other convex DNA recognition surfaces of "major groove-binders" which favor DNA bending towards the protein.<sup>56b</sup> The radical nature of the DNA bend is proposed to enhance strand separation events necessary for transcription.<sup>56</sup> In this motif, the TBP-DNA complex has been viewed as a highly distorted transition state (resulting in localized DNA melting) leading to transcription as the catalytic result.

The N-terminus of the DNA binding domain of Hin recombinase enzyme and the N-terminal arm of engrailed homeodomain proteins both rely upon the helix-turn-helix (HTH) motif for DNA recognition *via* minor groove contacts. This was the first DNA-recognition motif discovered and structures have been determined for many HTH proteins and protein-DNA complexes. Comparative amino acid analysis suggested that the homeodomain would contain a HTH motif and this has in fact been confirmed.<sup>66</sup> The engrailed homeodomain contains an extended N-terminal arm and three  $\alpha$ -helices.<sup>50a</sup> Helices 1 and 2 pack against each other in an antiparallel arrangement. Helix 3 is roughly perpendicular to the first two thus allowing its hydrophobic face to form the interior of the protein. The vast majority of DNA contacts are made by helix 3 and these reside predominantly within the major groove although residues in the extended N-terminal arm make contacts also with the minor groove (Figure 3-2).<sup>50a</sup> The exposed face of helix 3 fits into the major groove, allowing side chain-to-DNA contacts involving both the DNA bases and phosphodiester backbone.<sup>50a</sup> Other critical contacts arise from residues 3-9 of the N-terminal arm. This arm fits tightly into the minor groove and supplements the major groove contacts of helix 3.<sup>50a</sup>

Hin recombinase also possesses the HTH binding motif with helices 1 and 2 positioned in an antiparallel orientation with an approximate 25° angle between them.<sup>67</sup> This configuration, along with the arm extending from helix 1 that protrudes into the minor groove, is quite similar to the homeodomain motif. Helix 3, possessing only eight residues, is inserted into the major groove perpendicular to the DNA helical axis.<sup>67</sup> This

helix is locked into the major groove by amino acid-phosphodiester contacts involving Arg142, Tyr179 and Arg178.<sup>67</sup> Additional phosphate contacts involve the side chain of Thr175 and the amide NH of Gly172. Only two of the helix 3 residues make hydrogen bond contacts to DNA bases within the major groove. These are the serine at position 174 and arginine at position 178. The N-terminal arm of Hin is connected to the hydrophobic pocket *via* Ile144, and then reaches into the minor groove.<sup>68</sup> Arg 142 anchors the peptide onto the phosphate backbone, and the peptide chain then turns into the minor groove at Pro141.<sup>67</sup> Arg140 then makes a contact with the adenine at base pair 6 and the main chain NH is hydrogen bonded to its complement thymine. This amide is preferentially hydrogen bonded as a direct result of considerable propellor twisting at base pair 6 of the DNA recognition sequence.



**Figure 3-2.** Summary of all contacts in the engrailed homeodomain-DNA complex. The DNA is represented as a cylindrical projection, and the shading emphasizes the TAAT subsite that occurs in many homeodomain-binding sites. Phosphates are represented by black balls: hatched balls show phosphates that are contacted by the homeodomain.



Benefiting from the N-terminal arm and its specific minor groove contacts, Hin recombinase also demonstrates extensive minor groove interactions as a consequence of its C-terminal arm.<sup>58a</sup> Extending from helix 3 of the HTH, the C-terminal crosses the phosphodiester backbone and is inserted into the minor groove at the outer edge of the recombination site.<sup>58,67</sup> The six residue run Ile-Lys-Lys-Arg-Met-Asn follows the groove with the peptide main chain packed against the bases and the side chains pointing out of the groove.<sup>67</sup> Hydrogen bonding to bases from the peptide backbone occurs between the CO of Ile185 and G14 and between the NH at Lys187 and Asn190 to the T at base pair 12 and the A at base pair 10.<sup>58b</sup> In this fashion, the Hin C-terminal arm displays a similar hydrogen bonding motif to that known for minor groove-binding ligands netropsin and Hoechst 33258. Notably, studies involving deletion of the 6 C-terminal residues indicate that binding and recombination are largely unaffected by the absence of this fragment.<sup>67</sup> Alternatively, deletion of N-terminus residues showed the absolute requirement for the N-terminal binding manifold.<sup>67</sup> As such, the exact role played by the C-terminus in Hin binding is unclear. It is significant however, that the C-terminal arm affords a DNA-binding interaction reminiscent of the high mobility group I and Y proteins. This poses interesting evolutionary questions linking the two classes of proteins and their respective functions.

### **3.1.2. High Mobility Group (HMG) Proteins**

Perhaps the most well studied of the minor groove protein-DNA motifs are the HMG proteins. The HMG I proteins belong to the "high mobility group" (HMG) class of mammalian chromatin proteins and are present in higher eukaryotes.<sup>69</sup> These non-histone chromosomal proteins are preferentially expressed in undifferentiated, neoplastically transformed, and rapidly proliferating cells.<sup>70</sup> Their sequence conservation and ubiquity imply a great deal of importance. The HMG nucleoproteins may be divided into three groups based on their size, sequence homology and DNA binding properties: HMG-1/-2, HMG-14/-17 and HMG-I/Y.<sup>71</sup> HMG-1 and HMG-2 each have molecular weights of

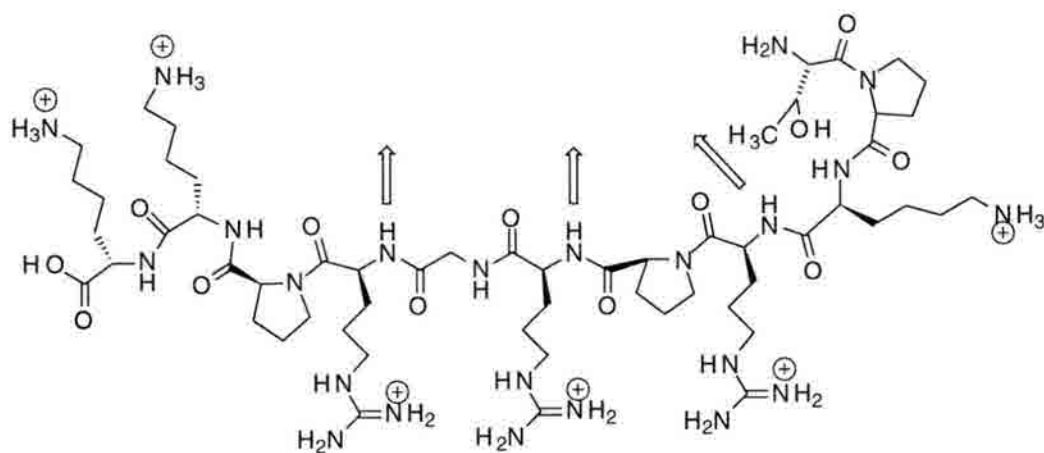
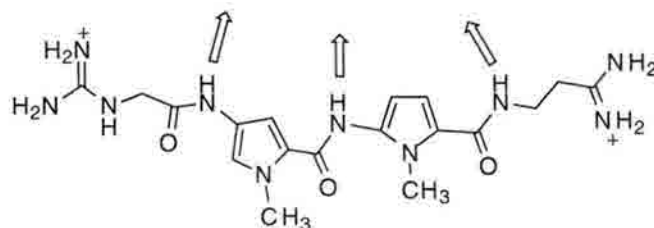


approximately 25 kDa and a distinct tripartite structure.<sup>72</sup> The N-terminal A-domain (amino acids 1-79) and the central B-domain (residues 90-163) are both highly basic and conform to a  $\beta$ -helix conformation.<sup>72</sup> Conversely, the C-terminus C-domain starting at residue 164, is very acidic in nature with some 30 aspartic and glutamic acid residues. This domain readily interacts with histones.<sup>72</sup> The A and B domains are homologous; each containing three  $\alpha$ -helices accounting for 75 % of the total residues in each "HMG" box. HMG-1 and HMG-2 bind both single- and double-stranded DNA and show a marked preference for non-B-DNA structures.<sup>73</sup> Despite structural similarities to known transcription activators, HMG-1 is not capable of transcription activation in transfected yeast cells.<sup>72</sup> It does, however, facilitate the formation of transcription initiation complexes of RNA polymerases II and III.<sup>74</sup>

HMG-14/-17 also facilitate polymerase II and II transcription.<sup>75</sup> Bustin *et al.* have shown that deletion of the 22 C-terminal amino acids from HMG-17 or 26 C-terminal residues of HMG-14 significantly reduces the ability of these chromatin-associated proteins to enhance transcription.<sup>75</sup> Similar deletions at the N-terminus had no effect upon transcription viability. Chromatin transcription enhancement assays revealed further, that the minimal nucleosomal binding domain of human HMG-17 is a 24 residue stretch from residue 17 to 40.<sup>75</sup> These studies suggest that, like the closely related proteins HMG-1/2, HMG-14/17 have a modular structure containing distinct functional domains. Strikingly, HMG-14 and HMG-17 possess molecular weights in the same range as those of the HMG-I(Y) proteins (approximately 10 kDa).<sup>69</sup>

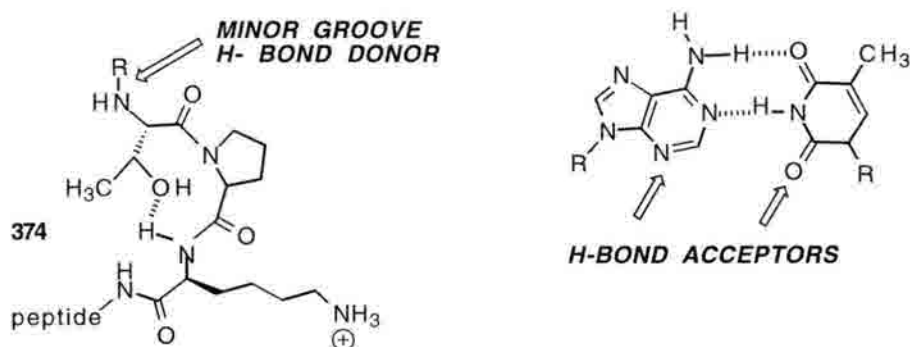
HMG I is the most heavily studied of the isoform nonhistone chromosomal proteins. With the exception of an internal 11 amino acid deletion, HMG-Y is identical to HMG-I.<sup>70</sup> Like the other HMG proteins, HMG-I has been implicated in the regulation of gene transcription.<sup>76</sup> Additionally, HMG-I(Y) have been implicated in the proper maintenance of structure and expression of chromatin.<sup>77</sup> Bearing both a DNA-binding domain and a negatively charged surface (at the C-terminus) these proteins fulfill the

requirements of a Ptashne-type activator protein.<sup>69</sup> Therapeutically significant is that high HMG-I levels are a consistent feature of rat and mouse malignant cells and have been suggested to be a protein marker for neoplastic transformation and metastatic potential.<sup>78</sup> HMG-I(Y) are distinguished from other HMG proteins by their ability to specifically bind double-stranded DNAs containing sequences of at least four continuous AT-bases (ideally, 5'-AATT-3').<sup>79</sup> Binding is sensitive to the local conformation of the minor groove of DNA instead of the specific nucleotide sequence, though sequence-dependent DNA conformation clearly plays a role.<sup>45</sup> Binding affinity and specificity results from three homologous DNA-binding domains (BD) with the consensus sequence TPKRP-RGRPKK.<sup>78,80</sup> Molecular modeling and NMR structural data has revealed that the domain possesses a crescent shape reminiscent of netropsin and distamycin (**373**) resulting from the predominantly *trans*-prolines at either end of the palindromic PRGRP.<sup>88</sup>

**372****373**

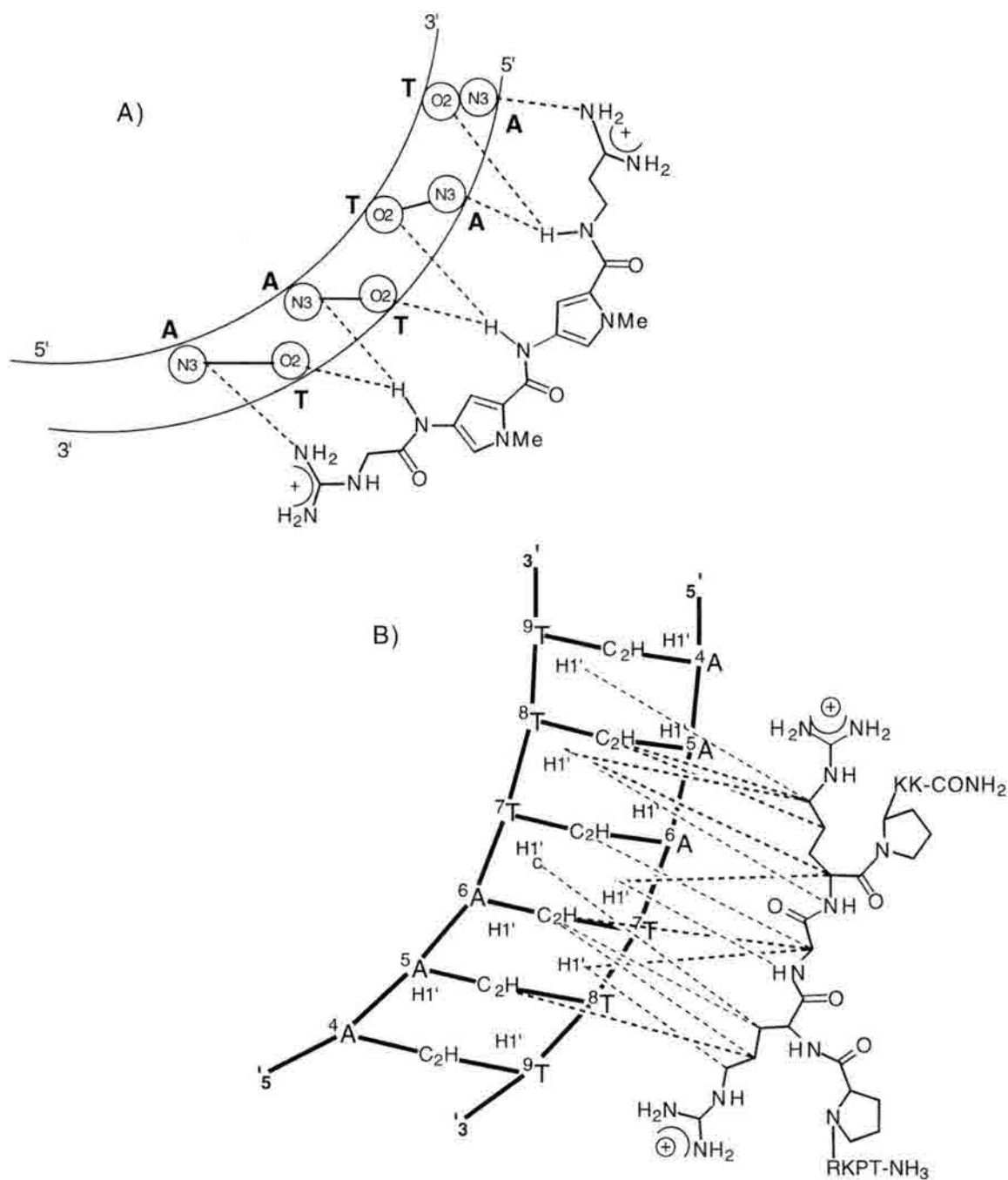
Binding to the minor groove of A-T rich DNA occurs *via* replacement of the inner spine of hydration by the donation of bifurcated hydrogen bonds from the appropriately placed amide NH residues in the peptide backbone.<sup>78,80</sup> Additionally, the non-specific ionic interactions of lysine and arginine with the anionic DNA backbone are responsible for most of the DNA binding energy.<sup>78</sup> This is consistent with the proteins's salt-dependent DNA binding affinity.

The "AT-hook" motif inherent to TPKRPRGRPCK (372) results from the synergism of the N-terminus TPK hook and the proline-induced crescent conformation of the RPRGRPCK fragment.<sup>77</sup> The N-terminal "hook" results from an Asx-turn (374) *resulting partly* from intramolecular hydrogen bonding between the threonine hydroxyl and



the lysine-to-proline amide hydrogen.<sup>77,81</sup> The intramolecularly stabilized tripeptide fits tightly into the wide minor groove of AT/GC junctions and has been implicated as a major factor in DNA binding by TPKRPRGRPCK.<sup>77,78</sup>

Reeves and Nissen have shown that substitution of alanine for threonine at this position results in retention of the hook motif and analogous DNA-binding affinities.<sup>77</sup> As such, the main contributor to the hook motif observed is proposed to be the neighboring proline which results in pronounced kinking of the N-terminus. This kink specifically orients the peptide amide one residue ahead of the proline into a strong hydrogen bond in the minor groove, most likely with the N<sup>3</sup> of deoxyadenosine or the O<sup>2</sup> of deoxythymidine.



**Figure 3-3.** A) 5'-AATT-3' binding motif for distamycin in which amide protons undergo bifurcated H-bonds with deoxyadenosine N<sup>3</sup> and deoxythymidine O<sup>2</sup>. B) Schematic representation of the intermolecular peptide-DNA (5'-AAATTT-3') contacts for intact HMG I binding domain TPKRPRGRPKK as determined from <sup>1</sup>H NOESY spectra in H<sub>2</sub>O and D<sub>2</sub>O.<sup>80</sup>

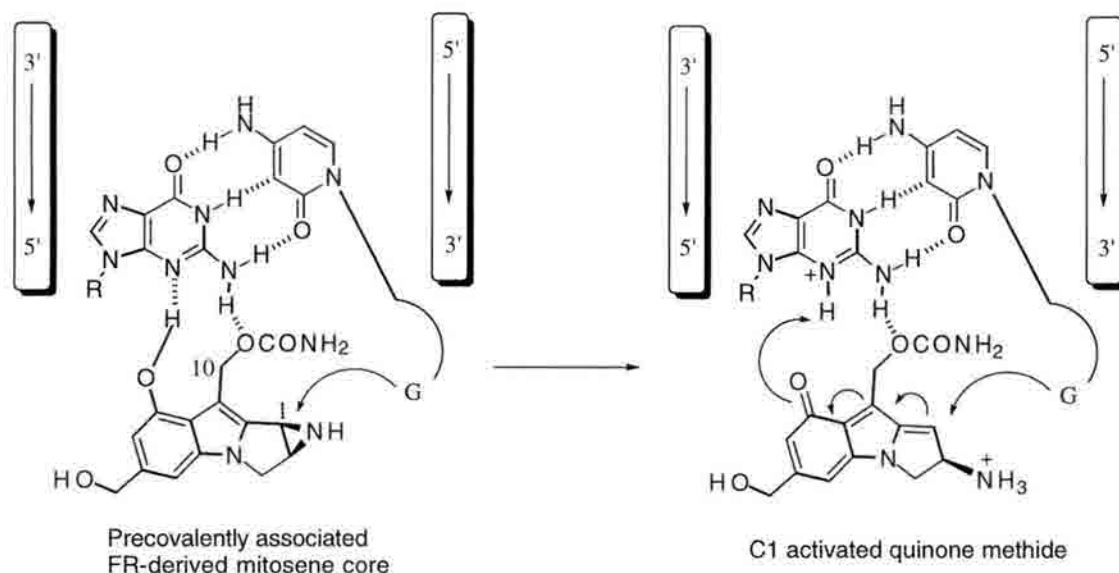
Threonine incorporation in the native protein allows for regulatory phosphorylation thus markedly reducing DNA affinity.<sup>82</sup> Once thought to abrogate Asx-turn formation, threonine phosphorylation most likely reduces DNA affinity through a combination of steric and electrostatic repulsive interactions with the DNA backbone.<sup>77</sup> Zhao *et al.* have shown that HMG-I(Y) effects displacement of histone H1 from scaffold-associated regions (SARs) *in vitro*.<sup>83</sup> In so doing, one proposed role of these small (10 kDa) proteins is to activate the genes associated with SARs. Cell cycle-dependent phosphorylation of both HMG-I(Y) by cdc2/histone H1 kinase may coordinatively alter relative binding affinities leading to regulation of gene activation from one interphase to the next.<sup>83</sup> This rationale is consistent with the presence of these proteins in rapidly proliferating cells.

### **3.2- Results & Discussion**

#### **3.2.1. DNA monoalkylation model studies pertinent to DNA-protein cross-linking by reductively activated 314**

Paramount to the ability of any agent to form DNA-protein cross-links is the amenability of the agent to monofunctionally bind the target DNA thus allowing the second binding event to arise *via* protein-drug interactions. The obvious difficulty in this process is that most compounds capable of such reactivity preferentially form the DNA interstrand cross-link following DNA mono-alkylation. MC is one example of this. Once alkylated at the optimum mono-alkylation site 5-CG-3', activated MC undergoes facile C10 alkylation by the complementary strand.<sup>25</sup> Tomasz and co-workers have shown that while loss of the carbamate functionality from C10 is the major obstacle to cross-link formation by MC (**163**), its presence is crucial to the ability of MC to efficiently alkylate the 5'-dCG.<sup>84</sup> Hydrogen bonding between the C-10-O of the activated form of MC and one of the exocyclic amines within the 5'-dCG box aligns the drug properly for ring-opening of the

aziridine by the "non-associated" guanosine of the opposing strand thus imparting initial monoalkylation with the 5'-dCG specificity necessary for ultimate interstrand cross-linking (Fig. 3-4).<sup>85</sup>



**Figure 3-4.** Proposed model of pre-covalent association of FR-66979 (**314**) core to 5'-CG-3'. Critical H-bonds are designated with arrows. Phenolic interaction with N<sup>3</sup> of guanine proposed for MC by Kohn, but debated by Tomasz.<sup>84,87</sup> Carbamate-to-N<sup>2</sup> (guanosine) interaction is mutually agreed upon by both Kohn and Tomasz.

Given the established mechanistic similarities between **314** and MC we felt that such interactions might have a bearing on the ability of **314** and related compounds to monoalkylate DNA substrates *enroute* to DNA-protein cross-linking. To determine the degree of analogy between MC and **314** (with respect to monoalkylation properties) reactions were carried out with <sup>32</sup>P-5'-end-labeled 5'-TGTTGAATACTCATACGTCTCTTGCTGAGGG-3' (**ODN 4**) annealed to the following complementary strands in which various guanosines were replaced by inosine.

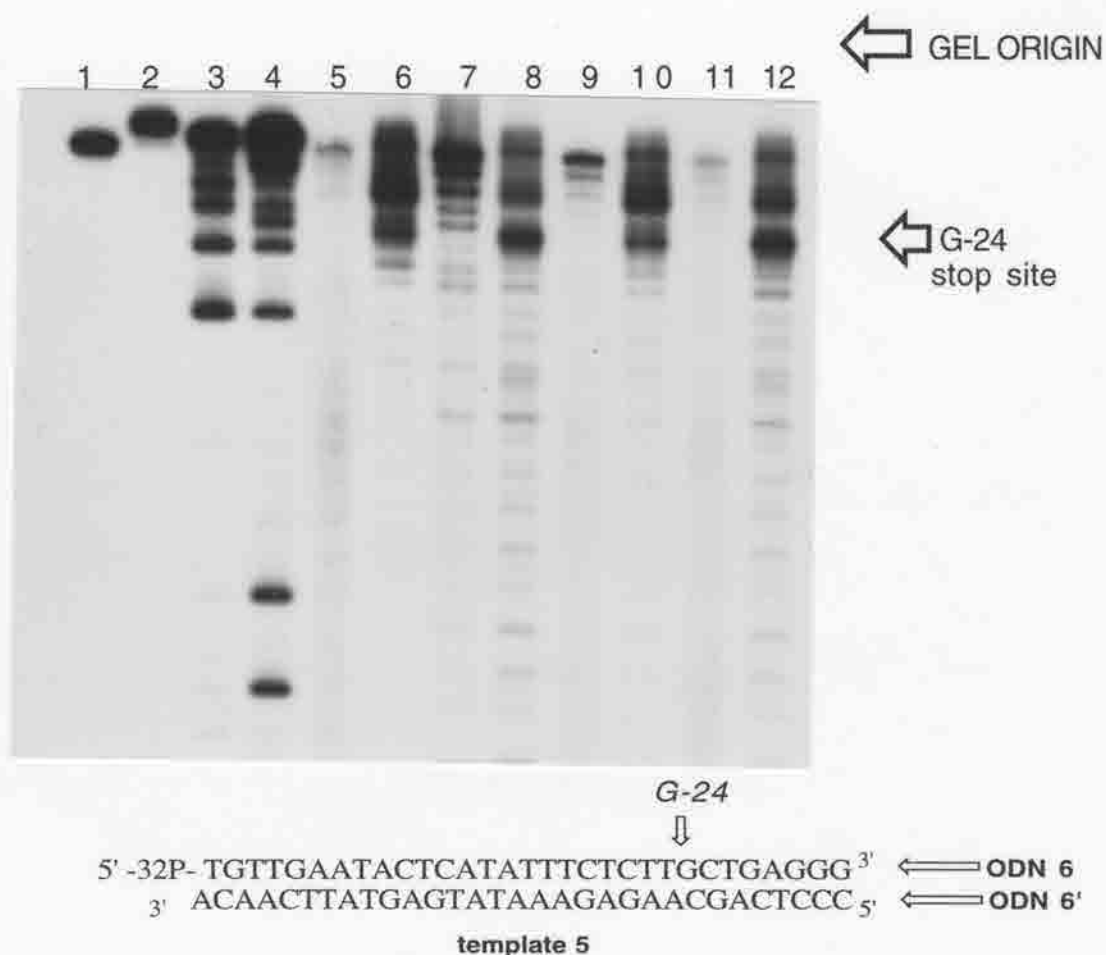
5'-CCCTCAGCAAGAGACGTATGAGTATTCAACA-3' (**ODN 4'**)

5'-CCCTCAICAAIAIACGTATIAITATTCAACA-3' (**ODN 10**)

5'-CCCTCAGCAAGAGACITATGAGTATTCAACA-3' (**ODN 11**)

5'-CCCTCAICAAIAIACITATIAITATTCAACA-3' (**ODN 12**)

Verification that the bands assigned as mono-adducted DNA (as judged by electrophoretic mobility) were indeed mono-alkylated was obtained by snake venom phosphodiesterase (SVPD) digestion using FR-66979 mono-alkylated **ODN 6** (following 20% DPAGE purification). Following methodology developed by Cosman *et al.*, the observed enzyme stop site unique to **314**-modified **ODN 6** was assigned as G-24 which had undergone monoalkylation by reductively activated **314** (Fig. 3-5).<sup>86</sup> The site of drug



**Figure 3-5.** Snake venom phosphodiesterase (SVPD) digestion analysis of **314** mono-alkylated **ODN 6** (5'-labeled). Samples were heated to 90°C prior to 3 hour digestion to insure the single-stranded nature of the substrate. **Lane 1**- standard ss **ODN 6**. **Lane 2**, "monoalkylated" **ODN 6** standard. **Lanes 3**, and **4**; Maxam-Gilbert G, G+A respectively. **Lanes 5**, **6** standard DNA and monoalkylated DNA subjected to 0.6 units SVPD respectively. **Lanes 7**, **8** standard DNA and monoalkylated DNA subjected to 1.2 units SVPD respectively. **Lanes 9-12** same as **lanes 5-8** except samples were not heated prior to digestion.

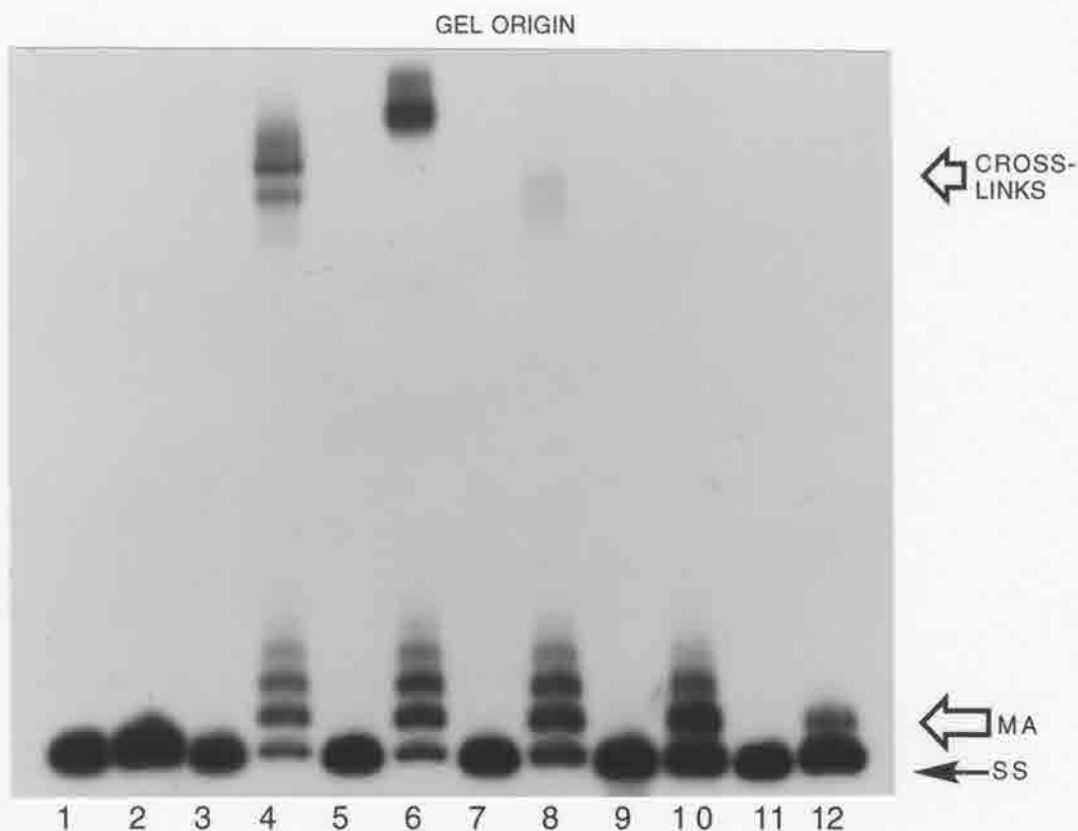


attachment to 5'-end-labeled ODNs gives rise to slight perturbations in the DNA base stacking and thus gives rise to enzyme stop-sites. As such, the sites unique to alkylated DNA which are not encountered in native unmodified oligos are attributable to sites of DNA alkylation. The stop site encountered in lanes 6,8,10, and 12 of Figure 3-5 (the fastest moving intense band denoted as G-24) was consistent for 5'-GC-3' monoalkylation despite considerably slower mobility than that seen in the Maxam-Gilbert sequencing lanes for strand cleavage corresponding to the G-24 residue. Altered mobility was due to drug attachment to the 5'-labeled remainder of the ODN resulting in mass and charge alterations not associated with SVPD digestion of native DNA. Attempts to obtain mass spectral data on such adducts (using **template 3**) failed, but the assignment of monoadduction was further supported as follows.

Efforts to assign the structural origin of cross-link orientational isomerism involved isolation of both fast and slow mobility cross-links and subsequent analysis by non-denaturing polyacrylamide electrophoresis (non-DPAGE). Also isolated from the FR-66979 reactions was the 5'-<sup>32</sup>P-labeled **ODN 4** which appeared to be monoalkylated. Analysis of these samples by non-DPAGE revealed no difference in mobility between the two cross-links. More troubling however, was that the monoalkylated band possessed identical electrophoretic mobility to that demonstrated for both cross-links despite having been rigorously denatured prior to electrophoresis (Appendix Fig. 5-16). Further analysis showed that the complement to radiolabeled monoalkylated **ODN 4** migrated with the same DPAGE mobility as the presumably monoalkylated material. Thus, the isolation of both unlabeled **ODN 4'** and the radiolabeled monoalkylated **ODN 4** gave rise to the interstrand cross-link. As such, the band tentatively assigned as monoalkylated material had to have been in line with this assignment to have afforded the **template 3** interstrand cross-link.

The results depicted in Figure 3-6 show very clearly that use of **ODNs 4'** (lanes 3,4) , **10** (lanes 5,6) or **11** (lanes 7,8) as the complements, resulted in nearly identical

patterns of monoadduct formation. Reaction of the **ODN 4/12** duplex (lanes 11,12) resulted in greatly diminished yields of mono-adduct and surprisingly a good deal of mono-alkylation was seen in the single-strand (**ODN 4**) control reaction (lanes 9,10). The ability to form the interstrand cross-link with **ODN 4/10** duplex in comparable yields to those using **ODN 9** as the complement of **ODN 4** demonstrated that inadvertent denaturing of **ODN 4/10** duplex was not a factor in these reactions. That substitution of inosine for guanosine at the 5'-dCG site had no effect on the relative amounts of monoalkylation, represents an interesting departure from the mitomycin C pathway with respect to "non-covalent" drug-DNA recognition. These results suggest that in the case of reductively activated **314** additional "non-covalent" associations may be operative which bear greater influence upon sequence specificity than that exerted by carbamoyl -to- dG-N<sup>2</sup> interactions inherent to the MC system. Of considerable interest are the potential H-bond donating properties of the phenol as well as the benzylic alcohol of C-12. Indeed, molecular modeling of **314** cross-linked 5'-CG-3' reveals that the benzylic alcohol (a potential H-bond donor/acceptor) resides proximal to the phosphate backbone periphery of duplex DNA (Fig. 2-30).



**Figure 3-6.** Reaction of  $^{32}\text{P}$ -5'-end-labeled 5'-TGTTGAATACTCATACGTCTCTTGC-TGAGGG-3' (ODN 4) annealed to complementary ODNs 4',10-12 with reductively activated FR66979 (**314**). Lanes 1, and 2 are radiolabeled oligo and oligo+ DTT standards respectively. Lanes 3,5,7,9,11 are control lanes containing substrate and FR66979. Lanes 4,6,8,10,12 are reaction lanes containing substrate after reaction with 10 mM FR66979 + 100 mM DTT. Lanes and corresponding complements to 5' labeled strand are as follows: Lanes 1-4 (ODN 4'), lanes 5,6 (ODN 10), lanes 7,8 (ODN 11), lanes 9,10 (single strand 5' labeled oligo control), lanes 11,12 (ODN 12). MA denotes monoalkylation products. Bands slower in mobility than bands noted as MA represent multiply alkylated species.

These results provide a basis for not only an explanation of the enhanced cross-linking efficacy of **314** over **312** and **313** (Appendix Fig. 5-7), but may also explain the unaltered monoalkylation patterns of inosine-substituted templates *versus* those bearing the native dG bases. The phenolic interaction of activated MC with  $\text{N}^3$  of an adjacent G prior to alkylation had been suggested by Kohn (based on modeling studies) and may play a much larger role with the FR-series compounds than with the mitomycins given the invariant oxidation state of the phenol ring of the FR drugs.<sup>87</sup> Importantly, the ability of **314** to efficiently monoalkylate 5'-CG-3 (and other dG containing sequences as well, based on

Fig. 3-5) with or without the native dG of the complementary strand in place indicated that elucidation of a potential DNA-protein cross-linking motif might be more likely with **314** than with other agents of similar structure and reactivity (ie.- mitomycins, pyrrolizidine alkaloids). This was particularly intriguing given the Fujisawa reports of extensive DNA-protein cross-linking by **312-314**.

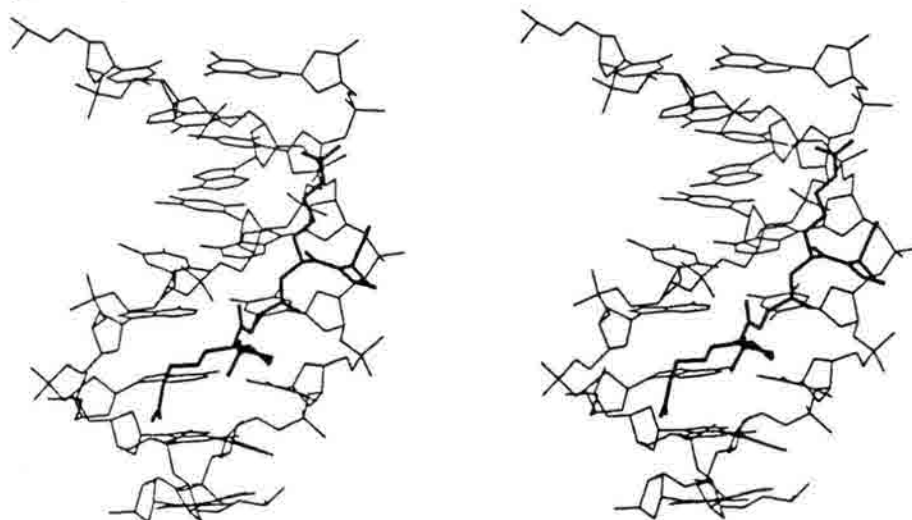
### **3.2.2. Initial Efforts towards DNA-peptide cross-linking by reductively activated 314; Modeling and Rationale**

Initial efforts had focused on the interaction of the  $\lambda$  phage 434 repressor protein with the operator (recognition) DNA sequence 5'-ACAAAAAGTTTGT-3'(OR1).<sup>88</sup> The failure of FR-66979 to mediate either DNA-DNA or DNA-protein cross-linking was attributed to the minor groove predisposition of FR-66979 with respect to 5'-CG-3' alkylation. Although select contacts of the 434 repressor-OR1 complex involve the minor groove, these were deemed unlikely sites for FR-66979 reaction.<sup>89</sup> Most repressor-OR1 contacts reside within the major groove thus suggesting that such a model system was not a viable choice for reactions with the FR-drugs.

Wemmer and co-workers had shown by <sup>1</sup>H NMR that the short binding domain peptide fragments derived from HMG-I/Y proteins (TPKRPRGRPKK; PRGRPKK; and PRGRP) bind specifically to the central AT sites of the self-complementary ODNs 5'-CGCAA-ATTTGCG-3' and 5'-CGCGAATTCGCG-3'.<sup>80</sup> The arginine side chains of each peptide protrude deep into the minor groove in a fashion similar to that known for the antibiotic netropsin.<sup>80</sup> The PRGRP run of each peptide bound specifically to the 5-AAATTT-3 region of the ODN duplexes examined with parts of the longer peptides associated with the flanking CG base pairs.<sup>80</sup> The minor groove nature of the disclosed peptide-DNA interactions and the known amenability of the FR drugs to react within the minor groove of DNA suggested that this motif may be one of potential significance. This

was further supported by the preferential expression of HMG-I(Y) proteins in rapidly proliferating, undifferentiated cells (such as those of cancerous tissues).<sup>78</sup>

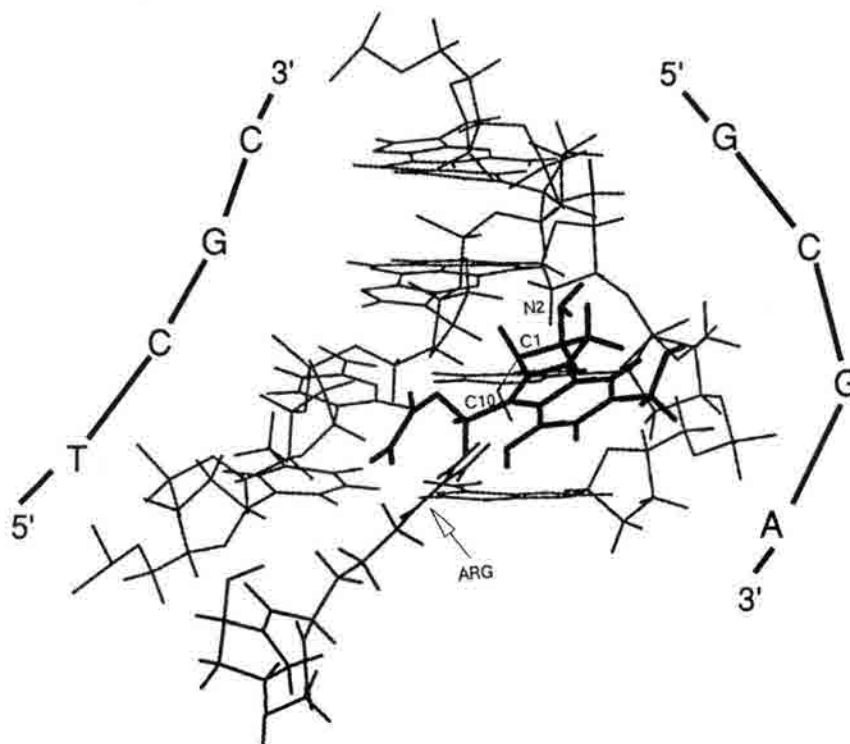
The <sup>1</sup>H NMR-derived structure for peptide-DNA binding revealed that one of the two arginines within the site-recognizing PRGRP sequence came within close proximity to the exocyclic N<sup>2</sup> amine of the 5'-AATT-3' abutted dG shown in the stereoview diagram below (Figure 3-7).<sup>80</sup> Further, minimization of this complex (coordinates courtesy of Wemmer and co-workers) with the FR-66979-derived mitosene at a dG mono-alkylation site flanking the 5'-AATT-3' revealed minimal distortion of the DNA duplex by the bound drug (Figure 3-8).



**Figure 3-7.** Stereoview diagram of molecular model consistent with the NOESY data of PRGRP bound to 5'-CGCGAATTCGCG-3'. All protons omitted for clarity. Bold faced dG is that which is proximal to the guanidine side chain. Only the central eight base pairs are shown. Peptide is shown in thick solid lines.<sup>80</sup>

Modeling revealed that the C10 of the mitosene is within 2 Å of a guanidine from one of the two palindromic arginines of PRGRP; not unexpected based upon Figure 3-7. An interesting feature revealed by the modeling involved the disposition of the amino group at N2 (from aziridine ring opening of reductively activated **314**). Using a cross-linkable 5'-CG-3' site, this amine is within 2 Å of the exocyclic N<sup>2</sup> of the opposing G residue. Presumed repulsive interactions between the two thus suggested that a 5'-GG-3' monoalkylation site may be optimal since, it positions the amino group in perfect H-

bonding distance (2-4Å) of the carbonyl on the opposing C-residue and may facilitate formation of the DNA-peptide lesion. Indeed the 5'-GG-3' box and numerous other monoalkylation sites were incorporated into synthetic ODNs throughout the course of these studies.



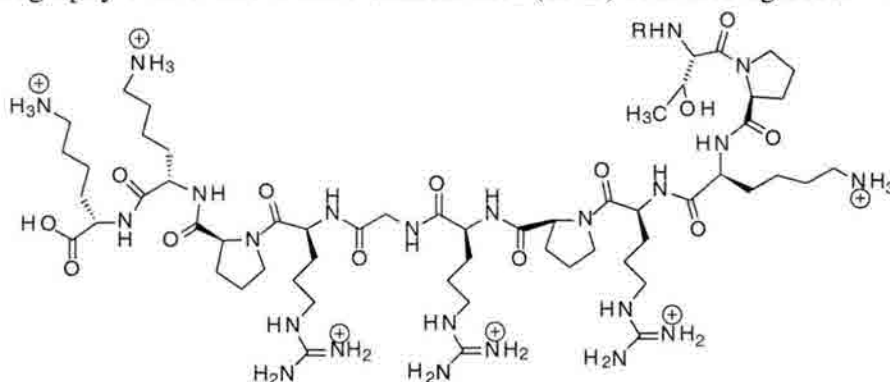
**Figure 3-8.** Molecular mechanics calculations for the proposed DNA-drug monoalkylation adduct. DNA backbone is shown in light gray, **314** derived mitosene (dark, bold lines) is covalently attached *via* C1 to N<sup>2</sup> of the dG residue of the right side strand; the HMG peptide is shown in dark, medium lines. The guanidine side chain of the Arg is indicated and positions the guanidino-N atom within 2Å of the mitosene C10.

Initial attempts to visualize a **314** induced DNA-peptide cross-link involved the use of small oligos some of which were identical to those employed by Wemmer. These efforts proved fruitless in that no detectable DNA-peptide species were ever generated, despite the incorporation of FR-66979 monoalkylation sequences. Suspected problems with these systems involved inordinately low  $T_m$  values which may have hindered the ability of the chosen binding domain (BD) peptide to bind double-stranded DNA. To overcome difficulties associated with low  $T_m$ s, we opted to examine larger ODN duplexes

such as the self-complementary **ODNs 13-15**. Each substrate bore the centrally located 5'-AATT-3' flanked on either side with CG rich runs (cross-linkable dGs are bold-faced below). In the **ODN 14** case 5'-CG-3' interstrand cross-linking would be averted *via* incorporation of inosine opposite the monoalkylated dG (monoalkylation target dG residues are italicized below).



Anticipated problems associated with the ability to visualize DNA-peptide cross-links *via* electrophoretic methods led to the generation of peptides **375 a/b**.<sup>90</sup> Bearing the N-terminal cysteine, **375a** was expected to give rise to a DNA-protein cross-link isolable by chromatography over 5-thio-2-nitro-benzoic acid (TNB) activated agarose.<sup>91</sup> Reaction

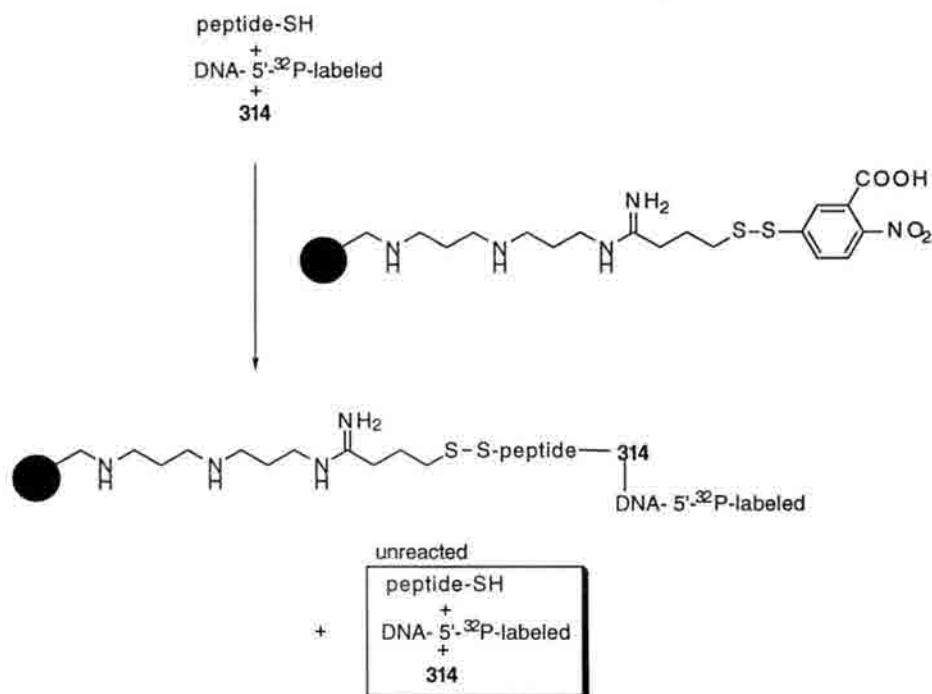


375  
a, R = N-Ac-Cys  
b, R = ε-Dansyl-L-Lys

of the TNB disulfide of the affinity matrix with the thiolated peptide adduct was envisioned to covalently link the peptide-DNA complex to the derivatized matrix *via* thiol-disulfide exchange (Fig. 3-9). The ability to radiolabel either strand of the duplex target DNA in conjunction with this methodology, would afford a means of rapid cross-link detection and purification were electrophoretic methods to fail. Alternatively the  $\epsilon$ -dansylated lysine of



**375b** would allow a readily detectable fluorescent species which could be isolated either electrophoretically or chromatographically (presumably by size exclusion).<sup>92</sup>



**Figure 3-9.** Thiol-disulfide interchange methodology as applied to affinity chromatography. The alkylamine linker is attached to agarose (denoted by the black ball) while the terminal disulfide is TNB activated.

Reactions of **375 a** with DNA substrates **ODN 13** and **14** were observed to give rise to electrophoretically shifted materials (Appendix Fig. 5-17). No such band shifting was obtained for **ODN 15**. Unexpectedly, the most noticeable gel-shift was found in those **ODN 13** reactions not involving **314**. Efforts to elucidate the nature of this species involved attempted oxidation of the presumed thiol-containing peptide species. Since reactions giving rise to the observed shifting involved DTT (to reductively activate **314**), any resulting peptide adduct was expected to be in the thiol oxidation state. Thus, one means of establishing peptide connectivity involved oxidation of the gel-shifted species (after isolation and purification) to the corresponding disulfide which would further shift the mobility of the already retarded species. This was found not to be the case. Oxidation failed to afford slower adducts than originally isolated. More surprising was that treatment

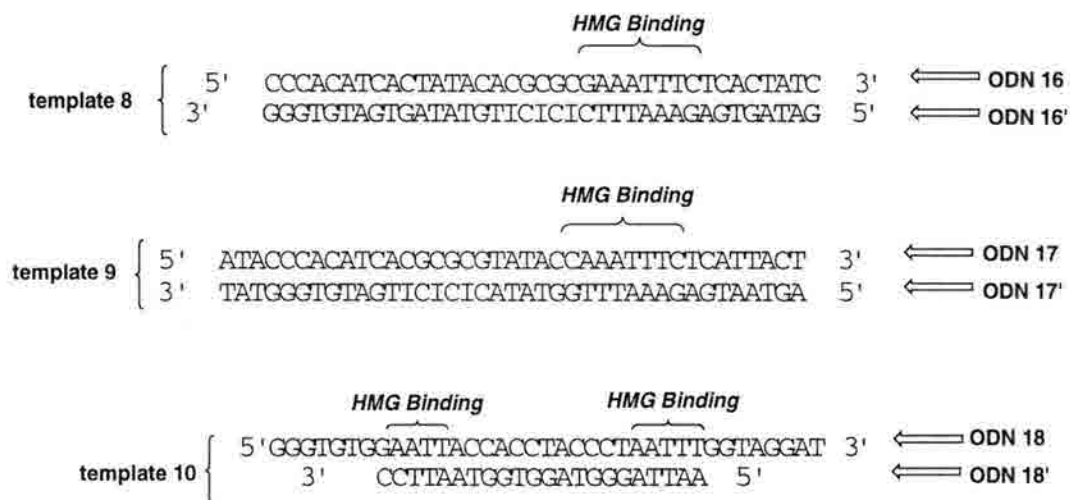
of the gel-shifted material with 100 mM DTT following attempted oxidation yielded conversion of slow mobility material to what appeared (based on electrophoretic mobility) to be monoalkylated **ODN 13**. This suggested that what was isolated, was in fact a disulfide peptide dimer bound to the self-complementary DNA. Dimerization of DNA-binding peptides results in substantial increases in binding affinity (approaching the square of the monomeric binding affinity).<sup>93</sup> As such, dimerization of **375a** would potentially afford a very tightly bound complex which could explain the retarded mobilities observed.

Attempts to elucidate the nature of this slow mobility band involved the reaction of **ODN 13** with **375a** in the absence of DTT. Surprisingly, the absence of DTT did not enhance the band shift (*via* facilitation of the dimerization event), but instead caused severe streaking of the sample and considerable loss in resolution. DNase I and Fe(II)-EDTA footprinting reactions of the gel-shifted material (before and after gel purification) revealed no regions of peptide-dependent DNA protection. Additionally, the gel-shifted control lanes completely lacked slow mobility material thus suggesting that the complex isolated had undergone substantial decomposition prior to footprinting. Alternatively, the complex isolated was due not to a specific binding event, but rather the simple electrostatic interactions between the cationic lysine and arginine residues of the peptide with the anionic phosphate backbone of the ODN. The known predilection of self-complementary oligos for retention of the duplexed state upon DPAGE, coupled with the described peptide-associated problems ultimately led to the examination of other potential DNA substrates.

### **3.2.3. Reactions of non-self-complementary DNA substrates with 375 a/b.**

In addition to the peptide-associated difficulties with **ODNs 13-15** we had observed that self-complementary ODNs were much more difficult to denature prior to electrophoresis and that this often led to artifactual band patterns. Efforts to avoid these problems entailed the synthesis of **ODNs 16-18** and their respective complements. As

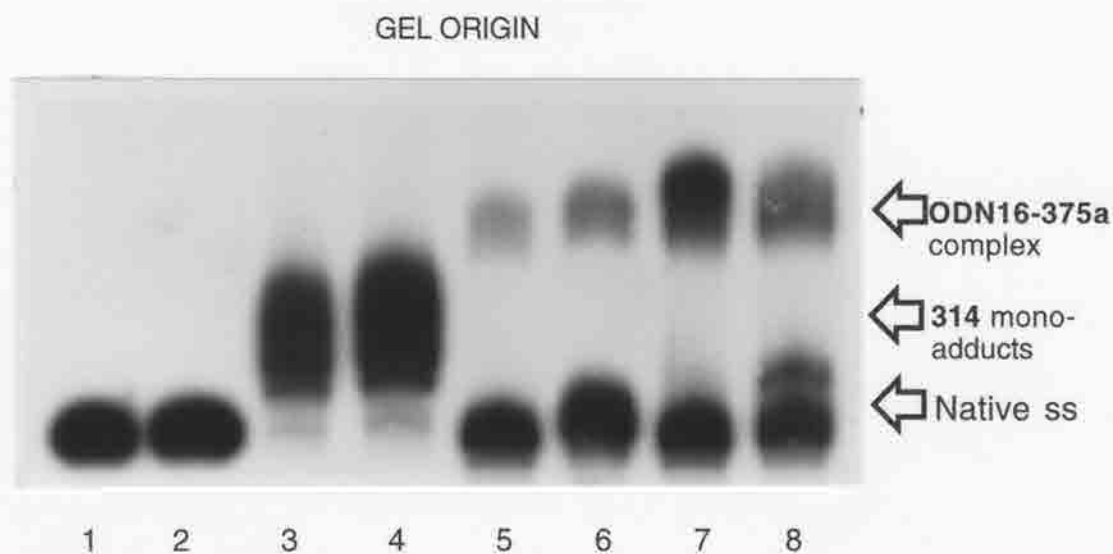
with previous substrates, these duplexes lacked the interstrand cross-linkable 5'-CG-3' due to incorporation of inosine on the complementary strands. Runs of 5'-CG-3' were placed immediately next to (**ODN 16**) and six base pairs upstream (**ODN 17**) of the 5'-AATT-3' or 5'-AAATTT-3 HMG recognition sequences. Alternatively, **ODN 18** placed the HMG domain next to single-stranded regions of dG rich runs since such regions had proven themselves effective monoalkylation sites for reductively activated **314** (Fig. 3-6)



Reactions of **templates 8-10** with **375a** afforded gel-shifted materials similar in mobility to those seen with **ODN 13**. Formation of these complexes was not dependent upon **314** or DTT although **template 8** gave rise to a second more slowly moving band which was present only in drug-containing reactions. Masking of the drug-dependent complexes (potentially with all three of the new templates) by this non-drug-dependent material facilitated identification of the contacts/functionalities responsible for the undesired bands observed.

**Template 8** appeared to be the most promising substrate (based on the second slow mobility band seen in drug-containing reactions). We therefore opted to study this duplex's interaction with both **375a** and **375b** in order to identify and delete the undesired protein-DNA interactions. Generation of gel-retarded material upon reaction of **template**

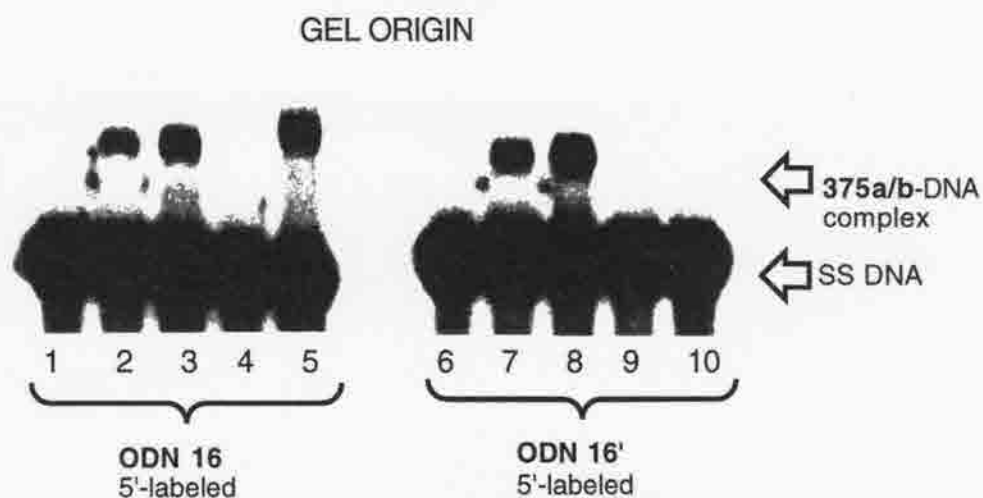
**8** with cysteinylated HMG **375a** (both in the presence and absence of reductively activated **314**) was probed *via* reaction of purified gel-shifted bands with DTT. This was intended to support or refute the possibility of peptide dimerization (*via* disulfide formation) leading to the undesired gel-shift. As shown in Figure 3-10, neither retarded band showed reductively mediated DNA strand release suggesting that disulfide formation was not responsible for the retarded mobility. However, a high degree of decomposition was observed in both control and DTT lanes. Significantly, decomposition of the **375a**-ODN **16** complex returned native single-stranded DNA and did not result in detectable strand



**Figure 3-10.** Reactions of ODN **16**-**375a** complex (following purification) reactions with DTT. **Lane 1** is standard 5' labeled ODN **16** annealed to its complementary unlabeled strand ODN **16'**. **Lane 2** 100mM DTT control. **Lane 3** is ODN **16** monoadducts formed upon reaction with **314** +DTT. **Lane 4** is ODN **16**-**314** monoadducts reacted with 100mM DTT. **Lane 5** is ODN **16** -**375a**. **Lane 6** is gel-shifted band reacted with 100 mM DTT. **Lane 7** is gel shifted band isolated from reaction of ODN **16** with 5mM **375a** + DTT + FR-66979. **Lane 8** is ODN **16** -**375a** isolated from reaction of ODN **16** with 5mM **375a** + DTT + FR-66979 followed by subsequent reaction with 100 mM DTT.

scission (hydrolytic or radical-induced). The bands isolated from reactions containing **314** revealed similar decomposition characteristics to the shifted material from those peptide reactions not containing drug. This supported the idea that the observed gel shifts in **314** reactions was due not to a drug-mediated cross-link but rather, the binding of monoalkylated ODN **16** by **375a**. Alternatively, drug-mediated peptide-DNA cross-

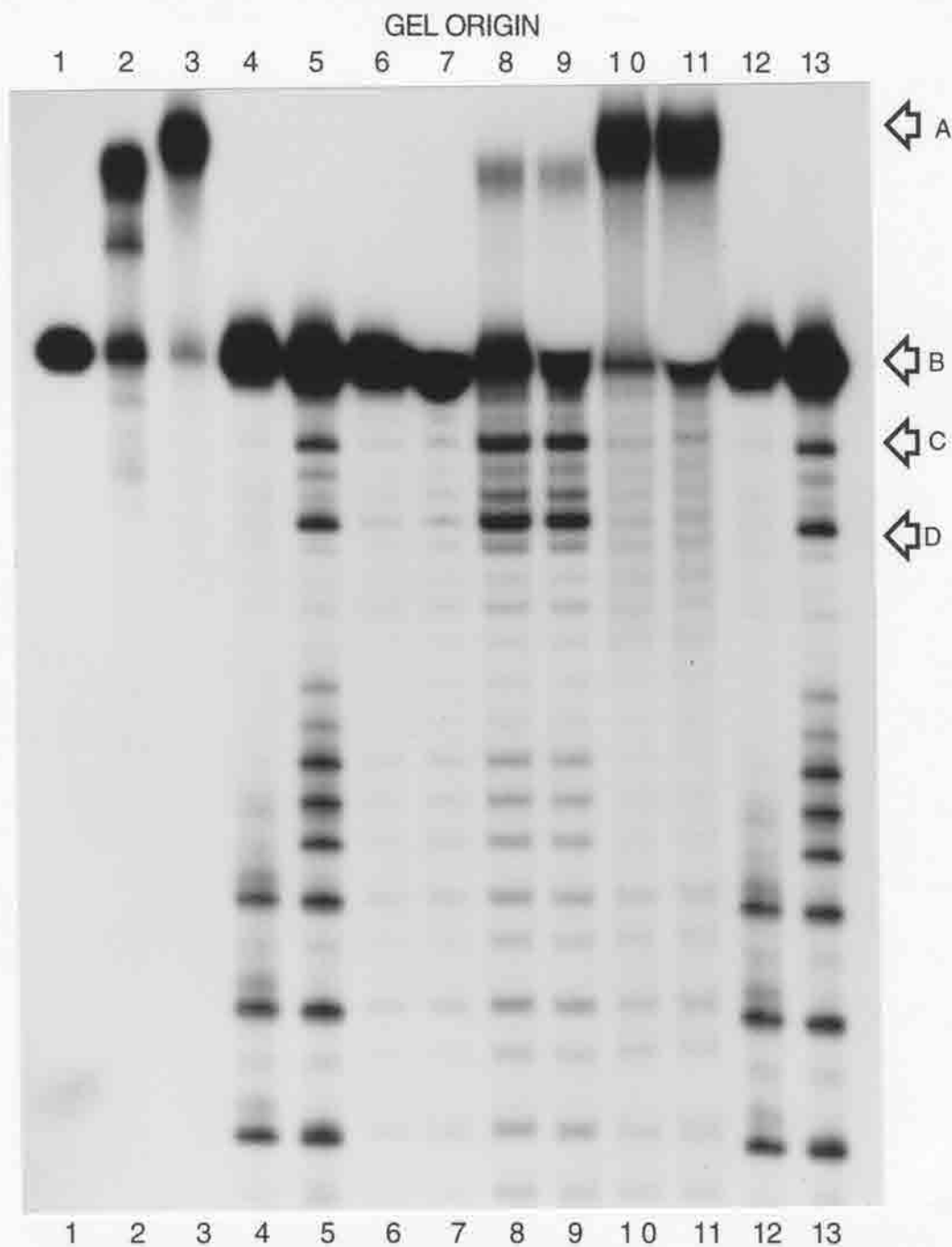
linking was masked by the undesired complex. Similar experiments using crude peptide-DNA reactions gave the same result. Extensive efforts to ensure sample denaturation (heating in 10M urea at 90°C, 5 min.) failed to effect disappearance of the slow mobility band. Retention of this complex suggested that the adduct of interest was not the result of non-covalent associations, but resulted rather, from a DNA-peptide covalency. This was supported not only by the inability to abrogate its presence *via* denaturation, but also was substantiated by the adduct's ability to at least partially withstand isolation and reanalysis. Ligand exchange reactions wherein the **375a**-ODN **16** (5'-<sup>32</sup>P-labeled) complex (formed in the absence of **314**) was allowed to incubate with increasing amounts of unlabeled **template 8** showed no loss of gel-shifted radiolabeled material even in the presence of a >100 fold molar excess of unlabeled competitor DNA. The inability of the radiolabeled DNA to be exchanged with unlabeled material further substantiated the belief that the complex of interest was due to actual covalent attachment of the cysteinylated peptide to ODN **16**.



**Figure 3-11.** Reactions of BD peptides **375a** and **375b** with differentially end-labeled **template 8**. Lane 1; **template 8** control 5' labeled on ODN **16**. Lanes 2,3; 5'-ODN **16** labeled **template 8** reacted with 0.5, 5 mM **375a** respectively. Lanes 4,5; same as lanes 2 & 3 except **template 8** was reacted with **375b**. Lane 6; **template 8** control 5'-end-labeled on ODN **16'**. Lanes 7,8; **template 8** reacted with 0.5, 5 mM **375a** respectively. Lanes 9,10; **template 8** reacted with 0.5, 5 mM **375b** respectively.

Differential radiolabeling of each **template 8** strand revealed that **375a** attachment could occur *via* either strand of the duplex (Fig. 3-11). Conversely, binding of **375b** was relegated only to **ODN 16** and was negligible at concentrations 10 fold more dilute than those which allowed **375a** to readily bind **ODN 16**. Interestingly, the adduct obtained upon reaction of **375b** with **template 8** proved to be much more stable upon isolation and re-analysis than did the thiol-containing peptide. This suggested that the cysteine of **375a** played a large role in the preferential binding over that of **375b** and that it might be involved in the proposed covalency of **375a** to **ODN 16**. However, the mutual binding of either peptide to **ODN 16** suggested that some substitution pattern common to both peptides was responsible for the observed gel-shifts.

A final round of experiments designed to detect potential base-labile lesions specific to each peptide-DNA cross-link obtained with **375a** and **375b** was performed. Each complex of **375a** and **375b** shifted **template 8** was isolated (5'-<sup>32</sup>P-labeled on both **ODN 16** and **ODN 16'**) and subjected to Maxam-Gilbert piperidine digestion conditions (Figure 3-12). To establish that cleavage was selective for 5'-labeled material to which each peptide was bound, piperidine digestions were performed on each radiolabeled complex in the presence and absence of unlabeled competitor DNA. Examination of piperidine control lanes 6 (without competitor) and 7 (with competitor), revealed no difference in cleavage intensities (Figure 3-12). As such, the observation that piperidine digestion of each peptide-DNA complex yielded similar cleavage patterns for reactions with and without competitor DNA did not give any further insights into the covalent nature of the adducts formed. The **375a** peptide complex resulted in markedly increased cleavage patterns over those of control DNA for both **ODN 16** 5'-labeled (Fig. 3-12) and **ODN 16'** 5'-labeled (Appendix Fig. 5-18) substrates. Interestingly, **ODN 16** cleavage due to the dansylated peptide was minimally enhanced over that of either control (lanes 6 & 7) suggesting a potentially weaker DNA association than observed with the thiolated complex. Piperidine



**Figure 3-12.-** Piperidine digestion of 375a/b complexes with 5'-labeled ODN-16 (base numbering starts at 5' end of ODN-16). **Lane 1** - standard template 8. **Lane 2-375a** complex with ODN-16; **Lane 3-375a** complex with ODN 16. **Lanes 4,12**-Maxam-Gilbert G ; **lanes 5, 13** Maxam-Gilbert G+A. **Lane 6**-piperidine control; **lane 7** -piperidine control with unlabeled competitor DNA. **Lane 8-375a-ODN 16** complex treated with piperidine; **Lane 9-375a-ODN 16** complex treated with piperidine and unlabeled competitor DNA. **Lane 10 375b-ODN 16** complex treated with piperidine; **Lane 11-375b-ODN 16** complex treated with piperidine. Annotations beside arrows denote: A) DNA-peptide complex; B) native DNA; C) base-labile lesion at adenine 35; D) base-labile lesion at adenine 32.



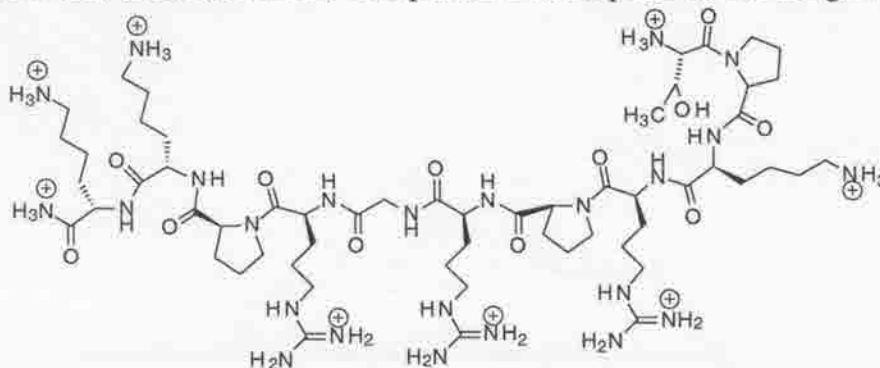
digestion of the **375b** complex also yielded a light protection pattern (as compared to control DNA in lanes 6,7) extending over the 5'-AAATTT-3' region of the bound oligo. Attempted Fe(II)-EDTA footprinting of the seemingly stable dansylated complex failed to reveal any similar protection regions.

The attenuated cleavage patterns between the **375a** and **375b** cases suggested that the cysteine of **375a** not only plays a role in formation of the DNA-protein complex, but also facilitates the piperidine-mediated strand scission of its "host" ODN. Particularly striking are the two site-specific adenine lesions (A-32, A-35) (unique to **375a**-bound material) inflicted upon **ODN 16** proximal to the HMG binding region. The exact nature/origin of these lesions was not pursued but may represent part of a novel DNA-protein interaction not previously observed with the HMG I(Y) protein-binding domain. Indeed, the ability of HMG I(Y) peptides/proteins to form covalent adducts with DNAs bearing 5'-AATT-3' has not been previously reported. The fact, however, that both N-terminally substituted BD peptides were able to form apparently covalent adducts with DNA substrates of interest suggested that substitution to the N-terminus side of the Asx hook TPK provides an efficient means of reactive agent delivery to adenines canted to the 3' side of 5'-AAATTT-3'. Although this represents an interesting finding, the masking effect of such undesired complexes warranted the synthesis of a BD peptide lacking any functionalities not necessary for DNA binding, particularly with respect to the N-terminal side of the Asx turn.

#### **3.2.4. HMG peptide-DNA cross-linking by reductively activated 314.**

The frustrating, albeit interesting, experiences involving TPK modified BD peptides **375a/b** facilitated the synthesis of **376**. This peptide was identical to the full length BD peptide originally described by Wemmer. The studies involving **375a/b** demonstrated quite clearly that a DNA-peptide complex would be easily detectable and separable from other reaction products *via* electrophoresis. As such, the lack of additional functionalities

within **376** (fluorescent chromophores, affinity matrix handles, etc.) was not anticipated to be a concern with respect to peptide-DNA complex visualization/isolation. As discussed in section 3.2.2., those cases in which the 5'-AAATTT-3' of the DNA recognition domain is flanked to the 5' side by a **314** monoalkylated dG were expected to most readily react with an arginine side chain of PRGRP. This provided the impetus for the design of the non-self-

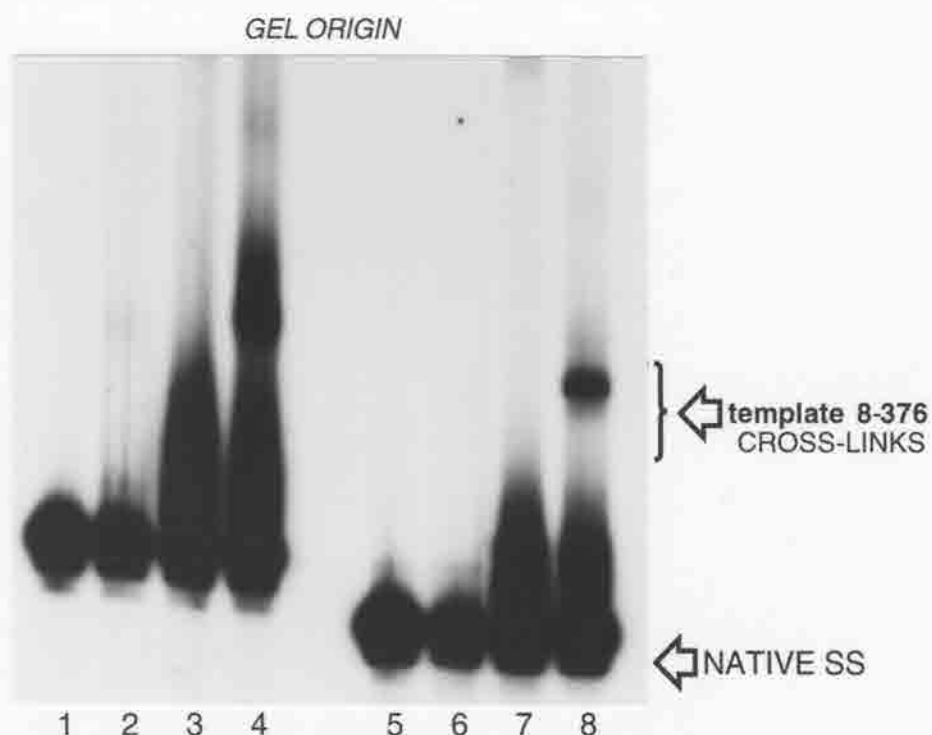


376

complementary **template 8** and was the motivation for using **template 8** in the initial studies with **376**. Efforts involving the simultaneous reaction of FR-66979, DTT, **376** and **template 8** failed. This was not surprising in light of earlier efforts with **375a** and **375b** in which simultaneous additions of drug, thiol, peptide and DNA afforded no peptide cross-link, but also demonstrated radically decreased yields of DNA monoalkylation. This was attributed to one of two phenomena; a) either the peptide shielded the DNA from alkylation *via* tight binding; or b) the peptide underwent alkylation with comparable or better efficiency than the DNA substrate. Given the salt dependence of BD peptide binding to 5'-AAATTT-3', the latter proposal was favored. Significantly, the formation of non-drug-dependent peptide-DNA complexes was not apparent in any reactions of **template 8** with **376**.

An alternative approach aimed at assessing the ability of **314** to covalently cross-link **376** to **template 8** involved a stepwise strategy. It was believed that initial alkylation of **template 8** followed by rigorous purification and desalting would give rise to a species capable of peptide binding. This approach was successful.

Monoalkylation of **template 8** followed by repeated EtOH precipitation and Sephadex G-50 size exclusion chromatography yielded the mixture of native and alkylated substrate in good yields ( $\geq 90\%$ ). Of the radiolabeled material isolated, 20-40% had suffered monoalkylation. Dilution of the alkylated substrate to a concentration of 20 pmol/ $\mu$ l (20  $\mu$ M in duplex) in 10 mM Tris (pH=8.0) yielded the desired DNA stock solution. Equal volumes of this stock solution and 10  $\mu$ M, 100 $\mu$ M, 1 mM, and 10 mM solutions of **376** in DDH<sub>2</sub>O were incubated at 37°C for 12 h. in glass-lined vials. Despite the use of glass-lined vials for the peptide reactions, the vast majority of material was unrecoverable for reactions in which the overall concentration of peptide exceeded 50 $\mu$ M.<sup>94</sup>



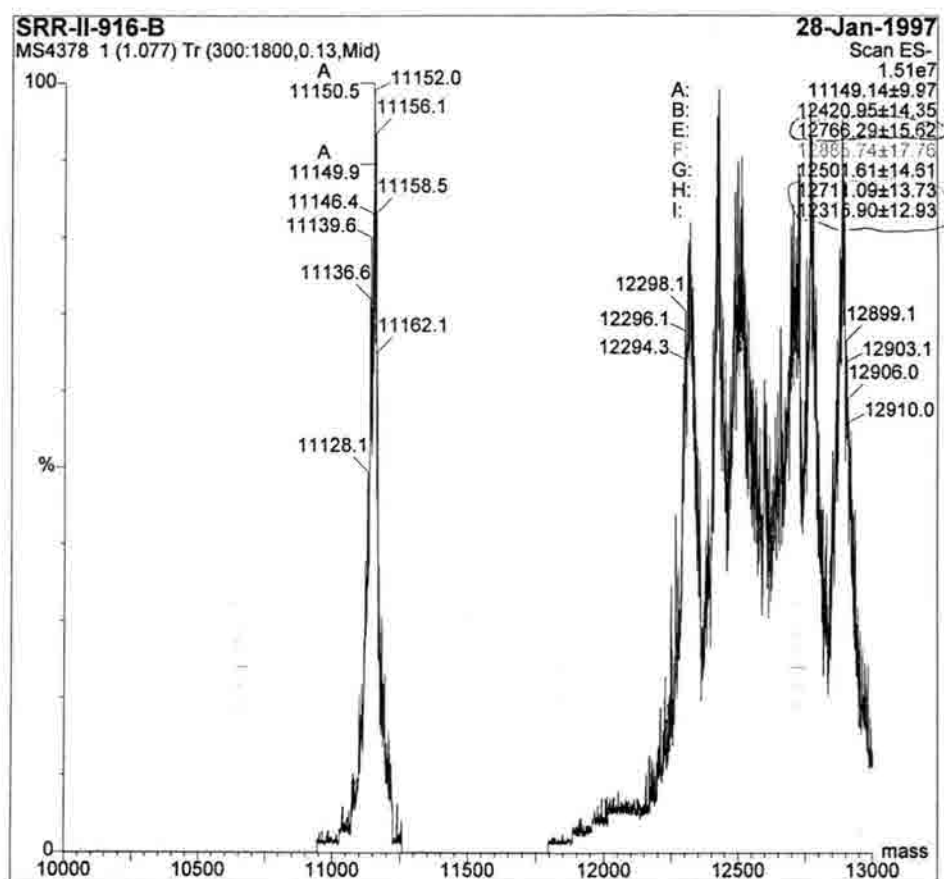
**Figure 3-13.** DNA-protein cross-linking by reductively activated **314**. All reactions were incubated 37°C in 5 mM Tris (pH = 8.0) for 12 hours. All DNAs were desalted by sephadex G-50 chromatography and subsequent EtOH precipitations prior to peptide addition. **Lanes 1-4** : reactions of **template 8** (5'-end-labeled **ODN-16'**). **Lanes 5-8**: reactions of **template 8** (5'-end-labeled **ODN-16**). **Lanes 1 & 5**- **template 8** standards. **Lanes 2 & 6**- 50 $\mu$ M HMG peptide + DNA controls. **Lanes 3 & 7**; DNA + FR-66979/DTT controls. **Lanes 4 & 8**; FR-66979 alkylated **template 8** + 50  $\mu$ M HMG peptide.

Optimal amounts of gel-retarded, drug-dependent material were obtained in reactions wherein the overall peptide concentration was 50  $\mu$ M. From these reactions it appears that a ratio of **314** alkylated DNA:**376** of 1:5 was optimal for formation of the observed gel-shift. Differential radiolabeling of either strand of **template 8** revealed that cross-link formation was not relegated to **ODN 16** as originally proposed (Figure 3-13). That residues other than the anticipated dG immediately to the 5' side of 5'-AAATTT-3' underwent drug-mediated DNA-peptide cross-linking represented a surprising, but important result. The incorporation of inosine (in **ODN 16'**) across from the 5'-CG-3' run proximal to 5'-AAATTT-3' of **ODN 16** was anticipated to facilitate identification of the HMG-DNA cross-link by abrogating interstrand cross-linking and allowing the formation of the peptide-DNA cross-link. As such, the argument that the **template 8** scenario was not representative of a naturally occurring situation was certainly valid and difficult to refute. Drug-dependent peptide cross-linking to both strands of **template 8** thus demonstrates the generality of this motif.

To confirm the covalency of the adduct formed, ligand/DNA-exchange reactions were performed. The purified radiolabeled complexes of **376** with **ODN 16** and **ODN 16'** were incubated with unlabeled competitor **template 8**. Incubation of each drug-mediated complex with increasing amounts of unlabeled competitor DNA **template 8** at 37°C for 24 h. failed to exchange **376** from either radiolabeled strand. Complete retention of each radiolabeled complex was observed with a >100 fold molar excess of unlabeled competitor **template 8** (Appendix Figure 5-20). This supported the belief that the peptide-DNA complexes formed were covalent in nature and not due to simple non covalent interactions. In contrast to the previously described **375a-ODN 16** adduct, the drug-dependent complexes showed only minimal decomposition to single-stranded material during the course of the 24 h. incubation.

Verification of the ligand-exchange result was sought *via* negative ion electrospray mass spectral analysis of the 20% DPAGE purified complex. Numerous high mass signals (much higher than for either DNA strand alone or their peptide-bound congeners) were obtained in the  $m/e=12,700\text{--}12,950\text{Da}$  range. The calculated mass of an **ODN 16-drug-376** conjugate is 12,721.3Da assuming that the covalencies involved are relegated to the mitosene 1 and 10 positions. Additionally, this mass takes into account that the peptidic portion (corresponding to the isotopically averaged species) of a possible drug-mediated conjugate would be neutral and not positively charged during the course of MS analysis. Were the peptide to be charged (very likely due to the  $\text{NH}_4\text{OAc}$  work-up procedure employed for oligo mass spectral analysis) it is proposed that the lysines, arginines, the free N-terminus and the C-terminal amide could all be protonated thus affording a +8 charge on the peptide. This would result in an increase in mass of 8 units thereby giving an expected mass of 12,729.3Da. More importantly, protonation of any one of these residues would enable the drug-mediated peptide-DNA cross-link to ion pair with acetate (an interaction not accessible to only native DNA). Such an interaction would increase the observed mass of the DNA-peptide cross-link by a factor of 59 per negatively charged OAc counterion. As such, potential masses of interest might be in the order of 12,781.3Da (one positive charge on **376** along with one OAc counterion) 12,841.3Da (two positive charges both ion paired with OAc), 12,901.3Da (three positive charges all ion paired with OAc.) and so on. In line with this rationale, it is interesting to note that **376** possesses 3 arginine groups each of which bears the extremely basic guanidine group. Protonation of each guanidine (preferential to the other amine functionalities within **376**), followed by OAc ion-pairing would be expected to afford a drug-mediated DNA-peptide conjugate of mass 12,901.3Da. Indeed the negative ion electrospray mass spectral analysis (Figure 3-14 shown below) of the suspected conjugate afforded intense signals corresponding to masses of 12,899.1, 12,903.1, 12,906.0, and 12910.0Da all of which are well within the typical standard deviation of  $\pm 10$  mass units. Although this is highly speculative, the results of the

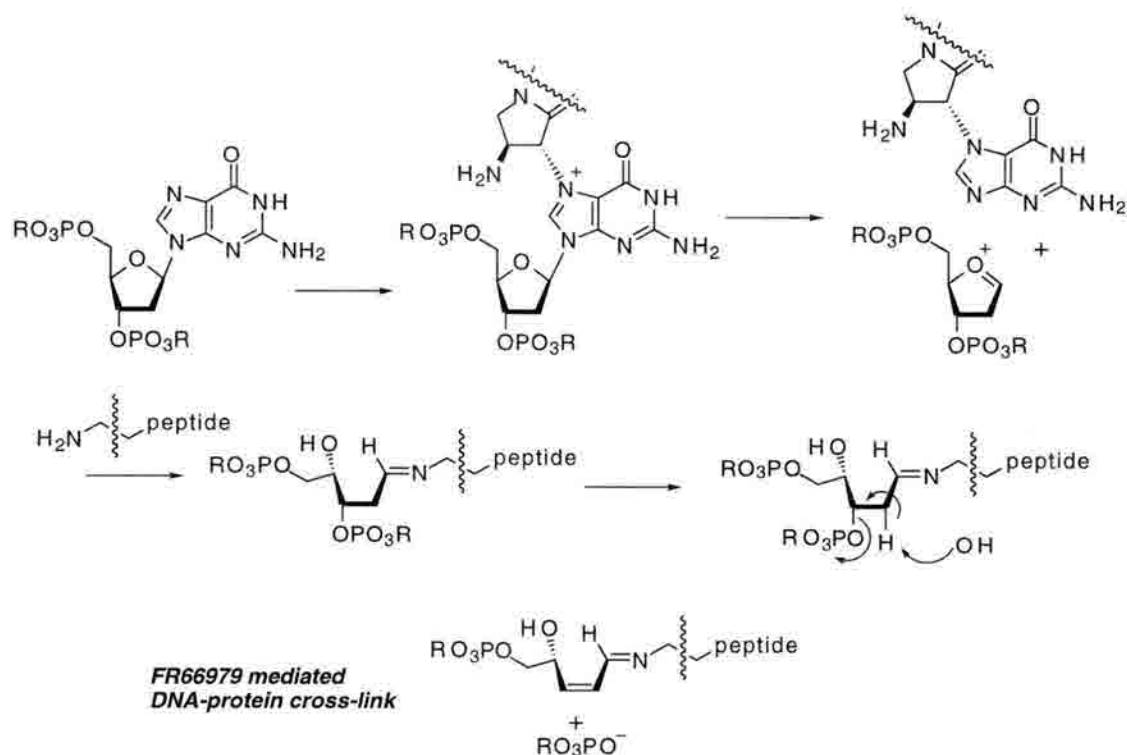
ligand exchange and mass spectral analysis suggest, that the complex formed between **376** and ODNs **16** and **16'** is in fact covalent and not due simply to enhanced non-covalent binding of the BD peptide to FR-66979 alkylated DNA.



**Figure 3-14.** Negative ion electrospray mass spectral analysis of FR-66979-mediated ODN **16-376** cross-link. The signals to the left side of spectrum (mass range 11,128.1-11,162.1Da) correspond to the parent mass for unmodified ODN **16** whereas the multiple signals in the range 12,294.3-12,910.0Da correspond predominantly to unknown adducts. The signals from 12,899.1-12,910.0Da are proposed to correspond to the +3 charged peptide-DNA adduct with each cationic species (from guanidine protonation) involved in ion-pairing with OAc.

One concern with respect to mass spectral analysis of the peptide-DNA involved the generation of abasic sites within the substrate DNA thus altering the expected mass (and thus giving rise to the unidentifiable high mass species in Figure 3-14). Additionally, the ability of an N<sup>7</sup> alkylated dG residue to undergo depurination and subsequent imine formation with a lysine on **376** (Figure 3-15) was an important consideration.

Depurination has been shown to very efficiently induce DNA-histone cross-links *via* lysine addition to the resulting aldehyde of the abasic site.<sup>96</sup> The ability of MC to induce abasic sites (section 1.5.5.) thus led to great concern regarding the nature of the FR-66979 mediated cross-links. To probe this possible means of cross-linking and to determine the minor or major groove nature of the observed complex, piperidine digestion of the complexes formed between **376** and both strands of **template 8** was performed.



**Figure 3-15.** Proposed depurination route to DNA-peptide cross-linking by reductively activated **314**

Isolation of both **ODN 16-376** and **ODN 16'-376** complexes was followed by 3'-end-labeling of each single-stranded species. Digestion of each complex in 1M piperidine at 90 °C was expected to reveal any abasic lesions. Examination of the resulting cleavage patterns (Appendix Figure 5-20) revealed that peptide-bound DNAs did not undergo significant strand cutting over that seen in the piperidine control reactions. This suggests that the peptide-DNA lesion formed does not go through a depurination pathway



since significant DNA cutting would have been observed at such a site. More importantly, this substantiates the anticipated minor groove nature of the drug-induced DNA-peptide cross-link and indicates that mass spectral analysis of these adducts is not likely to be complicated by sites of drug-induced depurination.

### **3.3 Conclusion**

The only reported instance of HMG protein-DNA cross-linking to date involved the reaction of the B-domain of HMG 1 with cisplatin modified DNA. HMG 1 binds *cis*-platin modified DNA 100 times greater normal DNA.<sup>73b</sup> Exploiting this high affinity ( $K_b = 4 \times 10^7 M$ ), Lippard and Kane showed that photolysis of the drug-DNA-protein complex afforded a DNA-protein cross-link which was reversible upon ligand exchange with NaCN or thiols.<sup>97</sup> Photosubstitution of one of the ligands on Pt(II) (likely to be a purine involved in either inter- or intrastrand cross-linking) with Lys-6 of the HMG 1 B domain is the proposed means by which protein attachment occurs.

Detailed herein is a synthetic DNA substrate, which upon monoalkylation by reductively activated **314**, readily forms a DNA-peptide cross-link. This represents the first documented case of mitosene-based cross-linking of a DNA-binding peptide to a DNA substrate bearing the peptide recognition sequence. Unlike the *cis*-platin case, little mechanistic information pertaining to FR-66979 mediated DNA-protein cross-linking has been generated. The cross-link fails to undergo DNA exchange in the presence of competitor DNA and is resistant to denaturation at 90°C for 3 minutes prior to denaturing gel electrophoresis. Negative ion electrospray mass spectral analysis reveals that a number of signals are obtained with some masses possibly corresponding to the tri-acetate salt of the FR-66979-mediated DNA-peptide cross-link (wherein each guanidinium of **376** is ion-paired with OAc). As such, the proposed covalency of the mitosene-based cross-link has been supported. Additionally, the cross-link does not appear to operate *via* a depurination mechanism as piperidine digestion failed to render any base-labile lesions within the cross-

linked DNA sequence. The relative importance of this finding is yet to be determined. However, given the preponderance of HMG-I(Y) proteins in rapidly proliferating undifferentiated cells, this may offer additional insights into how the mitomycins and related compounds exert biological activities which are selective for cancerous cell lines.

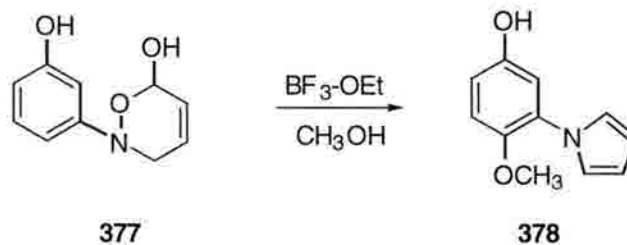
## **Chapters 2 & 3 References**

1. (a) *Structure of FR-900482, a Novel Antitumor Antibiotic from a Streptomyces*, Uchida, I.; Takase, S.; Kayakiri, H.; Kiyoto, S.; Hashimoto, M.; Tada, T.; Koda, S.; Morimoto, Y., *J. Am. Chem. Soc.* (1987) **109**, 4108; (b) *A New Antitumor Antibiotic, FR-900482, I. Taxonomic Studies on the Producing Strain: A New Species of the Genus Streptomyces*, Iwami, M.; Kiyoto, S.; Terano, H.; Kohsaka, M.; Aoki, H.; Imanaka, H., *J. Antibiotics* (1987) **40**, 589. (c) *A New Antitumor Antibiotic, FR-900482, II. Production, Isolation, Characterization and Biological Activity*, Kiyoto, S.; Shibata, T.; Yamashita, M.; Komori, T.; Okuhara, M.; Terano, H.; Kohsaka, M.; Aoki, H.; Imanaka, H., *J. Antibiotics* (1987) **40**, 594; (d) *Precursors in the Biosynthesis of FR-900482, A Novel Antitumor Antibiotic Produced by Streptomyces Sandaensis*, Fujita, T.; Takase, S.; Otsuka, T.; Terano, H.; Kohsaka, M., *J. Antibiotics* (1988) **41**, 392.
2. (a) *A New Antitumor Antibiotic, FR-900482, III. Antitumor Activity in Transplantable Experimental Tumors*, Shimomura, K.; Hirai, O.; Mizota, T.; Matsumoto, S.; Mori, J.; Shibayama, F.; Kikuchi, H., *J. Antibiotics* (1987) **40**, 600; (b) *A New Antitumor Antibiotic, FR-900482, IV. Hematological Toxicity in Mice*, Hirai, O.; Shimomura, K.; Mizota, T.; Matsumoto, S.; Mori, J.; Kikuchi, H., *J. Antibiotics* (1987) **40**, 607; (c) *Antitumor Activity and Hematotoxicity of a New, Substituted Dihydrobenzoxazine, FK973, in Mice*, Shimomura, K.; Manda, T.; Mukumoto, S.; Masuda, K.; Nakamura, T.; Mizota, T.; Matsumoto, S.; Nishigaki, F.; Oku, T.; More, J.; Shibayama, F., *Cancer Res.* (1988) **48**, 1116; d) *A New Antitumor Antibiotic, FR-900482: V. Interstrand DNA-DNA Cross-Links in L1210 Cells*, Masuda, K.; Makamura, T.; Shimomura, K.; Shibata, T.; Terano, H.; Kohsaka, M., *J. Antibiotics* (1988) **41**, 1497;
3. (a) *Interstrand DNA-DNA and DNA-Protein Cross-Links by a New Antitumor Antibiotic, FK973, in L1210 Cells*, Masuda, K.; Nakamura, T.; Mizota, T.; Mori, J.; Shimomura, K., *Cancer Res.* (1988) **48**, 5172; (b) *Effect of FK973, a New Antitumor Antibiotic, on the Cell Cycle of L1210 Cells In Vitro*, Nakamura, T.; Masada, K.; Matsumoto, S.; Oku, T.; Manda, T.; Mori, J.; Shimomura, K., *Japan J. Pharmacol.* (1989) **49**, 317.
4. (a) *FR66979 Requires Reductive Activation to Cross-Link DNA Efficiently*, Huang, H.; Rajski S.R.; Williams, R.M.; Hopkins, P.B., *Tetrahedron Lett.* (1994) **35**, 9669; b) *DNA-DNA Interstrand Cross-Linking by FR66979 and FR-900482: Requirement of Metal Ions During Reductive Activation*, Paz, M.M.; Hopkins, P.B., *Tetrahedron Lett.* (1997) **38**, 343.
5. *Generation of Reactive Oxygen Radicals through Bioactivation of Mitomycin Antibiotics*, Sartorelli, A.C.; Pristos, C.A., *Cancer Research* (1986) **46**, 3528.
6. For an excellent review pertinent to mechanisms of oxidative DNA strand cleavage due to Fenton/Haber Weiss redox cycling see: (a) *Mechanisms of Bleomycin-induced DNA Degradation*, Stubbe, J.; Kozarich, J.W., *Chem. Rev.* (1987) **87**, 1107; (b) *Oxidative Degradation of Nucleic Acids*, Knorre, D.G.; Fedorova, O.S.; Frolova, E.I., *Uspekhi Khimii* (1993) **62**, 70; (c) *The chemistry of single-stranded 4'-DNA radicals: influence of the radical precursor on anaerobic and aerobic strand cleavage*, Giese, B.; Beyrich-Graf, X.; Erdmann, P.; Petretta, M.; Schwitter, U., *Chemistry and Biology* (1995) **2**, 367.

7. (a) *Nucleotide Derivatives of 2,7-Diaminomitosene*, Iyengar, B.S.; Door, R.T.; Remers, W.A.; Kowal, C.D., *J. Med. Chem.* (1988) **31**, 1579; (b) *Conformations of Complexes between Mitomycins and Decanucleotides. 3. Sequence Specificity, Binding at C-10, and Mitomycin Analogues*, Remers, W.A.; Rao, S.N.; Wunz, T.P.; Kollman, P.A., *J. Med. Chem.* (1988) **31**, 1612; (c) *New 2- Substituted Indoloquinone Mitomycin Analogues*, Iyengar, B.S.; Remers, W.A.; Catino, J.J., *J. Med. Chem.* (1989) **32**, 1866; (d) *Synthesis, Mechanism of Action, and Biological Evaluation of Mitosenes*, Orlemans, E.O.; Verboom, W.; Scheltinga, M.W.; Reinhoudt, D.N.; Lelieveld, P.; Fiebig, H.H.; Winterhalter, B.R.; Double, J.A.; Bibby, M.C., *J. Med. Chem.* (1989) **32**, 1612; (e) *Full Structure of a Mitomycin C Dinucleoside Phosphate Adduct. Use of Differential FT-IR Spectroscopy in Microscale Structural Studies*, Tomasz, M.; Lipman, R.; Snyder, J.K.; Nakanishi, K., *J. Am. Chem. Soc.* (1983) **105**, 2059; (f) *Reassignment of the Guanine-Binding Mode of Reduced Mitomycin C*, Tomasz, M.; Lipman, R.; Verdine, G.; Nakanishi, K., *Biochemistry* (1986) **25**, 4337; (g) *Unusual CIS Stereoselectivity in an Aziridine Cleavage Reaction of Mitomycin C*, Verdine, G.L.; McGuinness, B.F.; Nakanishi, K.; Tomasz, M., *Heterocycles* (1987) **25**, 577; (h) *Synthesis of Guanine Derivatives Substituted in the 06-Position by Mitomycin C*, McGuinness, B.; Nakanishi, K.; Lipman, R.; Tomasz, M., *Tetrahedron Lett.* (1988) **29**, 4673; (i) *Structures of Modified Nucleotides Isolated From Calf Thymus DNA Alkylated with Reductively Activated Mitomycin C*, Hashimoto, Y.; Shudo, K.; Okamoto, T., *Tetrahedron Lett.* (1982) **23**, 677; (j) *Covalent Binding of Mitomycin C to Nucleosides Under Reductive Conditions*, Zein, N.; Kohn, H., *J. Am. Chem. Soc.* (1987) **109**, 1576; (k) *Electrophilic and Nucleophilic Character of the Carbon 10 Methylene Group in Mitosenes Revealed*, Zein, N.; Kohn, H., *J. Am. Chem. Soc.* (1986) **108**, 296; (l) *Modeling of the Electrophilic Activation of Mitomycins: Chemical Evidence for the Intermediacy of a Mitosene Semiquinone as the Active Electrophile*, Egbertson, M.; Danishefsky, S.J., *J. Am. Chem. Soc.* (1987) **109**, 2204; (m) *Observations on the Activation of Mitomycin C. Requirements for C-10 Functionalization*, Kohn, H.; Hong, Y.P., *J. Am. Chem. Soc.* (1990) **112**, 4596 (n) *Determination of the DNA Cross-Linking Sequence Specificity of Reductively Activated Mitomycin C at Single-Nucleotide Resolution-Deoxyguanosine Residues at CpG are Cross-Linked Preferentially*, Millard, J.T.; Weidner, M.F.; Raucher, S.; Hopkins, P.B., *J. Am. Chem. Soc.* (1990) **112**, 3637.
8. For recent total syntheses see (a) *Total Synthesis of (+)-FR-900482*, Fukuyama, T.; Xu, L.; Goto, S., *J. Am. Chem. Soc.* (1992) **114**, 383; (b) *Total Synthesis of (+)-FR-900482*, Schkeryantz, J.M.; Danishefsky, S.J., *J. Am. Chem. Soc.* (1995) **117**, 4722.
9. For additional synthetic studies, see (a) *Enantiospecific Synthesis of an Aziridinobenzoazocinone, an Advanced Intermediate Containing the Core Nucleus of FR900482 and FK973*, Jones, R.J.; Rapoport, H., *J. Org. Chem.* (1990) **55**, 1144; (b) *Novel Photochemical Route to the Mitomycin and FR-900482 Series*, McClure, K.F.; Benbow, J.W.; Danishefsky, S.J., *J. Am. Chem. Soc.* (1991) **113**, 8185; (c) *Cycloaddition Reactions of Aromatic Nitroso Compounds with Oxygenated Dienes. An Approach to the Synthesis of the FR-900482 Family of Antibiotics*, McClure, K.F.; Danishefsky, S.J., *J. Org. Chem.* (1991) **56**, 850; (d) *A New Approach to the Bicyclic Hydroxylamine Hemiketal Ring System of Antitumour-Antibiotic FR900482 Via Oxidative Ring Expansion of a Tetrahydropyrrolo[1,2-a]Indole*, Dmitrienko, G.I.; Dehnart, D.; Mithani, S.; Prasad, G.K.B.; Taylor, N.J., *Tetrahedron Lett.* (1992) **33**, 5705; (e)

*Intramolecular Cycloaddition Reactions of Dienyl Nitroso Compounds: Application to the Synthesis of Mitomycin K*, Benbow, J.W.; McClure, K.F.; Danishefsky, S.J., *J. Am. Chem. Soc.* (1993) **115**, 12305; (f) *A Novel Heck Arylation Reaction: Rapid Access to Congeners of FR 900482*, McClure, K.F.; Danishefsky, S.J., *J. Am. Chem. Soc.* (1993) **115**, 6094; (g) *A Novel Approach to FR-900482 Via Ring Forming Metathesis*, Martin, S.F.; Wagman, A.S., *Tetrahedron Lett.* (1995) **36**, 1169; (h) *Catalytic Ring-Closing Metathesis of Dienes: Application to the Synthesis of Eight-Membered Rings*, Miller, S.J.; Kim, S.H.; Chen, Z.R.; Grubbs, R.H., *J. Am. Chem. Soc.* (1995) **117**, 2108; (i) *Synthetic Approaches Toward FR-900482. I. Stereoselective Synthesis of a Pentacyclic Model Compound*, Fukuyama, T.; Goto, S. *Tetrahedron Lett.* (1989) **30**, 6491; (j) *Cycloaddition Reactions of Aromatic Nitroso Compounds with Oxygenated Dienes. An Approach to the Synthesis of the FR-900482 Family of Antibiotics*, McClure, K.F.; Danishefsky, S.J., *J. Org. Chem.* (1991) **56**, 850; (k) *Synthetic Studies of FR900482: Promising Method to Construct the Bicyclic Hydroxylamine Hemi-Ketal Ring System*, Yasuda, N.; Williams, R.M., *Tetrahedron Lett.* (1989) **30**, 3397 and disclosed patent entitled "Tricyclo Compounds, a Process for the Preparation Thereof, and Pharmaceutical Compositions Containing the Same," Nobuyoshi Yasuda and Robert M. Williams, jointly with Colorado State University and Fujisawa Pharmaceutical Co.

10. Additional mechanistic studies published to date : (a) *DNA Cross-Linking Studies on FR900482: Observations on the Mode of Activation*, Williams, R.M.; Rajski, S.R., *Tetrahedron Lett.* (1992) **33**, 2929; (b) *Determination of DNA Cross-Linking Sequence Specificity of FR66979: Observations on the Mode of Action of the FR900482 Class of Anti-tumor Compounds*, Williams, R.M.; Rajski, S.R., *Tetrahedron Lett.* (1993) **34**, 7023; (c) *Covalent Structure of the DNA-DNA Interstrand Cross-Link Formed by Reductively Activated FR66979 in Synthetic DNA Duplexes*, Huang, H.; Pratum, T.K.; Hopkins, P.B., *J. Am. Chem. Soc.* (1994) **116**, 2703; (e) *DNA Interstrand Cross-Linking by Reductively Activated FR900482 and FR66979*, Woo, J.; Sigurdsson, S. Th.; Hopkins, P.B., *J. Am. Chem. Soc.* (1993) **115**, 1199.
11. *DNA Cross-Linking by Intermediates in the Mitomycin Activation Cascade*, Cinzia, C.; Egbertson, M.; Teng, S.P.; Crothers, D.M.; Danishefsky, S.J., *Biochemistry* (1989) **28**, 5665.
12. This proposal stemmed partly from the observed transformation **377** to **378**.



Additional examples of Lewis acid mediated aromatic additions involving N-O cleavage have been reported in : (a) Shimada, M.; Kikugawa, Y., *J. Chem. Soc., Chem. Commun.* (1989) 1440; (b) Hutchins, C.W.; Coates, R.M., *J. Org. Chem.* (1979) **44**, 4742.



13. *Alkaline Gel Electrophoresis of Deoxyribonucleic Acid Photoreacted with Trimethylpsoralen: Rapid and Sensitive Detection of Interstrand Cross-Links*, Cech, T.R., *Biochemistry* (1981) **20**, 1431.
14. For example: the intracellular level of glutathione in mammalian cells is in the millimolar range (0.5 mM-10 mM). See: *Glutathione*, Meister, A.; Anderson, M.E., *Ann. Rev. Biochem.* (1983) **52**, 711.
15. (a) *Generation of Superoxide Free Radical during the Autoxidation of Thiols*, Misra, H., *J. Biol. Chem.* (1974) **249**, 2151; (b) *The Iron-Catalyzed Oxidation of Dithiothreitol is a Biphasic Process: Hydrogen Peroxide is Involved in the Initiation of a Free Radical Chain of Reactions*, Netto, L.E.S.; Stadtman, E.R., *Archives of Biochemistry and Biophysics* (1996) **333**, 233.
16. (a) *Fe<sub>3</sub>O(OAc)<sub>6</sub>(Py)<sub>3</sub> Mediated Reduction of Aromatic Nitro Compounds with 2-Mercaptoethanol*, Murata, S.; Miura, M.; Nomura, M., *Chem. Lett.* (1988) 361; (b) *Reduction of Aromatic Nitro Compounds with 2-Mercaptoethanol and Oxidation of Thiophenol with Molecular Oxygen Mediated by Trinuclear Iron Acetate Complexes*, Murata, S.; Miura, M.; Nomura, M., *J. Chem. Soc. Perkin Trans. II* (1989) 617.
17. (a) *Reduction of Cyclic Compounds Having an N-O Linkage by Dihydrolipoamide-Iron (II)*, Kijima, M.; Nambu, Y.; Endo, T.; *J. Org. Chem.* (1985) **50**, 1140; (b) *Reductive Cleavage of Hydroxylamine Derivatives by Dihydrolipoic Acid-Iron(II)*, Nambu, Y.; Kijima, M.; Endo, T.; Okawara, M., *J. Org. Chem.* (1982) **47**, 3066.
18. *Structure-Reactivity Relations for Thiol-Disulfide Interchange*, Houk, J.; Whitesides, G.M., *J. Am. Chem. Soc.* (1987) **109**, 6825.
19. *Iron catalysis of the reduction of oxime-bound nickel (IV) by hydroxylamine*, Mandal, S.; Bose, R.N.; Reed, J.W.; Gould, E.S., *J. Chem. Soc. Dalton Trans.* (1996)
20. The presence of adventitious Fe<sup>3+</sup> in supplies of DDH<sub>2</sub>O had been noted by Mark E. Flanagan (C.S.U.- R.M. Williams group) in studies pertaining to quinocarcin . More recent (1997) corroboration of this theory has been noted by Eric Dodson (C.S.U.- C.M. Elliot group)
21. (a) *Oxygen radical injury in the presence of desferal, a specific iron-chelating agent*, Gupta, M.; Singal, P.K., *Biochemical Pharmacology* (1987) **36**, 3777; (b) Graf, E.; Mahoney, J.R.; Bryant, R.G.; Eaton, J.W., *J. Biol. Chem.* (1984) **259**, 3620; (c) Graf, E.; Empson, K.L.; Eaton, J.W., *J. Biol. Chem.* (1987) **262**, 11647; (d) Lesko, S.A.; Lorentzen, R.J.; Ts'o, P.O., *Biochemistry* (1980) **19**, 3023.
22. Interestingly, cyclic voltametry of both natural products yielded irreversible reduction waves. FR-900482 possessed a reduction wave at -1.7V. while FR-66979 possessed a reduction wave at -1.83 Volts.
23. *Two Aspects of DNA Polymorphism and Microheterogeneity: Molecular Electrostatic Potential and Steric Accessibility*, Pullman, B.; Lavery, R.; Pullman, A., *Eur. J. Biochem.* (1982) **124**, 229.

24. (a) *Molecular Electrostatic Potential of the Nucleic Acids*, Pullman, A.; Pullman, B., *Q. Rev. Biophys.* (1981) **14**, 289; (b) *The Molecular electrostatic potential and steric accessibility of poly (dA-dT). poly (dA-dT) in various conformations: B-DNA, D-DNA and "alternating-B" DNA*, Lavery, R.; Pullman, B.; Corbin, S., *Nucleic Acids Research* (1981) **9**, 6539.
25. *Mitomycin C: small, fast and deadly (but very selective)*, Tomasz, M., *Chemistry & Biology* (1995) **2**, 575.
26. *Sequence-Selective Alkylation and Cross-Linking Induced by Mitomycin C upon Activation by DT-Diaphorase*, Prakash A.S.; Beall, H.; Ross, D.; Gibson, N.W., *Biochemistry* (1993) **32**, 5518.
27. (a) Verdine, G.L., Ph.D. thesis. Columbia University, 1986; (b) *Alkylation Reactions of Mitomycin C at Acid pH*, Tomasz, M.; Lipman, R., *J. Am. Chem. Soc.* (1979) **101**, 6063.
28. *Hydroxyl Radical "Footprinting" : High-resolution Information About DNA-protein Contacts and Application to  $\lambda$  Repressor and Cro Protein*, Tullius, T.D.; Dombroski, B.A., *Proc. Natl. Acad. Sci. U.S.A.* (1986) **83**, 5469.
29. (a) *DNA Affinity Cleaving: Sequence Specific Cleavage of DNA by Distamycin-EDTA-Fe(II) and EDTA-Distamycin-Fe(II)*, Taylor, J.S.; Schultz, P.B.; Dervan, P.B., *Tetrahedron* (1984) **40**, 457; (b) *Cleavage of Double Helical DNA by (Methidiumpropyl-EDTA)iron(II)*, Hertzberg, R.P.; Dervan, P.B., *J. Am. Chem. Soc.* (1982) **104**, 313; (c) *Cleavage of DNA with Methidiumpropyl-EDTA-Iron (II); Reaction Conditions and Product Analyses*, Hertzberg, R.P.; Dervan, P.B., *Biochemistry* (1984) **23**, 3934.
30. (a) *Determination at Single-Nucleotide Resolution of the Sequence Specificity of DNA Interstrand Cross-linking Agents in DNA Fragments*, Weidner, M.F.; Millard, J.T.; Hopkins, P.B., *J. Am. Chem. Soc.* (1989) **111**, 9270; (b) *Sequence Preferences of DNA Interstrand Crosslinking Agents: Quantitation of Interstrand Crosslink Locations in DNA Duplex Fragments Containing Multiple Crosslinkable Sites*, Millard, J.T.; Weidner, M.F.; Kirchner, J.J.; Ribeiro, S.; Hopkins, P.B., *Nucleic Acids Res.* (1991) **19**, 1885; (c) *Sequence Preferences of DNA Interstrand Cross-Linking Agents: Importance of Minimal DNA Structural Reorganization in the Cross-Linking Reactions of Mechlorethamine, Cisplatin, and Mitomycin C*, Hopkins, P.B.; Millard, J.T.; Woo, J.; Weidner, M.F.; Kirchner, J.J.; Sigurdsson, S.T.; Raucher, S., *Tetrahedron* (1991) **47**, 2475; (d) *Sequence Preferences of DNA Interstrand Cross-Linking Agents: dG-to-dG Cross-Linking at 5'-CG by Structurally Simplified Analogues of Mitomycin C*, Weidner, M.F.; Sigurdsson, S.T.; Hopkins, P.B., *Biochemistry* (1990) **29**, 9225.
31. *FR900482: Close Cousin of Mitomycin C Exploiting Mitosene-Based DNA Cross-Linking Chemistry*, Williams, R.M.; Rollins, S.B.; Rajski, S.R., *Chemistry & Biology* (1997)- in press.
32. P.B. Hopkins, personal communication.
33. *On the Characterization of Intermediates in the Mitomycin Activation Cascade: A Practical Synthesis of an Aziridinomitosene*, Egbertson, M.; Danishefsky, S.J., *J. Am. Chem. Soc.* (1986) **108**, 4648.



34. For additional studies relevant to the reductive activation pathway of mitomycins see: (a) *Leucomitomycins*, Ciufolini, M.; Danishefsky, S.J., *J. Am. Chem. Soc.* (1984) **106**, 5665; (b) *On the Remarkable Stability of Derivatives of Leucomitomycin F. Novel Mitomycin Analogues*, Egbertson, M.; Danishefsky, S.J., *J. Org. Chem.* (1987) **52**, 4424.
35. *Structure of the DNA Interstrand Cross-Link of 4,5',8-Trimethylpsoralen*, Kumaresan, K.R.; Ramaswamy, M.; Yeung, A.T., *Biochemistry* (1992) **31**, 6774.
36. *Orientation Isomers of the Mitomycin C Interstrand Cross-Link in Non-Self-Complementary DNA. Differential Effect of the Two Isomers on Restriction Endonuclease Cleavage at a Nearby Site*, Kumar, S.; Johnson, W.S.; Tomasz, M., *Biochemistry* (1993) **32**, 1364.
37. (a) *Autocatalytic Quinone Methide Formation from Mitomycin C*, Peterson, D.M.; Fisher, J., *Biochemistry* (1986) **25**, 4077; (b) *Duplex Oligodeoxyribonucleotides Cross-Linked by Mitomycin C at a Single Site: Synthesis, Properties, and Cross-Link Reversibility*, Borowy-Borowski, H.; Lipman, R.; Chowdary, D.; Tomasz, M., *Biochemistry* (1990) **29**, 2992;
38. (a) *Solution Structure of a Cisplatin-Induced DNA Interstrand Cross-Link*, Huang, H.; Zhu, L.; Reid, B.R.; Drobny, G.P.; Hopkins, P.B., *Science* (1995) **270**, 1842; (b) *Structural Aspects of Platinum Anticancer Drug Interactions with DNA*, Sherman, S.E.; Lippard, S.J., *Chem. Rev.* (1987) **87**, 1153; (c) *Base sequence-independent distortions induced by interstrand cross-links in cis-diamminedichloroplatinum (II)-modified DNA*, Leng, M. Perez, C.; Malinge, J.M., *Nucleic Acids Research* (1994) **22**, 3834.
39. For excellent references describing T4 DNA ligase ligation protocols in the detection of distorted DNA structures see: (a) *DNA bending at adenine-thymine tracts*, Koo, H.S.; Wu, H.M.; Crothers, D.M., *Nature* (1986) **320**, 501; (b) *DNA bending induced by covalently bound drugs: Gel electrophoresis and chemical probe studies*, Leng, M., *Biophysical Chemistry* (1990) **35**, 155; (c) *DNA bend direction by phase sensitive detection*, Zinkel, S.S.; Crothers, D.M., *Nature* (1987) **328**, 178.
40. Ligation of blunt-ended templates is typically very difficult. Approaches to facilitate such reactions are described in: (a) *Hexamine cobalt chloride promotes intermolecular ligation of blunt end DNA fragments by T4 DNA ligase*, Rusche, J.R.; Flanders, P.H., *Nucleic Acids Research* (1985) **13**, 1997; (b) *Rapid and efficient method for cloning of blunt-ended DNA fragments*, Upcroft, P.; Healey, A., *Gene* (1987) **51**, 69.
41. (a) *Distortions Induced in DNA by cis-Platinum Interstrand Adducts*, Sip, M.; Schwartz, A.; Vovelle, F.; Ptak, M.; Leng, M., *Biochemistry* (1992) **31**, 2508; (b) *Chemical Probes of the Conformation of DNA Modified by cis-Diamminedichloroplatinum (II)*, Marrot, L.; Leng, M., *Biochemistry* (1989) **28**, 1454.

42. (a) *Chemical Probes of DNA Conformation: Detection of Z-DNA at Nucleotide Resolution*, Johnston, B.H.; Rich, A., *Cell* (1985) **42**, 713; (b) *Unusual conformational effect exerted by Z-DNA upon its neighboring sequences*, Kohwi-Shigematsu, T.; Manes, T.; Kohwi, Y., *Proc. Natl. Acad. Sci. U.S.A.* (1987) **84**, 2223.
43. *Detection of an altered DNA conformation at specific sites in chromatin and supercoiled DNA*, Kohwi-Shigematsu, T.; Gelinas, R.; Weintraub, H., *Proc. Natl. Acad. Sci. U.S.A.* (1983) **80**, 4389.
44. *Diethylpyrocarbonate: A chemical probe for secondary structure in negatively supercoiled DNA.*, Herr, W., *Proc. Natl. Acad. Sci. U.S.A.* (1985) **82**, 8009.
45. (a) *Sequence-dependent DNA structure*, Hunter, C.A., *BioEssays* (1996) **18**, 157; (b) *B-DNA twisting correlates with base-pair morphology*, Gorin, A.A.; Zhurkin, V.B. Olson, W.K., *J. Mol. Biol.* (1995) **247**, 34.
46. (a) Hurley, L.H.; Reck, T.; Thurston, D.E.; Lanley, D.R., *Chem. Res. Toxicol.* (1988) **1**, 258; (b) *Steady-State Fluorescence in Molecular-Modeling Studies of Tomamycin-DNA Adducts*, Barkley, M.D.; Thomas, T.J.; Maskos, K.; Remers, W.A., *Biochemistry* (1991) **30**, 4421; (c) Kohn, K.W.; Glaubiger, D.; Spears, C.L., *Biochim. Biophys. Acta* (1974) **361**, 288.
47. *Demonstration of the asymmetric effect of CC-1065 on local DNA structure using a site-directed adduct in a 117-base-pair fragment from M13mp1*, Hurley, L.H.; Needham-VanDevanter, D.R.; Lee, C.S., *Proc. Natl. Acad. Sci. U.S.A.* (1987) **84**, 6412.
48. *The Enfolding Arms of EcoRI Endonuclease: Role in DNA Binding and Cleavage*, Jen-Jacobson, L.; Lesser, D.; Kurpiewski, M., *Cell* (1986) **45**, 619.
49. An interesting macromolecular example of DNA-protein cross-linking by the pyrrolizidine alkaloids is described in; *Pyrrolizidine alkaloid-induced DNA-protein cross-links*, Kim, H.Y.; Stermitz, F.R.; Coulombe, R.A.Jr., *Carcinogenesis* (1995) **16**, 2691.
50. For excellent reviews see: (a) *Transcription Factors: Structural Families and Principles of DNA Recognition*, Pabo, C.O.; Sauer, R.T., *Ann. Rev. Biochem.* (1992) **61**, 1053; (b) *DNA-Binding Proteins*, Takeda, Y.; Ohlendorf, D.H.; Anderson, W.F.; Matthews, B.W., *Science* (1983) **221**, 1020; (c) *DNA Conformation and Protein Binding*, Travers, A., *Annu. Rev. Biochem.* (1989) **58**, 427; (d) *Sequence specific recognition of double helical nucleic acids by proteins*, Seeman, N.C.; Rosenberg, J.M.; Rich, A., *Proc. Natl. Acad. Sci. U.S.A.* (1976) **73**, 804.
51. Luisi, B., (1995) in *DNA-Protein: Structural Interactions* (Lilley, D.M.J., Ed.) pp 1-39, Oxford University Press Inc., New York.
52. (a) *Minor-Groove Width and Accessibility in B-DNA drug and Protein Complexes*, Neidle, S.O., *FEBS* (1992) **298**, 97; (b) *A Decapeptide Motif for Binding to the Minor Groove of DNA: A Proposal*, Turnell, W.G.; Satchwell, S.C.; Travers, A.A., *FEBS* (1988) **232**, 263.

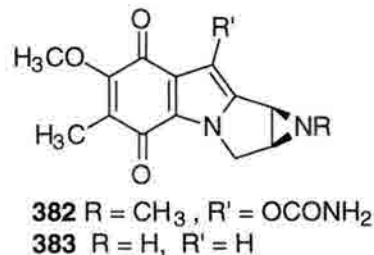
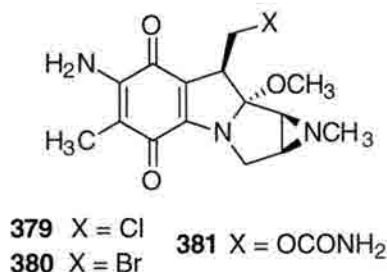
53. (a) *Histone H1-DNA Interactions and Their Relation to Chromatin Structure and Function*, Zlatanova, J.; Yaneva, J., *DNA and Cell Biology* (1991) **10**, 239; (b) *Preferential Binding of H1e Histone to GC-Rich DNA*, Wellman, S.E.; Sittman, D.B.; Chaires, J.B., *Biochemistry* (1994) **33**, 384; (c) *High-affinity binding sites for histone H1 in plasmid DNA*, Yaneva, J.; Schroth, G.P.; van Holde, K.E.; Zlatanova, J., *Proc. Natl. Acad. Sci. U.S.A.* (1995) **92**, 7060; (d) *'SPKK' motifs prefer to bind to DNA at A/T-rich sites*, Churchill, M.E.A.; Suzuki, M., *EMBO Journal* (1989) **8**, 4189.
54. (a) *A new protein domain for binding to DNA through the minor groove*, Freire, R.; Salas, M.; Hermoso, J.M., *EMBO Journal* (1994) **13**, 4353; (b) *A Novel Nucleoprotein Complex at a Replication Origin*, Serrano, M.; Salas, M.; Hermoso, J.M., *Science* (1990) **248**, 1012; (c) *Interaction of the bacteriophage  $\phi$ 29 protein p6 with double-stranded DNA*, Prieto, I.; Serrano, M.; Lazaro, J.M.; Salas, M.; Hermoso, J.M., *Proc. Natl. Acad. Sci. U.S.A.* (1988) **85**, 314.
55. *Structure refined to 2 Å of a nicked DNA octanucleotide complex with DNAase I*, Suck, D.; Lahm, A.; Oefner, C., *Nature* (1988) **332**, 464.
56. (a) *Co-crystal structure of TBP recognizing the minor groove of a TATA element*, Kim, J.L.; Nikolov, D.B.; Burley, S.K., *Nature* (1993) **365**, 520; (b) *Crystal structure of a yeast TBP/TATA-box complex*, Kim, Y.; Geiger, J.H.; Hahn, S.; Sigler, P.B., *Nature* (1993) **365**, 512.
57. (a) *DNA Recognition by Proteins with the Helix-Turn-Helix Motif*, Harrison, S.C.; Aggarwal, A.K., *Annu. Rev. Biochem.* (1990) **59**, 933; (b) *Crystal Structure of an engrailed Homeodomain-DNA Complex at 2.8 Å Resolution: A Framework for Understanding Homeodomain-DNA Interactions*, Kissinger, C.R.; Liu, B.; Martin-Blanco, Kornberg, T.B.; Pabo, C.O., *Cell* (1990) **63**, 579; (c) *Human and Drosophila Homeodomain Proteins That Enhance the DNA-Binding Activity of Serum Response Factor*, Grueneberg, D.A.; Natesan, S.; Alexandre, C.; Gilman, M.Z., *Science* (1992) **257**, 1089.
58. (a) *Hin recombinase bound to DNA: The origin of specificity in major and minor groove interactions*, Feng, J.A.; Johnson, R.C.; Dickerson, R.E., *Science* (1994) **263**, 348; (b) *Importance of minor-groove contacts for recognition of DNA by the binding domain of Hin recombinase*, Sluka, J.P.; Horvath, S.J.; Glasgow, A.C.; Simon, M.I.; Dervan, P.B., *Biochemistry* (1990) **29**, 6551; (c) *Sequence-specific interaction of the Salmonella Hin recombinase in both major and minor grooves of DNA*, Hughes, K.T.; Gaines, P.C.; Karlinsey, J.E.; Vinayak, R.; Simon, M.I., *EMBO Journal* (1992) **11**, 2695.
59. Eisenberg, D.; McLachlan, A.D., *Nature* (1986) **319**, 199.
60. *DNA structural variations in the E. coli tyrT promoter*, Drew, H.R.; Travers, A.A., *Cell* (1984) **37**, 491.
61. Satchwell, S.C.; Drew, H.R.; Travers, A.A., *J. Mol. Biol.* (1986) **191**, 659.
62. (a) *Flexibility of DNA*, Hagerman, P.J., *Ann. Rev. Biophys. Biophys. Chem.* (1988) **14**, 265; (b) *The mechanism of nucleosome assembly onto oligomers of the sea urchin 5 S DNA positioning sequence*, Hansen, J.C.; van Holde, K.E.; Lohr, D., *J. Biol. Chem.* (1991) **266**, 4276.

63. *The Interaction of E. coli IHF Protein with Its Specific Binding Sites*, Yang, C.C.; Nash, H.A., *Cell* (1989) **57**, 869.
64. Travers, A.A., (1995) in *DNA-Protein: Structural Interactions* (Lilley, D.M.J. Ed.) pp 58-59. Oxford University Press Inc., New York.
65. For an example of "edge-to-face" contacts involving aromatic amino acids see: *Structure of the HMG box motif in the B-domain of HMGI*, Weir, H.M.; Kraulis, P.J.; Hill C.S.; Raine, A.R.C.; Laue, E.D.; Thomas, J.O., *EMBO Journal* (1993) **12**, 1311.
66. Shepherd, J.C.W.; McGinnis, W.; Carrasco, A.E.; DeRobertis, E.M.; Gehring, W.J., *Nature* (1984) **310**, 70.
67. Johnson, R.C., (1995) in *DNA-Protein: Structural Interactions* (Lilley, D.M.J. Ed.) pp 151-155. Oxford University Press Inc., New York.
68. *The molecular origin of DNA-drug specificity in netropsin and distamycin*, Kopka, M.L.; Yoon, C.; Goodsell, D.; Pjura, P.; Dickerson, R.E., *Proc. Natl. Acad. Sci. U.S.A.* (1985) **82**, 1376.
69. *Cloning of cDNAs coding for human HMG I and HMG Y proteins: both are capable of binding the octamer sequence motif*, Eckner, R.; Birnstiel, M.L., *Nucleic Acids Research* (1989) **17**, 5947.
70. *The A-T-DNA-binding Domain of Mammalian High Mobility Group I Chromosomal Proteins; A Novel Peptide Motif for Recognizing DNA Structure*, Reeves, R.; Nissen, M.S., *Journal of Biological Chemistry* (1990) **265**, 8573.
71. *HMG domain proteins: architectural elements in the assembly of nucleoprotein structures*, Grosschedl, R.; Giese, K.; Pagel, J., *Trends in Genetics* (1994) **10**, 94.
72. *The HMG-I Box Protein Family: Classification and Functional Relationships*, Baxevanis, A.D.; Landsman, D., *Nucleic Acids Research* (1995) **23**, 1604.
73. (a) *Specific Recognition of Cruciform DNA by Nuclear Protein HMG I*, Bianchi, M.E.; Beltrame, M.; Paonessa, G., *Science* (1989) **243**, 1056; (b) *Specific Binding of Chromosomal Protein HMG I to DNA Damaged by the Anticancer Drug Cisplatin*, Pil, P.M.; Lippard, S.J., *Science* (1992) **256**, 234; (c) *Interaction between Cisplatin-modified DNA and the HMG boxes of HMG I: DNase I Footprinting and Circular Dichroism*, Locker, D.; Decoville, M.; Maurizot, J.C.; Bianchi, M.E.; Leng, M., *J. Mol. Biol.* (1995) **246**, 243.
74. *Activation of the TFIID-TFIIA complex with HMG 2*, Shykind, B.M.; Kim, J.; Sharp, P.A., *Genes & Development* (1995) **9**, 1354, and references therein.
75. *Molecular structure of chromosomal proteins HMG-14 and HMG-17: definition of a transcriptional enhancement domain distinct from the nucleosomal binding domain*, Trieschmann, L.; Psotnikov, Y.V.; Rickers, A.; Bustin, M., *Molecular Cell Biology* (1995) **15**, 6663.

76. (a) *Mechanism of Transcriptional Synergism between Distinct Virus-Inducible Enhancer Elements*, Du, W.; Thanos, D.; Maniatis, T., *Cell* (1993) **74**, 887; (b) *The High Mobility Group Protein HMG-I(Y) is Required for NF- $\kappa$ B-Dependent Virus Induction of the Human IFN- $\beta$  Gene*, Thanos, D.; Maniatis, T., *Cell* (1992) **71**, 777.
77. *Replacement of Conserved Threonines by Alanine Residues in High Mobility Group Protein HMG-I(Y): Effect on DNA Binding Affinity*, Siino, J.S.; Nissen, M.S.; Reeves, R., *Biochemical and Biophysical Research Communications* (1995) **207**, 497.
78.  *$^1\text{H}$  and  $^{13}\text{C}$  NMR Assignments and Molecular Modelling of a Minor Groove DNA-binding Peptide from the HMG-I Protein*, Evans J.N.S.; Zajicek, J.; Nissen, M.S.; Munske, G.; Smith, V.; Reeves, R., *Int. J. Peptide Protein Res.* (1995) **45**, 554.
79. *Substrate Structure Influences Binding of the Non-Histone Protein HMG-I(Y) to Free and Nucleosomal DNA*, Reeves, R.; Wolffe, A.P., *Biochemistry* (1996) **35**, 5063.
80. *Short Peptide Fragments Derived from HMG-I(Y) Proteins Bind Specifically to the Minor Groove of DNA*, Geierstanger, B.H.; Volkman, B.F.; Kremer, W.; Wemmer, D.E., *Biochemistry* (1994) **33**, 5347-5355.
81. For additional citations pertinent to Asx turns see: (a) *Structural and Functional Characterization of a Constrained Asx-Turn Motif*, Imperiali, B.; Spencer, J.R.; Struthers, M.D., *J. Am. Chem. Soc.* (1994) **116**, 8424; (b) *Involvement of Side Functions in Peptide Structures: The Asx Turn. Occurrence and Conformational Aspects*, Abbadi, A.; Mcharfi, M.; Premilat, S.; Boussard, G.; Marraud, M., *J. Am. Chem. Soc.* (1991) **113**, 2729; (c) *Asx-Turn conformation in the crystal structures of two tripeptides related to the sequence code for N-glycosylation*, Aubry, A.; Abbadi, A.; Boussard, G.; Marraud, M., *New Journal of Chemistry* (1987) **11**, 739.
82. *Phosphorylation of the DNA-binding domain of nonhistone high-mobility group I protein by cdc2 kinase: Reduction of binding affinity*, Reeves, R.; Langan, T.A.; Nissen, M.S., *Proc. Natl. Acad. Sci. U.S.A.* (1991) **88**, 1671.
83. *SAR-dependent mobilization of histone H1 by HMG-I/Y in vitro: HMG-I/Y is enriched in H1-depleted chromatin*, Zhao, K.; Kas, E.G.; Laemmli, U.K., *EMBO J.* (1993) **12**, 3237.
84. *Recognition of Specific DNA Sequences by Mitomycin C for Alkylation*, Kumar, S.; Lipman, R.; Tomasz, M., *Biochemistry* (1992) **31**, 1399.



85. The importance of the C-10-O to N<sup>2</sup> amino proton interaction has been further supported by the evaluation of **379-383** and their respective reactivities/specificities with a 3'-end-labeled BstNI-EcoRI 129bp restriction fragment of pBR322. See: *Role of the C-10 Substituent in Mitomycin C-I-DNA Bonding*, Li, V.; Choi, D.; Wang, Z.; Jimenez, L.S.; Tang, M.; Kohn, H., *J. Am. Chem. Soc.* (1996) **118**, 2326.



86. *Preparation and isolation of adducts in high yield derived from the binding of two benzo[a]pyrene-7,8-dihydroxy-9,10-oxide stereoisomers to the oligonucleotide d(ATATGTATA)*, Cosman, M.; Ibanez, V.; Geacintov, N.E.; Harvey, R.G., *Carcinogenesis* (1990) **11**, 1667.
87. (a) *Recognition of Mitomycin C-DNA Monoadducts by UVRABC Nuclease*, Kohn, H.; Li, V.; Tang, M., *J. Am. Chem. Soc.* (1992) **114**, 5501; (b) *Studies on the Bonding Specificity for Mitomycin C-DNA Monoalkylation Processes*, Li, V.; Kohn, H., *J. Am. Chem. Soc.* (1991) **113**, 275. (c) *On the Origins of the DNA Sequence Selectivity of Mitomycin Monoalkylation Transformations*, Kohn, H.; Li, V.; Shiltz, P.; Tang, M., *J. Am. Chem. Soc.* (1992) **114**, 9218.
88. References pertinent to reactions of FR-66979 with the 434 Repressor-Operator 1 complex : (a) *Recognition of a DNA Operator by the Repressor of Phage 434: A View at High Resolution*, Aggarwal, A.; Rodgers, D.W.; Drott, M.; Ptashne, M.; Harrison, S.C., *Science* (1988) **242**, 899; (b) *Cocrystals of the DNA-Binding Domain of Phage 434 Repressor and a Synthetic Phage 434 Operator*, Anderson, J.; Ptashne, M.; Harrison, S.C., *Proc. Natl. Acad. Sci. USA* (1984) **81**, 1307; (c) *Effect of Non-contacted Bases on the Affinity of 434 Operator for 434 Repressor and Cro*, Koudelka, G.B.; Ptashne, M.; Harrison, S.C., *Nature* (1987) **326**, 886; (d) *Substituting an  $\alpha$  - Helix Switches the Sequence-Specific DNA Interaction of a Repressor*, Wharton, R.P.; Ptashne, M.; Brown, E.L., *Cell* (1984) **38**, 361.
89. Arg<sup>43</sup> of the 434 repressor makes a water-mediated, bifurcated hydrogen bond to base pair 7 (adenine) in the minor groove of the OR1 DNA sequence.
90. The original peptide which had been used for the Wemmer-type DNA substrates was Ac-TPKRPRGRPKK-COOH.
91. Jayabaskaran, C., *et al.*, *Prep. Biochem.* (1987) **17**, 121.
92. Oray, B., *et al.*, *J. Chromatogr.* (1983) **270**, 253.

93. (a) *Sequence-Specific DNA Binding by a Short Peptide Dimer*, Kim, P.S.; McKnight, J.C.; Talanian, R.V., *Science* (1990) **249**, 769; (b) *Minimum Length of a Sequence-Specific DNA Binding Peptide*, Talanian, R.V.; McKnight, J.C.; Rutkowski, R.; Kim, P.S., *Biochemistry* (1992) **31**, 6871; (c) *Design of Peptides That Bind in the Minor Groove of DNA at 5'-(A,T)G(A,T)C(A,T)-3' Sequences by a Dimeric Side-by-Side Motif*, Wade, W.S.; Mrksich, M.; Dervan, P.B., *J. Am. Chem. Soc.* (1992) **114**, 8783; (d) *Artificial Sequence-Specific DNA Binding Peptides: Branched-Chain Basic Regions*, Pellegrini, M.; Ebright, R.H., *J. Am. Chem. Soc.* (1996) **118**, 5831.
94. It should be noted that addition of a 2% Triton X-100 aqueous solution to the reactions did not significantly improve the recovery of radiolabeled DNA-protein adducts.
95. The carbamate O10-dG contact involved in pre-covalent mitosene 5'-CG-3' binding (Figure 3-4) not only enhances alkylation specificity, but has also been proposed to help activate the carboxamide as a leaving group thus facilitating mitosene C10 alkylation.
96. (a) *The Method of Crosslinking Histones to DNA Partly Depurinated at Neutral pH*, Levina, E.S.; Bavykin, S.G.; Shick, V.V.; Mirzabekov, A.D., *Analytical Biochemistry* (1981) **110**, 93; (b) *Topography of Interaction of Escherichia Coli RNA Polymerase Subunits with lac UV5 Promoter*, Chenchick, A.; Beabealashvilli, R.; Mirzabekov, A., *FEBS LETTERS* (1981) **128**, 46; (c) *Primary Organization of the Nucleosome Core Particles: Sequential Arrangement of Histones along DNA*, Shick, V.V.; Belyavsky, A.V.; Bavykin, S.G.; Mirzabekov, A.D., *J. Mol. Biol.* (1980) **139**, 491.
97. *Photoreactivity of Platinum (II) in Cisplatin-Modified DNA Affords Specific Cross-Links to HMG Domain Proteins*, Kane, S.A.; Lippard, S.J., *Biochemistry* (1996) **35**, 2180.



## Chapter 4

### Experimental Procedures

FR-900482 was generously supplied by the Fujisawa Pharmaceutical Co.,Ltd.,Japan. FR-66979, FK973 were synthesized according to the Fujisawa patent Kokai 61-10590 and spectral data corroborated with the Fujisawa publication. All drug stock solutions were made up to 50mM in sterile DDH<sub>2</sub>O immediately prior to use unless otherwise noted. Oligodeoxynucleotides were synthesized on an Applied Biosystems 380B DNA synthesizer using standard phosphoramidite chemistry (reagents and phosphoramidites from GLEN Research). Plasmid DNA substrates (pBR322 and pBS+ were obtained from New England Biolabs) Only the pBS+ substrates were raised "in-house" *via* electroporation and large scale preparation/purification. Oligodeoxyribonucleotides (ODNs) were deprotected by heating 15 hrs. at 55°C in concentrated NH<sub>4</sub>OH, followed by filtering of the CPG resin and concentration of supernatant *in vacuo*. All oligos were purified by 20% Denaturing Gel Electrophoresis (DPAGE). ODNs of interest were 5' end-labelled with [ $\gamma$ -<sup>32</sup>P]ATP and T4 polynucleotide kinase (New England Biolabs) and then purified once more by 20% DPAGE. Labeled ODNs were then hybridized to their corresponding blunt ended complements in 200mM Tris (pH = 7.5) by heating the equimolar mixture of oligodeoxynucleotides to 75°C for 15 minutes then cooling to room temperature over 2 hrs. then to 4°C over another 2 hrs. 3'-end-labeling of DNA was performed using terminal deoxynucleotidyl transferase and  $\alpha$ -<sup>32</sup>P-ddATP. Nucleotidyl transferase and ddATP were obtained from Amersham radiochemicals and reactions were run as per manufacturer's instructions. 3'-end-labeled oligos were purified by Sephadex G-50 size exclusion chromatography and not 20% DPAGE. FeSO<sub>4</sub> (from Mallinkrodt) solutions were made up

to 4mM using 4mM EDTA 5 minutes before use. Mercaptoethanol (from Kodak) and dithiothreitol (from Gibco BRL) stock solutions were made using distilled deionized water immediately prior to use. Sodium acetate, tris, EDTA, and boric acid were also obtained from Gibco. Gel loading buffer contained .03% bromophenol blue, and .03% xylene cyanol in formamide. Dimethyl Sulfate and formic acid (88%) for Maxam-Gilbert sequence reactions were obtained from Mallinkrodt. Centrex MF .45um cellulose acetate spin filters were obtained from Schleicher & Schuell. Samples were counted on a Packard 1500 Tri-Carb liquid scintillation analyzer. All HMG BD peptides were prepared by solid phase synthesis by Macromolecular Resources (Dept. of Biochemistry, Colorado State University). TNB activated agarose was obtained from Pierce Chemicals.

#### **4.1. General Procedures.**

##### **4.1.1. Precipitation of nucleic acids**

Nucleic acids were routinely concentrated by precipitation with absolute ethanol. Precipitation was carried out by adjustment of the concentration of monovalent cations (NaOAc, pH 5.2) in the nucleic acid solution to 0.3M final and the addition of 3 volumes of ethanol. The contents were well mixed by either inversion and shaking of the eppendorf tube containing the ethanolic solution or by vortexing for 30 seconds at high speed. The mixture was then placed in dry ice acetone bath (-78°C) for 15 minutes followed by centrifugation at 14,000 RPM at 4°C for 12 minutes. The supernatant was carefully removed with a 0-200 µl sized Eppendorf pipetman and the remaining DNA pellet dried *in vacuo*. The nucleic acid was then redissolved in either DDH<sub>2</sub>O or an appropriate buffer.

##### **4.1.2. Quantitation of DNA.**

Pure samples of DNA (typically after 20% Denaturing polyacrylamide gel electrophoresis and subsequent extraction/isolation) were quantitated by measuring the absorbance at 260nm using a UV spectrophotometer. Molar extinction coefficients for the ODNs of

interest were calculated using the nearest neighbor method described by P. N. Borer in the Handbook of Biochemistry and Molecular Biology, CRC Press, 1975 in conjunction with optical density measurements obtained by ultraviolet absorption at 260 nm. Notably, quantitation of radiolabeled DNA in this fashion was not possible *via* UV spectrophotometric means. Quantitation of these ODNs was obtained by liquid scintillation of a given sample and comparison to the starting material's activity. Calculated molar absorptivity values for the ODNs of interest were as follows:

ODN 1	319,600 L/mol-cm
ODN 2	319,600 L/mol-cm
ODN 3	319,400 L/mol-cm
ODN 4	279,500 L/mol-cm
ODN 4'	295,800 L/mol-cm
ODN 5	305,300 L/mol-cm
ODN 5'	314,500 L/mol-cm
ODN 6	291,000 L/mol-cm
ODN 6'	317,700 L/mol-cm
ODN 7	316,200 L/mol-cm
ODN 9	293,100 L/mol-cm
ODN 9'	274,300 L/mol-cm
ODN 10	295,800 L/mol-cm
ODN 11	295,800 L/mol-cm
ODN 12	295,800 L/mol-cm
ODN 13	330,200 L/mol-cm
ODN 14	330,200 L/mol-cm
ODN 15	227,500 L/mol-cm
ODN 16	344,800 L/mol-cm
ODN 16'	374,700 L/mol-cm
ODN 17	369,700 L/mol-cm
ODN 17'	405,300 L/mol-cm
ODN 18	360,300 L/mol-cm
ODN 18'	236,600 L/mol-cm

For those instances involving plasmid DNA substrates, the conversion of 1 OD<sub>260</sub> = 50 µg of duplex was used.

#### 4.1.3. Hind III linearization of pBR322.

To 25 µg (100 µl) of ccc pBR322 DNA (New England Biolabs) was added 121.8 µl ddH<sub>2</sub>O, 25 µl of 10 X enzyme buffer (supplied with enzyme) and 3.2 µl of Hind III

restriction endonuclease ( New England Biolabs). The reaction was incubated 37°C for 18 hours and then analyzed by 0.8% neutral agarose gel to ensure that digestion was complete. The DNA was EtOH precipitated twice and then dried *in vacuo*. DNA was quantitated by OD<sub>260</sub> measurement.

#### **4.1.4. Electroporation/Large Scale of pBS+ into E. coli XL-1 Blue**

##### **Electroporation competent cells.**

Three 40 µl batches of XL-1 Blue electrocompetent cells (Stratagene Lot EX114) were added to pre-chilled (0°C) sterile eppendorf tube (0.65ml.). To these solutions were added 0.5, 1.0, and 2.0 µl aliquots of pBS+ plasmid DNA(10pg./µl.) respectively. The mixtures of DNA and cells were mixed by agitation and incubated on ice for one minute. Each mixture was then transferred to electroporation cuvettes (0.1cm gap size) and each was electroporated with settings of 1.7kV, 25mF and 200 ohms. The respective time constants were 4.6 msec., 4.5 msec., and 4.6 msec. for the 0.5, 1.0, and 2.0 µl DNA samples respectively. Immediately following poration each cuvette was rinsed with 1 ml. of pre-warmed (37°C) SOC broth. Each broth/cell/DNA mixture was then incubated 37°C for 1 hour. After incubation, 10<sup>2</sup> dilutions of each mixture were made and both the undiluted and 10<sup>2</sup> diluted SOC mixtures plated on LB-ampicillin (50µg/ml.)-tetracycline (12.5µg/ml.) plates. Incubation at 37°C was carried out for 12 h. after which time two colonies ( one from the 0.5 µl DNA 10<sup>2</sup> dilution plate and one colony from the 2.0 µl. DNA 10<sup>2</sup> dilution plate) were isolated and then plated onto new plates which had antibiotic and X-GAL/IPTG. Incubation at 37°C on the new plates was carried out 12 h. and the resulting transformants identified by their blue color. Using one of the blue transformants, cells were dissolved into 1 ml. sterile DDH<sub>2</sub>O and added to 1 L. of LB broth containing ampicillin (50µg/ml) and tetracycline (12.5µg/ml). Incubation was typically carried out for 16 h. after which time the cells were pelleted, supernatants discarded and the resulting ccc pBS+ isolated using Qiagen Maxi Prep Kits as per manufacturer's instructions. Linearization

of the resulting ccc plasmid was effected by digestion with Bam HI restriction endonuclease as per New England Biolabs protocol. Following incubation/linearization, DNA was EtOH precipitated, washed with 70% EtOH and dried *in vacuo*.

#### **4.1.5. Agarose gel purification of linearized pBS+**

Resuspension of linearized pBS+ into agarose loading dye was followed by 1.2% agarose gel purification (with ethidium bromide in gel (2 $\mu$ g/ml)). The band corresponding to linearized material was visualized by hand held-UV light. The agarose band was then excised and the DNA returned *via* electroelution in 1X TAE buffer. Following elution, the DNA was isoamyl alcohol extracted twice with 2 times the aqueous volume, EtOH precipitated and dried *in vacuo*. The DNA was then resuspended to a volume such that a DNA concentration of 0.97mM in base pairs (or 0.3  $\mu$ M in duplex) was obtained. This stock solution of linearized purified DNA was used to generate the data in Figures 2-7 and Appendix Figure 5-1. Reaction additions are detailed below.

#### **4.1.6. General Protocol for Alkaline Agarose Gel Electrophoresis**

1.2 % agarose gels were prepared as detailed in Maniatis. Gels were cast using 50mM NaCl, 2mM EDTA (pH = 8.0) in which to melt and dissolve the necessary quantity of agarose. For 50 ml volume gels this required 0.6 g agarose dissolved into 50 mls of saline/EDTA solution. Upon microwave dissolving of agarose, gels were poured ( without ethidium bromide) and allowed to solidify for 1 hour at room temperature. Combs were withdrawn from the gel and the gel then allowed to sit in 40mM NaOH + 1mM EDTA running buffer for at least 1 hour prior to electrophoresis. During this equilibration period the top of the gel was at least 4 mm below the surface of the NaOH solution. The basic running buffer was then discarded and new buffer placed in the gel chamber with no more than 2 mm above the top of the gel. Samples were traditionally dissolved in 15  $\mu$ l of alkaline agarose loading dye (50mM NaOH, 1mM EDTA, 2.5% (w/v) Ficoll, 0.25% (w/v)

bromocresol blue) to a concentration of approximately 0.05 µg plasmid DNA/µl. To each well was loaded 7.5-10 µl of DNA ( ~0.5 µg) and electrophoresis carried out at 25 Volts for 4 hours. In lieu of exact times and voltages, the distance traveled by the bromocresol tracking dye was routinely kept to 4 cm. from the well. The gels were then neutralized in 3 changes of 100 mM Tris (pH = 7.5) over the course of 2 hours. Using a 100 mM Tris (pH =7.5) 2µg/ml in ethidium bromide (obtained by diluting 200 µl of a 10mg/ml ethidium bromide solution into 1L of Tris buffer) the DNA bands were stained at room temperature for 1 hour. The gel was then destained ( to remove background staining) in 500 ml of 50 mM NH<sub>4</sub>OAc + 10mM β-mercaptoethanol for 15-20 minutes. Gels were visualized on a UV transilluminator and photographed using Polaroid Black % White film # 667.

#### **4.1.7. Maxam-Gilbert G Reactions**

5' or 3' end-labeled samples of DNA (typically 1 µg ) were dissolved into 10 µl ddH<sub>2</sub>O and to each sample was added 200 µl of Maxam-Gilbert G reaction buffer. To each 210 µl sample of DNA was added 1 µl of dimethyl sulfate (DMS) at room temperature. Each sample was aged at room temperature for 7-9 minutes folowed by the addition of 750 µls absolute EtOH, 10 µl tRNA ( 1mg/ml stock solution), and 30 µl 3M NaOAc (pH = 5.2). Reactions were kept at -80 °C for 15 minutes and centrifugation at 14,000 RPM carried out at 4°C for 10 minutes. The supernatant was discarded and the remaining pellet dissolved in 100 µls ddH<sub>2</sub>O followed by another EtOH precipitation (w/o tRNA addition). Following centrifugation the pellet was removed from the supernatant and the EtOH precipitation procedure repeated once more to ensure complete removal of G-reaction buffer salts. The pellet was dried *in vacuo*. To the pellet was added 100 µl 0.8 M piperidine ( prepared immediately prior to used) and the mixture heated to 80-90 °C for 20 minutes. The sample was then placed at -80°C and lyophilized to dryness. To the lyophilate was then added 100µl ddH<sub>2</sub>O and the lyophilization procedure repeated. Samples were dissolved in 50 µl DPAGE loading dye and the activity of each sample determined by liquid scintillation. Final activities of G reactions ranged from 2000 cpm/µl to 8000 cpm/µl.

#### **4.1.8. Maxam-Gilbert G+A Reactions**

5' or 3' end-labeled samples of DNA (typically 1  $\mu\text{g}$ ) were dissolved into 10  $\mu\text{l}$  ddH<sub>2</sub>O and to each sample was added 10  $\mu\text{l}$  of ddH<sub>2</sub>O. To each 20  $\mu\text{l}$  sample of DNA was added 50  $\mu\text{l}$  of formic acid (88%) at room temperature. Each sample was aged at room temperature for 7-9 minutes followed by the addition of 220  $\mu\text{l}$ s absolute EtOH, 10  $\mu\text{l}$  tRNA (1 mg/ml stock solution), and 15  $\mu\text{l}$  3M NaOAc (pH = 5.2). Reactions were kept at -80 °C for 15 minutes and centrifugation at 14,000 RPM carried out at 4°C for 10 minutes. The supernatant was discarded and the remaining pellet dissolved in 100  $\mu\text{l}$ s ddH<sub>2</sub>O followed by another EtOH precipitation (w/o tRNA addition). Following centrifugation the pellet was removed from the supernatant and the EtOH precipitation procedure repeated once more. The pellet was dried in vacuo. To the pellet was added 100  $\mu\text{l}$  1 M piperidine (prepared immediately prior to used) and the mixture heated to 80-90°C for 20 minutes. The sample was then placed at -80°C and lyophilized to dryness. To the lyophilate was then added 100  $\mu\text{l}$  ddH<sub>2</sub>O and the lyophilization procedure repeated. Samples were dissolved in 50  $\mu\text{l}$  DPAGE loading dye and the activity of each sample determined by liquid scintillation. Final activities of G + A reactions ranged from 2,000 cpm/ $\mu\text{l}$  to 16,000 cpm/ $\mu\text{l}$ .

#### **4.1.9. Recovery of radiolabeled DNAs from DPAGE (Crush and Soak method)**

Unless otherwise noted, all radiolabeled DNAs/DNA adducts were isolated as follows. Following drug and/or peptide reactions, samples were typically EtOH precipitated and then redissolved in a 1:1 mixture of DDH<sub>2</sub>O and DPAGE loading dye. Using analytical thickness DPAGE (4mm thickness), the samples were loaded to an appropriate number of wells (20  $\mu\text{l}$  maximum volume per well) and electrophoresis carried out at 50-75 Watts. Electrophoresis was traditionally carried out until the xylene cyanol dye (the slower mobility of the two dyes) was within 10 cm. of the gel bottom. The gel was removed from the apparatus and the plates separated so as to render the gel on only one plate. The gel was wrapped with plastic wrap and a clean glass plate placed on top so as to shield



radiation. Once in the darkroom, the top glass plate was removed and a piece of Kodak BioMax X-ray film placed on top of the gel. The top glass plate was placed on top of the X-ray so as to not completely cover the exposed gel surface. Using the top glass plate as a template, a razor blade was used to place cuts through both the X-ray and the gel below. Typical exposure times ranged from 2-5 minutes after which time the X-ray was developed, rinsed with DDH<sub>2</sub>O and then wiped dry. The bands of interest were cut out of the X-ray image. The slash marks through the X-ray and the gel were aligned and the band of interest excised from the gel using the X-ray as the template. DNAs were finely crushed using a glass rod and then eluted into 3-5 mls. of 500mM NH<sub>4</sub>OAc/1mM EDTA at 37°C for 1 hour. It is noteworthy that efficient elution ( $\geq 80\%$  recovery) may be achieved from 10% DPAGEs at room temperature in 10 minutes with occasional vortexing. Following elution, the crushed acrylamide matter was filtered off using centrex .45 $\mu$ m centrifugation filters (VWR Scientific). The eluant was butanol extracted to a volume of 200-300  $\mu$ l and then EtOH precipitated as described earlier.

#### **4.1.10. Piperidine digestion of DNAs (controls and alkylated adducts)**

DNAs (typically 1-3  $\mu$ g of radiolabeled material) were EtOH precipitated from DDH<sub>2</sub>O at least one time so as to ensure minimal salt content. Samples were then dried *in vacuo* and resuspended into 100 $\mu$ l 1M piperidine (prepared *via* 1:9 aqueous dilution of commercially available piperidine). Samples were rigorously vortexed for 2 minutes and then heated 80-90°C for 30 minutes with occasional vortexing. The samples were then withdrawn from the heating block and then placed in crushed dry ice and centrifuged so as to get all liquid into the bottom of the 1.7ml. eppendorf tube. Samples were frozen completely solid at -80°C and then a small hole melted into the top of the eppendorf tube. Samples were lyophilized to dryness (typically 12 hours) and then resuspended into 100  $\mu$ l of DDH<sub>2</sub>O and the freezing/lyophilization process repeated once more. Following the second lyophilization, samples were resuspended into 20  $\mu$ l DPAGE loading dye and 10-20  $\mu$ l of

this solution was transferred to a fresh tube. Samples were counted by liquid scintillation and then brought to an activity of 1000-3000 cpm/ $\mu$ l.

#### **4.1.11. Molecular Modeling**

Molecular mechanics were carried out using the cvff force-field in the molecular modeling package INSIGHT II ver. 2.3.5 (BIOSYM/Molecular Simulations, Inc.) For modeling of the orientation isomers in Figure 2-30 the double stranded hexamer was constructed using the Biopolymer program. The mitosene derived from FR-66979 was constructed using Macromodel software; DNA was constructed using Biosym insight II software. Once the mitosene was bonded to the duplex, 500 steps of energy minimization using the conjugate gradient algorithm were carried out by fixing the DNA strands and allowing the cross-linked drug to reach an energy minima. Modeling of the FR-66979 monoalkylated 5'-CGAATTCG-3' bound to PRGRP was facilitated by Wemmer et al. ( U.C. Berkeley). Coordinates for the peptide bound DNA was courtesy of Wemmer; the mitosene core of FR-66979 was bonded to the peptide-DNA complex and then minimized in a fashion similar to that used for the orientation isomer studies.

#### **4.2. Specific procedures ( as they appear in chapters 2 and 3)**

##### **4.2.1. FR-900482 cross-linking of Hind III linearized pBR322 DNA (results in Figures 2-4, 2-5)**

The 17.5  $\mu$ g of linearized pBR322 was dissolved in 1.94 mls of phosphate buffered saline (0.01 M PBS) to afford a stock DNA solution 13.8  $\mu$ M in base pairs (bp.). A stock solution 100mM in FR-900482 was made using DDH<sub>2</sub>O and stock solutions of dithiothreitol and  $\beta$ -mercaptoethanol were made immediately prior to use. Stock solutions were used to set up the reactions detailed below. Reactions were incubated 37°C for 24 h. Analysis of each series of FR-900482 reactions ( at 1, 10, and 50 mM concentrations respectively) with different reductants was carried out by 1.2% alkaline agarose gel

electrophoresis. Photography and subsequent 1D densitometry of the negative polaroid image was conducted to yield the results of depicted in Figures 2-4, 2-5.

**Table 4-1-** Composition of FR-900482/DTT/  $\beta$ -MET reactions (see Figure 2-4)

Reaction #	$\mu$ l pBR322 <sup>a</sup>	$\mu$ l FR900482	$\mu$ l DTT	$\mu$ l $\beta$ -MET
1	55.5	0.6	-	-
2	55.5	0.6	0.5 (12.5)	-
3	55.5	0.6	-	0.5(12.5)
4	55.5	0.6	0.6(100)	-
5	55.5	0.6	-	0.6(100)
6	55.5	0.6	0.7(800)	-
7	55.5	0.6	-	0.7(800)
8	55.5	6.2	-	-
9	55.5	6.2	0.5(12.5)	-
10	55.5	6.2	-	0.5(12.5)
11	55.5	6.2	0.6(100)	-
12	55.5	6.2	-	0.6(100)
13	55.5	6.2	0.8(800)	-
14	55.5	6.2	-	0.8(800)
15	55.5	55.5	-	-
16	55.5	55.5	0.4(25)	-
17	55.5	55.5	-	0.4(25)
18	55.5	55.5	0.6(200)	-
19	55.5	55.5	-	0.6(200)
20	55.5	55.5	1.4(800)	-
21	55.5	55.5	-	1.4(800)
22	55.5	-	0.7(800)	-
23	55.5	-	-	0.7(800)
24	55.5	-	-	-

<sup>a</sup> - The pBR322 stock solution was 14  $\mu$ M in base pairs.

Values in parenthesis denote stock solution concentrations (in mM) for the given reagent.

Drug and thiol stock solutions were prepared in sterile DDH<sub>2</sub>O immediately prior to reaction.

Figure 2-5 alkaline agarose gel image was generated similarly using the following reaction volumes and additions. Reactions were incubated 37°C 24 hours followed by the previously discussed electrophoretic analysis.

**Table 4-2-** Reactions of FR-900482 with  $\beta$ -MET/GSH and pBR322 (see Figure 2-5)

Reaction #	$\mu$ l pBR322 <sup>a</sup>	$\mu$ l FR900482	$\mu$ l MET	$\mu$ l GSH
1	25	0.5(50)	-	-
2	25	0.5(50)	1.1(25)	-
3	25	0.5(50)	-	1.1(25)
4	25	0.5(50)	0.6(200)	-
5	25	0.5(50)	-	0.6(200)
6	25	0.5(50)	1.3(200)	-
7	25	0.5(50)	-	1.3(200)
8	25	2.8(100)	-	-
9	25	2.8(100)	1.2(25)	-
10	25	2.8(100)	-	1.2(25)
11	25	2.8(100)	0.7(200)	-
12	25	2.8(100)	-	0.7(200)
13	25	2.8(100)	1.5(200)	-
14	25	2.8(100)	-	1.5(200)
15	25	25(100)	-	-
16	25	25(100)	1.0(50)	-
17	25	25(100)	-	1.0(50)
18	25	25(100)	1.3(200)	-
19	25	25(100)	-	1.3(200)
20	25	25(100)	1.3(400)	-
21	25	25(100)	-	1.3(400)
22	25	-	1.3(200)	-
23	25	-	-	1.3(200)
24	25	-	-	-

<sup>a</sup> - pBR322 stock solution was 14  $\mu$ M in base pairs. Values in parentheses denote stock solution concentrations in mM. All solutions were made up in sterile DDH<sub>2</sub>O immediately prior to reaction.

#### 4.2.2. Reactions of FR-900482 with linearized pBS+ plasmid DNA.

(Results depicted in Figures 2-7, and Appendix Fig. 5-1.)

Using the gel-purified linearized pBS+ substrate described above, the following reactions were set up and allowed to incubate for 4 h. at 37°C. Prior to incubation, all reactions were brought to a total reaction volume of 100µl with DDH<sub>2</sub>O. Reactions contained 10mM phosphate buffer (pH = 8.0). Following incubation, reactions were EtOH precipitated, dried *in vacuo* and then resuspended into 100 µl alkaline agarose gel loading buffer. To each well of a 1.2% alkaline agarose gel was added 10µl and electrophoresis/visualization carried out as described above.

**Table 4-3.** Reactions of FR-900482 with β-MET/Fe(III)-EDTA and linearized, gel purified pBS+ (see Figure 2-7).

Reaction #	µl pBS+	µl phosphate buffer <sup>a</sup>	µl 312	µl β-MET	µl Fe <sup>3+</sup> /EDTA
1	5	12.5	-	-	-
2	5	12.5	20(50)	-	-
3	5	12.5	20(50)	1(1M)	-
4	5	12.5	-	1(1M)	-
5	5	12.5	20(50)	-	1(100µM)
6	5	12.5	20(50)	-	1(1mM)
7	5	12.5	20(50)	-	1(10mM)
8	5	12.5	20(50)	-	1(100mM)
9	5	12.5	20(50)	1(1M)	1(100µM)
10	5	12.5	20(50)	1(1M)	1(1mM)
11	5	12.5	20(50)	1(1M)	1(10mM)
12	5	12.5	20(50)	1(1M)	1(100mM)

Values in parentheses denote stock solution concentrations. Both Fe<sup>3+</sup> and Fe<sup>2+</sup> solutions contained equimolar concentrations of EDTA (pH = 8.0) and iron. <sup>a</sup> - denotes an 80mM stock solution of phosphate buffer at pH=8.0.

**Table 4-4.** Reactions of FR-900482 with Fe(III)-EDTA or Fe(II)-EDTA in the presence of pBS+ (see Appendix Figure 5-1).

Reaction #	μl pBS+	μl phosphate	μl FR900482	μl Fe <sup>3+</sup> /EDTA	μl Fe <sup>2+</sup> /EDTA
1	4.6	6.2	-	-	-
2	4.6	6.2	10(50)	-	-
3	4.6	6.2	-	1(10μM)	-
4	4.6	6.2	-	1(100 μM)	-
5	4.6	6.2	-	1(1 mM)	-
6	4.6	6.2	-	-	1(10 μM)
7	4.6	6.2	-	-	1(100 μM)
8	4.6	6.2	-	-	1(1 mM)
9	4.6	6.2	10(50)	1(10μM)	-
10	4.6	6.2	10(50)	1(100 μM)	-
11	4.6	6.2	10(50)	1(1 mM)	-
12	4.6	6.2	10(50)	-	1(10μM)
13	4.6	6.2	10(50)	-	1(100 μM)
14	4.6	6.2	10(50)	-	1(1 mM)

Both Fe<sup>3+</sup> and Fe<sup>2+</sup> solutions contained equimolar concentrations of EDTA (pH = 8.0) and iron.

#### 4.2.3. FR-900482 and FR-66979 Reactions with pBR322

(see Figure 2-8)

**Table 4-5.** Reactions of FR-900482 (**312**) and FR-66979 (**314**) in the presence of pBR322 with and without  $\beta$ -mercaptoethanol. (see Figure 2-8). Reactions were incubated 37°C for 24 h. prior to analysis.

Reaction #	$\mu$ l pBR322 <sup>a</sup>	$\mu$ l <b>312</b>	$\mu$ l <b>314</b> <sup>b</sup>	$\mu$ l $\beta$ -MET
1	25	-	-	-
2	25	-	-	0.7(40)
3	25	1.3(20)	-	-
4	25	2.8(100)	-	-
5	25	25(100)	-	-
6	25	1.3(20)	-	0.7(40)
7	25	2.8(100)	-	0.7(400)
8	25	25(100)	-	0.6(800)
9	25	-	1.3(20)	0.7(40)
10	25	-	1.3(2)	0.7(4)
11	25	-	25(100)	-
12	25	-	2.8(100)	-
13	25	-	1.3(20)	-
14	25	-	1.3(2)	-
15	25	-	-	-
16	25	-	-	-

<sup>a</sup> -pBR322 stock solution was 10mM in phosphate buffered saline (pH = 7.0) and DNA concentration of stock solution was 14  $\mu$ M in base pairs. <sup>b</sup> - FR-66979 used for these reactions was obtained *via* Pd/C hydrogenation of FR-900482. By TLC and <sup>1</sup>H NMR, the sample appeared to contain no starting material or other contaminants and was therefore not chromatographed prior to use.

#### 4.2.4. Cross-link formation and subsequent Footprinting Reactions for "pre-activated" FR-66979 ( Fig. 2-14 & 2-15).

5'-<sup>32</sup>P-end-labeled 40  $\mu$ g of **ODN 1** and **ODN 2** separately as described above. T4 Polynucleotide kinase labeling reaction was incubated 45 minutes at 37°C and then phenol:CHCl<sub>3</sub> extracted three times with 1ml of fresh phenol each time. The oligos were passed through a Sephadex G-50 size exclusion column and the first radioactive fraction collected. To each lot of radiolabeled oligo was added an equimolar amount of the unlabeled complement ODN 3 and the resulting mixtures EtOH precipitated as before. The samples were dried in vacuo and then resuspended in 74.5  $\mu$ l of 10mM phosphate buffered saline (PBS). Strands were annealed by heating to 75°C 30minutes and then cooling



slowly ( over a 2 hour period) to room temperature. Samples were cooled even further to 4°C for an additional hour. To 55.9 µl of each selectively labeled duplex was then added 14 µl of 50mM crude FR-66979 (from hydrogenation of FR-900482). Reactions were kept on ice for 2 h. and then allowed to warm to room temperature for 10 hours. To each sample was then added 50 µl of formamide and the samples loaded to a 15% preparative DPAGE and electrophoresis carried out at 600 Volts for 5 hours. Bands were visualized by autoradiography, excised and returned via electroelution in 0.1 X TAE buffer ( 250V. for 2 h.). DNAs were EtOH precipitated and washed once with 70% EtOH. Samples were dried *in vacuo* and then resuspended into 40 µl DDH<sub>2</sub>O. To 15 µl of each sample was then added 7.5 µl of 80mM phosphate buffer (pH = 8.0), and 7.5 µl of 4 mM Fe(II)-EDTA (prepared immediately prior to use). Samples were agitated rigorously and allowed to incubate 37°C for 7.5 hours. To each sample was then added 10 µl tRNA (1mg/ml stock), 4 µl 3M NaOAc (pH=5.2), and 120 µl absolute EtOH. Samples were chilled -80°C for 10 minutes and then centrifuged 14,000 RPM at 4°C for 10 minutes. Supernatants were discarded and the resulting pellet resuspended into 100 µl DDH<sub>2</sub>O and EtOH precipitated again. Following the second EtOH precipitation, samples were dried *in vacuo* and resuspended into 10 µl DPAGE dye and analysed by 20% DPAGE to afford the image in Figure 2-13. Analysis of the complementary strand **ODN 3** was carried out in a similar fashion to yield Figure 2-15.

#### **4.2.5. Cross-link formation and subsequent Footprinting Reactions for FR-900482, FR-66979, and FK973 (Appendix Fig. 5-3).**

To 15 µl of a 90 µM (in duplex) stock solution (in 200 mM Tris pH=7.5) of 5'-<sup>32</sup>P-end-labeled DNA was added 50 mM drug stock solution to yield a drug concentration of 10 mM. To this mixture was added 1 µl of β-mercaptoethanol to afford a reaction concentration 500 mM in thiol. Reactions were incubated at 4 °C for 4 hours and were then allowed to warm to room temperature overnight. Modified ODNs were then ethanol

precipitated, dried *in vacuo*, and resuspended in 80  $\mu$ l DPAGE loading dye. Reactions were then loaded to a 20% DPAGE, electrophoresis was carried out for 5 hours at 2000 V, and the bands visualized by autoradiography. Cross-linked product bands were excised from the gel and the DNA recovered by electroelution (0.1 x TAE, 500V, 2 hours) using a Schleicher & Schuell Elutrap electro-separation system. The DNA isolated was once again ethanol-precipitated and then dried *in vacuo*. To each alkylation adduct was added 20  $\mu$ l distilled deionized water. From each ODN solution, a 5  $\mu$ l aliquot was removed for use as a standard. To the remaining 15  $\mu$ l of each product was added 7.5  $\mu$ l of 80 mM phosphate buffer (pH=8) and 7.5  $\mu$ l of a 4 mM FeSO<sub>4</sub>-EDTA solution to afford reactions 1 mM in Fe(II)-EDTA. Footprinting reactions were then incubated at 37 °C for 8 hours after which time samples were ethanol-precipitated, the pellets rinsed with cold 70% ethanol, and dried *in vacuo*. Dried pellets were then resuspended in 10  $\mu$ l DPAGE dye, and the samples counted by liquid scintillation (LSC). Samples were loaded such that standard duplex and standard cross-linked product lanes contained 500 counts, Fe(II)-EDTA lanes contained 5000 counts (for Fe(II)-EDTA standard and native duplex after cross-linking and Fe(II)-EDTA digestion) and 10,000 counts for inosine-substituted duplex after cross-linking and Fe(II)-EDTA digestion. To G and G+A Maxim-Gilbert sequencing lanes were added 4000 and 8000 counts respectively. Electrophoresis was carried out at 1500 V for 5 hours followed by autoradiography at -80 °C for 3 days. The results are depicted in Appendix Figure 5-2.

#### **4.2.6. Reactions of reductively activated FR-66979 with base substituted versions of template 1.**

10  $\mu$ g (1 nmol.) of each of the following oligodeoxyribonucleotides was 5'-<sup>32</sup>P-end-labeled and purified by analytical thickness 20% DPAGE. Note that **I** = inosine, and **DZG** = 7-Deazaguanosine (see Figure 2-15 for structures)

5'-TTTATTAACGTAATGCTTAATCGCAATGGGATT-3' (ODN 1)

5'-TTTATTAACITAATGCTTAATCGCAATGGGATT-3' (ODN 2)

5'-TTTATTAACITAATGCTTAATCICAATGGGATT-3' (ODN 1')

5'-TTTATTAAC<sup>DZ</sup>GTAATGCTTAATC<sup>DZ</sup>GCAATGGGATT-3' (ODN 1'')

Following purification (see above section 4.1.9.), each oligo was annealed to an equimolar amount of the unlabeled **ODN 3** mutual complement by heating to 85°C 15 minutes and then cooling to room temperature for 2 hours. Each sample was EtOH precipitated, dried *in vacuo* and then resuspended into 200 mM Tris (pH = 7.5) to afford each duplex stock solution 9 µM in duplex. To 5 µl of each solution was added 1.38µl 50mM FR-66979 (PTLC purified), and 0.5 µl 1376mM DTT so as to afford each reaction 10mM in FR-66979 and 100 mM in DTT. Analogous control reactions were set up in which DDH<sub>2</sub>O was added in place of drug and thiol. Additionally, DTT control reactions were also set up to which DDH<sub>2</sub>O was added instead of FR-66979. Reactions were set up at 4°C and then allowed to warm to room temperature overnight (10 h.). All duplexes were then EtOH precipitated, dried *in vacuo*, and resuspended in DPAGE dye to an activity of 5,799 cpm/µl. The contents of each FR-66979, DTT control, and DNA control was loaded to a 20% DPAGE (4ml sample/well) after heat denaturation at 90°C for 3 minutes. Electrophoresis was carried out for 3 h. at 50 Watts. Autoradiography was then conducted at -80°C for 12 hours to yield the image in Figure 2-15.

#### 4.2.7. Reactions of reductively activated FR-66979 and FR-900482 with base substituted versions of templates 1 and 2. (Quantitation of ISC efficiencies)

Using the stock DNA solutions described above in section 4.2.6., an additional set of **template 1** and **template 2** reactions were set up. One series of reactions involved the use of 50 mM FR-66979 while the other involved the use of a stock solution of 50mM FR-900482. Reaction additions, times, and work-up procedures were the same as in section

4.2.6. Following EtOH precipitation and drying, however, each sample was resuspended in DPAGE dye so as to afford a solution with activity of 11,398 cpm/ $\mu$ l. Using 3 ml of each reaction and its necessary control 20% DPAGE was carried out at 60 Watts for 4 hours so as to afford clean separation of each respective cross-linked species. Bands were visualized by autoradiography (8 h. at  $-80^{\circ}\text{C}$ ). The resulting X-ray and gel had been mutually cut prior to exposure. Thus, aligning of the slash marks allowed the use of the X-ray as a template by which to identify the location of each DNA containing fraction. Excision of the different bands was followed by liquid scintillation counting to afford the corresponding activities listed below. From these counts were calculated the relative efficiencies of FR-900482 and FR-66979 for each of the two possible 5'-CG-3' boxes contained within **template 1** and **template 2**.

**Table 5-6.** Liquid scintillation counting of **template 1** and **template 2** cross-links formed by reductively activated FR-66979 and FR-900482.

substrate	drug	native/ mono- adduct	G-10 cross-link	G-23 cross-link	% G-10 cross- linked	% G-23 cross- linked
<b>template 1</b>	<b>312</b>	23913	1639	645	6.2	2.4
<b>template 2</b>	<b>312</b>	37374	-	743	-	1.9
<b>template 1</b>	<b>314</b>	16834	11705	2678	37.5	8.6
<b>template 2</b>	<b>314</b>	24610	-	4097	-	14.3

**4.2.8. Reactions of template 3 with FR-66979 derived from FR-900482 via different reduction conditions. (Figure 2-21)**

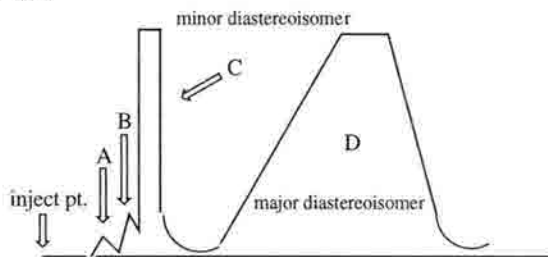
200  $\mu$ g (2.1 nmol.) of **ODN 4** was 5'-end-labelled and 20% DPAGE purified. The resulting oligo was then annealed to an equimolar amount of **ODN 4'** in 200 mM Tris (pH=7.5) as previously described. To 5 $\mu$ l aliquots of the duplex was added 1.38  $\mu$ l of FR-66979 and 0.5  $\mu$ l of 277 mM DTT so as to achieve final concentrations of 10mM drug and 20 mM DTT. Additionally, reactions were run in the presence of only drug. Reactions

were kept at 0°C for 3 hours and then allowed to warm to room temperature for an additional 12 hours. Following incubation, 2  $\mu$ l aliquots were withdrawn from each reaction and to each was added 3  $\mu$ l DPAGE loading dye. Samples were heated 90°C for 1 minute prior to loading and then each reaction was loaded to one well of a pre-warmed 20% denaturing acrylamide gel and electrophoresis carried out at 60 Watts for 4 hours. Autoradiography was conducted for 17 h. at -80°C to yield the image in Figure 2-21.

#### 4.2.9. Reactions of HPLC fractionated FR-66979 with template 1. (Appendix Figure 5-5.)

HPLC of crude FR-66979 prepared *via* hydrogenation at 1 atm H<sub>2</sub> pressure was carried out. A 2:8 mixture of H<sub>2</sub>O:CH<sub>3</sub>CN was used as mobile phase using isocratic runs at 2 mls./min. over a 10 cm x 4.7mm ID CHIRALPAK WH DAICEL COLUMN. The typical trace appeared similar to that depicted below. As such, fractions A and B were difficult to resolve out so these fractions were collected together for use in the **template 1** reactions.

CHARACTERISTIC LC TRACE OF  
CRUDE FR-66979



Fractions C and D were easily separable from each other though fraction C was likely tainted with small percentages of fraction B. The three fractions were collected, and the aqueous acetonitrile lyophilized off of each fraction overnight. 50mM stock solutions of each fraction were made by dissolution into DDH<sub>2</sub>O at 0°C. and these stock solutions used to compose reactions analagous in drug, DTT and **template 1** concentration to those reactions outlined in section. 4.2.8. Reaction additions were done at 0°C and kept at that

temperature for 1h. after which time they were allowed to warm to room temperature for 12 hours. From each sample was then withdrawn 3.4  $\mu$ l of each reaction and added to an equal volume of DPAGE dye. Samples were loaded to a 20% denaturing gel and the face-plate of the gel heated with a heat gun to ensure sample denaturation. Electrophoresis was carried out 5 h. at 45 Watts to ultimately yield Appendix Figure 5-5.

#### **4.2.10. HPLC monitoring of $\beta$ -MET reaction with PTLC purified FR-66979**

To 4.1mls. of 5 mM FR-66979 in DDH<sub>2</sub>O was added 300  $\mu$ l of B-MET. The sample was kept at room temperature for 48 h. HPLC analysis using conditions described above (section 4.2.9) revealed the appearance of two much slower moving peaks and no starting material. Differential detection at both 215 and 230 nm. revealed a much greater absorbance at 230 indicative of an indole structure. The reaction was therefore dried *in vacuo* at room temperature. The sample was dissolved into 1 ml. MeOH and purified by 1.5cm x 10 cm. silica column (pre-treated with 1% triethylamine) (eluted with 1:4 MeOH:CH<sub>2</sub>Cl<sub>2</sub>.) to afford a yellowish solid. The sample contained residual  $\beta$ -MET which proved difficult to avoid. Attempted PTLC was also performed but this too, failed to afford clean product. Given the undesired nature of the product based on DNA cross-linking reactions and spectral data, more material was not obtained due to the scarcity of the natural product.

#### **4.2.11. Analytical Scale Formation of Drug-DNA complexes for Orientation Isomer studies (Figure 2-22)**

Reactions were performed using 3 duplexes 5'-<sup>32</sup>P-end-labeled on the following strands of each duplex. "Template" numbers beside each oligodeoxyribonucleotide substrate refer to the corresponding ODN substrate annealed to their blunt-ended complements.

5'TGTTGAATACTCATACGTCTCTTGCTGAGGG3'      **template 3**

5'TGTTGAATACTCATACGTCTCTTGCTTTAAT3'      **template 4**

5'TGTTGAATACTCATATTTCTCTTGCTGAGGG3'      **template 5**

DNA concentrations were the same as those used for the footprinting studies outlined above. Reactions contained 10  $\mu$ l DNA, 2.76  $\mu$ l 50 mM drug and 1  $\mu$ l 277 mM DTT stock. Additions were done at 4 °C and mixtures were allowed to incubate at this temperature for 3 hours after which time they were allowed to warm to room temperature for an additional 21 hours for a net reaction time of 24 hours. Reactions were ethanol-precipitated, dried *in vacuo* and resuspended in 10  $\mu$ l DPAGE dye. Samples were counted and brought to a volume in loading dye such that samples were 6,692 counts/ml. To each well of a 20% DPAGE gel was loaded 13,384 counts and electrophoresis carried out 5 hours at 2500 V. Bands were visualized by autoradiography. The results are depicted in Figure 2-22.

#### 4.2.12.      **Preparation of FR-66979 cross-linked oligos for Mass Spectrometry (Figure 2-23)**

To 275  $\mu$ l of a 90  $\mu$ M (*in duplex*) solution of **template 3** ( dissolved in 200 mM Tris, pH=7.5) was added 75.9  $\mu$ l FR66979 and 27.5  $\mu$ l of 277 mM DTT at 0 °C. The reaction was allowed to warm to room temperature overnight (10 hours) and the contents ethanol-precipitated. Resuspension in 150  $\mu$ l DPAGE dye followed by 20% Preparative DPAGE at 800 V for 10 hours afforded clean separation of the two cross-linked species. Each band was excised from the gel, crushed and eluted for 2 hours at 37 °C in 500 mM NH<sub>4</sub>OAc, 1 mM EDTA buffer. The supernatant was passed through a Centrex centrifugal filter, butanol extracted to a volume of 200  $\mu$ l and ethanol-precipitated. Each resulting pellet was resuspended in 150  $\mu$ l DDH<sub>2</sub>O and to each solution was added 50  $\mu$ l 5 M NH<sub>4</sub>OAc (pH=5.2). Each sample was kept at room temperature for 10 minutes, followed by the addition of 600 ml ethanol and placed in a dry ice bath for 15 minutes. The products were re-pelleted by centrifugation at 14,000 rpm at 4 °C followed by removal of supernatant.



The series of steps starting with resuspension in 150  $\mu$ l ddH<sub>2</sub>O was performed once more followed by a 70% ethanol rinse and and drying *in vacuo*.

**4.2.13. Reversion of cross-linked template 3 substrate to native single-strand DNA and monoalkylation adducts (Figures 2-26, 2-27, 5-14)**

FR-66979 cross-linked DNA was prepared by 5' end-labeling 5.5 nmoles of either **ODN 4** or **ODN 4'** and then purifying the labeled oligo by 20 % DPAGE as previously described and annealing to an equimolar amount of unlabeled complementary DNA in 200 mM Tris (pH=7.5) to afford a stock solution 0.3 mM in duplex. To 150 $\mu$ l of this duplex stock was added 50mM FR-66979 to a final concentration of 10mM. 3125mM DTT was then added to a concentration of 20mM and the reaction allowed to warm to room temperature overnight (10hrs.). Following incubation, the reaction was ethanol precipitated, dried *in vacuo* and then redissolved in 100 $\mu$ l of DPAGE loading dye. The contents of the reaction was loaded to an analytical thickness gel (0.4 mm. thickness) and electrophoresis carried out for 8 h. at 60 Watts. The DNA bands were visualized by autoradiography and the two orientation isomers excised from the gel as was the band corresponding to standard single-stranded radiolabeled probe. DNA's were recovered by the crush and soak method of Maniatis, though elution from the gel was performed for only 1 hour as opposed to the prescribed 12 hrs. suggested in the Maniatis protocol. The crushed acrylamide matter was filtered off by passing through a Schleicher and Schuel centrex 0.45  $\mu$ m cellulose acetate spin filtration apparatus. The samples were then concentrated by butanol extraction to a volume of 300 $\mu$ l and the DNA's then EtOH precipitated by addition of 900 $\mu$ l of absolute ethanol and chilling to -78°C for 15 minutes. Centrifugation at 14,000 rpm for 10 minutes afforded small white pellets from which the supernatant was discarded. The DNA's were resuspended in 20  $\mu$ l ddH<sub>2</sub>O and from this was aliquoted a series of 5 $\mu$ l samples to which was added 95  $\mu$ l 200mM Tris (pH=7.5).

Each resulting 100  $\mu$ l sample of DNA ( standards and cross-linked substrates) was divided into three 33.3  $\mu$ l aliquots. Of the three aliquots, one was used as a control which was kept at room temperature while another was heated to 80°C for 15 minutes and then cooled to room temperature for 2 hrs. and then placed in an ice water bath for an additional 2 hours. The third aliquot was simply put through two rounds of the heating/cooling sequence described for aliquot #2. Each 33.3  $\mu$ l aliquot was then ethanol precipitated, dried *in vacuo* and then resuspended in DPAGE loading dye to afford solutions such that sample activities were 685 counts/ml. Denaturing polyacrylamide gel electrophoresis was carried out on 5ml of each reaction as well as the necessary control reactions. Electrophoresis was carried out at 60Watts for 8 h. after which time autoradiography was performed for 12h. at -80°C to yield Figure 2-26. Analagous experiments were performed with **template 3** 5'-end-labeled on **ODN 4** to yield Figure 2-27.

#### 4.2.14 **T<sub>m</sub> Determination of each Orientation Isomer of FR-66979 cross-linked template 3.**

Two stock solutions of **template 3** were set up. Neither strand of each duplex was radiolabeled. Each solution consisted of 2.1nmoles ( 200  $\mu$ g) of each synthetic ODN hybridized to an equimolar amount of its complement. Each lot of 21 nmoles of duplexed ODN was dissolved in 100  $\mu$ l 100 mM Tris (pH = 7.5) to afford DNA stock solutions 210 $\mu$ M in duplex ( 6.5 mM in base pairs). To each duplex ODN stock solution was added 25  $\mu$ l of 50 mM FR-66979 and 6.7  $\mu$ l of 2 M DTT at 0°C. These additions afforded DNA-FR66979 reactions 10mM in drug and 100 mM in thiol. Incubation of each reaction at 25°C for 24 hours was followed by EtOH precipitation followed by resuspension into 200  $\mu$ l of DPAGE loading dye. Samples were loaded to an 8% preparative DPAGE and electrophoresis carried out at 30 Watts for 4 hours. DNA bands corresponding to both fast and slow orientation isomers were visualized by UV-shadowing. The bands were excised and the modified ODNs isolated by the crush and soak method previously described. Following isolation, each band was rigorously desalted by washing with 500  $\mu$ l ddH<sub>2</sub>O in

an Amicon 30 kDa microconcentrator as per manufacturer's protocol. Analogously, a standard non-drug treated duplex was de-salted as well. ODNs were quantitated by OD<sub>260</sub> measurements. Roughly 2 nmoles of each orientation isomer was obtained as was standard non-alkylated duplex. The extinction coefficient of each duplex was assigned as being the sum of the individual strands ( $\epsilon = 575,300$ ). Following desalting, each ODN was lyophilized and resuspended in 100 mM NaCl, 10 mM Tris (pH = 7.0) so as to afford solutions 2  $\mu$ M in duplex. Samples were dissolved immediately prior to  $T_m$  determination so as to avoid inadvertant decomposition of the cross-link. Absorbance versus temperature plots were obtained using 500pmoles (250  $\mu$ l of each ODN) per run. Data points were obtained on a Beckmann Quartz Spectrophotometer ( $\lambda = 260$  nm) in line with a Gilford Thermo Programmer # 2527 heat supply using the following parameters.

Recorder span: 100°C

Heat rate: 1°C/ min.

Upper set point: 99.3°C

Lower set point: -0.1°C

Set point: 26°C or 50°C as designated

Data was plotted using a Gilford Instruments # 6051 chart recorder set to 20 cm/hr. Points of hyperchromicity were obtained from each plot. The  $T_m$  of standard duplex was obtained from a single run. Duplicate runs of each orientation isomer were averaged to obtain the stated  $T_m$  values.

$T_m$  of standard duplex: 69.16 °C

$T_m$  of slow FR-66979 orientation isomer: 77.56 °C

$T_m$  of fast FR-66979 orientation isomer: 79.92 °C

#### **4.2.15. T4 DNA Ligase Experiments: orientation isomer ligation and analysis (Figure 5-11)**

20  $\mu$ g (2 nmoles) of the **ODN 4** was 5'-<sup>32</sup>P labeled as previously described and subjected to purification by 20 % analytical thickness DPAGE. The ODN was visualized by autoradiography, isolated by the crush and soak method described earlier and EtOH

precipitated. To the purified ODN was added an equimolar (2 nmoles) amount of the unlabeled complement **ODN 4'** in ddH<sub>2</sub>O and the sample dried *in vacuo*. The mixture of two ODNs was then resuspended into 22 µl of 200 mM Tris (pH = 7.5), heated to 80 °C for 10 minutes and then allowed to cool to room temperature over the course of 2 hours. To 20 µl of this stock duplex solution (at 0°C) was added 50mM FR66979 ( in ddH<sub>2</sub>O) and 1376 mM DTT so as to afford the reaction 10 mM in FR-66979 and 100 mM DTT. The reaction was allowed to warm to room temperature overnight ( 10 hours) and the contents then EtOH precipitated. Resuspension into 20 µl DPAGE dye was followed by 20 % DPAGE purification of each orientation isomer as previously discussed. Following isolation and precipitation , each cross-link orientation isomer ( approximately 1 µg (50 pmoles) of each) was resuspended into 210 µl of T4 DNA ligase reaction buffer. An equivalent amount of standard non-alkylated duplex was also dissolved into the said amount of reaction buffer. From each ODN stock solution was withdrawn 10µl for use as non-ligase controls. To 100 µl of each remaining ODN was added 4 µl of stock T4 DNA ligase ( 4000 U/µl). Additionally, ligase reactions involving 50 µl of standard ODN + 50 µl of either orientation isomer were set up. These "mixed" ligations were also run in the presence of 4 µl of ligase. All samples were kept at 16 °C for 24 hours followed by EtOH precipitation. Samples were dried *in vacuo* and then resuspended into 10 µl ddH<sub>2</sub>O. From each sample was withdrawn 5 µl and these samples counted by liquid scintillation. Each reaction was brought to an activity of 285.5 cpm/µl using DPAGE loading dye. To each well of a 20 % non-denaturing polyacrylamide gel was loaded an activity of 1710 cpm (6 µl) of each sample. Electrophoresis was carried out at 4°C in 1X TBE running buffer until the xylene cyanol tracking dye was 25 cm. from the gel origin. Autoradiography at -80 °C was carried out for 24 hours to afford the image depicted in Figure 5-11.

#### 4.2.16. **Alu I restriction digestion of FR66979 cross-link orientation isomers of template 7 (Figures 2-31, 5-15)**

As per the T4 DNA ligase experiments outlined above, roughly 1  $\mu$ g of each orientation isomer of FR66979 cross-linked **template 7** substrate was isolated as was purified control duplex. Each purified substrate was resuspended into 1X Alu I restriction enzyme buffer to an activity of 1656.9cpm/ $\mu$ l. From each lot was withdrawn 20 $\mu$ l. From this 20  $\mu$ l aliquot was then withdrawn 2 $\mu$ l to which was added 6  $\mu$ l of AluI quench dye (30 mM EDTA + 0.25% bromophenol blue, 0.25% xylene cyanol in formamide). These control samples were placed at -80°C immediately. To the remaining 18  $\mu$ l of each sample was added 5 $\mu$ l of Alu I restriction endonuclease ( 0.8 U/ $\mu$ l in 1X Alu I reaction buffer) to afford reactions .17U/ $\mu$ l in Alu I. Reactions were kept at 37°C for 12 hours. From each reaction was withdrawn 2 $\mu$ l aliquots at time intervals corresponding to 1,2,5,10,30min., 1 hr., and 12 hrs. respectively. Enzyme reactions were stopped upon addition of 6  $\mu$ l Alu I quench dye to each 2  $\mu$ l aliquot followed by immediate cooling to -80°C. After quenching of the 1 hour samples 20 % DPAGE was carried out on 4  $\mu$ l of each sample. Electrophoresis was carried out at 50 W for 2.5 hours followed by autoradiography of the gel at -80°C for 12 hours. Gel electrophoresis and autoradiography of samples including the 12 hour digestion was carried out in an analogous fashion.(data not shown) Similar experiments were performed using MC cross-linked **template 7** (see Figure 5-15). The MC digestions called for 4.8 units of Alu I in a total reaction volume of of 29 $\mu$ l ( 0.16U/ $\mu$ l of Alu I).

#### 4.2.17. **Cross-linking of template 7 by reductively activated Mitomycin C**

To 40  $\mu$ g(2 nmol.) of ODN 9 5'-labeled **template 7** was added 44  $\mu$ l of 105 mM de-gassed phosphate buffer. The solution had been bubbled through with Ar for 1 h. prior to use. The reaction was brought to 10 mM in MC ( 33% aqueous methanol solution 50 mM in MC). To this was added 4, 4ml aliquots of 277 mM sodium dithionite (in de-gassed

phosphate buffer 105 mM) at 20 minute intervals. Each addition of dithionite effected a purple to yellow color change thus indicating formation of the reduced MC species (the quinone state of MC is purple). Following the complete cycle of dithionite additions, the DNA was EtOH precipitated and then 20% DPAGE purified as was the FR-66979 modified DNA in section 2.4.16..

#### **4.2.18. Diethylpyrocarbonate/Chloroacetaldehyde footprinting of FR-66979 cross-linked template 3 (Figures 2-29, 5-12, 5-13)**

Cross-linking reactions were performed as in T4 DNA ligase reactions with the notable exception that 1 nmole of duplexed substrate was used instead of 2 nmoles/reaction. Two lots (1 nmole each) of duplex were set up. One was brought to 10 mM in FR-66979 + 100 mM DTT while the other was brought to the same volume using ddH<sub>2</sub>O instead of drug and DTT stock solutions. The drug and DTT stock solutions used for cross-linking were 50 mM and 1375 mM respectively. Both control and FR66979 reactions were incubated at room temperature overnight (10 hrs) and then EtOH precipitated and dried *in vacuo*. Samples were purified by 20% DPAGE as previously discussed. The band for single-stranded control was divided in half and to one half was added an equimolar amount of unlabeled complement in 30  $\mu$ l 100 mM Tris (pH = 7.5) and the strands annealed by heating to 80 °C 10 minutes followed by cooling to room temperature for 2 hours. This duplex was then EtOH precipitated and dried *in vacuo*. All samples (orientation isomers of cross-link, single stranded control and duplex control) were resuspended into 50  $\mu$ l ddH<sub>2</sub>O and from each was withdrawn seven 5 $\mu$ l aliquots. Additionally, 7.5  $\mu$ l aliquots were withdrawn from each sample for use in Fe(II)-EDTA footprinting reactions to be electrophoresed with the "hyper-reactive" sequence reactions. To six of the seven 5 $\mu$ l aliquots taken for each sample was added 15  $\mu$ l of 50 mM NaOAc (pH = 5.2). To 3 of these 20  $\mu$ l aliquots of each sample was added 5, 10, and 15  $\mu$ l of diethylpyrocarbonate respectively. To another two aliquots of each sample was added 2 and 5  $\mu$ l chloroacetaldehyde respectively. All six of the NaOAc containing samples for each ODN



(cross-linked species and unmodified ODNs) were aged at room temperature for 1.5 hours followed by EtOH precipitation and a 70 % EtOH rinse. Samples were then dried *in vacuo* and heated to 80°C with 100 µl 1M piperidine. Piperidine was removed by centrifugation under vacuum for approximately 10 hours. Piperidine treated samples were resuspended in 6 µl DPAGE dye, transferred to new eppendorf tubes and counted by liquid scintillation. Samples were then brought to 1000 cpm/µl in activity while the double-stranded DNA control and non-piperidine treated cross-link controls were brought to 500 cpm/µl activity. Maxam-Gilbert G+A and Fe(II)-EDTA reactions were brought to 2700 cpm/µl. Each 20% DPAGE analysis of these reactions required 4 µl of sample per well. Electrophoresis was carried out at 40 W for approximately 6 hours followed by autoradiography at -80°C for 3 days.

#### **4.2.19. SVPD Digestion of FR-66979 alkylated ODN 6 (Figure 3-5).**

FR-66979 alkylated **ODN 6** was obtained *via* reaction of **template 5** (5'-end-labeled on **ODN 6**) with 20mM DTT and 10 mM FR-66979 at room temperature for 12 hours. Reactions were EtOH precipitated and resuspended into 20 µl DPAGE dye. 20% DPAGE was carried out until the xylene cyanol was within 1 inch of the gel bottom. The band corresponding to monoalkylated product was visualized by autoradiography and excised. This corresponded to approximately 1 µg of DNA. The DNA was recovered via electroelution in 0.5X TAE (2h. 500V) and subsequent precipitation. The alkylated material was resuspended into 100 µl DDH<sub>2</sub>O. To 10µl aliquots of alkylated DNA was added 200 µl of SVPD reaction buffer. From standard **ODN 6** stock solution of similar concentration was withdrawn 10µl aliquots and to these too were added 200µl SVPD buffer. Two batches of alkylated DNA and two batches of standard DNA were heated to 90°C 5 minutes prior to enzyme addition. After heating, the DNA samples were segregated such that one series of alkylated and control DNA not previously heated underwent additions of 0.6 and 1.2 units of SVPD. This was repeated for the samples that had been



heated. All SVPD reactions were heated 37°C for 3 h. after which time they were EtOH precipitated, dried and resuspended such that activities of 1000cpm/ml was obtained for each sample. 20% DPAGE was carried out on the samples to afford Figure 3-5.

#### **4.2.20. Analytical Scale Formation of FR66979-DNA Monoadducts (Figure 3-6)**

Monoalkylation studies involved reactions 6.5  $\mu$ M in duplex (thus a stock DNA solution 9  $\mu$ M in duplex was used instead of the 90  $\mu$ M stock used previously). Reactions were set up as outlined for orientational isomer studies (section 4.2.11.) with the exception that reactions were 100 mM in DTT. Reaction conditions and workup were the same as discussed earlier except reaction contents were dissolved in DPAGE dye to afford solutions of 2000 counts/ml activity. Reactions were analyzed by 20% DPAGE (8000 counts/well) followed by autoradiography.

#### **4.2.21. ODN 13 binding by HMG BD peptide 375a (Figure 5-17)**

To 150 $\mu$ g (7nmol for duplex) of **ODN 13** was added 4 $\mu$ l of P<sup>32</sup>-ATP, 10 $\mu$ l of polynucleotide kinase (PNK) buffer (10X) 1 $\mu$ l of 500mM DTT (prepared immediately prior to addition), 6 $\mu$ l of PNK and sterile DDH<sub>2</sub>O to a total volume of 100 $\mu$ l. The reaction was incubated 37°C for 1 hour, followed by EtOH precipitation, sephadex G-50 column chromatography, and subsequent EtOH precipitation. The labeled ODN was resuspended in 35.7 $\mu$ l of 20mM Tris buffer (pH = 7.5) to afford a 100 $\mu$ M stock solution with respect to the duplexed substrate. Annealing was carried out by heating to 80°C for 10 minutes followed by cooling to 25°C over the course of 3 hours. Further cooling to 4°C was carried out for another 2 hours. Utilizing this stock solution of duplexed ODN the following reactions were set up at 4°C. Incubation at 4°C was carried out for 1 hr. and the reactions then incubated at 37°C for another 14 hours.

**Table 4-7.** Reactions of **375a** with FR-66979 and **ODN 13**.

Reaction #	$\mu\text{l}$ ODN	$\mu\text{l}$ FR66979	$\mu\text{l}$ HMG-cys	$\mu\text{l}$ DTT	$\mu\text{l}$ H <sub>2</sub> O
1	5	-	-	-	5
2	5	2 (50mM)*	-	0.5 (2 M)*	2.5
3	5	-	2.5 (2 mM)*	0.5 (2 M)*	2
4	5	2 (50mM)*	2.5 (2 mM)*	0.5 (2 M)*	-
5	5	-	2.5(20 mM)*	0.5 (2 M)*	2
6	5	2 (50mM)*	2.5(20 mM)*	0.5 (2 M)*	-

\* - Denotes concentration of given stock solution. All stock solutions composed of DDH<sub>2</sub>O as solvent unless otherwise noted.

Following incubation at 37°C reactions were EtOH precipitated, dried *in vacuo* and then resuspended in DPAGE loading dye to an activity of 50,000 cpm/ $\mu\text{l}$ . To each lane of a 20% denaturing polyacrylamide gel was loaded 5  $\mu\text{l}$  of each reaction and electrophoresis carried out at 60 W for 4 hours. Autoradiography was performed at -80°C for 2 hours to yield the image depicted by Figure 5-17.

#### 4.2.22. DTT Reactions of 375a complex with ODN 16 (Figure 3-10)

The reactions detailed in 4.2.21. above were performed using **template 8** and the contents loaded to an analytical thickness 20% DPAGE ( poured using the preparative size comb). Electrophoresis of the samples was carried out for 6 hours at 75 Watts, the bands of interest (see table below) were visualized by autoradiography, excised and isolated *via* the crush and soak method described previously (section 4.1.9.) Each DNA was resuspended in DDH<sub>2</sub>O to an activity of 10,000 cpm/ $\mu\text{l}$ . Utilizing these stock solutions, the following reactions with DTT were set up at 25°C and allowed to incubate at this temperature for 45 minutes. To 4  $\mu\text{l}$  of each sample was added either 1  $\mu\text{l}$  DDH<sub>2</sub>O or 1  $\mu\text{l}$  500mM DTT to obtain the concentrations outlined in Table 4-8. The reaction contents and corresponding DTT concentrations were as follows:

**Table 4-8.** DTT concentrations for attempted reduction of **375a** peptide dimer-DNA complexes

Reaction / entry	Reaction Contents	DTT Concentration (in mM)
1	control <b>ODN 16</b>	-
2	control <b>ODN 16</b>	100
3	<b>ODN 16</b> monoadduct w/ FR66979	-
4	<b>ODN 16</b> monoadduct w/ FR66979	100
5	<b>ODN 16</b> gel-shifted adduct	-
6	<b>ODN 16</b> gel-shifted adduct	100
7	<b>ODN 16</b> gel-shifted adduct from FR66979 reaction	-
8	<b>ODN 16</b> gel-shifted adduct from FR66979 reaction	100

Following incubation at 25°C for 45 minutes, each reaction was EtOH precipitated and resuspended in 15 µl of DPAGE loading dye. To each well of a 20% DPAGE was added 5 µl of each dye-reaction mixture (without heating prior to loading). The faceplate of the gel was heated for 3 minutes to about 90°C with a hand-held heat gun with concomittant electrophoresis. Electrophoresis was carried out at 60 Watts until the xylene cyanol was 10 cm down the gel. Autoradiography was performed at -80 °C for 8 hours to yield the image depicted in Figure 3-10.

#### 4.2.23. Differential radiolabeling of template 8 and reactions with **375a** (Figure 3-11).

Two stock solutions of **template 8** were used; one in which **ODN 16** was 5' labeled; and the other in which **ODN 16'** was labeled. Each duplex (4 nmol.) was dissolved in 41µl of 20 mM Tris (pH=8.0) so as to afford DNA stock solutions 0.1mM in duplex ( 3.7 mM in base pairs). Using the peptides **375a** and **375b** and DTT, the following reactions were set up and allowed to incubate 37°C for 12 hours.

**Table 4-9.** Reactions of HMG peptides **375a** and **375b** with **template 8**.

entry/reaction	$\mu\text{l}$ DNA <sup>a</sup>	$\mu\text{l}$ <b>375a</b>	$\mu\text{l}$ <b>375b</b>	$\mu\text{l}$ DTT	$\mu\text{l}$ DDH <sub>2</sub> O
1	5 (ODN 16)	-	-	-	5
2	5 (ODN 16)	2.5 (2mM)	-	1(1M)	1.5
3	5 (ODN 16)	2.5 (20mM)	-	1 (1M)	1.5
4	5 (ODN 16)	-	2.5 (2mM)	1(1M)	1.5
5	5 (ODN 16)	-	2.5 (20mM)	1 (1M)	1.5
6	5 (ODN 16')	-	-	-	5
7	5 (ODN 16')	2.5 (2mM)	-	1(1M)	1.5
8	5 (ODN 16')	2.5 (20mM)	-	1 (1M)	1.5
9	5 (ODN 16')	-	2.5 (2mM)	1(1M)	1.5
10	5 (ODN 16')	-	2.5 (20mM)	1 (1M)	1.5

<sup>a</sup> The notation in parentheses indicates which strand of **template 8** bore the 5'-end radiolabel. All values in parentheses represent stock solution concentrations.

Following incubation, samples were EtOH precipitated, dried, and then resuspended into DPAGE dye to an activity of 50,000 cpm/ml. Electrophoretic analysis as in the preceding section led to the autoradiogram depicted in Figure 3-11.

#### 4.2.24. Piperidine digestion of ODN 16 and ODN 16' complexes with **375a** and **375b** (Figure 3-12, 5-18)

The slow mobility adducts obtained from section 4.2.23, were isolated *via* 10% DPAGE purification, isolated by crush and soak and then EtOH precipitated. Each slow mobility band and corresponding **ODN 16** and **ODN 16'** standards were resuspended in DDH<sub>2</sub>O to an activity of 8000 cpm/ml. From each sample isolated (peptide complexes and standards) was withdrawn 4 ml and to it was added 200  $\mu\text{l}$  1M piperidine. To another 4  $\mu\text{l}$  aliquot of each sample isolated was added 12  $\mu\text{g}$  (1 nmol) of **ODN 18** as a competitor for piperidine/peptide mediated DNA cleavage. This accounted for a 20 fold molar excess of unlabeled competitor DNA. To these samples was also added 200  $\mu\text{l}$  1M piperidine. All reactions were then heated to 90°C for 25 minutes and the reactions then work-up as described in section 4.1.10. Following lyophilization, each reaction was dissolved in

DPAGE dye to an activity of 500 cpm/ml. 20% DPAGE analysis of the resulting cleavage patterns followed electrophoresis at 50 Watts for 4 hours. The activities loaded to gels depicted in Figure 3-10 are as follows: DNA and DNA-peptide controls: 1250 cpm/well, Maxam-Gilbert G: 3000 cpm/well, G+A: 6000 cpm/well, All piperidine reactions 2390 cpm/well. Activities loaded to Figure 5-18 autoradiogram are the same except only 2319 cpm/well was loaded per piperidine reaction.

#### 4.2.25. **FR-66979-mediated DNA-peptide cross-linking of template 8 and HMG BD peptide 376 (Figure 3-13).**

To 10 nmoles of 5'-<sup>32</sup>P-end-labeled oligos **ODN 16** and **ODN 16'** annealed to their correspondingly unlabeled complements was added 100  $\mu$ l 200mM Tris (pH = 7.5). This resulted in stock solutions 0.1mM in **template 8**. The ODNs were annealed as described previously and then divided into two 50 $\mu$ l aliquots. To one 50  $\mu$ l aliquot for each differently radiolabeled duplex was added 50 mM FR-66979 and 2M DTT to final concentrations of 10 mM drug and 100 mM thiol. To the other 50  $\mu$ l batches of each duplex was added DDH<sub>2</sub>O instead of drug. The same volume of thiol was added so as to achieve a final concentration of 100 mM DTT. Reactions were incubated at 25°C for 16 h. after which time the reactions were passed through a Sephadex G-50 size exclusion column and the first radioactive fraction of each reaction collected and EtOH precipitated. The pellets were resuspended into 100  $\mu$ l DDH<sub>2</sub>O once more and EtOH precipitated once more to ensure desalting. The samples were then dried *in vacuo* and then resuspended into 250  $\mu$ l 10 mM Tris (pH = 8.0). This afforded stock solutions of FR-66979 modified DNA 20  $\mu$ M in duplex (740 $\mu$ M in base pairs). The following DNA-peptide reactions were set up at room temperature and allowed to incubate 37°C for 12-24 hours. These reactions were done in glass-lined screw top autosampler vials (100  $\mu$ l volume) due to the known tendency of the peptide to adhere to the inside of plastic eppendorf tubes.

**Table 4-10** Reactions of FR-66979 alkylated **template 8** with HMG peptide **376**

entry/reaction	$\mu\text{l}$ <b>314</b> modified <b>template 8<sup>a</sup></b>	$\mu\text{l}$ HMG peptide <b>376</b>	$\mu\text{l}$ DDH <sub>2</sub> O
1	20 (ODN 16')	-	20
2	20 (ODN 16')	20 (100 $\mu\text{M}$ )	-
3	20 (ODN 16')	-	20
4	20 (ODN 16')	20 (100 $\mu\text{M}$ )	-
5	20 (ODN 16)	-	20
6	20 (ODN 16)	20 (100 $\mu\text{M}$ )	-
7	20 (ODN 16)	-	20
8	20 (ODN 16)	20 (100 $\mu\text{M}$ )	-

<sup>a</sup> ODN in parentheses denotes which strand of **template 8** was radiolabeled. Other parentheses values denote stock solution concentration.

Following 37°C incubation, 5  $\mu\text{l}$  aliquots were withdrawn from each reaction and added to 15  $\mu\text{l}$  of DPAGE dye. Samples were then analysed by 20% DPAGE. It is noteworthy that whether or not the samples were heated to 90°C for 3 minutes prior to loading did not affect the amount of gel retarded material in the peptide + drug reactions. To ensure denaturation, samples were typically loaded and then the gel faceplate heated with a heat gun during the first 5 minutes of electrophoresis.

#### 4.2.26. Ligand exchange reactions of ODN 16 and ODN 16' drug-mediated complexes with 376 (Figure 5-19)

The entire reaction contents from section 4.2.25. were added to an equal volume of DPAGE loading dye and then loaded to an analytical thickness 20% DPAGE. The DNAs 0.4 mm above the gel-shifted bands were purified as described previously and then subjected to re-labeling with terminal deoxynucleotidyl transferase and  $\alpha$ -<sup>32</sup>P-ddATP. The radiolabeled bands were then EtOH precipitated, resuspended and passed through a Sephadex G-50 column. The first radiolabeled fractions were collected and EtOH precipitated. It is particularly noteworthy that these bands did not contain the 5'-end-

labeled material as this would interfere with later sequencing methods. Additionally, single-stranded 3'-end-labeled **ODN 16** and **ODN 16'** were purified on the same gel and used as standards. Each gel-shifted ODN was then dissolved into 100  $\mu$ l DDH<sub>2</sub>O. From each peptide-DNA complex was then withdrawn 10  $\mu$ l and using these aliquots, the following reactions with unlabeled duplex competitor **template 8** set up.

**Table 4-11.** Reaction volumes and concentrations of DNA-exchange reactions of **ODN 16/ODN 16'** complexes with **376** and unlabeled duplex **template 8**.

entry/reaction	$\mu$ l <b>376</b> -DNA complex	$\mu$ l "cold" <b>template 8</b>	$\mu$ l 10mM Tris	["cold" <b>template 8</b> ]	% retention of gel-shift adduct <sup>a</sup>
1	10 (ODN 16)	-	10	-	N/A
2	10 (ODN 16)	-	10	-	74.6
3	10 (ODN 16)	10 (0.5 mM)	-	0.25 $\mu$ M	62.4
4	10 (ODN 16)	10 (5 $\mu$ M)	-	2.5 $\mu$ M	77.4
5	10 (ODN 16)	10 (50 $\mu$ M)	-	25 $\mu$ M	74.4
6	10 (ODN 16)	10 (500 $\mu$ M)	-	250 $\mu$ M	75.8
7	10(ODN 16')	-	10	-	N/A
8	10(ODN 16')	-	10	-	65.0
9	10(ODN 16')	10 (0.5 $\mu$ M)	-	0.25 $\mu$ M	64.8
10	10(ODN 16')	10 (5.0 $\mu$ M)	-	2.5 $\mu$ M	67.7
11	10(ODN 16')	10 (50 $\mu$ M)	-	25 $\mu$ M	70.0
12	10(ODN 16')	10 (500 $\mu$ M)	-	250 $\mu$ M	66.7

Values in parentheses denote stock solution concentrations. In the case of the **376**-DNA complexes, the parentheses denote which complex was used. Values based on band excision and subsequent liquid scintillation counting.

All reactions were approximately 0.2  $\mu$ M in peptide-DNA complex. This value was based on the fact that each reaction in the preceeding section contained 20 $\mu$ l of a 20pmol/ $\mu$ l DNA solution. From each reaction was obtained about 10% (by LSC) yield of the DNA-peptide conjugate. This would equate to 40pmol of the gel-shifted material. After radiolabeling and purification, this complex was resuspended into 100  $\mu$ l DDH<sub>2</sub>O thus affording 0.4 pmol of



complex per  $\mu\text{l}$ . Ten  $\mu\text{l}$  of this solution would afford 4 pmol to be ultimately dissolved in a total of 20  $\mu\text{l}$  for each "exchange" reaction. In short, each ODN-peptide stock solution was 0.4  $\mu\text{M}$ . All exchange reactions were incubated 37°C for 24 h. after which time 5 $\mu\text{l}$  aliquots were withdrawn and placed in 10  $\mu\text{l}$  DPAGE dye. Samples were heated 90°C 2 minutes prior to DPAGE analysis. 20% DPAGE analysis was carried out similarly to section 4.2.25. to yield the image in Appendix Figure 5-19.

#### **4.2.27. Piperidine digestion of FR-66979 mediated ODN 16 and ODN 16' complexes with 376 (Figure 5-20)**

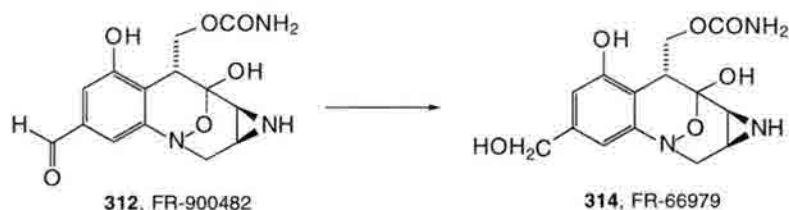
Using the remainder of the gel-shifted complexes in section 4.2.26 piperidine digestions were set up. 30  $\mu\text{l}$  of each complex was lyophilized to dryness to each was then added 100  $\mu\text{l}$  1M piperidine. Analogous control digestions were run alongside the peptide reactions. Samples were heated and then worked up as previously described. Following lyophilization each sample was resuspended into 10  $\mu\text{l}$  DPAGE dye, transferred to a new eppendorf tube and counted by LSC. Samples were then brought to an activity of 1000 cpm/ $\mu\text{l}$ . Standards for both native DNA and peptide complexes were brought to an activity of 725 cpm/ $\mu\text{l}$ , while G and G+A lanes were brought to activities of 1000, and 2000 cpm/ $\mu\text{l}$  respectively. The activities loaded to gels depicted in Figure 5-20 are as follows: DNA and DNA-peptide controls: 725 cpm/well, Maxam-Gilbert G: 2000 cpm/well, G+A: 4000 cpm/well, All piperidine reactions 3000 cpm/well. Electrophoresis was carried out at 60 Watts for 3.5 hours. Autoradiography was then conducted at -80°C for 18 h. to afford the image Figure 5-20. Notably, no prominent base labile sites were seen in peptide containing digestions that did not appear in the control digestions.

**4.2.27. Mass Spectral analysis of FR-66979 mediated ODN 16 and ODN 16' complexes with 376 (Figure 3-14)**

To 100 nmoles of **ODN 16** (unlabeled) was added 100 nmoles of **ODN 16'** The oligos were EtOH precipitated as described earlier and then dried *in vacuo*. Resuspension into 1 ml of 200 mM Tris (pH = 7.5) was performed and the strands annealed to each other by heating to 80 °C 10 min. and then cooling to room temperature over the course of a 2 h. time frame. To the resulting duplex was added 50 mM FR-66979 and 2M DTT so as to afford a final concentration of 10mM FR-66979 and 100 mM DTT. Reactions were kept at room temperature for 24 h. and the samples then EtOH precipitated. Resulting pellets were resuspended in 100 µl DDH<sub>2</sub>O and EtOH precipitation effected once again. This cycle was performed once more and the sample then dried *in vacuo*. The presumably alkylated species was then resuspended into 5 mls. 10mM Tris (pH = 8.0) so as to afford a stock solution of 20pmol/µl. To 4.5 mls. of this solution was added an equal volume of 0.1 mM **376** in DDH<sub>2</sub>O. To the remaining 0.5 ml of DNA was added an equal volume of DDH<sub>2</sub>O. Both reactions were heated 37°C for 24 hours followed by cooling to 4°C and subsequent butanol extraction down to a volume of 500 µl. To each 500 µl batch was added an equal volume of DPAGE dye and the samples loaded to a preparative 20% DPAGE. Samples were then worked up as described in section 4.2.12. Negative ion electrospray mass spectral analysis yielded the image depicted by Figure 3-14.

### 4.3. Representative Synthetic Methods

#### 4.3.1. FR-66979 (314) Pd/C Reduction methods



To a stirred solution of **312** (28.5 mgs., 09 mmol.) in de-gassed MeOH (2 mls.) was added 5 mgs. 10% Pd/C and the mixture bubbled through with H<sub>2</sub> at 1 atmosphere. The reaction was monitored periodically by TLC (4:9 MeOH:CH<sub>2</sub>Cl<sub>2</sub>). After 3 hours no **312** was visible by TLC and the reaction then passed through a pad of celite to remove the catalyst. Notably, both crude and PTLC purified (4:9 MeOH: CH<sub>2</sub>Cl<sub>2</sub>) samples gave rise to identical spectral characteristics and HPLC traces. PTLC purification afforded FR-66979 as a white solid in typical yields of 60 %. Notably, reduction at 60 psi or 90 psi afforded crude FR-66979 which possessed identical HPLC <sup>1</sup>H NMR, TLC and UV characteristics to all other samples of FR-66979. R<sub>f</sub> (4:9 MeOH:CH<sub>2</sub>Cl<sub>2</sub>) 0.24, 0.50

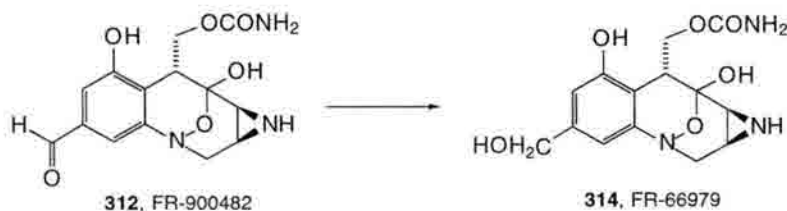
<sup>1</sup>H NMR (300 MHz.) (*major diastereoisomer* in D<sub>2</sub>O) 2.56 (m, 1H), 2.58 (d, J = 6.67 Hz., 1H) 3.31 (d, J = 5.7 Hz., 1H), 3.59 (d, J = 3.9 Hz. 2H), 4.40 (2H, s), 4.51 ( d , J = 11.3 Hz, 1H), 4.95 ( dd, J = 11.3, 4.8 Hz. 1H), 6.38 ( d, J = 1.35 Hz., 1H), 6.52 (d, J = 1.23 Hz., 1H).

IR (KBr) 3400, 1647, 1560, 1081, 670 cm<sup>-1</sup>

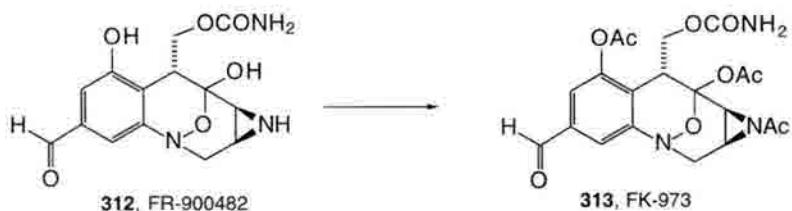
MS (ES) (% Total ion count) 324.2 (M+, 9.94), 279.2 (0.18), 214.1 (.79), 105 (4.20)

UV ( H<sub>2</sub>O); λ<sub>max</sub> nm. 215

#### 4.3.2. FR-66979 (314) $\text{NaBH}_4$ Reduction methods



To a stirred solution of **312** (29.2 mgs., 0.091 mmol.) in MeOH (2.9 mls.) was added 23 mgs.  $\text{NaBH}_4$  at  $-78^\circ\text{C}$ . The reaction was stirred for 15 minutes at  $-78^\circ\text{C}$ . TLC analysis (5:2  $\text{CH}_2\text{Cl}_2$ : MeOH) revealed consumption of starting material. To the reaction was then added saturated  $\text{NH}_4\text{Cl}$  (20mls) and the reaction allowed to warm to  $25^\circ\text{C}$ . The reaction contents were passed over a C18 Sep-Pak and the adsorbed compound washed with water. The product was eluted off the column with MeOH. The methanol was rotovapped off and the sample either PTLC purified as for the Pd derived material or used crude for the DNA-cross-linking reactions or HPLC analysis. This material (crude or purified) was identical to the material derived by catalytic hydrogenation.

4.3.3. Triacetylation of **312** to afford **313**

To a stirred solution of **312** (79.2 mgs., 25 mmol.) in pyridine (6.3 mls.) was added 3.2 mls. acetic anhydride at 25°C. The reaction was stirred overnight at room temperature. TLC analysis (1:1 Hexanes:MeOH; 1% Et<sub>3</sub>N) revealed consumption of starting material. The acetic anhydride/pyridine mixture was removed in vacuo and the resulting oil taken up in 5 mls. 1:1 EtOAc:CH<sub>2</sub>Cl<sub>2</sub>. To this was added 20mls. H<sub>2</sub>O. The resulting mixture was extracted 3 times with 20mls. EtOAc each time. The resulting organic was washed with saturated NaCl solution 3 times and then dried over anhydrous sodium sulfate. The sample was dried *in vacuo* and PTLC purified (15:1 CH<sub>2</sub>Cl<sub>2</sub>:MeOH) to afford **313** in an overall yield of 70% (78.2 mgs. recovered-major diastereoisomer) as a lightly colored yellowish powder.

<sup>1</sup>H NMR (300 MHz.) (*major diastereoisomer* in D<sub>2</sub>O) 1.75 (s, 3H), 2.13 (s, 3H) 2.26 (s, 3H), 2.98 (d, J = 6.48 Hz., 1H), 4.40 (2H, s), 3.62 (d, J = 6.44 Hz, 1H), 3.67 (dd, J = 6.6, 2.65 Hz. 1H), 3.87 (q, J = 15.2 Hz., 2H), 4.22 (dd, J = 2.66, 11.91 Hz., 1H), 4.38 (dd, J = 11.91, 5.3 Hz., 1H), 7.25 (d, J = 1.39 Hz., 1H), 7.31 (s, J = 1.42 Hz., 1H) 9.69 (s, 1H)

IR (KBr) 3600-3400, 1709, 1569(w), 1453, 1325, 1209 cm<sup>-1</sup>

MS (ES) (% Total ion count) 448.5 (M+, 0.46), 465.1 (M+NH<sub>4</sub>, 4.91), 391.3 (1.19)

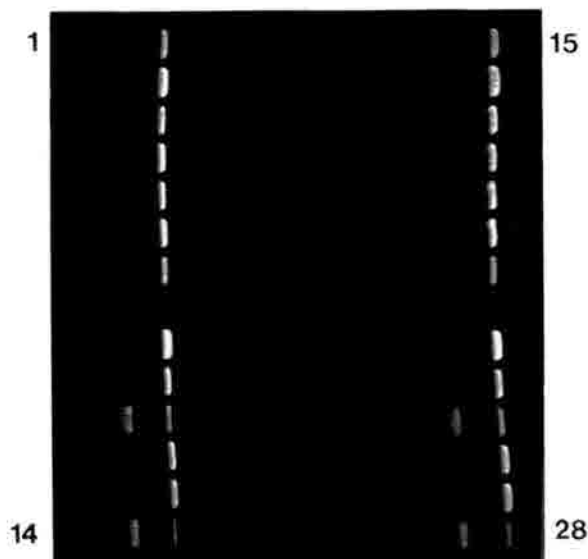
## APPENDICES

*Appendix Listing*

<b>Figure 5-1</b>	Desferal and Fe <sup>2+</sup> vs. Fe <sup>3+</sup> reactions of <b>312</b> with linearized pBR322	299
<b>Table 5-1.</b>	Summary of ISC yields from Figure 5-1.	300
<b>Figure 5-2</b>	Large format image of Fig. 2-14 (Fe(II)-EDTA footprinting of FR-66979 cross-linked <b>templates 1 and 2</b> )	301
<b>Figure 5-3</b>	Fe(II)-EDTA Footprinting for FR-900482, FR-66979, FK-973 cross-linked <b>templates 1 and 2</b>	302
<b>Figure 5-4</b>	Large format image of Fig. 2-15 (Fe(II)-EDTA footprinting of FR-66979 cross-linked <b>templates 1 and 2 - ODN 3</b> 5'-labeled)	303
<b>Figure 5-5</b>	Reactions of <b>template 1</b> with HPLC fractionated crude FR-66979	304
<b>Figure 5-6</b>	Reactions of <b>template 1</b> with FR-66979 derived mitosenes <b>352, 353</b>	305
<b>Figure 5-7</b>	Reactions of FR-66979, FR-900482, FK-973 with <b>template 3</b>	306
<b>Figure 5-8</b>	Reactions of FR66979 with self-complementary <b>ODN 7</b>	307
<b>Figure 5-9</b>	Fe(II)-EDTA Footprint analysis of orientation isomers of FR-66979 cross-linked <b>template 3</b>	308
<b>Figure 5-10</b>	UV vs. Temp. plots for orientation isomers of FR-66979 cross-linked <b>template 3</b>	309
<b>Figure 5-11</b>	T4 DNA Ligase reactions with orientation isomers of FR-66979 cross-linked <b>template 3</b>	310
<b>Figure 5-12</b>	DEPC hyperreactivity reactions of FR-66979 cross-link orientation isomers of <b>template 3</b> (5'-end-labeled on <b>ODN 4</b> strand)	311

<b>Figure 5-13</b> Chloroacetaldehyde (CAA) reactions with orientation isomers of cross-linked <b>template 3</b>	312
<b>Figure 5-14</b> Verification of C10 connectivity to slow orientation isomer of FR-66979 cross-linked <b>template 7</b>	313
<b>Figure 5-15</b> Alu I digestions of MC cross-linked <b>template 7</b> orientation isomers	314
<b>Figure 5-16</b> Non-Denaturing gel analysis of FR-66979 monoalkylated <b>template 3</b>	315
<b>Figure 5-17</b> Band-shifting of self-complementary <b>ODN 13</b> with cysteinylated BD peptide <b>375a</b>	316
<b>Figure 5-18</b> Piperidine digestions of <b>375a-ODN 16'</b> (5'-end-labeled) complex	317
<b>Figure 5-19</b> DNA exchange of radiolabeled drug-dependent DNA-peptide cross-link	318
<b>Figure 5-20</b> Piperidine digestions of <b>376-ODN 16'</b> and <b>376-ODN 16</b> drug-mediated complexes (each ODN 3' end-labeled)	319



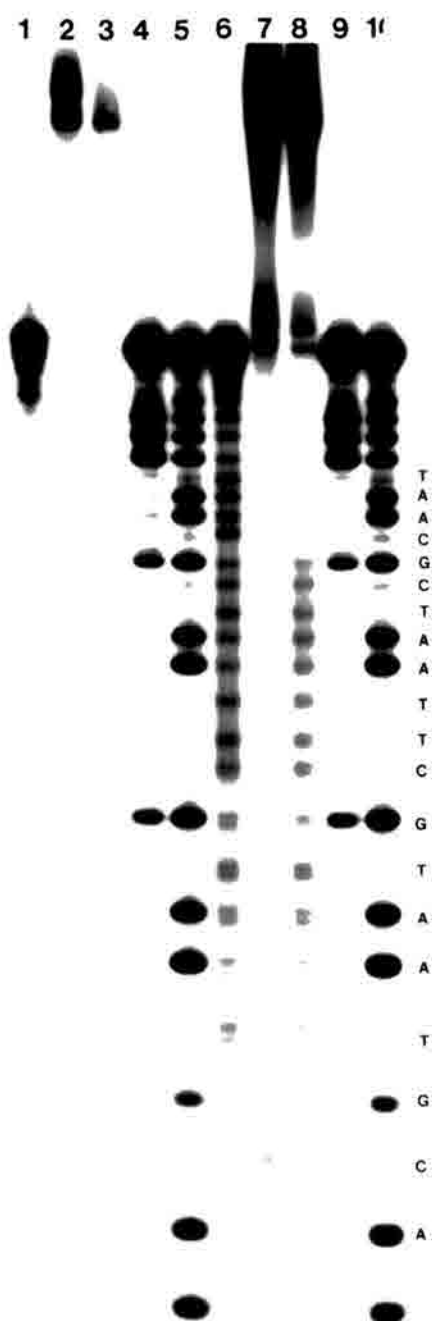


**Figure 5-1.** Reactions of **312** with linearized pBS+ in the presence of Fe(III)-EDTA and Fe(II)-EDTA in the absence and presence of desferal. All reactions carried out in 10mM phosphate buffer, pH 8.0. Gel origin is to the left of wells therefore the direction of electrophoresis is from left to right. Note that two series of wells were loaded; lanes 1-14 represent the first series of loadings and lanes 15-28 represent the second series of loadings. Reactions were incubated 37°C 4 hours prior to electrophoresis. **Lane 1**) DNA control ; **Lane 2**) 10mM **292** ; **Lane 3**) 0.2  $\mu$ M Fe(III)-EDTA; **Lane 4**) 2.0  $\mu$ M Fe(III)-EDTA; **Lane 5**) 20  $\mu$ M Fe(III)-EDTA; **Lane 6**) 0.2  $\mu$ M Fe(II)-EDTA; **Lane 7**) 2.0  $\mu$ M Fe(II)-EDTA; **Lane 8**) 20  $\mu$ M Fe(II)-EDTA. **Lane 9**) 10mM **312** + 0.2  $\mu$ M Fe(III)-EDTA ; **Lane 10**) 10mM **312** + 2.0  $\mu$ M Fe(III)-EDTA; **Lane 11**) 10mM **312** + 20  $\mu$ M Fe(III)-EDTA; **Lane 12**) 10mM **312** + 0.2  $\mu$ M Fe(II)-EDTA; **Lane 13**) 10mM **312** + 2.0  $\mu$ M Fe(II)-EDTA; **Lane 14**) 10mM **312** + 20  $\mu$ M Fe(II)-EDTA; **Lanes 15-28**; same loadings as **lanes 1-14** except these reactions also contained 10 $\mu$ M desferal.

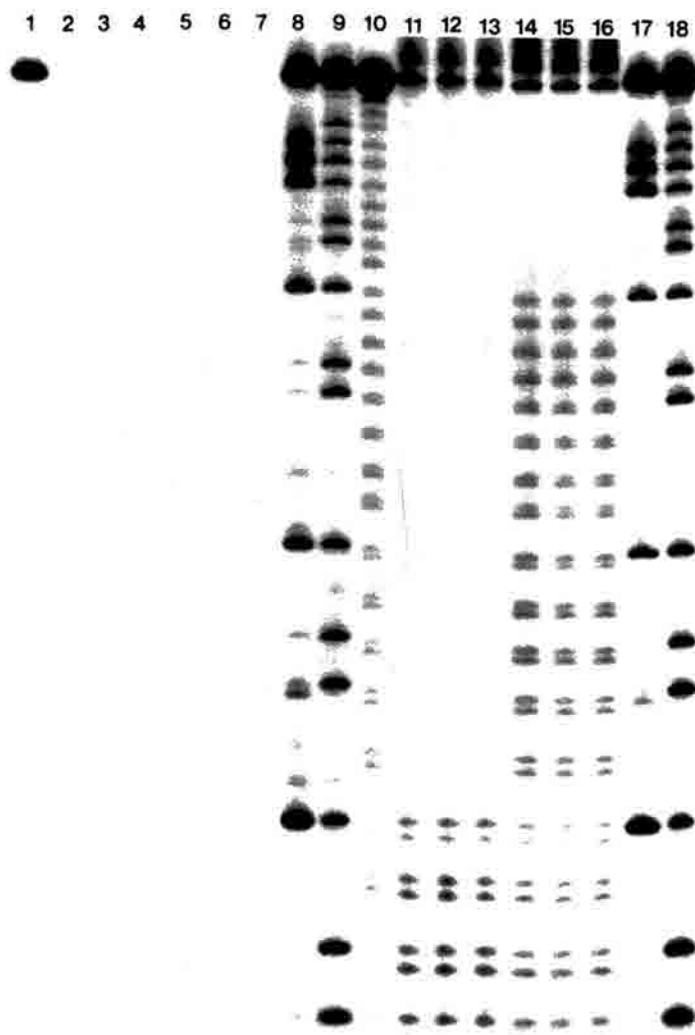
**Table 5-1.** Reactions of **312** in the presence of Fe(III)-EDTA and Fe(II)-EDTA

Entry/lane	[ <b>312</b> ]	[Fe(III)- EDTA]	Fe(II)-EDTA	% ISC <sup>a</sup>	% ISC <sup>b</sup>
1	-	-	-	-	-
2	10mM	-	-	8.3	5.9
3	-	0.2 $\mu$ M	-	-	-
4	-	2.0 $\mu$ M	-	-	-
5	-	20.0 $\mu$ M	-	-	-
6	-	-	0.2 $\mu$ M	-	-
7	-	-	2.0 $\mu$ M	-	-
8	-	-	20.0 $\mu$ M	decomp. <sup>c</sup>	decomp. <sup>c</sup>
9	10mM	0.2 $\mu$ M	-	16.7	11.6
10	10mM	2.0 $\mu$ M	-	28.8	16.6
11	10mM	20.0 $\mu$ M	-	59.0	61.3
12	10mM	-	0.2 $\mu$ M	10.9	16.3
13	10mM	-	2.0 $\mu$ M	28.9	26.3
14	10mM	-	20.0 $\mu$ M	70.3	74.5

<sup>a</sup> % ISC in the absence of desferal; <sup>b</sup> % ISC in the presence of 10mM desferal (represented by lanes 15-28 in Figure 5-1; <sup>c</sup> denotes decomposition resulting from Fenton/Haber-Weiss strand scission events mediated by Fe(II)-EDTA.



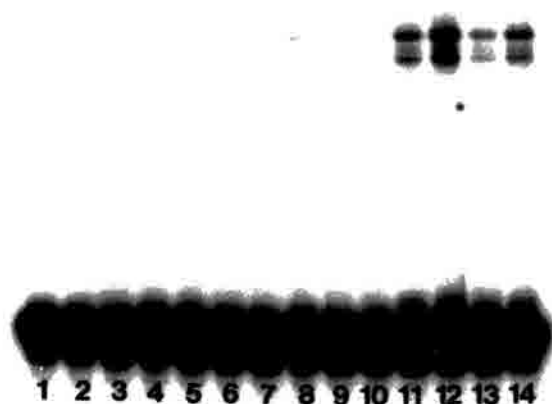
**Figure 5-2.** Autoradiogram of Fe(II)-EDTA footprinting of FR-66979 cross-linked **templates 1** and **2** (labeled at 5' terminus of ODNs **1** and **2** respectively). **Lanes 1-3**, standard DNA, cross-linked **template 1**, cross-linked **template 2**; **lanes 4 and 9** Maxam-Gilbert G; **lanes 5,10** Maxam-Gilbert G+A. **Lane 6**, 1mM Fe(II)-EDTA control; **Lane 7**, cross-linked **template 1** after 1mM Fe(II)-EDTA digestion; **Lane 8**, cross-linked **template 2** after 1mM Fe(II)-EDTA digestion. Slow mobility cross-link standards in **lanes 2 and 3** near gel origin.



**Figure 5-3.** Autoradiogram of Fe(II)-EDTA footprinting of cross-linked 5' end-labeled 5'-TTTATTAACGTAATGCTTAATCGCAATGGGATT-3' (ODN 1) and 5'-TTTATTAACITAATGCTTAATCGCAATGGGATT-3' (ODN 2) to their mutual complement ODN 3. **Lane 1** is standard 5'-labeled **template 1**. **Lanes 2,3,4** are **template 1** cross-linked with FR-900482 (312), FR-66979 (314), and FK973 (313) respectively. **Lanes 5,6,7**, are **template 2** cross-linked with 312, 314, and 313 respectively. **Lanes 8,9,10** are Maxam-Gilbert G, G+A, and 1 mM Fe(II)-EDTA lanes respectively. **Lanes 11,12,13** are **template 1** cross-linked by 312, 314, and 313 respectively, followed by Fe(II)-EDTA digestion. **Lanes 14,15,16**, are **template 2** cross-linked by 312, 314, 313 respectively, followed by Fe(II)-EDTA digestion. **Lanes 17** and **18** are Maxam-Gilbert G and G+A lanes respectively.



**Figure 5-4.** Autoradiogram of Fe(II)-EDTA footprinting of FR-66979 cross-linked **template 1** and **template 2** ( $^{32}\text{P}$  labeled at 5' terminus of ODN 3). **Lanes 1-3**, standard DNA, cross-linked **template 1**, cross-linked **template 2**; **lanes 4 and 5** Maxam-Gilbert G, G+A respectively. **Lane 6**, 1mM Fe(II)-EDTA control; **Lane 7**, cross-linked **template 1** after 1mM Fe(II)-EDTA digestion; **Lane 8**, cross-linked **template 1** after 1mM Fe(II)-EDTA digestion. **Lanes 9 and 10** Maxam-Gilbert G, G+A respectively. Slow mobility cross-link standards in **lanes 2 and 3** (outside of the sequencing region depicted) may be seen near gel origin.

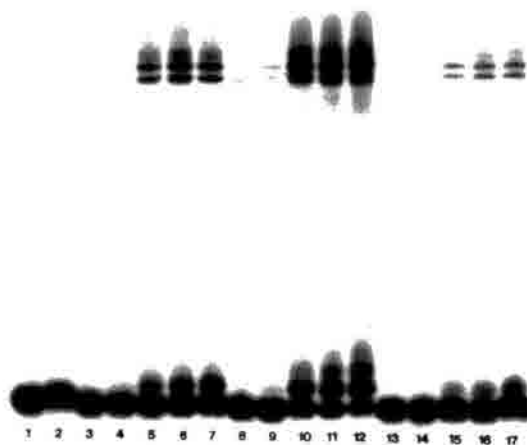


**Figure 5-5.** Autoradiogram of reactions of HPLC fractionated crude FR-66979 (**314**) from catalytic hydrogenation with **template 1** ( $^{32}\text{P}$  labeled at 5' terminus of **ODN 1**). **Lanes 1,2;** standard DNA, 10mM DTT control; **lane 3;** 1mM fraction A/B mixture **Lane 4,** 1mM fraction A/B mixture + 1 mM DTT; **Lane 5;** 1mM fraction C ; **Lane 6;** 1mM fraction C + 1 mM DTT; **Lane 7;** 1mM fraction D **Lane 8;** 1mM fraction D + 1mM DTT **Lane 9;** 10 mM fraction A/B mixture; **Lane 10;** 10 mM fraction A/B mixture + 10 mM DTT; **Lane 11;** 10 mM fraction C; **Lane 12;** 10 mM fraction C + 10 mM DTT; **Lane 13;** 10 mM fraction D; **Lane 14;** 10 mM fraction D + 10 mM DTT.



**Figure 5-6.** Autoradiogram of reactions of **352/353** with **template 3** ( $^{32}\text{P}$  labeled at 5' terminus of **ODN 4**). **Lanes 1,2**; standard DNA, 100mM DTT control; **lane 3**; 10mM FR-66979 **Lane 4**, 10 mM FR-66979 + 100 mM DTT; **Lane 5**; 20 mM FR-66979 ; **Lane 6**; 20 mM FR-66979 + 100 mM DTT; **Lane 7**; 10 mM **352/353** **Lane 8**; 10 mM **352/353** + 100mM DTT **Lane 9**; 20 mM **327/328** ; **Lane 10**; 20 mM **352/353** + 100 mM DTT.

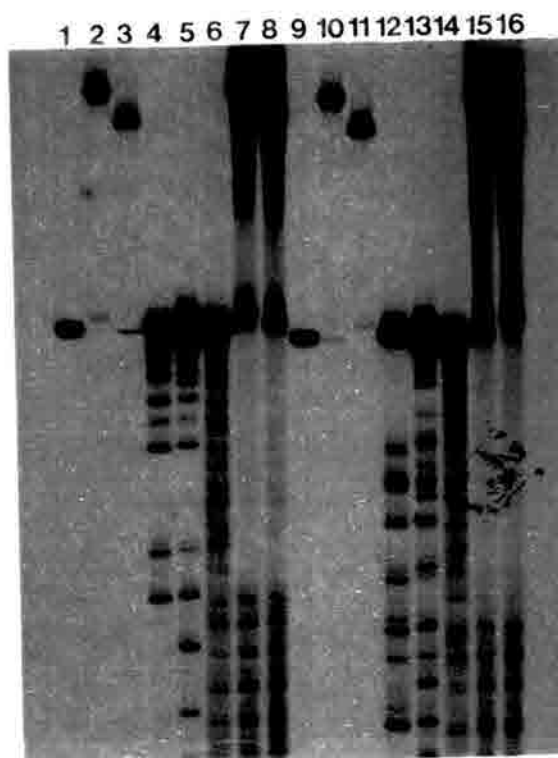




**Figure 5-7.** Autoradiogram of reactions of **312-314** with **template 3** ( $^{32}\text{P}$  labeled at 5' terminus of **ODN 4**). **Lanes 1,2**; standard DNA, 400mM DTT control; **lane 3**; 10mM **312** ;**Lanes 4-7** 10mM **312** + 10, 100, 200,400 mM DTT respectively; **lane 8**; 10mM **314** ;**Lanes 9-12** 10mM **312** + 10, 100, 200,400 mM DTT respectively; **lane 13**; 10mM **313** ;**Lanes 14-17** 10mM **313** + 10, 100, 200,400 mM DTT respectively.

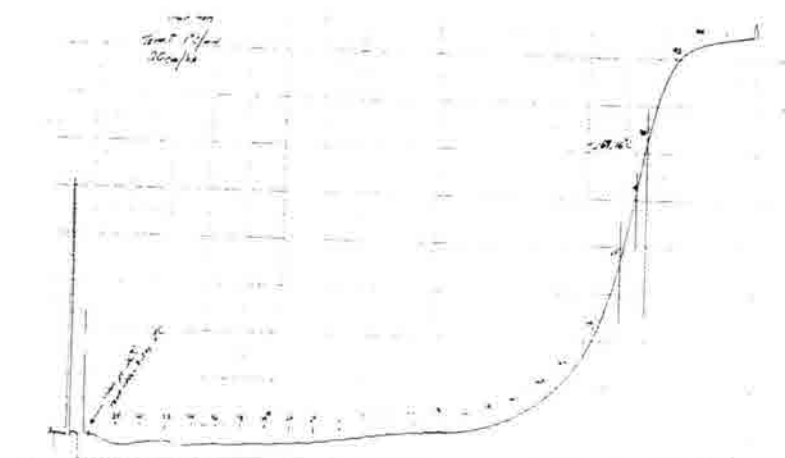


**Figure 5-8.** Reactions of reductively activated **314** with **template 3** (lanes 1,2), **template 4** (lanes 3,4) and the self-complementary **ODN 7** (lanes 5,6). **Lanes 1,2**; standard DNA, 10mM FR-66979 crude ; **Lane 3, 4**; standard DNA, 10mM FR-66979 crude; **Lanes 5, 6** standard DNA, 10mM FR-66979 crude

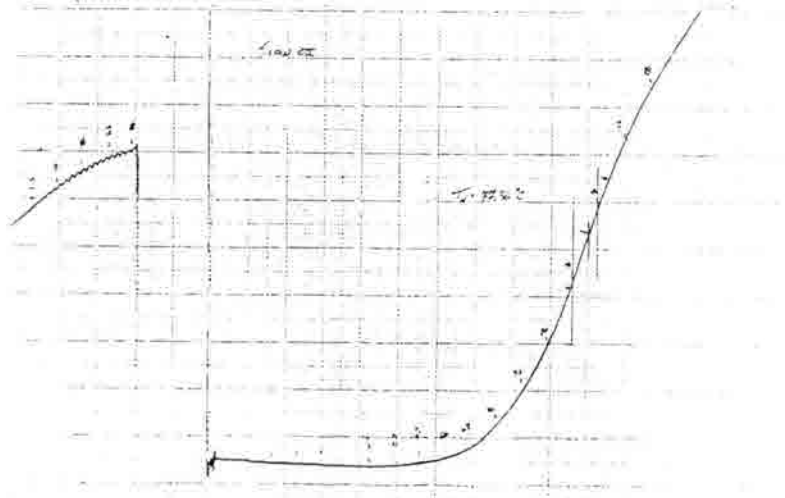


**Figure 5-9.** Fe(II)-EDTA footprinting of FR-66979 (**314**) cross-link orientation isomers of **templates 1** (lanes **1- 8** 5'-labeled on **ODN 4** whereas **lanes 9-16** are 5' labeled on **ODN 4'**) **Lanes 1-3**, standard DNA, slow cross-link, and fast cross-links respectively; **lanes 4,5** Maxam-Gilbert G and G+A lanes respectively; **lane 6** 1mM Fe(II)-EDTA control; **Lanes 7 and 8**, slow and fast orientation isomers subjected to 1mM Fe(II)-EDTA digestion. **Lanes 9-16** are the same as lanes 1-8 except **ODN 4'** is radiolabeled instead of **ODN 4**.

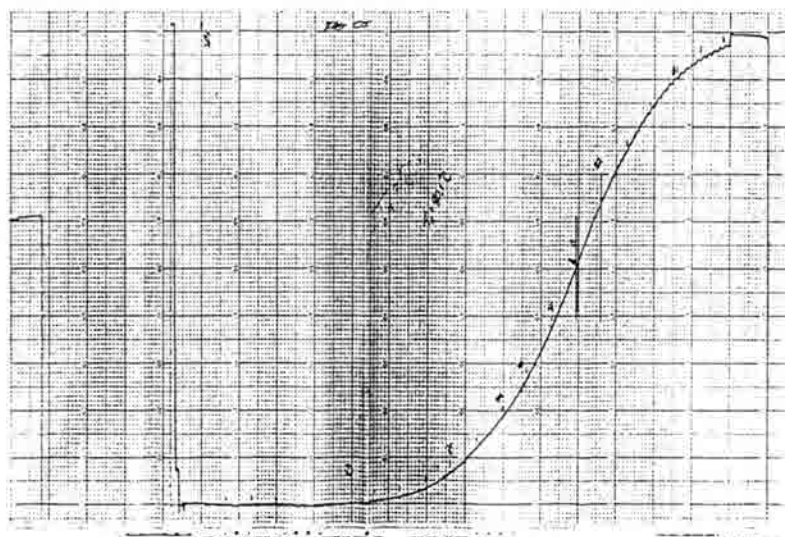
A)



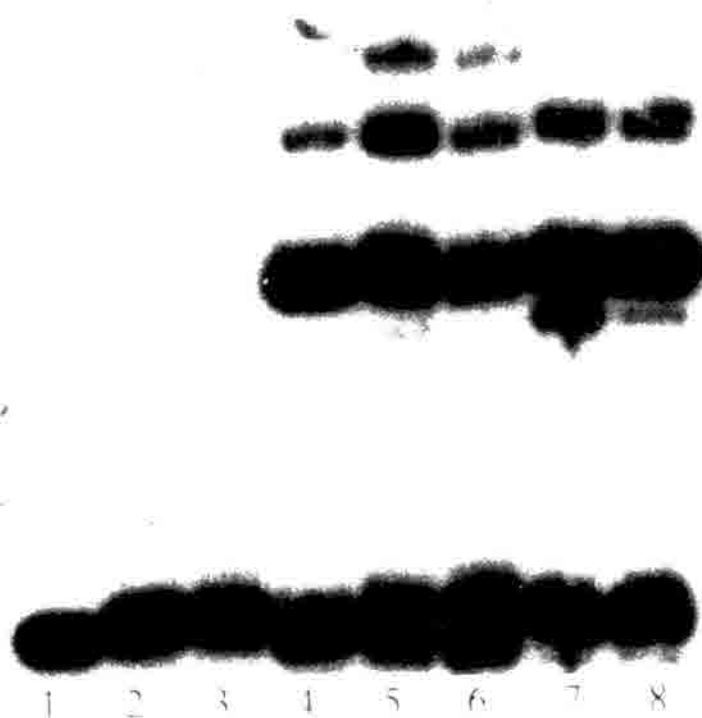
B)



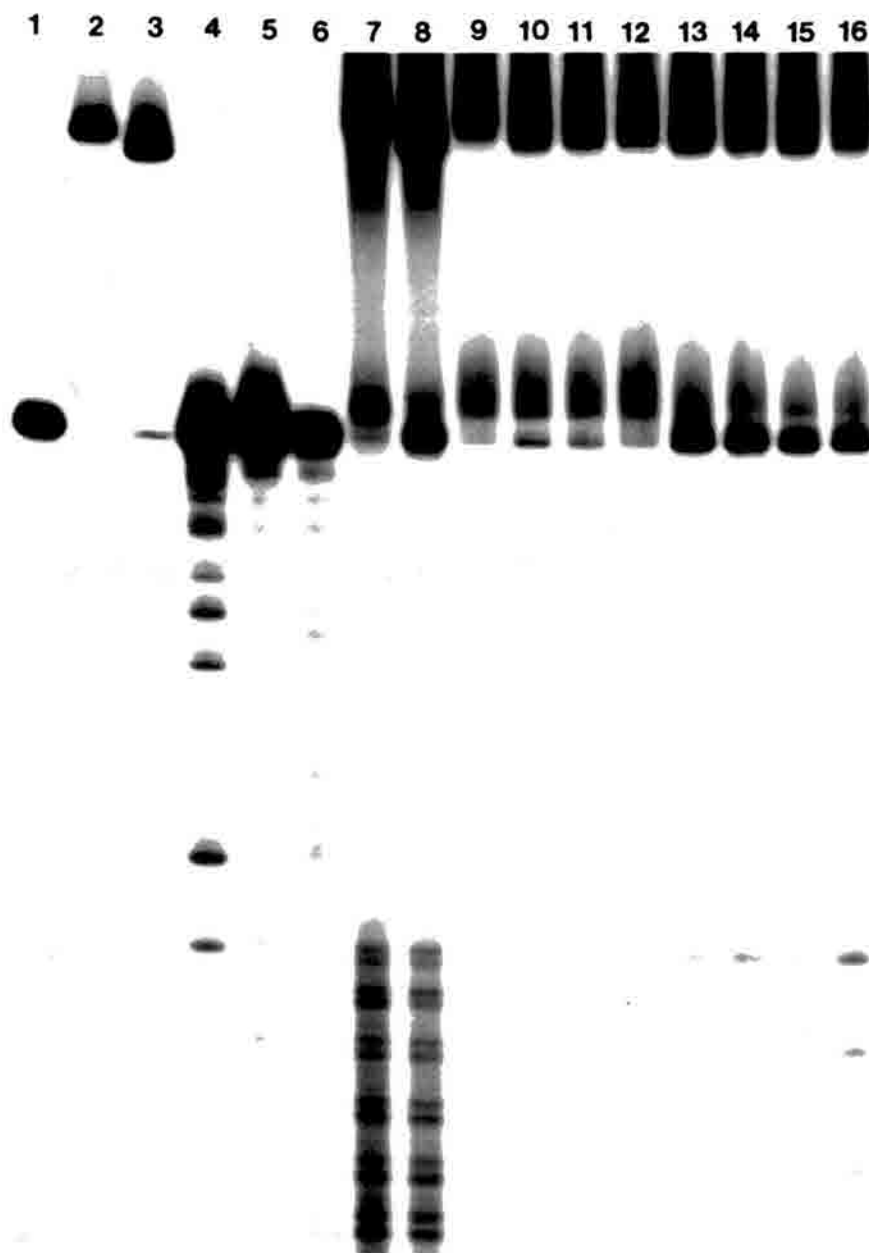
C)



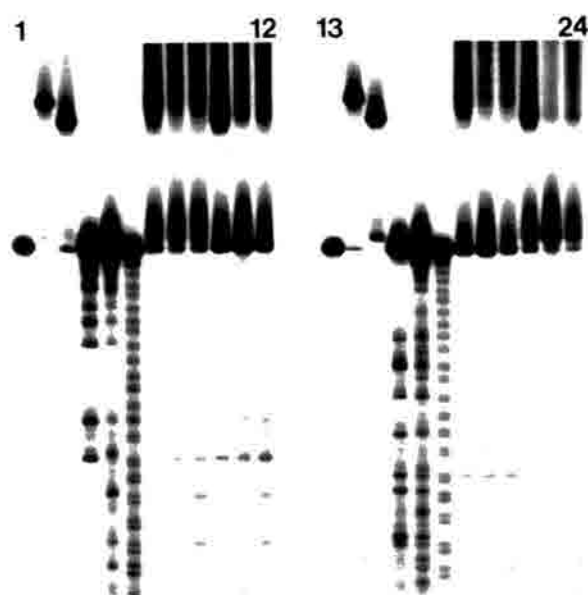
**Figure 5-10.** Hyperchromicity plots for fast and slow orientation isomers of FR-66979 cross-linked **template 3**. A) Plot of 260nm absorbance versus temperature for native template 3. B) Plot of 260nm absorbance versus temperature for slow isomer. C) Plot of 260 nm absorbance versus temperature for fast isomer.



**Figure 5-11.** Non-denaturing polyacrylamide gel electrophoresis of T4 DNA Ligase reactions of FR-66979 orientation isomers of cross-linked **template 1** ( $^{32}\text{P}$  labeled at 5' terminus of **ODN 1**). **Lanes 1-3**; standard DNA, slow and fast cross-link isomers respectively. **Lane 4**, **template 3** ligation standard; **Lane 5**; slow cross-link ligation; **Lane 6**; fast cross-link ligation; **Lane 7**; mixed native DNA and slow cross-link ligation; **Lane 8**; mixed native DNA and fast cross-link ligation.



**Figure 5-12-DEPC sequencing of hyperactive regions in 314 cross-linked template 3.** Template 3 was 5'-labeled on ODN 4. Base numbering is with respect to the 5' end of ODN 4. Lanes 1-3 are template 3 standard, slow cross-link and fast cross-link standards respectively; Lanes 4 & 5, Maxam-Gilbert G, G+A respectively, Lane 6, 1mM Fe(II)-EDTA digestion standard, Lanes 7 & 8 are fast and slow cross-links subjected to Fe(II)-EDTA digestion. Lane 9 is slow orientation isomer subjected to 1M piperidine 80°C; lanes 10-12 are slow cross-link treated with 5, 10, 15  $\mu$ l DEPC respectively then 1M piperidine. Lanes 13-16 are the same as lanes 9-12 except using the fast orientation isomer of cross-linked template 3.

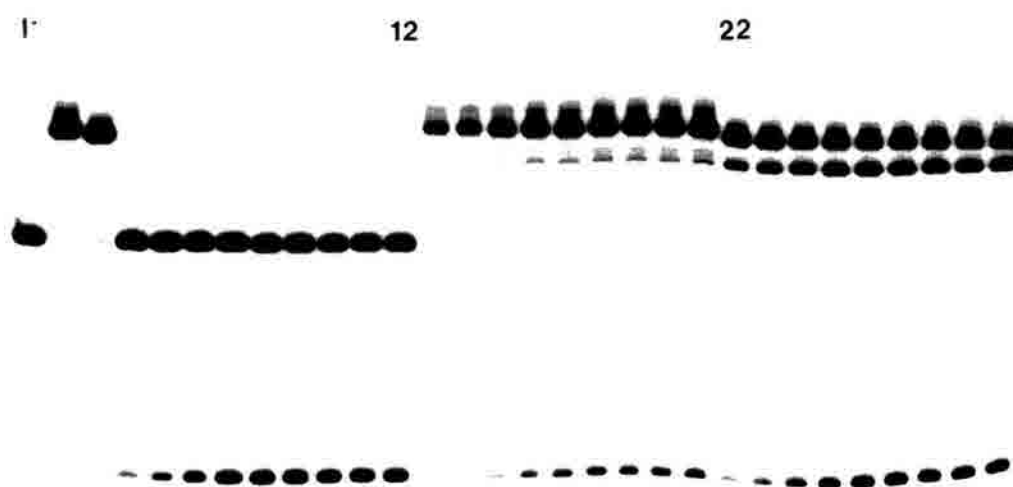


**Figure 5-13.** CAA sequencing of hyperactive regions in **314** cross-linked **template 3**. **Lanes 1-12** **template 3** was 5'-labeled on **ODN 4** while for **lanes 13-24** **ODN 4'** was 5' end-labeled. Base numbering is with respect to the 5' end of either radiolabeled ODN. **Lanes 1-3** are **template 3** standard, slow cross-link and fast cross-link standards respectively; **Lanes 4 & 5**, Maxam-Gilbert G, G+A respectively, **Lane 6**, 1mM Fe(II)-EDTA digestion standard, **Lanes 7** is slow cross-link subjected to 1M piperidine 80°C for 30 minutes. **Lanes 8,9** are slow orientation isomer subjected 2 and 5  $\mu$ l of chloroacetaldehyde respectively then 1M piperidine. **Lane 10** is fast cross-link subjected to 1M piperidine 80°C for 30 minutes. **Lanes 11,12** are fast orientation isomer subjected 2 and 5  $\mu$ l of chloroacetaldehyde respectively then 1M piperidine. **Lanes 13-24** were prepared analogously to **lanes 1-12**.

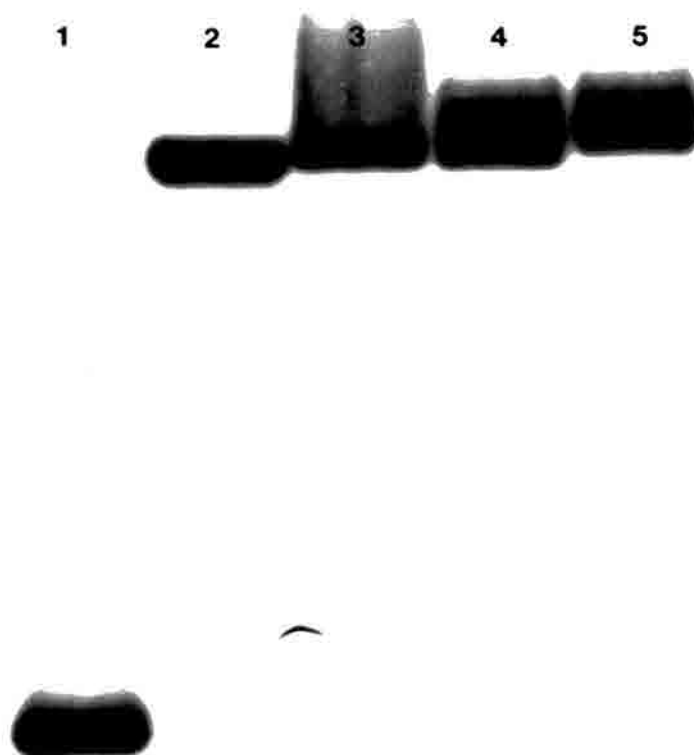




**Figure 5-14.** 20% DPAGE of sequential denaturing/renaturation reactions using orientation isomers of **template 7** (5' labeled on **ODN 9**) cross-linked with **314**. **Lanes 1-3**, standard duplex, slow orientation isomer of cross-linked substrate, fast orientation isomer standards. **Lanes 4-6** depict the products of heat denaturation at 80 °C for 10, 20, and 30 minutes respectively for the slow orientation isomer. **Lanes 7-9** depict the products of heat denaturation at 80 °C for 10, 20, and 30 minutes respectively for the fast orientation isomer.



**Figure 5-15.** 20% DPAGE analysis of Alu I restriction endonuclease reactions with MC cross-linked **template 7** (5' labeled on **ODN 9**). **Lanes 1-3**, standard duplex, slow orientation isomer of cross-linked substrate, fast orientation isomer standards. **Lanes 4-12**, reaction products of Alu I cleavage of native template 7 at 1,2,5,10, 20, 30, 40, 50 minutes and 1 h. respectively. **Lanes 13-21** reaction products of Alu I cleavage of slow MC isomer of cross-linked **template 7** at 1,2,5,10, 20, 30, 40, 50 minutes and 1 h. respectively. **Lanes 22-30** reaction products of Alu I cleavage of fast MC isomer of cross-linked **template 7** at 1,2,5,10, 20, 30, 40, 50 minutes and 1 h. respectively.



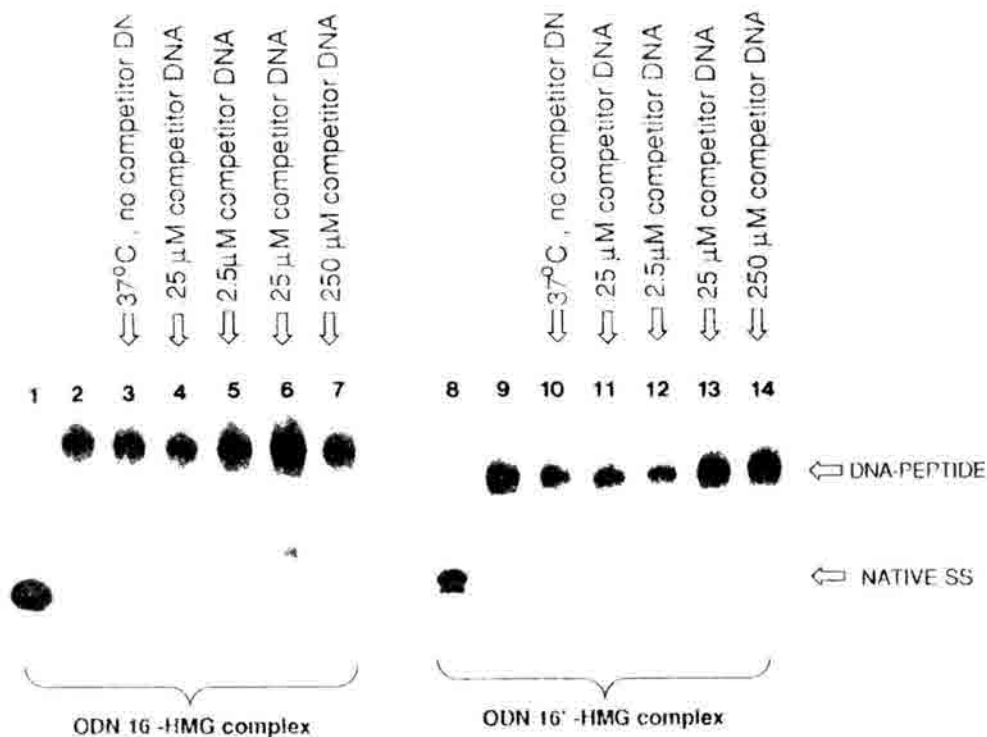
**Figure 5-16.** 20% non-DPAGE analysis of FR-66979 (**314**) cross-link orientation isomers of **template 3**. **Lanes 1,2**, standard duplex (heat denatured at 90°C 2 min. prior to loading), standard duplex (not denatured). **Lanes 3,4**, slow orientation isomer of cross-linked substrate, fast orientation isomer standards respectively. **Lane 6** FR-66979 monoadduct of **ODN 4** (after attempted denaturation at 90°C).



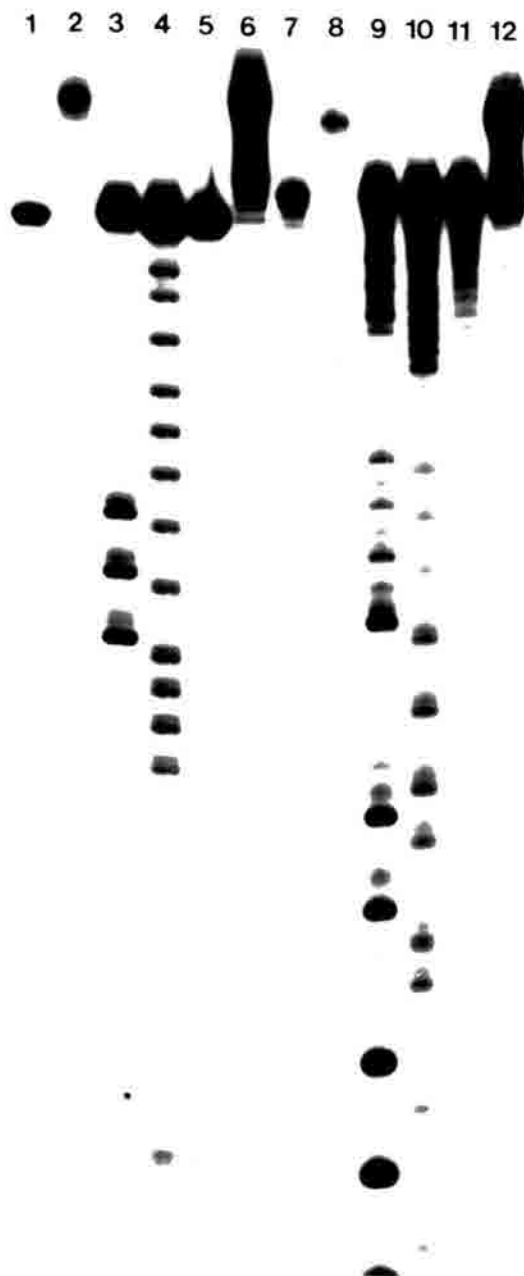
**Figure 5-17.** Autoradiogram of **ODN 13** reactions with **375a**. Reactions were conducted in 10mM Tris (pH = 8.0) at 37°C for 12 hours. **Lane 1** is standard 5' labeled self-complementary **ODN 13**. **Lane 2** is **ODN 13** reacted with 50mM FR-66979 + 100mM DTT. **Lane 3** is **ODN 13** reacted with 0.5 mM **375a** + 100mM DTT. **Lane 4** is **ODN 13** reacted with 0.5 mM **375a** + 100mM DTT + 10mM FR-66979. **Lane 5** is **ODN 13** reacted with 5 mM **375a** + 100mM DTT and **lane 6** is **ODN 13** reacted with 5 mM **375a** + 100mM DTT + 10 mM FR-66979.



**Figure 5-18.-** Piperidine digestion of 375a complex with 5'-labeled ODN-16'. **Lane 1 :** standard template 8. **Lane 2-** 375a complex with ODN-16; **Lane 3,** 375a complex with ODN 16'. **Lanes 4,12;** Maxam-Gilbert G ; **lanes 5, 13;** Maxam-Gilbert G+A. **Lane 6:** piperidine control; **lane 7;** piperidine control with unlabeled competitor DNA. **Lane 8:** 375a-ODN 16' complex treated with piperidine; **Lane 9:** 375a-ODN 16' complex treated with piperidine and unlabeled competitor DNA.



**Figure 5-19.-** DNA Exchange reactions of unlabeled **template 8** with **ODN 16** and **ODN 16'** complexes with HMG BD peptide **376**. All complexes were obtained after purification from FR-66979 reactions and subsequent 3'-end labeling with polynucleotidyl transferase. **Lane 1** : standard **template 8**. **Lane 2**: **376** complex with **ODN-16** control. **Lane 3**: **376-ODN 16 complex** incubation control (no unlabeled DNA included); **Lanes 4-7**: **376-ODN 16 complex** incubated with 2.5 $\mu\text{M}$ , 25 $\mu\text{M}$ , and 250 $\mu\text{M}$  unlabeled **template 8** respectively. **Lane 8**: **ODN 16'**; complex with **351** control, **lane 9**: **ODN 16'-376 complex** incubation control ( no unlabeled DNA). **Lanes 10-13**: **376-ODN 16 complex** incubated with 2.5 $\mu\text{M}$ , 25 $\mu\text{M}$ , and 250 $\mu\text{M}$  unlabeled **template 8** respectively.



**Figure 5-20.-** Piperidine digestion of FR-66979-mediated 376 complexes with 5'-labeled ODN-16 and ODN-16'. Lane 1: standard template 8; Lane 2: 376 complex with ODN-16 control; Lanes 3,4: Maxam-Gilbert G, G+A respectively; Lane 5: 1M piperidine control reaction, Lane 6: 376-ODN 16 complex subjected to 1M piperidine at 80°C 30 minutes. Lanes 7-12: same as lanes 1-6 except using 376-ODN 16' complex.